

WL-TR-95-4108

**HIGH TEMPERATURES COATINGS
FOR TITANIUM ALUMINIDES**



**J. C. Schaeffer
R. L. McCarron**

**GENERAL ELECTRIC COMPANY - AIRCRAFT ENGINES
ENGINEERING MATERIALS TECHNOLOGY LABORATORIES
CINCINNATI, OHIO 45215-6301**

13 December 1995

FINAL REPORT FOR 22 January 1991 - 13 December 1994

Approved for public release; distribution unlimited

DTIC QUALITY INSPECTED 4

**MATERIALS DIRECTORATE
WRIGHT LABORATORY
AIR FORCE MATERIEL COMMAND
WRIGHT-PATTERSON AIR FORCE BASE, OH 45433-7734**

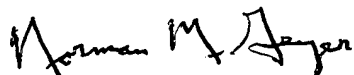
19970213 025

NOTICE

WHEN GOVERNMENT DRAWINGS, SPECIFICATIONS, OR OTHER DATA ARE USED FOR ANY PURPOSE OTHER THAN IN CONNECTION WITH A DEFINITELY GOVERNMENT-RELATED PROCUREMENT, THE UNITED STATES GOVERNMENT INCURS NO RESPONSIBILITY OR ANY OBLIGATION WHATSOEVER. THE FACT THAT THE GOVERNMENT MAY HAVE FORMULATED OR IN ANY WAY SUPPLIED THE SAID DRAWINGS, SPECIFICATIONS, OR OTHER DATA, IS NOT TO BE REGARDED BY IMPLICATION OR OTHERWISE IN ANY MANNER CONSTRUED, AS LICENSING THE HOLDER OR ANY OTHER PERSON OR CORPORATION, OR AS CONVEYING ANY RIGHTS OR PERMISSION TO MANUFACTURE, USE, OR SELL ANY PATENTED INVENTION THAT MAY IN ANY WAY BE RELATED THERETO.

THIS REPORT IS RELEASABLE TO THE NATIONAL TECHNICAL INFORMATION SERVICE (NTIS). AT NTIS, IT WILL BE AVAILABLE TO THE GENERAL PUBLIC, INCLUDING FOREIGN NATIONS.

THIS TECHNICAL REPORT HAS BEEN REVIEWED AND IS APPROVED FOR PUBLICATION.



NORMAN M. GEYER, Project Engineer
Ceramics Development & Materials
Behavior Branch
Metals and Ceramics Division



ALLAN W. GUNDERSON, Chief
Ceramics Development & Materials
Behavior Branch
Metals and Ceramics Division



WALTER M. GRIFFITH, Asst. Chief
Metals, Ceramics & Nondestructive
Evaluation Division
Materials Directorate

IF YOUR ADDRESS HAS CHANGED, IF YOU WISH TO BE REMOVED FROM OUR MAILING LIST, OR IF THE ADDRESSEE IS NO LONGER EMPLOYED BY YOUR ORGANIZATION, PLEASE NOTIFY, WL/MLLN, WRIGHT-PATTERSON AFB OH 45433-7817 TO HELP US MAINTAIN A CURRENT MAILING LIST.

COPIES OF THIS REPORT SHOULD NOT BE RETURNED UNLESS RETURN IS REQUIRED BY SECURITY CONSIDERATIONS, CONTRACTUAL OBLIGATIONS, OR NOTICE ON A SPECIFIC DOCUMENT.

DISCLAIMER NOTICE



**THIS DOCUMENT IS BEST
QUALITY AVAILABLE. THE
COPY FURNISHED TO DTIC
CONTAINED A SIGNIFICANT
NUMBER OF PAGES WHICH DO
NOT REPRODUCE LEGIBLY.**

REPORT DOCUMENTATION PAGE			Form Approved OMB No. 0704-0188	
<small>Public reporting burden for this collection of information is estimated to average 1 hour per response, including the time for reviewing instructions, searching existing data sources, gathering and maintaining the data needed, and completing and reviewing the collection of information. Send comments regarding this burden estimate or any other aspect of this collection of information, including suggestions for reducing this burden, to Washington Headquarters Services, Directorate for Information Operations and Reports, 1215 Jefferson Davis Highway, Suite 1204, Arlington, VA 22202-4302, and to the Office of Management and Budget, Paperwork Reduction Project (0704-0188), Washington, DC 20503.</small>				
1. AGENCY USE ONLY (Leave blank)		2. REPORT DATE 13 December 1995		3. REPORT TYPE AND DATES COVERED FINAL 22 Jan 91 - 13 Dec 94
4. TITLE AND SUBTITLE HIGH TEMPERATURE COATINGS FOR TITANIUM ALUMINIDES			5. FUNDING NUMBERS C - F33615-90-C-5960 PE - 62102F PR - 2418 TA - 01 WU - 56	
6. AUTHOR(S) J. C. SCHAEFFER; R. I. MCCARRON				
7. PERFORMING ORGANIZATION NAME(S) AND ADDRESS(ES) GENERAL ELECTRIC AIRCRAFT ENGINES ENGINEERING MATERIALS TECHNOLOGY LABORATORIES CINCINNATI OH 45215-6301			8. PERFORMING ORGANIZATION REPORT NUMBER	
9. SPONSORING/MONITORING AGENCY NAME(S) AND ADDRESS(ES) MATERIALS DIRECTORATE WRIGHT LABORATORY AIR FORCE MATERIEL COMMAND WRIGHT-PATTERSON AFB OH 45433-7734 POC: Steve Balsone, WL/MLLN, WPAFB OH 45433; 937-255-1346			10. SPONSORING/MONITORING AGENCY REPORT NUMBER WL-TR-95-4108	
11. SUPPLEMENTARY NOTES				
12a. DISTRIBUTION AVAILABILITY STATEMENT approved for public release; distribution is unlimited			12b. DISTRIBUTION CODE	
13. ABSTRACT (Maximum 200 words) The objective of this program was to select and evaluate environmentally protective coatings for alpha-2 and gamma titanium aluminide intermetallics. Many different coatings were selected including TiCrAl's, Alloy 718, APS YSZ, Cermet coatings (MCrAlY + Alumina), Modified Gamma TiAl compositions and MCr's. After a series of cyclic oxidation (760 and 900°C), burner rig (760 and 900°C) and hot salt stress corrosion cracking tests (400 to 565°C), the cermet coatings were selected for further evaluation. Different cermet coatings containing NiCoCrAlY, CoCrAlY and NiCrAlY were evaluated in similar tests. The best overall performer was the NiCrAlY/Alumina system. An optimized system applied to gamma and alpha-2 was mechanically tested in creep, fatigue and thermomechanical fatigue. Pretreatments included cyclic oxidation, salt and a CVD-W diffusion barrier. The final coating recommended for both gamma and alpha-2 Ti-aluminides is composed of 40-50% by volume alumina with the remainder Ni-20Cr-10Al-0.3Ywt% and is 50-75µm thick.				
14. SUBJECT TERMS			15. NUMBER OF PAGES 464	
			16. PRICE CODE	
17. SECURITY CLASSIFICATION OF REPORT UNCLASSIFIED	18. SECURITY CLASSIFICATION OF THIS PAGE UNCLASSIFIED	19. SECURITY CLASSIFICATION OF ABSTRACT UNCLASSIFIED	20. LIMITATION OF ABSTRACT SAR	

TABLE OF CONTENTS

REPORT DOCUMENTATION PAGE.....	i
FOREWORD	ii
TABLE OF CONTENTS	
LIST OF FIGURES	vii
LIST OF TABLES	xxx
1.0 Executive Summary	1
1.1 Introduction	1
1.2 Problem Definition	1
1.3 Summary of Results.....	1
1.3.1 Task 1 Coating/Substrate Selection.....	1
1.3.2 Task 2 - Environmental Screening.....	2
1.3.3 Task 3 - Mechanical Property Testing.....	3
1.3.4 Task 4 - Thermal Mechanical Fatigue Testing.....	4
1.3.5 Ti-Aluminide Environmental Coating Recommendation.....	5
2.0 Results and Discussion	6
2.1 Task 1 - Selection of Alloys, Coatings and Coating Processes	6
2.1.1 Alloy Selection - Task 1.1.....	6
2.1.2 Coating Selection - Task 1.2.....	6
2.1.3 Coating Process Selection-Task 1.3.....	7
2.1.4. Gamma Substrate-Task 1.4	8
2.1.4.1 Gamma Substrate-Task 1.4.....	8
2.1.4.2 Alpha-2 Substrate-Task 1.4.....	9
2.1.5 Coating Fabrication - Task 1.5.....	10
2.2 Task 2-Coating Performance Under Environmental Attack	10
2.2.2. Cyclic Oxidation Procedure - Task 2.2	10
900°C (1650°F) Cyclic Oxidation Test	11
Coated Gamma Ti-Aluminide	11
Coated Alpha-2 Ti-Aluminide	12
760°C (1400°F) Cyclic Oxidation Test	13
Coated Gamma Ti-Aluminide	14
Coated Alpha-2 Ti-Aluminide.....	14
2.2.3 X-ray Analysis of Coated/Uncoated Ti-Aluminides - Task 2.5.....	15
X-ray Analysis of Initial Coated/Uncoated Gamma.....	15

X-ray Analysis of Oxidized Coated/Uncoated Gamma	16
X-ray Analysis of Initial Coated/Uncoated Alpha-2	16
X-ray Analysis of Oxidized Coated/Uncoated Alpha-2	17
Summary of X-ray Analysis	17
Metallography of Coated/Uncoated Ti-aluminides - Task 2.5.....	18
Metallography of Gamma Ti-aluminides After Cyclic Oxidation	18
Sputtered Ti-44Al-28Cr/Gamma - 900°C.....	18
Sputtered Ti-55Al-8.5Cr/Gamma - 900°C.....	19
Cermet (NiCrAlY + Al ₂ O ₃)/Gamma - 900°C	19
APS YSZ/Gamma - 900°C	19
LPPS Ti-44Al-28Cr/Gamma - 900°C.....	20
Gamma - 900°C.....	20
Cermet (NiCrAlY/Al ₂ O ₃)/Gamma - 760°C.....	20
Sputtered Ti-44Al-28Cr/Gamma - 760°C.....	21
YSZ/Gamma - 760°C	22
Sputtered Ti-55Al-9Cr/Gamma - 760°C	22
HVOF TiCrAl/Gamma - 760°C.....	23
LPPS TiCrAl/Gamma - 760°C.....	23
Sputtered Alloy 718/Gamma - 760°C.....	23
HVOF CoCr(WSiC)/Gamma - 760°C	24
Gamma - 760°C.....	24
Metallography of Alpha-2 Ti-aluminides After Cyclic Oxidation	25
Sputtered Ti-44Al-28Cr/Alpha-2 - 900°C	25
Sputtered Ti-55Al-8.5Cr/Alpha-2 - 900°C	25
LPPS Ti-44Al-28Cr/Alpha-2 - 900°C.....	25
APS Alloy 718/Alpha-2 - 900°C.....	26
Alpha-2 - 900°C	26
Sputtered Ti-44Al-28Cr/Alpha-2 - 760°C	26
APS Alloy 718/Alpha-2 - 760°C.....	27
Sputtered Ti-55Al-9Cr/Alpha-2 - 760°C.....	27
LPPS Ti-44Al-28Cr/Alpha-2 - 760°C.....	28
Cermet (50%Al ₂ O ₃ &René 80)/Alpha-2 - 760°C	28
Alpha-2 - 760°C	29
2.2.4 Cyclic Hot Corrosion/Oxidation Testing (CHC/O) - Task 2.3	29
2.2.4.1 High Pressure Compressor (HPC) Test.....	30
Test Measurements.....	30
Metallography.....	31
Uncoated Gamma	31
Sputtered Ti-44Al-28Cr/Gamma	32
Cermet (50%Al ₂ O ₃ +NiCrAlY)/Gamma.....	32
APS YSZ/Gamma.....	32
Monolithic Alloy 718	33
Uncoated Alpha-2	33
Sputtered Ti-44Al-28Cr/Alpha-2	33
APS Alloy 718/Alpha-2	34
2.2.4.2 Low Pressure Turbine Test	35
Test Measurements.....	35
Metallography.....	36
Uncoated Gamma	36
Sputtered Ti-44Al-28Cr/γ.....	36
LPPS cermet (50%Alumina+50%NiCrAlY)/γ.....	37

APS YSZ/ γ	37
Uncoated Alpha-2	37
Sputtered Ti-44Al-28Cr/ α 2	37
APS Alloy 718/ α 2	38
LPPS Ti-48Al-2Cr-6Nb-0.1B/ α 2.....	38
Burner Rig Summary	39
2.2.5 Hot Salt Stress Corrosion Cracking Testing-Task 2.4.....	39
HSSCC Summary for Uncoated/Coated Gamma.....	39
Interstitial Embrittlement of Uncoated Gamma.....	39
HSSCC Metallography/Fractography of Gamma.....	40
Gamma Summary	41
Uncoated Gamma.....	41
Coated Gamma.....	42
HSSCC Summary of Uncoated/Coated Alpha-2	42
Interstitial Embrittlement of Uncoated Alpha-2	42
HSSCC Metallography/Fractography of Alpha-2	43
Alpha-2 Summary	44
Uncoated Alpha-2	44
Coated Alpha-2	45
2.2.6 Environmental Testing Iteration #2, Sub-Task 2.6.....	45
2.2.6.1 Hot Salt Stress Corrosion Cracking.....	46
HSSCC of Coated Gamma.....	47
HSSCC of Coated Alpha-2	48
2.2.6.2 Cyclic Hot Corrosion/Oxidation.....	48
Compressor Burner Rig Test - Task 2.6	49
Uncoated Alloys.....	50
Coated Alloys.....	51
Cermets Coatings on Alpha-2	51
Composite Coatings on Gamma.....	51
Reaction Zone.....	51
Low Pressure Turbine Burner Rig Test - Task 2.6	52
Metallography of Uncoated Alloys.....	54
Metallography of Coated Alloys.....	55
Cermets Coatings on Gamma	55
Cermets Coatings on Alpha-2.....	56
2.2.6.3 High Velocity Cyclic Oxidation Test - Task 2.6.....	57
Metallography of Uncoated Alloys.....	58
Cermets Coatings on Gamma	59
Cermets Coatings on Alpha-2.....	61
2.2.7 Coating Selection for Mechanical Tests in Task 3	62
Cermets Coating Selection.....	62
Diffusion Barrier Selection	62
2.3 Task 3 - Effect of Coating on Mechanical Properties.....	63
2.3.1 Mechanical Test Plan for Task 3.....	63
2.3.2 Coating Philosophy	63
2.3.3 Diffusion Barrier Application	64
2.3.4 Cermets Application	64

2.3.5	Mechanical Test Bar Exposure	65
2.3.6	Tensile Test Results	65
	Gamma	66
	Gamma Metallography	66
	Gamma Tensile Summary	67
	Alpha-2	68
	Alpha-2 Metallography	68
	Alpha-2 Tensile Summary	69
2.3.7	HSSCC Results	70
	Gamma Summary	70
	Gamma Metallography	70
	Gamma HSSCC Summary	72
	Alpha-2	72
	Alpha-2 Metallography	72
	Alpha-2 Summary	74
2.3.8	Fatigue 72	74
	Gamma Summary	74
	Gamma Metallography	75
	Alpha-2 Summary	77
	Alpha-2 Metallography	77
2.4	Task 4 - Coating Performance Under TMF	79
2.4.1	Optimized Cermet Coating Procedure	79
2.4.2	Coating Demonstration on Hardware	79
2.4.3	TMF Results	80
	Gamma	80
	Alpha-2	81
2.5	Coating Recommendations	82
3.0	Summary	84
Task 1	Alloy/Coating Selection	84
Task 2	Iteration #1.	84
Task 2	Iteration #2.	86
Task 3	Mechanical Testing.	88
Task 4	Thermal Mechanical Fatigue Testing.	90
	Ti-Aluminide Environmental Coating Recommendation	91
4.0	References	92

LIST OF FIGURES

Figure 1.	Schematic of a gas turbine engine showing the associated types of environmental attack for potential applications of alpha-2 and gamma alloys.....	95
Figure 2.	Schematic showing the task structure of the coatings program..	96
Figure 3.	Micrograph of the cermet coating after 500 hr of testing in cyclic hot corrosion/oxidation conditions.....	97
Figure 4.	Graphs showing the creep behavior of gamma and alpha-2 substrates with an applied cermet coating.....	98
Figure 5.	Cross-section of cermet coated gamma after 200K cycle runout at 760°C and 0.25% strain control with A=1.....	99
Figure 6.	Micrograph of a cermet coated cast gamma low pressure turbine blade.....	100
Figure 7.	Optical micrographs showing Ti-48Al-2Cr-2Nb after forging, heat treating and machining. The samples are etched in a solution of 2%HF and methanol.....	101
Figure 8.	Backscattered electron images (BEI) showing Ti-48Al-2Cr-2Nb after pancake forging and heat treatment. The microstructure is duplex and composed of primary gamma grains and transformed alpha.....	102
Figure 9.	Backscattered electron images (BEI) of Ti-48Al-2Cr-2Nb showing the alignment of phases in the "T" or transverse direction. "N" stands for the normal direction.	103
Figure 10.	Location of mechanical and environmental samples relative to the plane of the pancake gamma forging. Fibering or banding occurred in the plane of the forging.	104
Figure 11.	Schematic showing the location of the samples from the alpha-2 bar forging.	105
Figure 12.	Optical micrographs showing the Ti-24.5Al-12.5Nb-1.5Mo alloy after forging and heat treatment. Banding of the primary alpha-2 precipitates is observed. The area fraction of primary alpha-2 by image analysis in the higher magnification micrograph is 0.07.....	106
Figure 13.	Backscattered electron images showing the Ti-24.5Al-12.5Nb-1.5Mo alpha-2 alloy after forging and heat treatment. The dark imaging phase is metastable orthorhombic and the light imaging phase is stabilized beta.....	107

Figure 14.	Graph showing the results of cyclic oxidation testing at 900°C (1652°F) in air for 500 hr (a) gamma; (b) alpha-2	108
Figure 15.	Low magnification optical micrographs showing the surface of uncoated Ti-48Al-2Cr-2Nb after 100, 300 and 500 hr of cyclic oxidation at 900°C (1652°F). Spalling was observed especially on the edges of the sample.....	109
Figure 16.	Low magnification optical micrographs showing the surface of the LPPS Ti-44Al-28Cr coating on Ti-48Al-2Cr-2Nb after 100, 300 and 500 hr of cyclic oxidation in air at 900°C (1650°F).....	110
Figure 17.	Low magnification optical micrographs showing the surface of the HVOF Ti-44Al-28Cr coating on Ti-48Al-2Cr-2Nb after 100, 300 and 500 hr of cyclic oxidation in air at 900°C (1650°F).....	111
Figure 18.	Low magnification optical micrographs showing the surface of the Sputtered Ti-44Al-28Cr coating on Ti-48Al-2Cr-2Nb after 100, 300 and 500 hr of cyclic oxidation in air at 900°C (1650°F).....	112
Figure 19.	Low magnification optical micrographs showing the surface of the Sputtered Ti-55Al-8.5Cr coating on Ti-48Al-2Cr-2Nb after 100, 300 and 500 hr of cyclic oxidation in air at 900°C (1650°F).....	113
Figure 20.	Low magnification optical micrographs showing the surface of the APS YSZ coating on the Ti-47Al-2Cr-4Ta after 100, 300 and 500 hr of cyclic oxidation in air at 900°C (1650°F).....	114
Figure 21.	Low magnification optical micrographs showing the surface of the HVOF Co-Cr(W,Si,C) coating on the Ti-48Al-2Cr-2Nb after 100, 300 and 500 hr of cyclic oxidation in air at 900°C (1650°F).	115
Figure 22.	Low magnification optical micrographs showing the surface of the cermet coating (NiCrAlY and Al ₂ O ₃) on the Ti-48Al-2Cr-2Nb after 100, 300 and 500 hr of cyclic oxidation in air at 900°C (1650°F).....	116
Figure 23.	Low magnification optical surface micrographs of the uncoated Ti-24.5Al-12.5Nb-1.5Mo substrate after 100, 300 and 500 hr of cyclic oxidation in air at 900°C (1650°F).....	117
Figure 24.	Low magnification optical micrographs showing the surface of the sputtered Ti-44Al-28Cr on Ti-24.5Al-12.5Nb-1.5Mo after 100, 300 and 500 hr of cyclic oxidation in air at 900°C (1650°F).....	118
Figure 25.	Low magnification optical micrographs showing the surface of sputtered Ti-55Al-8.5Cr on Ti-24.5Al-12.5Nb-1.5Mo after 100, 300 and 500 hr of cyclic oxidation in air at 900°C (1650°F).....	119

Figure 26.	Low magnification optical surface micrographs of APS 718 on Ti-24.5Al-12.5Nb-1.5Mo after 100, 300 and 500 hr of cyclic oxidation in air at 900°C (1650°F).....	120
Figure 27.	Cyclic oxidation kinetics a for coatings on gamma Ti-aluminide substrate (top) and alpha-2 substrates (bottom) after 600 hr at 760°C (1400°F). (a) gamma; (b) alpha-2.....	121
Figure 28.	Backscattered electron micrographs of the sputtered Ti-44Al-28Cr on Ti-48Al-2Cr-2Nb. The top micrograph is the as deposited coating showing a very sharp coating/substrate interface. The bottom micrograph is after 500 one hour cycles at 900°C (1650°F) and shows a continuous Cr-rich reaction zone (arrow).....	122
Figure 29.	Microprobe traces for the elements that compose the sputtered Ti-44Al-28Cr coatings on Ti-48Al-2Cr-2Nb. The dotted lines represents the initial chemistry while the solid lines are after the 500 hr exposure at 900°C (1650°F).	123
Figure 30.	Graph showing the change in composition of the sputtered Ti-44Al-28Cr coatings on Ti-48Al-2Cr-2Nb. The change is relative to the amount of the element that was initially present.	124
Figure 31.	Backscattered electron micrographs of the sputtered Ti-55Al-8.5Cr on Ti-48Al-2Cr-2Nb. The top micrograph is the as deposited coating showing a very sharp coating/substrate interface. The bottom micrograph is after 500 one hour cycles at 900°C (1650°F) and shows a discontinuous Cr rich reaction zone (arrow).	125
Figure 32.	Microprobe traces for the elements that compose the sputtered Ti-55Al-8.5Cr coatings on Ti-48Al-2Cr-2Nb. The dotted lines represents the initial chemistry while the solid lines are after the 500 hr exposure at 900°C (1650°F).....	126
Figure 33.	Graph showing the change in composition of the sputtered Ti-55Al-8.5Cr coatings on Ti-48Al-2Cr-2Nb. The change is relative to the amount of the element that was initially present.....	127
Figure 34.	Optical micrographs showing a cermet coating of Al ₂ O ₃ (dark) and NiCrAlY (light) on Ti-48Al-2Cr-2Nb. The mixture of the constituents can be tailored to match the thermal expansion coefficient of the substrate.	128

Figure 35.	Backscattered electron micrographs showing the cermet coating of Al_2O_3 (dark) and NiCrAlY (light) on Ti-48Al-2Cr-2Nb. The top micrograph is as-coated and the bottom is after cyclic oxidation at 900°C (1650°F). A reaction layer occurs at the coating/substrate interface (arrow).....	129
Figure 36.	Microprobe traces for the elements that compose the cermet coating of Al_2O_3 (dark) and NiCrAlY (light) on Ti-48Al-2Cr-2Nb. The dotted lines represents the initial chemistry while the solid lines are after the 500 hr exposure at 900°C (1650°F).	130
Figure 37.	Graph showing the change in composition of the cermet coating of Al_2O_3 (dark) and NiCrAlY (light) on Ti-48Al-2Cr-2Nb. The change is relative to the amount of the element that was initially present. Oxygen was ignored in this analysis.....	131
Figure 38.	Backscattered electron micrographs of the yttria stabilized zirconia coating on Ti-47Al-2Cr-4Ta. The top micrograph is as-coated and the bottom is after cyclic oxidation at 900°C (1650°F). Oxide growth occurs at the coating/substrate interface (arrow).	132
Figure 39.	Microprobe traces for the elements that compose the of the yttria stabilized zirconia (YSZ) on the Ti-47Al-2Cr-4Ta substrate. The dotted lines represents the initial chemistry while the solid lines are after the 500 hr exposure at 900°C (1650°F).	133
Figure 40.	Graph showing the change in composition of the yttria stabilized zirconia (YSZ) coating on the Ti-47Al-2Cr-4Ta substrate. The change is relative to the amount of the element that was initially present. Oxygen was ignored in this analysis.....	134
Figure 41.	Secondary electron micrographs of the yttria stabilized zirconia coating on Ti-47Al-2Cr-4Ta. The top micrograph is as-coated and the bottom is after cyclic oxidation at 900°C (1650°F). The white line indicates where a line scan for oxygen was made. The fine white dots indicate the relative level of oxygen. The oxygen content of the YSZ is about 67 atom percent.....	135
Figure 42.	Electron micrographs of the LPPS Ti-44Al-28Cr coating applied to Ti-48Al-2Cr-2Nb. The initial microstructure (top) displays a typical plasma spray appearance. Copper and Ni-base superalloy contamination were noted in the sample (arrow). The exposed microstructure (bottom) shows areas where a protective alumina scale has formed and areas where non-protective rutile dominates.	136

Figure 43.	Microprobe traces for the elements in the LPPS Ti-44Al-28Cr coating on Ti-48Al-2Cr-2Nb. The dotted lines represents the initial chemistry while the solid lines are after the 500 hr exposure at 900°C (1650°F).	137
Figure 44.	Graph showing the change in composition of LPPS Ti-44Al-28Cr coating on Ti-48Al-2Cr-2Nb. The change is relative to the amount of the element that was initially present. Oxygen was ignored in this analysis.	138
Figure 45.	Secondary electron micrographs of the oxide scale formed on Ti-48Al-2Cr-2Nb. The oxide had locally thick areas that were associated with spallation.....	139
Figure 46.	Surface optical micrographs of the cermet (80%Alumina + NiCrAlY) coated gamma sample at various intervals throughout the 760°C (1400°F) cyclic oxidation test in air.	140
Figure 47.	Backscattered and secondary electron micrographs from a cross-section of the cermet (80%Alumina + NiCrAlY) coated gamma sample after the 760°C (1400°F) cyclic oxidation test in air.	141
Figure 48.	Chemical composition of the cermet coating on Ti-48Al-2Cr-2Nb before and after cyclic oxidation for 1000 hr at 760°C (1400°F) in air. Nickel has diffused into the substrate resulting in reaction layers.	142
Figure 49.	Surface optical micrographs of the sputtered Ti-44Al-28Cr gamma sample at various intervals throughout the 760°C (1400°F) cyclic oxidation test in air. Some thermal expansion mismatch cracks are observed.	143
Figure 50.	Backscattered and secondary electron micrographs from a cross-section of the sputtered Ti-44Al-28Cr gamma sample after the 760°C (1400°F) cyclic oxidation test in air.	144
Figure 51.	Microprobe results showing the difference in chemistry for a sputtered Ti-44Al-28Cr coating before and after cyclic oxidation exposure.	145
Figure 52.	Surface optical micrographs of the APS YSZ gamma sample at various intervals throughout the 760°C (1400°F) cyclic oxidation test in air. Coating spallation was evident at the edges.....	146
Figure 53.	Backscattered and secondary electron micrographs from a cross-section of the APS YSZ/gamma sample after the 760°C (1400°F) cyclic oxidation test in air	147
Figure 54.	Surface optical micrographs of the sputtered Ti-55Al-9Cr/gamma sample at various intervals throughout the 760°C (1400°F) cyclic oxidation test in air. Some thermal expansion mismatch cracks are observed.	148

Figure 55.	Backscattered electron micrograph from a cross-section of the sputtered Ti-55Al-9Cr gamma sample after the 760°C (1400°F) cyclic oxidation test in air.	149
Figure 56.	Surface optical micrographs of the HVOF Ti-44Al-28Cr coated gamma sample at various intervals throughout the 760°C (1400°F) cyclic oxidation test in air.	150
Figure 57.	Backscattered and secondary electron micrographs from a cross-section of the HVOF Ti-44Al-28Cr/gamma sample after the 760°C (1400°F) cyclic oxidation test in air.....	151
Figure 58.	Backscattered and secondary electron micrographs from a cross-section of the LPPS Ti-44Al-28Cr/gamma sample after the 760°C (1400°F) cyclic oxidation test in air	152
Figure 59.	Backscattered and secondary electron micrographs from a cross-section of the sputtered Alloy 718/gamma sample after the 760°C (1400°F) cyclic oxidation test in air.....	153
Figure 60.	Backscattered electron micrographs from a cross-section of the HVOF CoCr(WSiC)/gamma sample after the 760°C (1400°F) cyclic oxidation test in air.	154
Figure 61.	Surface optical micrographs of the uncoated Ti-48Al-2Cr-2Nb sample at various intervals throughout the 760°C (1400°F) cyclic oxidation test in air.	155
Figure 62.	Backscattered micrographs of the uncoated Ti-48Al-2Cr-2Nb sample after the 760°C (1400°F) cyclic oxidation test in air. One micrograph shows a microprobe trace for oxygen.	156
Figure 63.	Backscattered electron micrographs of the sputtered Ti-44Al-28Cr on Ti-24.5Al-12.5Nb-1.5Mo. Some through thickness defects are noted in the coating.	157
Figure 64.	Microprobe traces for the elements that compose the sputtered Ti-44Al-28Cr coating on Ti-24.5Al-12.5Nb-1.5Mo.	158
Figure 65.	Backscattered electron micrographs of the sputtered Ti-55Al-8.5Cr on Ti-24.5Al-12.5Nb-1.5Mo. Some through thickness defects are noted in the coating.	159
Figure 66.	Microprobe traces for the elements that compose the sputtered Ti-55Al-8.5Cr coating on Ti-24.5Al-12.5Nb-1.5Mo.	160

Figure 67.	Graph showing the linear expansion coefficients of TiCrAl coatings compared to the Ti-48Al-2Cr-2Nb and Ti-24.5Al-12.5Nb-1.5Mo substrates. The mismatch is greater between the alpha-2 alloys and the coating compositions.	161
Figure 68.	Backscattered electron micrographs of the LPPS Ti-44Al-28Cr on Ti-24.5Al-12.5Nb-1.5Mo. Layers at the coating substrate interface are associated with oxidation and contamination.	162
Figure 69.	Microprobe traces for the elements that compose the LPPS Ti-44Al-28Cr coating on Ti-24.5Al-12.5Nb-1.5Mo.	163
Figure 70.	Electron micrographs of the air plasma sprayed (APS) coating on the Ti-24.5Al-12.5Nb-1.5Mo alpha-2 substrate. Porosity and oxide inclusions are found in the coating.	164
Figure 71.	Microprobe traces for the elements that compose the APS 718 coating on Ti-24.5Al-12.5Nb-1.5Mo.	165
Figure 72.	Electron micrographs of the scale formed on Ti-24.5Al-12.5Nb-1.5Mo after cyclic oxidation for 500 hr at 900°C (1650°F) in air.	166
Figure 73.	Surface optical micrographs of the sputtered Ti-44Al-28Cr alpha-2 sample at various intervals throughout the 760°C (1400°F) cyclic oxidation test in air. Many thermal expansion mismatch cracks are observed.	167
Figure 74.	Backscattered and secondary electron micrographs from a cross-section of the sputtered Ti-44Al-28Cr alpha-2 sample after the 760°C (1400°F) cyclic oxidation test in air.	168
Figure 75.	Change in the composition of a sputtered Ti-44Al-28Cr coating after 1000 hr of cyclic oxidation at 760°C (1400°F) in air.	169
Figure 76.	Surface optical micrographs of the APS Alloy 718 on alpha-2 at various intervals throughout the 760°C (1400°F) cyclic oxidation test in air.	170
Figure 77.	Backscattered and secondary electron micrographs from a cross-section of the APS Alloy 718 on alpha-2 after the 760°C (1400°F) cyclic oxidation test in air.	171
Figure 78.	The change in composition of an air plasma sprayed Alloy 718 coating on a Ti-24.5Al-12.5Nb-1.5Mo alpha-2 alloy. After 1000 hr at 760°C (1400°F), there is a 35mm thick reaction layer.	172

Figure 79.	Surface optical micrographs of the sputtered Ti-55Al-9Cr gamma sample at various intervals throughout the 760°C (1400°F) cyclic oxidation test in air. Large thermal expansion mismatch cracks are observed along with coating spallation.	173
Figure 80.	Backscattered electron micrograph from a cross-section of the sputtered Ti-55Al-9Cr/alpha-2 sample after the 760°C (1400°F) cyclic oxidation test in air.	174
Figure 81.	Surface and cross-section micrographs of the LPPS Ti-44Al-28Cr coating on the alpha-2 sample after the 1000 hr 760°C cyclic oxidation test in air.	175
Figure 82.	Surface and cross-section micrographs of the cermet coating on the alpha-2 sample after the 1000 hr 760°C cyclic oxidation test in air.	176
Figure 83.	Surface optical micrographs of the uncoated Ti-24.5Al-12.5Nb-1.5Mo sample at various intervals throughout the 760°C (1400°F) cyclic oxidation test in air. Locally thick oxides that spalled are evident.	177
Figure 84.	Secondary electron micrographs of the uncoated Ti-24.5Al-12.5Nb-1.5Mo sample after the 760°C (1400°F) cyclic oxidation test in air. One micrograph shows a microprobe trace for oxygen.	178
Figure 85.	A schematic of the high velocity hot corrosion/oxidation rig used to test coated and uncoated Ti-aluminides in engine simulative environments. Photograph of the CHC/O rig in operation. The samples rotate on a carousel in front of a combustor.	179
Figure 86.	Graphs showing the temperature distribution of the environmental pins used to test the coated and uncoated Ti-aluminides in high pressure compressor conditions.	180
Figure 87.	Weight change/area data for unrinsed coated and uncoated Ti-aluminides during the high pressure compressor burner rig test. Thermally sprayed coatings had large spallation events early in the test. The other coatings exhibited little weight change.	181
Figure 88.	Weight change/area data for unrinsed coated and uncoated Ti-aluminides during the high pressure compressor burner rig test. The y-axis has been enlarged to differentiate the behavior of systems that showed little weight change.	182
Figure 89.	Color photograph shows the coated and uncoated Ti-aluminide samples after 3200 cycles or 550 hr under high pressure compressor (CHC/O) environmental conditions. The notched side faced the combustor.	183

Figure 90.	Color photograph shows the coated and uncoated Ti-aluminide samples after 3200 cycles or 550 hr under high pressure compressor (CHC/O) environmental conditions. This side of the pins faced away from the combustor.	184
Figure 91.	Cross-sectional micrographs taken from the hot spot of the uncoated gamma alloy after the HPC environmental test.	185
Figure 92.	Cross-sectional micrographs taken from the hot spot of the sputtered Ti-44Al-28Cr gamma alloy after the HPC environmental test. Through-thickness defects were observed in the coating, but did not penetrate the substrate.....	186
Figure 93.	Cross-sectional micrographs taken from the hot spot of the cermet (50%NiCrAlY +alumina) coating on the gamma alloy after the HPC environmental test. The coating shows no cracking, spalling or signs of degradation.....	187
Figure 94.	Micrographs of the APS YSZ coating on the gamma alloy at the hot spot after the HPC environmental test.	188
Figure 95.	Cross-sectional micrographs taken from the hot spot of the monolithic Alloy 718 after the HPC environmental test.	189
Figure 96.	Cross-sectional micrographs taken from the hot spot on the uncoated alpha-2 after the HPC environmental test. The alloy has a thick layered scale that might spall.	190
Figure 97.	Micrographs of the cross-section of the sputtered Ti-44Al-28Cr coating on alpha-2 after the HPC environmental test.	191
Figure 98.	Micrographs of the cross-section of the APS Alloy 718 coating on alpha-2 after the HPC environmental test.	192
Figure 99.	Micrographs of the cross-section of the LPPS modified gamma coating on alpha-2 after the HPC environmental test. No thermal fatigue cracks were seen on the coating.	193
Figure100.	Temperature profile of the specimens in the low pressure turbine environmental test. The "hot" area is located 1cm from the top of the pin. A section of the pin 3.3cm from the tip provides the same cycle as the hot spot from the HPC test except with a high concentration of salt.	194
Figure 101.	Color photograph shows the coated and uncoated Ti-aluminide samples after 498 cycles or 50 hr under low pressure turbine (CHC/O) environmental conditions. The notched side faced the combustor.	195

Figure 102.	Color photograph shows the coated and uncoated Ti-aluminide samples after 498 cycles or 50 hr under low pressure turbine (CHC/O) environmental conditions. This side of the pin faced away from the combustor.	196
Figure 103.	Cross-sectional micrographs taken from the hot spot (top) and the 3.3cm sections (bottom) of the uncoated gamma alloy after the LPT environmental test.	197
Figure 104.	Cross-sectional micrographs taken from the hot spot (top) and the 3.3cm sections (bottom) of the sputtered Ti-44Al-28Cr coating on the gamma alloy after the LPT environmental test.	198
Figure 105.	Cross-sectional micrographs taken from the hot spot (top) and the 3.3cm sections (bottom) of the cermet coating on the gamma alloy after the LPT environmental test. No significant degradation was observed.	199
Figure 106.	Cross-sectional micrographs taken from the hot spot (top) and the 3.3cm sections (bottom) of the APS YSZ coating on the gamma alloy after the LPT environmental test. The coating spalled during the test.	200
Figure 107.	Cross-sectional micrographs taken from the hot spot (top) and the 3.3cm sections (bottom) of uncoated alpha-2 after the LPT environmental test.	201
Figure 108.	Cross-sectional micrographs taken from the hot spot (top) and the 3.3cm sections (bottom) of sputtered Ti-44Al-28Cr coating on the alpha-2 alloy after the LPT environmental test.	202
Figure 109.	Cross-sectional micrographs taken from the hot spot (top) and the 3.3cm sections (bottom) of the APS Alloy 718 coating on the alpha-2 alloy after the LPT environmental test.	203
Figure 110.	Cross-sectional micrographs taken from the hot spot (top) and the 3.3cm sections (bottom) of the LPPS modified gamma coating on the alpha-2 alloy after the LPT environmental test.	204
Figure 111.	Cross-sectional micrographs taken from the hot spot (top) and the 3.3cm sections (bottom) of the René 80 after the LPT environmental test.	205
Figure 112.	Low magnification cross-sections of uncoated gamma (Ti-48Al-2Cr-2Nb) specimens showing the fracture path and little secondary tensile cracking after various salt free exposures.	206
Figure 113.	Higher magnification cross-sections of uncoated gamma (Ti-48Al-2Cr-2Nb) specimens showing the a very thin external scale.	207

Figure 114.	The UTS response surface is flat (~50-60 ksi) for gamma samples as a function of coating and exposure. Only the 1050°C/40 ksi/750 hr salt exposure of the bare gamma sample resulted in total embrittlement.	208
Figure 115.	Post exposure low magnification fractographs of gamma samples after tensile testing showing a difference in crack initiation. The sample exposed without salt has a single origin, while the salt exposed sample has multiple origins.	209
Figure 116.	Low magnification cross-sections of coated and uncoated gamma (Ti-48Al-2Cr-2Nb) specimens showing the fracture path and little HSSCC cracking after a 750°C/50 ksi/100h exposure.	210
Figure 117.	High magnification cross-sections of coated and uncoated gamma (Ti-48Al-2Cr-2Nb) specimens showing coating attack, substrate attack and cracking after a HSSCC exposure for 750°C/50 ksi/100h.	211
Figure 118.	Low magnification cross-sections of coated and uncoated gamma (Ti-48Al-2Cr-2Nb) specimens showing the morphology of the fracture path and cracking after a HSSCC exposure for 1050°C/40 ksi and different times.	212
Figure 119.	High magnification cross-sections of coated and uncoated gamma (Ti-48Al-2Cr-2Nb) specimens showing the morphology of HSSCC attack in the substrate and on coatings after a 1050°C/40 ksi exposure for different times. The attack is most notable on the uncoated gamma where a thick Cl-rich external scale and intergranular attack are observed.	213
Figure 120.	Curves showing the creep behavior of coated and uncoated gamma alloys during 100h exposures at 750°C/50 ksi and 1050°C/40 ksi. The gamma alloys crept at nearly the same rate for the two exposures.	214
Figure 121.	Low magnification cross-sections of uncoated alpha-2 (Ti-24.5Al-12.5Nb-1.5Mo) specimens showing the fracture path and secondary tensile cracking after various exposures.	215
Figure 122.	High magnification cross-sections of uncoated alpha-2 (Ti-24.5Al-12.5Nb-1.5Mo) specimens showing the thin external scale and secondary tensile cracking after various exposures. A regular distribution of secondary tensile cracks is observed (arrows).	216
Figure 123.	Low magnification cross-sections of coated and uncoated alpha-2 (Ti-24.5Al-12.5Nb-1.5Mo) specimens showing a flatter fracture path and one large HSSCC crack after a salt exposure at 750°C/50 ksi.	217

Figure 124.	Higher magnification cross-sections of coated and uncoated alpha-2 (Ti-24.5Al-12.5Nb-1.5Mo) specimens showing the surfaces after a salt exposure at 750°C/50 ksi.	218
Figure 125.	Low magnification fractographs of uncoated alpha-2 (Ti-24.5Al-12.5Nb-1.5Mo) specimens exposed with and without salt at 1050°C/40 ksi/100h. The sample exposed with salt had multiple fracture origins.	219
Figure 126.	Plot showing the potency of the air plasma sprayed Alloy 718 as a coating for HSSCC resistance. The Alloy 718 coating achieves a local maxima on the UTS response surface of coating vs. test. "LT" means long time exposure.	220
Figure 127.	Low magnification cross-sections of coated and uncoated alpha-2 (Ti-24.5Al-12.5Nb-1.5Mo) specimens showing a flatter fracture path and a large HSSCC crack in the bare sample after a salt exposure at 1050°C/40 ksi.....	221
Figure 128.	Higher magnification cross-sections of coated and uncoated alpha-2 (Ti-24.5Al-12.5Nb-1.5Mo) specimens showing cracking at the surface after various salt exposures at 1050°C/40 ksi.	222
Figure 129.	Higher magnification cross-sections of alpha-2 (Ti-24.5Al-12.5Nb-1.5Mo) specimens showing attack at primary α_2 islands and prior β grain boundaries after a salt exposure at 1050°C/40 ksi.	223
Figure 130.	Creep curves for 100h exposures at 750°C/50ksi and 1050°C/40 ksi of coated and uncoated alpha-2 showing greater deformation for samples undergoing HSSCC damage.....	224
Figure 131.	Micrographs of low pressure plasma sprayed FeCrAlY on cast and forged gamma alloys after 1500 hr of cyclic oxidation at 900°C (1652°F). Thermal fatigue cracks and coating spallation were observed.....	225
Figure 132.	Backscattered and secondary micrographs showing the morphology of the sea salt after application on a steel tensile bar.	226
Figure 133.	Curves showing the 750 hr creep behavior of cermet coated gamma and alpha-2 alloys at 1050°C/40 ksi. Only one of the coated alpha-2 alloys survived the exposure.	227
Figure 134.	Micrographs showing the Alloy 718 cermet specimen on gamma after a 750 hr HSSCC exposure at 1050°C/40 ksi. The sample failed in the radius during the post exposure tensile test.	228

Figure 135.	Micrographs showing the CoCrAlY cermet specimen on gamma after a 750 hr HSSCC exposure at 1050°C/40 ksi. The sample failed in the radius during the post exposure tensile test.	229
Figure 136.	Micrographs showing the NiCoCrAlY cermet specimen on gamma after a 750 hr HSSCC exposure at 1050°C/40 ksi. The sample failed in the radius during the post exposure tensile test.	230
Figure 137.	Micrographs showing the fractured cross-section of the NiCoCrAlY composite coating on the gamma Ti-48Al-2Cr-2Nb alloy after a 1050°C/40 ksi exposure with salt followed by a room temperature tensile test. The coating was adherent.	231
Figure 138.	Micrographs showing the fractured cross-section of the CoCrAlY composite coating on the gamma Ti-48Al-2Cr-2Nb alloy after a 1050°C/40 ksi exposure with salt followed by a room temperature tensile test. The coating was adherent.	232
Figure 139.	Micrographs showing the fractured cross-section of the Alloy 718 composite coating on the gamma Ti-48Al-2Cr-2Nb alloy after a 1050°C/40 ksi exposure with salt followed by a room temperature tensile test. The coating was adherent.	233
Figure 140.	Micrographs of the Alloy 718 cermet/alpha-2 specimen after 1.1H of HSSCC exposure. Large HSSCC cracks are observed throughout the cross-section. The intergranular nature of the fracture cannot be overlooked.	234
Figure 141.	Micrographs of the Alloy 718 cermet/alpha-2 specimen after 1.1H of HSSCC exposure showing the morphology of the crack in the coating, at the coating/substrate interface and at the crack tip in the substrate. The crack tends to propagate down prior b grain boundaries.	235
Figure 142.	Micrographs showing the fracture surface of the CoCrAlY cermet/alpha-2 coating after 62H of HSSCC exposure. The sample had a large origin that was associated with Cl.	236
Figure 143.	Micrographs of the CoCrAlY cermet/alpha-2 specimen after 62H of HSSCC exposure at 1050°C/40 ksi. Cracks are observed to penetrate in regions of the coating where alumina is concentrated. Internal attack is noted in the substrate (arrow).	237
Figure 144.	Micrographs showing the NiCrAlY cermet specimen on alpha-2 after a 750 hr HSSCC exposure at 1050°C/40 ksi. No HSSCC attack was observed in the substrate.	238

Figure 145.	Color photographs showing the flame-side of coated and uncoated Ti-48Al-2Cr-2Nb gamma after 3749 cycles (625 hr) of burner rig testing using a 760°C/648°C with 1ppm sea salt.....	239
Figure 146.	Color photographs showing the back-side of coated and uncoated Ti-48Al-2Cr-2Nb gamma after 3749 cycles (625 hr) of burner rig testing using a 760°C/648°C with 1ppm sea salt.....	240
Figure 147.	Color photographs showing the flame-side of coated and uncoated Ti-24.5Al-12.5Nb-1.5Mo alpha-2 after 3749 cycles (625 hr) of burner rig testing using a 760°C/648°C with 1ppm sea salt.....	241
Figure 148.	Color photographs showing the back-side of coated and uncoated Ti-24.5Al-12.5Nb-1.5Mo alpha-2 after 3749 cycles (625 hr) of burner rig testing using a 760°C/648°C with 1ppm sea salt.....	242
Figure 149.	Micrographs showing particulate found on filter paper after rinsing. The particles were mainly MgO.	243
Figure 150.	Graph showing the temperature profile of the pins during the 760/648°C burner rig test. Careful cross-sectioning allows different conditions to be analyzed on the same pin.....	244
Figure 151.	Micrographs showing cross-sections of the Ti-24.5Al-12.5Nb-1.5Mo alpha-2 as a function of peak temperature attained during burner rig testing.....	245
Figure 152.	Micrographs showing cross-sections of the Ti-48Al-2Cr-2Nb gamma as a function of peak temperature attained during burner rig testing.....	246
Figure 153.	Micrographs showing cross-sections of the Hastelloy X as a function of peak temperature attained during burner rig testing.....	247
Figure 154.	Micrographs showing cross-sections of the NiCrAlY composite coated alpha-2 as a function of peak temperature attained during burner rig testing.....	248
Figure 155.	Micrographs showing cross-sections of the CoCrAlY composite coated alpha-2 as a function of peak temperature attained during burner rig testing.....	249
Figure 156.	Micrographs showing cross-sections of the Alloy 718 composite coated alpha-2 as a function of peak temperature attained during burner rig testing.....	250

Figure 157.	Micrographs showing cross-sections of the NiCoCrAlY composite coated gamma as a function of peak temperature attained during burner rig testing.....	251
Figure 158.	Micrographs showing cross-sections of the CoCrAlY composite coated gamma as a function of peak temperature attained during burner rig testing.....	252
Figure 159.	Micrographs showing cross-sections of the Alloy 718 composite coated gamma as a function of peak temperature attained during burner rig testing.....	253
Figure 160.	Graph summarizing reaction zone thickness as a function of peak exposure temperature. An equation that fits the line drawn through the data is shown in the Figure.	254
Figure 161.	Color photograph of the back-side all of the pins after rinsing and 516 hr of burner rig testing at 871/760°C in 1-2ppm of sea salt. The figure allows comparisons between alpha-2 and gamma systems.	255
Figure 162.	Color photograph of the flame-side of rinsed coated and uncoated alpha-2 after 516H of burner rig testing at 871/760°C in 1-2ppm of sea salt.	256
Figure 163.	Color photograph of the flame-side of rinsed coated and uncoated gamma after 516H of burner rig testing at 871/760°C in 1-2ppm of sea salt.	257
Figure 164.	Graph showing the temperature distribution along the length of the pin for the 871/760°C burner rig test.	258
Figure 165.	Graph showing the weight change after rinsing for coated and uncoated samples during the 871/760°C burner rig test.....	259
Figure 166.	Micrographs showing cross-sections of uncoated gamma after the 871/760°C burner rig test.....	260
Figure 167.	Micrographs showing the attack of uncoated gamma in the 871°C section. Thick oxide scales formed as well as a lacy microstructure in the gamma substrate that was prone to cracking..	261
Figure 168.	Micrographs showing cross-sections of uncoated alpha-2 after the 871/760°C burner rig test.....	262
Figure 169.	Micrographs showing cross-sections of Codep coated R'80 after the 871/760°C burner rig test.....	263

Figure 170.	Micrographs showing the detail of the attack on Codep coated R'80 in the 871°C section. A lacy microstructure has formed similar to the uncoated gamma.	264
Figure 171.	Micrographs showing cross-sections of the NiCoCrAlY composite coated gamma after the 871/760°C burner rig test.....	265
Figure 172.	Micrographs showing cross-sections of the CoCrAlY composite coated gamma after the 871/760°C burner rig test.....	266
Figure 173.	Micrographs showing cross-sections of the Alloy 718 composite coated gamma after the 871/760°C burner rig test.....	267
Figure 174.	Micrographs showing cross-sections of the NiCrAlY composite coated alpha-2 after the 871/760°C burner rig test.....	268
Figure 175.	Micrographs showing cross-sections of the CoCrAlY composite coated alpha-2 after the 871/760°C burner rig test.....	269
Figure 176.	Micrographs showing cross-sections of the Alloy 718 composite coated alpha-2 after the 871/760°C burner rig test.....	270
Figure 177.	Graph showing the temperature distribution in pins tested in the 900/760°C burner rig test without salt.....	271
Figure 178.	Color photograph showing the alpha-2 systems after the 900/760°C burner rig test with no salt.	272
Figure 179.	Color photograph showing the gamma systems after the 900/760°C burner rig test with no salt.	273
Figure 180.	Graph showing the weight change of all the samples during the 900/760°C burner rig test with no salt.	274
Figure 181.	Micrographs showing the 900°C section of the uncoated gamma after 900/760°C burner rig testing with no salt. The lacy or cellular morphology develops under the scale.....	275
Figure 182.	Micrographs showing cross-sections of the uncoated alpha-2 as a function of peak temperature attained during 900/760°C burner rig testing with no salt.....	276
Figure 183.	Micrographs showing cross-sections of the uncoated alpha-2 as a function of peak temperature attained during 900/760°C burner rig testing with no salt.....	277

Figure 184.	Micrographs showing cross-sections of the uncoated R'80 as a function of peak temperature attained during 900/760°C burner rig testing with no salt.....	278
Figure 185.	Micrographs showing cross-sections of the NiCoCrAlY composite coated gamma as a function of peak temperature attained during 900/760°C burner rig testing with no salt..	279
Figure 186.	Micrographs showing cross-sections of the CoCrAlY composite coated gamma as a function of peak temperature attained during 900/760°C burner rig testing with no salt...	280
Figure 187.	Micrographs showing cross-sections of the Alloy 718 composite coated gamma as a function of peak temperature attained during 900/760°C burner rig testing with no salt..	281
Figure 188.	Micrographs showing cross-sections of the NiCrAlY composite coated alpha-2 as a function of peak temperature attained during 900/760°C burner rig testing with no salt.	282
Figure 189.	Micrographs showing cross-sections of the CoCrAlY composite coated alpha-2 as a function of peak temperature attained during 900/760°C burner rig testing with no salt.	283
Figure 190.	Micrographs showing cross-sections of the Alloy 718 composite coated alpha-2 as a function of peak temperature attained during 900/760°C burner rig testing with no salt.	284
Figure 191.	Micrographs showing cross-sections of the Codep coated R'80 as a function of peak temperature attained during 900/760°C burner rig testing with no salt.	285
Figure 192.	Optical micrograph of W diffusion barrier deposited by CVD.	286
Figure 193.	Photograph of alpha-2 and gamma tensile samples after the cyclic exposure at 760°C for 100 hr.....	287
Figure 194.	Cross-sections of uncoated unexposed gamma tensile samples as a function of temperature.	288
Figure 195.	Cross-sections of uncoated unexposed gamma tensile samples as a function of temperature.	289
Figure 196.	Cross-sections of uncoated gamma tensile samples cyclically exposed at 760°C/100 hr as a function of temperature.....	290

Figure 197.	Cross-sections of uncoated gamma tensile samples cyclically exposed at 760°C/100 hr as a function of temperature.....	291
Figure 198.	Cross-sections of cermet coated gamma tensile samples tested at 704°C.	292
Figure 199.	Cross-sections of cermet coated gamma tensile sample cyclically exposed at 760°C/100 hr tested at 704°C.	293
Figure 200.	Cross-sections of unexposed cermet W CVD coated gamma tensile sample after tensile testing.....	294
Figure 201.	Cross-sections of unexposed cermet W CVD coated gamma tensile sample cyclically exposed at 760°C/100 hr tested at 704°C after tensile testing.....	295
Figure 202.	Cross-sections of uncoated unexposed alpha-2 tensile samples as a function of temperature.	296
Figure 203.	Cross-sections of uncoated unexposed alpha-2 tensile samples as a function of temperature.	297
Figure 204.	Cross-sections of uncoated alpha-2 tensile samples cyclically exposed at 760°C/100 hr as a function of temperature.....	298
Figure 205.	Cross-sections of uncoated alpha-2 tensile samples cyclically exposed at 760°C/100 hr as a function of temperature.....	299
Figure 206.	Cross-sections of unexposed cermet coated alpha-2 tensile sample after testing.....	300
Figure 207.	Cross-sections of unexposed cermet coated alpha-2 tensile sample after testing.....	301
Figure 208.	Cross-sections of cermet coated alpha-2 tensile sample cyclically exposed at 760°C/100 hr before testing.	302
Figure 209.	Cross-sections of cermet coated alpha-2 tensile sample cyclically exposed at 760°C/100 hr before testing.	303
Figure 210.	Cross-sections of unexposed cermet coated CVD W alpha-2 tensile sample after testing.....	304
Figure 211.	Cross-sections of unexposed cermet coated CVD W alpha-2 tensile sample after testing.....	305
Figure 212.	Cross-sections of cermet coated CVD W alpha-2 tensile sample cyclically exposed at 760°C/100 hr before testing.	306

Figure 213.	Cross-sections of cermet coated CVD W alpha-2 tensile sample cyclically exposed at 760°C/100 hr before testing.	307
Figure 214.	Micrograph of salt distribution on a steel tensile sample.....	308
Figure 215.	Cross-sections of uncoated unexposed gamma samples after HSSCC testing.....	309
Figure 216.	Cross-sections of uncoated unexposed gamma tensile samples after HSSCC testing.	310
Figure 217.	Cross-sections of uncoated gamma samples cyclically exposed at 760°C/100 hr after HSSCC testing.....	311
Figure 218.	Cross-sections of uncoated gamma samples cyclically exposed at 760°C/100 hr after HSSCC testing.....	312
Figure 219.	Cross-sections of unexposed cermet coated gamma tensile samples after HSSCC testing.	313
Figure 220.	Cross-sections of unexposed cermet coated gamma tensile samples after HSSCC testing.	314
Figure 221.	Cross-sections of cermet coated gamma tensile sample cyclically exposed at 760°C/100 hr after HSSCC testing.....	315
Figure 222.	Cross-sections of cermet coated gamma tensile sample cyclically exposed at 760°C/100 hr after HSSCC testing.....	316
Figure 223.	Cross-sections of unexposed cermet W CVD coated gamma tensile sample after HSSCC testing.....	317
Figure 224.	Cross-sections of unexposed cermet W CVD coated gamma tensile sample after HSSCC testing.....	318
Figure 225.	Cross-sections of cermet W CVD coated gamma tensile sample cyclically exposed at 760°C/100 hr after HSSCC testing.....	319
Figure 226.	Cross-sections of cermet W CVD coated gamma tensile sample cyclically exposed at 760°C/100 hr after HSSCC testing.....	320
Figure 227.	Graph showing creep behavior of unexposed coated and uncoated gamma samples.	321

Figure 228.	Graph showing creep behavior of cyclically exposed coated and uncoated gamma samples.	322
Figure 229.	Graph showing the change in creep behavior of alpha-2 when stress was reduced from 20 to 10 ksi at 760°C.	323
Figure 230.	Cross-sections of uncoated unexposed alpha-2 samples after HSSCC testing.....	324
Figure 231.	Cross-sections of uncoated unexposed alpha-2 tensile samples after HSSCC testing.	325
Figure 232	Cross-sections of uncoated alpha-2 samples cyclically exposed at 760°C/100 hr after rupture during HSSCC testing.....	326
Figure 233.	Cross-sections of uncoated alpha-2 samples cyclically exposed at 760°C/100 hr after rupture during HSSCC testing.....	327
Figure 234.	Cross-sections of unexposed cermet coated alpha-2 tensile samples after HSSCC testing.	328
Figure 235.	Cross-sections of unexposed cermet coated alpha-2 tensile samples after HSSCC testing.	329
Figure 236.	Cross-sections of cermet coated alpha-2 tensile sample cyclically exposed at 760°C/100 hr after rupture during HSSCC testing.....	330
Figure 237.	Cross-sections of cermet coated alpha-2 tensile sample cyclically exposed at 760°C/100 hr after rupture during HSSCC testing.....	331
Figure 238.	Cross-sections of unexposed cermet W CVD coated alpha-2 tensile sample after HSSCC testing.....	332
Figure 239.	Cross-sections of unexposed cermet W CVD coated alpha-2 tensile sample after HSSCC testing.....	333
Figure 240.	Cross-sections of cermet W CVD coated alpha-2 tensile sample cyclically exposed at 760°C/100 hr after rupture during HSSCC testing.....	334
Figure 241.	Cross-sections of cermet W CVD coated alpha-2 tensile sample cyclically exposed at 760°C/100 hr after rupture during HSSCC testing.....	335
Figure 242.	Graph showing creep behavior of unexposed coated and uncoated alpha-2 samples without salt.....	336

Figure 243.	Graph showing creep behavior of cyclically exposed coated and uncoated alpha-2 samples with salt.	337
Figure 244.	Cross sections of cyclically exposed and uncoated gamma tested at RT and 0.4% strain for 200,000 cycles.....	338
Figure 245.	Cross sections of cyclically exposed and uncoated gamma tested at 760°C (1400°F) and 0.4% strain for 282641 cycles.	339
Figure 246.	Cross sections of cyclically exposed and uncoated gamma sample tested at 760°C (1400°F) and 0.4% strain for 200,000 cycles.....	340
Figure 247.	Cross section of the cyclically exposed, uncoated gamma sample tested at 648°C and 0.4% strain for 1549 cycles.....	341
Figure 248.	Cross sections of unexposed cermet coated gamma samples fatigue tested at 760°C and 0.4% strain for 345 cycles.....	342
Figure 249.	Cross sections of unexposed cermet coated gamma samples fatigue tested at 760°C and 0.25% strain for 248746 cycles.....	343
Figure 250.	Cross sections of cyclically exposed cermet coated samples fatigue tested at 648°C at 0.25% strain for 43825 cycles.....	344
Figure 251.	Cross sections of cyclically exposed cermet coated gamma sample fatigue tested at 648°C and 0.4% strain for 1 cycle.....	345
Figure 252.	Color photograph of failed gamma blade and an auger micrograph of the fracture surface.....	346
Figure 253.	Cross section of CVD W + cermet coated gamma sample fatigue tested at RT and 0.3% strain for 3 cycles.....	347
Figure 254.	Cross section of cyclically exposed CVD W + cermet coated gamma sample fatigue tested at 760°C and 0.3% strain for 5168 cycles.	348
Figure 255.	Cross section of uncoated unexposed alpha-2 fatigue tested at RT and 0.8% strain for 200,000 cycles.....	349
Figure 256.	Cross section of uncoated unexposed alpha-2 fatigue tested at 648°C and 0.8% strain for 200,000 cycles.....	350
Figure 257.	Cross section of uncoated cyclically exposed alpha-2 fatigue tested at RT and 0.8% strain for 323 cycles.....	351

Figure 258.	Cross section of uncoated cyclically exposed alpha-2 fatigue tested at 648°C (1200°F) and 0.8% strain for 3608 cycles.	352
Figure 259.	Cermet coated unexposed alpha-2 sample cross sections tested at RT and 0.8% strain for 378 cycles.	353
Figure 260.	Cermet coated unexposed alpha-2 sample cross sections tested at 426°C and 0.8% strain for 3608 cycles.....	354
Figure 261.	Cermet coated cyclically exposed alpha-2 samples tested at RT and 0.8% strain for 172 cycles. The coating spalled.	355
Figure 262.	Cermet coated cyclically exposed alpha-2 samples tested at 648°C and 0.8% strain for 530 cycles.	356
Figure 263.	Cermet coating with W CVD diffusion barrier fatigue tested at RT at a strain of 0.8% for 523 cycles.....	357
Figure 264.	Micrograph of steel tape used to masked cermet coated samples used in Task 3.	358
Figure 265.	Micrographs of microstructures obtained using various preheat cycles.....	359
Figure 266.	Micrographs of cermet coated gamma LPT blade.....	360
Figure 267.	Microprobe results are shown for the cermet coating on a cast gamma LPT blade.....	361
Figure 268.	Plots showing loading profile for the uncoated gamma alloy tested in TMF.	362
Figure 269.	Plot of TMF results for coated and uncoated gamma.....	363
Figure 270.	Plot of TMF results for coated and uncoated alpha-2.....	364
Figure 271.	Fractography of the uncoated gamma sample that failed after 108 TMF cycles.	365
Figure 272.	Cross-section of the uncoated gamma sample that failed after 108 TMF cycles..	366
Figure 273.	Surface and cross-section of a cermet coated gamma sample that failed during the first TMF cycle	367
Figure 274.	Fractography of an uncoated alpha-2 sample that failed after 1508 TMF cycles..	368

Figure 275.	Cross-section of the uncoated alpha-2 sample that failed after 1508 TMF cycles.	369
Figure 276.	Fractography of a cermet coated alpha-2 sample that failed after 952 TMF cycles.	370
Figure 277.	Cross-section of the cermet coated alpha-2 sample that failed after 952 TMF cycles.	371

LIST OF TABLES

Table 1.	Coating candidates for alpha-2 and gamma substrates for program.	373
Table 2.	The table indicates the class, composition and coating process for the coatings applied to the substrates for the first round of environmental testing in Task 2.	374
Table 3.	The test plan for Task 2. HSSCC stands for hot salt stress corrosion cracking and CHC/O refers to cyclic hot corrosion -oxidation burner rig testing.	375
Table 4.	Summary of the normalized weight change/area for the coated gamma alloy substrates after 500 hr of cyclic oxidation at 760°C (1400°F) and 900°C (1650°F) in air. The rank represents the magnitude of the data with 1 being the lowest and presumably the best since visually little spalling was noted. Delta (Δ) rank is a relative measure of change in coating behavior between test temperatures.....	376
Table 5.	Summary of the maximum weight change/area for the coated alpha-2 alloy substrates after 500 hr of cyclic oxidation at 760°C (1400°F) and 900°C (1650°F) in air. The rank represents the magnitude of the data with 1 being the lowest and presumably the best since little spallation was noted. Delta (Δ) rank is a relative measure of change in coating behavior between test temperatures.....	377
Table 6.	X-ray diffraction results for some as-processed coatings on the Ti-48Al-2Cr-2Nb gamma alloy substrate. Lattice parameters are given in angstroms.	378
Table 7.	X-ray diffraction results for coated Ti-48Al-2Cr-2Nb alloys after cyclic oxidation testing in air at 900°C (1652°F) for 500 hr. Identification was made in conjunction with microprobe and metallographic results. Lattice parameters are in angstroms.....	379
Table 8.	X-ray diffraction data from as-coated alpha-2 samples. Lattice parameters are given where appropriate in angstroms.....	380
Table 9.	X-ray diffraction results for various coated alpha-2 samples after cyclic oxidation for 500 hr in air at 900°C(1650°F). The phases were identified in combination with metallography and energy dispersive analysis.	381
Table 10.	Composition of reaction layer phases after an exposure of 1000 hr in air at 760°C (1400°F).....	382

Table 11.	Table showing the weight change of samples during a rinsing procedure that removed salt and debris after the high pressure compressor test. The last column indicated rinsed weight change/area data.	383
Table 12.	Weight change data for candidate coating systems after the 498 cycle low pressure turbine test and rinsing. Large negative weight changes indicate systems that had coating spallation. The chart also indicates the amount of water soluble debris (salt) that was rinsed off the surface and the change in diameter of the sample during the test..	384
Table 13.	Results of HSSCC testing for coated and uncoated gamma substrates as part of Task 2.4. Based on the data here, salt totally embrittled the bare gamma alloy after a 1050°C/40 ksi/750 hr exposure.	385
Table 14.	Results of HSSCC testing for coated and uncoated alpha-2 substrates as part of Sub-Task 2.4. The alpha-2 was severely embrittled in the presence of sea salt. The only sample to survive both 1050°C creep exposures with salt was coated with air plasma sprayed Alloy 718. "NA" means non-applicable because of failure during creep exposure.....	386
Table 15.	Depth and distribution of cracks in exposed (without salt) and unexposed bare alpha-2. The secondary cracking was an indication of interstitial embrittlement at the surface.....	387
Table 16.	Time to 0.1, 0.2, 0.5 and 0.75% creep for the alpha-2 exposed at 1050°C/40 ksi. Approximate values listed were linearly extrapolated from data at shorter times. A transient loading strain of 0.224% was subtracted from one of the alpha-2 coated with Alloy 718 data sets.....	388
Table 17.	Average linear expansion coefficients are shown for Ti-aluminides over the temperature range of expected application. Mismatch between MCrAlY and Ti-aluminides is a strong function of refractory metal content.	389
Table 18.	The compositions of composite coatings applied to the Ti-aluminide substrates. The composite compositions are listed in terms of volume percent of constituent. The MCrAlY compositions are listed in weight and atomic percent (parentheses). A NiCrAlY-based composite coating had previously been determined to be protective on gamma substrates in the first iteration of environmental testing.....	390
Table 19.	Table shows the tests used for the second iteration of environmental testing under Sub-Task 2.6.....	391
Table 20.	Results of a 1050°C/40 ksi HSSCC exposure followed by a RT tensile test of cermet coatings on Ti-aluminide substrates. All of the gamma samples failed in the radius away from the salt coating.....	392

Table 21.	The average amount of salt deposit removed duringCHC/O test rinsing is displayed with the standard deviation.	393
Table 22.	Summary of the attack observed on the uncoated Ti-24.5Al-12.5Nb-1.5Mo Alpha-2 alloy after 520 hr of testing.....	394
Table 23.	The average amount of deposit removed during rinsing is displayed with the standard deviation. The deposit taken after 50 hr was ~2-4X the values listed because of the extra salt and was ignored in the calculations.....	395
Table 24.	The test plan for Task 3. Tensile, fatigue and HSSCC tests will be performed to determine the effect of coating (CTG), exposure (EXP), salt and diffusion barrier (DB) at room (RT) and elevated temperature (ET).	396
Table 25.	Table summarizing color, spalling and W/A observations for mechanical specimens that were cyclically exposed at 760°C in air for 100 1-hour cycles. Nomenclature: N=No; Y=Yes; B=blue; Y=yellow; and YW=yellowish white.	397
Table 26.	Tensile Results for Coated and Uncoated Gamma and Alpha-2 Under Task 3.0.....	398
Table 27.	Summary of Task 3 HSSCC Test Results.	399
Table 28.	Task 3 Fatigue Results.....	400
Table 29.	Auger Spectroscopy Results on Tinted Oxides.....	401
Table 30.	Summary of Task 4 TMF Results for coated and uncoated Ti-aluminides.....	402

FOREWORD

This Final Report covers the work performed by the General Electric Company under Air Force Contract F33615-90-C-5960. The objective of this program was to select and evaluate environmentally protective coatings for alpha-2 and gamma titanium aluminide intermetallics for possible demonstration in IHPTET. The program consisted of four tasks. The selection of alloys, coatings and coating processes was accomplished in Task 1. Coating performance under environmental attack was investigated under Task 2. Under Task 3 the effects of selected coatings on mechanical properties was evaluated in environments which simulate intended applications. Coating demonstration under thermal-mechanical fatigue was investigated in Task 4.

Over the course of the program, excellent technical monitorship was provided by Stephen Balsone, Dr. Shiro Fujishiro and Karen Teal of the Air Force Wright Laboratory Materials Directorate, Wright-Patterson AFB, Ohio. The program was conducted by the Engineering Materials Laboratory (EMTL) at GE Aircraft Engines (GEAE) in Evendale, Ohio. Dr. Russell L. McCarron was the program manager. Dr. Jon C. Schaeffer was the principal investigator. The authors would like to thank the following people for their contributions:

technical consultants: Dan Krueger & Brian Marquardt from EMTL and Dr. Gerald H. Meier at the University of Pittsburgh;

cermet coating application: Dennis Gray at GE-Corporate Research and Development Center;

air and low pressure plasma spraying: Jeff Sloan, Bob Zimmerman and Tom Mantkowski at Materials Technology Laboratories (MTL);

gamma: J. Chesnutt, D. Shih, C. Austin and T. Kelly;

alpha-2: B. J. Marquardt;

sputtered coatings: Ted Grossman and John Moorhead;

burner rig: J. Leopold and B. Mounce;

mechanical sample exposures: R. Whitacre;

electron microscopy: Mike Cannon, Dr. H. P. Yan and E. Lanman;

auger electron spectroscopy: R. Smashey;

metallographic preparation: K. Chaney, T. Gillespie, R. Durvelius and B. Davis; and

report preparation: J. Geraci, S. Boone and K. Chaney.

1.0 Executive Summary

1.1 Introduction

Advanced titanium alloys based on alpha-2 (Ti_3Al) and gamma (TiAl) titanium aluminide intermetallics are under development for structural applications in gas turbine engines. Ti-aluminides have the potential for application to a large number of components because of their significantly increased strength- and modulus-to-density ratios compared to currently available materials. However, these components must operate in a variety of aggressive environments in which they are susceptible to surface and mechanical property degradation. For many components, successful application of the Ti-aluminides will require the use of protective coatings. The objective of this program was to evaluate protective coatings for both alpha-2 (Ti_3Al) and gamma (TiAl) titanium aluminide intermetallics.

1.2 Problem Definition

Environmental problems for Ti-base alloys include: excessive oxide growth; oxide spallation; oxygen and nitrogen embrittlement; hot corrosion; sulfidation; or hot salt stress corrosion cracking due to salt deposition at elevated temperatures. Environments to be considered include those typical of the compressor and exhaust for alpha-2 and gamma titanium aluminides and the low pressure turbine for gamma titanium aluminides. The types of environmental attack associated with various applications for titanium aluminides in advanced gas turbine engines are shown schematically in Figure 1.

Concern for environmental resistance of binary titanium aluminide intermetallics is partly based upon the higher oxidation rates compared to the coated superalloys that they would replace. These isothermal oxidation rates are two or three orders of magnitude greater at temperatures between 740°C (1300°F) and 982°C (1800°F). The titanium aluminide intermetallics may form layered, nonprotective mixed oxide scales (TiO_2 and Al_2O_3) that spall and are penetrated by oxygen and nitrogen causing embrittlement. Factors that contribute to the oxidation behavior include: 1) rapid growth of TiO_2 ; 2) similar thermodynamic stability of the oxides of Ti and Al; 3) low solubility of TiO_2 (titania) and Al_2O_3 (alumina); and 4) different oxide molar volumes.

Beyond simple oxidation behavior is the consideration of the effects of more complex environments including exposure to cyclic oxidation/hot corrosion and mechanical load in the presence of salt that can lead to hot salt stress corrosion cracking. Effort in this program was directed at evaluation of the baseline response of the selected Alpha-2 and Gamma alloys in the environments discussed above and evaluating the effectiveness of protective coatings which may inhibit degradation under these conditions.

1.3 Summary of Results

1.3.1 Task 1 Coating/Substrate Selection

The task structure for the program is shown in Figure 2. The selection of alpha-2 and gamma substrates and coating processes was completed under Task 1. The approved gamma and alpha-

2 substrates were Ti-48Al-2Cr-2Nb and Ti-24.5Al-12.5Nb-1.5Mo, respectively. The coating/process selections are summarized in Tables 1 and 2. The processes selected were sputtering, low pressure plasma spray (LPPS), air plasma spray (APS) and high velocity oxygen fuel (HVOF). Only physical deposition processes were used because chemical deposition processes were unavailable or assessed as ineffective because the process removed Al from the substrate.

1.3.2 Task 2 - Environmental Screening

Under Task 2, environmental testing was used to screen candidate coatings and processes (selected under Task 1) to determine preferred candidates for evaluation in subsequent tasks. In Table 3 the test plan for the first iteration of environmental testing in Task 2 is summarized. Subtask 2.1 was the coating of the specimens.

In the first iteration of testing, the cyclic oxidation test was used for screening to reduce the number of coating candidates to three on both the alpha-2 and gamma substrates prior to the more costly cyclic hot corrosion and oxidation (CHC/O) and hot salt stress corrosion cracking (HSSCC) tests. In general, the effectiveness of coatings in iteration #1 on the alpha-2 substrate changed with each type of test making the selection of a new coating imperative for the second iteration of environmental testing in Subtask 2.6. The results indicated that the coating on alpha-2 should combine the properties of the LPPS cermet coating in the CHC/O test with the properties of APS Alloy 718 in the HSSCC test. The best means to combine these different properties is a composite coating. The three variations of the composite coating used for application to alpha-2 in the second iteration (Subtask 2.6) are shown in Table 18.

In Table 3 the test plan for the second iteration of environmental testing under Subtask 2.6 is presented. The selected conditions allowed comparison to the first iteration of environmental testing. Hot salt stress corrosion cracking tests showed that for alpha-2, only the 60%NiCrAlY + 40%Alumina composite coating survived the 565°C/40 ksi/750 hr HSSCC exposure. In addition, the sample retained significant strength (148 ksi) as measured by an RT tensile test. Regarding gamma, all the composite coating variants survived the 565°C/40 ksi/750 hr exposure, but failed in the radii during the RT tensile test. The failure location was located away from the salt deposits and may indicate resistance to the effects of salt.

The cermet or cermet (Micro Metal Matrix NiCrAlY + Alumina) coating on the gamma substrate had superior performance in all of the iteration #1 tests and, therefore, three different variations were evaluated in Subtask 2.6 as shown in Table 18. Figure 3 shows a composite coating on a gamma Ti-aluminide substrate following a CHC/O test.

The cyclic hot corrosion/oxidation tests under Subtask 2.6 at 900°C/760°C (1650°F/1400°F) and 1-2ppm of sea salt were completed after 3000 cycles or 500 hr of hot time. The composite coatings not containing Co showed no spallation or cracking regardless of substrate or test conditions. MCrAlY-based composite coatings were visually more protective than Alloy 718-based systems. The concept of more closely matching the thermal expansion behavior of the coating with the substrate was validated as the Alloy 718 composite coating did not spall off the alpha-2 substrate.

1.3.3 Task 3 - Mechanical Property Testing

Mechanical property tests were performed under Task 3. The tests performed were: tensile, salt/creep exposures at high temperature (760°C) and strain controlled low cycle fatigue. The downselected coating system for the tests was a 50 vol% Ni-20Cr-10Al-0.3Y wt% + 50 vol% alumina. The system was applied using low pressure plasma spray to both Ti-aluminide substrates. A tungsten (W) diffusion barrier applied by chemical vapor deposition was attempted in an effort to slow interdiffusion between the substrate and coating, but was found to be ineffective because of incomplete sealing from the environment and the poor oxidation resistance of W.

Tensile results as a function of temperature for gamma indicated that the trade for improved high temperature environmental resistance involves a reduction in ultimate tensile strength and ductility. Thread failures were particularly evident at lower test temperatures and if a sample had thermal exposure prior to the tensile test. Results for alpha-2 indicated that the cermet coating reduces ductility but may increase strength at higher test temperatures. The cermet coating was susceptible to spalling when the substrate necked. Since most applications of alpha-2 will involve loading to stresses under yield, it is likely that the cermet coating could be applied with little impact on tensile properties. In addition, the residual ductility of alpha-2 after coating application and thermal exposure is generally above 3% over the usable temperature range.

The cermet coating significantly improved the creep properties of the gamma alloy. Figure 4 shows the lower creep deformation on cermet coated gamma and alpha-2. One bare gamma sample underwent a creep deformation of 20% during the 760°C/20 ksi/500 hr exposure, while another sample cyclically exposed at 760°C/100 hr prior to the test ruptured at 499.6 hr. Cermet coated samples all survived the 500 hr creep exposure regardless of pre-exposure and showed creep deformations of only 10%. The large reduction in creep deformation indicates that the cermet coating is preventing deformation that is dependent on surface cracking. It is not clear if this is an environmental or mechanical effect. The coating would have a mechanical effect because it is stronger in creep than gamma and an environmental effect if it prevented cracking of the gamma substrate due to oxide formation. For alpha-2, a similar improvement in creep strength was observed for coated samples. The initial condition of 760°C/20 ksi was causing rapid creep so a change was made to 760°C/10 ksi where possible. The 20 ksi condition resulted in rupture failures, while all samples loaded at 10 ksi survived 500 hr. Salt deposits lowered the time to rupture and the residual tensile properties of bars that survived the exposure. The cermet coating should be considered on applications of alpha-2 where creep is a limiting property and environmental attack can occur.

The fatigue life of the baseline uncoated Ti-48Al-2Cr-2Nb was excellent. Unexposed gamma ranout (200,000 cycles) at strains of 0.4% at $A=1$ ($A=\Delta\sigma_{alt}/\Delta\sigma_{mean}$) at all test temperatures (22, 568, and 760°C). These stresses were equivalent to 50 ksi and larger. Exposed gamma (cycled at 760°C/100 hr in air) had reduced fatigue capability. Nonetheless, exposed gamma material at all temperatures survived a cyclic tensile stress of lower than 41 ksi. Unexposed cermet coated gamma was tested at 22 and 760°C. The fatigue life was reduced when stresses were higher than 42 ksi. A runout, however, was observed at 0.25% total strain (41.5 ksi max. stress) at 760°C

indicating that the coating is best applied on components stressed below this value. Figure 5 shows a cross-section of this coating on the fatigue bar. Exposed coated gamma was tested at 568 and 760°C. Poor fatigue properties relative to uncoated gamma were observed at high strain ranges (0.4%). The sample tested at 568°C and 0.25% strain, however, was headed for a runout before a thread failure occurred. Gamma will likely be applied at lower stress levels than those tested here; therefore, load controlled high cycle fatigue testing on cermet coated gamma is recommended.

The fatigue life of unexposed alpha-2 (Ti-24.5Al-12.5Nb-1.5Mo) tested at RT, 426°C and 648°C and a strain of 0.8% ranout at a cycle count of 200,000 or greater. The maximum stress level corresponding to the strain was 98 ksi at 648°C to ~125 ksi at RT. Environmentally exposing the uncoated alpha-2 (760°C/100 hr) reduced the fatigue capability to 300-5000 cycles at strain levels of 0.6-0.8% (75-115 ksi max. stress). The reduction is the result of oxidation and interstitial dissolution. Additionally the possibility of aging during the pre-exposure can't be ignored since some coarsening of the primary alpha-2 was observed. The cermet coatings did not improve the fatigue behavior of the alpha-2 alloy. In the exposed and unexposed condition, the life of the coatings tested at 0.6-0.8% strain was from 300-3500 cycles. The similarity in cycle count to the cyclically exposed uncoated alpha-2 cannot be overlooked. It appears that the coating or coating processing has the same effect as the environmental exposure. This is possible because the LPPS process involves preheating to temperatures near 704°C. The cermet coatings were generally adherent to the alpha-2. Optimization of preheating was thus a major concern in the thermal mechanical fatigue testing performed in Task 4.

1.3.4 Task 4 - Thermal Mechanical Fatigue Testing

Results from Task 3 indicated that the cermet coating processing on gamma and alpha-2 could be optimize to limit exposure to gas species that might cause embrittlement. A matrix to optimize the Low Pressure Plasma Spray (LPPS) was performed and the conditions chosen to spray the cermet coating were:

Voltage=50;
Amps=1800;
Pressure=60Torr;
Preheat passes=15;
Rotation=320 rpm;
Substrate Traverse=5in/sec; and
Glass bead peening to 100% Coverage and 18-20N.

As a demonstration, the selected cermet coating with these conditions was applied to a cast gamma Ti-aluminide low pressure turbine blade. The coating is shown in Figure 6.

Out-of-phase (tension cold - compression hot) thermal mechanical fatigue tests were performed on coated and uncoated gamma Ti-aluminide. The TMF was controlled by maintaining strain (thermal+mechanical) constant between temperatures of 760°C and under 204°C from a neutral temperature of ~482°C. Strain levels of 0.3 and 0% resulted in tensile stresses greater than 40 ksi during the lower temperature part of the cycle and failures occurred at low cycle counts.

Uncoated gamma generally had larger cycle counts than cermet coated gamma, but no cycle count exceeded 108. The scatter in the data may not have allowed a true comparison to be made between coated and uncoated gamma, but it is clear that the cycle was very severe for gamma.

The tests were run in the same fashion for alpha-2 as for gamma except the peak temperature was 704°C. In the case of alpha-2, usable data was obtained that correlated nicely with the peak tensile stress experienced during the low temperature part of the cycle. For these TMF tests, the coating reduced the cyclic life of alpha-2 by 50% at a constant tensile stress level. This is a great improvement compared to the 2 order of magnitude reduction observed for coated samples during LCF testing. The improvement may be related to optimized coating processing.

1.3.5 Ti-Aluminide Environmental Coating Recommendation

The coating recommended for both gamma and alpha-2 Ti-aluminides is composed of 40-50% by volume alumina with the remainder Ni-20Cr-10Al-0.3Ywt% and is 50-75µm thick. It is applied using an LPPS process with a -400Mesh powder mixture. One change that might be performed is switching the NiCrAlY to a FeCrAlY to perhaps impart more ductility to the coating for enhanced tensile and fatigue properties. In addition, the elastic modulus of the coating might be measured and optimized to increase the coating strain-to-cracking. The TMF results in Task 4 indicated that masking, preheating and peening are potential areas for further performance enhancement especially on alpha-2. The cermet coatings still need demonstration under HCF conditions where lower system strains might prevent cracking of the coating. Environmentally, the cermet coatings provide superior resistance to oxidation, hot corrosion and hot salt stress corrosion cracking. A patent application has been made by GE Aircraft Engines for these coatings on Ti-aluminides in which the USAF shares rights.

2.0 Results and Discussion

2.1 Task 1 - Selection of Alloys, Coatings and Coating Processes

2.1.1 Alloy Selection - Task 1.1

The USAF approved the selection of Ti-48Al-2Cr-2Nb as the gamma alloy and Ti-24.5Al-12.5Nb-1.5Mo as the alpha-2 alloy.* These compositions are benchmark alloys for GEAE and have balanced mechanical and environmental properties when processed properly.

2.1.2 Coating Selection - Task 1.2

The coatings to be used in the program had to be available and readily applied to the Ti-aluminides without any further detailed development. To further aid in the selection of candidates, the key qualities or attributes of a coating were identified. These were:

- 1) a small thermal expansion mismatch (<10%) between the coating and substrate that minimizes the magnitude of the stresses caused by thermal cycling;
- 2) limited interdiffusion with the substrate to avoid the formation of brittle phases or a decrease in the protective properties of the coating;
- 3) strain accommodation in the substrate or coating without cracking;
- 4) the ability to form a protective oxide that has a slow oxide growth rate, high thermodynamic stability and low volatility; and
- 5) a coating process that is efficient, economical and can handle the geometry of the Ti-aluminide components.

The initial set of coating candidates tried in the program were presented in Table 1. The reasons for the selection of the various coatings based on the above attributes were summarized in Interim Report #1.¹ The following is a short excerpt from that report.

Ti-base environmental coatings are attractive because attributes 1, 2, 5 and sometimes 4 (above paragraph) are fulfilled. Cracking, attribute 3, might be a problem because of the low ductility of compositions that form protective oxides. The coating candidates for Ti-aluminides that best fulfill these attributes are TiCrAl's since they have the same phases and elements as the substrates.

Gamma alloy compositions modified for oxidation resistance instead of mechanical properties can be used as coatings for alpha-2 and gamma substrates. For example, a modified gamma composition of Ti-50Al-2Cr-12Nb was superior to the selected substrate materials and, therefore, could be used as a coating.² These gamma coatings would likely be compatible with alpha-2 and gamma alloys for reasons 1, 2 and 4.

* Compositions are in atom percent unless otherwise specified.

Oxide thermal barrier coatings (TBC's) are another coating candidate. These coatings are being used to insulate Ni-alloy substrates from high temperatures. The insulation must be supplemented with backside or internal cooling to produce a temperature gradient in the component. If no cooling is present, then no temperature advantage is obtained. TBC's may also act as a physical barrier to salt and lower the transient temperature response of the Ti-aluminides to the point where an environmental coating is not necessary.

A variation of the plasma sprayed TBC is the micro-laminated cermet coating developed at GE-CRD that consists of a plasma sprayed metal mixed with a plasma sprayed oxide. This system would consist of alumina mixed with an environmentally resistant metal like NiCrAlY. In essence, the bond coat is mixed with the TBC. The bond coat oxidizes to seal fast transport paths. The proportions of oxide and bond coat control the thermal expansion coefficient of the coating. The advantages of this system are a reduced temperature and oxygen potential at the surface of the substrate.

Ni-base superalloys in the temperature range of interest, 648-843°C (1200-1550°F), are environmentally resistant because they form protective Cr_2O_3 or Al_2O_3 oxide scales. A superalloy could thus be used as a coating on a Ti-aluminide or as a bond coat for TBC's applied on Ti-aluminides. Ni alloys with low coefficients of thermal expansion Ni-alloys might also have an advantage (IN903). Disadvantages are higher density and possible reactions with the Ti-aluminide substrate.

Work in the early 90's at GE-CRDC has shown that MCrAlY (M=Ni, Co, Fe) and MCr overlay coatings developed for Ni-base superalloys can also protect Ti, Ti-6242 and gamma alloys.(McKee) The compositions of these systems are such that Cr_2O_3 or Al_2O_3 oxide scales form. Low pressure plasma spraying of these alloys on Ti-aluminides has been demonstrated and provides environmental protection. The MCrAlY's, however, are sensitive to thermal fatigue and readily interdiffuse with Ti-aluminides. At temperatures in the range of 740 to 815°C (1300 to 1500°F), the above concerns may be minimal.

2.1.3 Coating Process Selection-Task 1.3

Coating processes can be broadly classified as either overlay or diffusion (conversion). This classification is based on the relative amount of diffusion between the substrate and coating that is required to form the final composition and structure.

Overlay coatings require little diffusion with the substrate and, therefore, can have compositions essentially independent of substrate chemistry. Overlay coating processes typically used on gas turbine components are air plasma spray (APS), low pressure plasma spray (LPPS) and electron beam physical vapor deposition (EB PVD). Overlay coatings are easy to apply and are likely to be important for gamma and alpha-2 substrates especially if radically different compositions are required for environmental protection.

All of the coating candidates in this program were initially applied as overlays. The reason for this choice is that diffusional processes were not fully developed for the selected coatings in Table 1. The two overlay processes to be used are plasma spray and sputtering.

The plasma spray process uses a gas to suspend and direct powder of the coating composition toward an arcing electrode. At the electrodes, the powder melts, and the gas is ionized forming a pressurized plasma that is directed toward the substrate. The substrate is a heat sink and the molten powder solidifies on the surface to form the coating. APS refers to using the torch in an air environment. This is useful for large parts that can't be placed in the vacuum chamber necessary to do LPPS. APS has been used to apply partially stabilized zirconia and superalloys. LPPS utilizes a vacuum chamber or an inert gas environment to avoid oxidation of oxygen active elements like Ti, Al and Y that may be part of the coating composition. LPPS would be required for applying cermet, MCrAlY and TiCrAl candidate coatings. In the case of the cermet coating, a dual plasma spray process mixes together two different coating compositions to better achieve a composition and structure that is most compatible with the substrate.

Sputtering is another process that can be used to produce overlay coatings. Sputtering requires a target of the desired coating composition. The target is placed in a sputtering unit in a direct line with the sample to be coated. The unit is sealed, backfilled with an inert gas and a potential is applied between the target and the sample. The inert gas ionizes and impacts the negatively biased target. The impact causes the atoms from the target to be ejected and "sputtered" onto the nearby substrate. Substrate heating and biasing can improve the integrity and microstructure of the sputtered coating and magnets can control charged particle motion. Sputtering was initially used in the coating composition screening activities because of short lead times. Sputtering can be used for the TiCrAl's, superalloys, partially stabilized zirconia, modified gamma compositions and MCrAlY's. Plasma spray processes were used in preference to sputtering because spraying is a more flexible production process because of deposition rate and widespread use by suppliers.

One disadvantage in the consideration of overlay coatings for production parts is that the processes are line-of-sight, and uniformity can be a problem. This shortcoming did not impact work on this program, and the final recommended coating was processed on a gamma low pressure turbine airfoil.

2.1.2 Substrate Selection - Task 1.4

2.1.4.1 Gamma Substrate-Task 1.4.1

The Ti-48Al-2Cr-2Nb substrate was induction skull melted at Duriron, Dayton Oh. as a 30lb heat. The actual chemical composition of the Ti-48Al-2Cr-2Nb was analyzed to be:

Element	Ti	Al	Cr	Nb	Fe	W	Co
Atom %	47.64	48.22	2.08	1.99	0.034	0.002	0.006

The interstitial analysis of the ingot was:

Element	O	N	H	C
PPM Wt.	512	53	23	140

The gamma ingot was cut into fourteen 2.8" X 2.0" (O.D.) cylinders, each of which were isothermally forged at Wyman-Gordon at 1176°C (2150°F) to a final thickness of 0.5". The forged pancakes were heat treated in flowing Ar at 1300°C (2372°F) for 2 hr and furnace cooled.

The processing resulted in a gamma alloy with a duplex microstructure. The duplex microstructure is composed of 30-40µm primary gamma grains and 10µm transformed alpha grains. Transformed alpha is a microstructure composed of α_2 (Ti₃Al-base) laths and gamma. Some β or bcc stabilized phase is found at grain boundaries, especially triple points. The duplex microstructure has been found to give the best balance of strength and ductility at temperatures less than 650°C (1202°F). A fully transformed microstructure has some advantages at temperatures greater than 650°C (1202°F).³ Figure 7 shows optical micrographs of the Ti-48Al-2Cr-2Nb after etching in a 2%HF-methanol solution. Figure 8 shows backscattered electron images (BEI) of the gamma alloy. The darker phase is gamma and the light colored phase is α_2 . The very bright phase at the grain boundaries is β .

Figure 9 shows that some fibering occurs during the forging operation. The BEI image marked with an "N" is normal to the major plane of the forging and the micrograph with a "T" is transverse to the plane of the forging. The "N" microstructure is nearly equiaxed and shows little fibering of the phases. The "T" structure, however, shows fibering of the phases in the direction of the metal flow. The fibering was not observed to affect program results.

The mechanical and environmental specimens for the program were taken from the heat treated and forged pancakes. A schematic of where the samples were removed is shown in Figure 10. Blanks of the specimens were electrodischarge machined and machined into final form by low stress grinding. Standard sized tensile (1.25" gage, 0.160"dia.), fatigue (0.75" gage, 0.200"dia.) and thermomechanical fatigue (0.75" gage, 0.200"dia.) samples with fine threads were chosen over smaller samples with button heads.

2.1.4.2 Alpha-2 Substrate-Task 1.4.2

The Ti-24.5Al-12.5Nb-1.5Mo alpha-2 alloy was produced at Timet (Henderson, Nevada) from a large triple melted, 18" dia., 1800lb. ingot. An average chemistry for the ingot using top and bottom measurements was:

Element	Ti	Al	Nb	Mo	Fe	O	N
Atom %	61.5	23.7	13.18	1.37	0.06	0.21	0.02

This ingot was thermomechanically processed into a 2.9" dia. bar. GEAE has shown that quenching of the bar can lead to section size effects. Therefore, it was decided to heat treat smaller blanks of the environmental and mechanical samples rather than a 2.9" dia. bar segment. Figure 11 illustrates where the blanks were removed. The blanks were heat treated at GEAE using the following parameters: 1079°C (1975°F)/1 hr followed by salt quenching to 843°C (1550°F)/30 min. and finally a stabilization at 704°C (1300°F)/8 hr. After heat treatment, the samples were final machined by low stress grinding methods. The sample sizes were identical to those used for the gamma alloy.

Figure 12 shows optical micrographs of the alpha-2 substrate after forging and heat treatment. The low magnification micrograph shows some banding of the white imaging primary alpha-2 islands. The primary alpha-2 grains are $\sim 15\mu\text{m}$ in size. The prior β grains are $\sim 75\mu\text{m}$ in diameter and are equiaxed. Figure 13 shows BEI of the alpha-2. The microstructure is duplex with ~ 5 -10% primary alpha-2 grains and the rest transformed β . Transformed β is composed of fine alpha-2 or orthorhombic laths precipitated in beta. The β can be ordered or disordered depending on the heat treatment parameters.

2.1.5 Coating Fabrication - Task 1.5

The Materials Technologies Laboratory (MTL) at GEAE in Evendale, OH. plasma sprayed the TiCrAl, Alloy 718 and yttria-stabilized zirconia (YSZ) using typical process parameters. Threads on mechanical samples were masked with metal foil tape. The TiCrAl powder, -325 mesh, used in the plasma spraying processes was produced at Crucible Research in Pittsburgh, Pa. using a gas atomization process. The same powder was hipped into sputtering targets by Cerac in Milwaukee, Wi. using standard powder metallurgical techniques. The Engineering Materials Technologies Laboratory (EMTL) at GEAE in Evendale, OH. sputtered the TiCrAl alloys using an Materials Research Corporation (MRC) DC magnetron sputtering unit operating in a diode configuration. The cermet coatings were made using a low pressure plasma spray process at the Corporate Research and Development Center (GE-CRDC) in Schenectady, N.Y. GE-CRDC also applied the Co-Cr-W-Si-C coating using a HVOF process. Two coatings were applied to another similarly processed Ti-47Al-2Cr-4Ta gamma alloy in order to meet program objectives. The coatings applied to this substrate were the APS YSZ and the Co-Cr-W-Si-C coating. The Ti-47Al-2Cr-4Ta alloy has better oxidation resistance than the Ti-48Al-2Cr-2Nb alloy. Table 2 summarizes the initial coating processes.

2.2 Task 2-Coating Performance Under Environmental Attack

The objective of Task 2 was to use environmental tests to screen candidate coatings and processes in order to determine the best candidates for application to the substrates in the following tasks. The environmental screening tests were cyclic oxidation, hot salt stress corrosion cracking (HSSCC) and cyclic hot corrosion/oxidation (CHC/O) testing. The design of the program allowed a second iteration after the first round of testing. The second iteration refined the coating process and composition for inclusion in Task 3 mechanical tests. Table 3 summarizes the test plan for Task 2.

2.2.2. Cyclic Oxidation Procedure - Task 2.2

Cyclic oxidation tests were performed on button samples 1" dia. and 0.125" thick. Only one side of the buttons was coated since all of the processes considered were line-of-sight and total surface coverage would lead to experimental difficulty and added expense. The problem with coating only one side of the button was that oxidation kinetics now represent the behavior of both the coating and uncoated substrate. This problem was addressed by characterizing the kinetics of the uncoated substrates and using this behavior to normalize the weight change on

coated samples. The normalized weight/area for a coated sample was twice the observed weight/area less the weight/area for an uncoated baseline sample. An example of the use of this formula is given in a following section. All results reported are normalized. The metallography of oxide thickness, cracking and spalling were much more important in determining if desired coating attributes were present.

The edges of the button samples in the cyclic oxidation test were placed on the bottom and side of 50ml pure alumina crucibles. The crucibles and samples were carefully loaded into the 12" X 12" X 12" chamber of a CM Rapid Temp furnace. The furnace uses a mechanical lift to periodically raise the samples into the MoSi₂ lined hot zone that ramps to test temperature in 5-10 minutes. After an isothermal hold of one hour, the lift lowers the samples to a position where a high speed fan cools the sample to room temperature in less than 10 minutes. The cycle was repeated for at least 500 one-hour soaks at temperature. The samples were weighed, examined and photographed at various intervals during the test in order to document changes during the exposure.

900°C (1650°F) Cyclic Oxidation Test

The results of cyclic oxidation testing in air at 900°C (1650°F) are shown in Figure 14. The oxidation temperature is at the upper end of where monolithic gamma alloys might be used and ~140°C (250°F) higher than the temperature where monolithic alpha-2 might be applied. The coated alpha-2 samples were tested at 900°C (1650°F) in order to accelerate oxidation attack for screening of coating candidates.

Coated Gamma Ti-Aluminide

The weight change data in Figure 14 show parabolic behavior for most of the coupons tested. The uncoated gamma gained ~3.3 mg/cm² during the 500 hr test. The tan-yellow oxide on the gamma substrate spalled in circular patches periodically throughout the test and especially at the edges of the oxidation coupon. Figure 15 shows low magnification micrographs that typify the oxide scale during the test.

Unacceptable behavior was exhibited by the gamma alloys coated with plasma sprayed Ti-44Al-28Cr. These samples had nodular growths of titania on the surfaces as seen in Figures 16 and 17.

The sputtered Ti-44Al-28Cr, on the other hand, exhibited a total weight change of +2.2 mg/cm² and a very thin scale of alumina on the surface. The sample had some cracking with titania growing out of the cracks. Despite the oxidation associated with the cracking, the magnitude of the weight change is what might be expected if oxidation was negligible on the coated side of the button. Normalization of the weight change was accomplished by doubling the total weight change (4.4mg/cm²) and then subtracting the weight change of the uncoated alloy (3.3 mg/cm²) to obtain the normalized weight change (1.1mg/cm²). The surface of the coating reflected these lower kinetics, and visually the sample appeared tinted. Optical micrographs are shown in Figure 18. The large disparity in the oxidation behavior of the Ti-44Al-28Cr shows that the protective nature of this type of coating is strongly dependent on the coating process. The sputtered Ti-55Al-8.5Cr coating (TiCrAl) on the gamma alloy performed similarly to the sputtered Ti-44Al-

28Cr. The surface of this sample appeared tinted during the oxidation exposure and is shown in Figure 19. Some fine surface cracking on the surface was noted. Of the coatings, the sputtered TiCrAl performed the best in the cyclic oxidation test. The sputtered Ti-44Al-28Cr coating was chosen for further testing under CHC/O and HSSCC conditions in Tasks 2.3 and 2.4 over Ti-55Al-8.5Cr on the basis of lower oxidation kinetics.

The plasma sprayed yttria stabilized zirconia coating on the gamma alloy exhibited a typical as-sprayed morphology throughout the cyclic oxidation test. The yttria stabilized zirconia (YSZ) coating prevented the spallation of the oxide scale that was observed on the uncoated gamma substrate. The lower oxidation kinetics were likely the result of a more oxidation resistant substrate (Ti-47Al-2Cr-4Ta) that was used to meet program schedule. The surface of the YSZ coating is shown in Figure 20. The APS YSZ coating was chosen for further testing in Tasks 2.3 and 2.4. The reasons for this selection are 1) good adhesion possibly due to a good thermal expansion mismatch with the Ti-aluminides, 2) lower ΔT compared to Ni-alloys, 3) reduced Ti-aluminide oxide spallation, and 4) the presence of a physical barrier to salt deposition.

The Co-Cr coating on Ti-47Al-2Cr-4Ta substrate exhibited oxide spallation after 200 cycles. The sample appeared dark gray on one half and black on the other indicating some inhomogeneity. The surface of the coating is shown in Figure 21. The CoCr(W,Si,C) coating did not warrant further testing as better candidates were available.

The cermet coating fabricated from Al_2O_3 /NiCrAlY had rapid initial oxidation kinetics that then slowed down to rates comparable with the sputtered TiCrAl alloys. The coating showed no cracking or spalling during the test as shown in Figure 22. The René 80 based cermet coating turned green early in the test and exhibited oxidation kinetics similar to uncoated gamma; therefore, it was dropped as a coating for gamma. The NiCrAlY-base cermet coating was chosen for further evaluation for reasons similar to those used for the APS YSZ. An additional reason is that oxygen ingress is stopped on cermet coatings because oxidation resistant NiCrAlY seals short circuit diffusion paths with alumina.

The sputtered IN 718 coating did not protect the gamma substrate. A large amount of oxidation was observed at the coating/substrate interface. The coating was not selected for further evaluation.

Coated Alpha-2 Ti-Aluminide

The uncoated alpha-2 gained $\sim 4 \text{ mg/cm}^2$ after 500 hr of cyclic oxidation as shown in Figure 14. Although the alpha-2 sample showed a weight gain, surface metallography shown in Figure 23 indicated that spallation was occurring throughout the test. The spall starts as an area of oxide that loses adhesion to the substrate resulting in a light colored region not unlike a bubble under a patch of ice. Upon further oxidation, the stresses produced by cycling or by oxide growth crack the scale resulting in a pocket or crater morphology on the surface.

The sputtered TiCrAl alloys did not perform as well on alpha-2 as on gamma. Most of the surface exhibited thin adherent layers of α -Al₂O₃, however, a large amount of thermal expansion mismatch cracking was observed. The thermal mismatch cracking will be discussed later. Figures 24 and 25 show that nodules of TiO₂ form in the cracks as oxidation proceeds. The sputtered Ti-44Al-28Cr sample exhibited more cracking than the sputtered Ti-55Al-8.5Cr sample. An interesting feature of Figure 25 was the lack of titania nodule formation near large thermal expansion mismatch cracks. The large cracks apparently relieve stresses and no nodules were observed. Away from the crack a lot of nodules were observed. The weight change/area for these coatings was approximately half that of the uncoated sample indicating reduced oxidation on the coated surface.

The LPPS Ti-44Al-28Cr coating on alpha-2 performed poorly and spalled off the substrate. The LPPS TiCrAl was discontinued from the program.

On the basis of these results, the sputtered Ti-44Al-28Cr coating will represent the TiCrAl alloys in Task 2.3 and 2.4 on alpha-2. In an attempt to address the CTE mismatch problem for the TiCrAl coatings on alpha-2, it was noted that gamma alloys have expansion coefficients closer to alpha-2 alloys than TiCrAl and could be effective as a coating for alpha-2. Using this logic, a composition of Ti-48Al-2Cr-6Nb-0.1B was chosen as a coating for alpha-2 since it was available and had been shown to be highly oxidation resistant.² This modified gamma powder was applied by LPPS.

The cermet coatings based on NiCrAlY/Al₂O₃ and René 80/Al₂O₃ reduced the oxidation kinetics compared to the uncoated alpha-2 sample. These coatings had thermal expansion coefficients more closely matched with the alpha-2 substrate and, therefore, did not show the cracking seen in the TiCrAl type coatings. The weight change/area produced on samples with these coatings was equivalent to the sputtered TiCrAl alloys after 500 hr. It was decided not to use the cermet coating on alpha-2 for Tasks 2.3 and 2.4 since one had already been selected for gamma.

The air plasma sprayed Alloy 718 coating displayed kinetics similar to the uncoated alpha-2 sample. Spallation was evident on the rough plasma sprayed surface as shown in Figure 26. The oxidation resistance of 718 is suspect at 900°C (1650°F), but improves as temperatures are lowered. A coating of Alloy 718 composition was included in Task 2.3 and 2.4 since Ni-base alloys are regarded as being resistant to HSSCC. In addition, many of the components that alpha-2 might replace operate in the same environment as Alloy 718. The primary concern with the coating is that the APS process results in a brittle form of Alloy 718. This concern might be alleviated by using a LPPS or sputtering process.

760°C (1400°F) Cyclic Oxidation Test

The cyclic oxidation test of coated and uncoated Ti-aluminides at 760°C (1400°F) are shown in Figure 27. The reduced test temperature extended the lives of the coatings as evidenced by smaller weight changes. Differentiation between the coatings required a test to 1000 hr. The test temperature was in the range targeted for gamma alloy application and is near the upper use limit of monolithic alpha-2 alloys.

For gamma, the weight change/area for the coated substrates was lower than for the uncoated substrates indicating that some protection occurred. The thermally sprayed coatings were all a little unstable with respect to oxidation kinetics because the process introduces porosity and cracks which result in more surface area and a higher propensity to spall. Specific system performance will be addressed in the following section.

Coated Gamma Ti-Aluminide

Cyclic oxidation results for the uncoated gamma substrate at 760°C (1400°F) are shown in Figure 27. The gamma alloy started the test with behavior similar to coated alloys, however, after 50 hr of oxidation a large positive weight change occurred. No change in surface morphology was observed in connection with the weight gain and little spallation was observed. The coated buttons did not show a similar change in behavior even though one-half of the button was uncoated. The scale on the gamma alloy had a dull grayish white appearance with little surface relief.

Coating behavior evaluated at 760°C (1400°F) in Figure 27 was different from that observed at 900°C (1650°F) shown in Figure 14. The weight changes at 760°C (1400°F) from lowest to highest were modified as shown in Table 4. The disparity in coating ranking may be a result of the test temperature being near the ductile to brittle transition (~704°C or ~1300°F) for the gamma substrate which may affect coating/substrate interactions. In addition, the lower temperature likely causes a change in oxidation mechanism for many of the systems studied.

The rankings show that the cermet coating had the largest change in behavior as a function of test temperature even though the magnitude of the weight change is similar at the two temperatures. This behavior may be caused by initial oxidation of the larger amount of surface area intrinsic in the intermixed microstructure. The behavior should stabilize as all exposed metal forms protective oxide scales. Another coating chosen for further study, APS YSZ, also showed a large change in behavior. In this case, visual observation indicated that some of the coating spalled near the edges of the sample resulting in a weight loss at 760°C (1400°F) that was not observed at higher temperatures. The slow oxidation kinetics of sputtered Alloy 718 were a pleasant surprise since the coating is likely to be ductile. X-ray analysis of this coating will show that it had an FCC structure which generally exhibits excellent ductility. The sputtered 718 was therefore a coating to be considered for gamma operating at lower temperatures.

Oxidation testing of coated gamma at 760°C (1400°F) reinforced the coating selections made using the 900°C (1650°F) data. The coatings to be included in Task 2.3 (HSSCC) and Task 2.4 (CHC/O testing) are sputtered Ti-44Al-28Cr, Cermet NiCrAlY/Al₂O₃ and APS YSZ.

Coated Alpha-2 Ti-Aluminide

The 760°C (1400°F) cyclic oxidation results for coated alpha-2 are shown in Figure 27. The uncoated substrate exhibits a thin, darkly tinted oxide on most of the surface with a small portion showing spallation or small white oxide nodules. Image analysis of a low magnification surface

micrograph indicates that ~5-10% of the area on the sample is spalling similar to that reported for 900°C oxidation. The spallation appears to be the primary reason for the weight change/area data for alpha-2 at 760°C (1400°F) being less than that for gamma under identical conditions.

A summary of the kinetics for the coatings on alpha-2 is shown in Table 5. The data show that the weight change at lower temperature was smaller as expected. The ranking of the coating behavior at 760°C (1400°F) is nearly the same as that observed at higher temperature. Only the cermet coating with René 80 shows a significant deviation which may be a result of the high amount of exposed surface area characteristic of the coating process and a change in the oxidation behavior of the René 80 in the coating.

The results of the cyclic oxidation test support the selection of coatings for Tasks 2.3 and 2.4 made using 900°C (760°C) data which are sputtered Ti-44Al-28Cr, APS Alloy 718 and LPPS Ti-48Al-2Cr-6Nb-0.1B. The selection of Ti-44Al-28Cr was based on weight change data. The APS 718 coating was selected even though it had poor oxidation behavior. The oxidation behavior of this coating will likely improve at lower temperature as indicated in Table 5. Results of sputtered Alloy 718 on the gamma alloy are better and suggest that the poor coating performance on alpha-2 may be the result of the coating process which could deplete critical scale forming elements. The modified gamma alloy, Ti-48Al-2Cr-6Nb-0.1B, addresses the issue of thermal expansion mismatch cracking that was observed on TiCrAl coatings on alpha-2 at both test temperatures.

2.2.3 X-ray Analysis of Coated/Uncoated Ti-Aluminides - Task 2.5

X-ray diffraction was performed on the coated and uncoated surfaces of the buttons before and after cyclic oxidation testing. The Philips 3100 x-ray generator used Cu-K α radiation, a data acquisition unit, and was in excellent calibration with a systematic error of 0.002Å. In one case, diffractometer measurements on a sputtered coating showed a high degree of preferred orientation, therefore, the Debye-Scherrer technique was used on a powder specimen taken from the sample. The x-ray results are summarized in Tables 6-9.

X-ray Analysis of Initial Coated/Uncoated Gamma

X-ray diffraction was used to characterize the phases in the coatings, alloys and oxidation products. Phase identification is important in the prediction of alloy and coating stability based on known thermochemical data. The X-ray analysis of the as-processed coatings on the Ti-48Al-2Cr-2Nb substrate are shown in Table 6. The substrate is a TiAl-base alloy with the characteristic L1₀ structure. There were weak peaks indicative of the DO₁₉ structure of alpha-2, but a crystal structure was not determined. Microstructurally the presence of the alpha-2 is confirmed in Figure 8. The TiCrAl coatings on the gamma alloys were similar those on alpha-2 alloys and are discussed in that section.

The HVOF processing of Ti-44Al-28Cr alloy produced a phase constitution much different than LPPS of the same composition. The HVOF process involves a more uniform plume and less heat than the LPPS process. The HVOF coating produce two BCC phases. One appears to be similar

to Cr and may reflect unmelted or segregated powder particles caused by the reduced heat input. The other BCC phase may be a Cr-Ti solid solution or AlCr_2 .

The sputtered Alloy 718 coating exhibits only a gamma, FCC- (Ni,Fe) matrix. This is exciting since FCC crystal structures generally exhibit ductility from 5 independent slip systems. A ductile coating might be effective in applications limited by low cycle fatigue.

X-ray Analysis of Oxidized Coated/Uncoated Gamma

The x-ray diffraction results for uncoated and coated gamma samples after the 900°C cyclic oxidation test are shown in Table 7. The uncoated gamma alloy exhibits major amounts of rutile and minor amounts of alumina. The gamma substrate is observed because spalling during the test thins the oxide scale.

The sputtered TiCrAl coatings displayed $\alpha\text{-Al}_2\text{O}_3$ scales with some contribution from the underlying coating. The sputtered Ti-44Al-28Cr coating has transformed from an amorphous state into a $\gamma\text{-TiAl}$ alloy during the course of the oxidation test. The sputtered Ti-55Al-8.5Cr coating has transformed from cubic TiAl_3 to a TiCrAl-Laves phase. The sputtered coatings on the gamma substrate showed no rutile which was different from the same coating on alpha-2 alloys. Recall that the thermal expansion mismatch is large enough between the TiCrAl and the alpha-2 to cause cracking of the coating and the formation of TiO_2 . The plasma sprayed TiCrAl coatings formed TiO_2 and Al_2O_3 . In each case the titania was in abundance rather than the alumina. The alumina was modified with other elements such as Cr since the lattice parameter was larger than expected. The cermet coatings retained their as-processed phase composition of NiO, gamma or FCC - Ni, a spinel of variable composition and α -alumina.

X-ray Analysis of Initial Coated/Uncoated Alpha-2

X-ray diffraction results from coated and uncoated alpha-2 substrates are shown in Table 8. Most of the heat treated alpha-2 substrates exhibited orthorhombic- Ti_3AlNb (O) and bcc- β . The O phase represents a distortion of the ordered hexagonal phase (DO_{19}) which is the equilibrium microstructure of the binary compound Ti_3Al . The appearance of $\text{O}+\beta$ is supported by the isothermal transformation diagrams published in a recent USAF report entitled "Microstructure/Processing Effects on Properties of Titanium Aluminides" by B. Marquardt. According to the T-T-T diagram for Ti-24.5Al-14.5Nb-1.5Mo, a solution temperature of 1085°C (1985°F) for 30min. may not have been long enough for decomposition of ordered β into ordered hexagonal (DO_{19}) alpha-2. The diagram also indicates that the other heat treatment temperatures used in this program also result in the formation of various O phases. The only sample with the DO_{19} structure was low pressure plasma sprayed. The heating of the sample under vacuum may have allowed the sample to attain times and temperatures where DO_{19} could form.

X-ray analysis of as-processed coatings on the alpha-2 samples revealed many different phases and crystal structures as shown in Table 8. The sputtered Ti-44Al-28Cr coating formed as an amorphous solid with diffraction intensity centered around a d-spacing of $\sim 2.2\text{\AA}$. This type of

structure is frequently encountered when sputtering is done at low temperatures since atoms lack the mobility to arrange themselves into a crystalline structure. The sputtered coating of Ti-55Al-8.5Cr formed an FCC phase. It is worthwhile to note that the L1₀ structure of TiAl is tetragonal with lattice parameters of $a_0=3.987\text{\AA}$ and $c_0=4.07\text{\AA}$. The similarity in lattice parameter between the observed FCC phase and the TiAl phase may not be coincidence and the processing may have resulted in a disordered TiAl crystal form or the tau phase (Cr-modified TiAl₃). Another possibility is that the FCC phase could be similar to Al₁₉Cr.⁴ Remarkably, the microprobe showed concentrations of Al and Ti that are expected for single phase gamma.

The low pressure plasma sprayed Ti-44Al-28Cr coating had a Laves phase (MgZn₂-type), FCC- γ TiAl and a weak unidentified cubic phase. Microprobe of the coating near the surface indicated a composition close to TiCrAl_{1.5}. A search of Laves phases in this range of compositions yields equiatomic TiCrAl with $a_0=5.01\text{\AA}$ and $c_0=8.22\text{\AA}$ and Ti₅Cr₈Al₂ with $a_0=4.956\text{\AA}$ and $c_0=8.090\text{\AA}$.⁵ The phase observed in the coating is closer to the equiatomic TiCrAl. Apparently Laves phases in this area of the ternary can have variable composition. The unidentified cubic phase may result from reaction of the coating with residual gas in the chamber and the formation of a Ti(O,N,C) NaCl-type compound.⁶

The air plasma sprayed IN 718 coating contained four phases. Two of the phases were FCC-based gamma Ni-Fe matrices. The oxide is a result of the air processing and reflects oxidation of Cr and Fe into an AlMg₂O₄-type spinel structure. The amorphous phase was weak and could be an oxide or splat cooled metal.

X-ray Analysis of Oxidized Coated/Uncoated Alpha-2

X-ray analyses performed on some of the coated alpha-2 samples after exposure in the 900°C (1650°F) cyclic oxidation test are shown in Table 9. The surface of the uncoated sample was a mixture of tetragonal rutile (TiO₂) with a small amount of rhombohedral alumina (Al₂O₃). The rutile peaks were skewed to lower 2 θ values indicating the incorporation of other atoms into the lattice or a solid solution rather than a pure phase. One thought is that Nb dissolves into both the alumina and titania to make the scales dense and more resistant mass transport.⁷ The oxidized sputtered Ti-44Al-28Cr coating showed contributions from titania, alumina and the Laves phase in the coating. The observation of the Laves phase indicates that the oxide scale is thin, ~0.1 μm . The sputtered Ti-55Al-8.5Cr shows a large contribution from titania and a small contribution from alumina.

Summary of X-ray Analysis

X-ray analysis was an effective way of determining the important phases in the substrates and coatings. The gamma substrates were composed of L1₀ tetragonal gamma-TiAl and DO₁₉ ordered hexagonal Ti₃Al. The alpha-2 substrate was composed of primary alpha-2 and a transformed beta phase composed of ordered orthorhombic Ti₂NbAl and a BCC stabilized phase. The low volume fraction of primary alpha-2 and banding might explain why hexagonal Ti₃Al was not observed to a larger extent in the alpha-2 substrate.

X-ray analysis of the coatings allowed identification of beneficial and detrimental phases in as-received and exposed coatings. Possible metastable phases were observed in the TiCrAl coatings which depended on the particular coating process conditions. The other coatings were shown to have phases expected for the coating application process. After exposure, the coatings all displayed oxides on the surface. In Ti-base coating systems and the uncoated alloys, the scale was a mixture of alumina and titania. The sputtered TiCrAl coatings on gamma were special in that only alumina was formed. The oxides on all of the sputtered TiCrAl coatings were thin enough to analyze coating phases indicating protective behavior. Phase transformations in TiCrAl coatings were evident after exposure and may be a cause of cracking. The cermet coating was basically unchanged by exposure.

Metallography of Coated/Uncoated Ti-aluminides - Task 2.5

Metallography on cyclically oxidized samples is as important as the kinetic data. Specifically the samples are examined for signs of protective and nonprotective oxides, oxide/coating cracking and spallation, and the formation of detrimental phases in the coated system. Metallography was performed on cross-sections of the coatings before and after cyclic oxidation testing. Samples for metallography were cut in half with a cut off wheel and mounted in alumina reinforced epoxy or conductive bakelite and polished to 0.5 μ m. Optical or scanning electron microscopy was used to characterize the microstructure of the coatings. Chemical profiles through the coatings were made using a microprobe equipped with a wavelength dispersive spectrometer and calibrated with suitable standards. Readings were taken in 5 μ m steps with a 5x7 μ m raster. Coatings selected for Tasks 2.3 (HSSCC) and 2.4 (CHC/O) were emphasized.

Metallography of Gamma Ti-aluminides After Cyclic Oxidation

Sputtered Ti-44Al-28Cr/Gamma - 900°C

The microstructure and chemistry of the sputtered Ti-44Al-28Cr coating on gamma is shown in Figures 28-30. Figure 28 shows the as-coated thickness to be 40 μ m thick with a featureless amorphous microstructure. The exposed coating is only 25 μ m thick with a 10 μ m thick reaction zone which has a similar contrast to the coating. Separating the coating is a dark Cr-depleted layer that seems to demarcate the substrate interface before coating. The difference in coating thickness with exposure may be sample to sample coating variation or a sectioning effect. Generally, the coating thickness was very uniform on any individual sample. The reaction zone is Cr-rich as indicated in Figure 29 and 30 with a composition similar to the coating. The presence of Nb in this zone indicates that it is a reaction layer and not part of the deposited coating. Aluminum decreases by 5 atom percent in the coating due to interdiffusion with the Ti-48Al-2Cr-2Nb substrate and oxidation into a α -Al₂O₃ scale. Titanium is enriched in the coating. Most of these atom movements can be predicted with a Fick's first law analysis where the flux of a species is proportional to the concentration gradient. It appears on the basis of Figure 30 that Ti diffuses quickly compared to the other species in the system. Some cracks were noted in the coating, but in general the coating microstructure had high integrity and the coating was adherent.

Sputtered Ti-55Al-8.5Cr/Gamma - 900°C

The microstructure and chemistry of the sputtered Ti-55Al-8.5Cr coating on gamma is shown in Figures 31-33. The as-deposited modified gamma coating was 30 μ m thick with no microstructural features. XRD showed a high degree of preferred orientation for the cubic phase. The Debye-Scherrer powder method was used to show that the coating was cubic and not oriented tetragonal TiAl. The exposed sample had a similar coating thickness, but had two phases. One of the phases was hexagonal Laves phase. The other, based on composition, is likely gamma. A bright imaging Cr-rich reaction zone is seen at the coating/substrate interface. The reaction layer was not continuous. Thus there might be an advantage for TiCrAl alloys with lower Cr concentrations if the reaction layer turns out to be brittle or detrimental for other reasons. The other atom movements are similar to those discussed for Ti-44Al-28Cr. This can be observed by comparing the ordinates in Figures 30 and 33. Equalizing the concentration of elements in the coating with the substrate appears to have reduced the overall segregation and interdiffusion.

Cermet (NiCrAlY + Al₂O₃)/Gamma - 900°C

The microstructure and chemistry of the LPPS cermet coating composed of NiCrAlY and Al₂O₃ on gamma is shown in Figures 34-37. The as-deposited coating shown in Figure 34 was 100 μ m thick, and was composed of a intermixed metallic phase (FCC γ matrix) and ceramic (α -Al₂O₃). Porosity was evident in the structure and may be provide a large amount of surface area that is responsible for the rapid initial oxidation kinetics observed in Figures 14 and 27. Figure 35 shows the coating after oxidation testing at 900°C (1650°F). The coating is about 75 μ m thick with a reaction layer from 1-20 μ m thick at the coating/substrate interface. Figure 36 shows that the reaction layer is Ni-rich and could be a Ti-Ni compound or a brittle Ni-Ti-Al intermetallic. No distinct oxide scale is evident at the gas/coating interface or at the coating/substrate interface, although a Ti enrichment occurs at the latter. Figure 37 shows the coating chemistry which reflects the complex microstructure of the dual constituent coating.

APS YSZ/Gamma - 900°C

The microstructure and chemistry of the APS YSZ coating on the Ti-47Al-2Cr-4Ta gamma alloy substrate is shown in Figures 38-41. The different substrate was required to meet the program schedule. The thickness of the ceramic coating was ~90 μ m as shown in Figure 38. The coating is porous and contains interfaces produced by consecutive passes made by the plasma torch. The exposed coating in the same figure shows that oxide forms at the coating/substrate interface since oxygen is easily transported through the porous ceramic. The yttria stabilized zirconia has a high conductivity for O²⁻ anions. Figures 39 and 40 show the chemical composition of the coating excluding oxygen. The 20 μ m thick scale is Al-rich at the YSZ interface and Ti-rich at the gamma interface. Titanium is found at a depth of at least 25 μ m in the YSZ indicating a high permeability. The diffusion coefficient for this type of transport is on the order of 2.5x10⁻¹² cm²/sec at 900°C (1650°F). An enrichment of Ta and Cr is noted beneath the oxide scale next to the gamma substrate. Figure 41 shows an oxygen profile at the coating substrate interface. The

initial coating shows little oxygen penetration into the gamma alloy even though the coating was applied using an air plasma spray process. The cycled coating shows high oxygen in the cracks of the coating and in the oxide, but only a $2\mu\text{m}$ penetration into the substrate in the Cr-Ta enriched area. This corresponds to a diffusivity of oxygen of $\sim 1 \times 10^{-14} \text{ cm}^2/\text{sec}$. The YSZ did not spall on the gamma substrate at 900°C (760°F) and may be a barrier to salt induced degradation modes.

LPPS Ti-44Al-28Cr/Gamma - 900°C

The microstructure and chemistry of the LPPS Ti-44Al-28Cr coating are shown in Figures 42-44. In Figure 42, the initial coating is about $75\mu\text{m}$ thick. Alumina grit used to roughen and clean the surface was noted at the coating/substrate interface. Nickel-base superalloy and Cu contamination were found in the coating and traced to previous runs in the vacuum chamber. The coating has a typical plasma spray appearance with significant porosity and some through thickness cracks. The same figure shows the coating after cyclic oxidation at 900°C (1652°F). The coating has desirable and undesirable regions. In desirable regions, a $1\mu\text{m}$ $\alpha\text{-Al}_2\text{O}_3$ oxide scale is present at the gas/coating interface and the coating has a similar appearance to the sputtered coating shown in Figure 28. In undesirable regions, the coating has experienced accelerated oxidation as a protective scale has not formed. The large rutile crystals observed on the surface correspond to these regions. This may be related to contamination or unmelted powder particles in the as-sprayed coating. Figures 43 and 44 show chemistries associated with desirable areas.

Gamma - 900°C

The oxide that formed on the uncoated Ti-48Al-2Cr-2Nb alloy is shown in Figure 45. The scale on the alloy is generally planar and $10\text{-}15\mu\text{m}$ thick with little evidence of cracking. In areas associated with spallation, however, the oxide is $30\text{-}40\mu\text{m}$ thick and has large rutile (TiO_2) crystals at the gas/oxide interface. Under the rutile are dark crystals of an Al-rich oxide. The body of oxide is layered and composed mostly of TiO_2 with some Al_2O_3 interspersed. At the oxide/alloy interface, a $0.75\mu\text{m}$ layer is enriched in elements that participate to a limited extent in the scale forming reaction, namely, Cr and Nb.

Hardness profiles were taken on a few gamma systems. The uncoated alloy had a Vicker's hardness numbers (100g load) between 240 and 280, while the scale that formed was between 900 and 1200. Hardness readings weren't able to detect a significant thickness of interstitial embrittlement in uncoated or coated alloys. The sputtered TiCrAl coatings had Vicker's hardness values between 500 and 700.

Cermet NiCrAlY/ Al_2O_3 /Gamma - 760°C

The cermet coating had the highest weight change/area in the cyclic oxidation test for a coated system. The large weight change is thought to be the result of oxidation of the Ni-24Cr-12AlY associated with open porosity in the coating. Figure 46 shows the surface of the coating

throughout the test. No cracks were observed and the morphology did not change with increased exposure. Some of the bright areas in the micrographs may be oxide spalls.

Figure 47 shows the coating in cross-section. The 85 μ m thick coating showed no through-thickness cracking, spallation or environmental attack. X-ray diffraction indicated that the major phase in the coating was an FCC Ni-alloy. Minor phases included δ -Al₂O₃ that possibly contained g-Al₂O₃, α -Al₂O₃ and NiO. The only evidence that the coating had been exposed to 760°C (1400°F) for 1000 hr was the 6 μ m reaction layer at the coating/substrate interface where NiCrAlY borders the Ti-48Al-2Cr-2Nb. In areas where Al₂O₃ bordered the gamma, there is little reaction indicating that oxygen did not penetrate through the coating and that alumina is stable in contact with the gamma alloy at these temperatures and times.

Figure 48 shows the change in chemical composition of the coating shown in Figure 47. The reaction zone is forming by the diffusion of Ni into the gamma alloy substrate. Using these data, the interdiffusion coefficient for Ni in the temperature range of the tests is $\sim 2 \times 10^{-13} \text{ cm}^2/\text{sec}$. The microprobe was also used to get a more accurate chemistry for the reaction layer. Figure 47 shows that two distinguishable phases have formed. The lighter one nearest the coating has a composition of Ni-24.5Ti-27Al which is near Ni₂TiAl. The darker phase bordering the gamma has a composition Al-33Ti-19Ni-3Cr-2Nb which is near Al(Ni,Ti).

The cermet coating was selected for evaluation in burner rig and hot salt stress corrosion cracking testing after the 900°C cyclic oxidation test.

Sputtered Ti-44Al-28Cr/Gamma - 760°C

The sputtered Ti-44Al-28Cr coating on gamma had very little weight change/area during the course of the cyclic oxidation test. Visually the sample was tinted blue throughout the test indicating that a very thin oxide layer was present on the surface. Figure 49 shows that the surface of the alloy had some cracks which segmented the coating into elongated areas with dimensions on the millimeter scale. The cracking is a means of stress relief caused by thermal expansion mismatch. The bright circular features on the surface are associated with an oxide that has overgrown the thin scale. No observations of coating spallation could be made, therefore, the weight gain of $\sim 0.25 \text{ mg/cm}^2$ might indicate a parabolic rate constant, k_p , of $\sim 1.7 \times 10^{-14} \text{ g}^2 \text{ cm}^{-4} \text{ sec}^{-1}$. This value is 30X smaller than that observed on a spalling uncoated gamma substrate.

Figure 50 shows cross-sectional micrographs of the coating. The 33 μ m thick coating is multiphase with submicron precipitates. At the coating/substrate interface, a dark phase has formed which microprobe indicates is Ti-50Al-10Cr. This phase may be gamma with a maximum of Cr in solution and would be expected to form since the coating has less Al (on a concentration basis) than the substrate. The bright continuous reaction zone, analyzed to be Ti-41Al-24Cr, is the Laves phase. This continuous layer may be beneficial if the coating spalls or cracks at the original interface since it has a composition that is still capable of forming alumina.⁸

X-ray diffraction on the surface of the coating indicates an α - Al_2O_3 scale and a coating comprised of a MgZn_2 Laves phase, gamma TiAl and a BCC phase. The Laves phase was discussed previously and is thought to be a variation of TiCrAl . The BCC phase is β (Cr-Ti solid solution) or Cr_2Al . A recent ternary diagram proposed by workers at Michigan Technological University indicates that the BCC phase is Cr_2Al .⁹ In addition, these researchers have found that Al_3Ti when modified with 7-13 atom percent Cr forms an L_{12} tau-phase. The similarity in lattice parameters between the L_{10} gamma and the L_{12} phase would make observation difficult because major peaks overlap and the superlattice lines might be weak. The compositional analysis did not indicate the high Al phase, but perhaps this was beyond the micron resolution of the microprobe.

Figure 51 shows that on a $5\mu\text{m}$ scale little or no chemistry change occurred during the cyclic oxidation exposure. Chemistry changes on a finer scale did occur at the coating/substrate interface as explained above and that is why specific chemistries were given for reaction product phases. The results discussed here support the selection of the sputtered Ti-44Al-28Cr as a coating for further evaluation.

YSZ/Gamma - 760°C

The YSZ coating had a negative weight change/area at the beginning of the test. Visual observations of the surface indicated that the YSZ had spalled at the edges. Figure 52 shows little change in the surface morphology away from the edges.

Figure 53 shows a cross-section of the coating after the test. There is a $3\text{-}4\mu\text{m}$ oxide that forms at the alloy/coating interface from oxygen ingress through the porous YSZ. The oxide is thinner on the Ti-47Al-2Cr-4Ta compared to the Ti-48Al-2Cr-2Nb substrate. This effect has been discussed and may be due to a larger Al/Ti ratio or the ability of the YSZ to incorporate or dissolve any TiO_2 that forms. X-ray diffraction of the surface indicated only a random tetragonal ZrO_2 phase. The APS YSZ on Ti-48Al-2Cr-2Nb was selected for further evaluation, but the edge spallation observed in this test is a concern.

Sputtered Ti-55Al-9Cr/Gamma - 760°C

The weight change/area data for the sputtered Ti-55Al-9Cr coating on Ti-48Al-2Cr-2Nb were extremely small. The surface was tinted blue to purple throughout the exposure indicating a very thin oxide. Figure 54 shows that thermal expansion mismatch cracks did form on the surface, but did not lead to coating spallation. Grinding marks are apparent on the surface, but the mismatch cracks do not follow their direction.

Figure 55 shows the $37\mu\text{m}$ thick coating in cross-section. The major differences between this coating and the Ti-44Al-28Cr is the diffuse reaction layer at the coating/substrate interface and the larger amount of gamma in the coating. The reaction layer in the present case does not form a discontinuous Cr-rich phase at the interface which may be advantageous if this phase leads to cracking or coating spallation. In addition, there is no dark (Al-rich) gamma phase on the coating side of the interface, because the coating has more Al than the substrate. Instead Al is diffusing

into the $\gamma + \alpha_2$ substrate and dissolving the α_2 or Ti_3Al -based phase into $\gamma + \beta$. The β is present as bright (Cr+Nb) particles that form in the wake of converted α_2 laths. X-ray diffraction of the surface indicated the presence of gamma TiAl and the AB_2 -type of Laves phase in the coating. The only oxide phase detected was $\alpha\text{-Al}_2\text{O}_3$. This coating was not selected for further evaluation despite excellent performance because a similar coating, sputtered Ti-44Al-28Cr, was already selected.

HVOF TiCrAl/Gamma - 760°C

The HVOF Ti-44Al-28Cr coating exhibited the smallest weight change/area in the 760°C (1400°F) test despite poor behavior at 900°C (1650°F). Visual observations in Figure 56 indicated little spallation on the surface. Some TiO_2 nodule formation was apparent at longer times as well as a heterogeneous scale character.

Figure 57 shows the coating to be a dense, 12-20 μm thick layer with a 3 μm reaction zone with the substrate. The coating appears to be a mixture of metal and oxide similar to the cermet coating, but with very little porosity. The incorporation of oxides into this coating would lower any thermal expansion mismatch with the gamma substrate. X-ray diffraction of the surface indicated that many phases existed including: TiO_2 (rutile), the MgZn_2 Laves phase, TiN, a $\text{Cr}_2\text{O}_3\text{-Al}_2\text{O}_3$ solid solution and several unidentified weak phases. The coating was not selected for further evaluation based on poor results from the 900°C (1650°F) cyclic oxidation test.

LPPS TiCrAl/Gamma - 760°C

The LPPS Ti-44Al-28Cr coating, like the HVOF Ti-44Al-28Cr coating performed much better at 760°C (1400°F) than at 900°C (1652°F). The main difference at 760°C (1400°F) was that only a few small TiO_2 nodules formed during the exposure resulting in much smaller weight changes.

Figure 58 shows that the 65 μm thick coating had a typical structure with dense TiCrAl coating between regions with many defects. The coating shows high integrity with the exception of a few through-thickness cracks that penetrate into the substrate. As expected for the Ti-44Al-28Cr composition, a continuous 4 μm thick reaction layer (likely Cr-rich Laves) formed at the coating/substrate interface. X-ray diffraction on the surface indicated that the external oxide was composed of $\alpha\text{-Al}_2\text{O}_3$ and TiO_2 and that the coating was almost entirely the AB_2 Laves phase ($a_0=5.053\text{\AA}$ and $c_0=8.259\text{\AA}$). The through-thickness cracks and poor behavior at high temperature resulted in this coating not being selected for further evaluation.

Sputtered Alloy 718/Gamma - 760°C

The sputtered 718 on the Ti-48Al-2Cr-2Nb substrate displayed low weight change/area kinetics at 760°C (1400°F). Alloy 718 is regarded as having good oxidation resistance to 815°C (1500°F) in addition to having good stability, strength and fatigue crack growth. Visual examination of the

surface indicated that a thin dark gray oxide had formed on the surface during the test but this oxide did not spall. The as-coated surface morphology was preserved through most of the test until long times when dark striations appeared on the surface.

Figure 59 shows the cross-section of the Alloy 718 coating. The coating was 175 μ m thick with a 15 μ m reaction zone between the coating and substrate. The reaction layer has three distinct phases. The dark phase bordering the bright coating in the microstructure may be an oxide which would indicate rapid oxidation in from the edge of the sample. This possibility is mentioned because a phase bordering the Ni-rich coating should have enough Ni to image brightly in the BEI mode. X-ray on the surface of the coating indicated a Cr₂O₃ scale with the coating being comprised of a textured FCC Ni solid solution phase and the δ -Ni₃Nb phase. The coating was not selected for further evaluation because of the debonding at the substrate/coating interface at 900°C (1652°F).

HVOF CoCr(WSiC)/Gamma - 760°C

The weight change/area for the HVOF Co-32Cr-5C-2Si-1W coating on a Ti-47Al-2Cr-4Ta gamma alloy substrate was unstable at early times as some spallation of the coating was observed. After these perturbations, the weight change stabilized and a continuous Cr-rich scale was observed on the surface with internal oxidation of Si. Visual examination of the sample indicated that half of the sample was much darker in color than the other half indicating a heterogeneous system.

Figure 60 shows the HVOF CoCr(WSiC) coating on a Ti-47Al-2Cr-4Ta gamma alloy substrate. The coating is nearly 100 μ m thick with little reaction between the coating and substrate. The dark zone or gap between the coating and substrate may mean that the coating was not adherent to the substrate. No explanation for this behavior was found and the coating was not selected for further testing.

Gamma - 760°C

The uncoated Ti-48Al-2Cr-2Nb gamma alloy gained ~1.4mg/cm² after 1000 hr. If spallation is ignored and parabolic kinetics assumed, the parabolic rate constant for scale growth was ~5.4 X 10⁻¹³ g²cm⁻⁴s⁻¹. This value is near levels expected for alumina-formers at temperatures between 1000 and 1150°C (1832 and 2102°F).

The surface of the sample had a yellowish tan scale that had signs of spallation especially near edges. Figure 61 shows the surface of the gamma sample at various times during the test. An increase in roughness and titania outgrowths is noticeable at longer times. Figure 62 shows cross-sectional micrographs of the uncoated gamma sample. The oxide is ~8 μ m thick and x-ray diffraction (XRD) shows it to be composed of pure rutile and (Al,Cr)₂O₃. In addition XRD indicates the presence of γ -TiAl, Ti(C,N,O) and a weak unidentified phase with a peak at d=2.25Å. The bright TiN phase is located underneath the dark external oxide.

The backscattered electron image (BEI) in Figure 62 has a line scan for oxygen. The trace indicates that oxygen penetrates only 1.5 μ m into the substrate. The depth of enrichment is small, but it is yet to be determined how mechanical properties might be affected. The trace also shows that dark features in the unetched substrate are possibly oxygen rich. These areas may be associated with artifacts that look like microcracks that are observed in gamma alloys when etched.

Metallography of Alpha-2 Ti-aluminides After Cyclic Oxidation

Metallography of alpha-2 systems tested at 900°C will not be discussed in great detail. The reason is that the alloy will not be applied in this temperature regime. The tests were performed at 900°C to accelerate oxidation and interdiffusion for exposure of any problems with the coating system.

Sputtered Ti-44Al-28Cr/Alpha-2 - 900°C

The as-coated microstructure of sputtered Ti-44Al-28Cr on the alpha-2 alloy is shown in Figure 63. The coating is 30 μ m thick and has some through thickness cracks and porosity. The chemistry of the coating is presented in Figure 64.

Sputtered Ti-55Al-8.5Cr/Alpha-2 - 900°C

The as-coated microstructure of sputtered Ti-55Al-8.5Cr on the alpha-2 alloy is shown in Figure 65. The coating is 30 μ m thick and had some through thickness cracks and porosity. The chemistry of the coating is presented in Figure 66. The sputtered TiCrAl coatings on alpha-2 cracked more than on the gamma substrate, e.g. compare Figures 54 and 60. The reason is the better match of thermal expansion coefficients for the gamma substrate as illustrated in Figure 67. The difference between the curves for alpha-2 and TiCrAl coatings is greater than 10%. Figure 67 also shows that expansion coefficients of gamma alloys are within ~10% of those for alpha-2. Environmentally resistant gamma alloys, therefore, might be useful as coatings for alpha-2. X-ray analysis and visual observations of these samples indicate that α -Al₂O₃ scales form on the majority of the surface.

LPPS Ti-44Al-28Cr/Alpha-2 - 900°C

The as-coated microstructure and chemistry of LPPS Ti-44Al-28Cr on Ti-24.5Al-12.5Nb-1.5Mo are shown in Figures 68 and 69. The coating is 70 μ m thick with a structure similar to that already described. The complex layer at the coating/substrate interface is associated with contamination and oxidation.

APS Alloy 718/Alpha-2 - 900°C

The as-coated microstructure and chemistry of APS Alloy 718 on Ti-24.5Al-12.5Nb-1.5Mo are shown in Figures 70 and 71. The coating is 50 μ m thick with a structure expected for an APS superalloy. Some oxide is noted in the coating. A small 4 μ m reaction layer formed at the interface during the processing of the coating. The interface may be the result of interstitial embrittlement or the diffusion of Fe and Ni.

Alpha-2 - 900°C

The oxide produced on uncoated alpha-2 after 500 hr of cyclic oxidation at 900°C (1650°F) is shown in Figure 72. The oxide is ~15 μ m thick and planar. The mixed oxide scale is Ti-rich, porous and layered. The only Al-rich areas on the scale are discrete dark particles located at the gas/metal interface. Under the mixed scale, there is a phase where Nb and Mo are enriched and intermixed with a Ti-rich oxide. An alpha case is not obvious, perhaps because the oxide scale is spalling.

Vicker's hardness measurements (100g load) were taken on uncoated and coated alpha-2 substrates. The Vicker's hardness for the baseline substrate is from 350 to 400 which is larger than gamma. A hardness increase was always detected at the oxide/substrate interface in uncoated samples and at the coating/substrate interface in plasma sprayed samples. The embrittlement extended 25-30 μ m into the substrate. The hardness of the sputtered TiCrAl coatings was from 500-700 which was the same as that reported for the coatings on gamma. No increase in hardness was found on alpha-2 alloys with protective coatings after exposure.

Sputtered Ti-44Al-28Cr/Alpha-2 - 760°C

The sputtered Ti-44Al-28Cr coating on the Ti-24.5Al-12.5Nb-1.5Mo alpha-2 substrate had a weight change/area of ~0.6mg/cm² after 1000 hr at 760°C (1400°F). This translates roughly to a k_p of $1 \times 10^{-13} \text{g}^2 \text{cm}^{-4} \text{s}^{-1}$. The values for the sputtered Ti-Cr-Al coatings were the smallest in the test despite thermal expansion mismatch cracks. Figure 73 shows low magnification micrographs of the surface of the sample throughout the test. A large number of cracks are seen throughout the test which were much worse than those on gamma (See Figure 49). The difference between gamma and alpha-2 is that alpha-2 has a lower coefficient of expansion. The cracking at 760°C indicates that Ti-Cr-Al coatings will crack in service on alpha-2 at this temperature despite a lower ΔT . Previously, only 900°C data were available. The cracks on the surface allowed some oxidation of Ti and this resulted in a larger weight change/area of the coating on alpha-2 than expected from results on gamma. The Ti-44Al-28Cr coating was tinted purple for most of the test indicating that a very thin protective scale had formed. X-ray diffraction showed that the scale was $\alpha\text{-Al}_2\text{O}_3$.

Figure 74 shows the 29 μ m thick TiCrAl coating in cross-section. The micrograph is taken away from a cracked region where the coating has high integrity and a highly developed 13 μ m thick reaction layer. X-ray diffraction shows that the coating is a combination of the Laves MgZn₂-

type TiCrAl phase, γ -TiAl and a BCC phase. The phase that comprises the body of the coating has a composition of Ti-40Al-27Cr which is lower in Al than the nominal composition. In Figure 74, the dark phase is gamma, the precipitate is the BCC phase and the gray phase is TiCrAl.

The complex reaction zone required microprobe analysis. The change in chemical composition of the coating is shown in Figure 75. The microprobe results indicate that the dark band in the reaction zone where the original interface resided has a gamma composition with substantial Cr+Nb content from a bright imaging precipitate. The phase bordering the alpha-2 substrate has a composition of Ti-33Al-11Nb-2Cr-1.5Mo. This phase is likely either hexagonal or orthorhombic alpha-2. Microprobe also clearly shows that the coating had high Al at the surface and the reaction layer, but lower Al in the body. One might expect a completely opposite profile as Al is being depleted at the surface by oxidation and at the coating/substrate interface by interdiffusion. The performance of this coating in the cyclic oxidation tests was such that it was selected for further evaluation.

APS Alloy 718/Alpha-2 - 760°C

The air plasma sprayed Alloy 718 coating on the Ti-24.5Al-12.5Nb-1.5Mo alloy displayed parabolic kinetics and a weight change/area of 1.7mg/cm². This value is high and reflects the oxidation of pores and cracks in the coating.

The surface of the Alloy 718 coating at various times during the 760°C (1400°F) cyclic oxidation test is shown in Figure 76. The surface is very rough and bright shiny areas are indicative of oxide spalling to bare coating.

Figure 77 shows the Alloy 718 coating in cross-section. The coating had a thickness that ranged from 30-50µm. The coating had many cracks and large oxide inclusions. X-ray diffraction determined the oxide to be composed of Cr₂O₃, a (Cr,Ni,Fe) oxide spinel and NiO. The coating phases were determined to be a randomly oriented FCC Ni solid solution and possible δ -Ni₃Nb. The Alloy 718 reacted with alpha-2 to form a 30-40µm thick reaction zone during the exposure. Figure 77 labels four of the phases in the reaction zone 16, 17, 18 and 19; and Table 10 lists the compositions of these phases in atom percent. The change in chemical composition in the coating after exposure is shown in Figure 78.

The APS Alloy 718 was selected for further evaluation in the environmental testing performed in Tasks 2.3 and 2.4. The selection was based on engine application experience that shows that Alloy 718 is insensitive to HSSCC.

Sputtered Ti-55Al-9Cr/Alpha-2 - 760°C

The sputtered Ti-55Al-9Cr coating on the Ti-24.5Al-12.5Nb-1.5Mo alpha-2 substrate showed a very small weight change/area of ~0.4mg/cm². The behavior of this system was similar to the Ti-44Al-28Cr coating except that larger thermal expansion mismatch cracks lead to coating spallation. Figure 79 shows the surface of the coating after the 1000 hr 760°C (1400°F) cyclic oxidation test. In spite of the cracking, the coating maintained a tint throughout the test which

indicated that a very thin protective oxide had formed. X-ray diffraction verified that the oxide was α - Al_2O_3 with a weak contribution from TiO_2 . The rutile (TiO_2) may have come from a brief transient oxidation stage or from areas where the coating had spalled.

Figure 80 shows a cross-section of the 25 μm thick coating away from a cracked region. The outer coating phases were shown by x-ray diffraction to be γ -TiAl and the Laves TiCrAl phase. Comparing this coating to Ti-44Al-28Cr in Figure 74, the coating has much more of the dark gamma phase as is to be expected from the higher Al content. The reaction zone is about 8 μm which also is similar to the Ti-44Al-28Cr. This coating was not chosen for further evaluation because a TiCrAl-type of coating had already been selected. This coating composition did suggest that a modified gamma composition could be used as a coating for alpha-2. To this end, a Ti-48Al-2Cr-6Nb-0.1B coating was selected for evaluation due to powder availability and the elevated Nb content which is known to improve oxidation resistance.

LPPS Ti-44Al-28Cr/Alpha-2 - 760°C

The low pressure plasma sprayed Ti-44Al-28Cr on the Ti-24.5Al-12.5Nb-1.5Mo alpha-2 alloy gained $\sim 1.2\text{mg}/\text{cm}^2$. Figure 81 shows both the surface of the alloy and cross-section of the alloy after the 1000 hr 760°C cyclic oxidation test. The surface shows thermal expansion mismatch cracking that formed after 600 cycles. The surface had indications of some TiO_2 nodule formation. The cross-section shows that the coating was $\sim 32\mu\text{m}$ thick and was heavily cracked. The figure shows a through-thickness crack that penetrated into the alpha-2 substrate. The crack was heavily oxidized and must be considered a poor microstructure. The reaction layer for this coating was very irregular and varied in thickness from 4-30 μm . X-ray diffraction revealed that the oxide phase on the surface was mostly α - Al_2O_3 with a weak contribution from rutile. The major phase in the coating was the Laves TiCrAl phase observed in other TiCrAl coatings. The LPPS coating was not chosen for further environmental test evaluation because of the cracking.

Cermet (50% Al_2O_3 &René 80)/Alpha-2 - 760°C

The air plasma sprayed cermet coating (50% Al_2O_3 and René 80) on the Ti-24.5Al-12.5Nb-1.5Mo alpha-2 alloy exhibited a weight change/area of $\sim 2.1\text{mg}/\text{cm}^2$ in the 760°C cyclic oxidation test. Figure 82 shows the surface and cross-section of the sample after the test. The surface had typical plasma spray roughness and a green oxide was observed to form and spall from the surface. X-ray diffraction indicated the presence of α , γ and δ - Al_2O_3 oxides and NiO. The oxide that was observed to spall was thus green colored NiO. Surprisingly, no Cr_2O_3 was observed as expected when René 80 oxidizes. The cross-section shows that the coating was 84 μm thick and had a limited reaction zone. No through-thickness cracking or poor microstructures were observed on the coating. X-ray indicated that the bright phase in the coating was a FCC Ni solid solution. The cermet was not selected for further evaluation on alpha-2 because a cermet coating was already selected for the gamma substrate.

Alpha-2 - 760°C

The uncoated Ti-24.5Al-12.5Nb-1.5Mo alloy gained $\sim 0.9\text{mg/cm}^2$. The surface of the alpha-2 is shown in Figure 83. The alloy formed TiO_2 nodules on top of a thin protective scale. At longer times, oxide patches turned white as they lost adhesion to the underlying substrate. Further thermal cycling caused these patches to crack and spall reducing weight gain. Thus the low magnitude and high stability of the weight change/area data for alpha-2 versus coated systems is a little misleading as the oxide on most coatings did not spall.

The oxide on the alpha-2 was determined by x-ray diffraction to be Nb-doped TiO_2 , with a weaker contribution from $\alpha\text{-Al}_2\text{O}_3$. The substrate phases were ordered hexagonal Ti_3Al , cubic TiN and weak contributions from a $\beta\text{-Ti}$ phase and an orthorhombic phase (Ti_2AlNb). The cubic TiN phase is more correctly $\text{Ti}(\text{O}, \text{N}, \text{C})$.

Figure 84 shows cross-sectional micrographs of the scale on the alpha-2 alloy. The scale is $3\text{-}7\mu\text{m}$ thick. There is also a $13\mu\text{m}$ region under the scale that has exhibited a refinement or dissolution of the α_2 precipitates. One micrograph shows a line trace for oxygen across the scale and "a denuded" zone. Little oxygen ingress was observed.

2.2.4 Cyclic Hot Corrosion/Oxidation Testing (CHC/O) - Task 2.3

The program provided an opportunity to assess the environmental performance of coated and uncoated Ti-aluminides in testing simulative of an engine. Environmental tests of this sort are very valuable if they can approximate engine conditions. To do so requires a very special apparatus that can 1) produce combustion gases at high velocity and temperature, 2) heat and cool samples rapidly, and 3) introduce contaminants such as sea salt. At GE Aircraft Engines, high velocity burner rigs can be programmed to simulate various mission cycles. These are very specialized rigs that heat cylindrical pin samples that rotate at 500rpm into and out of a 0.8 Mach gas stream produced by combusting Jet A fuel that can heat samples as fast as $20\text{-}30^\circ\text{C/sec}$. After exposure, the samples are mechanically withdrawn from the gas path and high pressure air is used to cool the samples. The rig also has the capability of injecting sea salt into the gas to produce hot corrosion conditions. The cylindrical pins used in the rig have a temperature gradient along their length which allows many different temperature conditions to be analyzed using special sectioning techniques. Temperature control in the rigs is performed with a calibrated turbine pyrometer. Figure 85 shows a schematic of the rig in operation.

The testing of the coated Ti-aluminides in the CHC/O burner rig was a challenge. The rigs are generally used to test coated and uncoated superalloys at temperatures greater than 1093°C (2000°F) and are not commonly used on Ti-based systems. In consideration of program objectives, test missions were designed to represent and accelerate the conditions found in the gas path for high pressure compressors and the low pressure turbines where Ti-aluminides might be used.

The high pressure compressor test was chosen to accelerate the environmental degradation in current military compressor materials that cycle between 593°C (1100°F) and 482°C (900°F). The selected thermal cycle begins with rapid heating to 760°C (1400°F) which accelerates environmental degradation since it is higher than typical take-off temperatures. During the heat up, 0.25ppm of sea salt was injected for 30 seconds into the gas stream to represent the possibility of salt contamination from various aerosols located near oceans. Upon reaching 760°C (1400°F), the temperature is held constant for 5min; cooled via reduced fuel flow to a temperature of 648°C (1200°F) which represents cruise; held for 5min; and then cooled to room temperature by high pressure air. A monolithic sample of cast Alloy 718 was included in this test as a baseline.

A more severe low pressure turbine (LPT) cycle was also selected. The cycle starts with a rapid heat up to 900°C (1650°F) with 2.0ppm of sea salt injected into the combustion gas stream. The salt injection in this test is continuous. The rotating samples are held for 5min and then the fuel is cut back until the samples attain 760°C (1400°F). The samples are held at this temperature for 5min and then cooled rapidly to room temperature. Two common low pressure turbine materials, René 77 and René 80, were included as baselines.

2.2.4.1 High Pressure Compressor (HPC) Test

The high pressure compressor test was run for 550 hr at temperatures between 648-760°C (1200-1400°F) or 3200 cycles. The diameter, weight and visual observations of the pins were taken throughout the test to indicate the amount of oxidation, spalling or metal loss. After the test, the samples were water rinsed and the deposits were analyzed and were weighed again. These samples were then photographed and metallographically evaluated. The temperature gradient along the length of the pin in this particular test is shown in Figure 86.

Test Measurements

Figure 87 shows the weight change/area data for the coated and uncoated Ti-aluminides in the high pressure compressor burner rig test. The figure shows that the thermally sprayed coatings spall loosely adherent particles during the first few thermal cycles. After the initial spallation, the APS Alloy 718 and the cermet-(50%Al₂O₃ and NiCrAlY) exhibit very little weight change. The APS YSZ on gamma, on the other hand, continued to exhibit spallation. The other coated and uncoated samples exhibited very little weight change.

Figure 88 shows the plot with a different range on the y-axis. The coated and uncoated Ti-aluminides showed very protective behavior with little weight change. The apparent exceptions are the LPPS Ti-48Al-2Cr-6Nb-0.1B coating on alpha-2 and monolithic Alloy 718, however, their weight change was small suggesting formation of a protective oxide.

After the test, the samples were rinsed of any salt or debris with distilled water. The weight loss that occurs during this stage was an indicator of the propensity of a coating to retain salt and other contaminants. Table 11 shows the change in weight after the rinsing process. The table indicates that thermally sprayed coatings retained more salt than the monolithic substrates and

sputtered coatings, because the sprayed coatings had a larger amount of porosity. The salt from the rinsings was analyzed and composed of 29%Na, 5%Ca and 2%Mg cations and 50% SO₄ and 14%Cl anions.

The measurements summarized in Table 11 mean that the samples had from 0.05-0.35 mg/cm² of salt on their surfaces. This range is about 5X greater than measurements performed on the uncoated high pressure compressor blades of a T39 engine flying out of Charleston AFB¹⁰. The test, therefore, deposits more salt on the samples than expected in the field. This is bad for field simulation but good for test acceleration as corrosion is often related to the quantity of salt deposited. Also included in Table 11 are the final rinsed weight change/area measurements for the samples. There is little difference between these values and those shown in Figures 87 and 88.

Diameter measurements were taken on all of the samples during the test in a consistent manner with a micrometer. A diameter change of less than 25.4µm (0.001") was recorded for all of the specimens at the hot spot except for the APS YSZ which showed a loss during the course of the test. This is consistent with the gradual loss in weight for the YSZ shown in Figure 87. The small change in diameter of the samples meant that metallography was necessary to characterize the environmental attack on the various coating candidates.

Metallography

Figures 89 and 90 show the rinsed samples after the 550 hr HPC cyclic hot corrosion/oxidation test. The front side of the pin has a notch at the bottom and faces the combustor. The backside has no notch and faces away from the combustor. The samples show only slight signs of degradation and are discussed in the following paragraphs.

Uncoated Gamma

The uncoated gamma alloy developed a gray oxide at areas that experienced temperatures greater than approximately 732°C (1350°F). The thin gray oxide has a "fingerprint" morphology, where islands of oxide have formed between distinct boundaries. Elsewhere on the pin, a shiny tint indicates the formation of a thin protective interference film or oxide.

A cross-section of the sample taken from a section at the hot spot is shown in Figure 91. The scale had a uniform thickness of 6µm with the outer layer generally cracked. Underneath the oxide, a submicron alpha-2 layer forms either by interstitial enrichment or Al depletion. Figure 91 also shows an area of "lath attack," where environmental attack of the bright imaging alpha-2 phase was observed. This attack extends 7µm into the substrate and was not frequently observed on the sample. The uncoated gamma sample looked good after the test, but it was not clear how the lath attack, interstitial embrittlement and oxide formation affect mechanical properties.

Sputtered Ti-44Al-28Cr/Gamma

The sputtered Ti-44Al-28Cr coating in Figures 89 and 90 has a dull tint across the entire length of the pin with little or no spalling. No thermal expansion mismatch cracks were noticeable with a 10X eyepiece even though they were observed during the 760°C cyclic oxidation test.

Figure 92 shows a cross-section of the coating at the hot section of the pin. The coating had many evenly spaced oxidized leaders or through-thickness defects that may be the missing expansion mismatch cracks. These defects were not observed to penetrate in to the substrate. In one of the micrographs, a oxidized defect was viewed at a perpendicular angle. Most of the sputtered coating, however, had high integrity with no cracks with the two phase microstructure observed in the cyclic oxidation test. The alumina thickness on the surface of the coating was submicron.

Cermet (50%Al₂O₃ +NiCrAlY)/Gamma

The cermet coating did not change appearance throughout the test with the exception of green NiO that formed at longer times. Figures 89 and 90 show that the tip of the pin was polished to remove extra coating thickness. The polished region was tinted throughout the test and shows that this coating can be finished to various aerodynamic requirements.

Figure 93 shows the cermet coating in cross-section at the hot spot. The 125µm coating was remarkable in that no cracks or defects were observed around the entire circumference. The figure shows that a very thin 0.2µm oxide is at the surface and that the reaction zone varies between 0 and 6µm. The cermet coating was the best performer in the high pressure compressor environmental test.

APS YSZ/Gamma

Figures 89 and 90 show that the APS YSZ coating spalled on both the front and backside of the pin. Spalling was not observed to this extent in cyclic oxidation tests, therefore, the geometry of the pin and the more severe thermal transients have affected the coating behavior.

Figure 94 shows the cross-section of the APS YSZ after the test. The micrograph shows that a large continuous crack has developed 8-15µm above the oxide that formed at the coating/substrate interface. This type of cracking causes the spallation that was observed macroscopically. It is clear that the YSZ cannot be a good barrier to contaminants if it cracks and spalls off. A YSZ thermal barrier coating will most likely have to be used with an environmentally resistant bond coat.

Monolithic Alloy 718

The monolithic Alloy 718 represents a material that Ti-aluminide may replace. The Ni-Fe superalloy exhibited a thin oxide at the hot spot. Interestingly, there was an area of enhanced degradation 37mm (1.5") from the tip of the pin where a rust colored Fe-rich oxide was observed. The temperatures at this region of the sample had a maximum temperature of 565°C (1050°F).

Figure 95 shows a cross-section of Alloy 718 at the hot spot. The 4µm thick external oxide has a spinel composition and there are some internal oxides as deep as 6µm into the substrate. The 718 is protective under these conditions and is an attractive material because of good potential ductility over the entire temperature range.

Uncoated Alpha-2

The uncoated Ti-24.5Al-12.5Nb-1.5Mo alloy had a dark blue-black tint over most of the sample. In areas of the pin that saw temperatures higher than 675°C (1250°F), bright patches of thick oxides formed that were prone to spallation. Under this temperature, the oxide was very thin and no spallation was observed.

Figure 96 shows a cross-section of the alpha-2 alloy at the hot spot. The external scale is 9µm thick and EDS shows that it is composed of more Nb than what was observed in cyclic oxidation tests. The high magnification micrograph shows the layered nature of the scale. There was a zone of internal attack under the scale that is 2µm deep.

Sputtered Ti-44Al-28Cr/Alpha-2

The outward appearance of the Ti-44Al-28Cr sputtered coating on alpha-2 was the same as that observed for the same coating on the gamma substrate. None of the spallation or thick oxide growth seen on the uncoated alpha-2 was observed. At longer times, the sample did develop a fine striated structure on the surface that were thermal expansion mismatch cracks consistent with cyclic oxidation results.

Figure 97 shows the coating in crosssection at the hot spot. The coating had a set of evenly spaced through-thickness defects around the circumference. These defects have oxidized through to the substrate and caused substrate cracking. The crack is heavily oxidized and shows signs of trifurcating (one crack becomes three) at the coating/substrate interface. The bright phase around the crack was rich in interstitials and will not blunt the crack tips. The defects may initially result from difficulties associated in sputtering cylindrical specimen geometries, but in combination with large thermal expansion mismatch strains they become substrate cracks. The effect of the defects are amplified in this test as compared to the cyclic oxidation test, because of the very high heating and cooling rates which increase the strain rate at the interface. The structure of the coating in other areas is excellent as a 0.4µm alumina scale forms on the surface. The major challenge in using this coating on alpha-2 will be to lower the thermal expansion mismatch and to find a coating process that minimizes defects.

APS Alloy 718/Alpha-2

The air plasma sprayed Alloy 718 coating on alpha-2 generally maintained the as-sprayed morphology throughout the test with no coating spallation. At longer times, the hotter regions showed some oxide spallation and gray patches.

Figure 98 shows this coating in cross-section at the hot spot. The coating is $\sim 90\mu\text{m}$ thick with $\sim 6\text{--}10\mu\text{m}$ thick external oxide on the surface. More importantly, the sample has a set of evenly spaced oxidized thermal fatigue cracks around the circumference. These cracks are similar to those observed on the alpha-2 coated with TiCrAl except that there is not a lot of evidence of the crack splitting into more branches. The cracks penetrated through the coating, propagated $30\text{--}40\mu\text{m}$ deep into the alpha-2 and were filled with a Ti-rich oxide. Also observed were alumina grit particles at the coating/substrate interface used to prepare the surface of the alpha-2 for coating. High magnification examination of these particles indicate that they did not nucleate cracks during the test. The cracks that occurred on this sample are the result of thermal expansion mismatch strains. The coefficient of thermal expansion, α , for alpha-2 ($\sim 10.5 \times 10^{-6}/^{\circ}\text{C}$) is much less than that for Ni-Fe superalloys ($\sim 15 \times 10^{-6}/^{\circ}\text{C}$). Application of this coating to alpha-2 will require a second phase to reduce thermal expansion mismatch. This type of coating is available with the cermet processing.

LPPS Ti-48Al-2Cr-6Nb-0.1B/Alpha-2

The LPPS modified gamma composition coating on alpha-2 maintained the as-sprayed morphology throughout the test. In the hot regions of the sample, a uniform oxide formed giving the sample a light gray color. Also noticeable at early times were locally thick rutile scales (white specks) similar to those observed on uncoated alpha-2. These local areas did not cause any problems.

Figure 99 shows a cross-section of the modified gamma coating at the hot spot after the test. The coating had many pores and a thickness that varied between $65\text{--}110\mu\text{m}$. There were no cracks or coating spallation observed along the circumference. The thick oxide that caused the light gray color was $12\mu\text{m}$ thick and was composed of a dark $5\mu\text{m}$ Al-rich layer at the surface and a light $7\mu\text{m}$ thick Ti-rich layer underneath. An accicular $10\mu\text{m}$ reaction layer formed between the coating and substrate along with the degeneration of some prior β grain boundaries in the alpha-2 substrate. The modified gamma coating was judged better than the other alpha-2 coating candidates since substrate cracking did not occur. This reduced cracking may be a direct result of using a weaker coating with a lower expansion coefficient ($\sim 12.6 \times 10^{-6}/^{\circ}\text{C}$).

2.2.4.2 Low Pressure Turbine Test

The low pressure turbine (LPT) test was performed for 50 hr at high temperature or 498 cycles. The same procedures for the high pressure compressor (HPC) test were used. The temperature gradient along the length of the pin in this particular test is shown in Figure 100. Recall that this test had 2ppm salt injected into the combustion path continuously throughout the test as compared to the HPC test that had 0.5ppm salt injected for only the first 30sec of each cycle.

Test Measurements

The LPT conditions used were much more severe than the HPC conditions and this resulted in a significant reduction in the length of the test. Table 12 presents the weight change/area of rinsed samples after the test. The coated samples with the largest weight loss/area ($>3\text{mg}/\text{cm}^2$) were visually observed to have coating spallation. The exception was the cermet coating that had no spallation. Comparison of Table 12 with Table 11 shows that the amount of weight change/area for the cermet was constant between the two tests.

Included in Table 13 is the weight of water soluble debris (mostly salt) removed from the surface. The metallic surfaces had less water soluble debris than thermally sprayed structures. This is directly related to the porosity and cracks found in the sprayed coatings after processing. This supports the observation that sprayed coatings gain more weight in static oxidation tests because of larger effective surface areas. The surface concentration of salt for the metallic dense surfaces was calculated to be $5\text{-}6\text{mg}/\text{cm}^2$ and that for sprayed surfaces was $7\text{-}9\text{mg}/\text{cm}^2$. Coating surfaces can be densified by using techniques like peening, HIPping and surface melting.

The water soluble salt composition was analyzed by a combination of capillary electrophoresis and plasma emission spectroscopy. The salt composition on all of the samples was nearly the same and was composed of 70% SO_4 , 27%Na, 1.5 %Ca, 1.0%Mg and traces of other alkalis. The insoluble debris from the uncoated gamma and René 80 was analyzed qualitatively by x-ray fluorescence. The debris on the gamma had in order of greatest contribution Mg, Al and Si with smaller amounts of P, S, Ca, Ti, Fe and Ni. The appearance of Ni indicates that small amounts of molten corrosion products from the Ni-base superalloys may have been transferred to other test samples in the carousel. The insoluble debris from the René 80 in order of highest contribution contained a lot of Mg, Si and Ni with smaller amounts of Na, Al, P, S, Ca, Ti, Cr, Fe, Co, Cu and W. The presence of many elements from the substrate was expected in the reaction product since hot corrosion reactions were occurring.

Diameter measurements in Table 12 indicated that the Ni-base superalloys, including the Alloy 718 coating, are attacked severely and lost a substantial amount of cross-section. The cermet coating contained Ni, but the composition of this Ni-alloy is such that a protective alumina scale formed and little change of the diameter was noticed. The APS YSZ lost cross-section because of coating spallation. The Ti-base systems were more resistant to reduction in cross-section.

Metallography

Color photographs of the samples after the LPT environmental test are shown in Figures 101 and 102. Figure 101 shows the front or notched side of the samples, while Figure 102 shows the backside. The severe nature of the attack under these conditions is evident when these figures are compared to Figures 89 and 90. The sputtered Ti-44Al-28Cr/ γ , the APS YSZ/ γ and the APS Alloy 718/ α 2 coatings spalled off their respective substrates. In addition, the Ni-alloys show evidence of a molten hot corrosion product in the hot spot. The uncoated Ti-aluminides had loosely adherent scales that were prone to spallation. The best coating system on the gamma was the cermet coating which showed no signs of attack. On the alpha-2 substrate, the Ti-48Al-2Cr-6Nb-0.1B and sputtered Ti-44Al-28Cr coatings looked the best. The coatings were cross-sectioned at the hot spot and 3.3cm from the tip of the specimen. The 3.3cm specimen shows the effect of higher salt concentration and a smaller number of thermal cycles at a temperature comparable to the HPC simulative environment.

Uncoated Gamma

The uncoated Ti-48Al-2Cr-2Nb substrate looked rough in appearance with a multi-colored scale that spalled during the test. This type of environmental attack was seen in areas of the pin that were hotter than 750°C (1382°F). The greenish color in the oxide may be Ni-rich products from the hot corroding René 80 and 77.

Figure 103 shows that a 30 μ m thick oxide had formed on the surface. The thickness of this oxide varied across the circumference and was heavily cracked. There was a zone of internal attack under this scale that was about 4 μ m thick. This subscale attack has Ti-rich black particles that contain some S indicating an oxidation/sulfidation type of attack.

The same Figure shows the 3.3cm cross-section. The scale was very thin (0.5 μ m thick) in most areas with the exception of locally thick areas that were 2.5 μ m thick. The general scale was thin compared to the HPC results because less time was spent at temperature. Under the locally thick area, there is internal attack of 2 μ m. The internal attack is dark and contains sulfur but did not look like "lath attack."

Sputtered Ti-44Al-28Cr/ γ

The sputtered Ti-44Al-28Cr coating spalled in less than 25 hr in the LPT test. The spalled areas of the coating resemble the uncoated gamma alloy. Figure 104 shows a cross-section of the alloy at the hot spot where the coating had spalled. The sputtered TiCrAl coating had dark precipitates in the coating and at the coating/substrate interface. The adherent coating formed a 1 μ m alumina scale. In areas where the coating was not adherent, a 15 μ m scale formed. This micrograph, therefore, shows the protective ability of the TiCrAl coating if it stays adherent. One possible way of improving the adhesion of the sputtered coating may be to give it an anneal at high temperature after coating to promote interdiffusion. The 3.3cm section shows the same type of morphology only on a finer scale.

LPPS Cermet (50%Alumina+50%NiCrAlY)/ γ

The 50% alumina + NiCrAlY cermet coating had no visible signs of environmental attack. Figure 105 shows the 125 μ m thick cermet coating at the hot spot and at the 3.3cm section. The observable scale on the hot section is 1 μ m thick and the reaction layer is 6 μ m thick. There were no cracks, spalling or evidence of environmental attack. The 3.3cm section shows the same morphology with the exception of a thinner 3 μ m reaction layer. This cermet coating on gamma was the best performer in both the LPT and HPC tests.

APS YSZ/ γ

The air plasma sprayed 8 weight percent yttria stabilized zirconia coating on gamma showed a large amount of spallation after 44 hr of testing. Figure 106 shows cross-sections at the hot spot and at the 3.3cm section. The hot section micrograph shows that a 10 μ m oxide formed at the coating/substrate interface. TBC spallation was observed on ~50% of the circumference. Under the oxide of the coating, there was an interstitial layer with sulfides. There was no spallation of the coating on the 3.3cm section. The coating on this section stopped sulfur ingress to the coating/substrate interface. The spallation of this coating was a disappointment and YSZ might have to be used with an environmental bond coat in the future.

Uncoated Alpha-2

The uncoated Ti-24.5Al-12.5Nb-1.5Mo substrate had a loosely adherent scale that spalled after 25 hr of testing. The heavy attack occurred on the sample on sections that were hotter than 700°C (1292°C). Figure 107 shows cross-sections of the substrate at the hot spot and the 3.3cm section. The scale in the hot spot was as thick as 40 μ m, layered and porous. There did not appear to be an interstitial layer under the external oxide. The lack of a layer was the result of rapid oxidation and spallation rather than interstitial dissolution. The 3.3cm section has a 1.8 μ m thick oxide with a distinct interstitial layer. The presence of the interstitial layer is associated with the thinner more protective oxides at lower temperatures.¹¹

Sputtered Ti-44Al-28Cr/ α 2

The sputtered Ti-44Al-28Cr coating on the alpha-2 substrate does not show substantial attack on the surface. The surface for the most part is reflective which indicates that a thin protective oxide has formed. Using 10X magnification, the sample shows thermal expansion mismatch cracks with rutile growing out from the crevices. Figure 108 shows the hot and 3.3cm sections of the coating. The hot section had the same through-thickness coating defects that were seen in the HPC test. Most of the defects showed the trifurcation of the crack, but others showed rapid attack of the coating/substrate interface. These defects dominated 25% of the circumference.

The reaction zone in the sample was 41 μ m thick away from cracked regions. The 3.3cm section shows the same cracks in the coating but with a 2 μ m reaction zone. The through-thickness defects compromise the microstructure and indicate incompatibility between the substrate and coating.

APS Alloy 718/ α 2

The air plasma sprayed coating on the alpha-2 alloy was totally consumed in regions that saw temperatures greater than 815°C (1500°F). The coating was heavily attacked between 0 and 44 hr of testing and then spalled after that point. Figure 109 shows the hot and 3.3cm sections of the coating. The micrograph from the hot section shows that the coating had been totally converted to oxide. The Ni-Fe rich oxide images lighter than the oxide indigenous to the alpha-2 substrate. The 3.3cm coating is intact and exhibits a protective oxide scale. Unfortunately, there were 10-15 cracks through the coating with most penetrating the substrate with a morphology similar to that observed in the HPC test. These cracks are caused by differences in expansion coefficients and form in less than 498 cycles.

LPPS Ti-48Al-2Cr-6Nb-0.1B/ α 2

The low pressure plasma sprayed modified gamma coating on the alpha-2 had no coating spallation and was peach colored with areas of green. The green oxide is thought to be from the René 77 that was located next to the sample in the rotating carousel. Figure 110 shows the hot and 3.3cm sections of the coating. The micrograph from the hot section shows a 42 μ m thick external oxide with a 11 μ m reaction layer. The scale has many cracks and would have likely spalled with more cycling. Importantly, there were no through-thickness cracks along the circumference of the sample. The micrograph from the 3.3cm section shows a coating that is roughening or "rumpling" with exposure. The roughness often leads to thermal fatigue cracks in other coating systems. The external oxide under these conditions is only 2 μ m thick. This coating performed the best on the alpha-2 substrate in the engine simulative testing.

René 80 and René 77

The monolithic current LPT Ni-base superalloys underwent severe hot corrosion in this test. Figures 101 and 102 show graphically that uncoated Ti-aluminides are more resistant to these conditions than the Ni-base superalloys. The hot corrosion attack occurs on sections of the pins that saw temperatures greater than 800°C (1500°F). Figure 111 shows the cross-section of the René 80 at the hot and the 3.3cm sections. The cross-section at the hot spot underwent an oxidation/sulfidation type of attack. In some areas the sulfides were molten and wetted grain boundaries (shown). The molten reaction products accelerate degradation in the Ni-alloys while this type of attack was not observed on the Ti-based materials. In another area, a large 0.75mm thick blister formed. In the 3.3cm section, a much thinner 3.6 μ m scale formed along with preferential attack of the carbides. The ductile Ni-base alloys had more attack than the Ti-alloys but the effect of the attack on mechanical properties may be less.

Burner Rig Testing Summary

The burner rig testing showed that uncoated alpha-2 and gamma Ti-aluminides are resistant to thermal cycling in the presence of salt at temperatures to 760°C. Coating systems, especially, the cermets offered additional protection. Concerns with the effects of salt on mechanical properties are addressed under Task 2.4.

Burner rig testing at temperatures to 900°C showed that uncoated alpha-2 and gamma Ti-aluminides are attacked at a rate that requires a coating. For alpha-2, thermal expansion mismatch between the substrate and coating is an issue and can cause cracking when not addressed. For gamma, the cermet coating offered the most protection.

2.2.5 Hot Salt Stress Corrosion Cracking Testing-Task 2.4

One of the types of environmental attack that Ti-base alloys can experience is hot salt stress corrosion cracking or HSSCC. HSSCC refers to the interaction between salt, tensile stress and temperature that results in the production of cracks that can reduce mechanical properties. HSSCC is thought to be caused by H₂ embrittlement at crack tips.¹² The evaluation procedure chosen for the coated and uncoated Ti-aluminides is a salt-stress exposure followed by a room temperature (RT) tensile test. The three HSSCC exposures were: 1) 400°C (750°F) at 50 ksi for 100 hr; 2) 565°C (1050°F) at 40 ksi for 100 hr; and 3) 565°C (1050°F) at 40 ksi for 750 hr. Samples that were salt coated were first cleansed in solvents, heated to 150°C (302°F), cooled and then weighed. The sample was then heated back to 150°C (302°F) and an aerosol of synthetic sea salt was then sprayed on to a 2.54cm section of the gage length after which the sample was cooled and reweighed. The salt concentrations used were ~0.1mg/cm² which is 5X greater than that observed on compressor blades and vanes. The RT tensile test was performed at a strain rate of 0.005/min with an extensometer used for the first 0.2% strain after which it was removed. The test was severe in that the long term isothermal exposure would not occur in service and is known to increase HSSCC susceptibility.¹³

HSSCC Summary for Uncoated/Coated Gamma

The results of the HSSCC testing on coated and bare gamma are presented in Table 13. The bare gamma alloy was sensitive to all exposures; however, the salt was only clearly detrimental after the 565°C (1050°F) 40 ksi/750 hr exposure where total embrittlement was observed. Under these conditions, all of the applied coatings proved beneficial.

Interstitial Embrittlement of Uncoated Gamma

The embrittlement of the Ti-48Al-2Nb-2Cr gamma substrate after exposures with no salt was thought to be a result of interstitial embrittlement. Creep damage to the microstructure was not thought to be responsible for the reduced tensile properties as the deformation was small for all exposures ($\epsilon < 0.2$) and no phase transformations were observed in the bulk. In addition, GEAE IR&D work has shown embrittlement with unstressed exposures at similar temperatures and times.¹⁴

Figure 112 shows cross-sectional micrographs of the fracture paths of tensile tested bars. The fracture path of the RT tensile tested bar was rougher and more tortuous than the exposed samples. The exposed samples displayed a flatter fracture, but the degree was not easily related to the length and temperature of exposure. Secondary tensile cracks were not frequent or distributed evenly when compared to alpha-2. Figure 113 shows higher magnification images of the surfaces of the tested samples. The secondary cracks illustrated in the micrographs were generally located near the final fracture path. The crack depths were $\sim 15\mu\text{m}$ and $\sim 60\mu\text{m}$ after the 400°C (750°F) 50 ksi and 565°C (1050°F) 40 ksi exposures, respectively. The infrequent nature of the cracks in the gamma may indicate a more complicated embrittlement mechanism that results in the rapid propagation of initiated cracks. One such mechanism could be moisture induced embrittlement where H_2O reduction results in the presence of H at crack tips at room temperature.¹² These effects will be studied under a recently awarded Naval Air Warfare Center contract.¹⁵

HSSCC Metallography/Fractography of Gamma

The gamma samples were more resistant to the HSSCC exposures than the alpha-2 systems, since bare gamma never failed during salt exposure. The HSSCC environments for gamma, however, produced a flatter fracture and lower tensile elongation than samples exposed without salt. The uncoated gamma sample after the 750 hr salt exposure, however, was totally embrittled and failed during insertion into the tensile machine for the RT tensile test. Further testing is necessary to determine the time, temperature and stress conditions where the gamma substrates become embrittled with statistical significance.

The coated gamma systems behaved similarly to bare gamma perhaps showing that embrittlement from coating processing or exposure is a large concern for a successful coating on gamma. Figure 114 summarizes the behavior by showing a flat plateau when the UTS is plotted as a function of exposure and coating system. The lack of total embrittlement for any of the coated systems was thought to show that the coating prevents salt damage of the substrate.

Low magnification fractographs of uncoated tensile bars with and without salt are shown in Figure 115. The micrograph with salt shows the flat nature of the fracture and the lack of a well defined initiation site. The lack of a well defined origin is consistent with a layer of salt attack along the circumference of the sample causing an extended defect. The sample exposed without salt showed a definite initiation site (arrow) and a rougher fracture surface.

Low magnification cross-sectional micrographs of the 400°C (750°F) 50 ksi HSSCC tested systems are shown in Figure 116. The TiCrAl and APS YSZ coatings spalled near the fracture, while the cermet sample was adherent. The fracture paths were similar and no HSSCC cracks were visible at low magnification. The TiCrAl sample failed in the radius rather than in the salt coated gage length. Generally this type of failure is usually attributed to stress concentration effects at defects but in this case the salt may augment the fracture process. Figure 117 shows higher magnification images of the samples. The sputtered TiCrAl and uncoated samples both show signs of cracking. The cracking on the uncoated gamma was $\sim 30\mu\text{m}$ deep. Cracking on the TiCrAl sample was associated with through-thickness defects in the coating. Little cracking was

observed under the APS YSZ and cermet coatings. The cermet sample may have shown signs of alpha-2 attack on the fracture path (arrow).

Figures 118 and 119 show low and high magnification micrographs of the samples tested using the 565°C(1050°F)40 ksi exposure. The low magnification images show features that have already been discussed. Micrographs in Figure 119 show signs of attack on every system tested except for cermet. The uncoated sample shows a thick TiO₂-based reaction product that penetrates along boundaries in the material. One of these penetrations included a crack (arrow) and seemed to be associated with the alpha-2 in the dual phase gamma alloy. EDS analysis of the internal corrosion shows Cl, Ca, Mg and K in addition to substrate elements. The sputtered TiCrAl coating shows signs of coating attack (product was Ti-rich with substantial Cl and Si), but no attack of the substrate. The APS YSZ sample exhibited an Al-rich scale (arrow) at the coating/alloy interface that had formed during the HSSCC exposure and some internal attack. Little attack was observed on the cermet (NiCrAlY/Alumina) coating system which showed superior resistance and adhesion.

Figure 120 shows 100h creep curves for the (400°C) 750°F/50 ksi and (565°C) 1050°F/40 ksi exposures of coated and uncoated gamma. The samples showed no signs of tertiary creep or accelerated deformation as a result of environmental cracking. The 750 hr exposures resulted in ~0.2% deformation. The minimum creep rate at (400°C) 750°F/50 ksi was 5.2×10^{-6} /min with a standard deviation of 1.7×10^{-6} and at (565°C) 1050°F/40 ksi was 5.4×10^{-6} /min with a standard deviation of 1.8×10^{-6} .

Gamma Summary

Uncoated Gamma

The uncoated Ti-48Al-2Cr-2Nb was not as sensitive to HSSCC as alpha-2 systems under the conditions of the current test (See Table 14). The resistance may be attributable to having a smaller volume fraction of the ordered α_2 (Ti₃Al) phase. Emphasis might be concentrated on the α_2 phase since it is known to cause HSSCC sensitivity in conventional Ti-alloys.¹⁶

The gamma alloys, however, underwent an embrittlement after the 400 and 565°C (750 and 1050°F) 100 hr stress exposures in air with no salt. The embrittlement is characterized by a lower σ_{UTS} , lack of a yield stress as measured by the extensometer and low ductility. No firm explanation for the air embrittlement is available. Note that a solid interstitial layer was observed with the SEM and x-ray diffraction during the cyclic oxidation test. Interestingly, some of the ductility appears to return after the 750 hr 565°C (1050°F) exposure. If an interstitial layer is the culprit, this revitalization might be explained by the diffusion of the interstitials away from the surface after a more effective oxide diffusion barrier has formed at the surface.

The uncoated Ti-48Al-2Cr-2Nb did not show sensitivity to salt except after the 750 hr exposure time. The fracture surface of Ti-based tensile specimens that prematurely fail as a result of HSSCC generally exhibit a "picture frame" corrosion product when examined at low power.

Examination of the 750 hr sample did not show this type of morphology indicating a different process.

Coated Gamma

The coating systems on gamma were most beneficial after the 750 hr, 565°C (1050°F) stress-salt exposure. Recall from Table 13 that the uncoated gamma failed before the room temperature tensile test. All of the coated systems retained strength to levels greater than 53 ksi, but this value was reduced from the 67.6 ksi observed for the unexposed sample. In the case of the cermet coating, the sample had measurable ductility in addition to retained strength.

The improvement from coating in the other tests was not as noticeable since the uncoated substrate survived the test with adequate tensile strength and similar ductility to coated systems. None of the coated systems reached the goal of maintaining the σ_{UTS} or percent elongation found for the unexposed room temperature tensile test. The sputtered TiCrAl coating at 565°C (1050°F) for 100 hr and the cermet at 400°C (750°F) for 100 hr each exhibited a reduced tensile stress compared to the uncoated substrate. These data show that long term exposures of gamma alloys to HSSCC conditions can benefit from coatings.

HSSCC Summary of Uncoated/Coated Alpha-2

The results of the HSSCC testing on coated and bare alpha-2 are presented in Table 14. The results indicated that uncoated alpha-2 was sensitive to both interstitial embrittlement and HSSCC because a reduction in both UTS and elongation was observed after exposure. It is believed that microstructural creep damage was not the major factor because the (400°C) 750°F/50 ksi/100h exposure caused minimal creep (0.01-0.05%) yet the UTS and elongation were reduced.

Interstitial Embrittlement of Uncoated Alpha-2

The stressed exposures without salt shown in Table 14 are thought to cause interstitial embrittlement (O, N, C) rather than bulk embrittlement. Interstitial embrittlement refers to a surface related effect where the concentration of O, N, and C is increased. Bulk embrittlement refers to an effect caused by high interstitial content in the alloy prior to exposure. Figures 121 and 122 show unexposed and exposed (without salt) uncoated alpha-2 substrates. The unexposed alpha-2 had a rough fracture surface that exhibited shear lips and little or no secondary tensile cracking. The exposed samples, however, had noticeable secondary cracking and a flatter fracture surface. Most secondary cracks on the exposed samples had a constant depth that may correlate to interstitial enrichment at the surface. A crude analysis of the secondary crack data using a simplistic diffusion model ($X \sim \sqrt{2Dt}$) indicates a diffusivity of the embrittling species to be $D = 0.00024 \exp\left(\frac{-20.5 \text{ KCal}}{RT}\right) \text{ cm}^2/\text{sec}$. This value was high compared to diffusivities of oxygen in α -Ti, but near values extrapolated for diffusion in β -Ti.¹⁷ The activation energy of 20.5 Kcal/mol was expected for a species diffusing interstitially. A (Mo and Nb-stabilized) β phase was present in this alloy and may explain how the embrittlement occurs, i.e., interstitial

diffusion through the β phase. Interestingly, oxygen microprobe data from another GEAE IR&D study also indicated that penetration in Ti-24.5Al-12.5Nb-1.5Mo alpha-2 sheet in the 565-648°C (1050-1200°F) temperature range was characterized by an activation energy of 20.5Kcal/mol.¹⁸ The tensile stresses during the creep exposure may also increase interstitial penetration by producing a strained or cracked external oxide that could be less protective. Table 15 summarizes the depth and distribution of secondary cracks. Some cracks propagated much deeper, but could not be correlated with any particular microstructural constituent like a prior β grain boundary.

The heat treatment of the alpha-2 involved a solution of 1975°F/1h followed by a salt quench to 1550°F/0.5 hr and a stabilization at 1300°F/8h. A TTT diagram for the Ti-24.5Al-12.5Nb-1.5Mo alpha-2 predicts that β , α_2 and O phases should be observed.¹⁹ X-ray diffraction of the as-coated buttons confirmed predictions from the TTT diagram. The low temperature creep exposures used in this work, however, are not predicted to drive any further transformation based on the diagram. The effect of stress during exposure, however, may be important. Recent GEAE IR&D tests of alpha-2 sheet material of the same composition and a finer microstructure, showed little effect of *unstressed* exposure in air at 1200°F/16h on room temperature ductility.

HSSCC Metallography/Fractography of Alpha-2

Figure 123 shows low magnification micrographs of the coated and uncoated samples after the 400°C (750°F) 50 ksi HSSCC exposure shown in Table 14. The modified gamma coating and uncoated alpha-2 samples showed a severe reduction in mechanical properties. The fracture paths for the uncoated and modified gamma coated samples contained large regions of relatively flat fracture which correlate with the low elongation. The modified gamma coating, however, was very adherent to the substrate throughout the tensile test. In the case of the Alloy 718 and TiCrAl coatings, the fracture path was rougher with more tearing. Each of these coatings spalled off the substrate near the fracture perhaps as a result of greater recorded strain to failure, necking or through-thickness cracking in the coating.

Figure 124 shows cross-sections at the coating/substrate interface at higher magnification. The TiCrAl and Alloy 718 which were protective during this test have interfacial morphologies similar to alpha-2 exposed without salt. The modified gamma sample, on the other hand, showed signs of cracking through the coating and into the substrate. The uncoated alpha-2 sample had a porous, relatively thick external scale (~2 μ m) with some attack at α_2/β interfaces (arrows). The thick external scale may be caused by salt accelerated oxidation which has been documented in the literature on Ti-6242.²⁰ The attack at the α_2/β interfaces might be preferential oxidation of boundary segregants leading to interfacial decohesion by an active species like Cl.

Figure 125 shows the appearance of the fracture surface for uncoated alpha-2 exposed with and without salt at 565°C (1050°F) 40 ksi/100h. The sample exposed with salt had multiple fracture origins (arrows) associated with a relatively thick corrosion product. The sample exposed without salt has a single origin with very little corrosion product.

The salt exposures at 565°C (1050°F)40 ksi were more severe than those at 400°C (750°F)50 ksi. In the former case, only the Alloy 718 coating did not fail through the creep exposure with salt. Figure 126 shows the potency of the Alloy 718 coating in more detail using a plot of the UTS versus test exposure and type of coating. The Alloy 718 coating shows up as a local maximum on the UTS response surface. The other samples, except for one of the modified gamma coatings, all failed in under 40h. Microstructures were similar among the samples, so section effects were ruled out. Note that the times of failure for these samples were fairly reproducible. Figure 127 shows cross-sections of the fracture surfaces of the coated and uncoated samples. For samples that failed during the exposure, secondary HSSCC cracks from 50-500µm (2-20mils) were observed and the fracture surfaces were flat with little tearing.

Figure 128 shows cross-sections at higher magnifications. The most notable feature associated with the HSSCC cracking of the coated and uncoated alpha-2 was the attack of primary alpha-2 islands and alpha-2 that precipitates along prior β grain boundaries. An example of this type of attack was shown in Figure 129. Chemical analysis using EDS of the attacked alpha-2 phase indicated elevated levels of Cl, Na, Mg, K and Ca with indications of oxygen.

Figure 130 shows 100h creep curves for the 400°C (750°F)50 ksi and 565°C (1050°F)40 ksi exposures of coated and uncoated alpha-2. Creep times for various deformations are shown in Table 16 for uncoated alpha-2 and Alloy 718 coated alpha-2. The samples showed no signs of tertiary creep. At 400°C (750°F)50 ksi, coating/alpha-2 combinations that suffered from HSSCC exhibited a larger amount of deformation, presumably due to crack displacements under load and creep of uncracked material due to higher stresses. The Alloy 718 exhibits larger deformations, but no signs of HSSCC were observed. The average minimum creep rate at times greater than 50h for the uncoated (no salt) and the sputtered TiCrAl samples at 400°C (750°F)50 ksi was 2×10^{-6} /min. At 565°C (1050°F)40 ksi, the curves exhibited the same behavior except more creep occurred and Alloy 718 did not exhibit larger deformations. The average minimum creep rate of the uncoated (no salt) and Alloy 718 coating sample was 2.2×10^{-5} /min. Standard deviations were not calculated due to the limited population of samples surviving HSSCC exposures.

Alpha-2 Summary

Uncoated Alpha-2

Table 14 shows that the Ti-24.5Al-12.5Nb-1.5Mo was very sensitive to the HSSCC exposures. Both of the uncoated alpha-2 samples tested at 565°C (1050°F) in salt failed before the RT tensile test. The uncoated sample at 400°C (750°F) failed with little ductility at a much reduced σ_{UTS} (61 ksi vs. 174 ksi). Visual examination of the fracture surface indicated the "picture frame" effect associated with HSSCC on Ti-base alloys. These data substantiate claims that the α_2 phase is susceptible to HSSCC. The data generated in this program show that alpha-2 alloys will need coatings to prevent mechanical property degradation in environments that cause HSSCC.

The uncoated alpha-2 at similar temperature and stress conditions without salt survived the exposures and were tensile tested. The sample exposed at 565°C (1050°F) for 100 hr had no measurable ductility. The 750 hr exposure at the same conditions has ductility, but the tensile

strength is greatly reduced (133 ksi vs. 174 ksi). The lower temperature exposure was not as detrimental as there was measurable ductility and a respectable UTS (165 ksi). The embrittlement here is related to dissolution of interstitials. The detrimental effects of interstitials were observed in the cyclic oxidation test and in other work.¹⁴

Coated Alpha-2

The APS Alloy 718 coating on the Ti-24.5Al-12.5Nb-1.5Mo alpha-2 substrate was beneficial under all HSSCC exposure conditions as shown by the survival of the samples after the various salt exposures. The Alloy 718 coated samples retained usable levels of strength, but had questionable ductility at the higher exposure temperature, 565°C (1050°F).

The sputtered TiCrAl coating on the alpha-2 failed in salt environments at 565°C (1050°F) and, therefore, was not tensile tested. The lack of protection is not a surprise given the through-thickness defects in the coating observed in the cyclic and engine simulative environmental tests. The fracture surfaces had "picture frame" corrosion in areas around the periphery. The TiCrAl at 400°C (750°F), however, did provide protection. This sample survived the test and had a usable UTS of 165 ksi with measurable ductility.

The LPPS modified gamma coating (Ti-48Al-2Cr-6Nb-0.1B) on alpha-2 was no better than the uncoated substrate and failed prior to tensile testing. This coating performed poorly in the HSSCC test and visually a "picture frame" was noted on the fracture surface. Since monolithic γ performed better, the results point to chemical inhomogeneity or microstructural changes from the coating process causing HSSCC sensitivity.

The severe embrittlement of alpha-2 resulting from exposures in HSSCC environments is evidence of the need for a coating. The only coating to survive all exposures was the Alloy 718, which in monolithic form is resistant to HSSCC.

2.2.6 Environmental Testing Iteration #2, Subtask 2.6

The first iteration of environmental testing screened 10 different coatings on both the gamma (Ti-48Al-2Cr-2Nb) and alpha-2 (Ti-24.5Al-12.5Nb-1.5Mo) substrates. Testing included cyclic oxidation, high velocity oxidation/hot corrosion and hot salt stress corrosion cracking (HSSCC). The first iteration results showed that a composite mixture of alumina and an MCrAlY provided superior resistance to all forms of environmental attack evaluated under this program.

The MCrAlY's (M=Fe, Co, Ni or combination) are a broad series of compositions that are heavily relied upon to provide oxidation and corrosion resistance in current land, air and marine gas turbines. The application of MCrAlY's directly to Ti-aluminides has been the subject of several patents and papers.²¹⁻²³ A diffusion barrier between the MCrAlY and Ti-aluminide has been proposed to prevent a decrease in mechanical properties at the interface.²⁴ The refractory metals and TiN are mentioned most often as the preferred barrier layers.²⁵

Work performed under this contract shows that alumina should be mixed with the MCrAlY to lower thermal expansion. Table 17 shows the linear thermal expansion coefficient for material systems of interest and compares them to a NiCrAlY. The need for alumina is particularly high for alpha-2 and orthorhombic alloys which have coefficients of thermal expansion 25-33% lower than that of the MCrAlY coating. Assuming stress relaxation at operating temperatures due to creep of the substrate or coating, the mismatch would put the coating in tension at the surface upon cooling. Surface tension is normally considered bad because flaws that initiate at the surface because of irregularities and geometry can grow. Tension on the surface in this case may mean that the brittle interdiffusion zone that forms between the coating and substrate is in tension. This may be a good situation if cracks nucleate but do not grow. To minimize thermal expansion mismatch effects, alumina with a low expansion coefficient is added to the MCrAlY to provide a better match. The result is the cermet coating.

Table 18 shows the composite coating compositions selected for the Ti-aluminide substrates during the second iteration of environmental testing. The coatings were formulated using two underlying principles. First, the thermal expansion mismatch should be minimized over the temperature range where the substrate is likely to see service. Emphasis was placed on temperatures where the Ti-aluminide substrate behaves like a brittle solid, i.e., under the ductile to brittle transition temperature range. The second principle was that the MCrAlY composition should be chosen to have good ductility since environmental resistance for MCrAlY's at these lower temperatures is excellent. Therefore, there was a conscious effort to choose MCrAlY's with lower Al contents when possible. The Alloy 718 composition was chosen because the Ni-Cr composition had shown resistance to hot salt stress corrosion cracking. It also represents a chromia former with a very small level of Al.

A FeCrAlY composition is not listed in Table 18. The reason for omitting FeCrAlY in the present study was that GEAE Internal Research and Development (IRD) data had shown cracking and rumpling during a cyclic oxidation test at 900°C (1652°F). Micrographs from this study are shown in Figure 131. Recent NASA data, however, indicate that FeCrAlY can be an effective coating for alpha-2.²⁶ The FeCrAlY in the NASA study was bcc and had only 4 atom percent Al resulting in measurable RT ductility which may be the most important coating property on that Ti-aluminide system.

In Table 19, the actual test plan for the second iteration of environmental testing under Subtask 2.6 (Iteration 2) is presented. The conditions selected allow comparison to the first iteration of environmental testing.

2.2.6.1 Hot Salt Stress Corrosion Cracking

The hot salt stress corrosion cracking exposure used in the second iteration was the 565°C (1050°F) 40 ksi/750 hr exposure with ~0.1mg/cm² of sea salt applied to the gage length. This exposure was shown to be the most severe in iteration #1 and uncoated Ti-aluminides were totally embrittled. The results of such a test are also directly comparable to results obtained in iteration #1. The simulative sea salt was sprayed on the samples by Joliet Metallurgical Laboratory using procedures co-developed under another program.²⁷ The distribution of the salt sprayed on a tensile sample of steel is shown in Figure 132. The salt tended to form spots from

0.01-0.1mm in diameter with 1-15mm crystals. EDS analysis of the salt on the surface revealed in order of highest to lowest contribution: Cl, K, S, Mg and Na. Table 20 shows creep and tensile results for the cermet systems on both gamma and alpha-2 substrates. All the cermets protected the gamma substrates, while only the NiCrAlY/alumina cermet protected alpha-2. The RT tensile properties of the Ti-aluminides were not retained, which might be expected after a 750 hr creep exposure since some microstructural damage is occurring.

Figure 133 shows the creep curves for the samples. The alpha-2 crept at a faster rate than the gamma samples. The alpha-2 minimum creep rate was $1.2 \times 10^{-5}/\text{min}$ which compares favorably to results from iteration #1. The gamma minimum creep rate was $3.9 \times 10^{-6}/\text{min}$ with a standard deviation of $1.2 \times 10^{-6}/\text{min}$ which is slightly lower than what was observed in iteration #1.

The results for the alpha-2 substrates in Table 20 were disappointing as the Alloy 718 and CoCrAlY cermet coatings failed early in the test. A positive result, however, was obtained for the NiCrAlY cermet coating which survived the 750 hr exposure and maintained a usable level of strength. A similar NiCrAlY cermet coating also performed well on the gamma substrate in the first iteration of testing.

Test results for the coatings on the gamma substrates were unclear because of failures in the coated radii. Apparently the cermet coatings protected the samples from HSSCC since the radii were located away from the location where the salt was deposited. Possible explanations for failures in the radii are stress concentration effects, sensitivity to a different stress state or a different population of defects.

HSSCC of Coated Gamma

Figures 134-136 show the cermet coatings on the gamma substrate. All of the samples failed in the radius away from the salt. The samples all had an ill-defined origin which is common in gamma alloys.⁸ The fracture was predominantly transgranular. The higher magnification images did not show any corrosion at the coating/substrate interface as expected since the failure occurred away from the salt deposit. Distinguishing between the different cermet coatings on gamma was difficult.

Figures 137-139 show cross-sections of the composite MCrAlY coatings on the gamma substrate after the exposure with salt at 565°C/40 ksi for 750 hr and a post-exposure tensile test. Low magnification micrographs show that the failures occurred in the radii. The figures show good adhesion between the composite MCrAlY coatings and the gamma substrate since the coating does not spall from the substrate even after an RT tensile test.

Higher magnification images show fracture and secondary cracking on grain boundaries in the substrate, i.e. intergranular fracture behavior. Secondary cracking was noted in the CoCrAlY/Al₂O₃ and the NiCoCrAlY/Al₂O₃ coatings. In the case of the CoCrAlY-type coating, the secondary cracking extended into the substrate (arrow), while it was contained within the coating for the NiCoCrAlY/Al₂O₃ coating. The NiCoCrAlY/Al₂O₃ coating had tensile properties nearly equivalent to unexposed gamma and, therefore, was regarded as being the best in this test.

The corrosion product on the NiCoCrAlY-type coating was 2-10 μ m and composed of mostly Cr and Al-rich with smaller amounts of Ni and Co. Contaminants from the salt and sample preparation included Si, Ca, Fe, S and Mg.

HSSCC of Coated Alpha-2

Figure 140 shows the Alloy 718 cermet/alpha-2 coating. The fractographs show multiple origins and the intergranular nature of the fracture. The oblate grain boundary precipitates (primary alpha-2) shown in the higher magnification micrograph are rich in Ti and equiatomic with respect to Nb/Al and, therefore, may be orthorhombic forms of alpha-2. No corrosion attack was found on this surface. In cross-section large HSSCC cracks are observed through out the sample. Figure 141 shows one of these cracks at higher magnification. The cracks in the coating were found to confine themselves to the alumina (black) and go around Alloy 718 islands. Future cermet coatings of this composition should have isolated islands of alumina. At the coating/substrate interface, the crack contains a corrosion product containing Cl and Fe. At the crack tip, oxidation was observed along a prior β grain boundary.

Figure 142 shows the CoCrAlY cermet/alpha-2 sample. The fracture appears to have initiated from a region (arrows) rather than a singular point. The region was associated with Cl. A higher magnification micrograph again shows the intergranular nature of the fracture at the origin. Figure 143 shows the coating in cross-section. Cracks appear to prefer the alumina and CoCrAlY areas that are thin rather than spherical in shape. A reaction zone between the coating and substrate was seen where the CoCrAlY was in contact with the alpha-2. In one such region, internal corrosion (arrow) and cracking were observed.

Figure 144 shows the NiCrAlY cermet/alpha-2 sample that did not fail during the 750 hr HSSCC exposure. The fractograph shows a distinct origin from the RT tensile test that had no corrosion and little intergranular fracture. The cross-section in the figure shows no HSSCC cracks. Much of the coating had spalled off this sample during the RT tensile test. The coating was not as adherent as the cermet coatings on gamma perhaps because of substantial necking. The higher magnification image of the coating/substrate shows little cracking and a reaction zone between metal in the cermet and the alpha-2. The NiCrAlY cermet coating performed the best in the HSSCC test.

2.2.6.2 Cyclic Hot Corrosion/Oxidation

Table 19 summarizes the conditions of the burner rig tests performed under the second iteration. The conditions were chosen to be simulative of gas path environments that Ti-aluminides will see during application, but temperatures were purposely increased by $\sim 100^{\circ}\text{C}$ to accelerate environmental degradation phenomena without changing the rate controlling mechanism. These tests were performed using the Becon burner rig. The recent successful engine test of cast Ti-48Al-2Cr-2Nb as low pressure turbine (LPT) blades validates the importance of such testing since Ti-aluminides are likely to be applied to the LPT.²⁸ Testing was performed according to the original work plan with one exception. The original plan specified a standard laboratory cyclic oxidation test that would have provided little new data. This test was replaced with a high

velocity cyclic oxidation burner rig test. The rig test was more severe as the heat transfer coefficient was much higher resulting in greater thermal stain rates and more damage to oxide scales and coatings.

Compressor Burner Rig Test - Task 2.6

Color photographs of the flame-side and back-side of the specimens after the 760°C/648°C test are shown in Figures 145-148. The samples went through 3749 cycles and had a hot time of 625 hr. One cycle was a rapid heat up to 760°C (1400°F), followed by a hold of 5 min, rapid cooling to 648°C (1200°F), followed by a hold of 5 min and then a rapid cool down to $T < 200^{\circ}\text{C}$. One ppm sea salt was continuously injected into the combustion stream. The photos were taken after the salt and debris were rinsed with warm water from the surface. No significant diameter change was measurable with a micrometer or caliper on any of the samples. Debris from the last rinsing was filtered and analyzed using a scanning electron microscope. The debris had a tan, gray or clear color. Figure 149 shows the particles on the filter paper. Regardless of color, EDS showed the particles to be mostly MgO with some Ca, Fe, Co and Ni depending on sample. The Mg is from the sea salt.

Degradation in Figures 145-148 was visible on the bare gamma, alpha-2 and Hasteloy X pins, especially in areas that experienced temperatures greater than $\sim 660^{\circ}\text{C}$ ($\sim 1220^{\circ}\text{F}$). The temperature distribution of the pins during the test is shown in Figure 150. The initial surface finish of the bare pins was better than that for coated specimens resulting in specular reflection of light versus diffuse reflection for the rougher coatings. As oxides grew and spalled on the surface of bare samples, the surface got rougher resulting in a duller appearance. Note that the Hasteloy X pins were included as a reference for temperature measurement purposes.

In the case of the gamma and alpha-2, the oxide was a mixture Mg, Na, Ti, Al and O. On the Hast X the scale was Cr, Fe, Mg, Na and O. The bare gamma had white striations of oxides on the surface. The cause of the striations was not clear, but it might be related to the deformation structure noted in the forged and heat treated Ti-48Al-2Cr-2Nb. The NiCoCrAlY and CoCrAlY/Alumina coatings were unaffected and revealed only a heat tint. Both the tinting and metallographic analysis revealed that a thin protective external alumina scale had formed. The Alloy 718-based cermet coatings were darker with no tint because of the formation of chromia and spinels in locations where the 718 in the coating was attacked.

The average weight of deposit per cycle removed from the various types of pins are shown in Table 21. The magnitude of the deposit was a strong function of surface area. The bare pins had better surface finishes with lower surface areas thus reducing the magnitude of the deposit. The standard deviation, however, suggests a lot of scatter for bare pins which is due to increased oxidation and spallation. The coated samples had larger deposits with remarkably similar standard deviations as a result of greater surface stability.

In all systems the weight loss appeared to follow a linear relationship with exposure time or cycling. The weight change of coated and uncoated gamma was less than that observed for alpha-2 systems. The greater loss for bare alpha-2 compared to bare gamma might simply be related to Al content, with more protective scales forming on gamma. Gamma with a larger amount of Al,

would be better able to reform Al-rich damaged or spalled scales.²⁹ The greater loss for cermets on alpha-2 is puzzling, since the composite coatings should have similar resistance to environmental attack. A major difference, however, is the amount of alumina in the composite coatings for alpha-2. The alumina near the external surface in these coatings may crack and spall leading to weight loss as cycling continues. Alumina spallation would suggest that more of the metallic component in the composite coating on alpha-2 might be better if thermal expansion can still be controlled.

Cross-sections were taken at 0.65, 1.125, 1.35 and 2" from the tip of each pin. These sections represented structures that were degraded for 5min at each of the following temperatures: 760/648°C (1400/1200°F); 704/604°C (1300/1120°F); 648/~565°C (1200/~1050°F), and 398°C (750°F) > T . The last cross-section was an important referee showing what the structure was before the test since the exposure temperature was too low to result in environmental attack or extensive interdiffusion.

Uncoated Alloys

Figures 151 and 152 show cross-sections of the uncoated Ti-24.5Al-12.5Nb-1.5Al and Ti-48Al-2Cr-2Nb samples. A more uniform attack was observed on alpha-2 than on gamma with less attack of gamma at lower temperatures.

Alpha-2

The attack of alpha-2 is summarized in Table 22 as a function of peak exposure temperature. Figure 151 shows that the attack on the alpha-2 was most visible in the 760/648°C (1400/1200°F) section and was uniform and multi-layered. The total attack was 5.7µm thick and composed of a 2µm external oxide, 3.3µm of substrate converted to oxide and a 0.5µm interstitial layer. The measured attack did not account for any product that may of spalled as a result of thermal cycling, however, the attack on alpha-2 was minimal under these conditions and the cylindrical specimen experienced no measurable diameter change. As the exposure temperature decreased, so did the extent of attack. Alpha-2 was environmentally resistant under these conditions, but the effects of the exposure on mechanical properties like fatigue remains undetermined.

Gamma

The uncoated gamma Ti-aluminide was resistant to attack under these new conditions. Figure 152 shows that a 3-6µm thick external scale formed on the section that was exposed to a peak temperature of 760°C. The thicker areas of oxide were localized rather than uniform. A subscale structure (1-2µm thick) composed of a Ti₃Al-like chemistry with some EDS indication of S was observed. One possibility is that S stabilizes Ti₃Al like O. At the 704°C peak temperature the maximum thickness of attack observed was 3µm. The subscale structure grew finer (0.8µm); however, oxide was observed to penetrate along lath boundaries in different areas. No attack was observed in the other cooler sections.

Hast X

Figure 153 shows the cross-section of the Hast X sample after exposure. The Hast X after this exposure has severe internal and intergranular oxidation/sulfidation attack. The Hast X shows that conditions in this test were sufficient to corrode an oxidation resistant superalloy. The intergranular attack penetrated to depths of 108 μ m at 760°C, 48 μ m at 704°C and 32 μ m at 648°C. Negligible diameter change was noted on this pin through the test. The test showed the superiority of engineering Ti-aluminide alloys compared to conventional Ni-base superalloys in this environmental test. The Hast X should be better environmentally than some of the materials currently being applied to high pressure compressors like stainless steels and Alloy 718.

Coated Alloys

Cermet Coatings on Alpha-2

Figures 154-156 show cross-sections for the composite coatings on alpha-2. The alumina in these coatings makes assessment of attack difficult, however, in the NiCrAlY and CoCrAlY-base coatings it is less than 2 μ m. Corrosion product on the Alloy 718-base coating was greater and approached 13 μ m in areas where Alloy 718 was exposed to highest peak temperatures. In other areas, the alumina protected the 718 from attack. In general, the composite coatings on alpha-2 were resistant to attack under these conditions and showed most importantly, no signs of cracking from thermal strains.

Cermet Coatings on Gamma

Figures 157-159 show cross-sections for the composite coatings on gamma. Again little attack was noted on the surface, with the exception of exposed Alloy 718. The other noteworthy observation was the thermal fatigue cracking in the CoCrAlY composite coating sample. This was the first observation of through-thickness cracking in the cermet coatings. The crack in Figure 158 was open to the environment during the test as oxidation was observed. The cracking was most severe in the 760°C (1400°F) section with a 100 μ m penetration into the substrate, while the crack in the 704°C (1300°F) section was 44 μ m deep. The cracks were observed only in the CoCrAlY-based composite coatings. The reason for the poor behavior of the CoCrAlY was not determined. The NiCoCrAlY and Alloy 718 coatings exhibited superior performance in this test.

Reaction Zone

The reaction zone between the MCrAlY and the substrate is a greater concern than environmental distress. Cracks could be found in the reaction zone. The cracks may have been caused by sample preparation, but the brittle nature of the layer cannot be ignored. Figure 160 summarizes the thickness of the reaction zone for the composite coatings on both alpha-2 and gamma after the exposure at the various peak temperatures for 1.125×10^6 sec. If growth is $x - x_0$, where x is instantaneous thickness and x_0 is initial thickness formed during spraying (estimated using the 398°C section) then the following relationship can be obtained:

$$(x-x_0) = 20464 * \exp(-8320/T) \mu\text{m} \quad (1)$$

where T is temperature in K. The major error in the expression comes from the fact that growth occurs at both the peak and lower temperature parts of the cycle. A growth rate for the reaction zone can be calculated if zone thickness is assumed to grow parabolically and volume changes are negligible, i.e. $(\Delta x)^2 = k*t$; where k is the growth rate and t is time at temperature, The expression is:

$$k = 1.8 \times 10^{-6} * \exp(-16640/T) \frac{\text{cm}^2}{\text{sec}} \quad (2)$$

At 760°C (1400°F) the k is $1.8 \times 10^{-13} \text{cm}^2/\text{sec}$. The activation energy, Q, for this layer growth is ~33Kcal/mol. The activation energy is likely related to interdiffusion between the MCrAlY and the substrate where Ti and Al are diffusing into the coating or the transition metal is diffusing into the gamma. This would explain the M₂AlTi and MTiAl-type compositions of the layers formed in the reaction zone. A comparison of Q to other measured values at higher temperatures is in order. Chemical diffusion of Ni in alloys containing 0-0.9Ti has a Q of 61.4Kcal/mol.³⁰ The Q for interdiffusion in Ti-Al is ~40Kcal/mol.³¹ The Q for Ni diffusion in Ni-Al is 41Kcal/mol.³² The value observed in equation (2) agrees more with diffusion in an Al containing intermetallic. The lower magnitude may indicate that short circuit paths for diffusing species are predominant or that the new phases that form allow rapid transport.

The reaction zones are observed only in areas where the metallic component are in contact with the Ti-aluminide substrate. No reaction zone is observed in areas where alumina is in contact with the substrate. The lack of reaction between alumina and the alloys means alumina is stable. The adhesion of the coating to the substrate is usually classified as mechanical or chemical. The reaction zones indicate that a strong chemical component is present in these coatings.

Low Pressure Turbine Burner Rig Test - Task 2.6

Color photographs of the flame-side and back-side of the specimens after the low pressure turbine test are shown in Figures 161-163. The samples went through 3000 cycles and had a hot time of 500 hr. One cycle was a rapid heat up to 871°C (1600°F), followed by a hold of 5min, rapid cooling to 760°C (1400°F), followed by a hold of 5min and then a rapid cool down to T<200°C. Salt at a level of 2ppm was continuously injected into the combustion stream for the first 50 hr to compare to iteration #1 results, then the salt concentration was lowered to 1ppm. The photos were taken after rinsing with hot water to remove salt and debris. A Codep coated (pack aluminide) Rene 80 specimen was included to compare the coated Ti-aluminide systems to a current LPT material system. The idea here is that Ni-base LPT blades are coated so this provides a better comparison. None of the samples lost measurable diameter during the course of the test.

Figure 164 shows the temperature profile of the pins for this test. Visible degradation occurred on the uncoated Ti-aluminides and the coated R'80 at T > 704°C (1300°F). Discoloration occurred on the composite coating systems if the peak T > 825°C (1517°F).

Figure 162 shows the alpha-2 systems. The bare alpha-2 shows scaling of TiO_2 which was white. The specimens coated with composite coatings have darkened in the hot regions, but no spalling or heavy attack was observed. The darkening may be a result of the exposure of an increasing fraction of alumina as the MCrAlY component was oxidized or spalled off. The Alloy 718 composite coating shows some hematite (Fe_2O_3) formation at the tip, characterized by the reddish brown color, but otherwise appears unaffected. Recall that testing of an air plasma sprayed (APS) Alloy 718 coating on the same alpha-2 alloy under nearly identical conditions (28°C greater for iteration#1) showed total spallation of the coating after only 50 hr! These observations indicated that the addition of alumina to the Alloy 718 coating has had a very beneficial effect. The other possible difference was that the Alloy 718 in the first iteration was air plasma sprayed rather than low pressure plasma sprayed. Metallography, however, indicated that the APS coating was adherent, did not have excessive amounts of oxides or porosity and was not depleted of Cr, i.e. the coating had chemical and microstructural integrity. Therefore, the inclusion of the alumina is thought to be the major reason for enhanced performance under these conditions. The Codep coated Rene 80 shows oxidation and spallation in the hot areas. Visually, the composite coatings on the alpha-2 look better than the coated Ni-base superalloy.

Figure 163 shows the gamma systems. The bare gamma shows heavy oxidation and spallation. The whitish oxide (TiO_2 -based) appears thinnest at the hottest portion of the pin. This can be explained in terms of oxide exfoliation under higher thermal or oxide growth stresses. The NiCoCrAlY and CoCrAlY composite coatings do not exhibit much degradation. Some darkening is noted in the hot regions which is likely the result of exposed alumina. The Alloy 718 coating shows some Fe-oxide formation giving it a brownish color, but appears to be in good shape. Visually, the composite coatings on gamma looked better than the coated Ni-base superalloy.

Figure 165 shows the weight change of the systems as a function of cycling. The bare Ti-aluminides, the Hast X and the coated R'80 had a weight loss of 25-40mg. The total surface area of the pins was $\sim 16.3\text{cm}^2$, but most of the loss occurred over an area of $\sim 7\text{cm}^2$. This corresponds to specific weight losses between ~ 3.6 - 5.7mg/cm^2 . These weight losses at first appear low compared to the composite coatings; however, a closer look shows that the coatings lost 25-50mg very rapidly as loosely adhering regions were removed as a result of oxidation, thermal cycling and the high velocity gas flow. After this initial loss, very little weight loss was observed (0-15mg). This rapid initial weight loss was observed on plasma sprayed coatings tested in the first iteration under Task 2.4.

Table 23 shows the average amounts of debris removed with rinsing after the first 50 hr. The rinsing contained in the first 50 hr was ignored because the salt concentration was 2ppm which resulted in the removal of 0.5-0.9mg/cycle. The data show that the salt deposition at 1ppm was nearly constant during both burner rig tests. One major difference was that the standard deviation in the bare alpha-2 and gamma systems was much less. The coated superalloy, with a good surface finish, was similar to the bare Ti-aluminide systems. Cross-sections were taken at 0.6, 1.1, 1.4 and 2" from the tip of each pin. These sections represent structures that were degraded for 5min at each of the following temperatures: $871/760^\circ\text{C}$ ($1600/1400^\circ\text{F}$); $821/710^\circ\text{C}$ ($1510/1310^\circ\text{F}$); $(760/648^\circ\text{C})$ $1400/1200^\circ\text{F}$, and 510°C (950°F) $> T$.

Metallography of Uncoated Alloys

Gamma

Gamma alloys are likely to see application in the temperature range of 760-900°C (1400-1650°F) especially if second generation alloys under development have improved creep properties.³³ Figure 166 shows cross-sections of the gamma as a function of the peak temperature. The corrosion product was multilayered and was ~25µm thick in localized areas. The local thickening of oxide has been related to the formation of a Ti-rich scale in nitrogen containing environments.³⁴ Spallation of these locally thick regions has introduced "chips" into the substrate. The oxide was also prone to spallation of entire layers at the higher temperatures. Diameter measurements suggested, however, that the loss was minimal.

Figure 167 shows the complicated attack in much greater detail. Focusing on the 871°C section, the external 4-5µm layer was MgO. This agrees with the rinsing analysis. The underlying 5-6µm of light gray product was a Ti-rich oxide with lesser amounts of Mg, Al, and Si. The 2-3µm thick underlying dark gray layer was an Al-rich oxide with a minor amounts of Ti and Cr. Finally, the grainy product next to the substrate was Ti-rich with Al (2:1 Ti:Al ratio), with smaller amounts of Cr and Nb and detectable S and O. A sulfidation-oxidation attack of the gamma was occurring.

The figure also clearly shows that a lacy phase has formed which was prone to many fine hairline cracks. The EDS of this phase indicates a 2:1 Ti:Al ratio with Nb, which is similar to what is expected for alpha-2 or Ti₃Al. No S was observed in this layer, although some overlap with Nb occurs. The morphology suggests that alpha-2 forms at grain, subgrain or phase boundaries in the gamma followed by lateral growth until a single layer is formed. The lighter imaging phase at the oxy-sulfide/substrate interface had a similar composition to the alpha-2, but was enriched in Nb and Cr. The last noteworthy feature of the attack was the presence of dark pegs and particles in the lacy structure. EDS confirmed that this phase was similar to the alpha-2 but was enriched with S. The effect of the brittle lacy structure on the mechanical properties of gamma is a concern.

Alpha-2

The mechanical properties of monolithic alpha-2 are such that application at temperatures greater than 760°C (1400°F) are doubtful. Still, much is to be learned about the environmental degradation of Ti-aluminides and the ability of the composite coatings to resist attack on an alloy with a lower relative coefficient of thermal expansion. Figure 168 shows cross-sections of the uncoated alpha-2. The corrosion product was uniform around the circumference of the pin; however, cracks and indications of spallation were prevalent in the oxide. The corrosion product was ~20, 8 and 5µm at 871, 821 and 760°C peak temperatures. EDS analyses were performed on the 871°C section. The external product was Al, Mg, O, Si with some Nb and Ti. This is consistent with the MgO found in the rinsings. The bulk of the scale was composed of Ti, Nb and Al. The layer under the bulk scale was a mixed nitride. The bright layer under the nitride was enriched in Nb. Substrate features were observed in the scale especially for the 821°C

specimen. This "ghost" of the substrate indicates the dissolution of oxygen and nitrogen into the substrate with subsequent conversion to an oxide, i.e. inward scale growth. No S was in the corrosion morphology, although overlap with the Mo peak would have made detection difficult.

Metallography of Coated Alloys

Coated R'80

Figure 169 shows the Codep coated Rene 80 after rig testing with under pressure turbine conditions. The coating was only 37 μ m thick which is considered thin. An oxidation/sulfidation attack was evident and sulfides were observed. There was one observation of diffusion zone attack in the 871°C section indicating that the coating was near failure, but still repairable with a strip and recoat cycle. The morphology of the attack observed is similar to that in Naval flight engines after service. The morphology of the attack on the Codep coated R'80 shows that the test was representative of low pressure turbine engine environments.

Figure 170 shows higher magnification images of the oxidation sulfidation attack. It is shown because some features are similar to the attack on the bare Ti-48Al-2Cr-2Nb, namely a lacy phase at grain boundaries and internal sulfides. EDS analysis of the lacy phase indicated it was enriched in bcc refractory metals like Cr, W and Mo with S possible. The formation of the phase at the grain boundaries may be common in intermetallics as the depletion of either of the major constituents through oxidation or interdiffusion results in the formation of another phase. Note that the Codep is a heavily alloyed, polycrystalline NiAl. The dark internal sulfides were TiS. Many hairline cracks were observed in the coating under the thick corrosion product.

Cermet Coatings on Gamma

NiCoCrAlY

Figure 171 shows the NiCoCrAlY composite coating on the Ti-48Al-2Cr-2Nb gamma substrate. These coatings were ~150 μ m thick. Very little environmental attack was observed, however, three through-thickness coatings cracks were observed in the hot section. The cracks appear to be surface initiated, and propagated through ~65 μ m of the coating. The cracks had oxide associated with them so they occurred during testing. The oxide in the crack depleted the Al and caused the formation of an FCC- γ phase which presumably would be more compliant to strain. There was also cracking associated with the 19 μ m reaction zone. These cracks had no oxide and may have resulted from surface preparation. The reaction zone on the gamma had two distinct layers. The layer near the coating had a chemistry of Ti:Ni:Co:Al in a ~3:2:1:1 ratio, while the coating near the substrate was Ti:Al:Ni of ~4:2:1. The reaction zone was much thinner in areas where alumina grit was embedded from the surface cleaning process. The alumina was an interdiffusion barrier.

CoCrAlY

Figure 172 shows the CoCrAlY composite coating on the Ti-48Al-2Cr-2Nb gamma substrate. The coatings were ~100μm thick. Again little environmental attack was observed on the composite coating; however, oxidized through-thickness cracks which propagated into the substrate were observed in every cross-section. In the hot section, the crack also propagated at the coating/substrate interface resulting in decohesion. The cracking either occurred before or during testing since oxide was observed. One puzzling observation was the very large crack in the coldest section. The crack ran approximately parallel to the fibering in the forged structure and may have been present in the originally forged and heat treated pancake. The reaction zone on the sample was ~13μm and again composed of two phases. The phase nearest the coating was Co:Ti:Al in a ratio of ~3:3:1 and the phase nearest the gamma was Ti:Al:Co in a ratio of ~2.5:1.25:1. The cracking in the sample was severe and was the reason that CoCrAlY composite coatings were dropped from the program.

Alloy 718

Figure 173 shows the Alloy 718 composite coating on the Ti-48Al-2Cr-2Nb gamma substrate. The coatings were ~150mm thick. Environmental attack was observed on the coating in the form of Nb, Fe, Cr and Ni-oxides and Cr-sulfides. The attack was observed in areas where Alloy 718 was not buried by the alumina. A heavily oxidized crack was observed to penetrate 63μm into the coating in the hot section. A 20μm thick reaction zone with two layers developed on the hottest cross-section. EDS showed the layer nearest the coating Ti:Ni:Al to be in a ratio of 4:3:1 with Fe and Nb detectable and the layer nearest the substrate to be Ti:Al:Ni in a ratio 4:2:1 with Fe and Nb present.

Cermet Coatings on Alpha-2

NiCrAlY

Figure 174 shows the NiCrAlY composite coating on the Ti-24.5Al-12.5Nb-1.5Mo alpha-2 substrate. The cross-sections show ~125μm thick coatings with environmental attack only evident in NiCrAlY that was not covered or buried by alumina. The lack of environmental attack means that thinner coatings might improve performance by lowering weight and thermal expansion mismatch stresses. The reaction zone in the hottest section was as large as 23μm thick using alumina grit particles as inert markers. The reaction zone had two major layers. The layer (phase) bordering the substrate was Ti:Nb:Al in a ~2:2:1 ratio with a small amount of Ni and Cr. The gray layer bordering the coating was really two phases, one was Ti:Ni:Al in a ratio of ~8:2.5:1 and the other was Ti:Ni:Al in a ratio of ~4:3:1. The 821°C section had a visible crack that penetrated into the substrate 28μm. The crack was not oxidized which may mean it was caused by subsurface initiation in the coating/reaction zone or as a result of sample preparation. With the exception of the single crack, the NiCrAlY coating on alpha-2 performed excellently in the LPT test and survived the HSSCC exposure.

CoCrAlY

Figure 175 shows the CoCrAlY composite coating on the Ti-24.5Al-12.5Nb-1.5Mo alpha-2 substrate. The coatings are again $\sim 125\mu\text{m}$ thick. There was very little environmental attack of the CoCrAlY, however, through-thickness coating cracks were observed on the 871 and 821°C sections. The 510°C section was replaced with a high magnification micrograph of a crack at the substrate/coating interface that penetrated $\sim 50\mu\text{m}$ into the substrate. As in the case with the NiCrAlY, no oxidation was observed indicating internal initiation or heavy handed specimen preparation. The morphology indicates that the crack may propagate by cracking the alpha-2 phase ahead of the crack front followed by fracture of the remaining ligaments. The crack also appeared to be present at the coating/substrate interface which could result in coating spallation if the crack formed during the test. The reaction zone in the hottest section was $\sim 10\mu\text{m}$ thick composed of two major phases. One had a Ti:Co:Al ratio of $\sim 4:3:1$ and the other had a Ti:Co:Al ratio of $\sim 8:4:1$. These chemistries were similar to those observed in the reaction zone for the NiCrAlY, with Co replacing Ni.

Alloy 718

Figure 176 shows the Alloy 718 composite coating on the Ti-24.5Al-12.5Nb-1.5Mo alpha-2 substrate. These coatings are $\sim 137\mu\text{m}$ thick and no cracking was observed. The only environmental attack observed was on Alloy 718 that was exposed to the gas stream. The external oxide was Fe-rich with Mg corresponding to earlier observations of hematite formation. The subscale was a Fe, Cr and Nb rich oxide. The reaction zone on the 871°C section was $\sim 15\mu\text{m}$ thick with two major components. One had a chemistry of Ti:Nb:Al of $\sim 4:4:1$ with a small amount of Ni and Cr the other, closer to the coating, was Ti:Ni:Al of $\sim 4:2.5:1$.

Reaction Zone

The reaction zone is not only important in the coating of Ti-aluminides, but also is a consideration in joining Ti-aluminides to transition metal based components. The average $\pm 1\sigma$ (standard deviation) for reaction zone thickness in the 871°C (1600°F) section for the alpha-2 systems was $16 \pm 6.5\mu\text{m}$ and for the gamma systems was $17.3 \pm 3.8\mu\text{m}$. Significant growth occurred at both temperatures in the cycle, therefore, if $T=1144\text{K}$ for $t=9 \times 10^5\text{s}$ and $T=1033$ for $t=9 \times 10^5\text{s}$, then equation (2) results in k 's of $8.67\text{E-}13\text{ cm}^2/\text{s}$ and $1.82\text{E-}13\text{ cm}^2/\text{s}$, respectively. These k 's lead to a reaction zone thickness of $12.7\mu\text{m}$ which is within 1σ of the measured values.

2.2.6.3 High Velocity Cyclic Oxidation Test - Task 2.6

The samples went through 1778 cycles of oxidation using a rapid heat up to 900°C (1650°F), followed by a hold of 5min, rapid cooling to 760°C (1400°F), followed by a hold of 5min and then a rapid cool down to $T < 200^\circ\text{C}$. After cycling under these conditions for 1778 cycles, it was decided that too little attack for differentiation was occurring on the composite coatings and so the 760°C (1400°F) part of the cycle was dropped. The rest of the test, therefore, consisted of 2639 cycles with heat up and 5min hold at 900°C followed by rapid air cooling. The total hot time was 516 hr. The temperature distribution of the pins as a function of length is shown in

Figure 177. Both coated and uncoated Rene' 80 were included in this test as a standard. No rinsing was necessary in this test. Cross-sections were taken at 0.6", 1.1", 1.4" and 2" from the tip representing regions that experienced 900/760°C (1652/1400°F), 828/710°C (1520/1310°F), 760/654°C (1400/1210°F), respectively. The cross-sections were examined using scanning electron microscopy and EDS analysis.

Figure 178 was a color macrograph the alpha-2 systems. The uncoated Ti-24.5Al-12.5Nb-1.5Mo shows a oxide spallation in regions of the pin that have been exposed to temperatures that exceed ~785°C (1445°F). The whitish areas are rutile flakes. The composite coating systems showed excellent resistance with darkening only at the hot spot. Optically, colors indicative of their base metal oxide could be observed. For example, the Alloy 718 is black and reddish-brown indicating that Fe-oxides are forming, the CoCrAlY is turning blue indicative of Co-oxides and the NiCrAlY is greenish indicating spinel and NiO formation. The base metal oxides are observed only in the region that reaches a peak temperature of 900°C (1652°F). The uncoated Rene' 80 shows spallation and green oxide formation (spinel and NiO) at temperatures on the pin exceeding ~745°C (1373°F). The Codep coated Rene' 80 appears very protective.

Figure 179 is a color macrograph of the gamma systems. The uncoated gamma has a white oxide in sections that experienced temperatures greater than 690°C (1274°F). The oxide appears thicker in localized areas on the surface and was mostly TiO₂. The composite coatings showed excellent oxidation resistance with no cracking or spalling of the coating. The hot areas of the pins are darker presumably because a thicker oxide formed. In the hot areas, the Alloy 718 shows some signs of Fe-oxide formation, while colder areas are dark gray indicating the predominance of protective alumina.

Figure 180 shows the weight change for the specimens as a function of cycling. The gamma sample gained the most weight which correlates to the cross-sections to be discussed later. The alpha-2 sample had erratic behavior and showed large weight losses as the number of thermal cycles grew. The composite coatings on gamma did not lose as much weight as the composite coatings on the alpha-2 samples. This behavior again may correlate to the amount of alumina in the coatings. The Rene'80 showed a linear weight loss as a function of time and thermal cycling, but the Codep coated Rene'80 had kinetics indicative of a system with good surface stability.

Metallography of Uncoated Alloys

Gamma

Figure 181 shows cross-sections of the uncoated Ti-48Al-2Cr-2Nb gamma alloy in the hottest section. In one area, a ~50µm thick oxide composed of two distinct layers was observed. The external oxide was cracked and layered and appeared to form from outward transport of cations. The gray regions were titania and darker regions of alumina. The internal oxide had features that indicated that the substrate was converted to oxide as an oxidation front moved inward, i.e., formed by anion movement. Ahead of the front, the alloy transformed to the lacy structure observed in other hot corrosion producing environments. EDS analyses indicated that the matrix of the cellular product had a Ti:Al ratio of 3:1 indicating alpha-2 with a trace of Cr and Nb. The fingers in the phase were a little richer in Al and Nb. No oxygen was observed in the cellular

product with EDS. At the oxidation front, the black oxide was alumina (Al, O) and the gray islands (converted fingers) in the oxide had Ti, Al and Nb cations. In other areas on the same cross-section, the oxide was much thinner ($\sim 15\mu\text{m}$) because of spallation. In these areas, breakdown of the uniform scale occurred and localized pits were observed.

Figure 182 shows lower magnification micrographs of the sections as a function of temperature. From the figure it is clear that a large change in metal loss occurs as the peak temperature is increased from 760°C (1400°F) to 900°C (1650°F). Using a criteria of $25\mu\text{m}$ of metal loss per 1000 hr, the coating temperature for gamma would be between 828°C (1520°F) and 900°C (1650°F). Linear interpolation puts the coating temperature at $\sim 830^\circ\text{C}$ (1527°F).

Alpha-2

Figure 183 shows cross-sections of the uncoated Ti-24.5Al-12.5Nb-1.5Mo alpha-2 alloy. The alpha-2 showed a thick layered oxide scale that was prone to cracking, spallation and exfoliation in the high temperature region. In adherent regions, the scale was $17\mu\text{m}$ thick and may represent the thickness attained before spallation. The embrittled layer under the scale was only $1\mu\text{m}$ thick. In cooler regions the scale was only $3\mu\text{m}$ thick. Some cracking was observed in these scales. The coarsening behavior of the alpha-2 substrate as a function of temperature was evident in the micrographs and would be a problem for applications over 760°C (1400°F).

Rene' 80

Figure 184 shows cross-sections of uncoated Rene'80 after the test. The 900°C (1652°F) cross-section shows an external oxide that was as thick as $30\mu\text{m}$ with intergranular oxidation/internal oxidation of Al and Ti to a depth of $76\mu\text{m}$. The 828°C (1520°F) section shows much less attack with $8\mu\text{m}$ observed in the micrograph. It appears that Rene'80 goes from acceptable surface stability to unacceptable stability over this temperature range. Furthermore, in the absence of salt, the Rene'80 shows less attack than the uncoated gamma at $T \leq 828^\circ\text{C}$ (1520°F).

Composite Coatings on Gamma

NiCoCrAlY

Figure 185 shows the composite NiCoCrAlY coating on the Ti-48Al-2Cr-2Nb gamma substrate after the test. The coating had a $3\mu\text{m}$ thick alumina scale at the external surface that provided excellent oxidation protection. Under the alumina scale, the $\gamma + \beta$ coating was depleted of Al resulting in a layer of γ . The coating showed some through-thickness cracking, cracking at the substrate/coating interface and cracking in the reaction zone. The cracks were not oxidized and may have been caused by sample preparation. The concentration of cracking in the 900°C section in the reaction zone implies that the phases are brittle and could be a problem during fatigue testing at the thicknesses used here. The reaction layer in the hottest section was $26\mu\text{m}$ thick which agrees well with other measurements in this report. EDS analysis of the reaction

zone was similar to those given in the LPT test. The NiCoCrAlY coating was protective, but the cracking was a concern. No cracking was observed on the 50 vol% NiCrAlY-50 vol% alumina coating on gamma in the shorter first iteration test.

CoCrAlY

Figure 186 shows the composite CoCrAlY coating on the Ti-48Al-2Cr-2Nb gamma substrate after the test. There was a thin 2-5 μ m alumina scale on the external surface of the 900°C section. The reaction zone observed in the hot section was ~12 μ m thick in agreement with measurements of the zone on alpha-2. The phases in the reaction zone were similar in chemistry to those reported for the LPT test.

Through-thickness cracks were present in each of the cross-sections which means they may have propagated along the length of the pin. Several of these cracks were observed in each section. The cracks are heavily oxidized indicating their formation during testing as a result of thermal fatigue (TF) or their presence before the test started. The crack morphology was similar to that observed in the first iteration of environmental testing on various coatings, with heavy oxidation along the length and at the coating/substrate interface resulting in a trifurcated appearance. The crack was observed to extend up to 112 μ m into the substrate. The cracking of the composite CoCrAlY coating in these rig tests indicates poor TMF resistance. The presence of Co in systems that crack was suspicious and this element was not used in coatings for Task 3.

The severe cracking of this coating on gamma and not on alpha-2 is puzzling. The thermal expansion behavior of the two aluminides are different, but the coatings were tailored to compensate for this effect by varying the amount of alumina. The mechanical properties of the two aluminides are different and may act to constrain the coating during temperature changes causing crack initiation at the surface. In any case, the CoCrAlY composite coating was dropped from further consideration in this program.

Alloy 718

Figure 187 shows the composite Alloy 718 coating on the Ti-48Al-2Cr-2Nb gamma substrate after the test. External oxides composed of Ni, Fe and Cr were observed to be up to 40 μ m thick on the 900°C section. Many through-thickness TF cracks were observed which had formed during the test. The TF crack in the figure did not penetrate deeply into the substrate and some cracks had not propagated through the coating. The reaction zone in the 900°C section was from 16-24 μ m and composed of the same phases analyzed after the LPT test. There were many unoxidized cracks in the reaction layer which may again be due to surface preparation but still indicative of brittle behavior. The TF cracking was the main reason the Alloy 718 coating was discontinued.

Cermet Coatings on Alpha-2

NiCrAlY

Figure 188 shows the composite NiCrAlY coating on the Ti-24.5Al-12.5Nb-1.5Mo alpha-2 substrate after the test. The coating had very little oxidation attack, showed no cracking and no signs of spallation. The reaction zone in the 900°C section was ~23µm thick. The substrate microstructure exhibited severe coarsening at temperatures greater than 760°C (1400°F).

CoCrAlY

Figure 189 shows the composite CoCrAlY coating on the Ti-24.5Al-12.5Nb-1.5Mo alpha-2 substrate after the test. Similar to the NiCrAlY coating, very little oxidation was observed as well as no cracking and coating spallation. There were many unmelted CoCrAlY particles in the coating which correlate to surface undulations in the coating. The unmelted particles increased the thickness of the reaction zone if they impinged upon the substrate presumably because there was a larger amount of Co than that present in the more prevalent thin layers. The reaction zone was ~15µm. In examining reaction zone thickness for the CoCrAlY composite coating in all three tests, it is clear that less interdiffusion occurs because of lower interdiffusion coefficients or thinner volumes of material in contact with the substrate.

Alloy 718

Figure 190 shows the composite Alloy 718 coating on the Ti-24.5Al-12.5Nb-1.5Mo alpha-2 substrate after the test. Oxidation was observed on Alloy 718 that was not buried by the alumina constituent in the coating. Although no through-thickness cracks were observed on the coating, cracks were observed in the reaction zone and along the coating/substrate interface. These cracks had no oxidation product associated with them and may be a result of surface preparation. The reaction zone thickness was 20-25µm thick.

Coated Rene '80

Codep coated Rene 80 is a material system currently used in military gas turbine engines. Figure 191 shows that oxidation attack can only be observed on the 900°C section. The alumina in this micrograph is 2-3µm thick. The only other sign of exposure was the formation of topologically close packed (TCP) phases at the coating/substrate interface. The extent of TCP formation was greater at higher temperatures. If the TCP zone is considered as a region of interdiffusion, then the extent is as great as 23µm at 900°C for 516 hr. This quantity can be used for comparison purposes to the reaction zones that form on composite coated Ti-aluminides. In general, the coated Ni-base superalloy was very resistant to attack under these conditions.

2.2.7 Coating Selection for Mechanical Tests in Task 3

Cermet Coating Selection

The results of both iterations of environmental testing indicated that the NiCrAlY [Ni-20Cr-10Al-0.3Ywt% (Ni-19.7Cr-19Al-0.2Yat%)] type of composite coating was the best choice for coating both gamma and alpha-2 Ti-aluminide. The reasons are:

- 1) **Excellent hot salt stress corrosion resistance** on alpha-2 in iteration 2 and gamma in iterations 1 and 2. Both alpha-2 and gamma coated with the NiCrAlY composite survived HSSCC exposures with usable strength. Uncoated substrates with the same exposure were totally embrittled.
- 2) **Excellent environmental resistance in burner rig testing** on alpha-2 in iteration 2; and gamma in iteration 1. The NiCrAlY composite coating was not tested for long times at 900°C on gamma, but the performance of the NiCoCrAlY composite on gamma was also good. The NiCoCrAlY was not chosen for gamma, because of the propensity of composite coatings with Co to undergo thermal fatigue cracking.

The volume percent of alumina to be sprayed with the Ni-20Cr-10Al-0.3Ywt% (Ni-19.7Cr-19Al-0.2Yat%) was chosen to be near 50. This amount was sprayed with the NiCrAlY on gamma in iteration 1 and within 5% of the amount used to spray alpha-2 in iteration 2. The advantage to spraying the same composition on both substrates was economic.

Diffusion Barrier Selection

The major concern for the selected NiCrAlY composite coating was the reaction zone that forms during exposure. The reaction zone was brittle and was frequently observed to crack during specimen preparation. One way of curtailing the zone is to apply a diffusion barrier. Diffusion barriers for Ti-aluminides are generally the refractory metals, TiN or TiC. Compared to ceramics, the refractory metals may have some ductility and stop the propagation of through-thickness cracks. Refractory metals include Cr, W, Mo and Ta. Chromium and Ta have the best environmental resistance; however, GE had experience in depositing W using a chemical vapor deposition (CVD) technique. A CVD technique was chosen because the low pressure plasma spray process used to apply the composite coating requires a grit blasted surface. Typical PVD (physical vapor deposition) processes like sputtering might produce non uniform layers with many defects on such a rough surface. The CVD technique on the other hand, would produce a more uniform layer with less of a dependence on surface roughness.

2.3 Task 3 - Effect of Coating on Mechanical Properties

Mechanical Test Plan for Task 3

The mechanical tests performed on the selected NiCrAlY composite coated specimens are shown in Table 24. The test matrix examines the tensile, fatigue and hot stress corrosion cracking (HSSCC) behavior of coated alpha-2 and gamma systems. All mechanical specimens had round cross-sections. The diameters in mm for the tensile, fatigue and creep specimens are 4.06, 6.35 and 6.35, respectively. The major variables were environmental exposures, the presence of the W diffusion barrier (DB), the presence of a coating (ctg), test temperature and strain level in the fatigue tests.

The exposure used was a 100 hr cyclic exposure at 760°C (1400°F) in air, because the alpha-2 and gamma could realistically see application at these temperatures. Inspections were performed during the exposure and included weight change and any visual signs of distress.

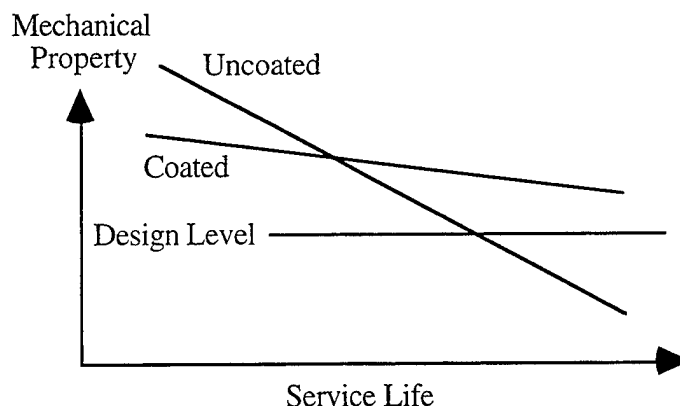
The initially planned mechanical test conditions were:

- 1) tensile tests of both coated and uncoated gamma and alpha-2 at RT, 400°F, 900°F and 1300°F at a strain rate of 5×10^{-3} /min.;
- 2) fatigue tests for coated and uncoated alpha-2 at $A=1^*$, 30cpm at RT, 800°F and 1200°F with a strain range of 0.8-1.0% with a runout of 200,000 cycles;
- 3) fatigue tests for coated and uncoated gamma at $A=1$, 30cpm at RT, 1200°F and 1400°F with a strain range of 0.2-0.4% with a runout of 200,000 cycles; and
- 4) hot salt stress corrosion cracking tests were performed by spraying synthetic sea water on the surface and drying to achieve 0.1-0.3mg/cm² coverage, followed by a creep exposure at 760°C(1400°F)/20 ksi for 500 hr. If the samples did not fail, a room temperature tensile test was performed to evaluate residual tensile properties.

2.3.2 Coating Philosophy

The application of a coating to an engineering material generally reduces mechanical properties. The engineer realizes, however, that the environmental degradation experienced during material application can be more severe than that produced during a mechanical test in a laboratory. The hope is that the coating can extend the useful life of the component as shown in the following schematic.

* A-ratio is defined as the alternating stress over the mean stress.



For alloys like gamma and alpha-2, the conditions that establish the axes, curves and the goals are still under debate and are application specific. In Task 3, test conditions were chosen so that more information on the unexposed and exposed properties of coated and uncoated Ti-aluminides could be measured.

2.3.3 Diffusion Barrier Application

The CVD W was applied by GE-CRDC to the samples indicated in Table 24. The surfaces were first grit blasted, cleaned in Alconox, rinsed, ultrasonically cleaned in water, rinsed in alcohol and air dried. The threads were mechanically masked using Mo sheet and Ni-chrome wire. Three CVD W runs were performed with 10 samples in each run.

The CVD gas mixture used was WF_6 and H_2 . Not unexpectedly, a low volatility Ti-fluoride species formed on surfaces at low temperatures and precluded W deposition. Only heating to temperatures greater than $700^\circ C$ causes volatilization of this compound and allowed W deposition. The Al activity in the Ti-aluminides was low enough to preclude the formation of a AlF_3 -type species. The final deposition was performed at $740^\circ C$ at 2Torr total pressure with a (H_2/WF_6) ratio of 12. The thickness of the deposits were measured by using a profilometer on a Si wafer. The W thickness was between 3.5 and $5\mu m$. The W deposit was adherent on the grit blast surface, but some spallation occurred in smooth areas. Figure 192 shows an optical micrograph of the deposit.

2.3.4 Cermet Application

Cermet coatings were applied to the mechanical test specimens by GE-CRDC. Samples were prepared by grit blasting with a coarse grit at 60psi and ultrasonically cleaning with propanol. The coating was applied using an LPPS unit with an EPI gun at 60Torr and spraying a -400Mesh powder mixture of 40% by volume alumina with the remainder Ni-20Cr-10Al-0.3Ywt%. The samples were preheated with the plasma torch with as many as 15 torch passes before deposition was started. The target coating thickness was 75-100 μm with the threads masked by a low carbon steel tape that was tack welded to the gripping section. The samples were rotated

while the gun was translated. The diameters of the samples were measured before and after coating application to determine coating thickness. Specimens with the diffusion barrier were oversprayed so that the cermet would seal the barrier from oxidation. Subsequent data will show that the overspray was not adequate.

2.3.5 Mechanical Test Bar Exposure

Coated and uncoated mechanical test bars were placed on alumina ceramic and cycled between $\sim 40^{\circ}\text{C}$ and 760°C for 100 one-hour cycles in air using the same apparatus as cyclic oxidation testing performed under Task 2. The weight and visual appearance of each sample was recorded before and after the exposure. Table 25 summarizes the data taken after 50 hr, and Figure 193 shows uncoated gamma and alpha-2 after the exposure.

Several observations were made from the data:

- 1) The specimen type was important for weight change data as the surface area varies considerably. The creep and fatigue samples had greater surface area than the tensile bars.
- 2) Another observation was the formation of a yellowish white oxide on uncoated gamma or alpha-2 which resulted in larger weight gains. GEAE's experience is that the yellow-white reflects the formation of a Ti-rich oxide scale which grows faster, hence, the larger weight gain. The yellow-white oxide on uncoated samples tends to be located at the threads which may indicate contamination from machining fluids or chemical segregation.
- 3) All coated samples lost weight. The weight loss is likely from the spallation of loosely adhering coating from the spraying process similar to that noted during burner rig testing in Task 2. It must also be noted that the threads on coated samples were masked and could form the Ti-rich oxide discussed in 2.
- 4) Coatings that included a W diffusion barrier could cause the formation of a thicker yellow oxide. This oxide was thought to be the result of oxidation of the W CVD diffusion barrier which was not totally sealed by the cermet coating. The only coatings judged to be unacceptable after the cyclic exposure had the W diffusion barriers and are listed as Y's under the cracking column.

2.3.6 Tensile Test Results

Tensile tests as a function of temperature were carried out on gamma and alpha 2 substrates under a strain rate of $5 \times 10^{-3}/\text{min}$ in air. Strain was monitored with an extensometer. Variables examined on each substrate were a $760^{\circ}\text{C}/100$ hr cyclic oxidation exposure, the W diffusion barrier and the cermet coating. The coating made measurement of elongation and yield strength difficult on several samples due to slippage so some data points are missing. The results are summarized in Table 26.

Gamma

The Ti-48Al-2Cr-2Nb (gamma) data set was marred by the high frequency of thread failures. Threads can act like a notch and locally increase the stress level to the point where a crack can nucleate, grow and cause failure. The thread failures were more prevalent on samples receiving a thermal exposure. The thermal exposure could be the cyclic oxidation exposure at 760°C or the application of the cermet or W diffusion barrier. The application of the cermet involved as many as 15 preheat passes of the torch to insure coating adhesion and the W CVD process was done at elevated temperature (740°C). The plasma spray process heats the substrate to temperatures near 598°C (1200°F). The lack of ductility in gamma after these types of exposures has been documented in the literature.¹⁴ That work did not point out any notch sensitivity after exposure. This subject will be investigated more thoroughly under a Navy contract recently awarded to GE Aircraft Engines.³⁵

Statistical analysis of the data, excluding samples with diffusion barriers, indicates that the cermet coating and cyclic exposure decreased the UTS of the gamma alloy by about 15 and 23%, respectively, and that any thermal exposure lowers the ductility by ~40%. The yield strength of the material does not depend heavily on the cyclic exposure or the presence of a coating indicating that the major difference between as-received gamma and thermally exposed gamma is the work hardening behavior of the alloy. In as-received gamma, some ductility is observed after yield, while in exposed material, less ductility is observed. Recall that coated gamma is thermally exposed from processing. The reasons for the loss of ductility with exposure are not yet known, but it may involve aging the microstructure, roughening the surface, recrystallization or the creation of some other critical defect.

Gamma Metallography

Figures 194 and 195 show cross-sections of the uncoated unexposed gamma tensile samples as a function of temperature. The fracture surfaces are relatively flat with no apparent necking except when tested at 704°C. Secondary tensile cracking was not evident on the samples tested at 22 and 204°C, but can be observed on bars tested at 482 and 704°C. The ductility of the latter two was greater which relates to the ability to withstand the nucleation of crack without catastrophic propagation. Some of the ductility in the latter two must be attributed to the accumulation of surface crack opening displacements.

Figures 196 and 197 show cross-sections of the uncoated and 760°C/100 hr cyclically exposed gamma as a function of temperature. The 22°C sample that had a thread failure was lost. The sample tested at 204°C shows that the gamma sample during the 760°C/100 hr cyclic exposure had formed a 1-1.5µm alpha layer under a 1-1.5µm oxide scale. The alpha layer was heavily cracked during the tensile test with cracks ~10-25µm apart. The samples tested at 482°C and 704°C show the same oxide and alpha layer morphology, but secondary cracks were found to extend up to 25µm into the substrate. Regions with high volumes of alpha-2 were most susceptible to cracking.

Figure 198 shows the cross-section of the cermet coated unexposed gamma samples tested at 704°C. The coating shows excellent adhesion to the gamma substrate; however, the fracture surface was flat. Higher magnification shows no secondary cracking in the reaction zone that develops between the substrate and coating. Some cracking in the alpha-2 phase in the substrate was observed. Figure 199 shows the cross-section of the cermet coated 760°C/100 hr cyclically exposed gamma samples after tensile testing at 704°C. The microstructure is similar to that in Figure 198, indicating that the 760°C exposure had little effect on the coating. The measurement of 0.5% strain and the observation of no coating cracking means that the strain to cracking of the coating is at least 0.5% at this temperature. The cermet coated samples tested at 22°C both had thread failures and weren't available for metallography.

Figure 200 shows cross-sections of the unexposed cermet W CVD coated gamma samples after tensile testing. The sample tested at 204°C shows a thread failure. The microstructure shown near the failure shows the bright 4µm W layer. Above the layer, however, was a remnant of the low C steel tape used to mask the threads indicating that work needs to be done with tape material removal and selection. The other micrographs show the coating in the gage section. The W CVD barrier had prevented interdiffusion between the substrate and coating during coating processing. The sample tested at 482°C shows delamination of the W CVD barrier at the gamma/diffusion barrier interface indicating that the layer may affect adhesion of the environmentally worthy cermet.

Figure 201 shows cross-sections of the 760°C/100 hr cyclically exposed cermet W CVD coated gamma samples after tensile testing. The sample tested at 204°C shows the loss of the cermet coating over a measurable length of gage section and that a brittle layer has formed on gamma. It is not clear if the layer is the alpha observed on uncoated gamma samples or a W stabilized phase like β. The microstructure shows that cracking has occurred in this layer similar to uncoated gamma. The sample tested at 482°C showed that the cermet coating had completely spalled and that the W barrier was not continuous. The sample tested at 704°C again showed a spalled cermet and locally spalled diffusion barrier. This sample showed a lot of voiding in the substrate and apparently was very ductile although no reading was given due to extensometer slippage on the decohering coating. The data indicate that the W was not properly sealed by the coating and oxidation of the W layer caused delamination of the coating. No overcoating can guarantee complete sealing so the use of W as a diffusion barrier is not recommended but, the use of a CVD Cr layer might be a useful alternative.

Gamma Tensile Summary

The cermet coating without a diffusion barrier has been shown to prevent oxidation, hot corrosion and hot salt stress corrosion cracking of the gamma alloy in Task 2. The tensile results indicate that the trade for improved high temperature environmental resistance involves a reduction in ultimate tensile strength and ductility. The reduction in tensile properties might be acceptable if gamma is being applied at stresses well below yield. The cermet coating stopped secondary cracking in the tension tests. The reaction zone between the coating and substrate was observed to be less brittle than the alpha layer found under the oxide scale in uncoated gamma. Effort in Task 4 will be to further improve the processing of the cermet on the Ti-aluminide substrates to prevent embrittlement.

Alpha-2

Alpha-2 samples were not observed to have thread failures so a complete data set was available for examination. Not taking into account samples with the W diffusion barrier, the cyclic exposure decreases the UTS and YS by about 8% and the ductility of alpha-2 by 44%. Coating on the other hand, increases the YS by 10% but decreases the ductility 54%. The strength increase provided by the coating might be expected as it comprises approximately 7-10% of the cross-section of the sample.

The general trend for alpha-2 was a maximum ductility observed for the 482°C test temperature. This might be the temperature range where slip system activation is maximized and dynamic embrittlement is minimized. Dynamic embrittlement refers to the absorption and diffusion of interstitials like O at the crack tip resulting in enhanced crack propagation.

The cermet coating without the diffusion barrier in Task 2 prevented oxidation, hot corrosion and hot salt stress corrosion cracking of alpha-2. The tensile data show that the coating will decrease ductility, but the residual levels of 3% are still high enough for application. In addition, the strength increase in thin sections might be put to great advantage if alpha-2 is applied at temperatures greater than 568°C (1200°F).

Alpha-2 Metallography

Figures 202 and 203 show cross-sections of the unexposed uncoated alpha-2 alloy after tensile testing at various temperatures. Structures after the 22°C and 204°C test revealed a flat fracture, cracking of the primary alpha-2 islands, few secondary tensile cracks and no observable oxide or alpha case layer. The structures after the 482°C and 704°C revealed a ductile fracture, primary alpha-2 cracking and a series of wedge shaped secondary cracks 5-25µm apart and 2-25µm deep.

Figures 204 and 205 show cross-sections of the cyclically exposed uncoated alpha-2 alloy after tensile testing at various temperatures. The samples had an oxide scale 1-5µm thick and a sublayer approximately 2µm thick. The sample tested at 22°C did not have primary alpha-2 cracking, but had a series of secondary cracks 10-20µm deep and 20-60µm apart. The samples at 204°C and 482°C showed primary alpha-2 cracking and wedge shaped secondary tensile cracks. The cracks are deeper (120µm) on the 482°C sample which agrees with the larger ductility. The sample tested at 704°C shows primary alpha-2 cracking and secondary cracking 25-50µm deep.

Figures 206 and 207 show cross-sections of the unexposed cermet coated alpha-2 alloy after tensile testing at various temperatures. The cermet coating does not appear to have the adhesion that was observed on the gamma sample and much of the coating was separated from the substrate. Compared to uncoated alpha-2 at 22°C, no cracking of primary alpha-2 was observed and secondary cracks were noted at the coating/substrate interface. The cracking may be a result of thermal exposure during coating application. The coating for the sample tested at 704°C showed greater adhesion. The micrographs show that the sample had necked near the failure causing the cermet to lose adhesion. Necking puts tensile stresses normal to the coating/substrate

interface resulting in spallation. The sample also displayed shallow secondary cracks at the coating/substrate interface.

Figures 208 and 209 show cross-sections of the cyclically expose cermet coated alpha-2 alloy after tensile testing at various temperatures. The 22°C section showed that an uncracked cermet coating had spalled from the substrate for a good portion of the gage length. Also evident was cracking of the coating/alpha-2 reaction zone and primary alpha-2 islands. These cracks are approximately 5-8µm deep, while others that propagated into the matrix were from 25-100µm deep. The sample tested at 704°C showed excellent coating adhesion with only a small chip near the fracture. The sample had reaction zone cracking, cracking of the cermet coating and a few deep cracks(150µm). The micrographs clearly showed that the cermet separates at the coating/alpha-2 interface.

Figures 210 and 211 show cross-sections of the unexposed CVD W cermet coated alpha-2 alloy after tensile testing at various temperatures. Coating adhesion was poor in these samples. The adhesion failure was at the W/alpha-2 interface. An array of secondary tensile cracks could be found on all of the samples the deepest and were on the sample tested at 22°C. The other samples showed cracks in the reaction zone. It is interesting to note that a classical cup-and-cone fracture was noted on the sample tested at 482°C. .

Figures 212 and 213 show cross-sections of the cyclically exposed CVD W cermet coated alpha-2 alloy after tensile testing at various temperatures. The sample tested at 22°C showed oxide formation under the W barrier and the spallation of the cermet coating. The oxidation of the W and the alpha-2 again indicated that the W barrier was not sealed properly with the cermet. The oxidation makes the assessment of W as a barrier difficult. The sample tested at 204°C shows no coating and an array of wedge shaped tensile cracks. Again, oxidation occurred under the W diffusion barrier. The 482°C sample showed more frequent and deeper secondary cracking commensurate with the greater ductility. The sample at tested at 704°C has the same features as those previously discussed. This sample had more cracking of the alpha-2 phase.

Alpha-2 Tensile Summary

The cermet coating without a diffusion barrier has been shown to prevent oxidation, hot corrosion and hot salt stress corrosion cracking of the alpha-2 alloy in Task 2. These tensile results indicated that the cermet coating reduces ductility, but may increase strength in thin sections. The cermet coating was susceptible to spalling when the substrate necks. Since most applications of alpha-2 will involve stresses under yield, it is likely that the cermet coating could be applied with little impact. In addition, the residual ductility of alpha-2 after application is still in excess of 3% over the usable temperature range. The CVD W barrier was not effective due to oxidation and overcoat sealing problems. An additional effort was made in Task 4 to further improve the processing of the cermet on the Ti-aluminide substrates to prevent embrittlement from coating application.

2.3.7 HSSCC Results

Hot salt stress corrosion cracking (HSSCC) testing of gamma and alpha-2 specimens was performed as a function of cyclic exposure, cermet coating, diffusion barrier and salt. Table 27 shows the results of this testing. Initially the exposure conditions were to be 760°C/20 ksi for both substrates; however, the creep rate for alpha-2 was excessive under these conditions. A decision was made to reduce the exposure for alpha-2 to 10 ksi during testing. Salt was applied to the substrates using a method identical to that discussed in Task 2. A micrograph of the salt distribution is shown in Figure 214. The test procedure was such that if a sample survived the stress exposure then it was room temperature tensile tested to measure residual strength. The exposure performed here is at a much higher temperature (111°C) than HSSCC exposures in Task 2. The increase in temperature was specifically directed at determining if the cermet coating could protect the substrate under creep in a salt laden environment.

Gamma

Uncoated gamma samples survived the 500 hr stress exposure with and without salt; however, there was a reduction in residual strength and ductility. One exception was the pre-exposed (760°C/100 hr cyclic oxidation) sample stress exposed without salt which ruptured after 499.6 hr of stress exposure. The sample exposed with salt survived and had good residual strength, 62 ksi. This may mean that the oxide produced during pre-exposure protects gamma against salt attack.

Cermet coated samples survived the 500 hr stress exposure under all conditions. Amazingly, the coated samples had 50% less deformation than the uncoated samples. This is an important result as dimensional change in certain engine components is very important. The residual strength of the cermet coated samples was ~51 ksi which is near that of uncoated gamma.

Cermet samples with a W diffusion barrier performed similarly to uncoated samples. The reason that the diffusion barrier is considered poor is that the W oxidizes and ruins the adhesion of the overlying cermet coating. Figure 211 shows this phenomena on an alpha-2 bar. The W layer has oxidized to WO₃ and unzips the cermet. The cermet holds its shape while the substrate creeps and all adhesion is lost. The net result is that the W diffusion barrier sample performs similarly to an uncoated sample. Pinholes and other paths through the cermet will never be totally prevented, therefore, a high temperature coating system for Ti-aluminides should not use a W diffusion barrier. Chromium with better environmental resistance maybe a better alternative.

Gamma Metallography

Figures 215 and 216 show cross-sections of the uncoated unexposed gamma after the HSSCC test. The sample exposed without salt had a flat fracture path, an 8µm thick oxide scale, a 0.5µm alpha layer under the scale and many secondary cracks. The cracks tended to follow alpha-2/gamma phase boundaries. The sample had reduced strength and ductility after the exposure.

The sample exposed with salt showed a similar crack morphology but a more complex reaction product. In this case the corrosion product was up to 90 μ m thick showing that sea salt can accelerate surface attack on gamma. The sample exposed in the salt environment had a lower UTS and ductility.

Figures 217 and 218 show cross-sections of the uncoated and cyclically exposed gamma samples after the HSSCC test. The sample without salt failed in rupture with 20min left in the planned 500 hr exposure. The sample showed heavy deformation and had an extensive neck. The sample had poor creep resistance compared to the unexposed sample, but the exact reason for the difference was not investigated. Possibilities include microstructural coarsening, segregation, inhomogeneous forging microstructure or a greater stress was applied than was recorded. The oxide scale on this sample was again about 8 μ m thick which was similar to the unexposed sample. The cyclically pre-exposed sample tested in the salt environment survived the 500 hr exposure and was tensile tested at RT. The sample did not show the heavy corrosion observed on the unexposed sample meaning that the oxide that formed during cyclic exposure protected the alloy from salt attack. The microstructure was that expected for RT tested gamma with the exception of the 9 μ m scale, however, lower tensile properties were observed.

Figures 219 and 220 show cross-sections of the unexposed cermet coated gamma sample after HSSCC testing. The sample tested without salt shows an adherent coating with many creep cracks. The coating had formed a 6 μ m thick reaction zone with the gamma. In areas where there was a creep crack in the coating, a 6 μ m oxide was present in the reaction zone. The substrate has a region on the fracture face that appears to be lower in Al resulting in a high volume fraction of alpha-2 phase. This is a concern but probably does not affect the favorable result that the coating reduced the deformation of gamma by 50% under the 760°C/20 ksi creep condition. The unexposed cermet coated sample exposed in a salt environment showed many of the same features. Again, the adherent coating reduced the deformation of the gamma by 50%! No inhomogeneity was noticed in the bar. The cracking in the coating resembles that found for the 22°C tensile test which may mean that the coating can improve the high temperature creep resistance of gamma by stopping metal loss and surface cracking. Surface cracking may raise the stress locally resulting in activation of a different mechanism for creep.³⁶

Figures 221 and 222 show cross-sections of the cyclically exposed cermet coated gamma substrate. Results again indicate a 50% reduction in creep deformation over uncoated gamma and a very adherent coating. Specimen ID numbers indicate that these bars were from the same pancake forging as the uncoated bars adding credence to the positive influence of the coating. Also note that these samples had 0.25" (6.4mm) gage diameter so the coating comprised only 4-5% of the cross-section. The sample exposed in the salt free environment had an adherent coating with creep cracks. The cracks in the coating occurred during the creep exposure as evidenced by the oxidation attack of the reaction zone. The sample exposed in the salt environment shows a very similar morphology, but examination of Table 27 shows very little RT residual strength (6.5 ksi). Both samples failed near or in the radius.

Figures 223 and 224 show cross-sections of the unexposed CVD W cermet coated gamma samples. The samples in terms of creep deformation and residual strength behaved like the unexposed uncoated gamma samples. The CVD W layer in each case was adherent to the

substrate, but the cermet coating spalled. For the sample exposed without salt, a 2-3 μ m oxide and a 1-3 μ m alpha layer was found under the W. For the sample exposed with salt, a 1-6 μ m oxide and a 2-6 μ m alpha layer was observed. The CVD W was a poor barrier to oxygen ingress.

Figures 225 and 226 show cross-sections of the cyclically exposed CVD W cermet coated gamma samples exposed without salt. The sample exposed with salt was lost. The sample exposed without salt performed similarly to the cyclically exposed uncoated gamma samples because the cermet spalled. The sample made it through the 500 hr creep exposure and was tensile tested. Visually the surface was yellow in appearance indicating oxidation to WO₃. The cyclic pre-exposure resulted in a thicker oxide scale and alpha layer under the W. Secondary cracks tended to follow alpha-2/gamma phase boundaries. The sample exposed with salt failed after 418 hr of creep exposure. These results were considered inferior to the cermet-only coating.

Gamma HSSCC Summary

The uncoated gamma underwent a creep deformation of 20% during the 760°C/20 ksi/500 hr exposure. A sample cyclically exposed at 760°C/100 hr prior to the test ruptured at 499.6 hr. Cermet coated samples all survived the 500 hr creep exposure regardless of pre-exposure and showed creep deformations of only 10%. The large reduction in creep deformation indicates that the cermet coating is preventing deformation that may be dependent on environmental interaction and surface cracking. Figures 227 and 228 graphically illustrate the large change in creep behavior for samples that were unexposed and pre-exposed for 100 cycles at 760°C in air. The W diffusion barrier was not effective. The W oxidized resulting in cermet spallation and, furthermore, allowed oxygen ingress into the substrate.

Alpha-2

The alpha-2 samples crept readily under the 760°C/20 ksi creep condition. A decision was made to reduce the stress to 10 ksi. Figure 229 shows how the change affected creep rate. Unfortunately, the testing vendor forgot this test condition change on a subsequent shipment of cyclically exposed samples resulting in many stress rupture failures. Samples exposed to only 10 ksi survived the stress exposure, while samples exposed at 20 ksi ruptured. Comparing these results to Task 2, the 760°C/10 ksi salt condition appears to be under the HSSCC threshold as no early failures were observed. Apparently creep deformation relaxes stress at crack tips resulting in slower crack propagation. There was strong evidence that the cermet coating prolonged the creep life of alpha-2 substrate.

Alpha-2 Metallography

Figures 230 and 231 show the uncoated unexposed alpha-2 substrates exposed at 760°C/10 ksi/500 hr and then RT tensile tested. The sample exposed in the salt environment had more creep deformation and cracking and less residual strength. The figures show that the sample exposed without salt had a 4-5 μ m oxide scale with a 2-4 μ m subscale zone. Secondary tensile cracks were most noticeable near the fracture and did not seem to follow any microstructural constituent. The fracture surface revealed an embrittlement layer approximately 30 μ m deep. Tensile properties after the exposure were similar to unexposed alpha-2. The sample exposed

with a salt deposit showed a corrosion product up to 30 μ m thick and many more secondary cracks. The cracks appeared to sever the primary alpha-2 island/transformed β interface. Residual tensile properties were reduced. The fracture surface had a larger embrittled region (flat fracture) 70 μ m thick.

Figures 232 and 233 show the uncoated cyclically exposed alpha-2 substrates after rupture at the 760°C/20 ksi condition. The time to rupture for the sample exposed without salt was 187.1 hr and with salt, 175.8 hr. The sample exposed without salt had a scale up to 13 μ m thick and many wedge shaped creep cracks. The thicker oxide was a by-product of the cyclic exposure. The sample exposed with salt had a thicker oxide with many more of the wedge shaped creep cracks. There was oxidation observed at the tip of the cracks that followed the stress field rather than any microstructural feature. The creep cracks were much deeper on this sample resulting in the larger creep deformation.

Figures 234 and 235 show the cermet coated unexposed alpha-2 substrates after the creep exposure and RT tensile test. Both samples failed in the threads. The sample exposed without salt was switched from 20 to 10 ksi during the test. The residual strength and ductility of this sample was lower than that expected for as-received alpha-2.

Figures 236 and 237 show cross-sections of the cyclically exposed cermet coated alpha-2 substrates after stress rupture at 760°C/20 ksi. The sample in a salt free environment failed after 244.3 hr and showed good adhesion of the coating to the alpha-2 substrate with wedge shaped creep cracks located mostly in the coating. The cermet was mostly spalled near the failure. High magnification shows oxidation of the alpha-2 and the reaction zone in areas where the coating cracked. The secondary cracks extend ~25 μ m into the alpha-2 substrate. The sample exposed with salt failed after 220.4 hr of exposure and had a very similar morphology. Compared to cyclically exposed uncoated alpha-2, the coated samples lasted 28% longer showing the positive impact of the coating on creep rupture strength.

Figures 238 and 239 show cross-sections of the unexposed W CVD diffusion barrier cermet coated samples after RT tensile testing. Both samples failed in the threads. The sample exposed with salt had properties similar to uncoated alpha-2 so the coating had no effect. The microstructure shows that the cermet coating spalled from the substrate leaving behind the W diffusion barrier. Visually, the W barrier was yellow green indicating oxidation to WO₃. Under the W is a 35 μ m thick corrosion product that selectively attacked prior β grain boundaries. The thread failure nucleated from a gage mark on the sample. The results here indicated that the W diffusion barrier was not effective.

Figures 240 and 241 show cross-sections of the cyclically exposed, W CVD diffusion barrier, cermet coated samples after rupture under 760°C/20 ksi conditions. These samples both failed after 131 hr on the stand regardless of salt application. These were the lowest rupture lives observed on alpha-2. Both microstructures show a lack of cermet adhesion and a thick corrosion product under the W barrier. Under the thick oxide was a brittle layer of internal oxidation that showed profuse cracking. Large wedge shaped cracks existed along the gage length which lead to the large deformation.

Alpha-2 Summary

The 760°C/10 and 20 ksi creep condition was below the stress-temperature threshold for hot salt stress corrosion cracking. The 20 ksi condition resulted in rupture failures, while the samples survived 500 hr at 10 ksi. Salt deposits lowered both the time to rupture and the residual tensile properties. The cermet coating improved the creep resistance of alpha-2 in environments with and without salt. This is shown in Figures 242 and 243. The cermet coating should be considered for applications of alpha-2 at $T > 704^{\circ}\text{C}$ where creep is a limiting property and environmental attack can occur.

2.3.8 Fatigue

Fatigue testing was performed on gamma and alpha-2 substrates using a $A=1$ ($R=0$), a 30cpm frequency under strain control and an arbitrary runout of 200,000 cycles. The variables tested were cyclic exposure (760°C/100 hr), cermet coating and the W diffusion barrier. Rapid coating spallation was observed with the W diffusion barrier so testing of these samples were curtailed to conserve program resources. Table 28 summarizes the fatigue results. The matrix was by no means a complete study of the fatigue behavior of these coated Ti-aluminide systems. Instead the matrix was directed at illustrating the conditions where the cermet coating might be applied without a reduction in LCF behavior.

Gamma Summary

The fatigue life of the baseline uncoated Ti-48Al-2Cr-2Nb was excellent. The gamma ranout (200,000 cycles) at strains of 0.4% or larger at $A=1$ at all test temperatures (22, 568, and 760°C). The maximum tensile stresses were equivalent to 50 ksi and larger. Examination of the stress-strain loops as a function of time showed that gamma softened slightly with increasing exposure. For exposed samples, the softening is most likely from the formation of cracks at the surface.

When the uncoated gamma was cyclically exposed at 760°C/100 hr in air and then tested, the fatigue life was reduced. A thread failure occurred at 22°C on one sample as might have been expected from the tensile testing. Another sample had a two order of magnitude reduction in life when tested at 568°C and 0.4% strain. The reduction in fatigue life, however, was not observed at 760°C. The difference apparently lies in the temperature activated plasticity for the gamma alloy and a change in the crack propagation behavior. Nonetheless, the exposed gamma material at all temperatures was able to survive a cyclic stress of lower than 41 ksi.

Fatigue strength is a mechanical property that is very sensitive to surface flaws and condition. The samples used to generate the uncoated gamma data had a 8 μin finish (polished). The application of the cermet coating involved a grit blast to roughening the samples which could have reduced the fatigue life of gamma. The cermet coating grit blast treatment was tested on unexposed gamma and no effect was observed on fatigue properties at 22 or 760°C.

Unexposed cermet coated gamma was tested at 22 and 760°C. The fatigue life was reduced drastically when stresses were higher than 42 ksi. This may indicate the stress where the coating begins to crack. One runout was observed at 0.25% total strain (41.5 ksi max. stress) at 760°C indicating that the coating is best applied in components where the stresses are below this value. Lower stress applications would require high cycle fatigue testing which was not performed under this program.

Cermet coated gamma that was cyclically exposed at 760°C/100 hr in air was tested at 568 and 760°C. Poor fatigue properties relative to uncoated gamma were observed at high strain ranges (0.4%). On the bright side, a sample tested at 568°C and 0.25% strain was headed for a runout before an uncoated thread failed. The maximum stress for this sample was 44.7 ksi. Uncoated exposed gamma showed a fatigue reduction at 50 ksi and a runout at 41 ksi; therefore, the coated sample may have similar fatigue properties.

The W CVD cermet coated samples both performed poorly. At 22°C, the sample failed after 2 cycles. The only thermal exposure this sample had was during coating processing. The sources of property reduction are hydrogen embrittlement during the CVD deposition and vacuum exposure during the preheat cycle for cermet application. When tested at 760°C, the coating spalled from the substrate after 5168 cycles.

Gamma Metallography

The cross-sections of the unexposed uncoated gamma samples are relatively featureless. These samples ran out (200,000 cycles) and no fatigue crack initiations were obvious. Figure 244 shows a cross-section of the sample tested at RT and 0.4% total strain. The micrograph shows what may be the crack initiation sites (1.3µm) in the alpha-2 phase of transformed α grain at the surface. Figure 245 shows the unexposed uncoated gamma after testing at 760°C and 0.4% strain. Some oxide intrusions (7µm) were observed on the surface that and a few 38µm deep cracks that followed no observable microstructural feature.

Micrographs of cyclically pre-exposed and uncoated gamma sample tested at 760°C (1400°F) and 0.4% total strain are shown in Figure 246. The higher strain level produced cracks through the 4µm thick oxide scale and 20µm into the substrate. The 760°C temperature apparently increases the size of a crack the gamma can tolerate before stage III crack growth. Figure 247 shows the cyclically pre-exposed gamma sample tested at 648°C (1200°F) and 0.4% strain. Cracks are observed through the 6µm oxide scale and extended 12µm into the substrate. The cracks typically had a jagged fracture path that did not follow any observable microstructural feature. At lower magnifications, the fracture was very flat and extended around the surface before overloading near the middle of the bar. The bar tested at 648°C (1200°F) and 0.25% strain (not shown), did not have cracking into the oxide and substrate. This explains why the 0.25% bar ranout at 200K cycles and the 0.4% bar failed in 1549 cycles.

The cross-section of the unexposed, grit blasted and uncoated gamma sample tested at RT and 0.4% total strain was examined. Cracks were not found to emanate from the rough surface or grit particles on the surface consistent with the runouts in the fatigue tests.

The cross-sections of unexposed cermet coated samples tested at 760°C are shown in Figures 248 and 249. The best comparison was between the samples tested at 0.4% and 0.25% total strain. The sample lasted only 345 cycles at 0.4% strain with a maximum stress of 52.1 ksi, but ran out at 248746 cycles at 0.25% strain and a maximum stress of 41.5 ksi. At the lower strain, no cracks were found in the cermet or substrate and the coating remained adherent. At the higher strain, the cross-sections show cracks 100µm long that follow α_2/γ phase boundaries in the substrate. It also appears that the cracks occur in areas of the cermet where there is a larger amount of the alpha alumina phase. This might be a coating process variable that can be used to improve the fatigue life.

The cross-sections of cyclically exposed cermet coated samples tested at 648°C are shown in Figures 250 and 251. The sample tested at 0.4% strain and a maximum stress of 49.5 ksi lasted only 1 cycle. The bar tested at 0.25% strain (~44.7 ksi) was on route to a runout when a thread failure ended the test. The sample tested at high strain did not show any secondary cracking in the coating indicating that the strain was high enough to nucleate and grow a single crack. A reaction layer is seen at the cermet/ γ interface that was a result of the cyclic exposure. The sample tested with low strain had the same general microstructure but with secondary crack evidence. The cracks may have been generated during sectioning of the unfailed part with a cutoff wheel as the result of bending stresses. The coating in the same micrograph shows partial exfoliation of the cermet which was likely the result of sectioning.

Another cyclically exposed cermet coated sample tested at 760°C and 0.4% strain lasted only 3 cycles before failure. Visually the sample displayed several regions with different heat tints, with a blue oxide tint at the coating in the center and a golden brown oxide tint at the middle radii. It was suspected that a pre-existing flaw may have existed. Auger spectroscopy was used to determine the difference in composition between the brown and blue oxides. The results are shown in Table 29 and Figure 252. The table shows that the composition of the two regions were similar. The spectra indicate an Al+Ti oxide which was thicker in the blue region as determined by crossover between Ti and O profiles.

Only two CVD W + cermet coated samples were tested because other tests had shown poor performance. The tests were performed at RT and 760°C and 0.3% strain. At RT, the unexposed sample failed outside the extensometer after 2 cycles. Figure 253 shows the cross-section. The coating maintained adhesion for the most part because there was no elevated temperature exposure in air that could oxidize the W. Cracks were found in the coating and substrate but did not follow any obvious microstructural feature. This indicates that the coating processing reduced the fatigue capability. Figure 254 shows the cross-section of the sample tested at 760°C. The coating and very little of the W CVD barrier is left in contact with the substrate. This was the same result seen in other exposed mechanical tests for this type of coating system.

Alpha-2 Summary

Uncoated unexposed alpha-2 (Ti-24.5Al-12.5Nb-1.5Mo) tested at RT, 426°C and 648°C and a total strain of 0.8% ran out at a cycle count of 200,000 or greater. The maximum stress level corresponding to 0.8% strain was 98 ksi at 648°C to ~125 ksi at RT. Data on unexposed alpha-2 (Ti-24Al-11Nb) at much lower stresses (35-75 ksi) indicate a life of 27,000 to 55,000 cycles.³⁷ This shows the superiority of the 12.5-1.5 composition and processing. The excellent behavior of the alpha-2 was also observed for samples receiving the same heavy grit blast as the cermet coated samples.

Cyclically exposed alpha-2 was another story. The 760°C/100 hr exposure prior to testing was enough to reduce the fatigue capability to 300-5000 cycles at strain levels of 0.6-0.8%. The reduction is the result of oxidation and interstitial dissolution. Additionally the possibility of microstructural aging from the exposure can't be ignored. Recall that the alpha-2 was given a 704°C stabilization heat treatment, so some coarsening was expected. The data produced here were similar to exposed Ti-24Al-11Nb referenced above where a similar exposure resulted in lives between 2000 and 6000 cycles, however, the stress levels here were higher.

The cermet coatings did not improve the fatigue behavior of the alpha-2 alloy. In the exposed and unexposed condition, the life of the coatings tested at 0.6-0.8% strain was from 300-3500 cycles. The similarity in cycle count to the cyclically exposed uncoated alpha-2 cannot be overlooked. It appears that the coating or coating processing has the same effect as the environmental exposure. This is possible because the LPPS process involves preheating to temperatures near 704°C and the CVD W process was performed at 740°C. The cermet coatings were generally adherent to the alpha-2 except when the CVD W was present or when the sample was tested at RT. The cermet coatings were disappointing in fatigue at high stresses and optimized processing was needed for Task 4 to improve performance.

Alpha-2 Metallography

Uncoated unexposed alpha-2 are shown in Figures 255 and 256. Samples that ran out (including grit blasted samples) did not show signs of fatigue cracking at the coating/substrate interface. These samples have an excellent microstructural appearance. Table 28 shows that increasing the strain range over 0.8% results in a large loss in fatigue life and implies a very shallow slope for the S vs. N curve for the alloy.

Uncoated cyclically exposed alpha-2 exposed at 0.8% strain are shown in Figures 257 and 258. At room temperature, a series of cracks can be observed in an interstitially enriched surface layer. The surface layer was 18µm thick and was discernible using backscattered electron imaging. The cracks that extend further than the enriched layer do not appear to follow any microstructural feature, although cleaving of the primary alpha-2 phase was observed. The fracture surface shows surface initiation, but no flat embrittled circumferential layer. At 648°C, a similar cross-sectional morphology was observed, but the fracture surface is much different. The fracture was surface initiated, but testing at 648°C has produced a discernible flat region on the surface that extends around the entire circumference. This layer was 200-500µm deep and reflects dynamic embrittlement during the fatigue test where air changes the fracture morphology and presumably

increases the crack propagation rate. Characteristically for LCF, there are multiple initiation sites joined by ratchets and a large area of overload in the middle of the sample. A half penny shape initiation site is clearly shown (arrow). The 200-500 μ m outer layer was caused by dynamic embrittlement because the secondary cracks due to interstitial embrittlement (cyclic exposure) were only 18 μ m deep similar to the RT sample. At 426°C, the cross-section had a similar morphology and fracture surface to the sample tested at 648°C.

Cermet coated unexposed alpha-2 sample cross-sections tested at 0.8% strain are shown in Figures 259 and 260. The sample tested at RT shows cracking associated with cermet/coating interface. One micrograph shows evidence that the cracking may be a form of internal oxidation in prior β grain boundaries. The fracture surface shows surface initiation and a circumferential flat region corresponding to the coating. The sample tested at 426°C showed 60 μ m cracks in the adherent coating and emanating from grit particles at the cermet/substrate interface. The cracks grow from particles that are embedded the deepest into the alloy presumably because the local stresses were highest. The fracture surface was similar to pre-exposed uncoated alpha-2 tested at 426°C except there were more ratchet marks on the coated sample perhaps indicating easier initiation. The coating was observed as a flat circumferential layer encompassing the region of dynamic embrittlement. The dynamic embrittlement extends from 100-500 μ m deep. This suggests that the coating cracks heavily under the 0.8% tensile strain in many circumferential locations in the same section of the bar. The associated cracking results in rapid crack growth and reduced fatigue capability. It suggests that the strain-to-cracking of this coating system is a very important quantity in connection with fatigue life. The cross-section of the sample tested at 648°C shows several large cracks as well as 5-10 μ m cracks at the coating/substrate interface. The coating was adherent. The fracture surface shows similar features to the sample tested at 426°C except the embrittlement was not as deep. The shallower embrittlement zone maybe the result of stress relaxation at crack tips as temperature increases. The maximum stresses tested here were from 95-120 ksi which may be high compared to where designers are planning to apply alpha-2 and similar materials.

Cermet coated cyclically exposed alpha-2 samples tested at 0.8% strain are shown in Figures 261 and 262. The sample tested at RT failed at 172 cycles because the coating came off. The micrographs show coating separation at the substrate/coating interface with only shallow cracking at the surface. The sample tested at 426°C had an adherent coating but many deep secondary cracks. Many of the cracks emanate from a singular origin while others concentrate in the coating substrate reaction zone. The fracture surface shows large regions of dynamic embrittlement 300-800 μ m deep. The sample tested at 648°C and shown in Figure 262 was similar to structures observed in other tests. The cross-sections show the microcracking of the reaction layer and very large secondary cracks that extend through nearly half of the radius. The fracture surface was similar to the unexposed cermet tested at the same temperature. The results and structures indicate that a greater effort needs to be made to stop the coating from cracking either by improved processing or by lowering loads.

Only one sample with the W CVD diffusion barrier and cermet coating was tested. It was unexposed and tested at RT at a strain of 0.8%. The coating did not maintain adhesion and the sample failed in 523 cycles. The micrographs are shown in Figure 263. The W CVD barrier has been discussed and is not recommended for alpha-2.

2.4 Task 4 - Coating Performance Under TMF

2.4.1 Optimized Cermet Coating Procedure

Tensile and fatigue results indicated that the cermet coating processing on gamma and alpha-2 needed to be optimized to limit exposure to gas species and temperature that cause embrittlement. The items targeted were 1) masking, 2) preheating, and 3) coating densification.

The masking material used for Task 3 samples was a low C steel tape. Figure 264 shows a picture of the tape. A switch to commercially pure (CP) Ti tape was made for the coating of Task 4 samples. The CP Ti was chosen because of compatibility with alpha-2 and gamma substrates.

An experimental matrix was performed on alpha-2 and gamma substrates to determine the minimum number of preheat passes and stroke length necessary to guarantee coating adhesion on a Ti-aluminide substrate in the LPPS chamber. Adhesion was tested by glass bead peening to 18-20N. Figure 265 shows the microstructures for various preheat cycles. The best adhesion was shown by a sample that had 15 preheat passes with a stroke length of 16".

The plasma spraying of NiCrAlY and alumina likely involves the incorporation of porosity. Regions of high porosity weaken the coating and lower the strain-to-cracking. To improve the cermet coating density, it was glass bead peened to 100% coverage at 18-20N on an Almen strip. The intent was to deform the NiCrAlY in the coating to better seal the alumina. Heat treatment to further densify the peened coating is usually performed at temperatures greater than 800°C. These temperatures might affect bulk stability so the heat treatment was avoided.

The Task 4 cermet coating conditions were:

40%Alumina + 60%NiCrAlY Powder /-400Mesh;
EPI Gun;
Voltage=50;
Amps=1800;
Pressure=60Torr;
Preheat passes=15;
Rotation=320 rpm;
Substrate Traverse=5in/sec; and
glass bead peening to 100% Coverage and 18-20N.

2.4.2 Coating Demonstration on Hardware

The coating conditions selected must be capable of applying the cermet coating to gas turbine hardware. To demonstrate this capability a gamma low pressure turbine blade was coated with the cermet coating. The coated blade is shown in Figure 266 and microprobe results in Figure 267. The coating had an excellent structure with no cracks or large regions of porosity.

2.4.3 TMF Results

Thermal mechanical fatigue (TMF) testing was performed using an out-of-phase cycle. This cycle is the hardest on materials as it involves tension when the material is cold and compression when the material is hot. This might occur in practice if slower cooling or thick Ni-base materials constrain faster cooling or thin Ti-aluminide components. The samples were tested using strain control where the total strain on the sample (mechanical and thermal) was maintained throughout the cycle. The data for the alpha-2 and gamma substrates that were supplied to approximate the thermal strains were:

Alloy	RT Modulus, msi	Peak Temp Modulus, msi	Mean CTE, °F ⁻¹
Gamma	23.7	21	8.5E-06
Alpha-2	16	14.2	6.4E-06

The test was performed by finding a neutral test temperature ~ 482°C (~900°F) and then fan cooling to under 204°C (400°F) under tension in 3-4 minutes. After a 30s hold at this temperature, rapid induction heating occurred to 760°C (1400°F) for gamma and 704°C (1300°F) for alpha-2, where a compressive load was applied to maintain constant strain and held for 30s. The sample was then fan cooled under constant strain within minutes to under 204°C (400°F) to comprise a single cycle. Figure 268 shows hysteresis loops for the three cycles before failure on an uncoated gamma sample.

The results of the TMF testing are shown in Table 30. All samples failed during the tensile part of the fatigue test; therefore, the tension at lower temperatures was most severe as expected. Plots were made of maximum tensile stress at $N_f/2$ versus N_f in order to compare uncoated Ti-aluminide to coated Ti-aluminide. These plots are shown in Figures 269 and 270.

Gamma

Figure 269 shows that uncoated gamma was better than the cermet coated gamma in the test. The tensile stress levels at low temperature were higher than 40 ksi in all tests, even in tests where the total strain was confined to 0%. Confining the samples to 0% total strain means that load was applied to balance the forces exerted by thermal contraction or expansion. LCF results for uncoated gamma from Task 3 showed that fatigue loading at larger stresses at RT and 760°C resulted in run outs of 200,000 cycles; therefore, the additional compression loading and temperature change appears to initiate surface flaws rapidly. An environmental influence may also aid in flaw initiation although not detected. Gamma will likely be applied at lower stress levels, but these tests are a warning that out-of-phase TMF may be a problem.

The low life for the cermet coated gamma was disappointing, but expected from LCF testing under Task 3. During LCF testing, only the sample tested at 760°C with 0.25% strain ran out. The other coated samples failed in relatively few cycles with little secondary cracking which is similar to the TMF results. The improved coating processing may not have sufficiently ameliorate embrittlement effects. One cermet coated sample lasted one full cycle compared to an

uncoated gamma sample lasting 3 cycles at similar stress levels. This result may indicate that the scatter in the test was too large to adequately evaluate the effect of the cermet coating. The large scatter in turn was promoted by testing under severe conditions.

Figure 271 shows some fractography on the uncoated gamma sample that lasted 108 cycles. The fracture was flat and many secondary cracks can be observed normal to the primary stress axis. The major initiation site appeared to be at a large gamma colony at the surface of the sample. The appearance is similar to LCF fractures discussed under Task 3.

Figure 272 shows cross-sections of the same uncoated gamma sample. The micrographs show secondary cracks approximately 50 μ m apart and ~25 μ m deep. The cracks do not follow any observable microstructural feature, which indicates that stress is dominating the fracture process.

Figure 273 shows fractography on the cermet coated sample that survived a quarter of a TMF cycle. The fracture was flat with no secondary cracks in the coating. Again it appears that in the case of the cermet on gamma that only one crack forms and all mechanical and environmental degradation is concentrated along that plane. The micrographs show that the cermet coating has excellent adhesion to the substrate. The micrograph of the coating/gamma interface shows features similar to a low temperature tensile test. One possible failure mechanism is that the higher modulus cermet coating forms a crack in tension that runs to the substrate and exposes fresh gamma to the lab test environment at temperatures lower than 204°C. At these temperatures, moisture in the environment might lead to a dynamic hydrogen embrittlement at the crack tip and rapid failure of the bar. Again the stresses used during testing of gamma were probably too high ($\sigma > 40$ ksi) relative to where gamma would be applied (~20 ksi) and a gentler TMF cycle might be explored for the cermet coating on gamma.

Alpha-2

Figure 269 shows that uncoated alpha-2 was better than cermet coated under the TMF conditions used here. In contrast to gamma, a useful number of cycles were achieved for alpha-2, indicating a greater resistance to out-of-phase TMF degradation. As in the case of gamma, both coated and uncoated alpha-2 failed during the tensile portion of the test at low temperature. The alpha-2 showed the expected correlation between the maximum tensile stress and the cyclic life, i.e. higher cyclic stress caused lower life. Perhaps most significantly, the cermet coating did not degrade the life as much as was found in LCF testing. In LCF testing, coated samples lowered lives by two-orders of magnitude. Using the "improved" cermet coating under more severe TMF testing reduced the life only by ~50%, which has to be considered a big improvement.

Figure 274 shows fractography on the uncoated alpha-2 sample that went 1508 cycles. Secondary cracks are observed on the side of the specimen. The low magnification of the cross-section shows three origins with a typical "thumbnail" shape. High magnification at one of these origins shows a flat region with a small amount of oxidation.

Figure 275 shows cross-sections of the same sample. An array of secondary cracks observed was at the surface with a depth of ~5 μ m and a spacing of ~15 μ m. The cracking appears independent of the phases in the alpha-2 but, backscattered imaging at high magnification shows a

region $\sim 5\mu\text{m}$ deep at the surface which may indicate interstitial enrichment of oxygen and nitrogen. The depth of enrichment was nearly equivalent to the crack depth.

Figure 276 shows fractography on the cermet coated alpha-2 sample that went 952 cycles. The side view of the surface shows secondary cracks in the coating and a region where the coating has spalled. The fracture surface shows that $\sim 85\%$ of the coating remains in contact with the alpha-2. A region of flat fracture exists in the alpha-2 immediately underneath the coating. Higher magnification shows that the embrittled region is $100\text{-}125\mu\text{m}$ thick and contains microstructural fatigue features (arrows) that have a $4\text{-}5\mu\text{m}$ spacing. A simple calculation shows that if one of these features is caused by one TMF cycle, then only 30 cycles would be needed to form a critical flaw (assumed to be $125\mu\text{m}$) that would propagate to failure. This indicates that flaw initiation dictates life in the out-of-phase TMF testing. The cermet coating apparently allows faster flaw initiation perhaps due to a higher modulus resulting in higher stresses in the coating per unit strain leading to coating failure in tension. In the future, the modulus and thermal expansion mismatch might be better balanced in these cermet coatings.

Figure 277 shows a cross-section of the same cermet coated alpha-2 sample. The micrographs show cracking of the cermet coating and of the substrate. In the cermet, cracks are observed to run through the coating thickness and either deflect at the coating/substrate interface leading to coating spallation or penetrate into the alpha-2. Penetrations into the substrate were often located at grit particles used to prepare the surface for application of the cermet. These cracks were about $60\text{-}75\mu\text{m}$ deep which is somewhat shallower than the $100\text{-}125\mu\text{m}$ thick flat fracture zone. No region on interstitial embrittlement comparable to the uncoated alpha-2 was observed at the coating/substrate interface. It is not clear if the coating is keeping interstitials out or if the length of exposure was less due to a failure at fewer cycles.

2.5 Coating Recommendations

The cermet coating examined under this contract had excellent oxidation and hot corrosion resistance which was demonstrated in the burner rig to temperatures of 900°C . The hot salt stress corrosion (HSSCC) resistance of the coating was demonstrated on both gamma and alpha-2 substrates at temperatures between 398°C and 760°C . The trade-off for the better environmental performance was a degradation in UTS, ductility and low cycle fatigue capability. On the other hand, the coating improved creep resistance on both substrates. The reduction of fatigue capability is not a surprise under the low cycle conditions examined under this program where a crack is quickly initiated in the coating. The cermet coating, however, would likely survive high cycle fatigue testing at lower stress and strain. The better behavior in HCF was suggested on the gamma substrates when runouts were observed at lower peak tensile stresses ($<42\text{ ksi}$). It is recommended that HCF testing be performed on the cermet coated gamma and alpha-2 using load control at an array of temperatures to further substantiate the above statements. The recommended cermet coating is applicable to components that operate at high temperatures ($T > 704^\circ\text{C}$ or 1300°F) and low stresses (50% of the materials yield strength) in or out of the gas flow path. A USAF/GEAE coating patent has been applied for using data produced by this contract.

The final recommended coating for Ti-aluminides is a LPPS mixture of 40-50% by volume alumina with the remainder Ni-20Cr-10Al-0.3Ywt%. The coating should be 50-75 μ m thick. The best results were obtained with a -400Mesh powder mixture. One change that might be performed is switching the NiCrAlY to a FeCrAlY to perhaps impart more ductility to the coating for enhanced tensile and fatigue properties. In addition, the modulus of the coating might be altered by substituting a different metal or ceramic component to reduce coating stress when the substrate is being strained. The TMF results in Task 4 indicated that masking, preheating and peening are potential areas for further performance enhancement.

3.0 Summary

The summary remarks for this contract are classified according to the work performed under each task. The net result of the contract was that a cermet coating was demonstrated on both gamma and alpha-2 Ti-aluminide alloys that protects them from environmental attack. Mechanically speaking, the cermet coating lowers properties at high stress levels and improves properties at low stress levels.

Task 1.

- 1) The base alpha-2 alloy selected and approved for the program was forged and heat treated Ti-24.5Al-12.5Nb-1.5Mo in atomic percent.
- 2) The base gamma alloy selected and approved for this program was forged and heat treated Ti-48Al-2Cr-2Nb in atomic percent.
- 3) Coating systems applied were cermet coatings, yttria-stabilized zirconia, TiCrAl, CoCrWSiC, modified gamma Ti-aluminide and Alloy 718. Coating deposition methods were thermal spray and sputtering.

Task 2 Iteration #1.

Cyclic Oxidation Results:

- 1) All coating candidates on the gamma (Ti-48Al-2Cr-2Nb) in the 1000 hr 760°C (1400°F) cyclic oxidation test provided oxidation protection as measured by weight change/area. The uncoated gamma exhibited some oxide spallation and thicker oxide scales. Coated samples formed reaction layers with the gamma, but had little oxide or coating spallation. Coatings selected for further evaluation in cyclic hot corrosion and oxidation (CHC/O) and hot salt stress corrosion cracking (HSSCC) tests were 1) low pressure plasma sprayed 50%Ni-23Cr-12Al-Y (atomic %) and alumina, 2) air plasma sprayed yttria (weight %) stabilized zirconia, and 3) sputtered Ti-44Al-28Cr.
- 2) All coating candidates on the alpha-2 (Ti-24.5Al-12.6Nb-1.5Mo) in the 1000 hr 760°C (1400°F) cyclic oxidation test provided protection as measured by weight change/area. The uncoated alpha-2 exhibited oxide spallation in contrast to the candidate coatings. Coatings selected for further evaluation in CHC/O and HSSCC tests were 1) air plasma spray Alloy 718, 2) low pressure plasma sprayed modified gamma (Ti-48Al-2Cr-6Nb-0.1B in atom %), and 3) sputtered Ti-44Al-28Cr (atomic %).
- 3) Sputtered TiCrAl coatings were prone to thermal expansion mismatch cracks especially on the alpha-2 substrate. The sputtered TiCrAl coatings, however, showed desirable thin protective alumina scales. The surfaces of these coatings appeared tinted throughout the test. Thermally sprayed Ti-44Al-28Cr coatings performed much better at 760°C (1400°F) than at 900°C (1650°F) because less TiO₂ was formed.
- 4) Cermet coatings were not observed to crack on either alpha-2 or gamma substrates. The mixture of alumina and an environmentally resistant MCrAlY leads to excellent oxidation

protection and favorable thermal expansion mismatch between the coating and the particular Ti-aluminide substrate.

- 5) Little interstitial penetration was observed on coated or uncoated gamma alloys.

Burner Rig Results:

- 1) The 648-760°C (1200-1400°F) high pressure compressor CHC/O test with periodic salt injection was performed on selected coatings for gamma substrates. The uncoated gamma showed thicker oxides and spallation at temperatures on the pin that exceeded 732°C (1350°F). Coating spallation was observed on the APS YSZ sample. Through-thickness coating defects were observed in the sputtered Ti-44Al-28Cr coating, but did not penetrate into the substrate. The cermet coating had little degradation and performed the best in the test.
- 2) The high pressure compressor CHC/O test was performed on the selected coatings for alpha-2 substrates. The uncoated alpha-2 showed locally thick oxides and spallation at temperatures greater than 675°C (1250°F). The air plasma sprayed Alloy 718 and sputtered Ti-44Al-28Cr coatings had thermal fatigue cracks that penetrated the substrate and failed the test. The modified gamma coating did not exhibit cracking and, therefore, passed the test.
- 3) The 760-900°C (1400-1650°F) low pressure turbine CHC/O test with continuous salt injection was performed on selected coatings for gamma alloys. The uncoated gamma sample showed thick loose scales and evidence of lath attack and sulfidation. The APS YSZ and sputtered Ti-44Al-28Cr coatings spalled off the substrate during the test. The cermet coating showed little evidence of degradation by the exposure and was clearly superior.
- 4) The low pressure turbine CHC/O test was performed on the selected coatings for alpha-2. At the highest temperature, the uncoated alpha-2 sample was severely degraded and formed thick unadherent oxide scales with no interstitial layer. The APS Alloy 718 coating was totally consumed by the environment, while the modified gamma and Ti-44Al-28Cr coatings were intact. Metallography revealed that thermal fatigue cracks had formed in the sputtered Ti-Cr-Al coating while none formed in the modified gamma coating. The cracking behavior indicated that the modified gamma coating was the best in this test because of a more favorable thermal expansion mismatch with the alpha-2.
- 5) Uncoated Ti-aluminides were more resistant to hot corrosion attack in the low pressure turbine CHC/O test than uncoated Ni-base superalloys. The better resistance is related to the absence of liquid reaction products on the Ti-aluminides.

HSSCC Results:

- 1) Uncoated gamma exhibited a reduction in tensile properties after a salt free stress exposure. The fracture surfaces were flatter with less tearing when compared to an

unexposed sample. The embrittlement of uncoated gamma did not manifest itself as a set of secondary tensile cracks. Instead relatively few (compared to alpha-2) cracks were found whose depth roughly correlated with time and temperature of the exposure. A complicated embrittlement phenomena may occur in gamma where fewer cracks extend to greater depths.

- 2) Uncoated gamma after the 565°C (1050°F) 40 ksi/750 hr HSSCC exposure had no strength illustrating a need for protective coatings. A thick contaminant modified Ti-rich oxide formed on the external surface of the gamma with 25µm of attack in the substrate. The coated samples all survived this exposure without a loss of strength. Typically coated samples had more retained strength than the bare gamma but, more testing is needed to validate the statistical significance. Metallography revealed little substrate attack in coated samples.
- 3) Alpha-2 is susceptible to interstitial embrittlement. The stressed exposures without salt resulted in a reduction in tensile properties but, were not severe enough to cause rupture. The fracture surface of exposed alpha-2 was more planar with less tearing than that of an unexposed sample. The interstitial embrittlement could be observed by examining the secondary tensile cracks after a prolonged exposure. The secondary tensile cracks had a constant depth and distribution. Using simplistic diffusion theory, the activation energy of diffusion for the embrittling species was calculated to be ~20.5KCal/mol. This value is consistent with extrapolated values of the activation energy for oxygen diffusion in β-Ti which may be part of the embrittlement mechanism.
- 4) HSSCC embrittlement of alpha-2 was much more severe than interstitial embrittlement and led to a rapid deterioration in mechanical properties with most samples failing during the stressed salt exposure. Uncoated samples failed in under 40h at 565°C (1050°F) 40 ksi, indicating that an environmental coating is needed if this alloy is applied in salt rich environments. Salt was found to accelerate the oxidation of the external surface by forming contaminant modified Ti-rich external scales. Internally the attack preferred primary alpha-2 islands and alpha-2 precipitates along prior β grain boundaries. Chlorine was typically associated with these attacked regions. The TiCrAl and modified gamma coatings were mostly unprotective due to cracking of the coating which allowed ingress of salt. The deformation rate of materials undergoing HSSCC was greater than those exposed in salt free environments most likely due to the accumulation of crack opening displacements near the surface and creep at higher stress on remaining material. The data indicate that the embrittlement was more severe at 565°C (1050°F) 40 ksi than at 398°C (750°F) 50 ksi. The only coating composition successful in prohibiting gross HSSCC was the air plasma sprayed Alloy 718.

Task 2 Iteration #2.

Cermet coatings were downselected for the second round of environmental testing in Subtask 2.6. The cermet compositions chosen were various volume fractions of alumina mixed with NiCrAlY, Alloy 718, CoCrAlY and NiCoCrAlY. The volume fraction was chosen such that thermal

expansion mismatch was minimized between the coating and substrate at temperatures where the substrate behaves as a brittle solid.

Burner Rig Results:

- 1) A burner rig test was performed using a 760°C/648°C cycle with 1ppm of sea salt continuously injected into the combusted gas for 3749 cycles or 625 hot hours. Uncoated substrates showed attack in regions of the pin that exceeded 660°C, with $\gamma < \alpha\text{-}2 < \text{Hast X}$. Composite coatings on the Ti-aluminides in the same test showed excellent environmental resistance with no thermal fatigue cracks. The only exception was the CoCrAlY composite coating on $\alpha\text{-}2$ which showed cracking.
- 2) A reaction or interdiffusion zone develops between the MCrAlY component of the composite coating and the Ti-aluminide during coating deposition and high temperature exposure. Equations were developed to describe the growth of this zone. These equations are:

$$(x-x_0) = 20464 * \exp(-8320/T) \mu\text{m} \quad (1)$$

$$k = 1.8 \times 10^{-6} * \exp(-16640/T) \frac{\text{cm}^2}{\text{sec}} \quad (2)$$

where x is thickness of zone, T is temperature in Kelvin and k is a parabolic growth rate constant. The activation energy of 33KCal/mol is near values determined for interdiffusion in NiAl and TiAl. The reaction zone is important because it is comprised of intermetallic compounds that were observed to crack easily during sample preparation. A W diffusion barrier between the substrate and coating was attempted to reduce the impact of this zone on mechanical properties in Task 3.

- 3) A burner rig test was performed using a 871°C/760°C cycle with 2ppm of sea salt continuously injected into the combusted gas for the first 50 hrs and 1ppm thereafter, for a total of 3000 cycles or 516 hot hours. Salt deposition was consistent between the two salt injected burner rig tests. Uncoated substrates showed attack in regions where temperatures exceeded 704°C, while the composite coatings showed visual attack at $T > 825^\circ\text{C}$. Composite coatings on the Ti-aluminides showed less attack than a pack aluminide coated Rene'80. The composite coatings showed some thermal fatigue cracking which was especially apparent on the CoCrAlY-based coatings. Cracking on the NiCoCrAlY and Alloy 718 coatings on gamma did not penetrate into the substrate.
- 4) Comparing the 900/760°C iteration #1 burner rig test to the 871/760°C iteration #2 test shows the effectiveness of adding alumina to reduce expansion mismatch between the MCrAlY-type coatings and Ti-aluminide substrates. The air plasma sprayed Alloy 718 coating in iteration #1 spalled from the $\alpha\text{-}2$ substrate after only 50 hr of testing. In iteration #2, the low pressure plasma sprayed Alloy 718 + alumina composite coating remained protective with no spallation for over 500 hr.

- 5) A burner rig test was performed using a 900/760°C cycle with no salt for 1778 cycles, and thereafter only the 900°C part of the cycle was continued for a total of 4417 cycles or 516 hot hours. The uncoated alpha-2 and R'80 showed visible degradation at $T > 745^{\circ}\text{C}$, while the uncoated gamma alloy showed degradation at $T > 704^{\circ}\text{C}$. A 25µm metal loss in 1000 hr criteria places the coating temperature for gamma at 830°C. The Codep coated R'80 and the composite coatings performed excellently and only showed visual degradation at $T = 900^{\circ}\text{C}$.

Cross-sectional analysis of the hot section of the pin revealed thick, layered scales on uncoated alpha-2, 30µm intergranular attack on bare R'80 and 50µm scales on bare gamma. The composite coatings on alpha-2 did not show signs of TF cracking and good integrity was maintained throughout the test. The pack aluminide coated R'80 showed very little environmental attack and no cracking. The composite coatings on gamma resisted environmental attack, but exhibited some cracking. The cracking in the case of the CoCrAlY and Alloy 718-base coatings appeared to be related to thermal fatigue, while cracking on the NiCoCrAlY-based coating may have been due to sample preparation. Oxidation in the crack was the major tool in determining which type of crack occurred.

HSSCC Results:

Hot salt stress corrosion cracking tests were completed for Subtask 2.6. For alpha-2, only the 60%NiCrAlY + 40%Alumina cermet coating survived the 565°C (1050°F) 40 ksi/750 hr HSSCC exposure. In addition, the sample had good strength (148 ksi) as measured by a RT tensile test. For gamma, all the cermet coated samples survived the 565°C (1050°F) 40 ksi/750 hr exposure, but failed outside the gage during the post-exposure RT tensile test. The failure away from the salt deposits may indicate good resistance of the coating to HSSCC.

Downselected Coating.

The downselected coating system for both gamma and alpha-2 for Task 3 was a 60vol% Ni-20Cr-10Al-0.3Ywt% + 40vol% alumina. The system was applied using low pressure plasma spray. A W diffusion barrier applied by chemical vapor deposition was attempted in an effort to reduce reaction with the substrate.

Task 3 Mechanical Testing.

Tensile Results:

- 1) Tensile results for coated gamma indicated that the trade for improved high temperature environmental resistance involves a reduction in ultimate tensile strength and ductility. The reduction in tensile properties might be acceptable if gamma is being applied at temperatures greater than 704°C and stresses well below yield. The cermet coating stopped secondary cracking in the tension tests. The reaction zone between the coating and substrate appeared to be less brittle than the alpha layer found under the oxide scale in uncoated gamma. The CVD W layer was not effective.

- 2) Tensile results for coated alpha-2 indicated that the cermet coating reduces ductility, but may increase strength in thin sections. The cermet coating was also susceptible to spalling when the substrate necks. Since most applications of alpha-2 will involve loading to stresses under yield, it is likely that the cermet coating could be applied with little impact. In addition, the residual ductility of alpha-2 after application is still in excess of 3% over the usable temperature range. Gamma was successfully applied as a LPT airfoil with unexposed RT ductility near 2%. The CVD W barrier was not effective due to oxidation and overcoat sealing problems.

High Temperature HSSCC Results:

- 1) The uncoated gamma underwent a creep deformation of 20% during the 760°C/20 ksi/500 hr exposure. A sample cyclically exposed at 760°C/100 hr prior to the test ruptured at 499.6 hr. Cermet coated samples all survived the 500 hr creep exposure regardless of pre-exposure and showed creep deformations of only 10%. The large reduction in creep deformation indicates that the cermet coating is preventing deformation that is dependent on surface cracking. The W diffusion barrier was not effective.
- 2) The 760°C/10 and 20 ksi creep condition was below the threshold for hot salt stress corrosion cracking observed in Task 2. The 20 ksi condition resulted in rupture failures, while all samples loaded at 10 ksi survived 500 hr. Salt deposits lowered both the time to rupture and the residual tensile properties. The cermet coating improved the creep resistance of alpha-2 in environments with and without salt. The cermet coating should be considered on applications of alpha-2 at $T > 704^{\circ}\text{C}$ where creep is a limiting property and environmental attack can occur. The W diffusion barrier was not effective.

Fatigue Results:

Gamma

- 1) The fatigue life of the baseline uncoated Ti-48Al-2Cr-2Nb was excellent. Unexposed gamma ran out (200,000 cycles) at strains of 0.4% at $A=1$ at all test temperatures (22, 568, and 760°C). These stresses were equivalent to 50 ksi and larger. Exposed gamma (760°C/100 hr in air) had reduced fatigue capability. Nonetheless, exposed gamma material at all temperatures survived a cyclic tensile stress of lower than 41 ksi.
- 2) Fatigue strength is a mechanical property that is very sensitive to surface flaws and condition. The samples used to generate the uncoated gamma data had a 8 μin finish (polished). The application of the cermet coating involved a grit blast to roughen the samples which could have reduced the fatigue life of gamma. The cermet coating grit blast treatment was tested on unexposed uncoated gamma and no effect was observed on fatigue properties at 22 or 760°C.
- 3) Unexposed cermet coated gamma was tested at 22 and 760°C. The fatigue life was reduced drastically when stresses were higher than 42 ksi. One runout was observed at 0.25% total strain (41.5 ksi max. stress) at 760°C indicating that the coating is best

applied in components stressed below this value. High cycle fatigue data for this coating at lower stress levels is needed.

- 4) Exposed coated gamma was tested at 568 and 760°C. Poor fatigue properties relative to uncoated gamma were observed at high strain ranges (0.4%). One sample tested at 568°C and 0.25% strain was headed for a runout before a thread failure occurred. The maximum stress for this sample was 44.7 ksi. Uncoated exposed gamma showed a fatigue reduction at 50 ksi and a runout at 41 ksi, therefore, the coated sample may have similar fatigue properties.
- 5) The W CVD cermet coated samples both performed poorly. At 22°C, the sample failed after 2 cycles. The only thermal exposure this sample had was during coating processing. The sources of property reduction are H embrittlement during the CVD deposition and vacuum exposure during the preheat cycle for cermet application. When tested at 760°C, the coating spalled from the substrate after 5168 cycles.

Alpha-2

- 1) Uncoated unexposed alpha-2 (Ti-24.5Al-12.5Nb-1.5Mo) tested at RT, 426°C and 648°C and a total strain of 0.8% ranout at a cycle count of 200,000 or greater. The maximum stress level corresponding to the strain was 98 ksi at 648°C to ~125 ksi at RT. Data on unexposed 14-21 alpha-2 (Ti-24Al-11Nb) at much lower stresses (35-75 ksi) indicated a life of 27,000 to 55,000 cycles.³⁷ This shows the superiority of the 12.5-1.5 composition and processing. The excellent behavior of the alpha-2 was also observed for samples receiving the same grit blast as the cermet coated samples.
- 2) Exposing the uncoated alpha-2 reduced the fatigue capability to 300-5000 cycles at strain levels of 0.6-0.8% (75-115 ksi max. stress). The reduction is the result of oxidation and interstitial dissolution. Additionally the possibility of microstructural aging from the exposure can't be ignored. The data produced here were similar to the 14-21 referenced above where a similar exposure resulted in lives between 2000 and 6000 cycles.
- 3) The cermet coatings did not improve the fatigue behavior of the alpha-2 alloy. In the exposed and unexposed condition, the life of the coatings tested at 0.6-0.8% strain was from 300-3500 cycles. The similarity in cycle count to the cyclically exposed uncoated alpha-2 cannot be overlooked. It appears that the coating or coating processing has the same effect as the environmental exposure. This is possible because the LPPS process involves preheating to temperatures near 704°C and the CVD W process was performed at 740°C. The cermet coatings were generally adherent to the alpha-2 except when the CVD W was present or when the sample was coated and tested at RT and necked. Fatigue tests at lower stress levels are needed on coated alpha-2 samples.

Task 4 Thermal Mechanical Fatigue Testing.

- 1) Tensile and fatigue results from Task 3 indicated that the cermet coating processing on gamma and alpha-2 needed to be optimize to limit exposure to gas species that might

cause embrittlement. The items targeted were 1) substrate masking, 2) substrate preheating, and 3) cermet coating densification through peening.

- 2) The selected cermet coating structure was applied to a cast gamma Ti-aluminide low pressure turbine blade demonstrating the ability to coat actual engine components.
- 3) Out-of-phase thermal mechanical fatigue tests were performed on coated and uncoated gamma Ti-aluminide. The TMF was controlled by maintaining strain (thermal + mechanical) constant between temperatures of 760°C and under 204°C from a neutral temperature of ~482°C. Strain levels of 0.3 and 0% resulted in tensile stresses greater than 40 ksi during the lower temperature part of the cycle and failures resulted at low cycle counts. Uncoated gamma generally had larger cycle counts than cermet coated gamma, but no cycle count exceed 108. The difference may have been that the higher modulus coating cracked revealing fresh metal and moisture induced embrittlement. The scatter in the data, however, may not have allowed a true comparison to be made between coated and uncoated gamma. Out-of-phase TMF may be a large consideration in the application of gamma alloys.
- 4) Out-of-phase thermal mechanical fatigue testes were performed on coated and uncoated alpha-2 Ti-aluminide. The tests were run in the same fashion as the gamma except the peak temperature was 704°C. In the case of alpha-2, usable data were obtained that correlated nicely with the peak tensile stress experienced during the low temperature part of the cycle. For these TMF tests, it appeared that the coating reduced the cyclic life of the sample by 50% at constant stress levels. This is a great improvement compared to the 2 order of magnitude reduction of coated alpha-2 observed during LCF tests. The improvement may be related to optimized coating processing.

Ti-Aluminide Environmental Coating Recommendation

The final recommended coating for Ti-aluminides is a LPPS mixture of 40-50% by volume alumina with the remainder Ni-20Cr-10Al-0.3Ywt%. The coating should be 50-75µm thick. The best results were obtained with a -400Mesh powder mixture. One change that might be performed is switching the NiCrAlY to a FeCrAlY to perhaps impart more ductility to the coating for enhanced tensile and fatigue properties. In addition, the modulus of the coating might be altered by substituting a different metal or ceramic component to reduce coating stress when the substrate is being strained. The TMF results in task 4 indicated that masking, preheating and peening are potential areas for further performance enhancement especially on alpha-2.

The cermet coatings still need demonstration under HCF conditions where lower system strains might prevent cracking of the coating. Environmentally, the cermet coatings provide superior resistance to oxidation, hot corrosion and hot salt stress corrosion cracking. A patent application has been made by GE Aircraft Engines for these coatings on Ti-aluminides in which the USAF shares rights.

4.0

References

- (1) Schaeffer, J. C.; McCarron, R. L. "Interim Report - High Temperature Coatings for Titanium Aluminides," GE Aircraft Engines, 1992.
- (2) McKee, D. W.; Huang, S.-C. "Oxidation Resistant Coatings of Gamma Titanium Aluminum Alloys Modified by Chromium and Tantalum," General Electric, 1992.
- (3) Shih, D. S.; Huang, S. C.; Scarr, G. K.; Jang, H.; Chesnutt, J. C. In TMS-AIME: 1991.
- (4) Warlimont, H.; Zingg, W.; Furrer, P. *Mat. Sci. Eng.* **1976**, *23*, 101-105.
- (5) Raman, A.; Schubert, K. *Zeitschrift Fuer Metallkunde* **1964**, *55*, 798-804.
- (6) Schuster, J. C.; Bauer, J. *Journal of Solid State Chemistry* **1987**, *68*, 124-127.
- (7) Welsch, G.; Kahveci, A. In *Oxidation of High Temperature Intermetallics*; TMS: 1989.
- (8) Schaeffer, J. C.; McCarron, R. L.; Meier, G. H.; Perkins, R.; Cullinan, J. F.; Berztiss, D. "Final Report - High Temperature Coatings for Gamma Titanium Aluminide Intermetallics," GE Aircraft Engines, 1995.
- (9) Nic, J. P.; Zhang, S.; Mikkola, D. E. *Scripta Met* **1990**, *24*, 1099.
- (10) Shamblen, C. E.; Redden, T. K. "Surface-Salt Concentrations in Jet Engine Compressors," GE Aircraft Engines, 1972.
- (11) Schaeffer, J. C. *Scripta Met* **1993**, *28*, 791-796.
- (12) Liu, C. T.; Kim, Y.-W. *Scripta Met* **1992**, *27*, 599-603.
- (13) Petersen, V. C. *Journal of Metals* **1971**, *40*.
- (14) Kelly, T. J.; Austin, C. M.; Fink, P. J.; Schaeffer, J. C. *Scripta Met.* **1994**, *30*, p.1105.
- (15) Schaeffer, J. C.; McCarron, R. L.; Smith, G. S. **1993**, 100.
- (16) Gray, H. *Met. Engr. Quarterly* **1972**, 10.
- (17) Liu, Z.; Welsch, G. *Met. Trans.* **1988**, *19A*, 1121.
- (18) Schaeffer, J. C. "Oxygen Diffusion in Titanium Aluminides," GE Aircraft Engines, 1992.
- (19) Bartz, A., M.S. Thesis, Wright State University, 1992.
- (20) Dumas, P.; St. John, C. *Journal Oxidation of Metals* *10*, 127.
- (21) Tobin, A. G. "Barrier Coatings For Oxidation Protection Incorporating Compatibility Layer," Grumman Aerospace Corporation, 1991.
- (22) McKee, D. W. "Oxidation Behavior of Gamma-Titanium Aluminide Alloys," GE Corporate Research and Development Center, 1990.
- (23) McKee, D. W. In *Proceedings of the 5th Symposium on High-Temperature Ordered Intermetallic Alloys*; Materials Research Society: Boston, Ma., 1993; pp 953-958.
- (24) Gibbons, T. B. *Adv. Materials* **1990**, *2*, 583-588.
- (25) Coad, J. P.; Rickerby, D. S.; Oberlander, B. C. *Material Science and Engineering* **1985**, *74*, 93-103.
- (26) Brindley, W. L.; Smialek, J. L.; Rouge, C. J. "Oxidation Resistant Coating For Titanium Alloys and Titanium Alloy Matrix Composites," NASA, 1992.
- (27) Johansen, E. W.; Woodfield, A. P.; Buttrill, W. H. "Mechanical Property Evaluation of IMI 834, Ti 1100, Ti-6242," GE Aircraft Engines, 1992.
- (28) Writer, Staff. In *Aviation Week and Space Technology*; 1993; pp 37.
- (29) Whittle, D. P. *Oxidation of Metals* **1972**, *4*, 171-179.
- (30) *Smithells Metals Reference Book*; Seventh ed.; Brandes; Butterworth-Heinemann Ltd.: London, 1992.
- (31) Ouchi, K.; Yoshiaki, I.; Hirano, K. In *Proceedings of the 4th International Conference on Titanium*; Kyoto, Japan, 1980; pp 559-568.

- (32) Jannsen, M. M. P.; Rieck, G. D. *Transactions of the Metallurgical Society of AIME* **1967**, 239, 1372-1385.
- (33) Austin, C. M. "Interim Report - Gamma Titanium Aluminide Alloy Development," GE Aircraft Engines, 1993.
- (34) Pettit, F. S.; Meier, G. H. "Oxidation Behavior of Gamma Ti-Aluminide," University of Pittsburgh, 1990.
- (35) Schaeffer, J. C.; McCarron, R. L. "Proposal - Environmental Effects and Coatings Assessment for Orthorhombic and Gamma Titanium Aluminide Alloys - Volume 1" GE Aircraft Engines: Cincinnati, Ohio, 1993; pp 68.
- (36) Frost, H. J.; Ashby, M. F. *Deformation-Mechanism Maps*; 1st ed.; Pergamon Press: 1982; Vol. 1, pp 165.
- (37) Barber, M. J.; Hensler, T. H.; Creech, G. E. "Interim Report - High Temperature Coatings for Titanium Aluminides," Allison Gas Turbine Division, 1993.

FIGURES

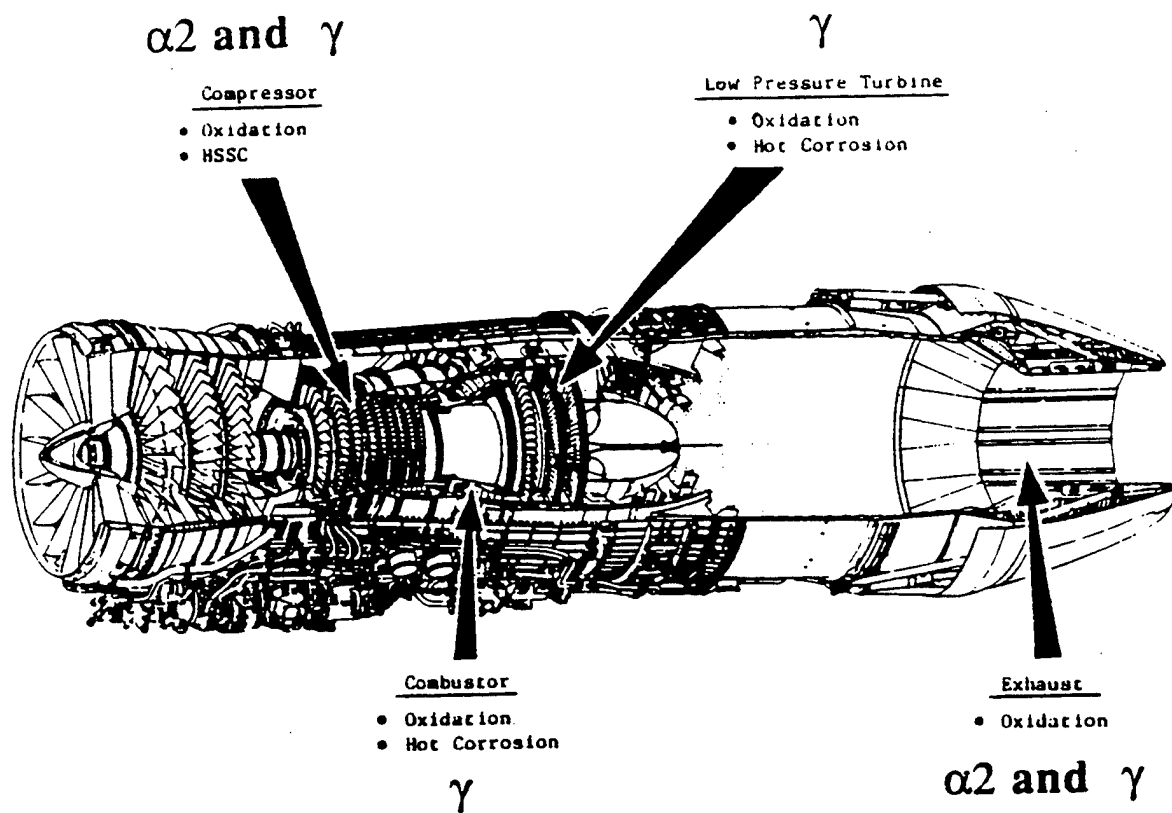


Figure 1. Schematic of gas turbine engine showing the associated types of environmental attack for potential applications of alpha-2 and gamma alloys.

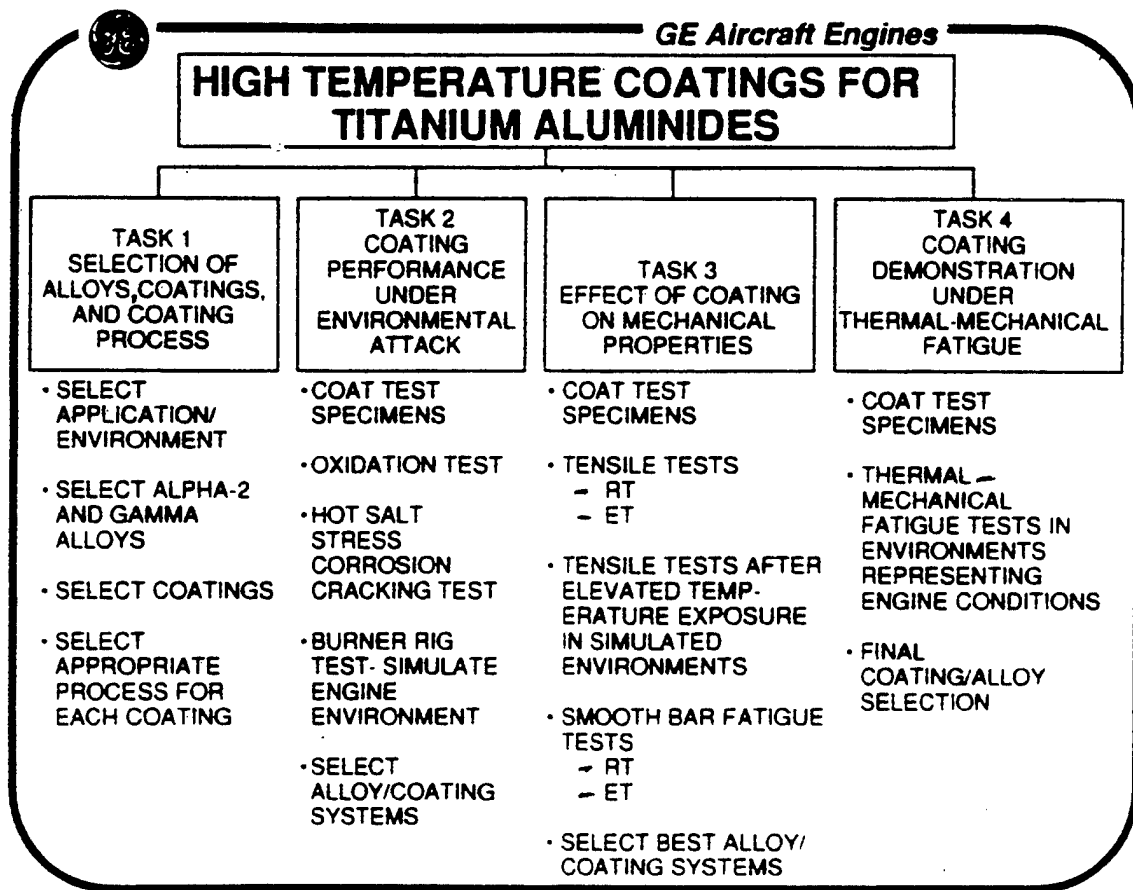


Figure 2. Schematic showing the task structure of the coatings program.

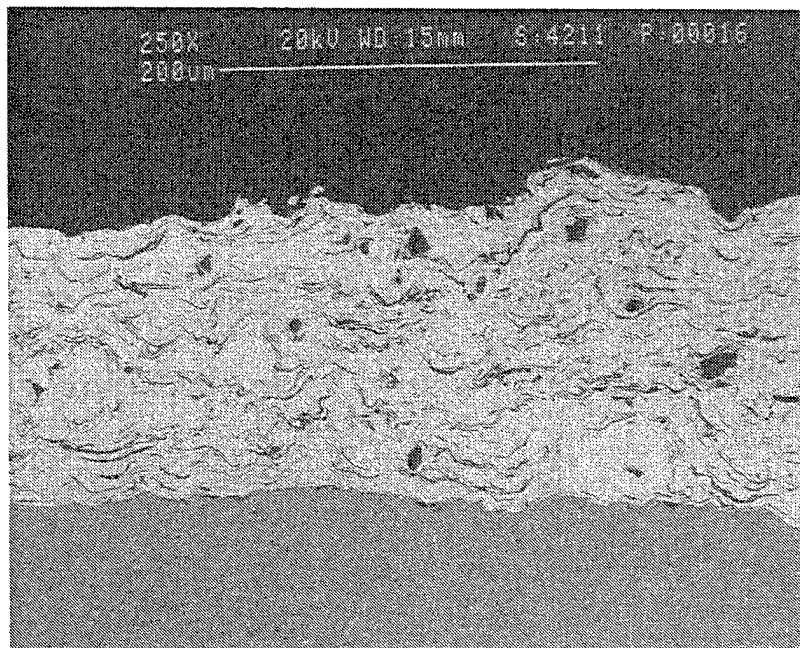
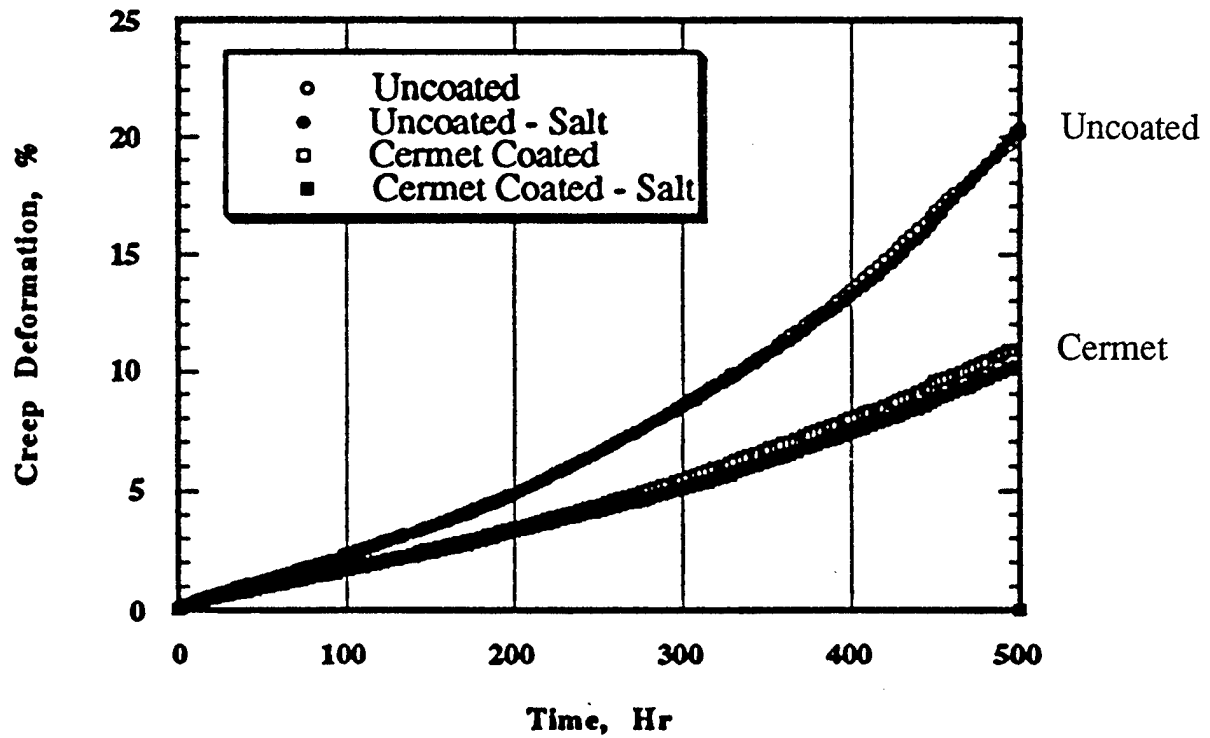


Figure 3. Micrograph of the cermet coating after 500Hr of testing in cyclic hot corrosion/oxidation conditions.

Gamma @ 760°C/20ksi in Air



Alpha-2 @ 760°C/10ksi in Air

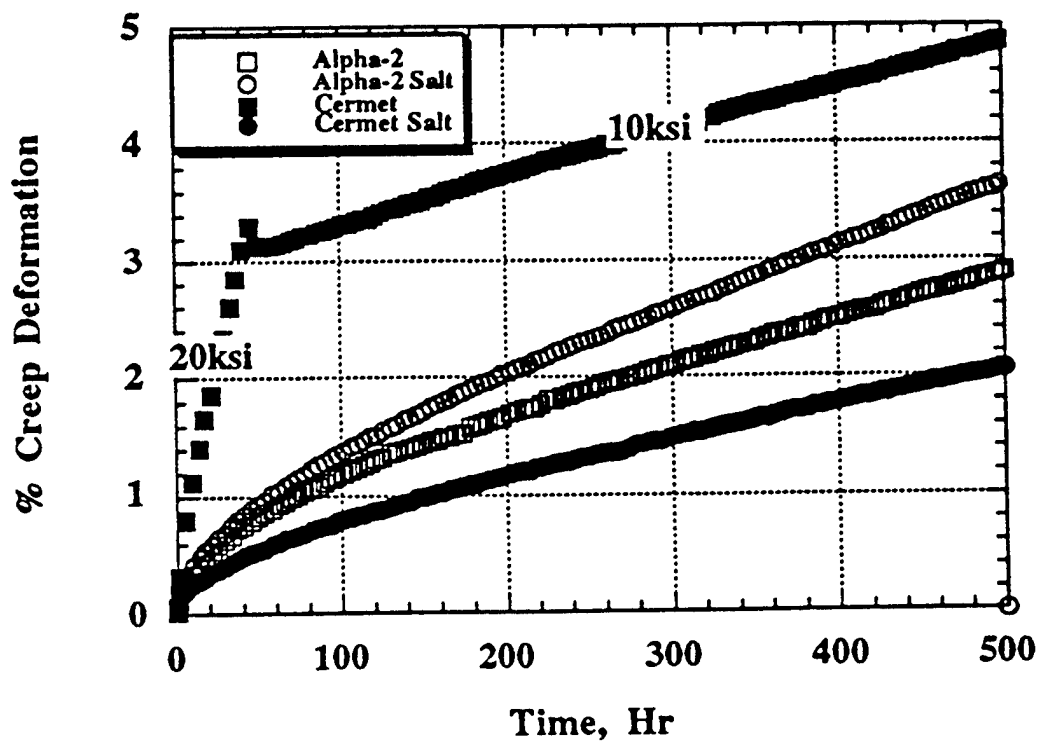


Figure 4. Graphs showing the creep behavior of gamma and alpha-2 substrates with an applied cermet coating.

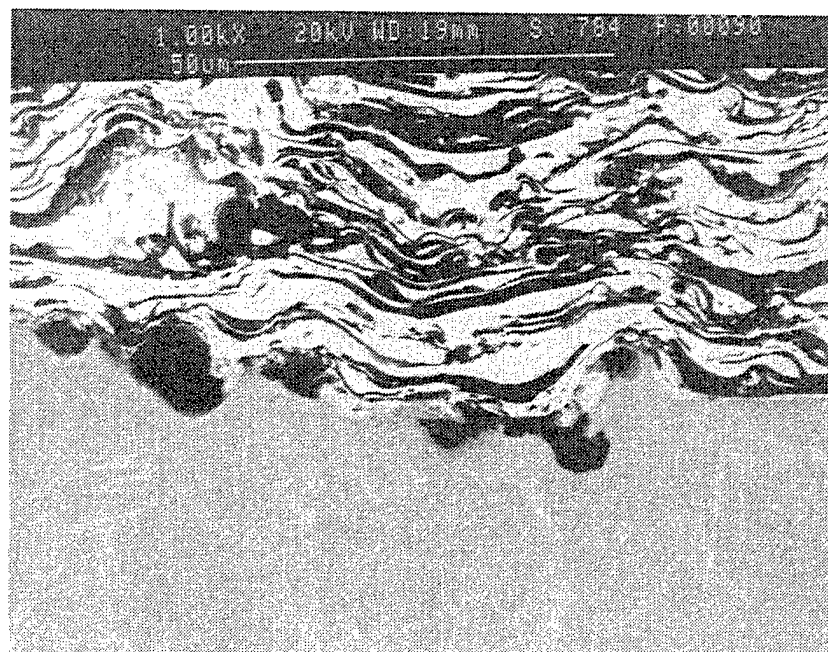
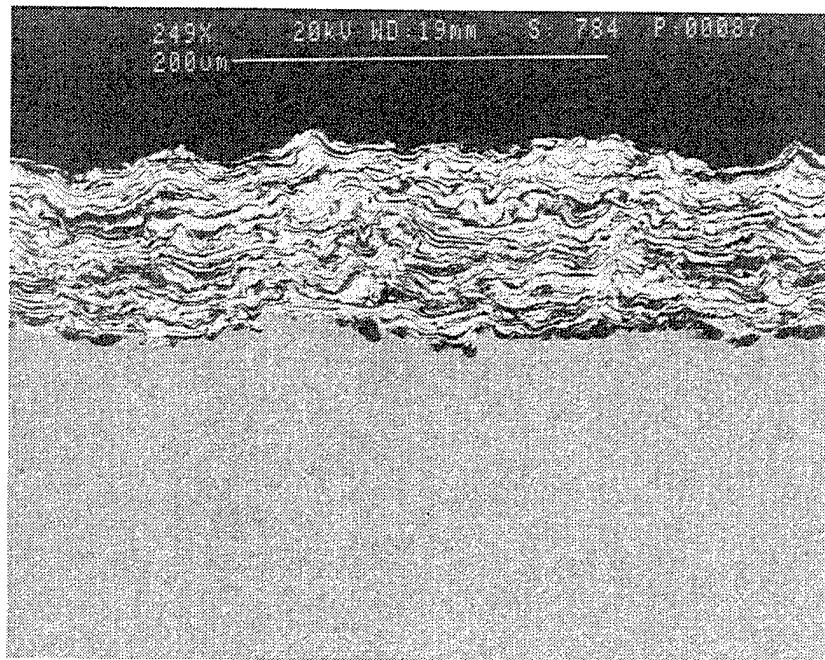


Figure 5. Cross section of cermet coated gamma after runout at 760°C and 0.25% strain control with A=1.

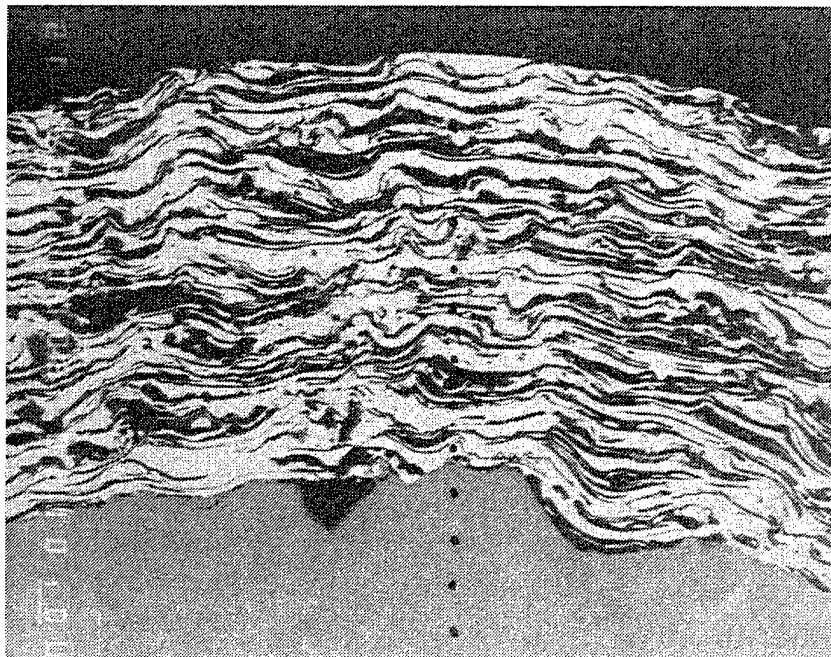
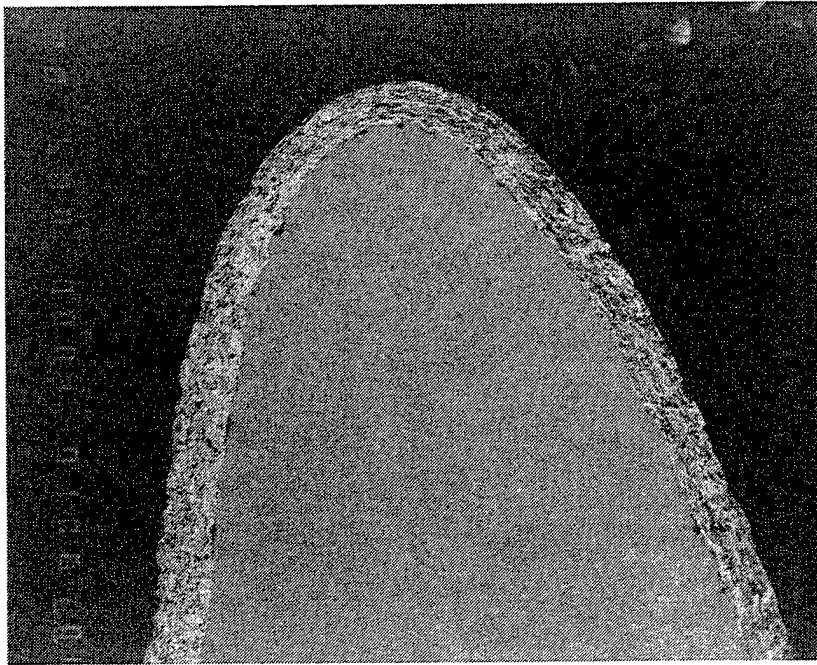
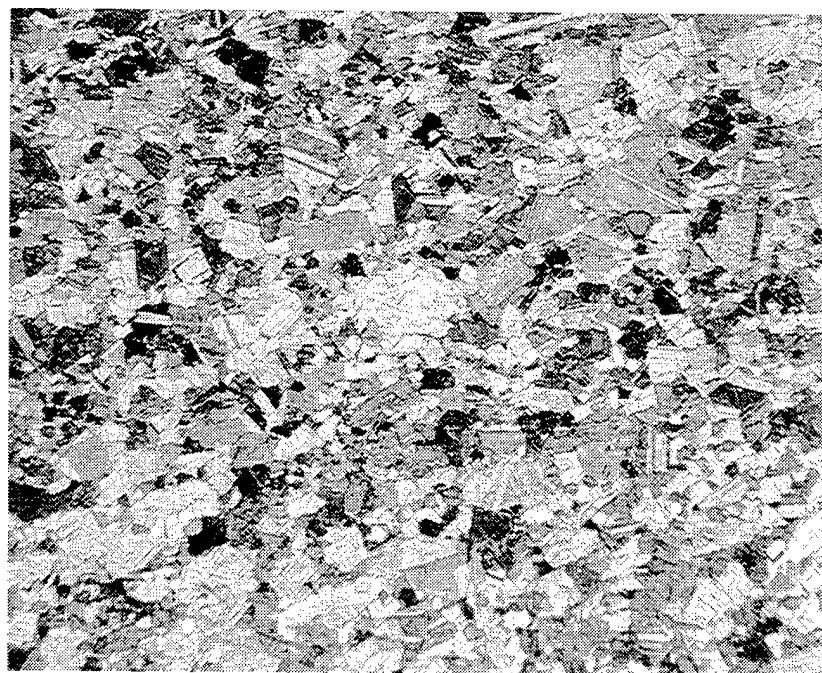


Figure 6. Micrograph of a cermet coated cast gamma low pressure turbine blade (LPTB).



250 μm



50 μm

Figure 7. Optical micrographs showing Ti-48Al-2Cr-2Nb after forging, heat treating and machining. The samples are etched in a solution of 2%HF and methanol.

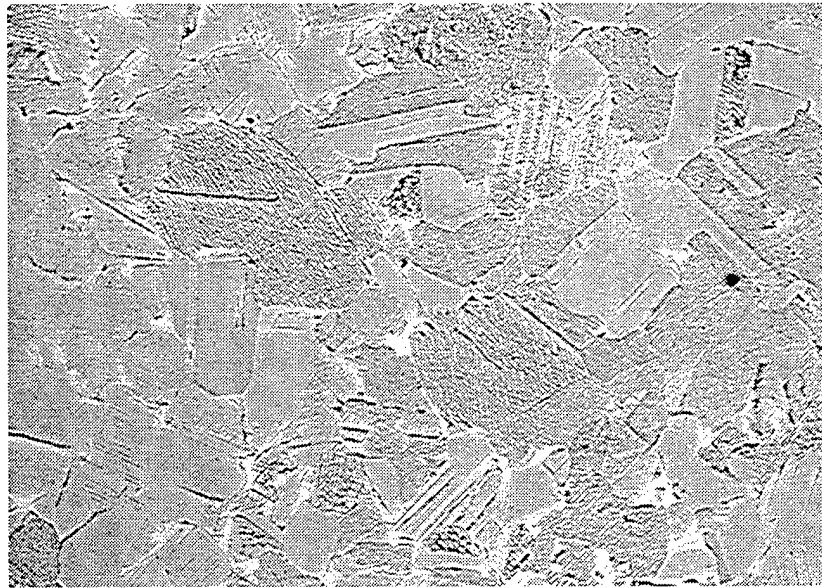


Figure 8. Backscattered electron images (BEI) showing Ti-48Al-2Cr-2Nb after pancake forging and heat treatment. The microstructure is duplex and composed of primary gamma grains and transformed alpha.

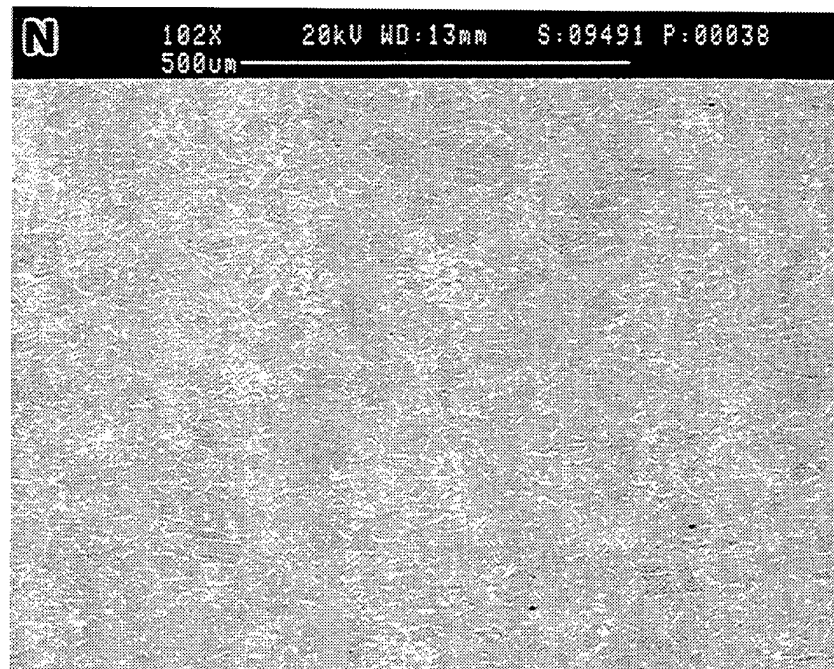
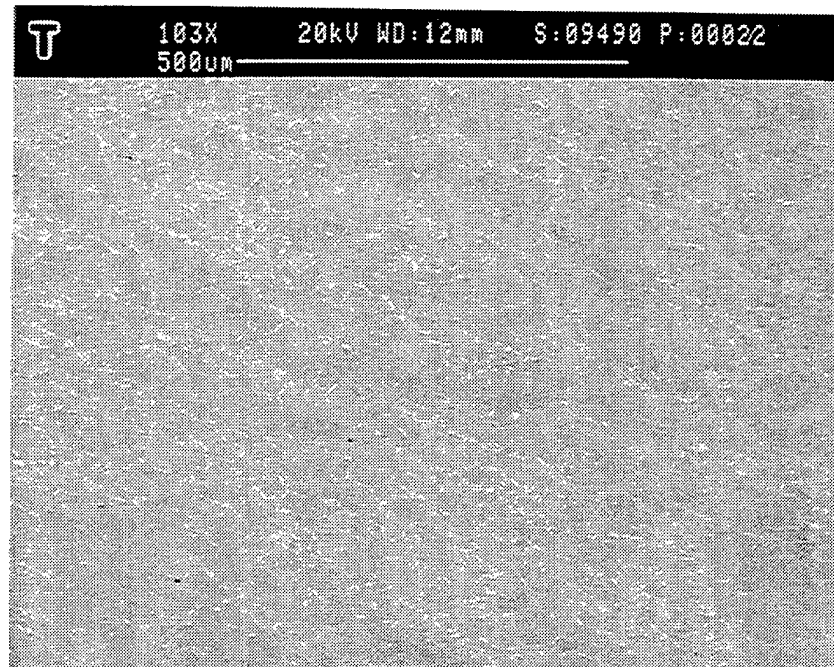


Figure 9. Backscattered electron images (BEI) of Ti-48Al-2Cr-2Nb showing the alignment of phases in the "T" or transverse direction. "N" stands for the normal direction.

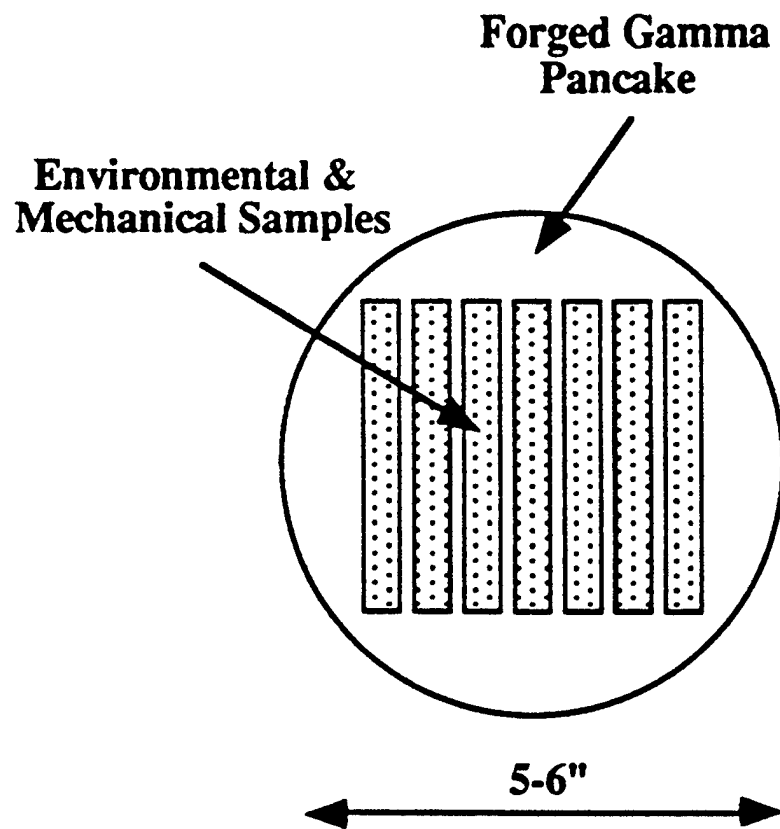


Figure 10. Location of mechanical and environmental samples relative to the plane of the pancake gamma forging. Fibering or banding occurred in the plane of the forging.

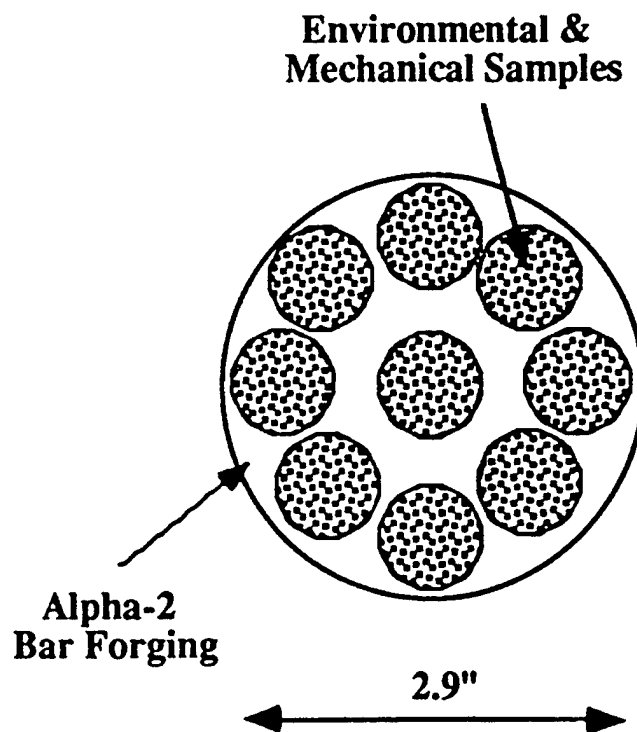
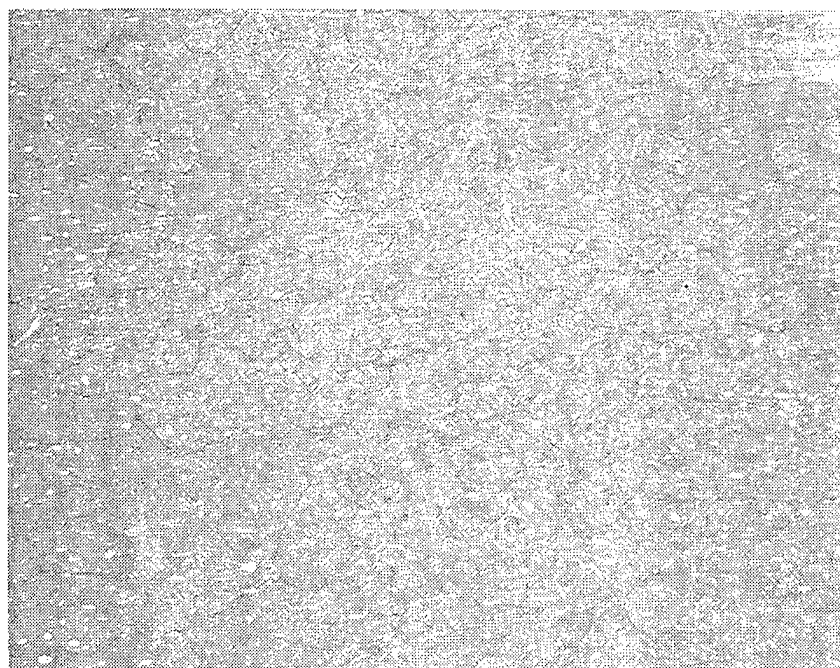
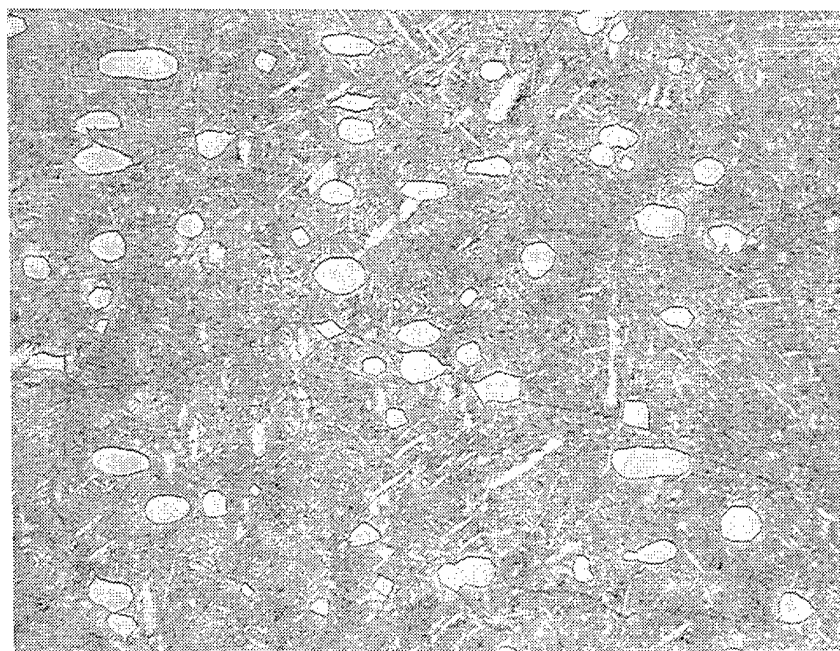


Figure 11. Schematic showing the location of the samples from the alpha-2 bar forging.



250 μm



50 μm

Figure 12. Optical micrographs showing the Ti_{24.5}Al-12.5Nb-1.5Mo alloy after forging and heat treatment. Banding of the primary α_2 precipitates is observed. The area fraction of primary α_2 by image analysis in the higher magnification micrograph is 0.07.

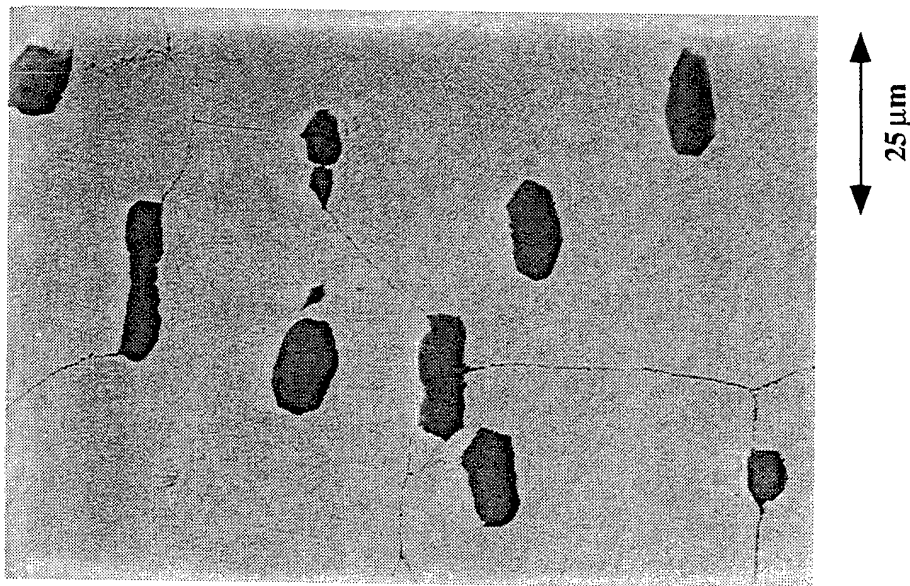
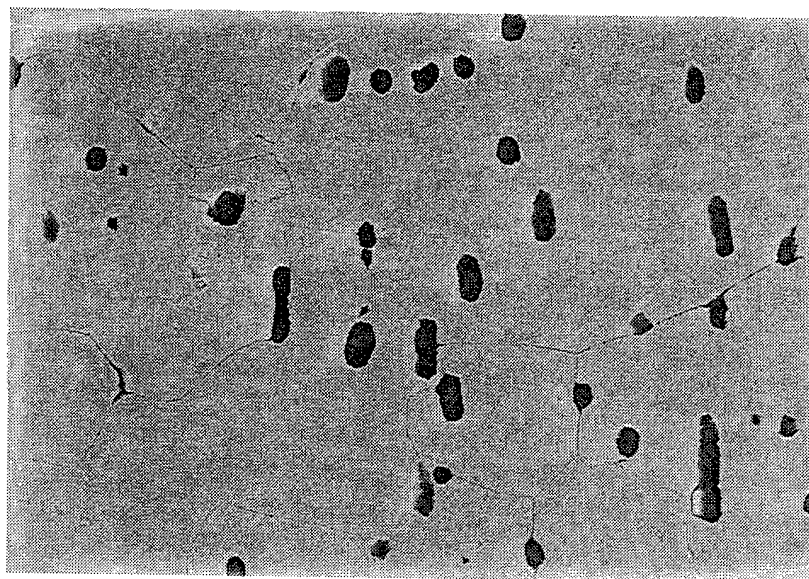
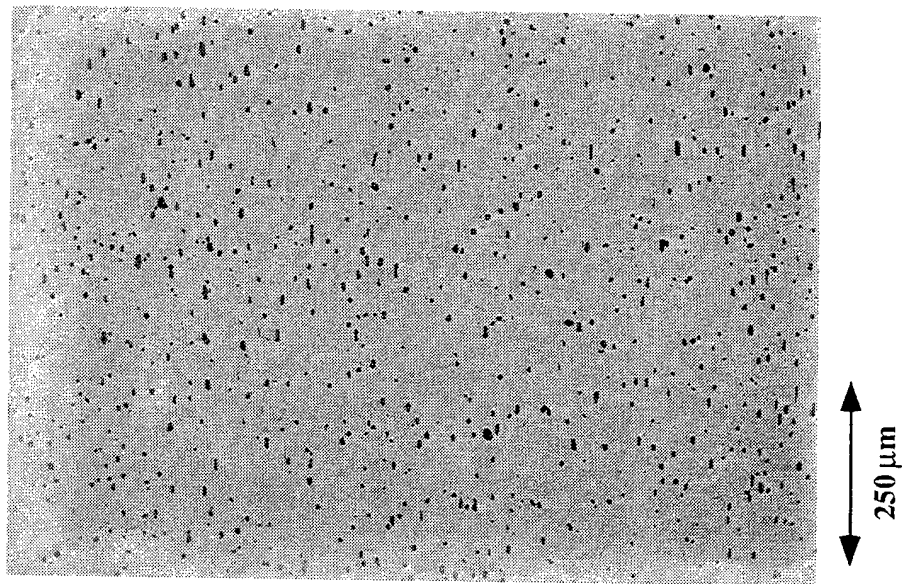


Figure 13. Backscattered electron images showing the Ti-24.5Al-12.5Nb-1.5Mo α -2 alloy after forging and heat treatment. The dark imaging phase is metastable orthorhombic and the light imaging phase is stabilized beta.

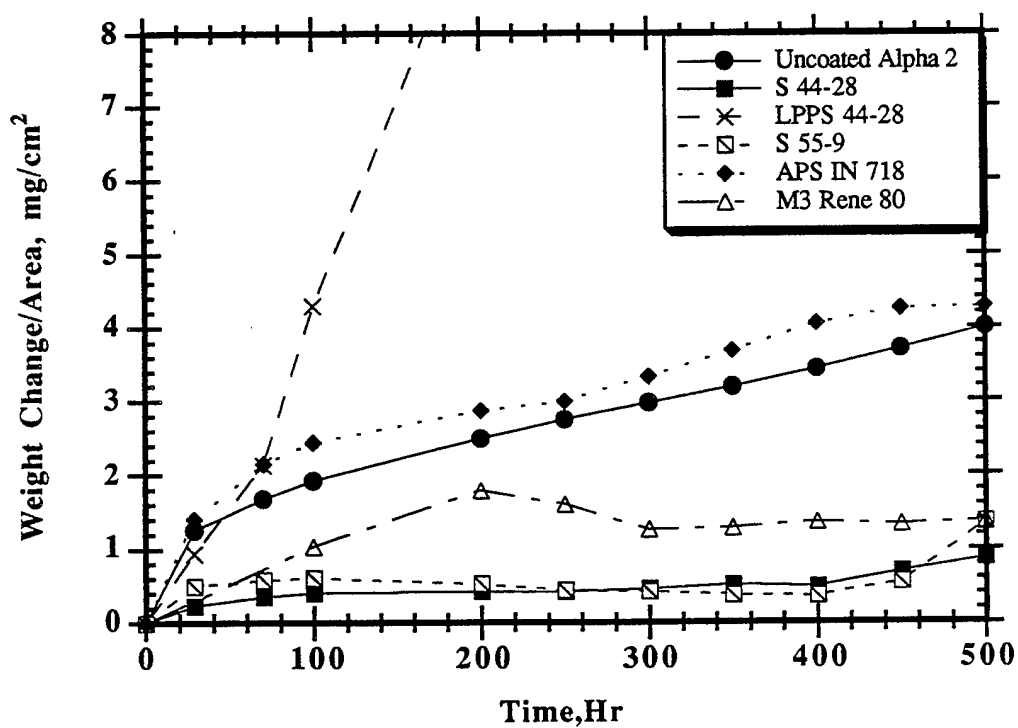
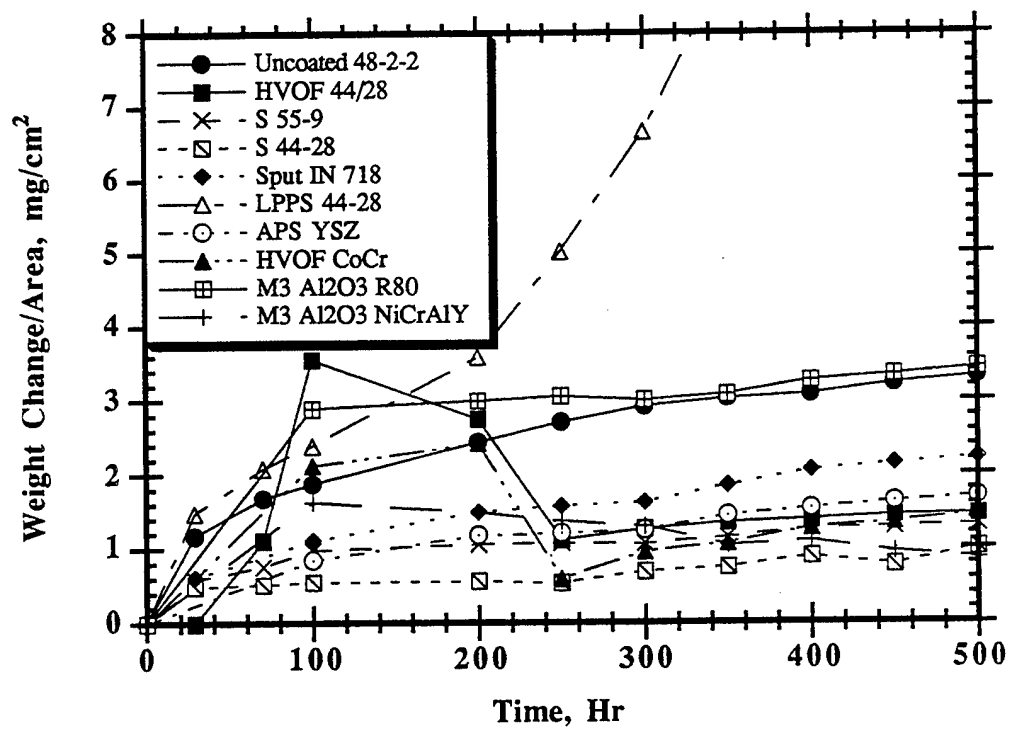
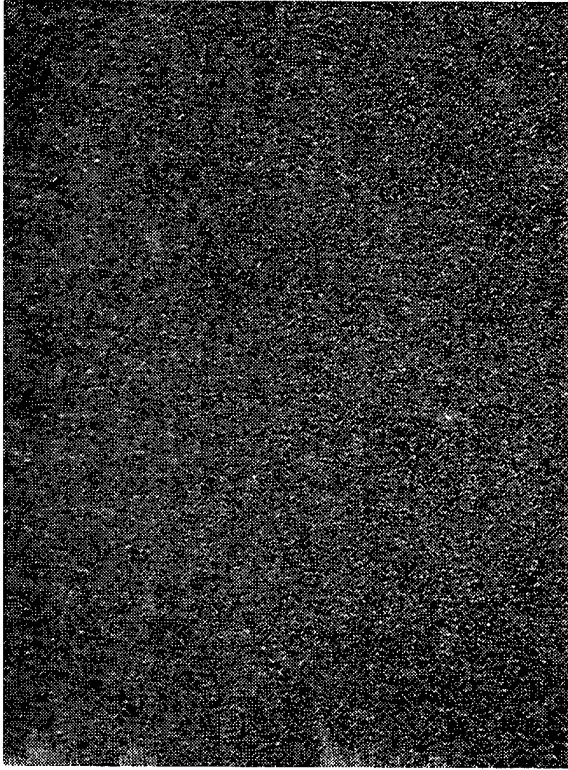
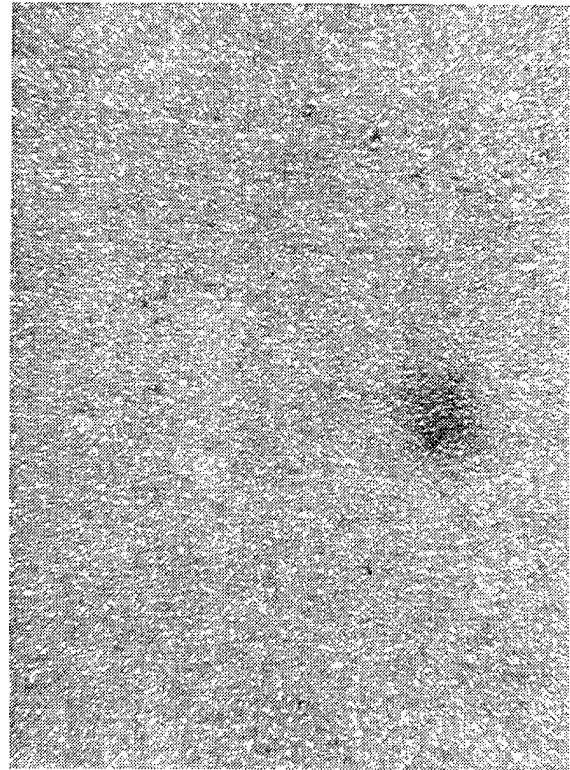


Figure 14. Graph showing the results of cyclic oxidation testing at 900°C (1652°F) in air for 500Hr. (a) Gamma; (b) Alpha-2

100 Cycles



300 Cycles



500 Cycles

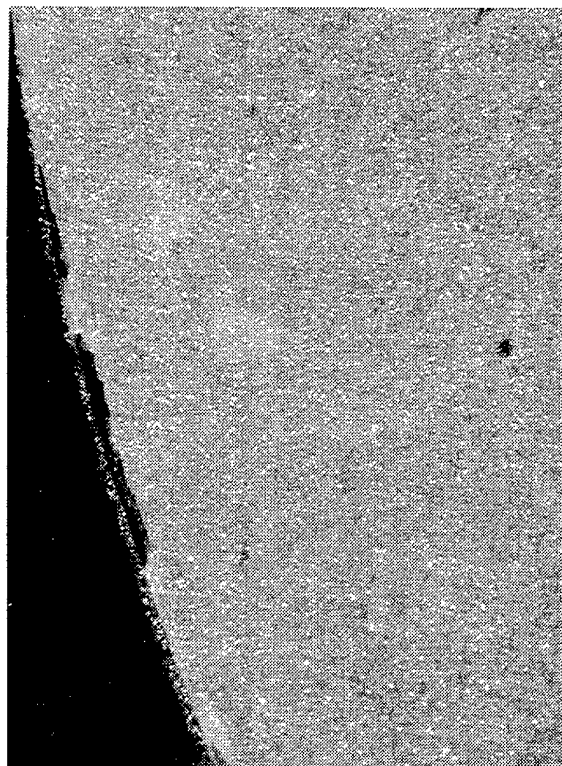
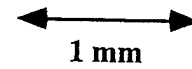
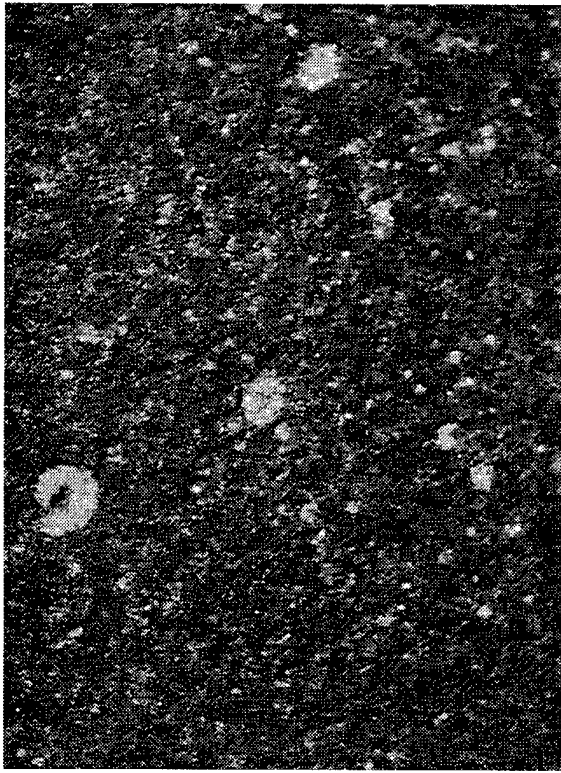
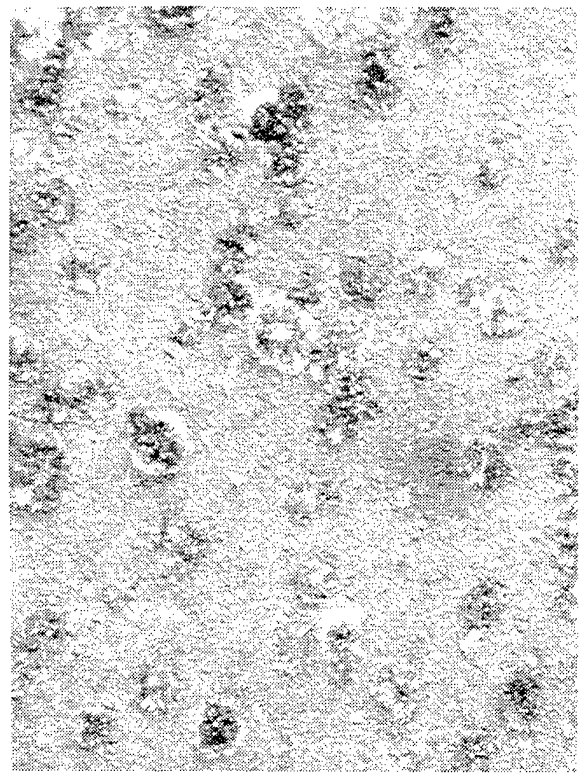


Figure 15. Low magnification optical micrographs showing the surface of uncoated Ti-48Al-2Cr-2Nb after 100, 300 and 500Hr of cyclic oxidation at 900°C (1652°F). Spalling was observed especially on the edges of the sample.

100 Cycles



300 Cycles



500 Cycles

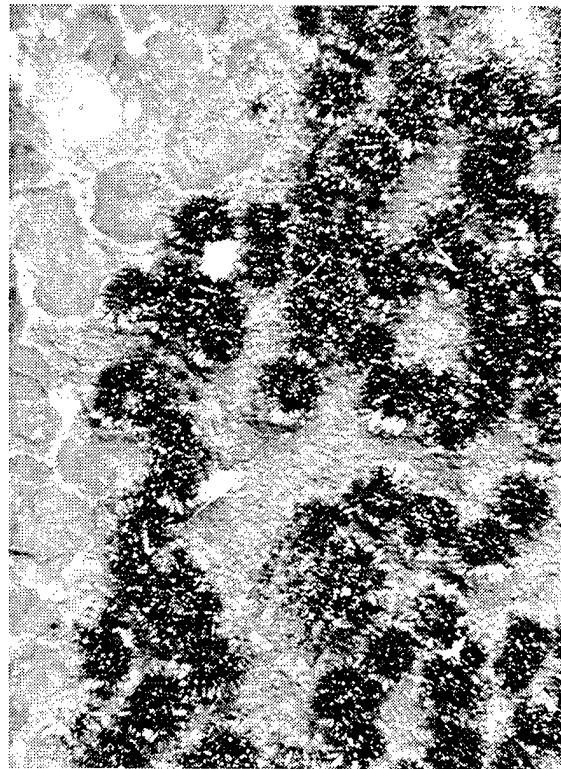
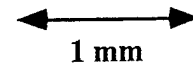
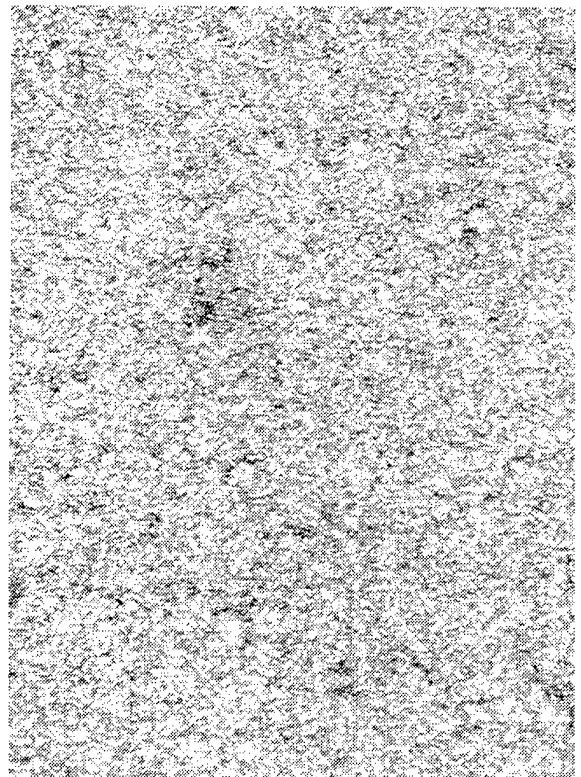


Figure 16. Low magnification optical micrographs showing the surface of the LPPS Ti-44Al-28Cr coating on Ti-48Al-2Cr-2Nb after 100,300 and 500Hr. of cyclic oxidation in air at 900°C (1652°F).

100 Cycles



300 Cycles



500 Cycles

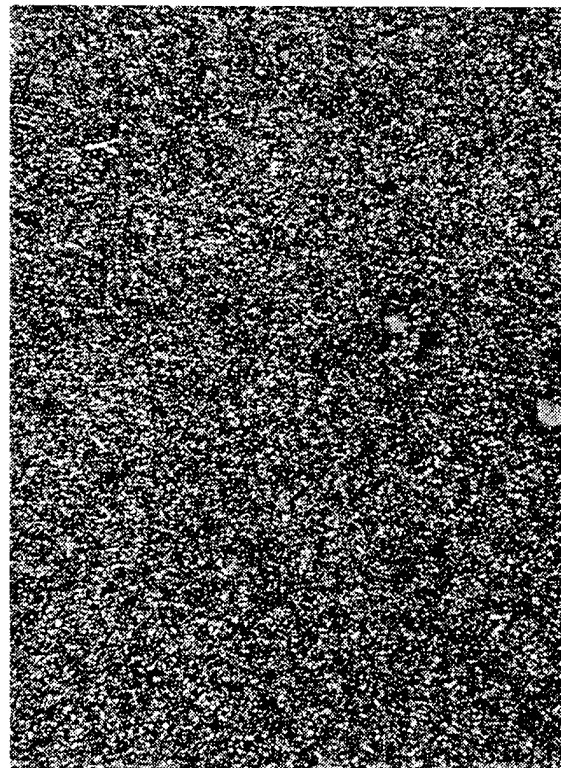
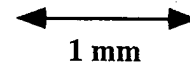
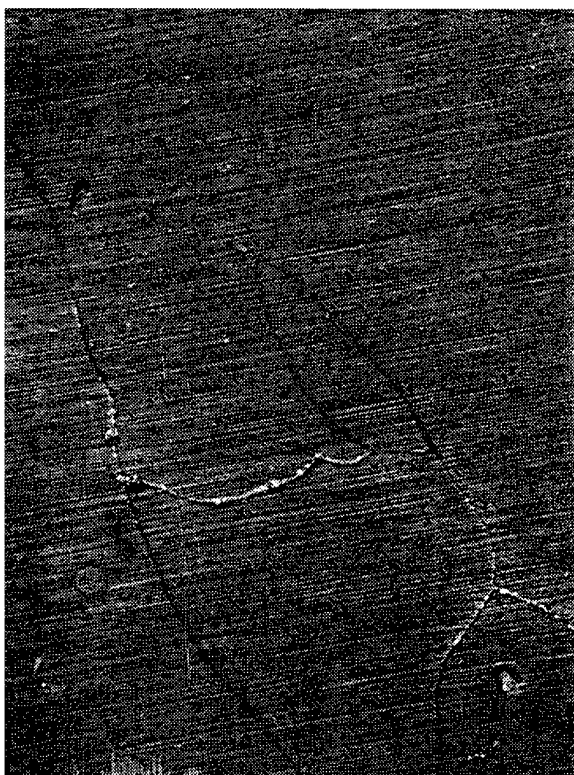


Figure 17. Low magnification optical micrographs showing the surface of the HVOF Ti-44Al-28Cr coating on Ti-48Al-2Cr-2Nb after 100, 300 and 500Hr. of cyclic oxidation in air at 900°C (1650°F).

100 Cycles



300 Cycles



500 Cycles

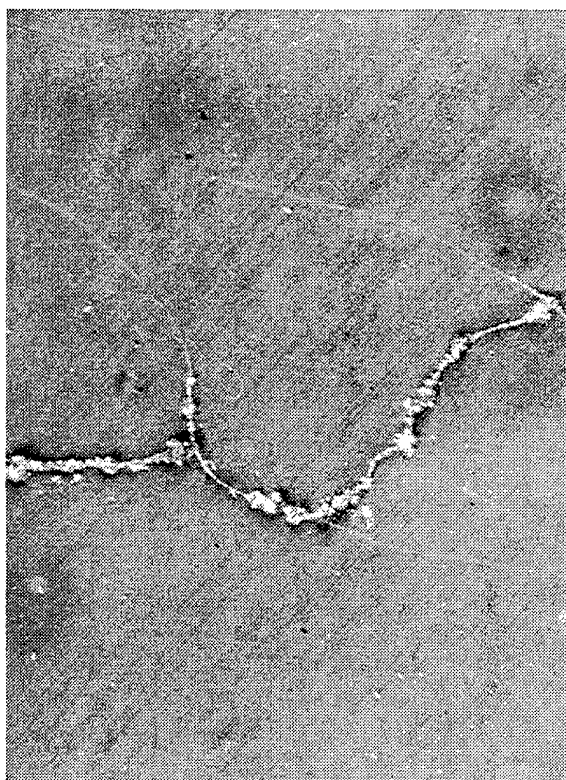
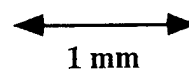
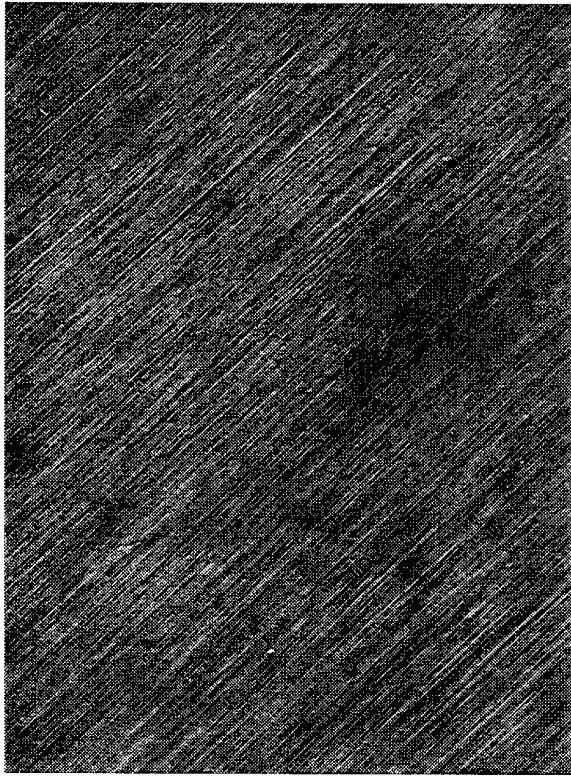


Figure 18. Low magnification optical micrographs showing the surface of the Sputtered Ti-44Al-28Cr coating on Ti-48Al-2Cr-2Nb after 100, 300 and 500Hr. of cyclic oxidation in air at 900°C (1652°F).

100 Cycles



300 Cycles



500 Cycles

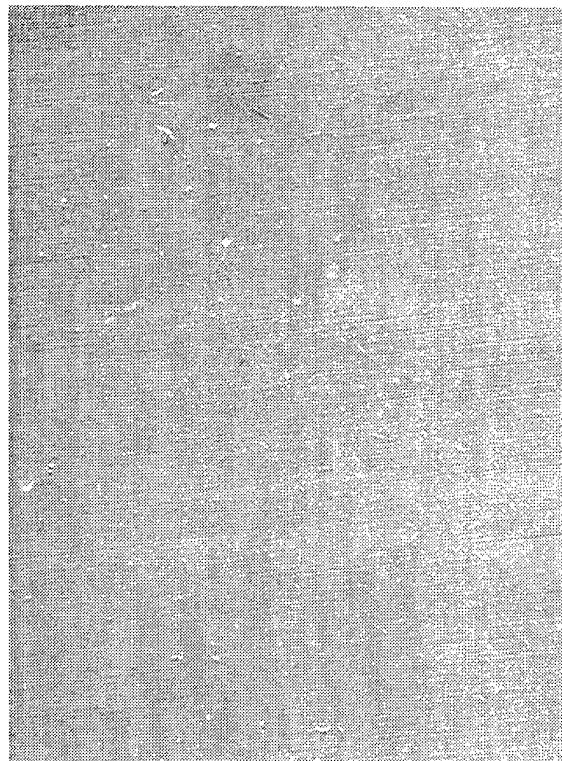
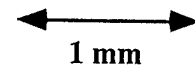


Figure 19. Low magnification optical micrographs showing the surface of the APS YSZ coating on the Ti-47Al-2Cr-4Ta after 100, 300 and 500Hr. of cyclic oxidation in air at 900°C (1652°F).

100 Cycles



300 Cycles



500 Cycles

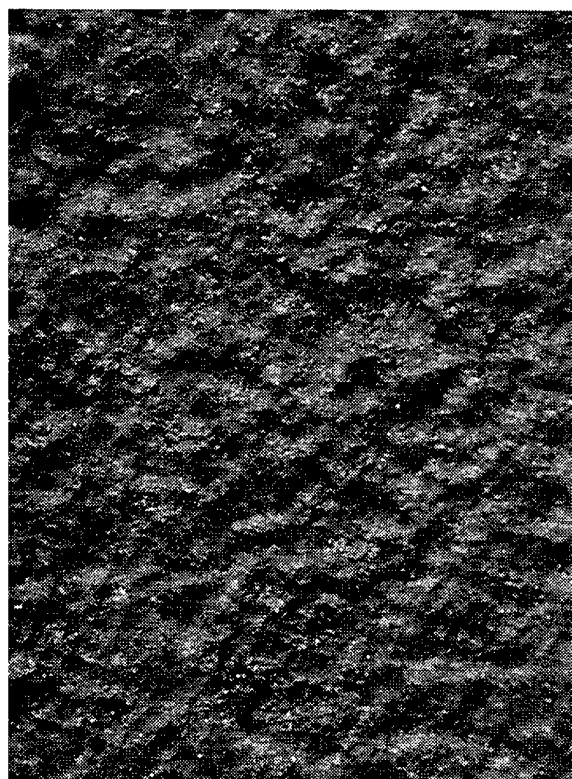
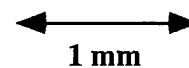


Figure 20. Low magnification optical micrographs showing the surface of the APS YSZ coating on the Ti-47Al-2Cr-4Ta after 100, 300 and 500Hr. of cyclic oxidation in air at 900°C (1652°F).

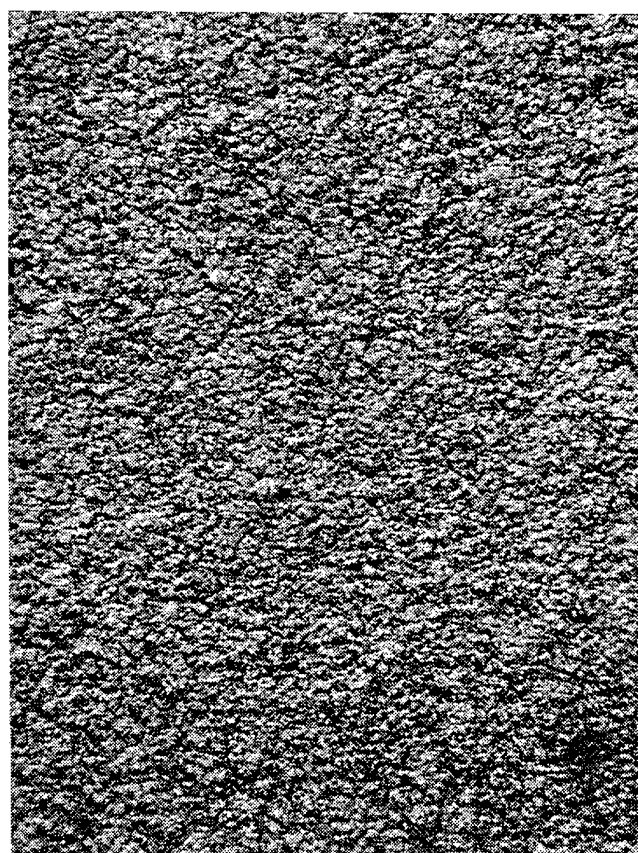
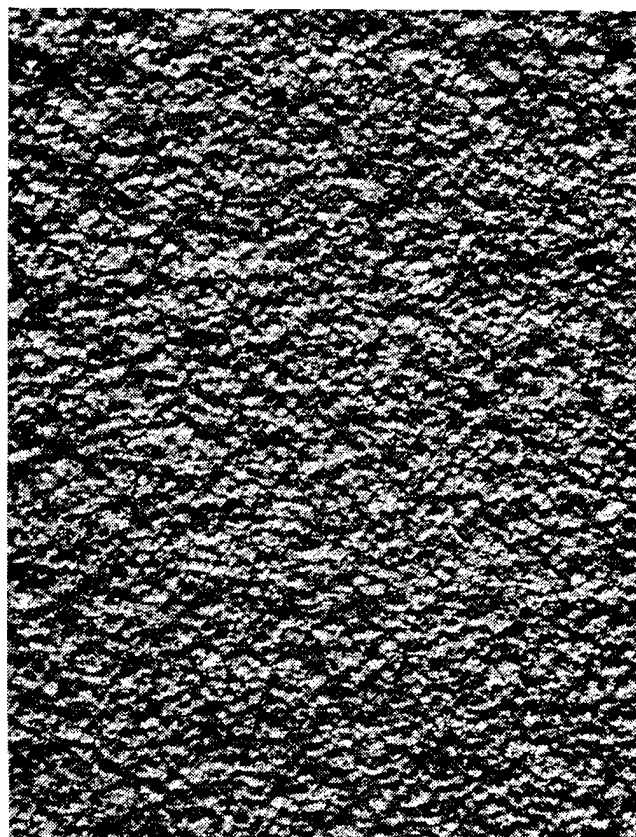
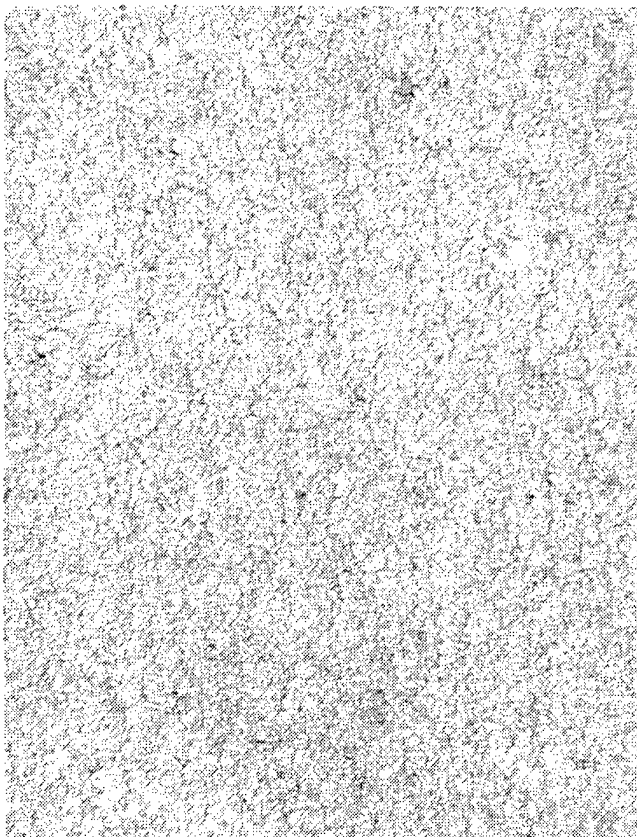
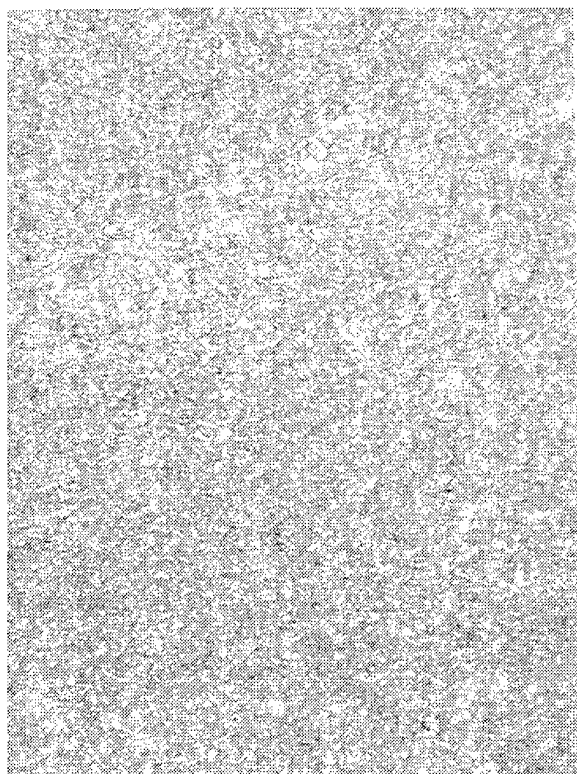


Figure 21. Low magnification optical micrographs showing the surface of the HVOF Co-Cr(W,Si,C) coating on the Ti-48Al-2Cr-2Nb after 100, 300 and 500Hr. of cyclic oxidation in air at 900°C (1652°F).

100 Cycles



300 Cycles



500 Cycles

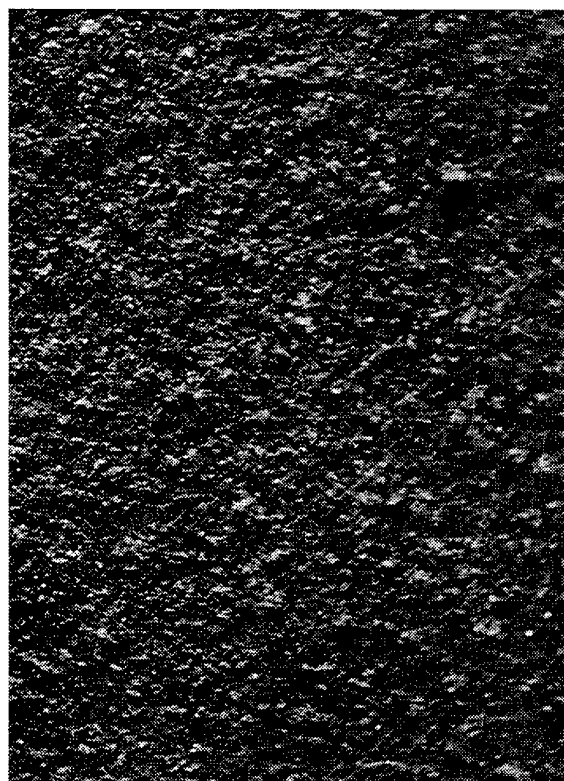
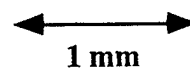
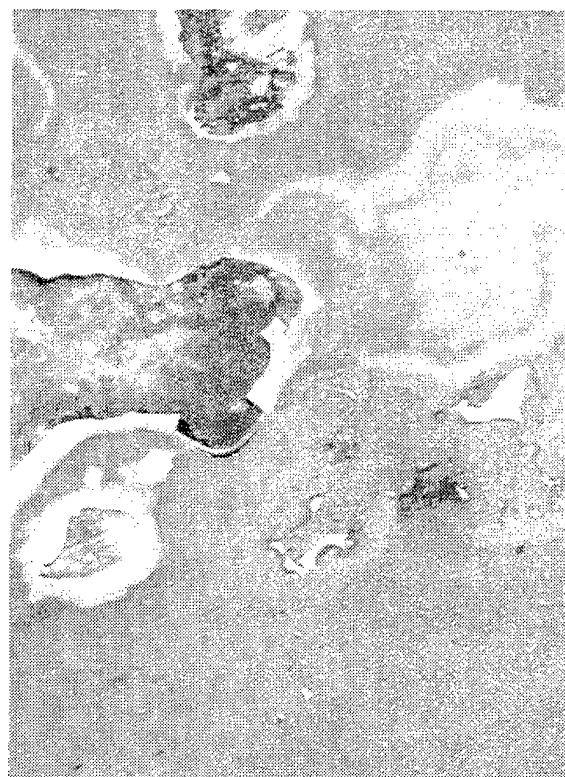


Figure 22. Low magnification optical micrographs showing the surface of the M³ coating (NiCrAlY and Al₂O₃) on the Ti-48Al-2Cr-2Nb after 100, 300 and 500Hr. of cyclic oxidation in air at 900°C (1652°F).

100 Cycles



300 Cycles



500 Cycles

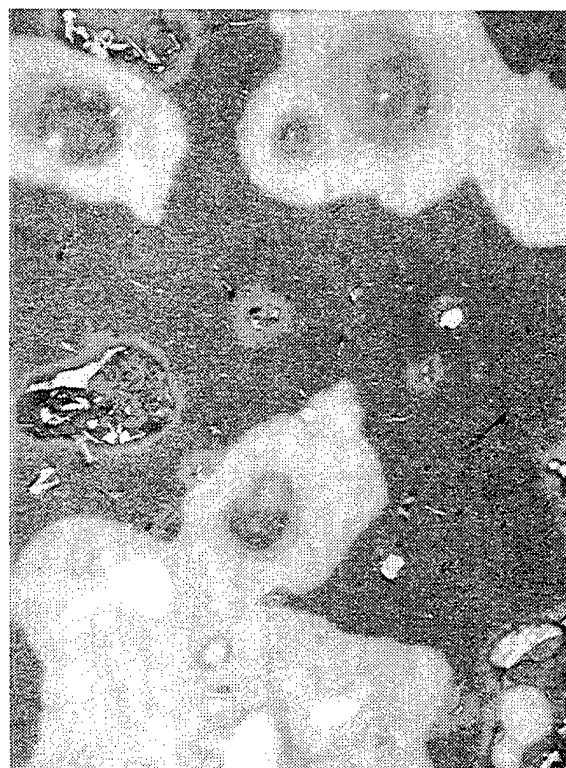
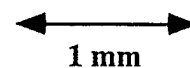
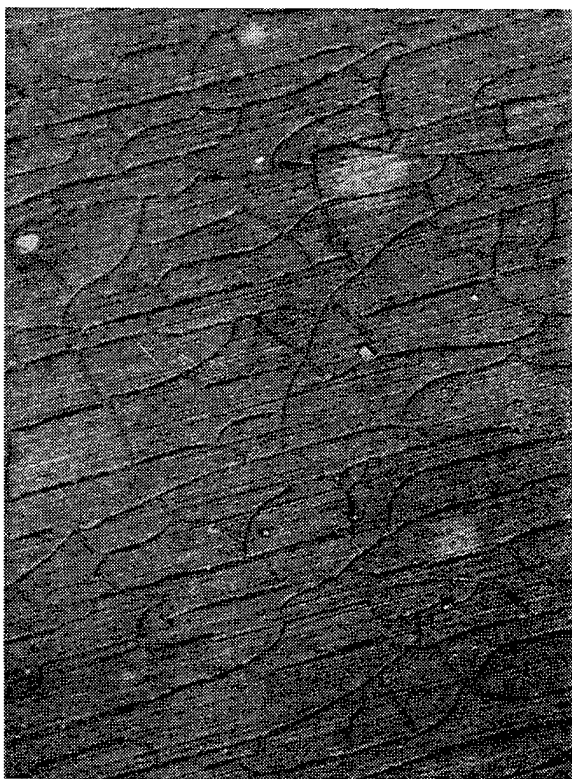
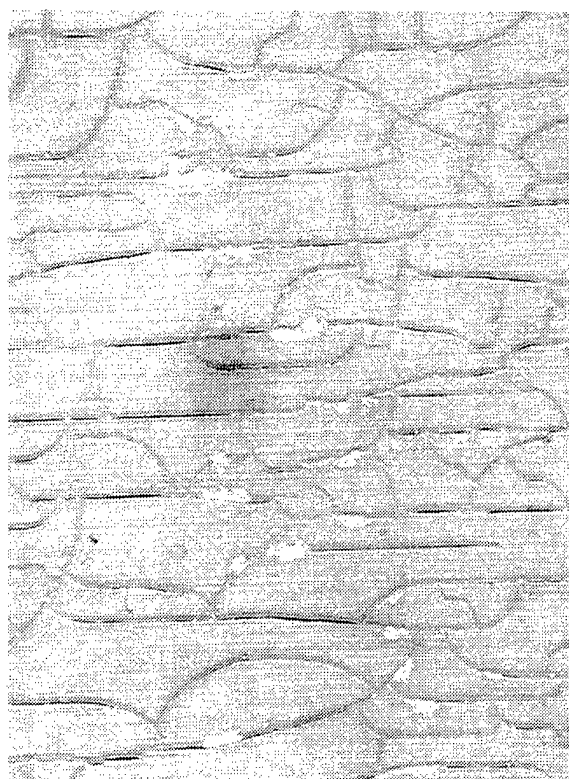


Figure 23. Low magnification optical surface micrographs of the uncoated Ti-24.5Al-12.5Nb-1.5Mo substrate after 100, 300 and 500Hr. of cyclic oxidation in air at 900°C (1652°F).

100 Cycles



300 Cycles



500 Cycles

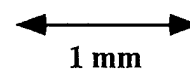
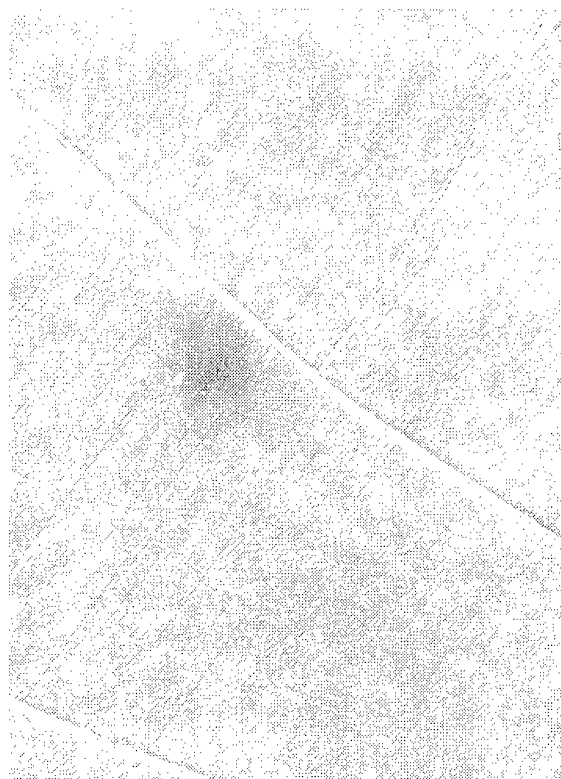


Figure 24. Low magnification optical micrographs showing the surface of the sputtered Ti-44Al-28Cr on Ti-24.5Al-12.5Nb-1.5Mo after 100, 300 and 500Hr. of cyclic oxidation in air at 900°C (1652°F).

100 Cycles



300 Cycles



500 Cycles

1 mm

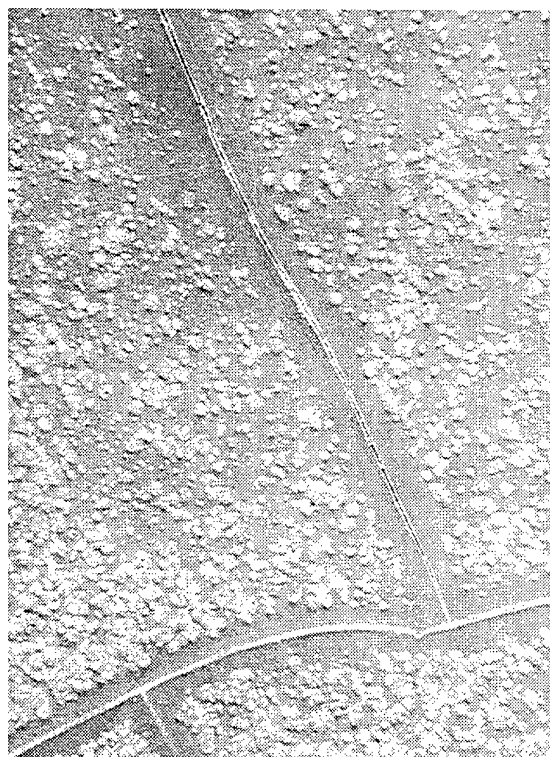
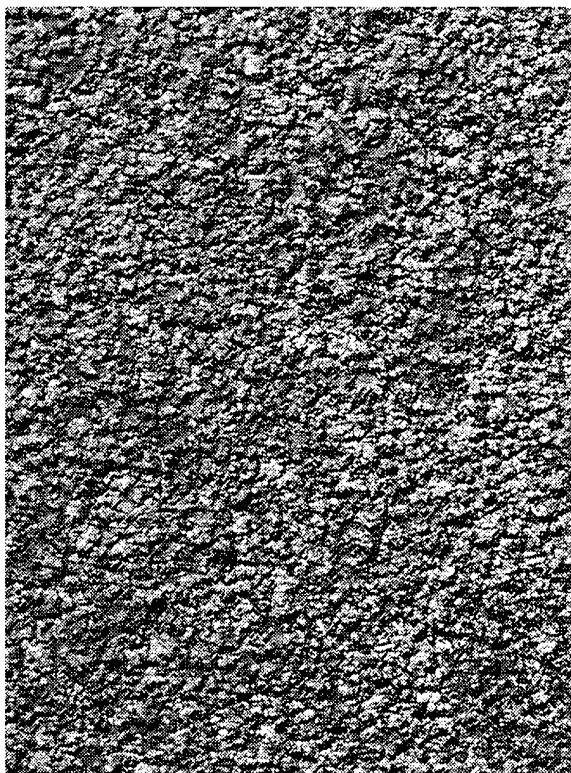
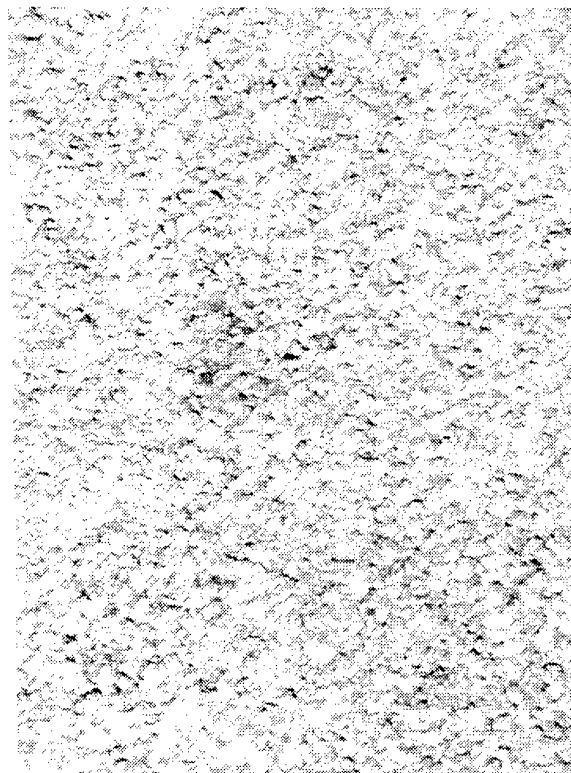


Figure 25. Low magnification optical micrographs showing the surface of sputtered Ti-55Al-8.5Cr on Ti-24.5Al-12.5Nb-1.5Mo after 100, 300 and 500Hr. of cyclic oxidation in air at 900°C (1652°F).

100 Cycles



300 Cycles



500 Cycles

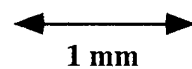
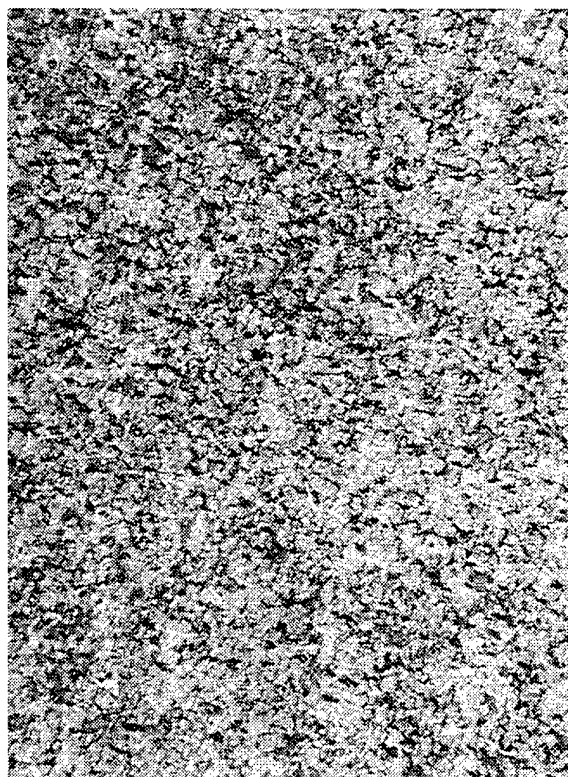


Figure 26. Low magnification optical surface micrographs of APS 718 on Ti-24.5Al-12.5Nb-1.5Mo after 100, 300 and 500Hr. of cyclic oxidation in air at 900°C (1652°F).

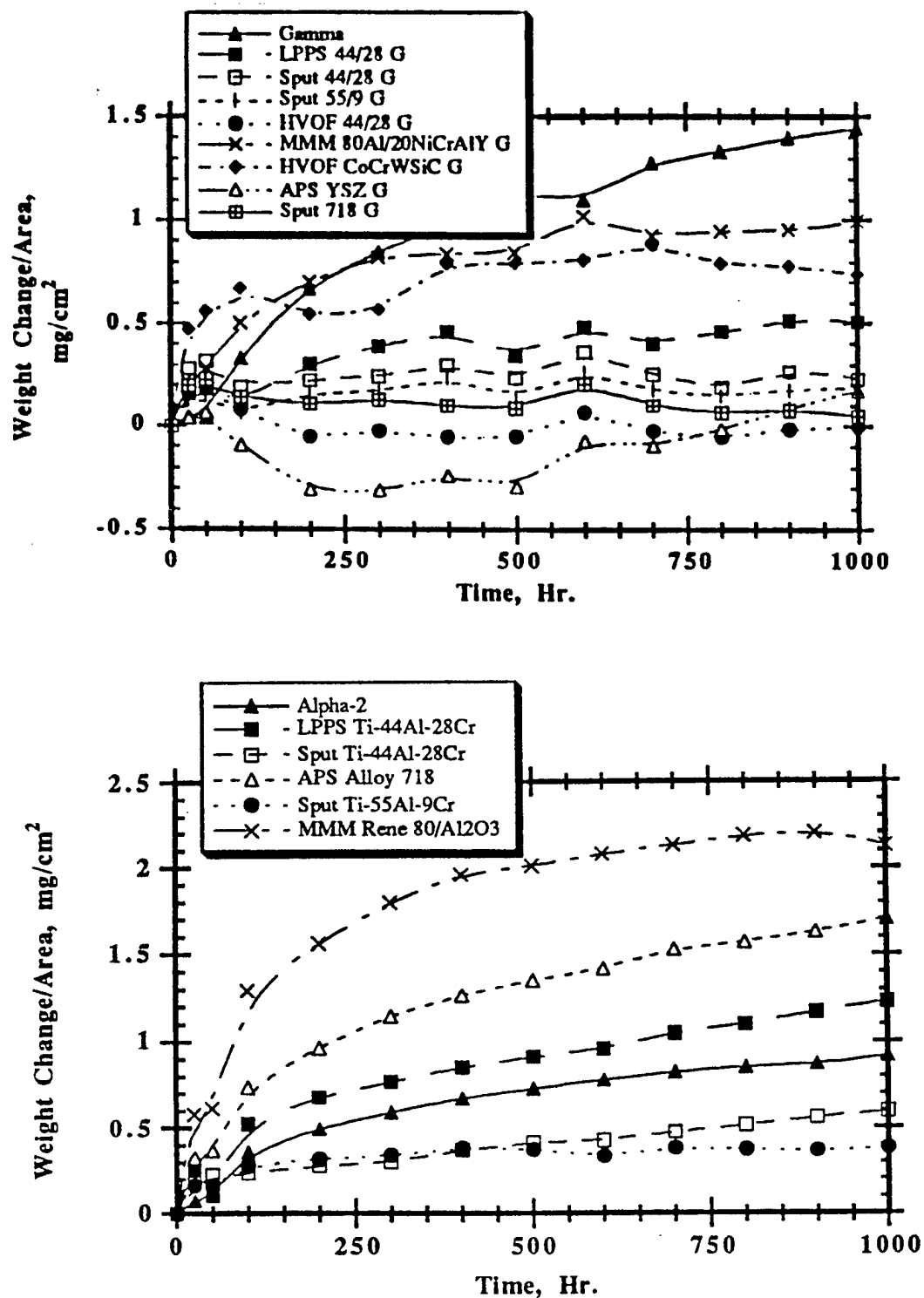
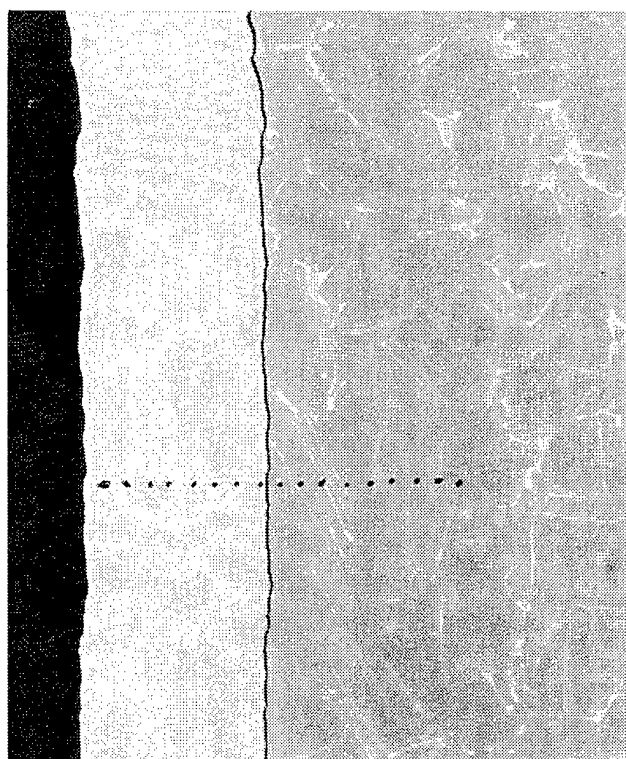


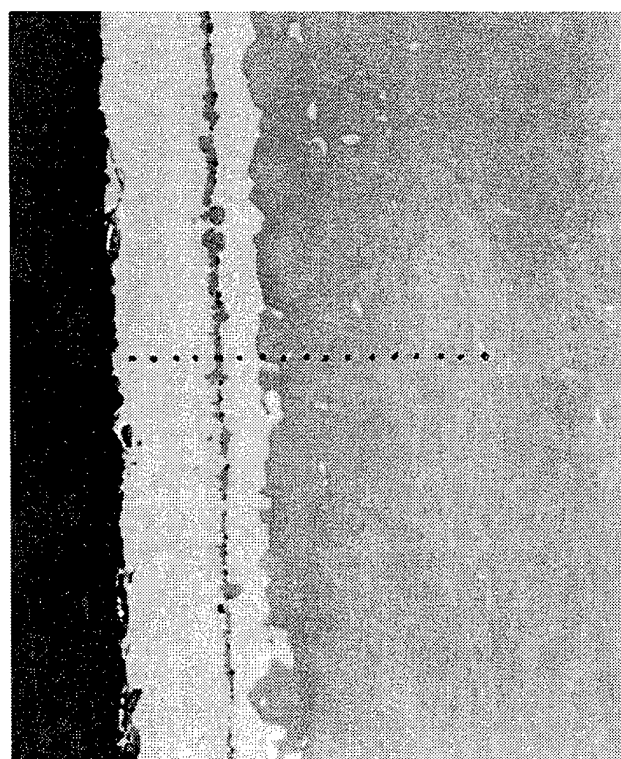
Figure 27. Cyclic oxidation kinetics a for coatings on gamma Ti-aluminide substrate (a) and alpha-2 substrates (b) after 1000 hr at 760°C (1400°F).

As-Coated



40 μm

500 Cycles



40 μm

Figure 28. Backscattered electron micrographs of the sputtered Ti-44Al-28Cr on Ti-48Al-2Cr-2Nb. The top micrograph is the as deposited coating showing a very sharp coating/substrate interface. The bottom micrograph is after 500 one hour cycles at 900°C (1650°F) and shows a continuous Cr-rich reaction zone (arrow).

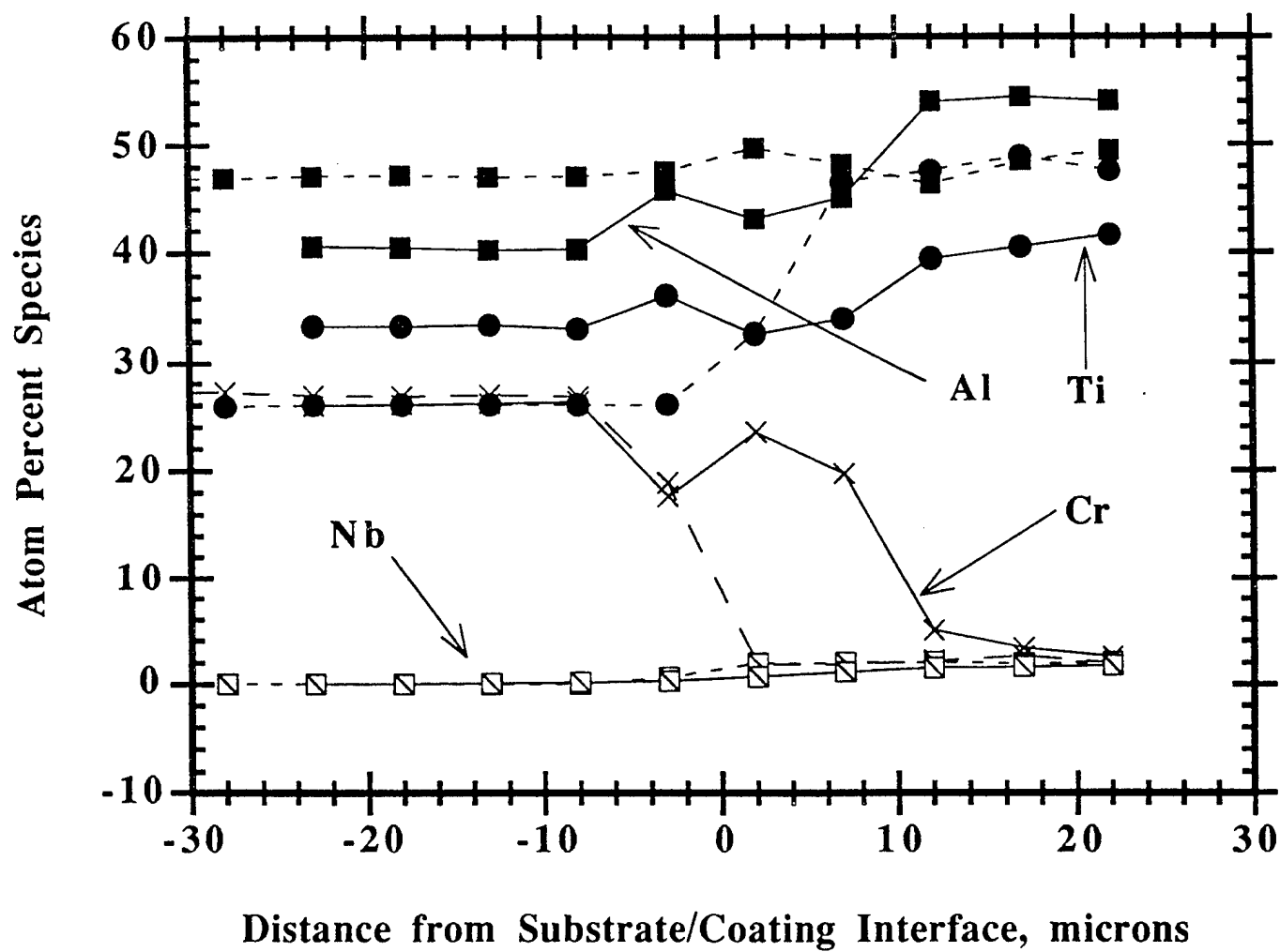


Figure 29. Microprobe traces for the elements that compose the sputtered Ti-44Al-28Cr coatings on Ti-48Al-2Cr-2Nb. The dotted lines represents the initial chemistry while the solid lines are after the 500Hr. exposure at 900°C (1650°F).

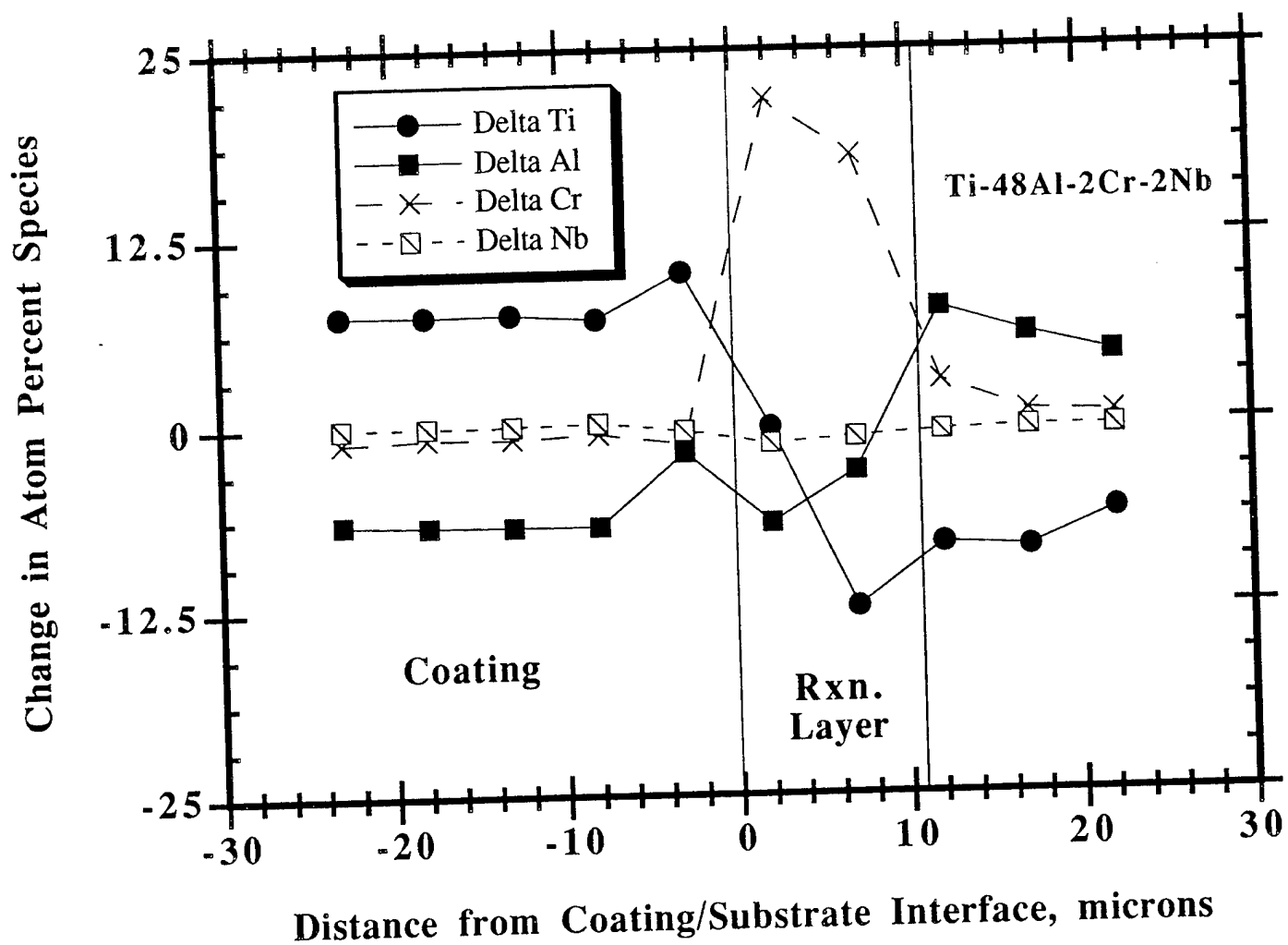
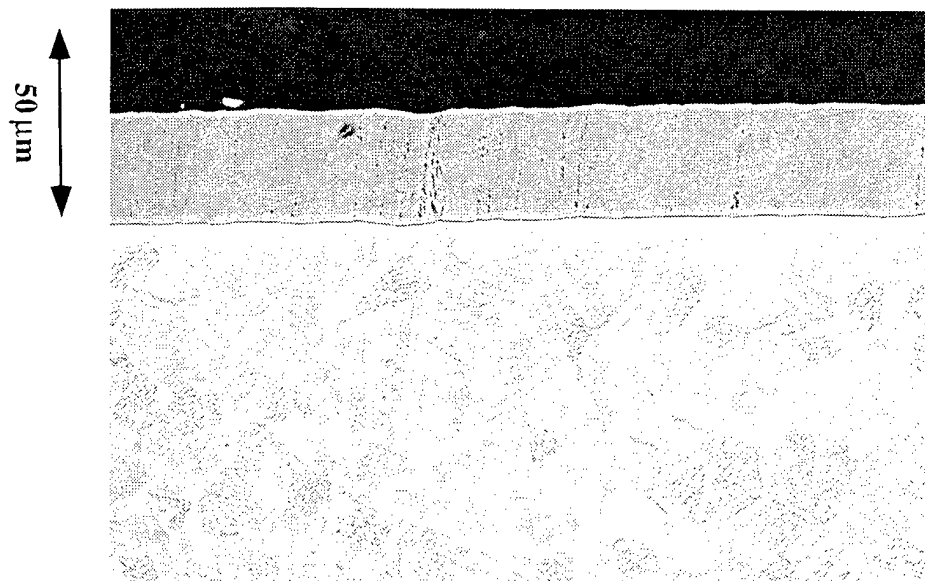
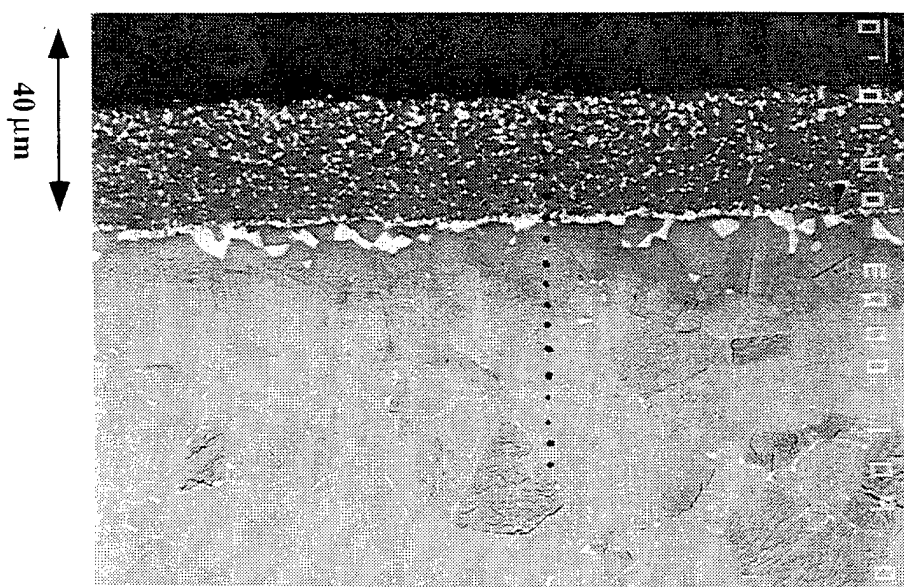


Figure 30. Graph showing the change in composition of the sputtered Ti-44Al-28Cr coatings on Ti-48Al-2Cr-2Nb. The change is relative to the amount of the element that was initially present.



As-Coated



500 Cycles

Figure 31. Backscattered electron micrographs of the sputtered Ti-55Al-8.5Cr on Ti-48Al-2Cr-2Nb. The top micrograph is the as deposited coating showing a very sharp coating/substrate interface. The bottom micrograph is after 500 one hour cycles at 900°C (1650°F) and shows a discontinuous Cr rich reaction zone (arrow).

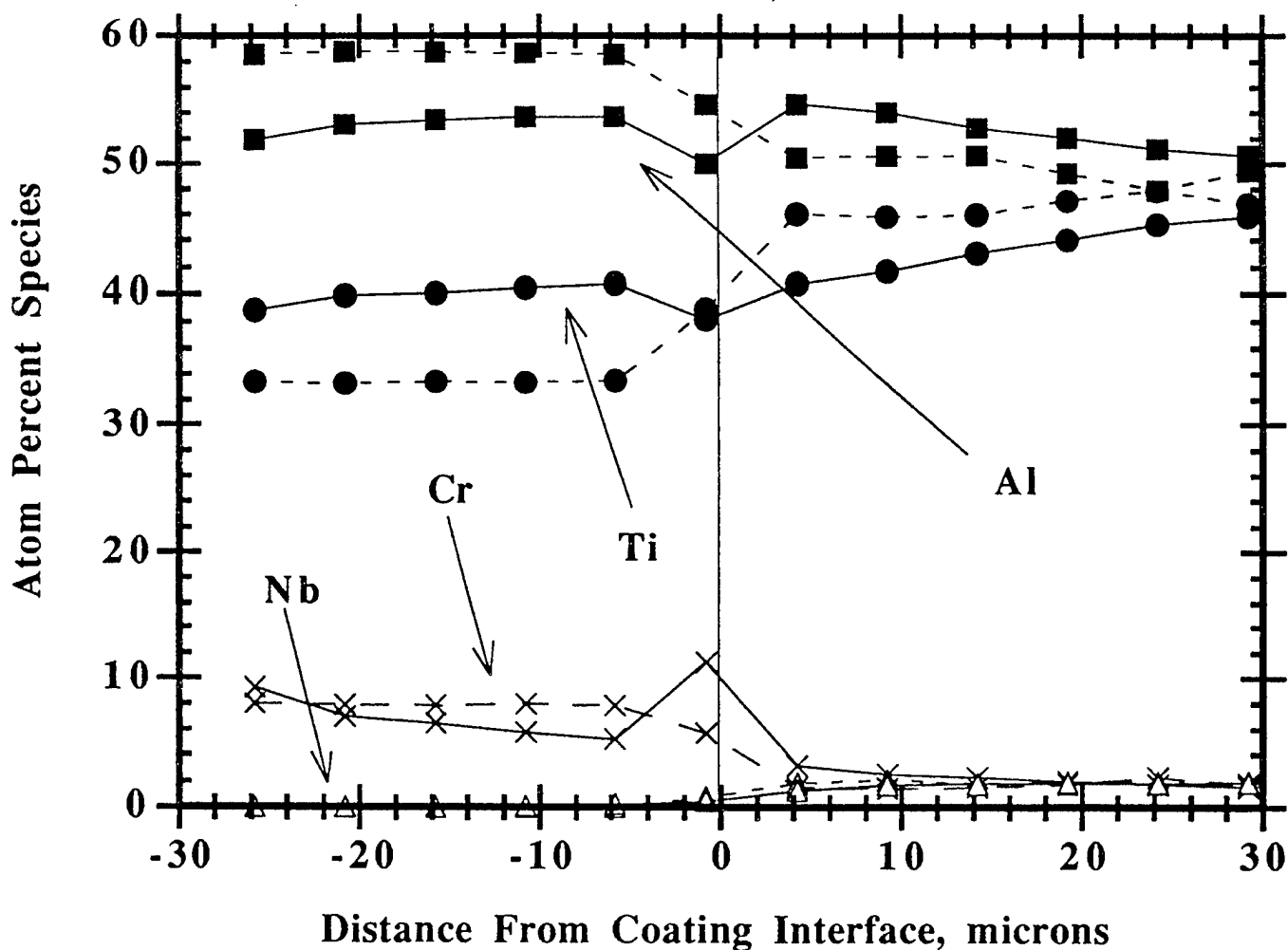


Figure 32. Microprobe traces for the elements that compose the sputtered Ti-55Al-8.5Cr coatings on Ti-48Al-2Cr-2Nb. The dotted lines represents the initial chemistry while the solid lines are after the 500Hr. exposure at 900°C (1650°F).

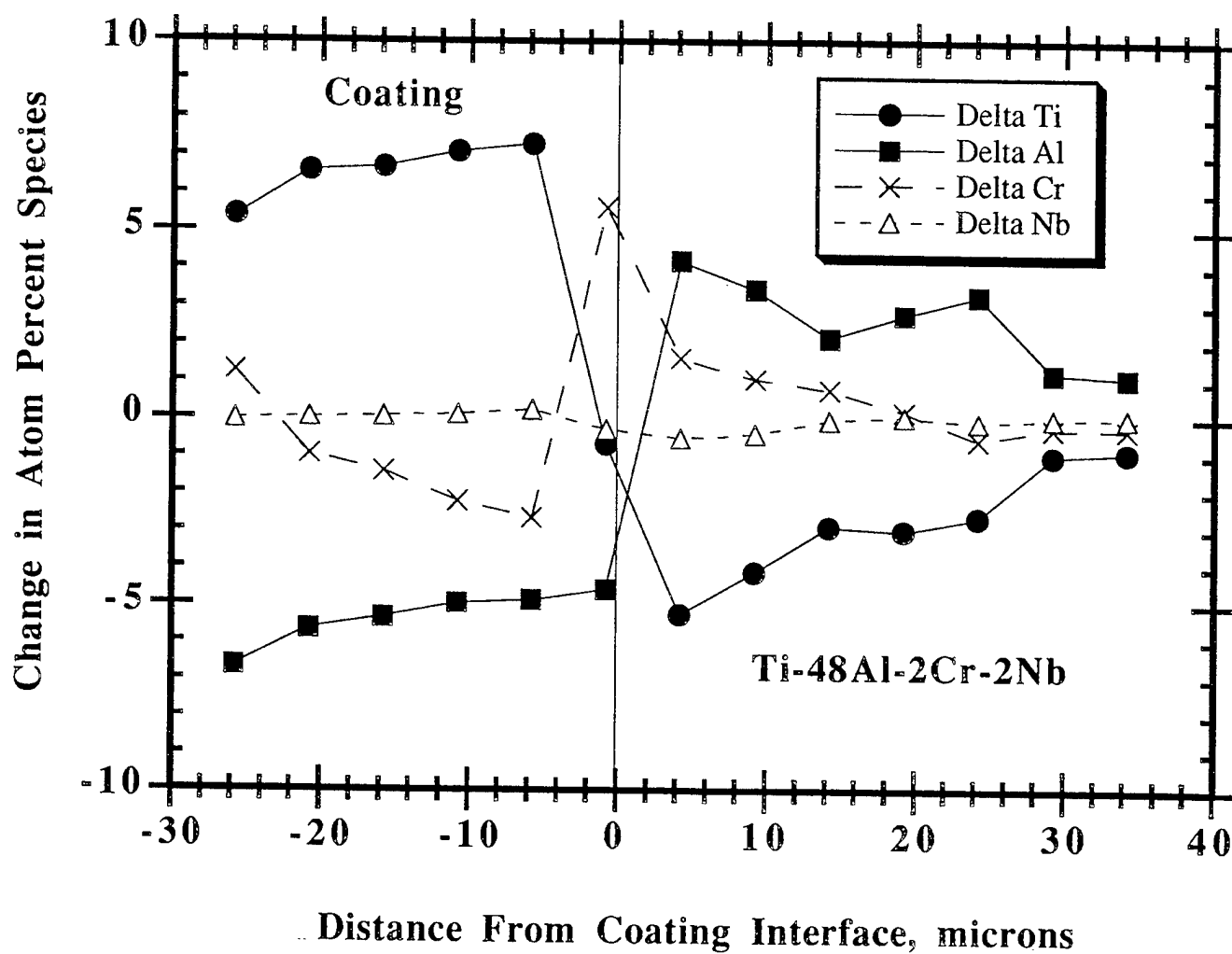
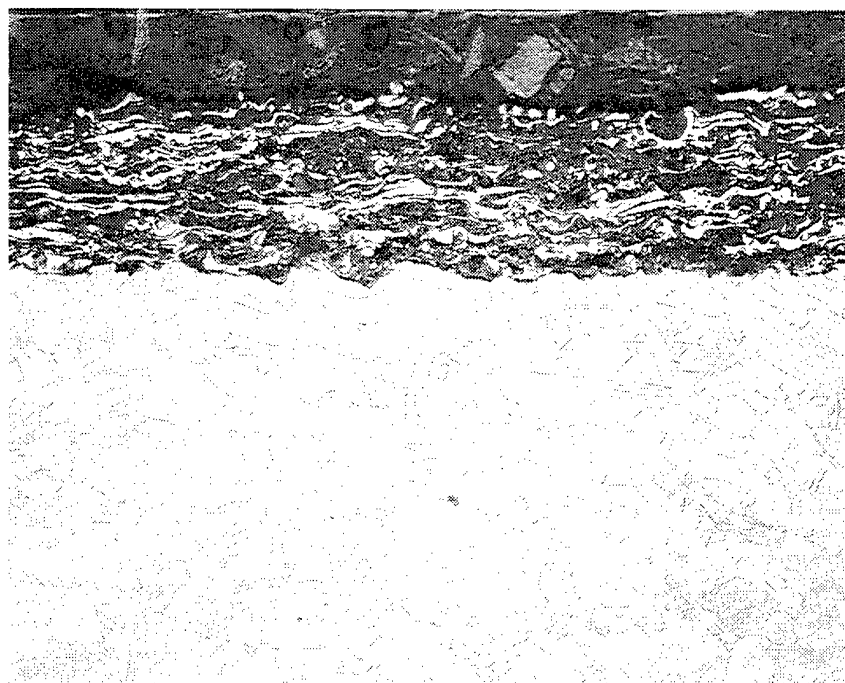
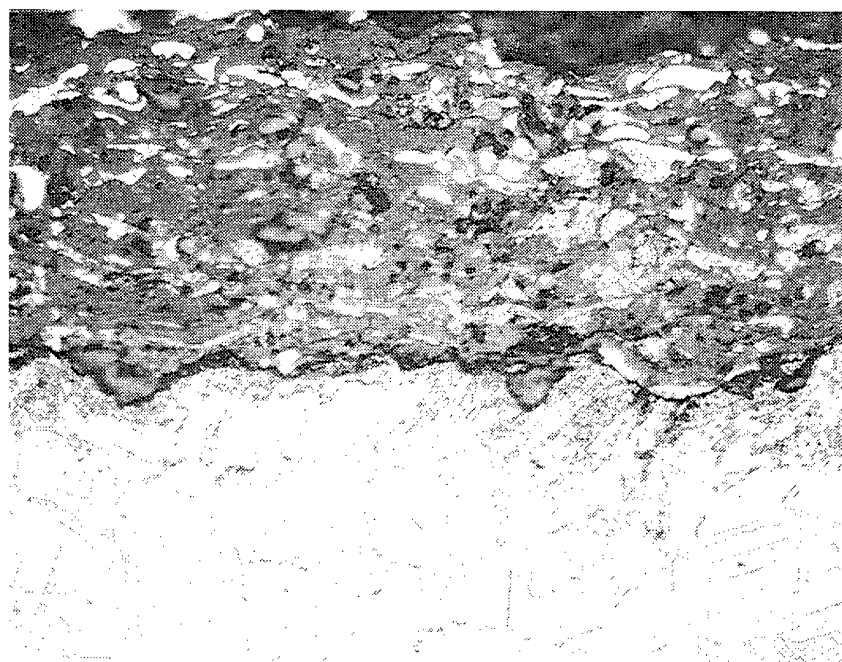


Figure 33. Graph showing the change in composition of the sputtered Ti-55Al-8.5Cr coatings on Ti-48Al-2Cr-2Nb. The change is relative to the amount of the element that was initially present.



125 μm



50 μm

Figure 34. Optical micrographs showing a cermet coating of Al_2O_3 (dark) and NiCrAlY (light) on Ti-48Al-2Cr-2Nb. The mixture of the constituents can be tailored to match the thermal expansion coefficient of the substrate.

As-Coated

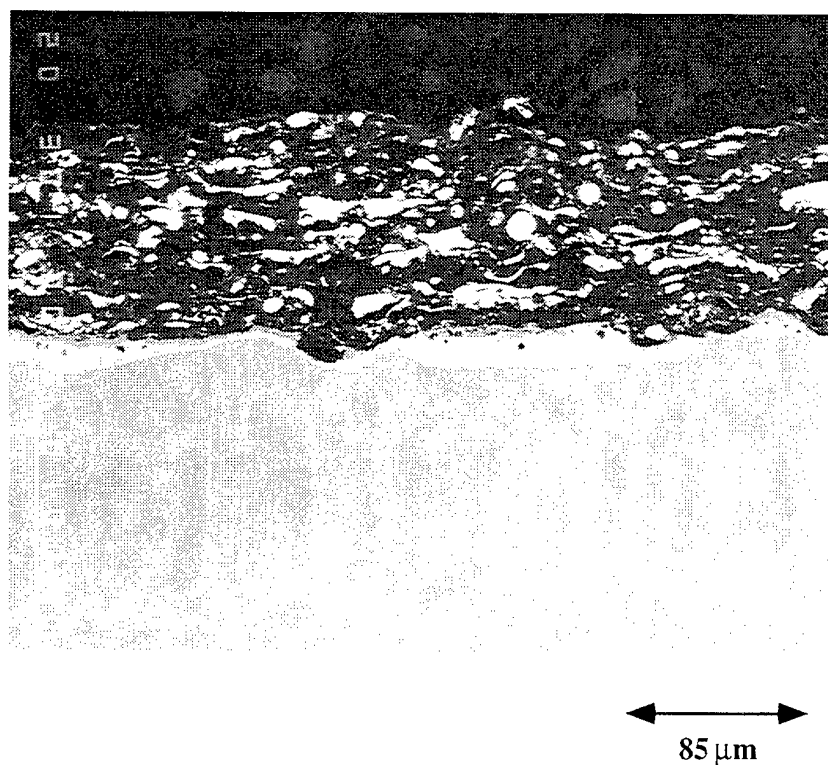
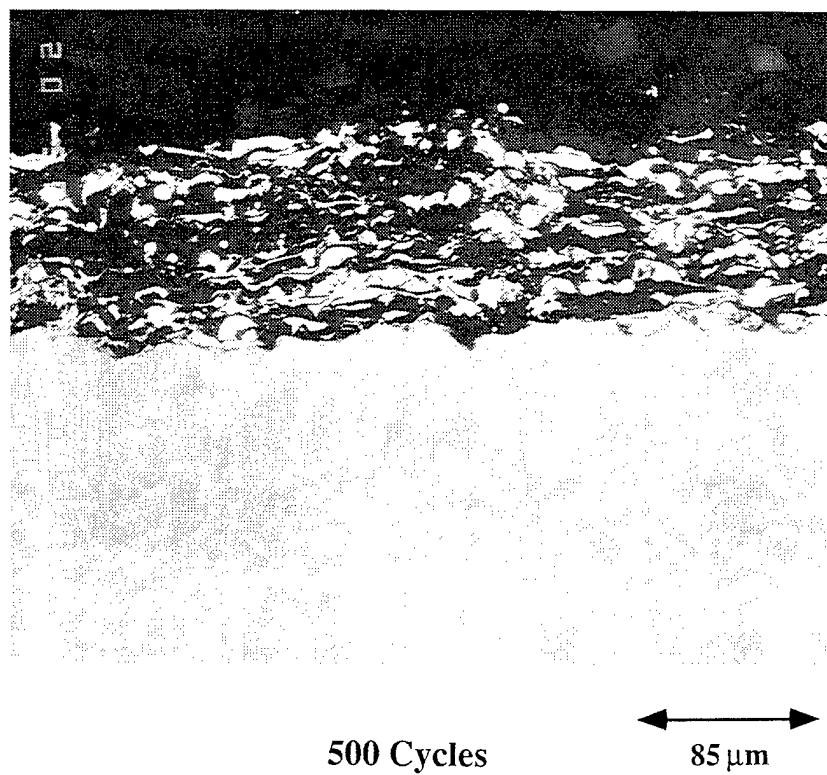


Figure 35. Backscattered electron micrographs showing the cermet coating of Al_2O_3 (dark) and NiCrAlY (light) on Ti-48Al-2Cr-2Nb. The top micrograph is as-coated and the bottom is after cyclic oxidation at 900°C (1650°F). A reaction layer occurs at the coating/substrate interface (arrow).

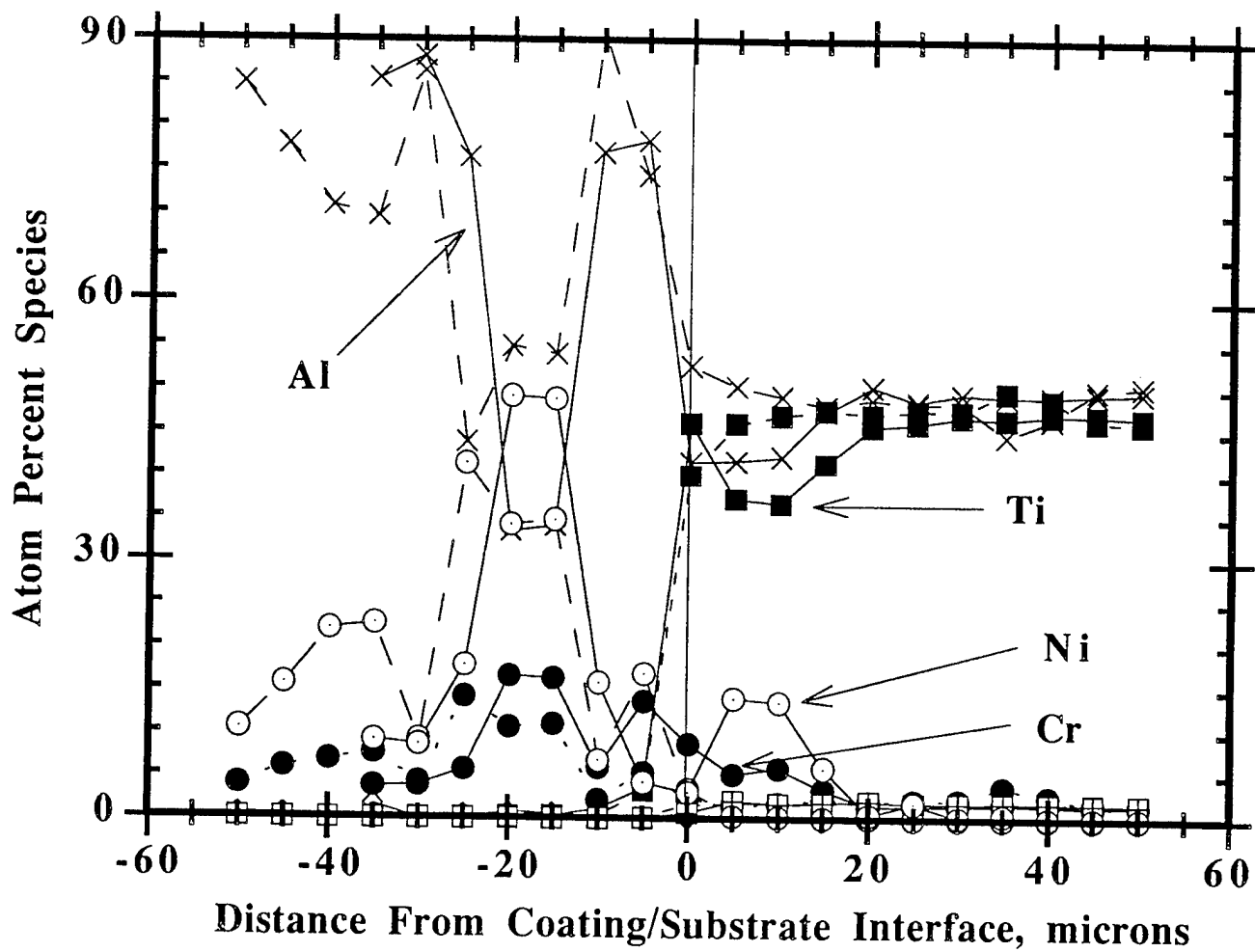


Figure 36. Microprobe traces for the elements that compose the cermet coating of Al_2O_3 (dark) and NiCrAlY (light) on Ti-48Al-2Cr-2Nb. The dotted lines represents the initial chemistry while the solid lines are after the 500Hr. exposure at 900°C (1650°F).

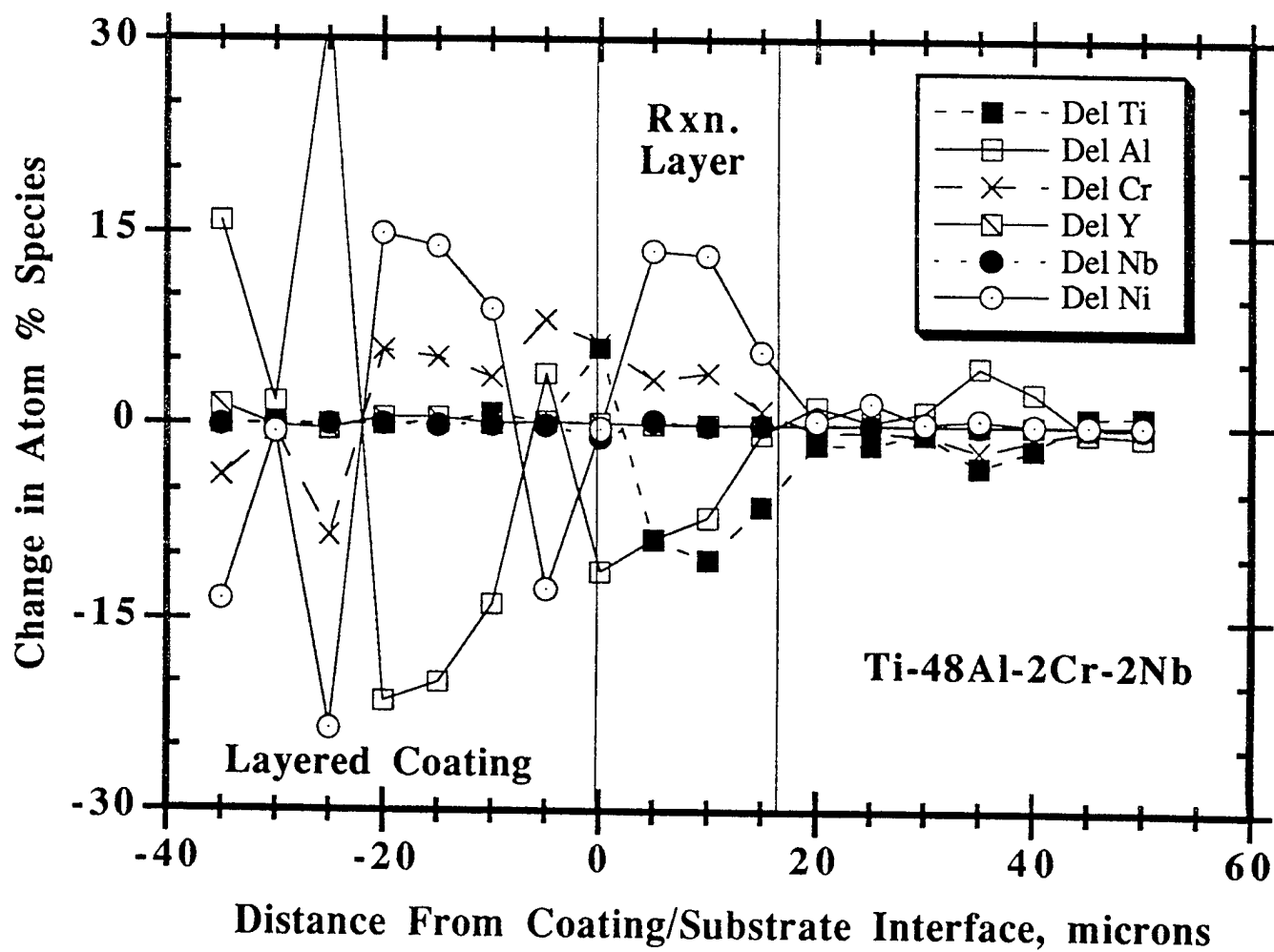
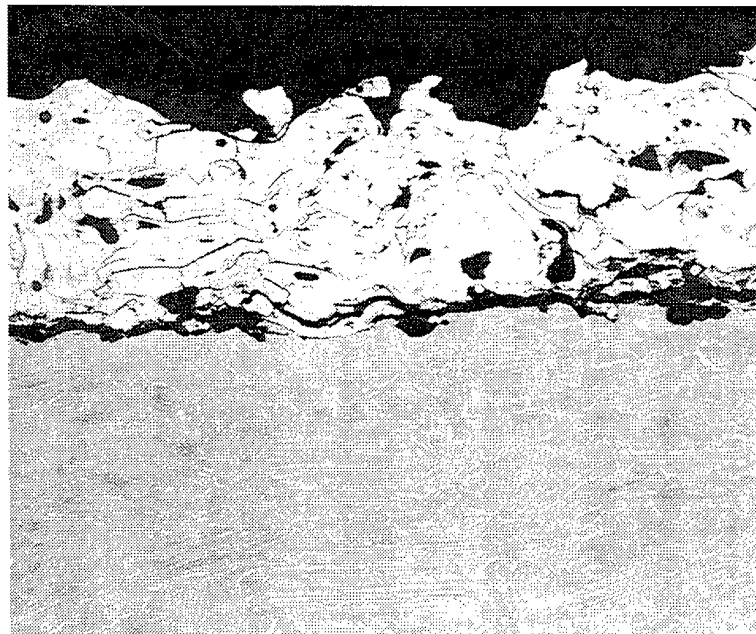
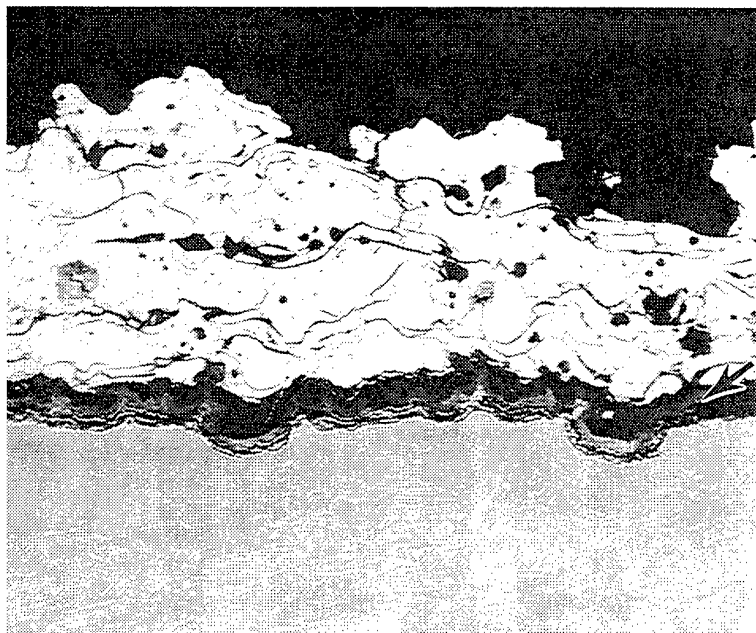


Figure 37. Graph showing the change in composition of the cermet coating of Al_2O_3 (dark) and NiCrAlY (light) on Ti-48Al-2Cr-2Nb. The change is relative to the amount of the element that was initially present. Oxygen was ignored in this analysis.

As-Coated



500 Cycles



85 μm

Figure 38. Backscattered electron micrographs of the ytria stabilized zirconia coating on Ti-47Al-2Cr-4Ta. The top micrograph is as-coated and the bottom is after cyclic oxidation at 900°C (1650°F). Oxide growth occurs at the coating/substrate interface (arrow).

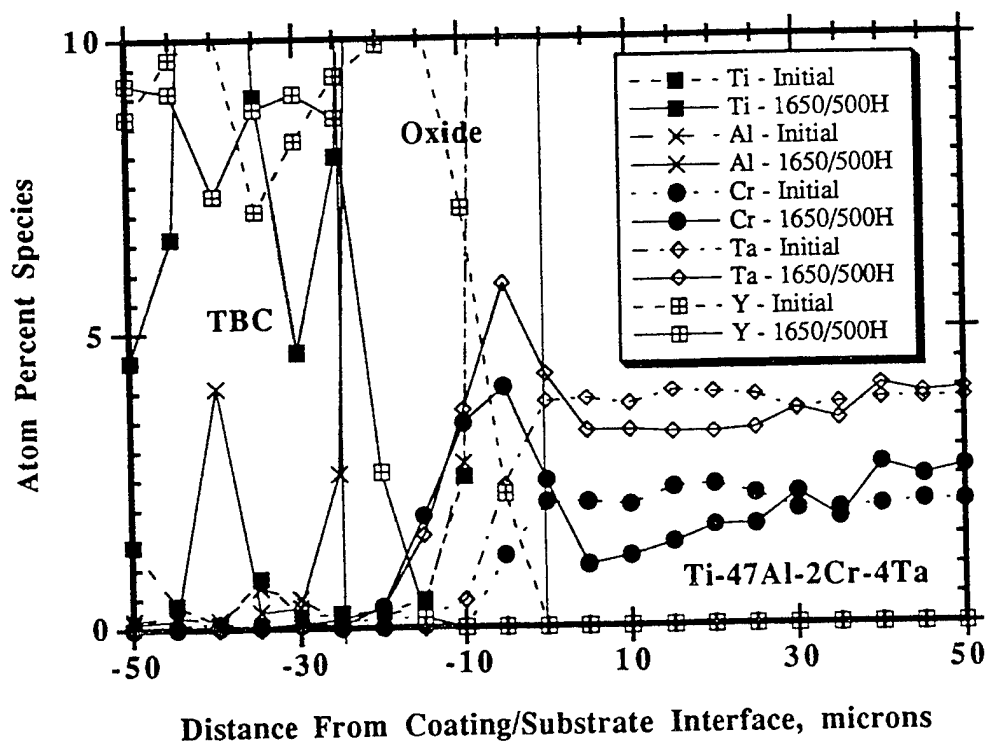
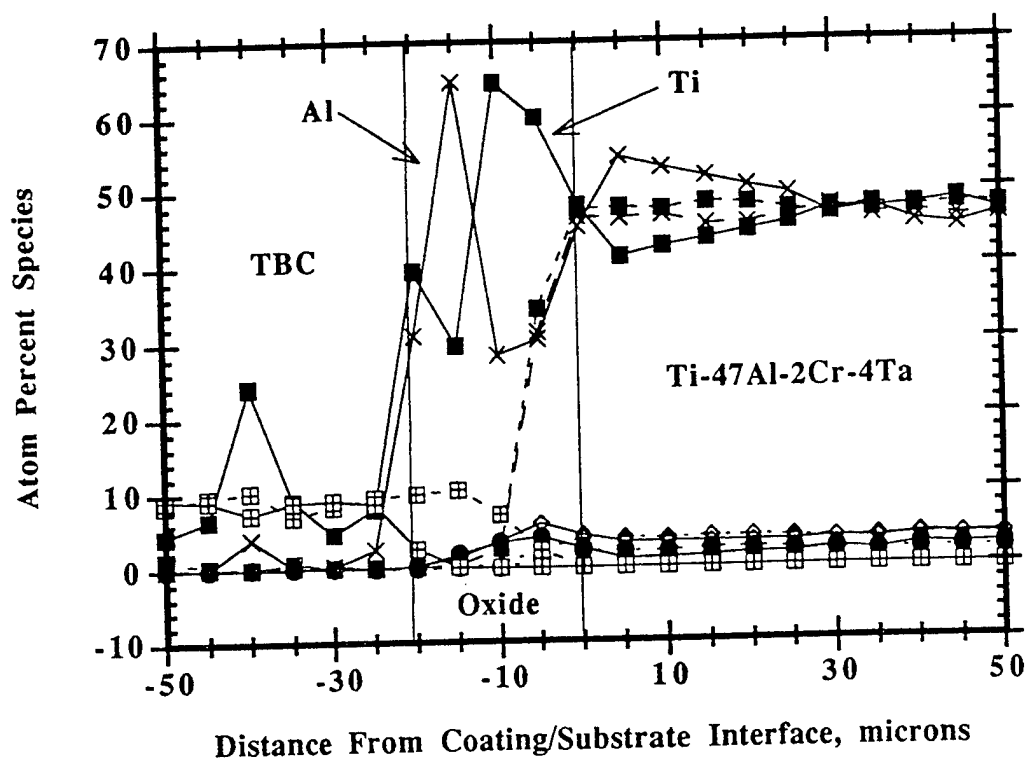


Figure 39. Microprobe traces for the elements that compose the of the yttria stabilized zirconia (YSZ) on the Ti-47Al-2Cr-4Ta substrate. The dotted lines represents the initial chemistry while the solid lines are after the 500Hr. exposure at 900°C (1650°F).

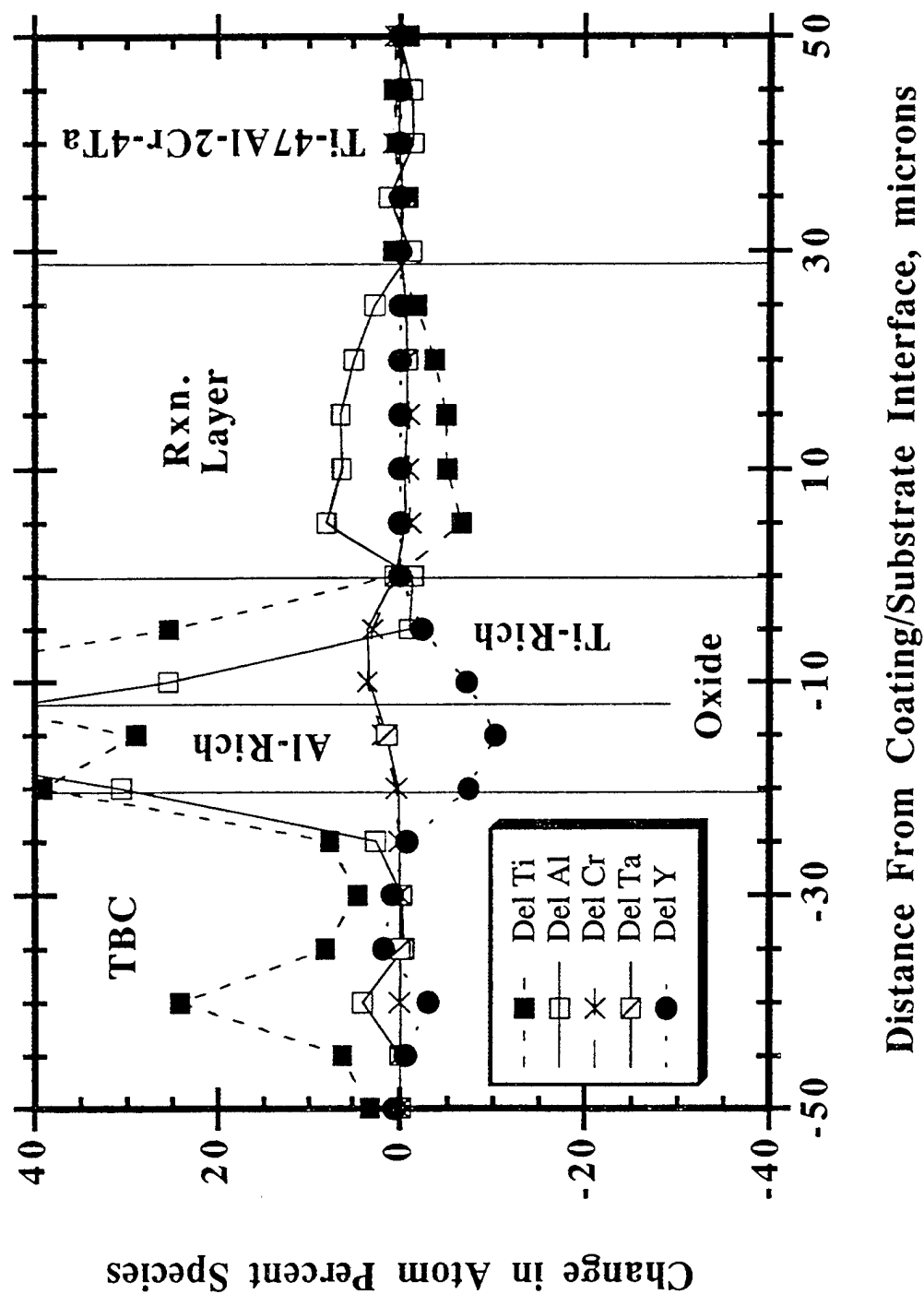
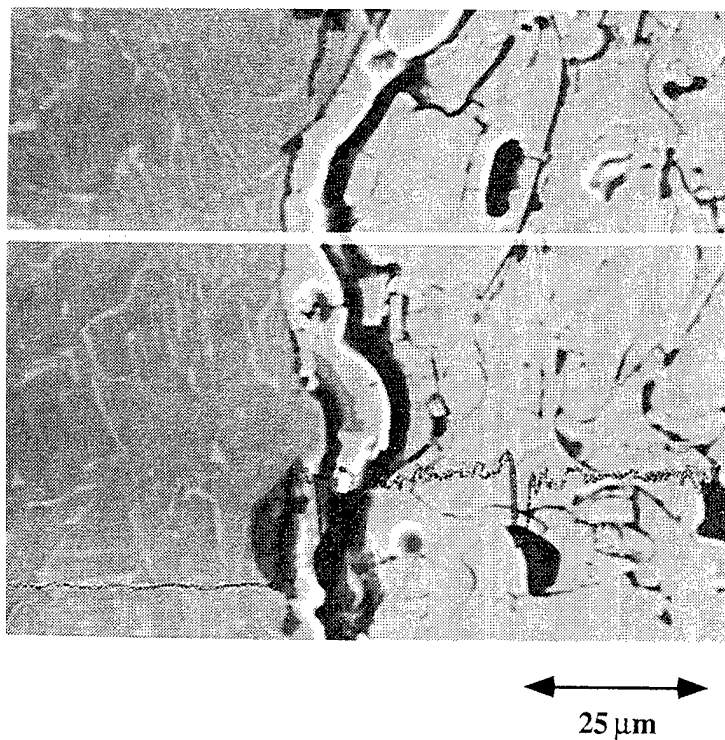


Figure 40. Graph showing the change in composition of the yttria stabilized zirconia (YSZ) coating on the Ti-47Al-2Cr-4Ta substrate. The change is relative to the amount of the element that was initially present. Oxygen was ignored in this analysis.

As-Coated



500 Cycles

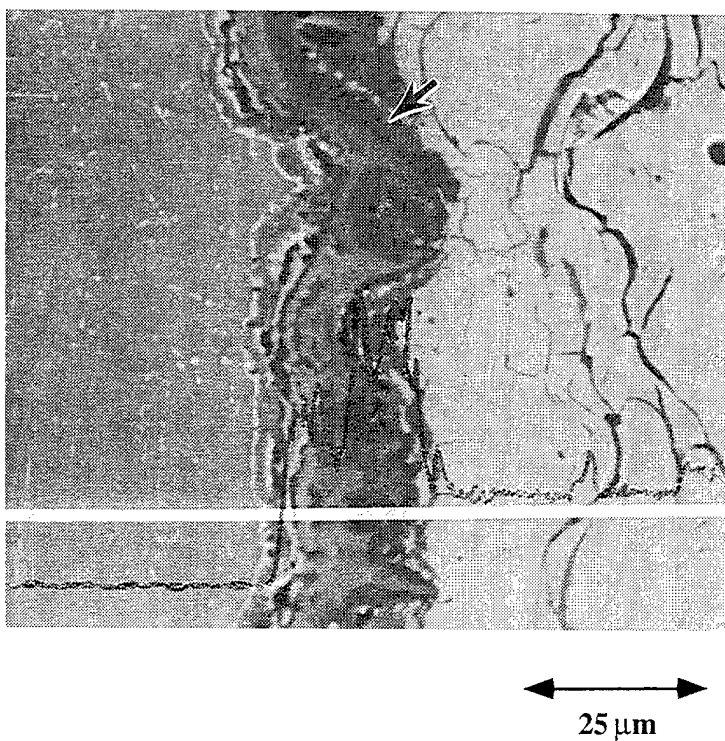
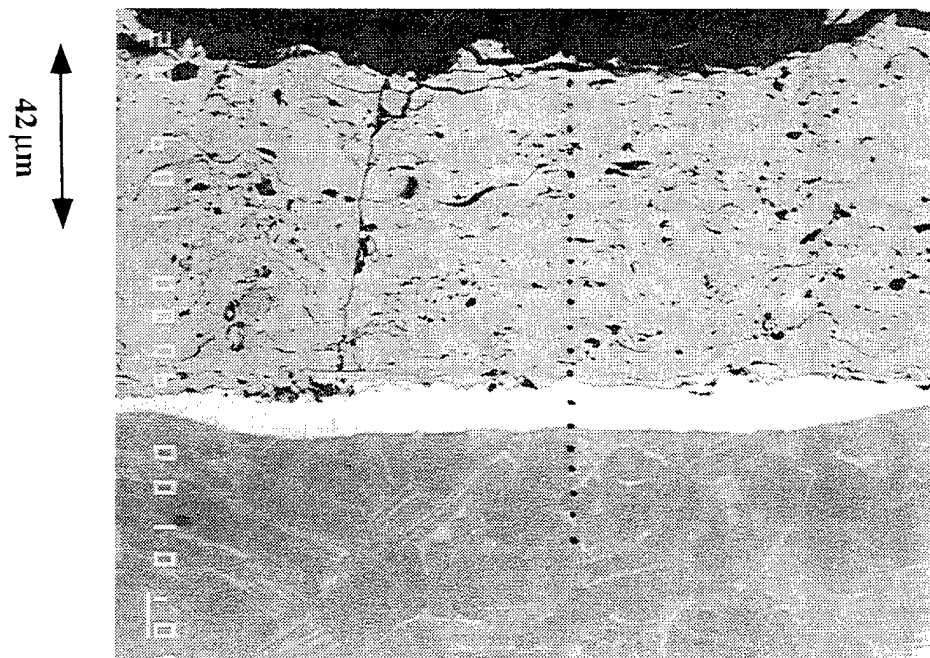
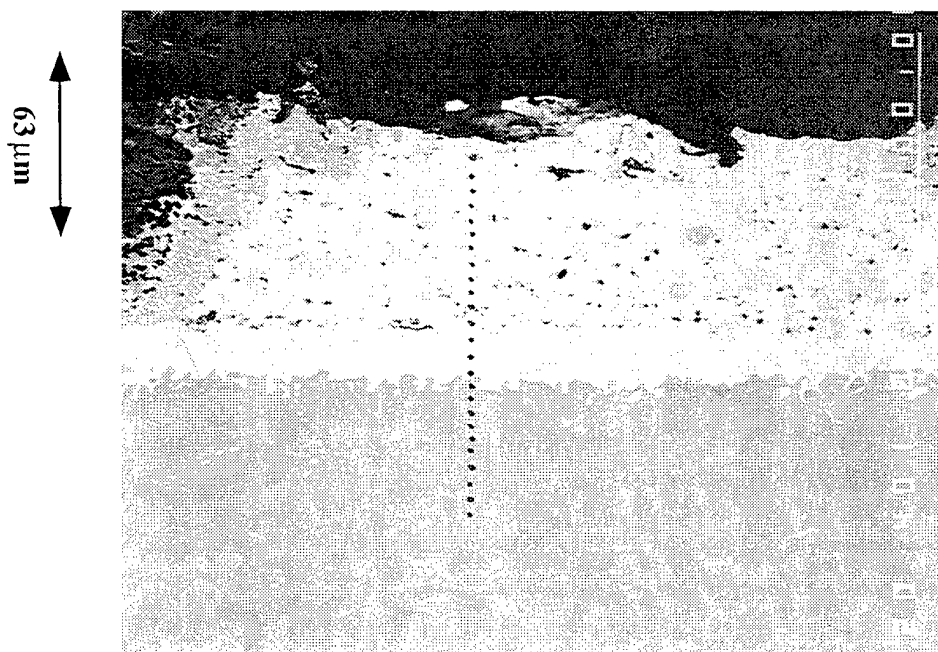


Figure 41. Secondary electron micrographs of the yttria stabilized zirconia coating on Ti-47Al-2Cr-4Ta. The top micrograph is as-coated and the bottom is after cyclic oxidation at 900°C (1650°F). The white line indicates where a line scan for oxygen was made. The fine white dots indicate the relative level of oxygen. The oxygen content of the YSZ is about 67 atom percent.



As-Coated



500 Cycles

Figure 42. Electron micrographs of the LPPS Ti-44Al-28Cr coating applied to Ti-48Al-2Cr-2Nb. The initial microstructure (top) displays a typical plasma spray appearance. Copper and Ni-base superalloy contamination were noted in the sample (arrow). The exposed microstructure (bottom) shows areas where a protective alumina scale has formed and areas where non-protective rutile dominates.

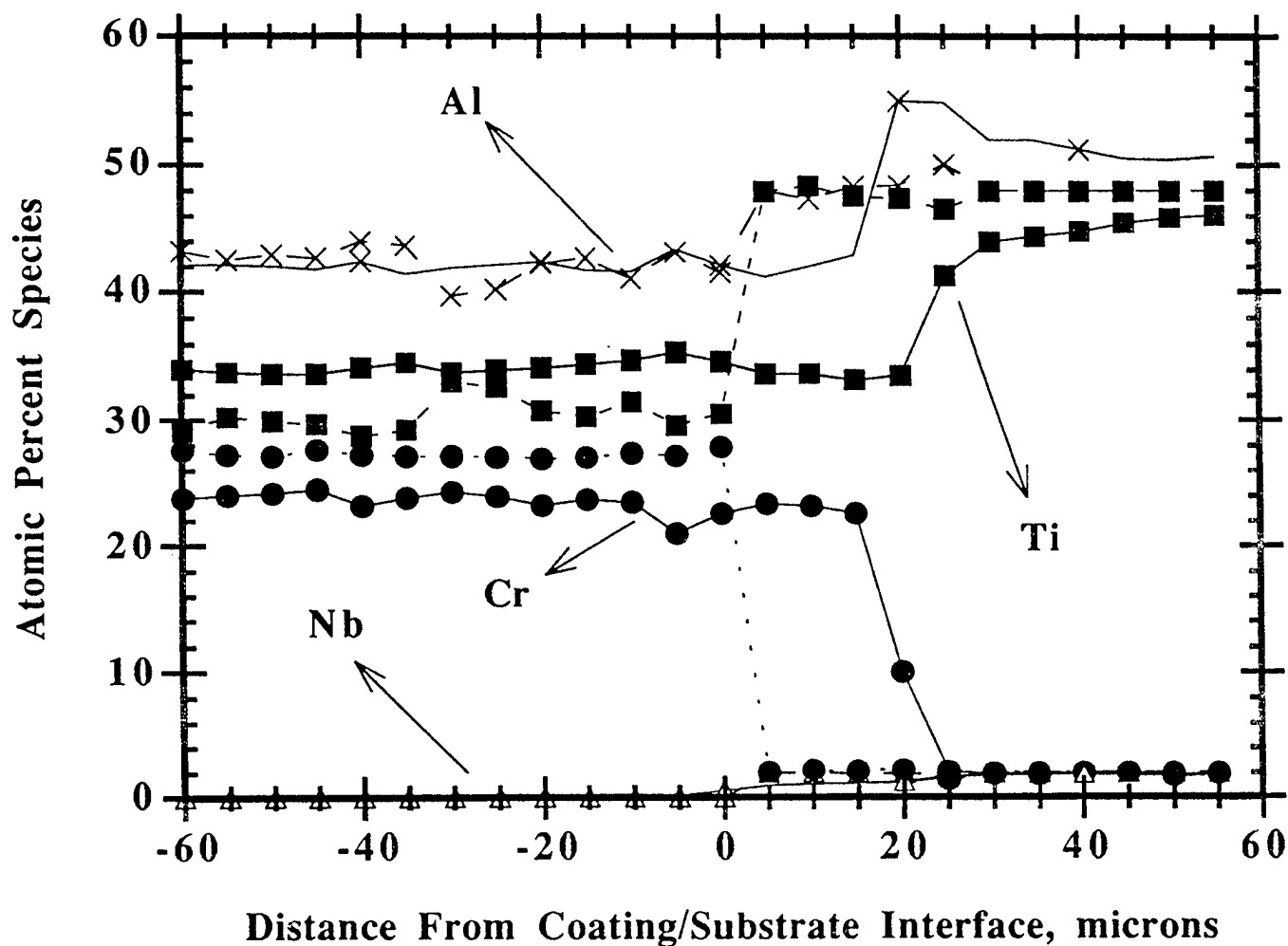


Figure 43. Microprobe traces for the elements in the LPPS Ti-44Al-28Cr coating on Ti-48Al-2Cr-2Nb. The dotted lines represents the initial chemistry while the solid lines are after the 500Hr. exposure at 900°C (1650°F).

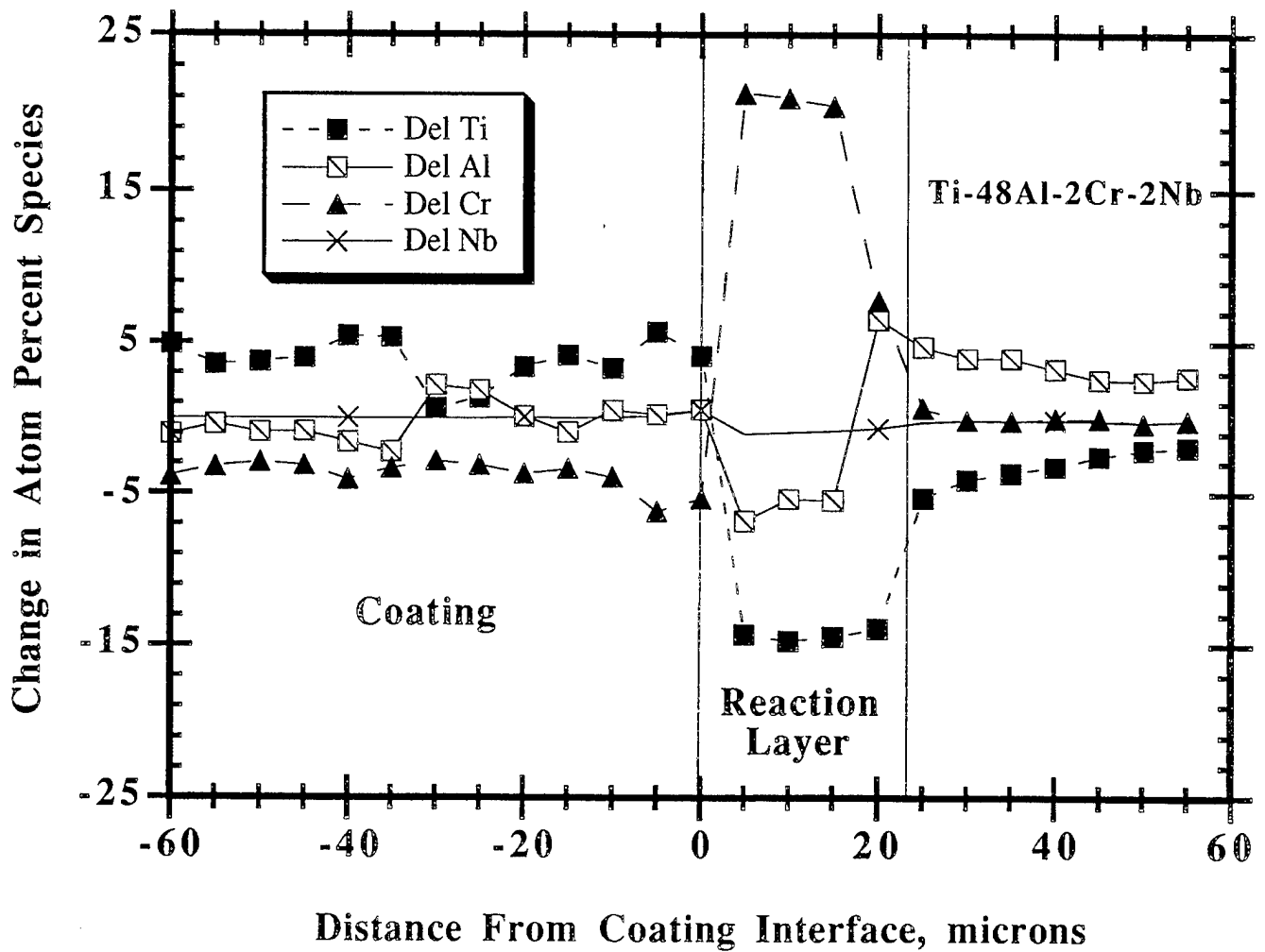


Figure 44. Graph showing the change in composition of LPPS Ti-44Al-28Cr coating on Ti-48Al-2Cr-2Nb. The change is relative to the amount of the element that was initially present. Oxygen was ignored in this analysis.

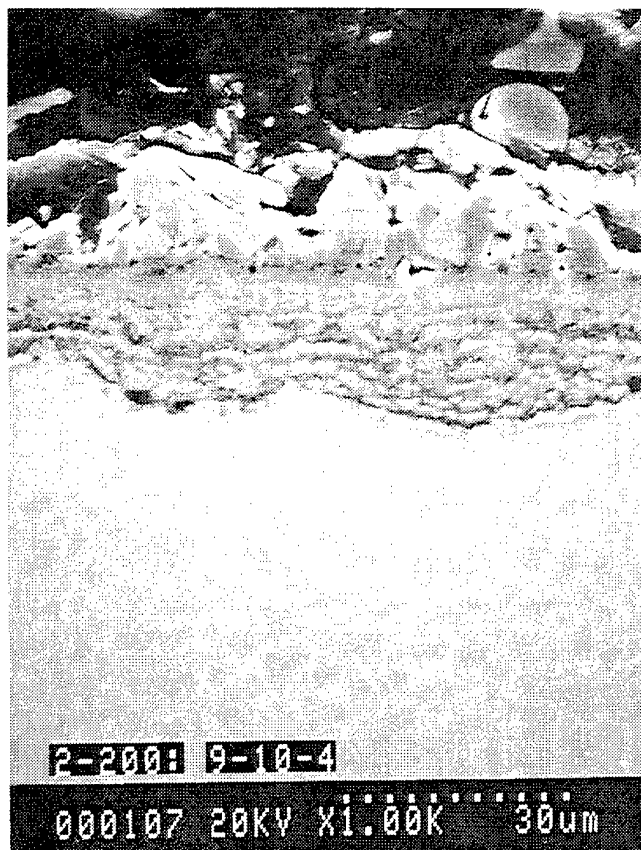


Figure 45. Secondary electron micrographs of the oxide scale formed on Ti-48Al-2Cr-2Nb. The oxide had locally thick areas that were associated with spallation.

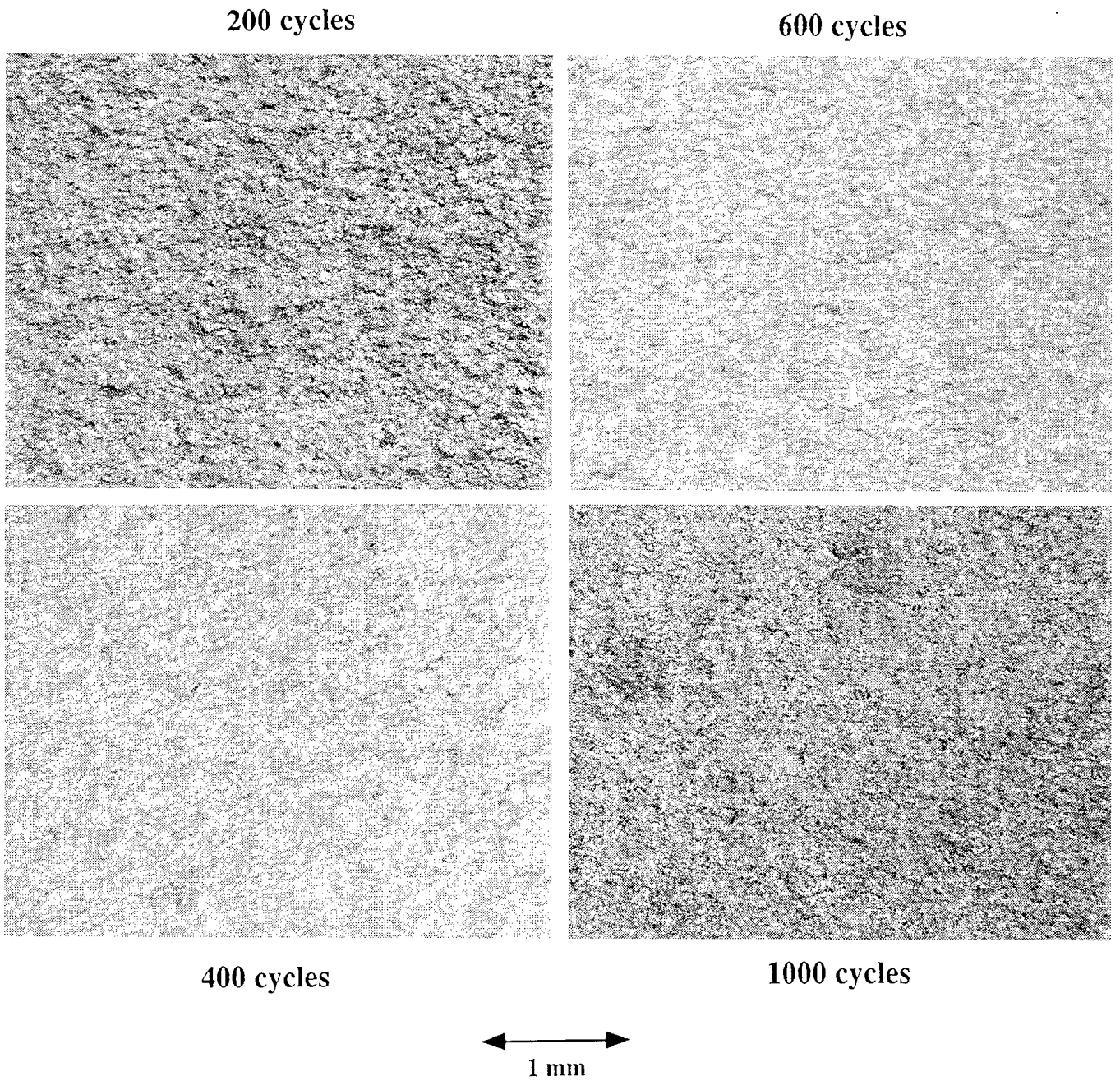


Figure 46. Surface optical micrographs of the cermet (80%Alumina + NiCrAlY) coated gamma sample at various intervals throughout the 760°C (1400°F) cyclic oxidation test in air.

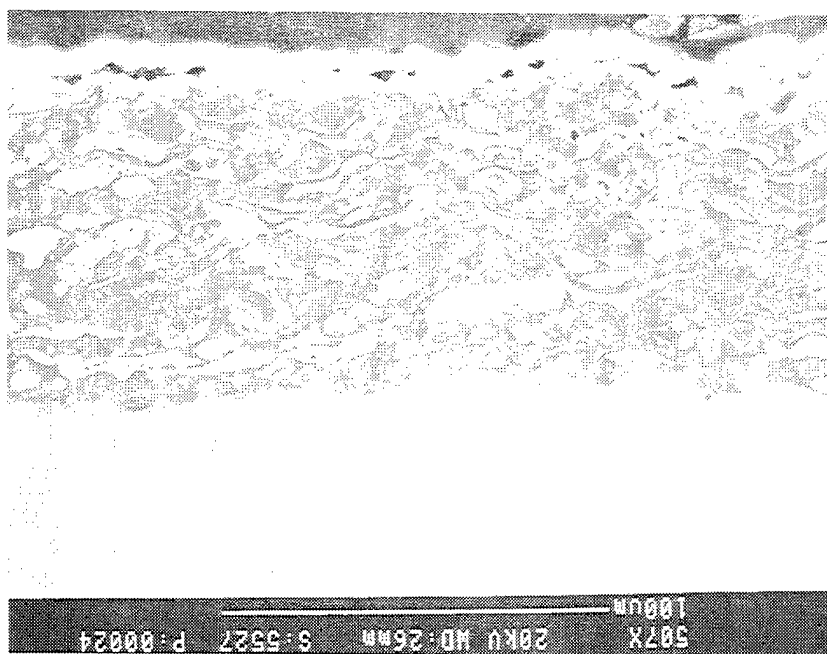
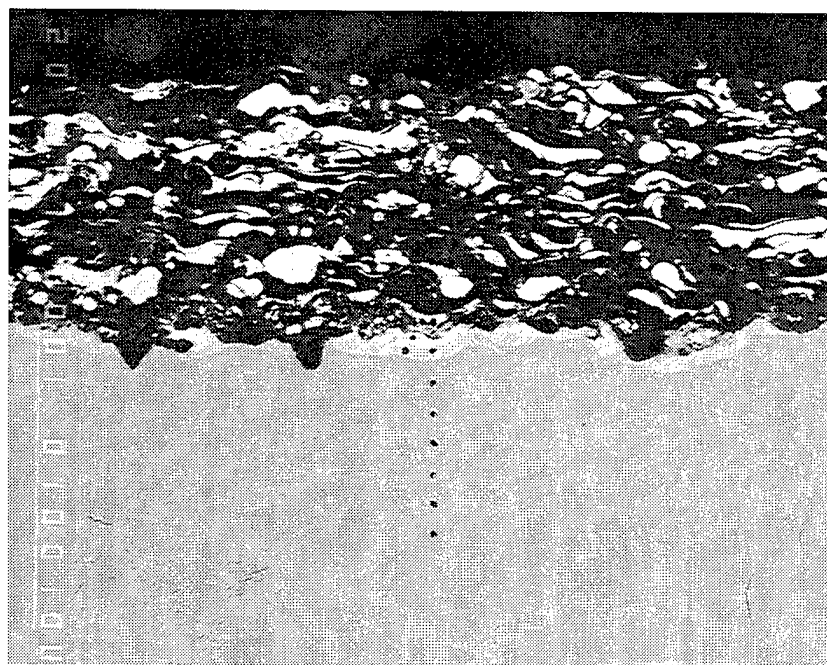


Figure 47. Backscattered and secondary electron micrographs from a cross section of the cermet (80%Alumina + NiCrAlY) coated gamma sample after the 760°C (1400°F) cyclic oxidation test in air.

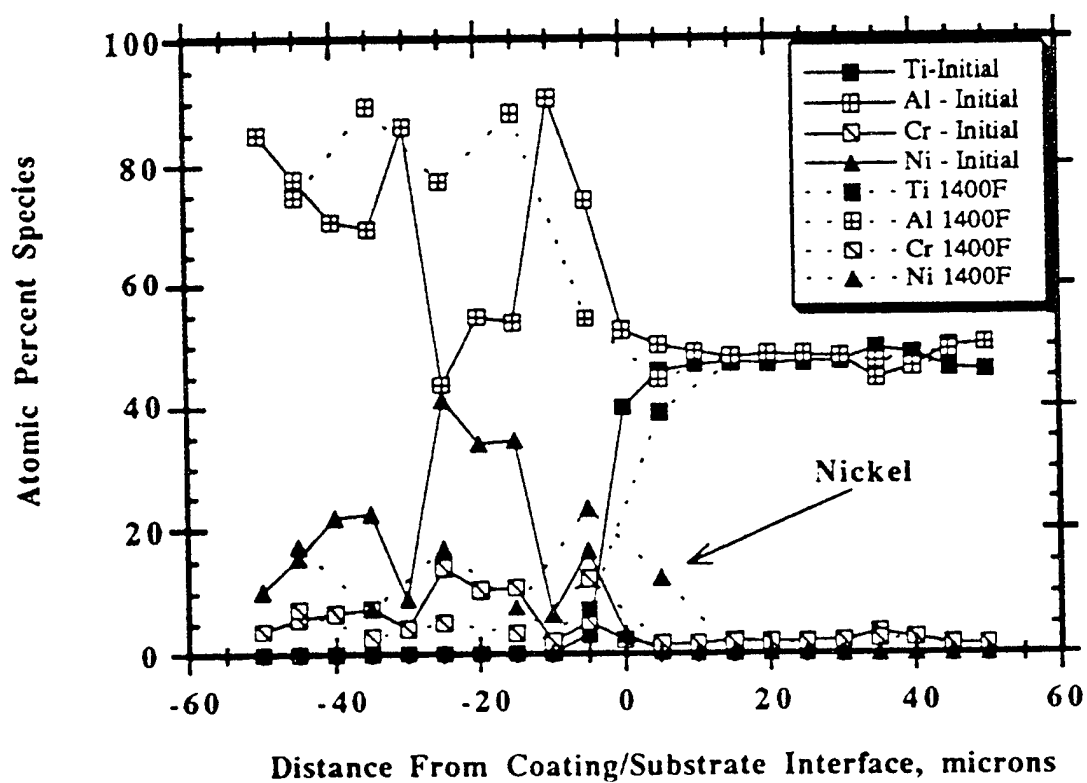
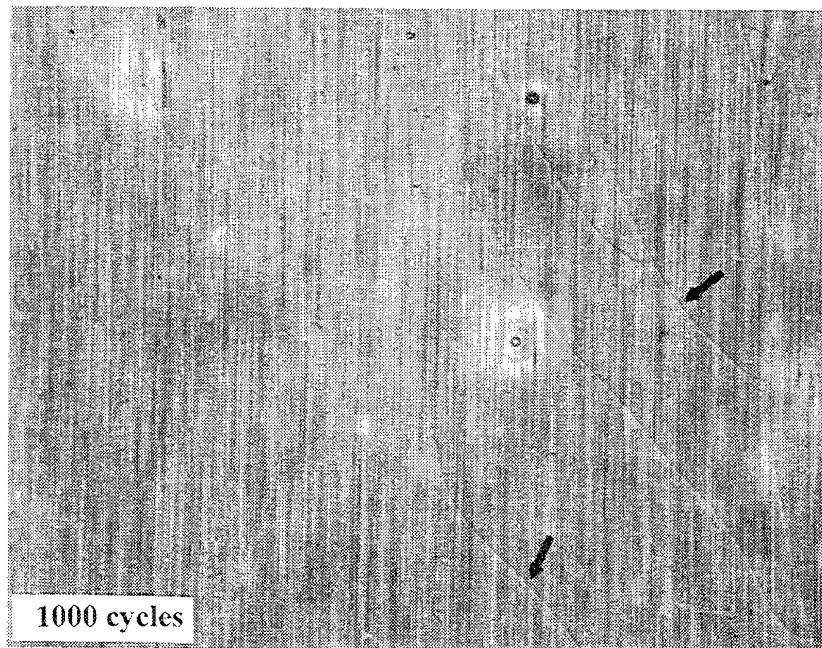
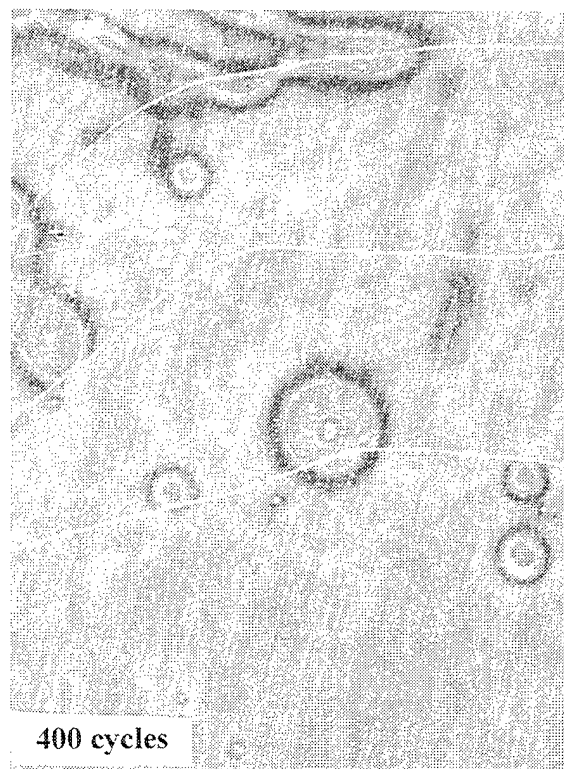


Figure 48. Chemical composition of the cermet coating on Ti-48Al-2Cr-2Nb before and after cyclic oxidation for 1000Hr. at 760°C (1400°F) in air. Nickel has diffused into the substrate resulting in reaction layers.



1 mm

Figure 49. Surface optical micrographs of the sputtered Ti-44Al-28Cr gamma sample at various intervals throughout the 760°C (1400°F) cyclic oxidation test in air. Some thermal expansion mismatch cracks are observed.

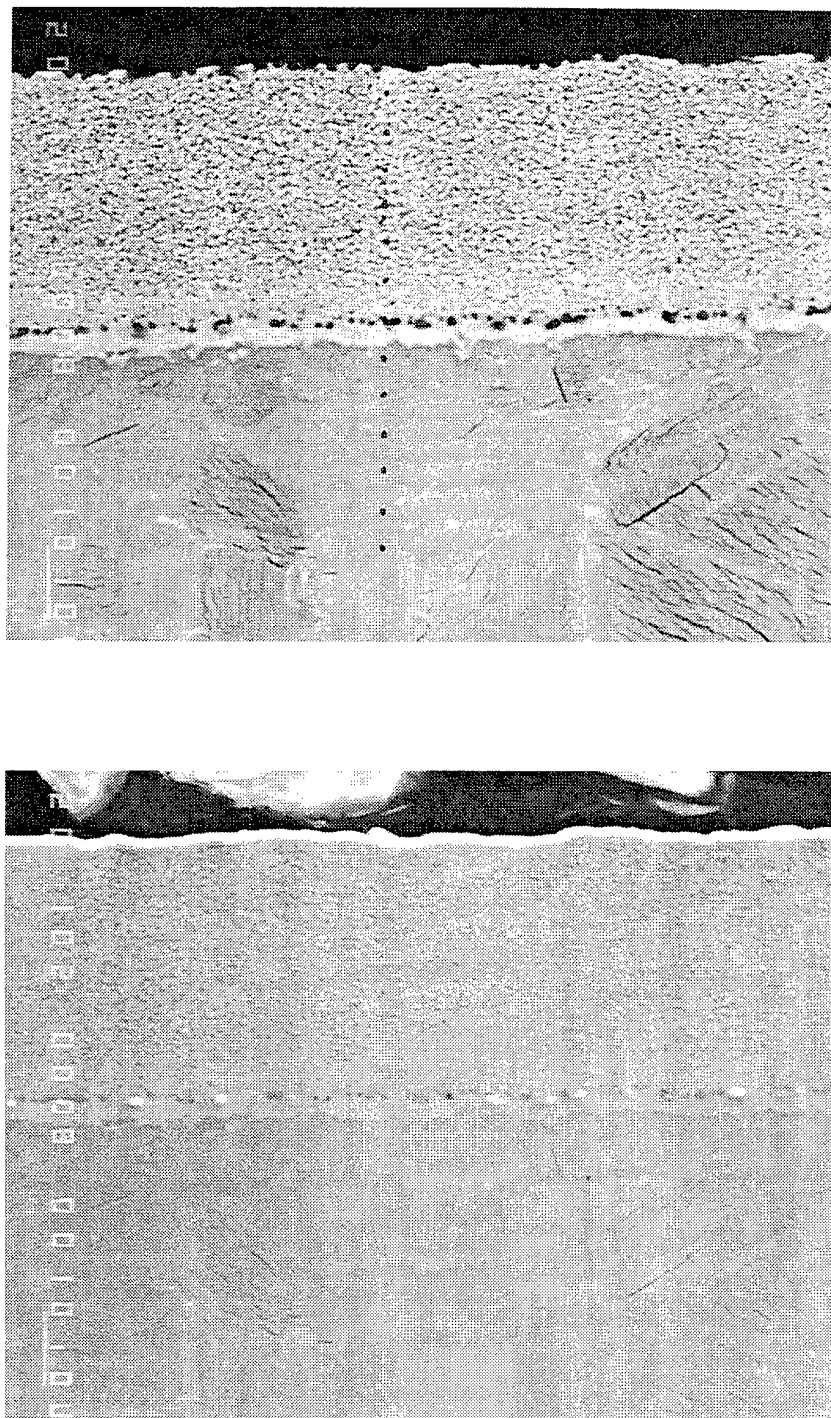


Figure 50. Backscattered and secondary electron micrographs from a cross section of the sputtered Ti-44Al-28Cr gamma sample after the 760°C (1400°F) cyclic oxidation test in air.

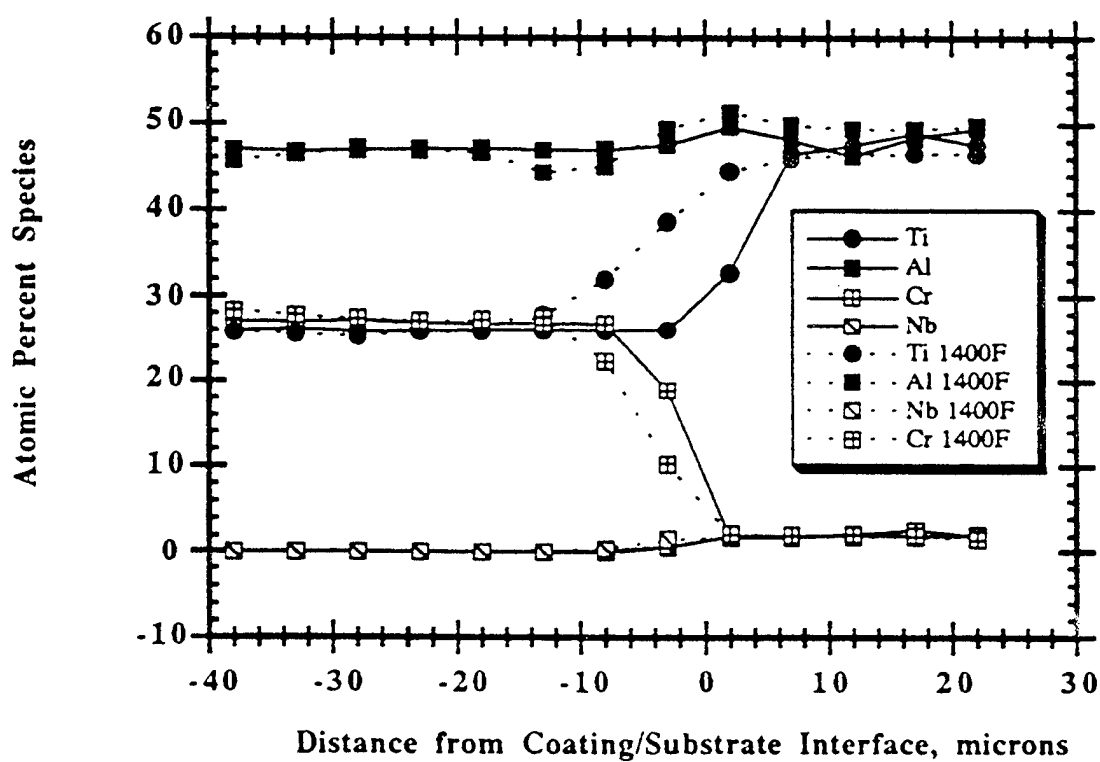


Figure 51. Microprobe results showing the difference in chemistry for a sputtered Ti-44Al-28Cr coating before and after cyclic oxidation exposure at 760°C (1400°F).

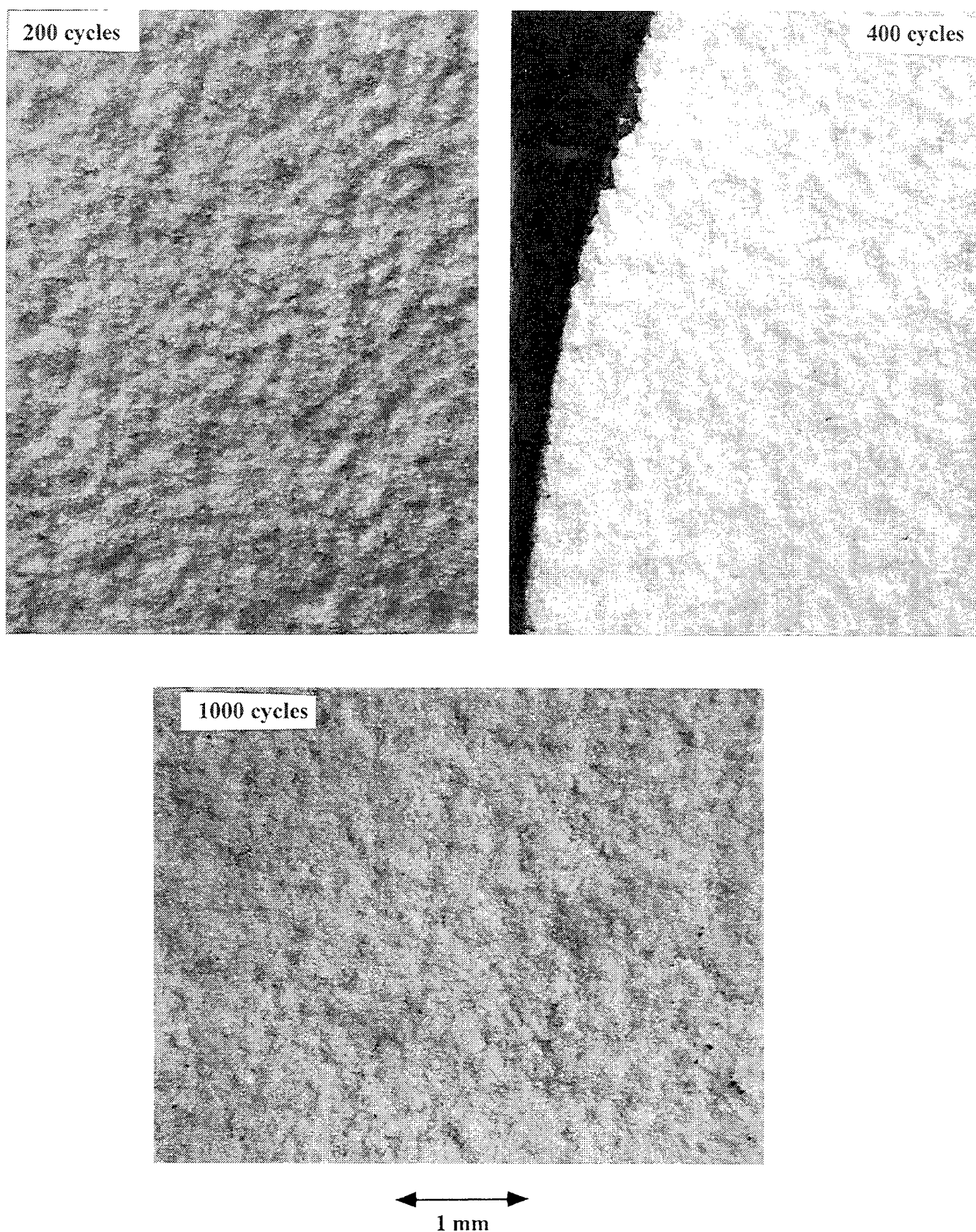


Figure 52. Surface optical micrographs of the APS YSZ gamma sample at various intervals throughout the 760°C (1400°F) cyclic oxidation test in air. Coating spallation was evident at the edges.

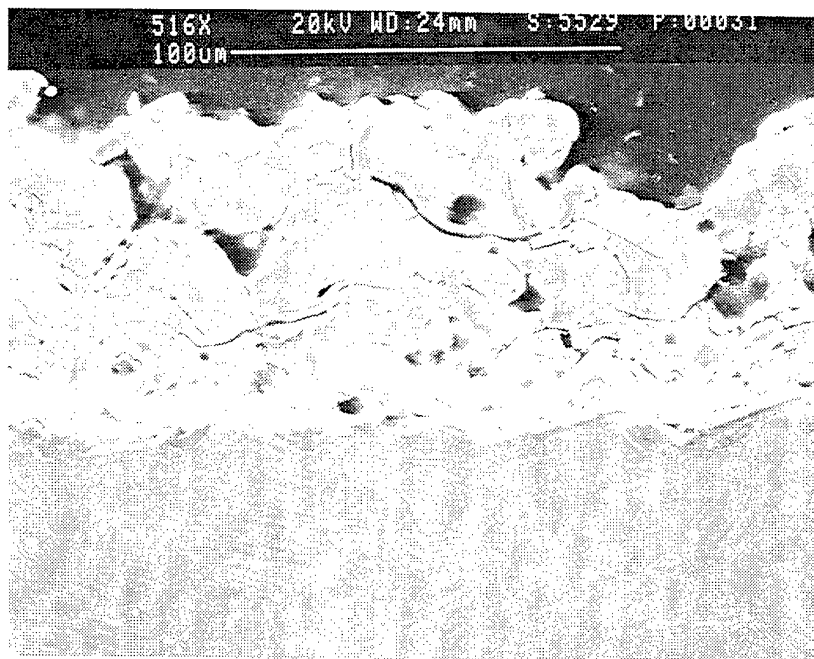
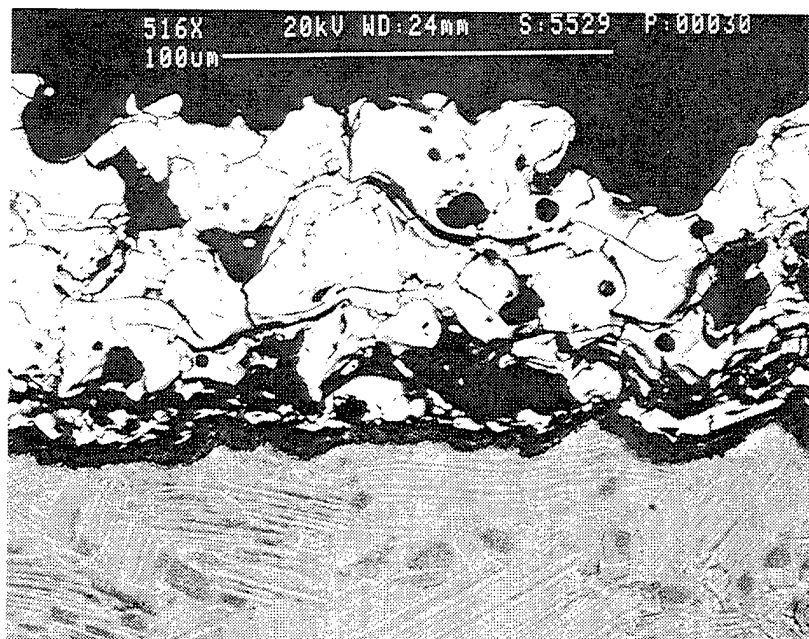
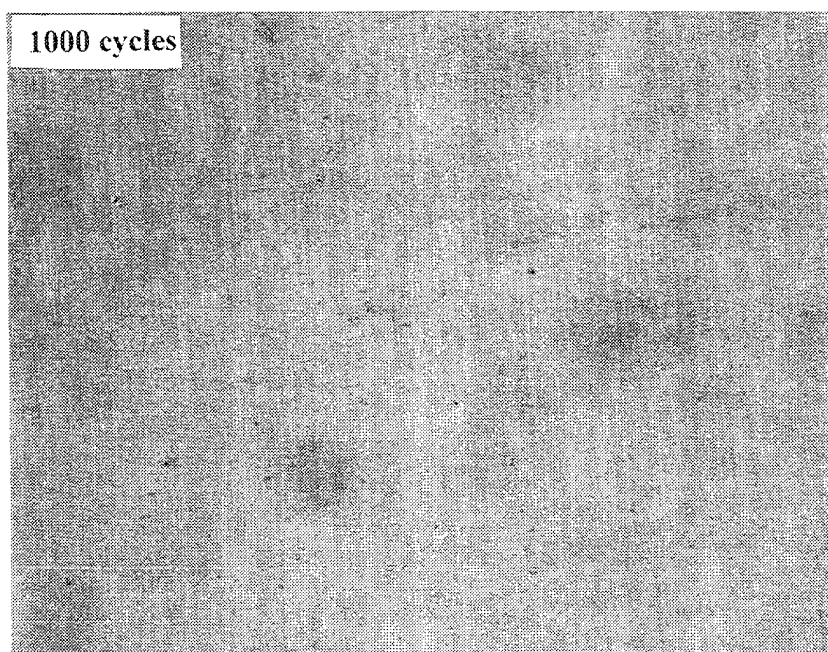
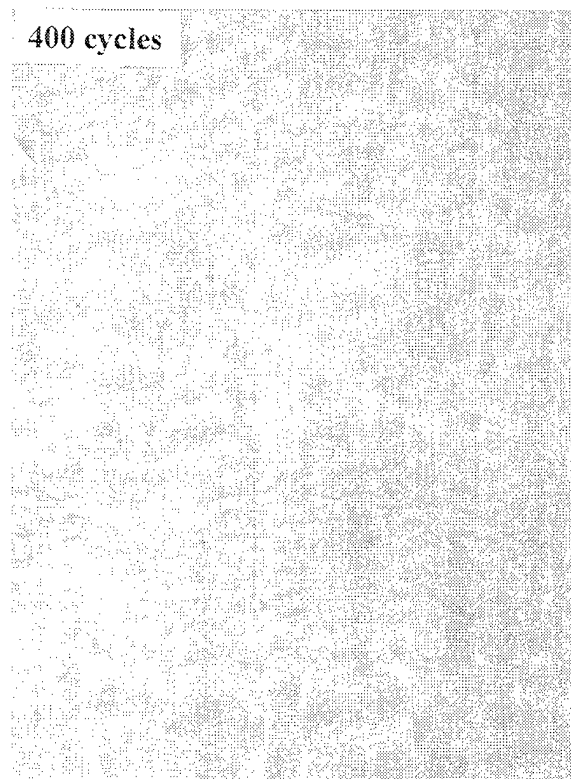
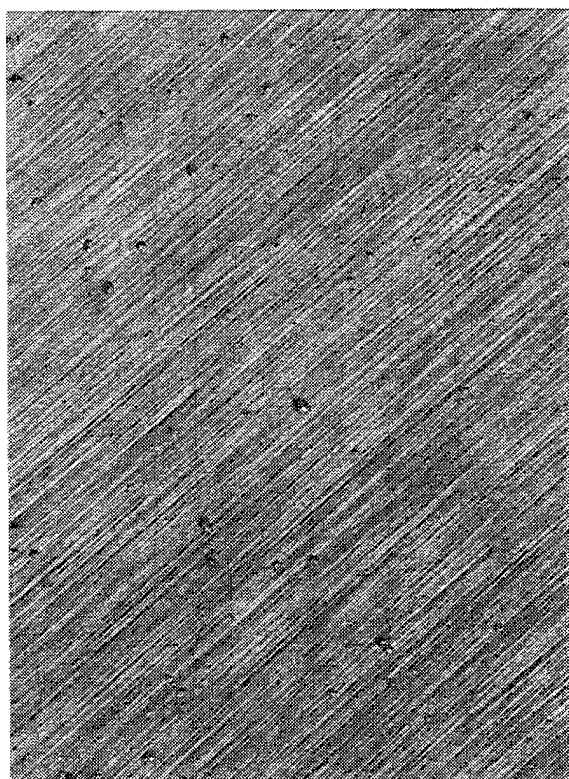


Figure 53. Backscattered and secondary electron micrographs from a cross section of the APS YSZ/gamma sample after the 760°C (1400°F) cyclic oxidation test in air.



1 mm

Figure 54. Surface optical micrographs of the sputtered Ti-55Al-9Cr/gamma sample at various intervals throughout the 760°C (1400°F) cyclic oxidation test in air. Some thermal expansion mismatch cracks are observed.

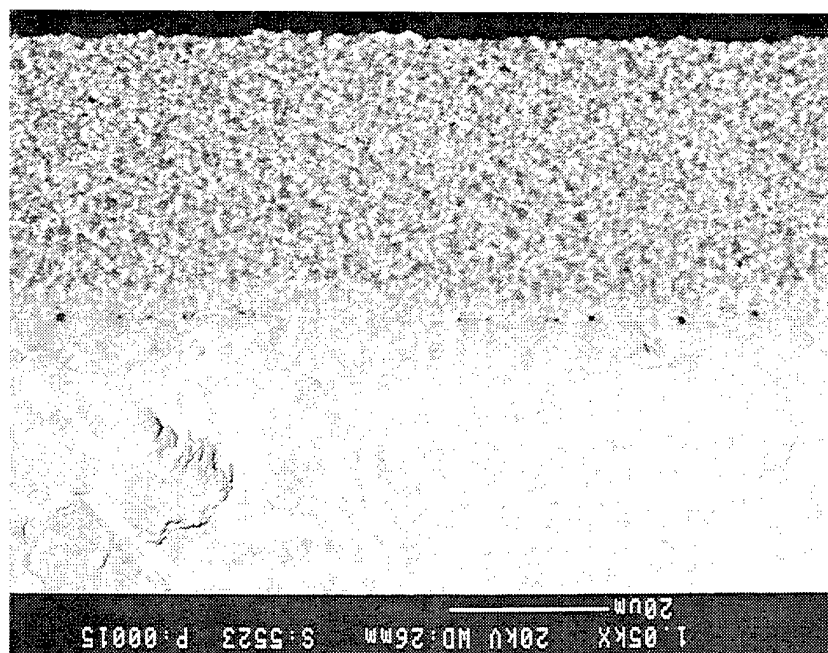


Figure 55. Backscattered electron micrograph from a cross section of the sputtered Ti-55Al-9Cr gamma sample after the 760°C (1400°F) cyclic oxidation test in air.

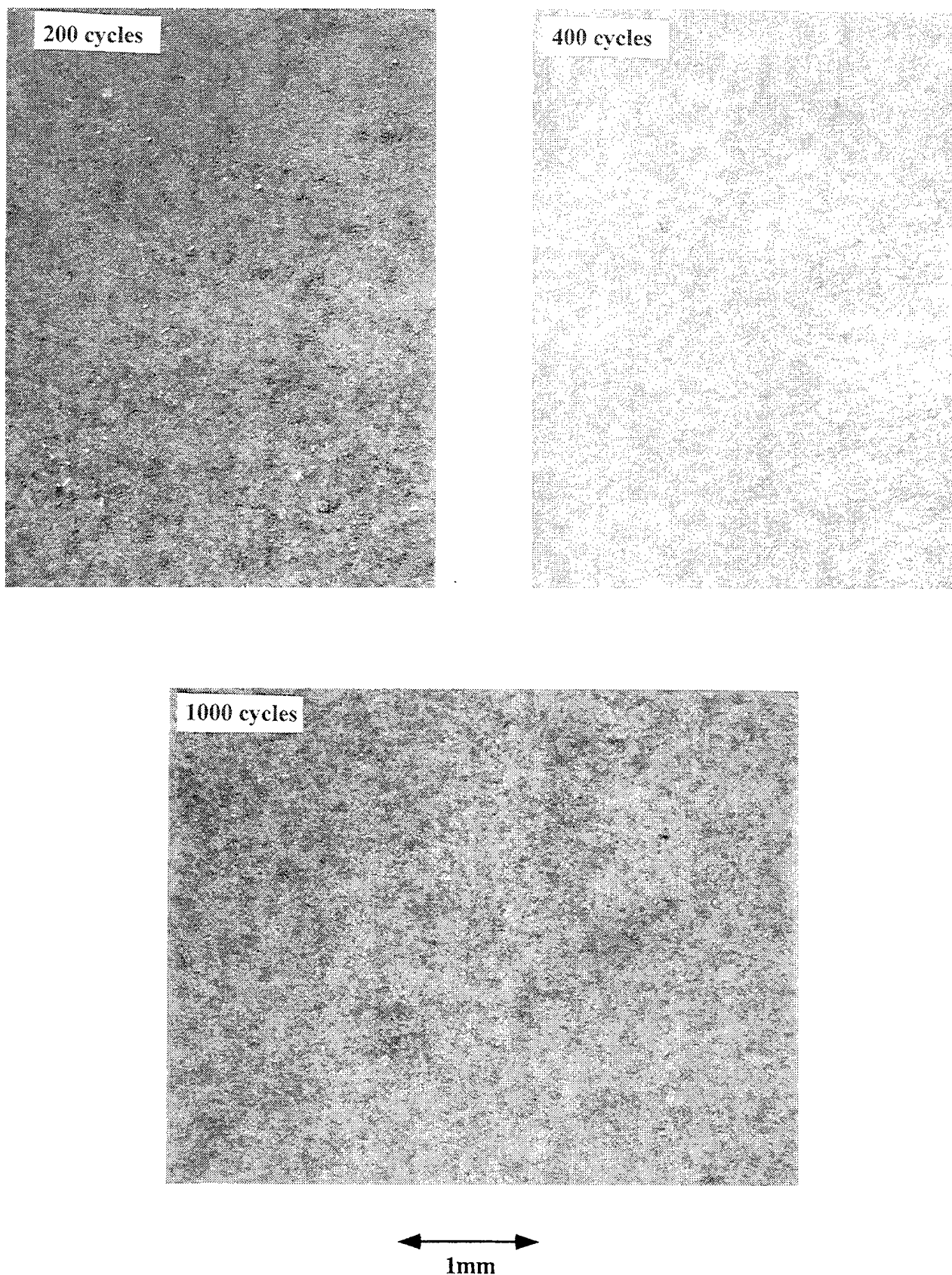


Figure 56. Surface optical micrographs of the HVOF Ti-44Al-28Cr coated gamma sample at various intervals throughout the 760°C (1400°F) cyclic oxidation test in air.

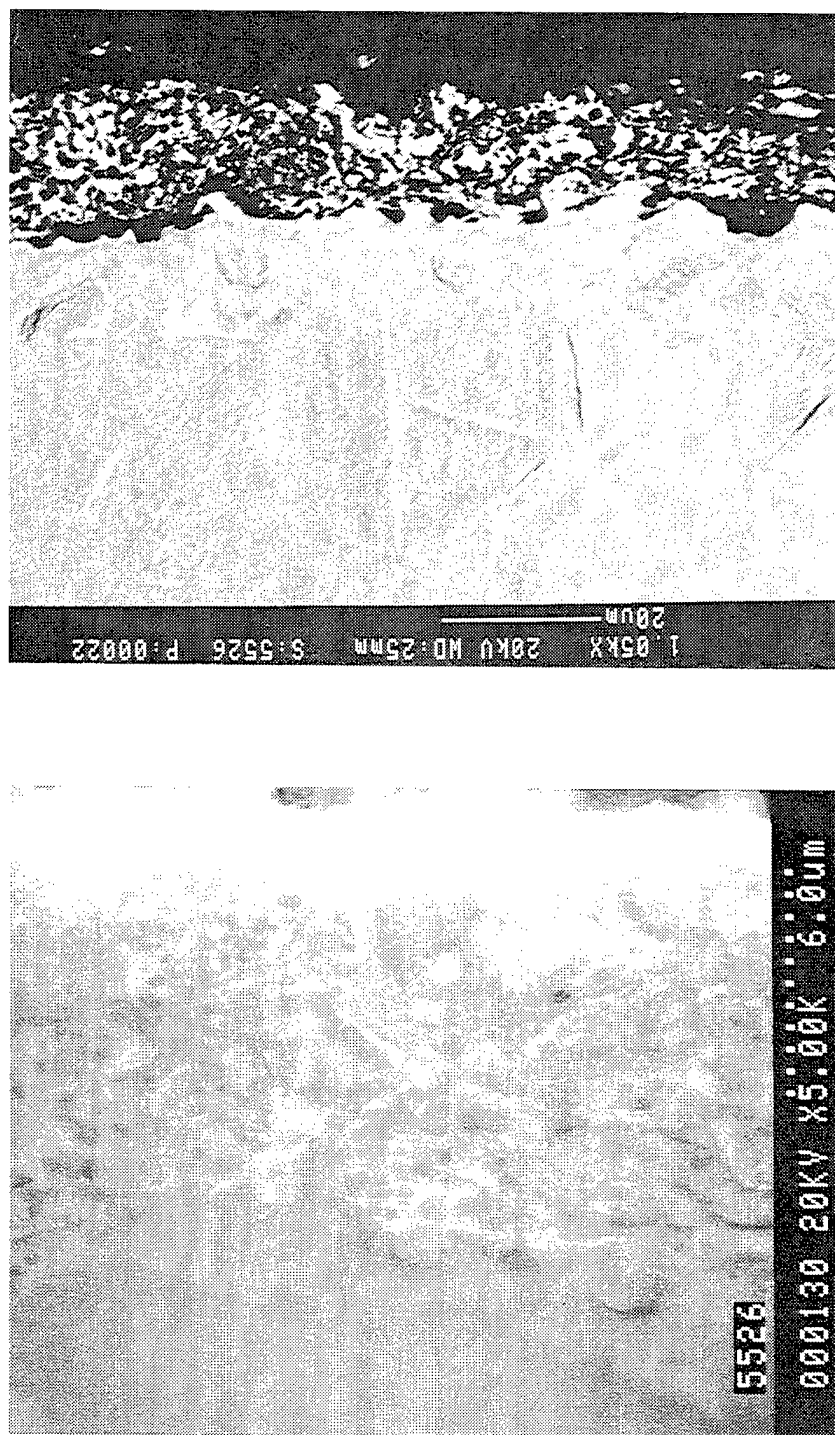


Figure 57. Backscattered and secondary electron micrographs from a cross section of the HVOF Ti-44Al-28Cr/gamma sample after the 760°C (1400°F) cyclic oxidation test in air.

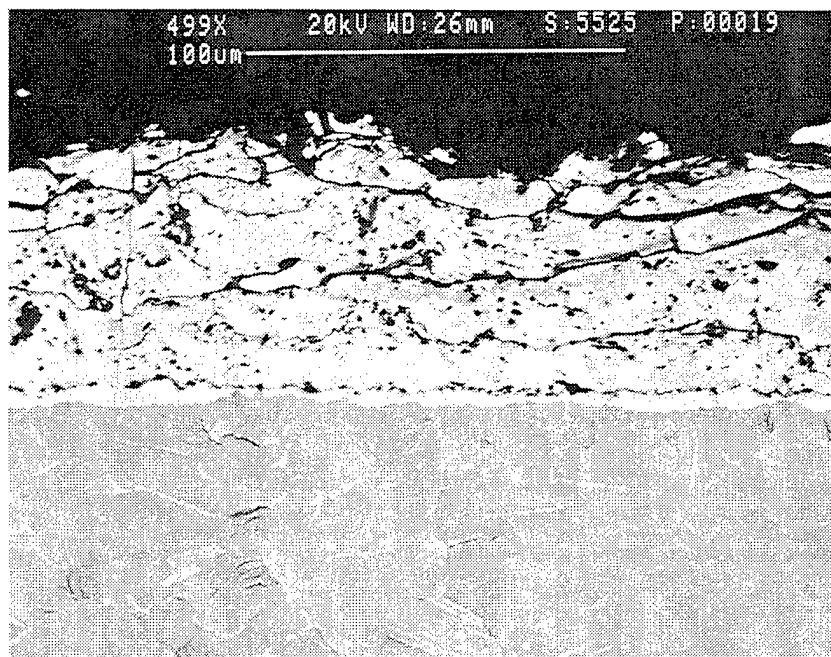
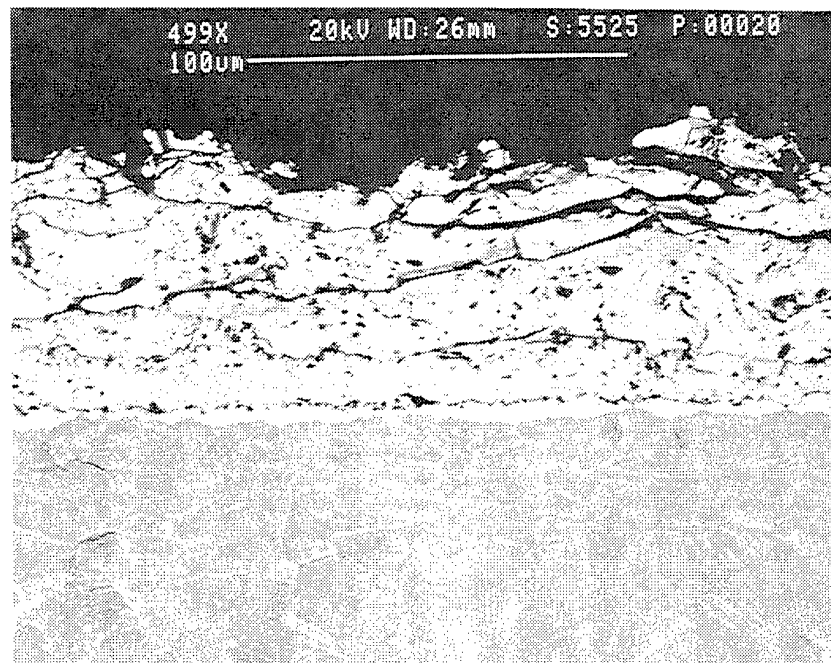


Figure 58. Backscattered and secondary electron micrographs from a cross section of the LPPS Ti-44Al-28Cr/gamma sample after the 760°C (1400°F) cyclic oxidation test in air.

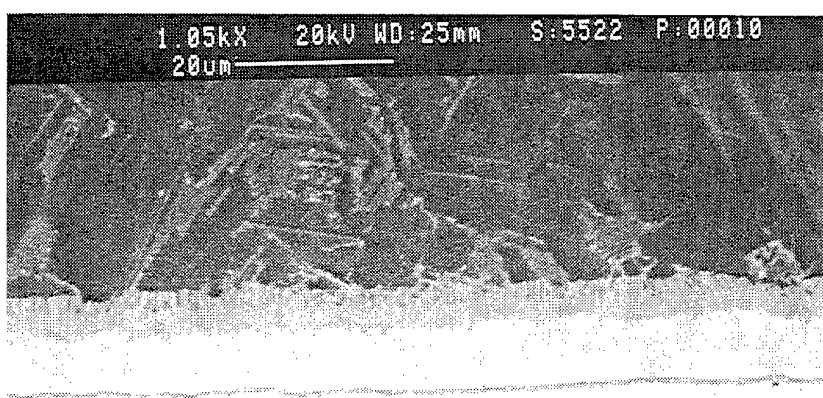
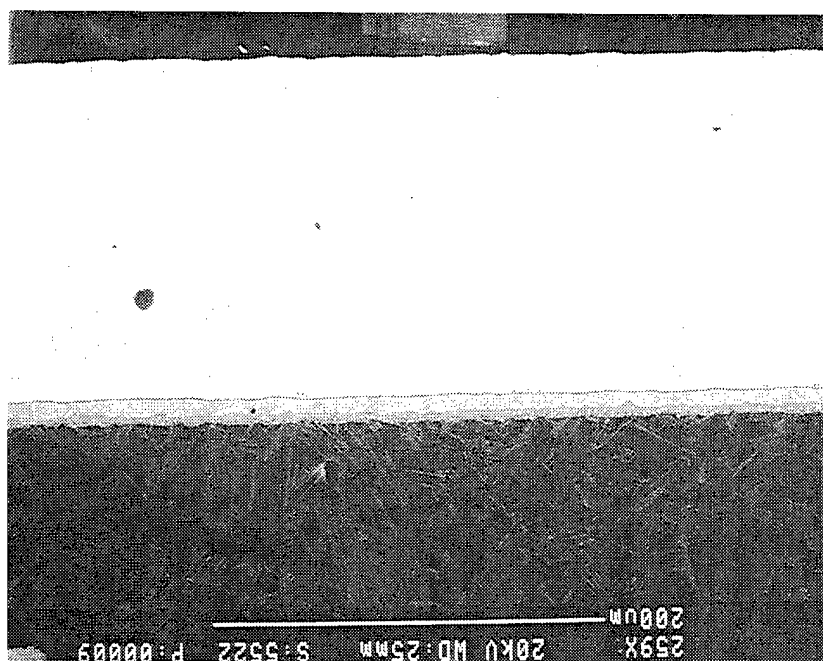


Figure 59. Backscattered and secondary electron micrographs from a cross section of the sputtered Alloy 718/gamma sample after the 760°C (1400°F) cyclic oxidation test in air.

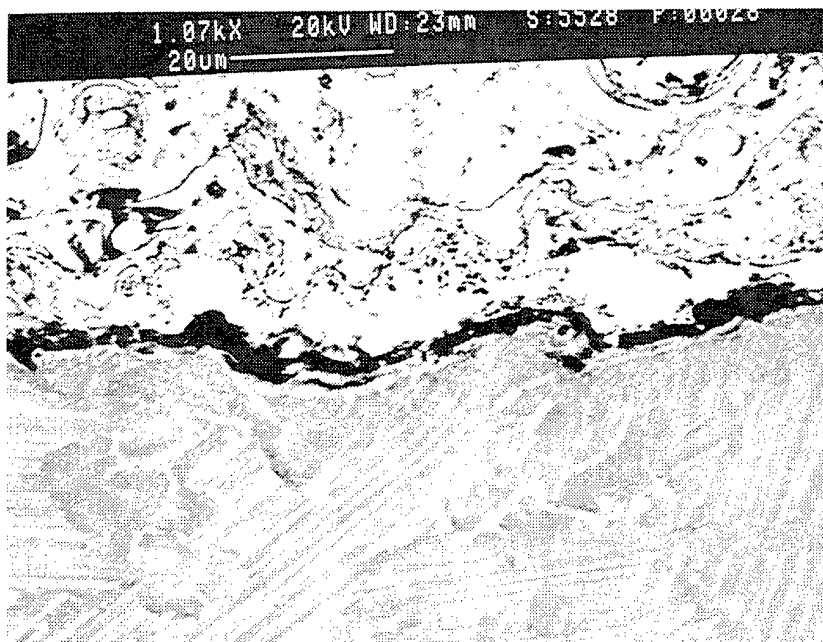
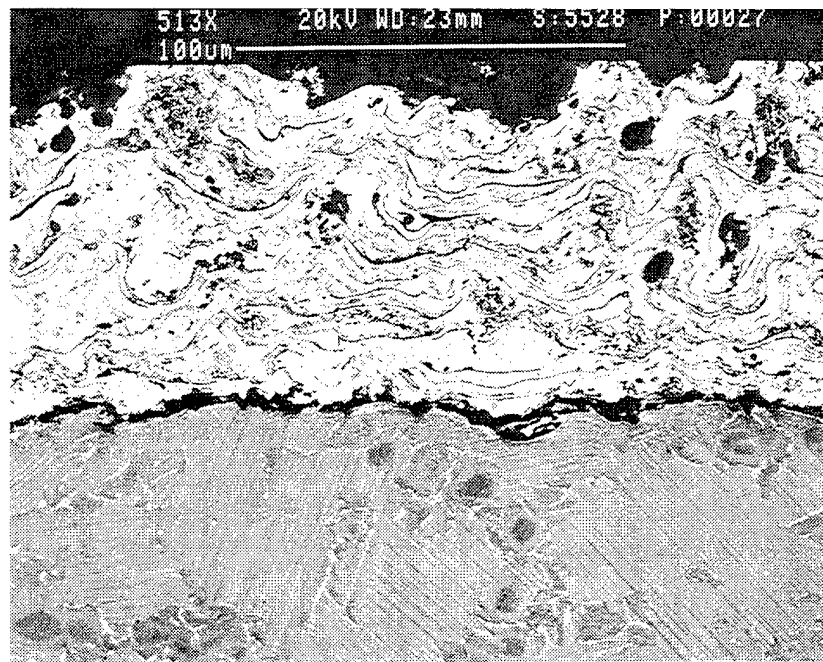
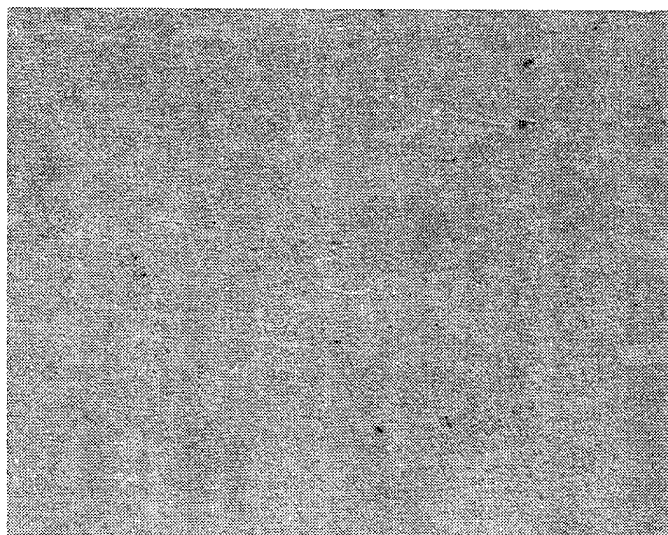
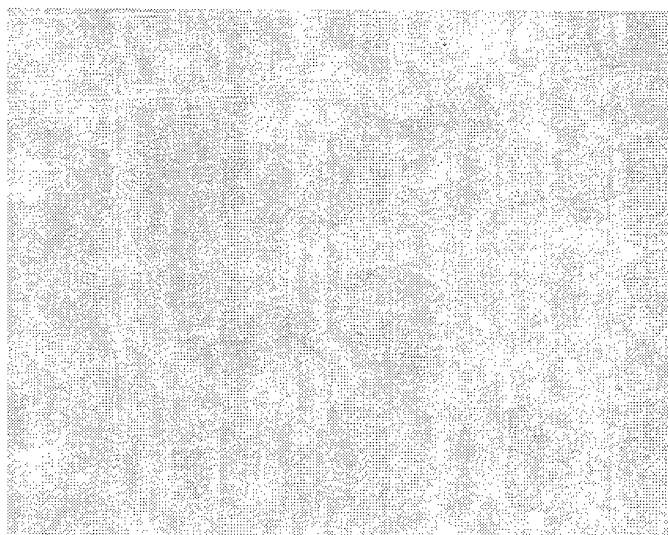


Figure 60. Backscattered electron micrographs from a cross section of the HVOF CoCr(WSiC)/gamma sample after the 760°C (1400°F) cyclic oxidation test in air.

200 cycles



600 cycles



400 cycles



1000 cycles

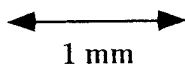
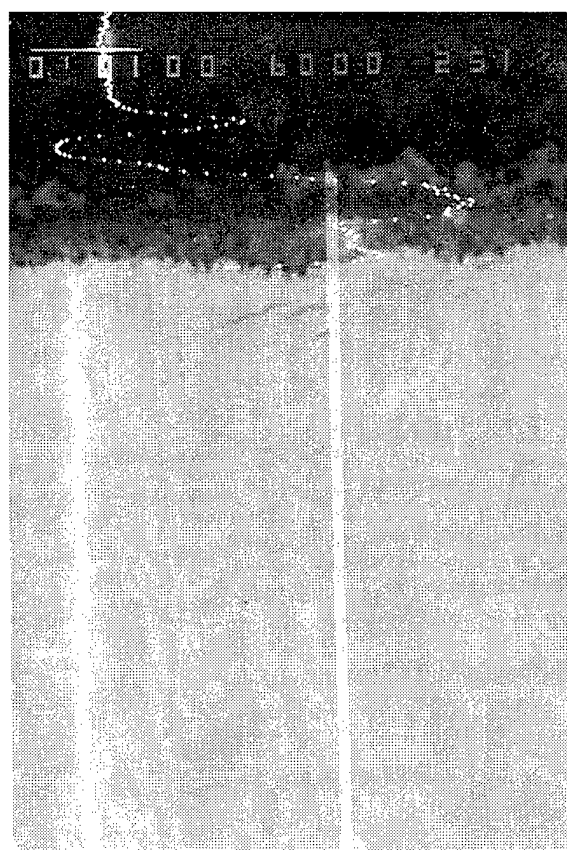
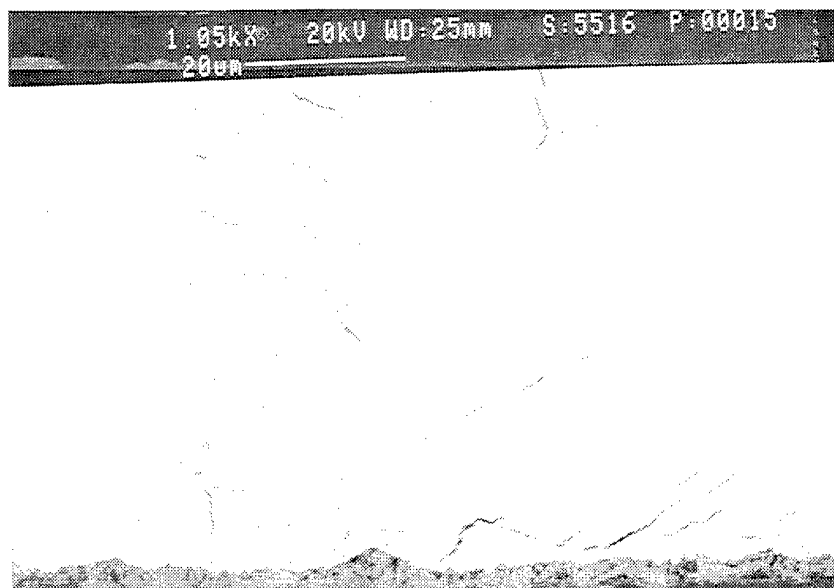


Figure 61. Surface optical micrographs of the uncoated Ti-48Al-2Cr-2Nb sample at various intervals throughout the 760°C (1400°F) cyclic oxidation test in air.



Oxygen →

Figure 62. Backscattered micrographs of the uncoated Ti-48Al-2Cr-2Nb sample after the 760°C (1400°F) cyclic oxidation test in air. One micrograph shows a microprobe trace for oxygen.

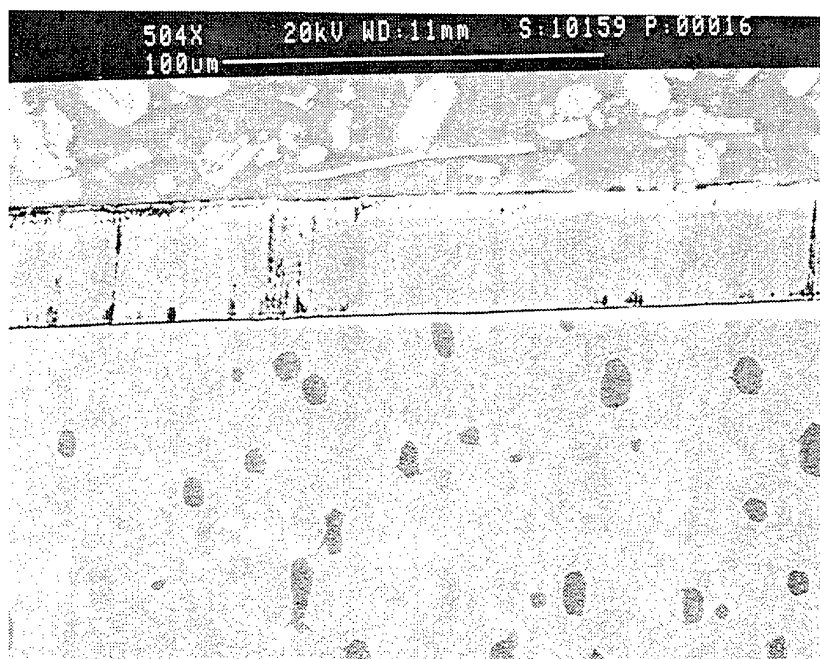
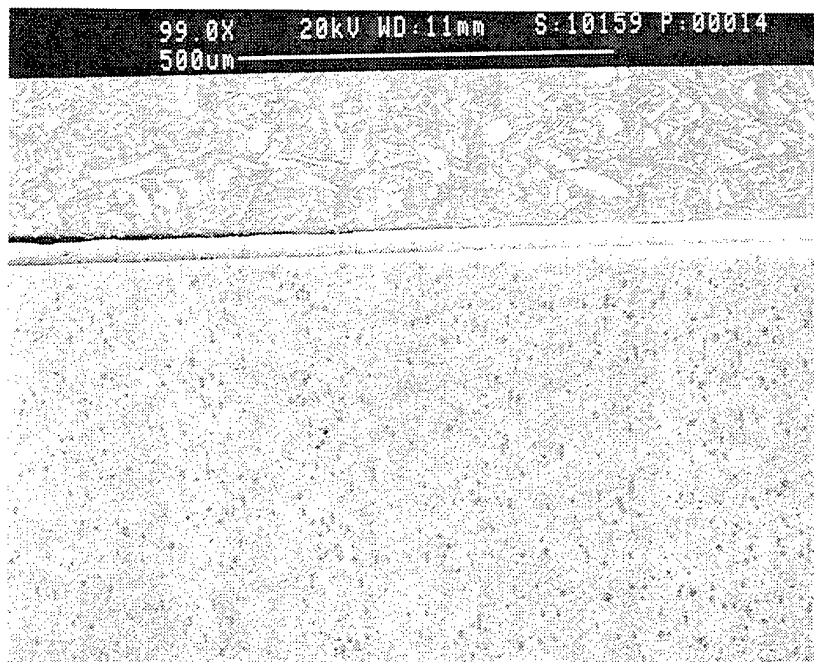


Figure 63. Backscattered electron micrographs of the sputtered Ti-44Al-28Cr on Ti-24.5Al-12.5Nb-1.5Mo. Some through thickness defects are noted in the coating.

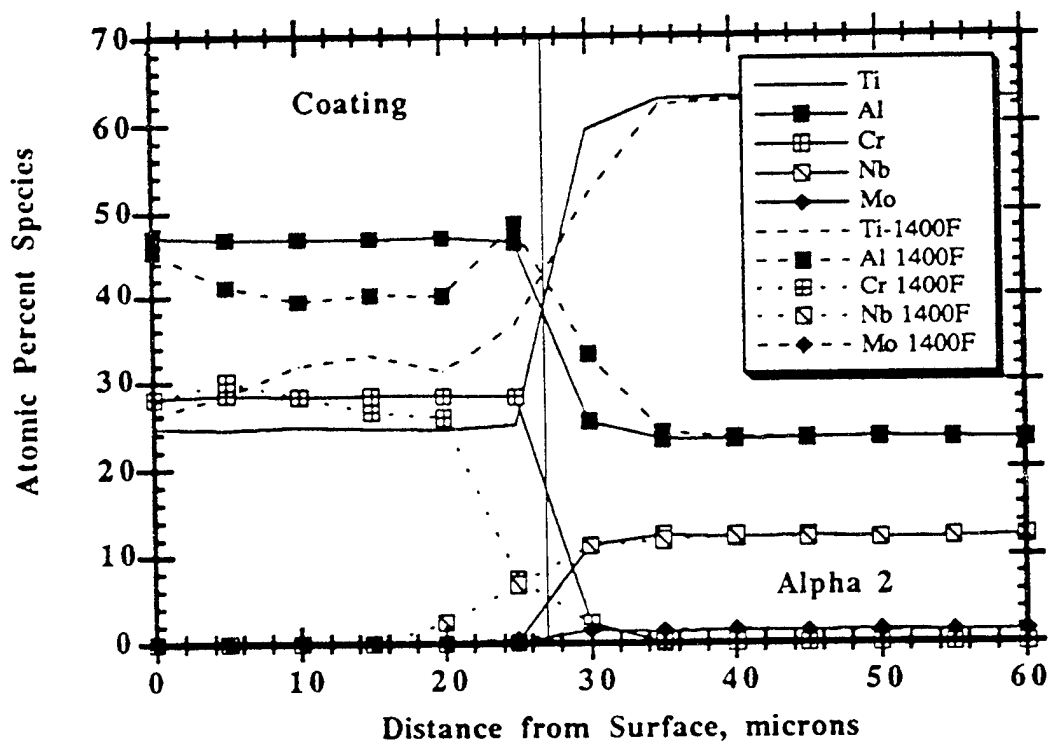


Figure 64. Microprobe traces for the elements that compose the sputtered Ti-44Al-28Cr coating on Ti-24.5Al-12.5Nb-1.5Mo.

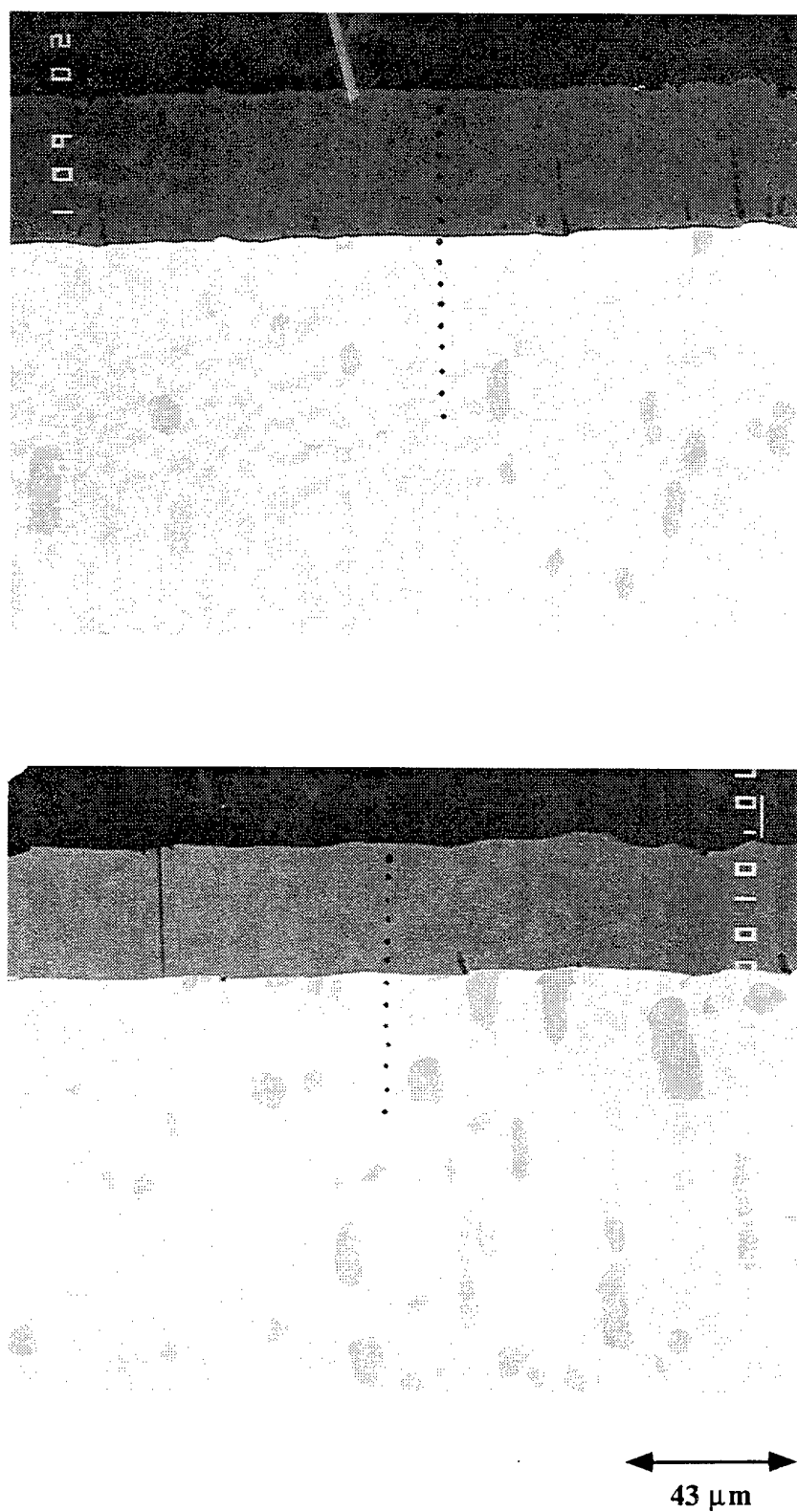


Figure 65. Backscattered electron micrographs of the sputtered Ti-55Al-8.5Cr on Ti-24.5Al-12.5Nb-1.5Mo. Some through thickness defects are noted in the coating.

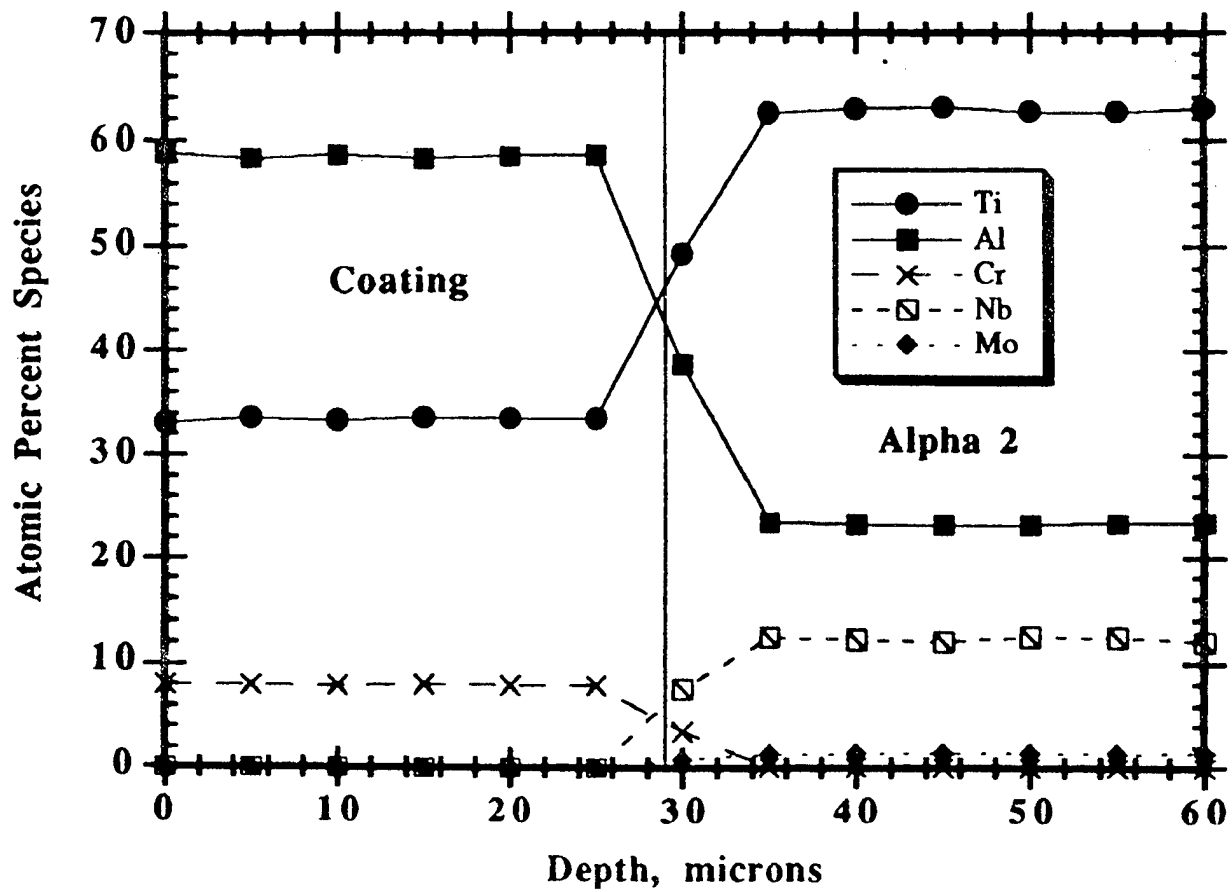


Figure 66. Microprobe traces for the elements that compose the sputtered Ti-55Al-8.5Cr coating on Ti-24.5Al-12.5Nb-1.5Mo.

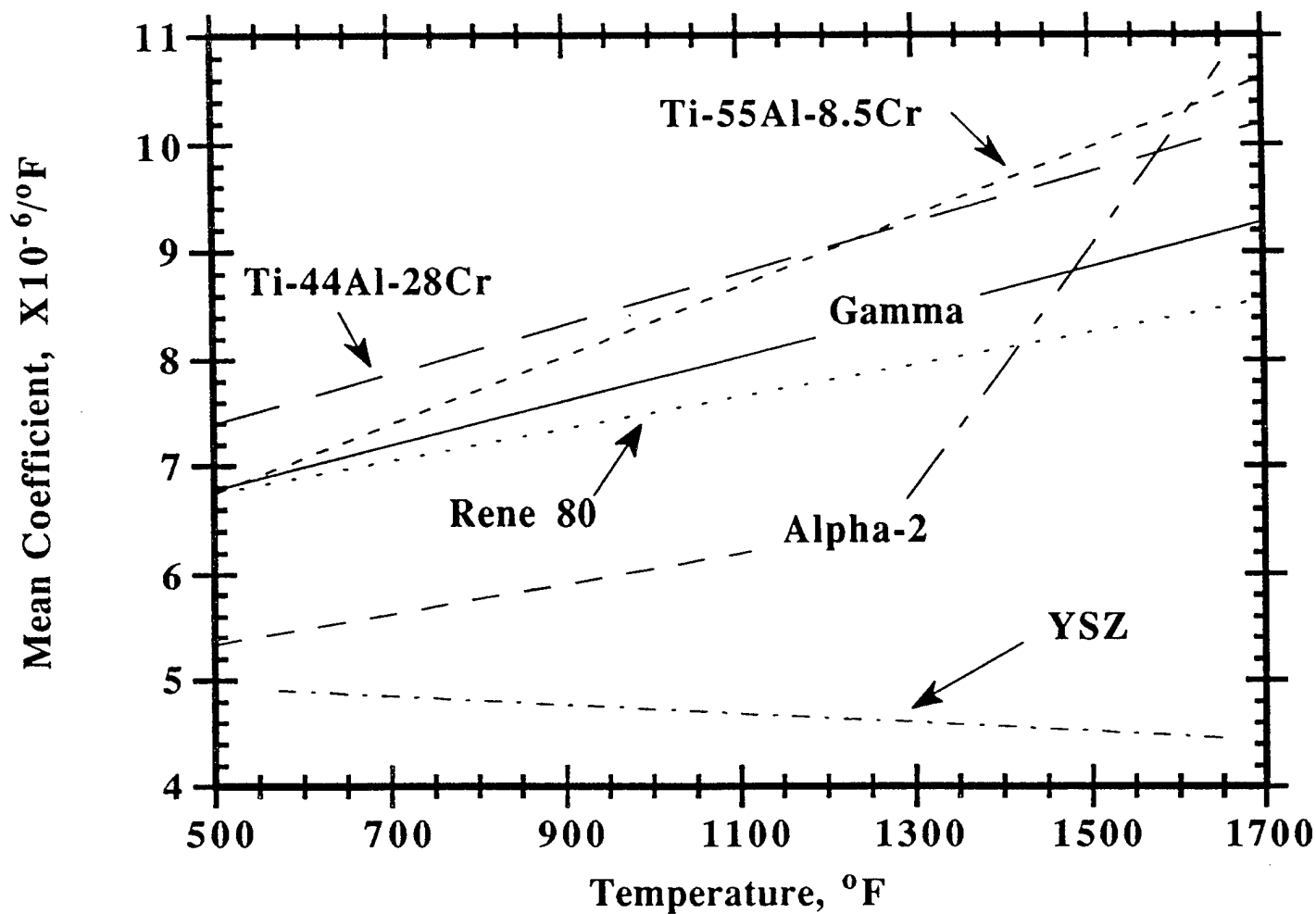


Figure 67. Graph showing the linear expansion coefficients of TiCrAl coatings compared to the Ti-48Al-2Cr-2Nb and Ti-24.5Al-12.5Nb-1.5Mo substrates. The mismatch is greater between the alpha-2 alloys and the coating compositions.

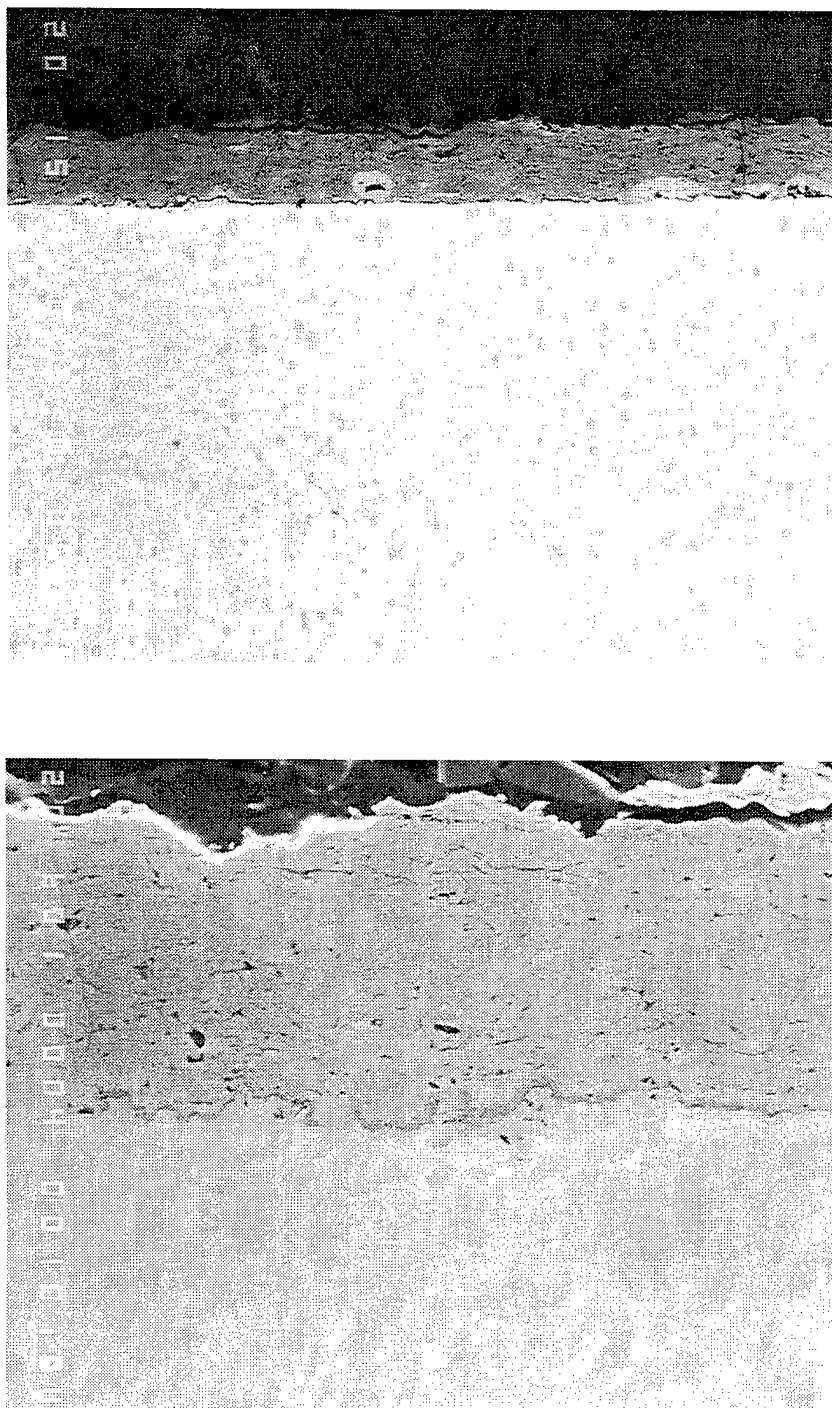


Figure 68. Backscattered electron micrographs of the LPPS Ti-44Al-28Cr on Ti-24.5Al-12.5Nb-1.5Mo. Layers at the coating substrate interface are associated with oxidation and contamination.

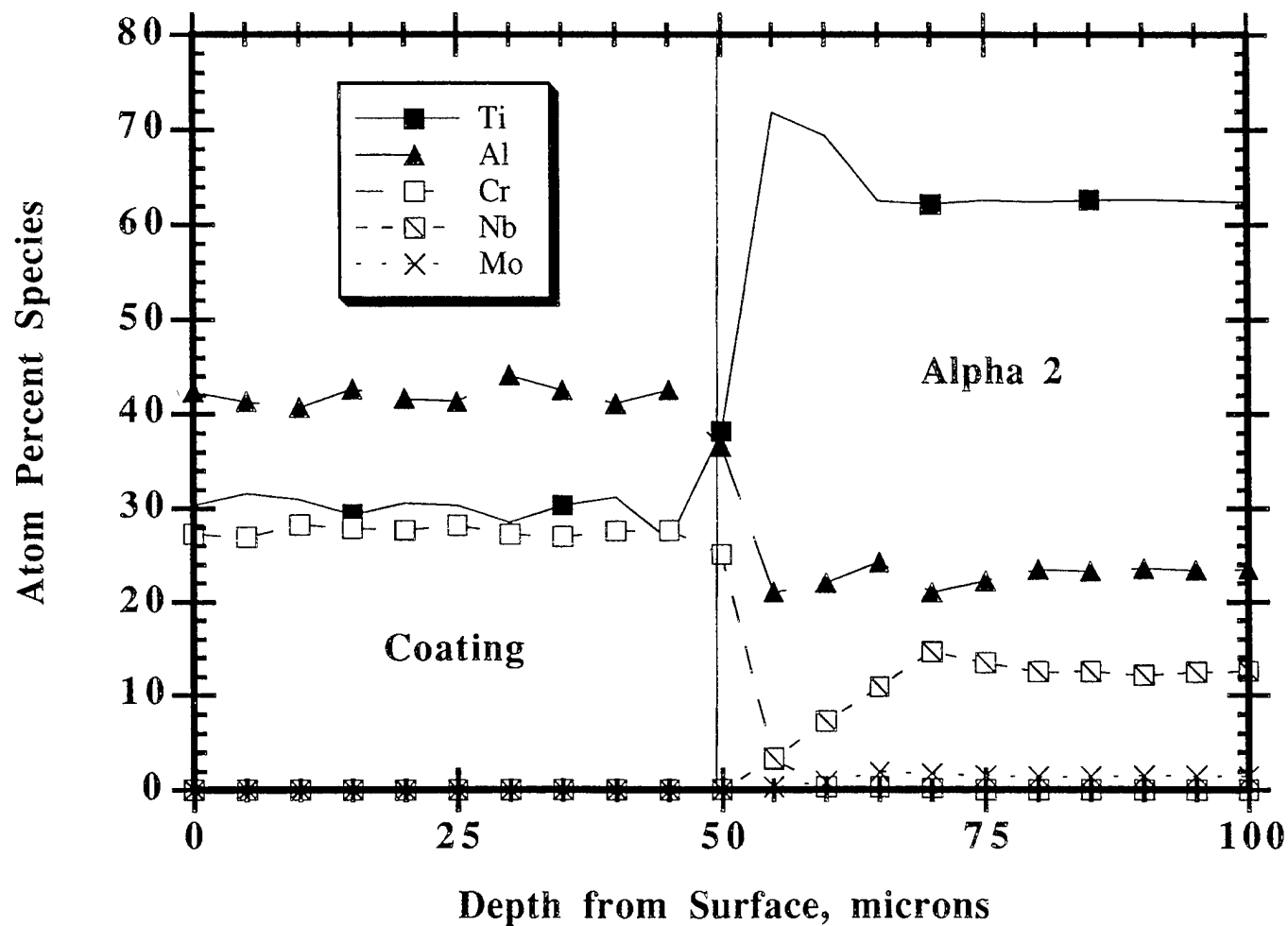


Figure 69. Microprobe traces for the elements that compose the LPPS Ti-44Al-28Cr coating on Ti-24.5Al-12.5Nb-1.5Mo.

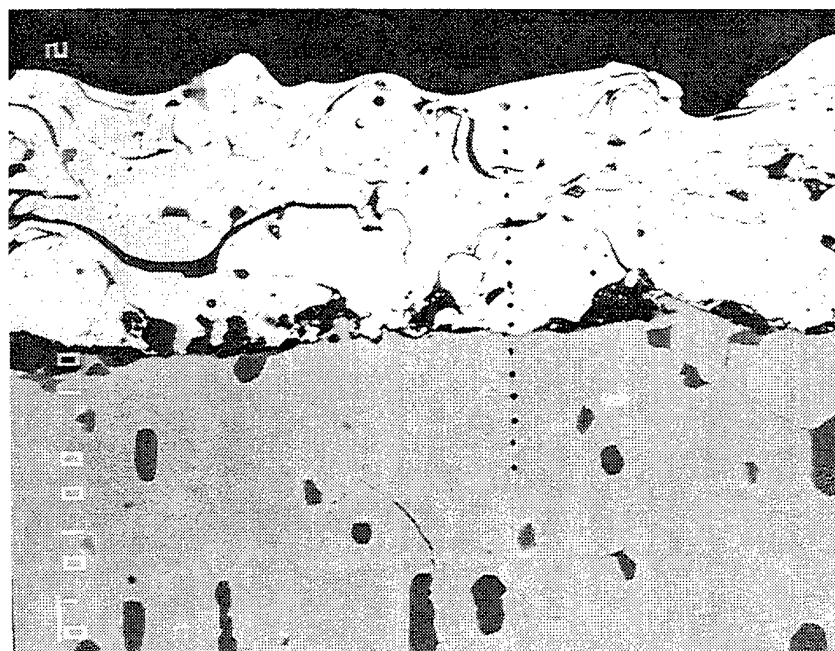
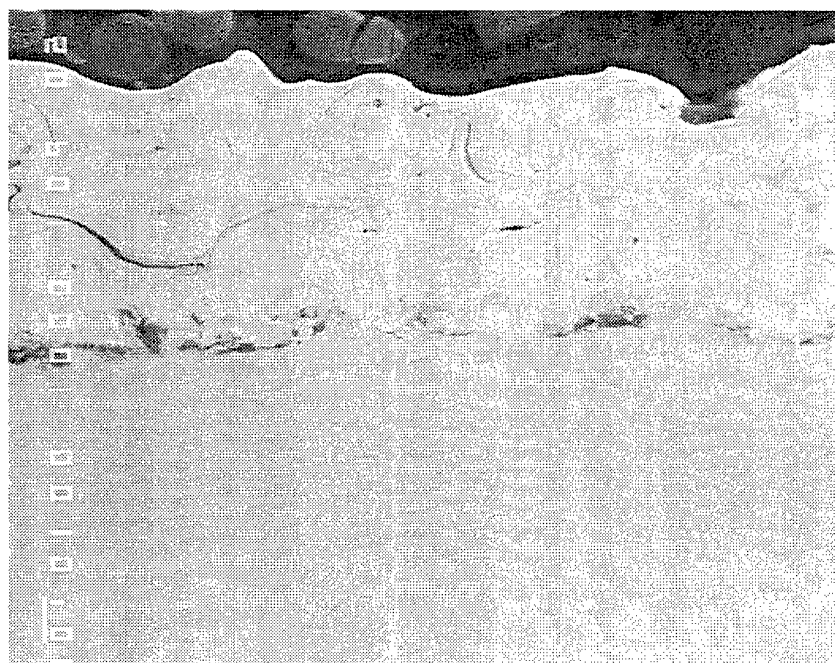


Figure 70. Electron micrographs of the air plasma sprayed (APS) coating on the Ti-24.5Al-12.5Nb-1.5Mo α -2 substrate. Porosity and oxide inclusions are found in the coating.

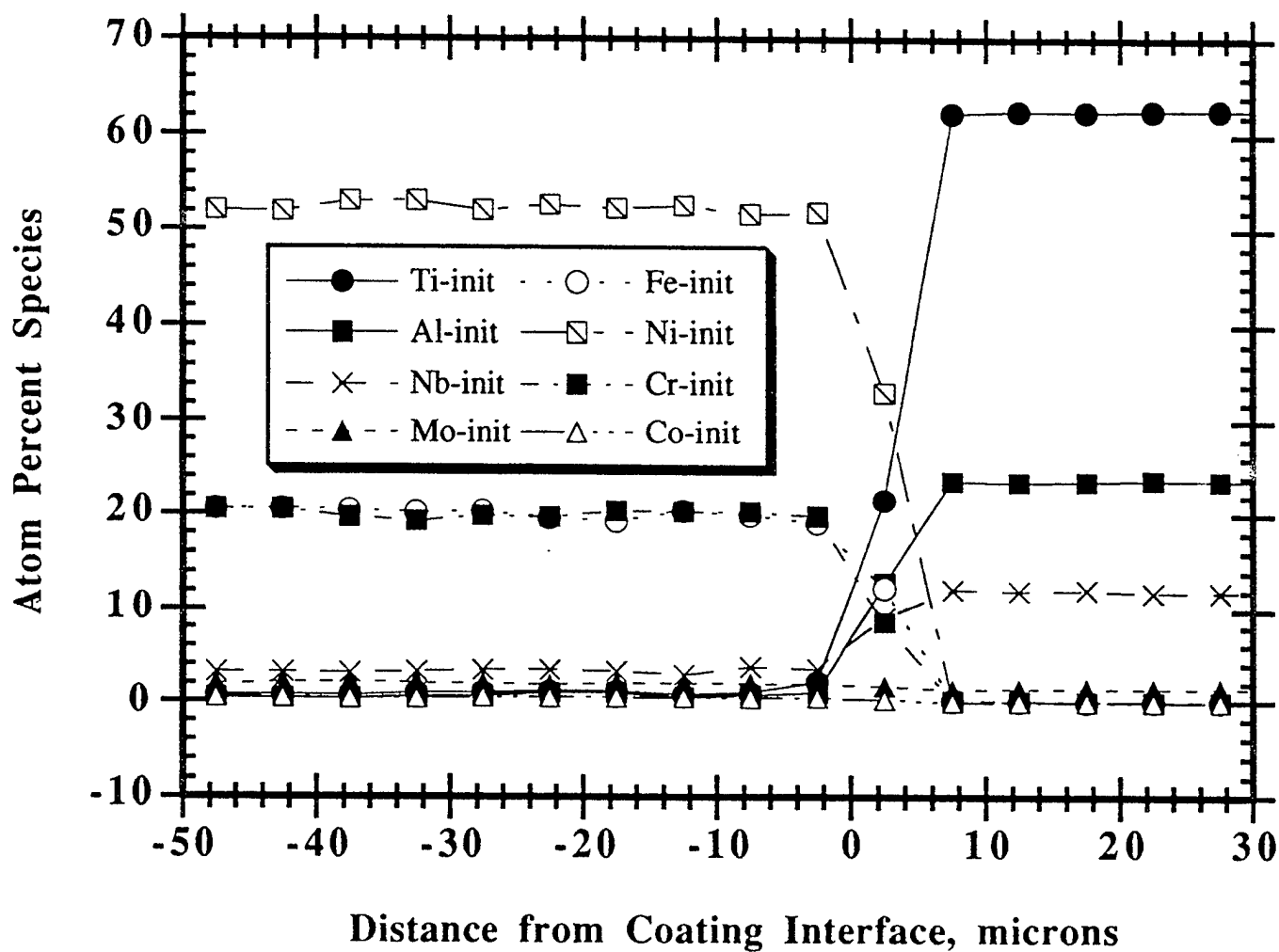


Figure 71. Microprobe traces for the elements that compose the APS 718 coating on Ti-24.5Al-12.5Nb-1.5Mo.

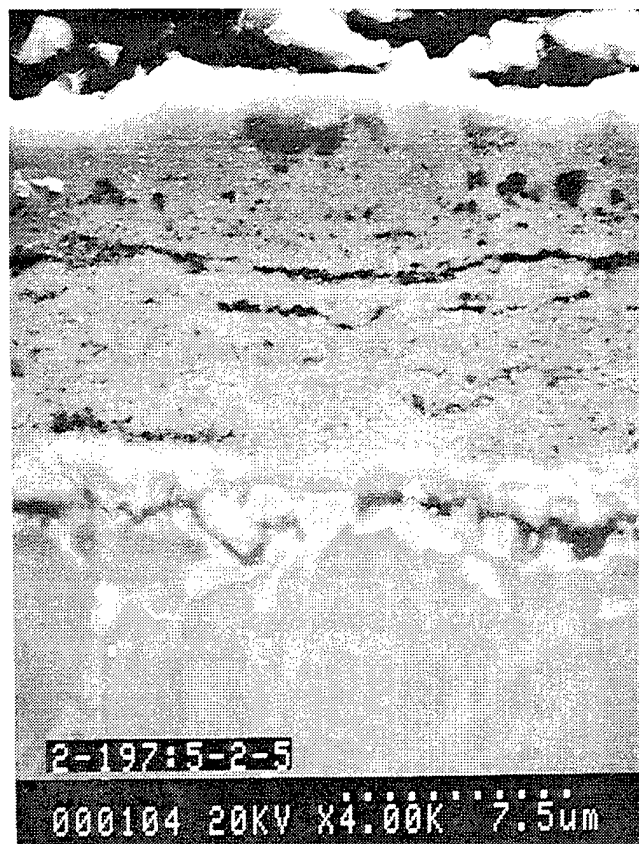
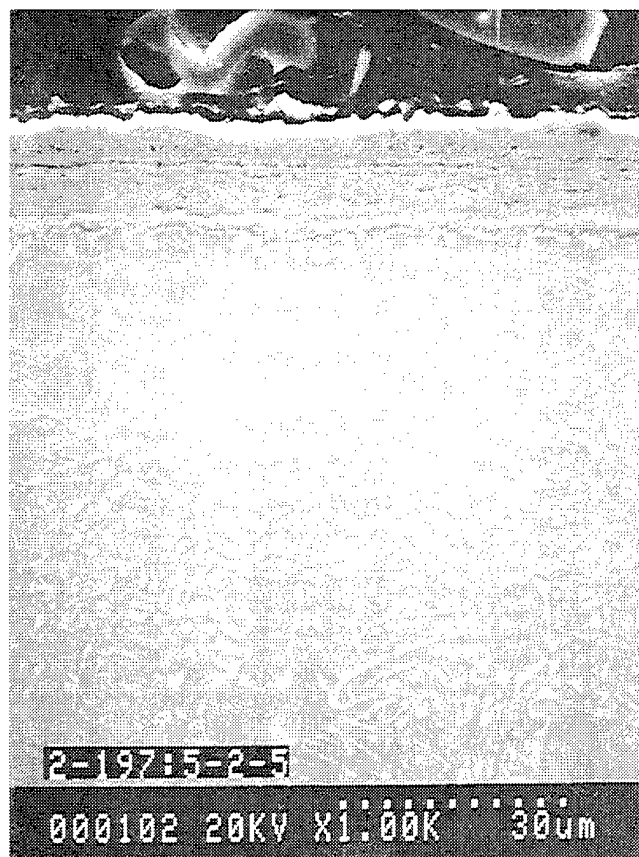
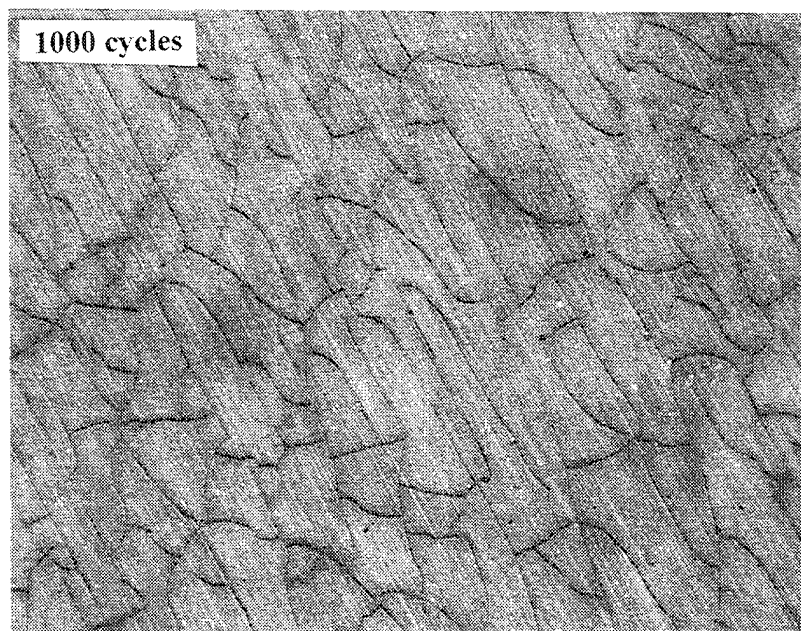
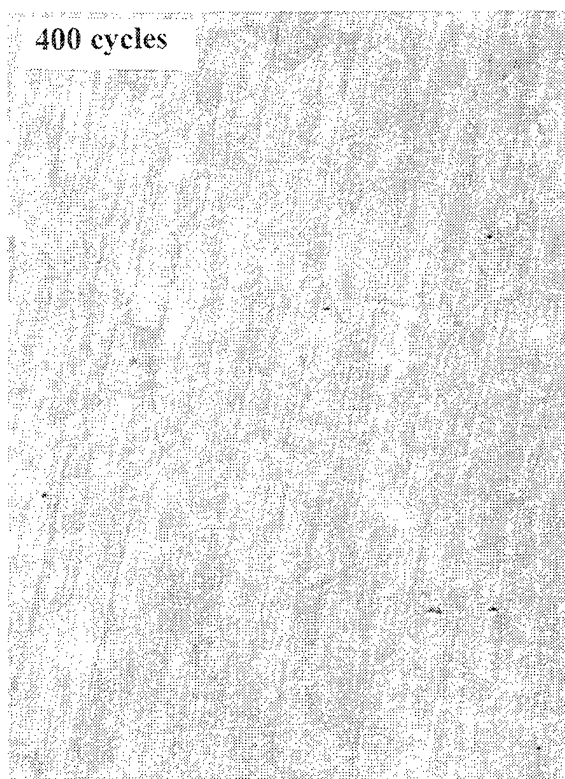
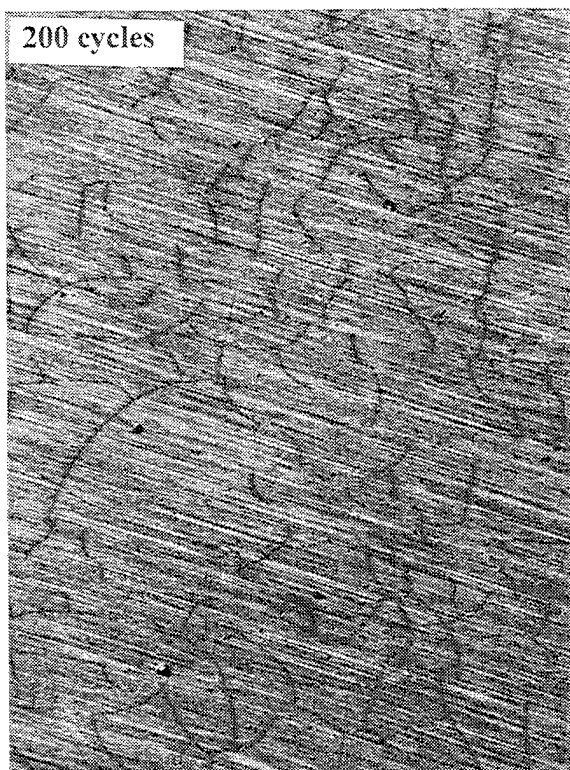


Figure 72. Electron micrographs of the scale formed on Ti-24.5Al-12.5Nb-1.5Mo after cyclic oxidation for 500Hr. at 900°C (1650°F) in air.



1 mm

Figure 73. Surface optical micrographs of the sputtered Ti-44Al-28Cr alpha-2 sample at various intervals throughout the 760°C (1400°F) cyclic oxidation test in air. Many thermal expansion mismatch cracks are observed.

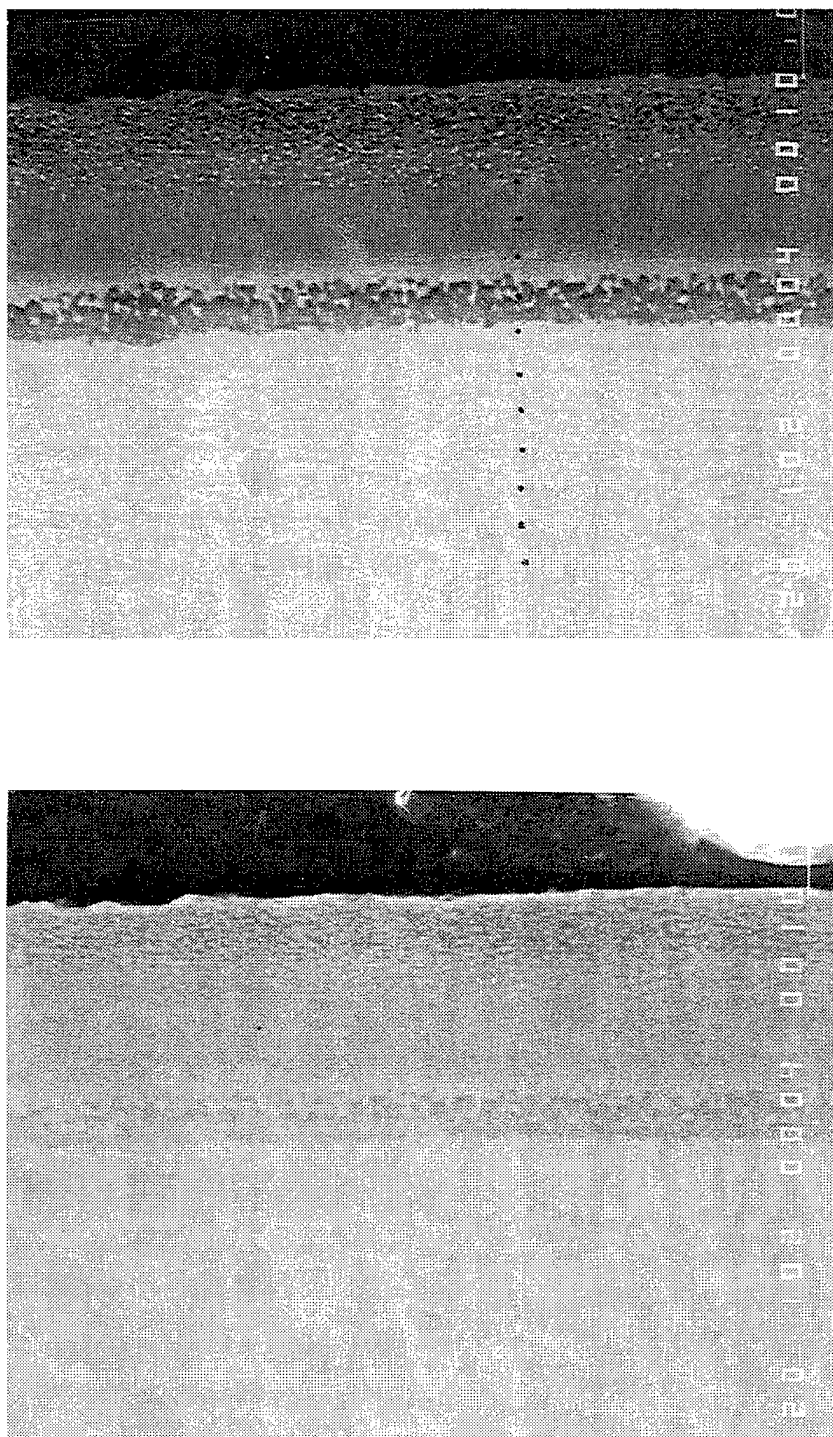


Figure 74. Backscattered and secondary electron micrographs from a cross section of the sputtered Ti-44Al-28Cr alpha-2 sample after the 760°C (1400°F) cyclic oxidation test in air.

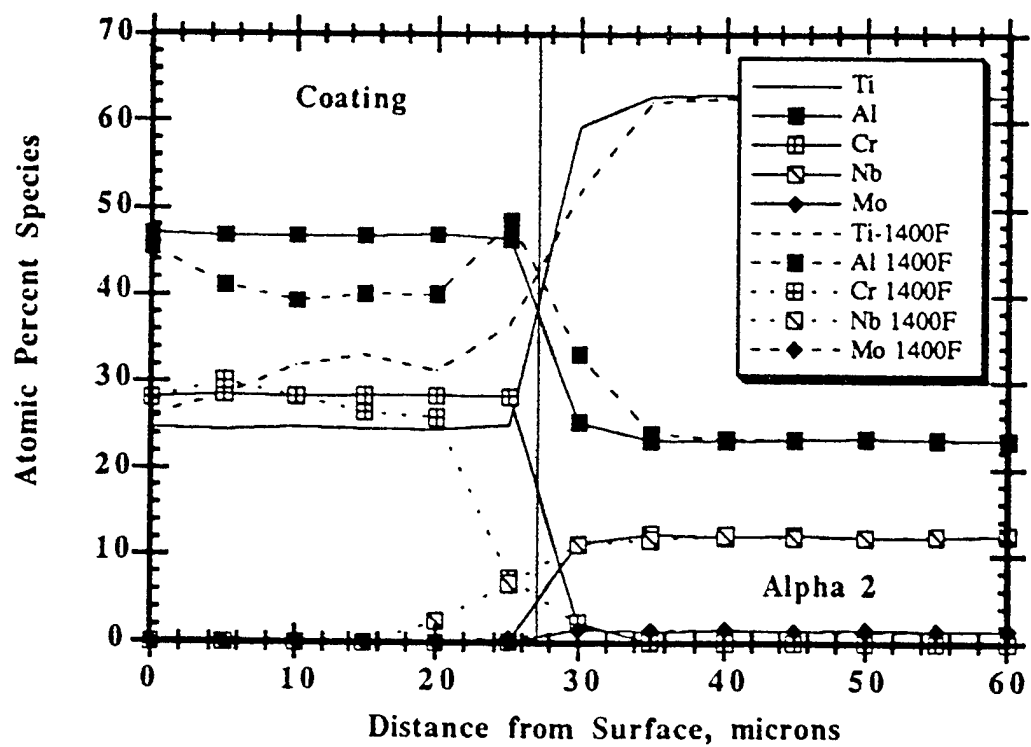
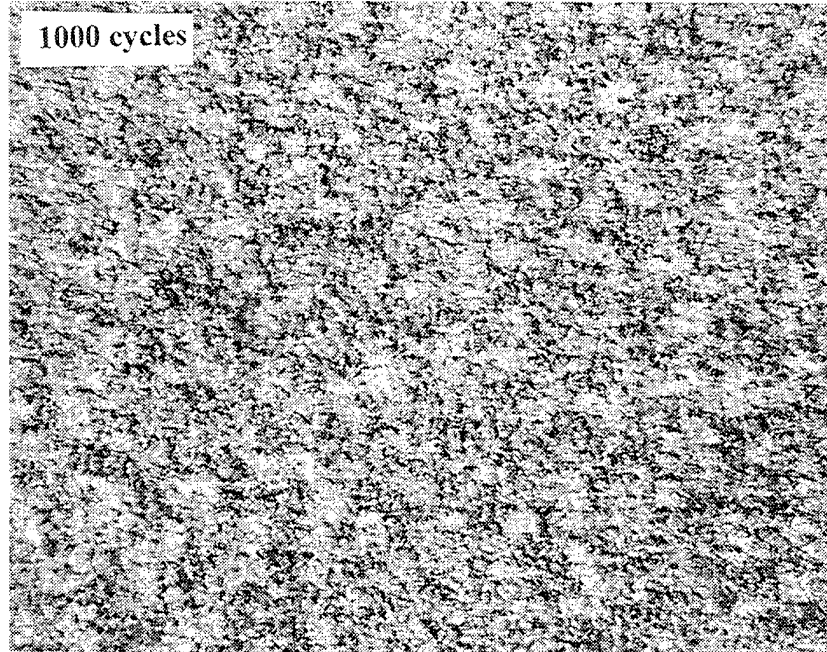
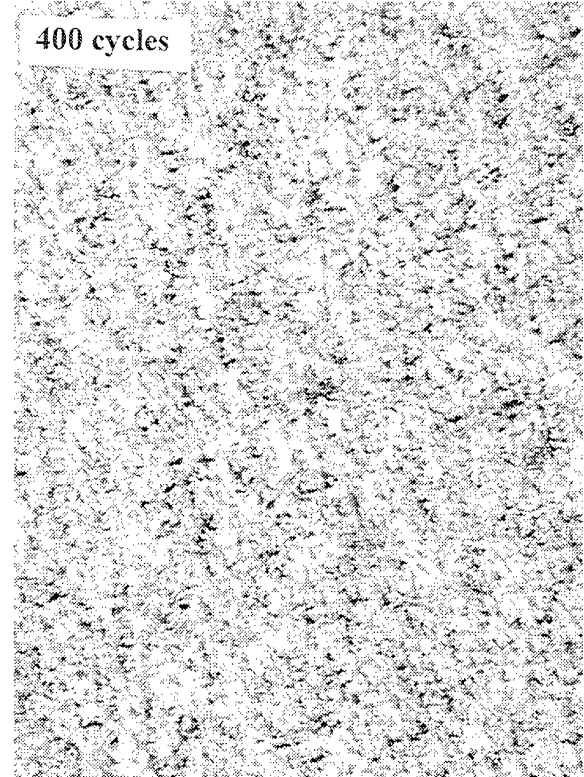
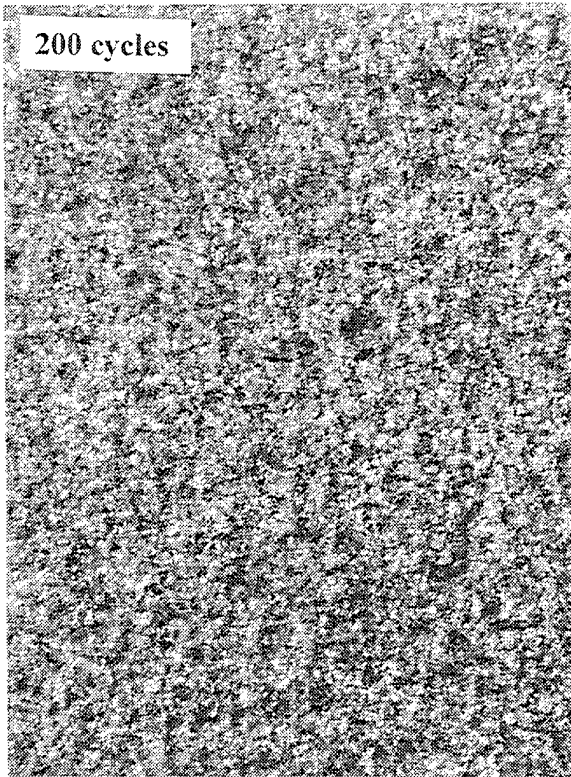


Figure 75. Change in the composition of a sputtered Ti-44Al-28Cr coating after 1000Hr. of cyclic oxidation at 760°C (1400°F) in air.



1 mm

Figure 76. Surface optical micrographs of the APS Alloy 718 on alpha-2 at various intervals throughout the 760°C (1400°F) cyclic oxidation test in air.

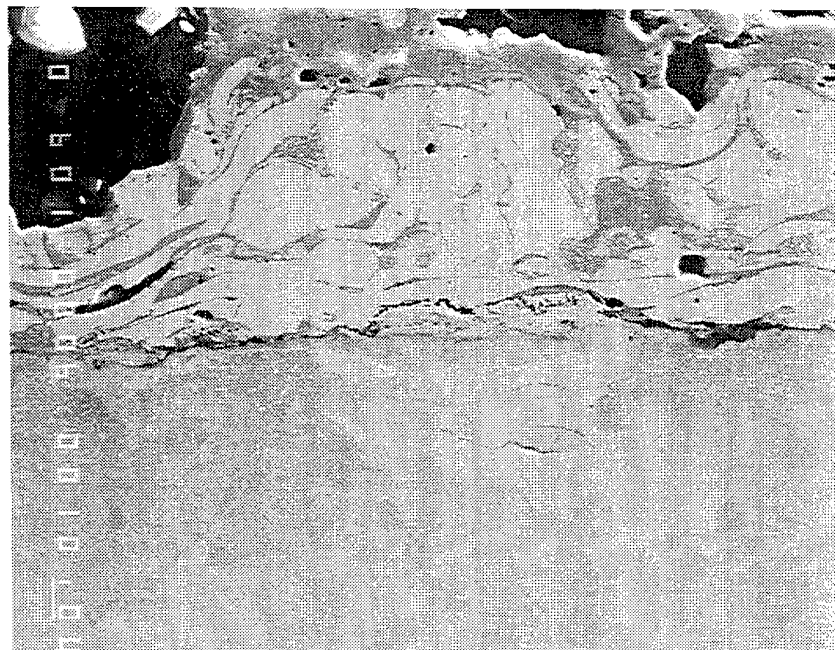
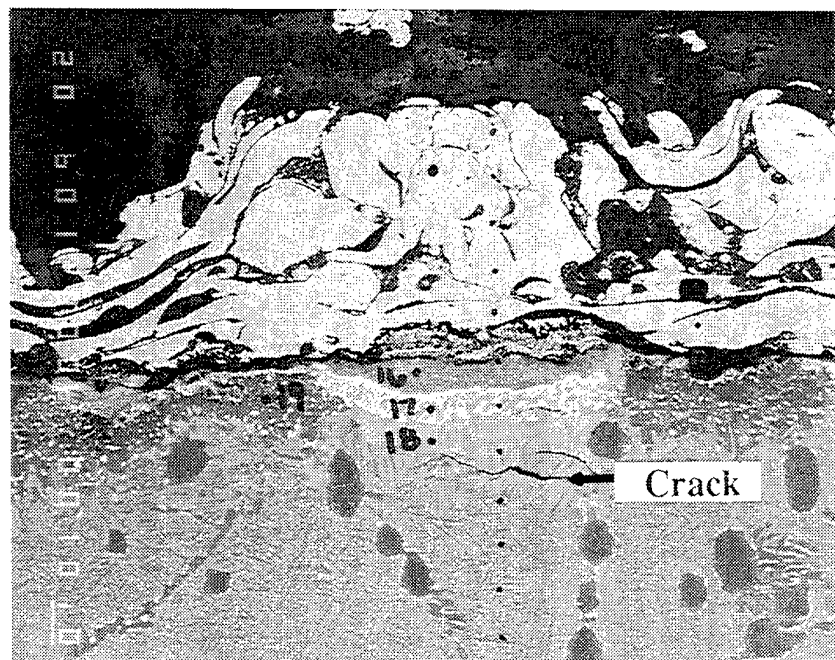


Figure 77. Backscattered and secondary electron micrographs from a cross section of the APS Alloy 718 on alpha-2 after the 760°C (1400°F) cyclic oxidation test in air.

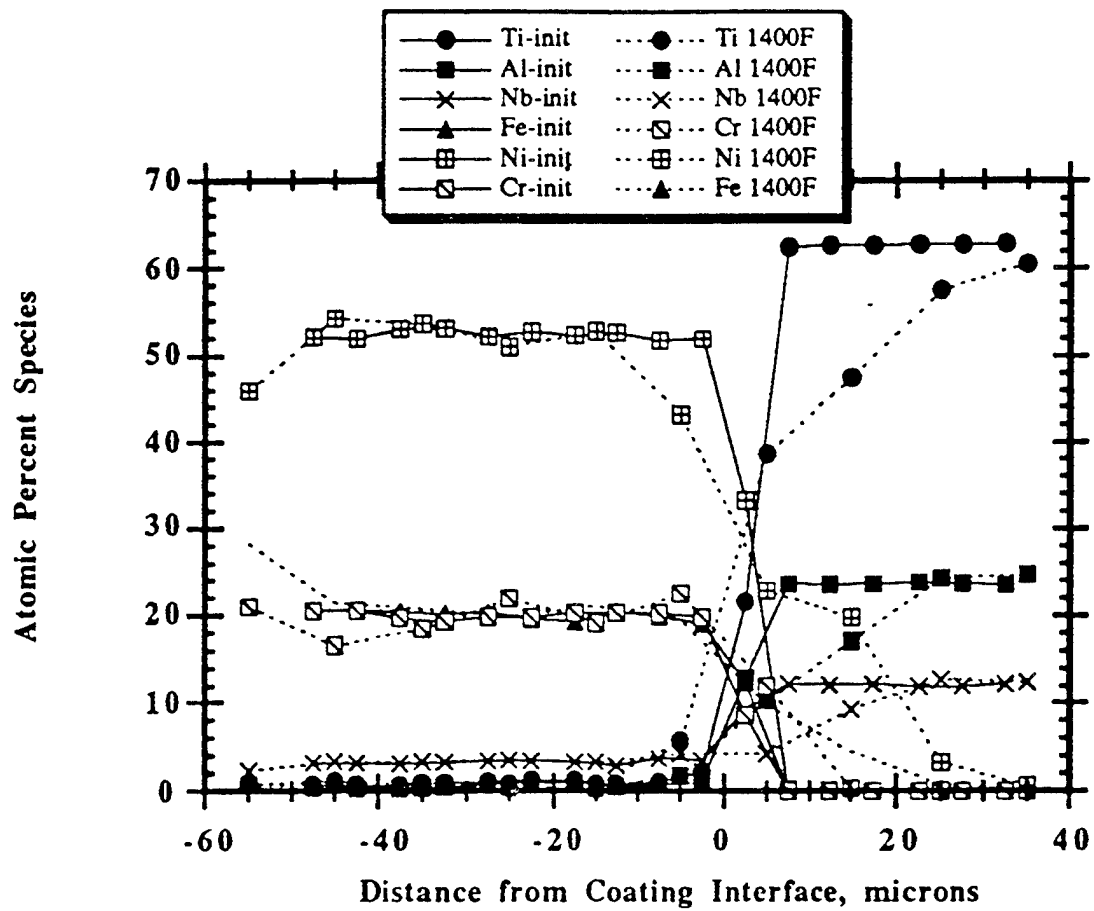


Figure 78. The change in composition of an air plasma sprayed Alloy 718 coating on a Ti-24.5Al-12.5Nb-1.5Mo alpha-2 alloy. After 1000Hr at 760°C (1400°F), there is a 35µm thick reaction layer.

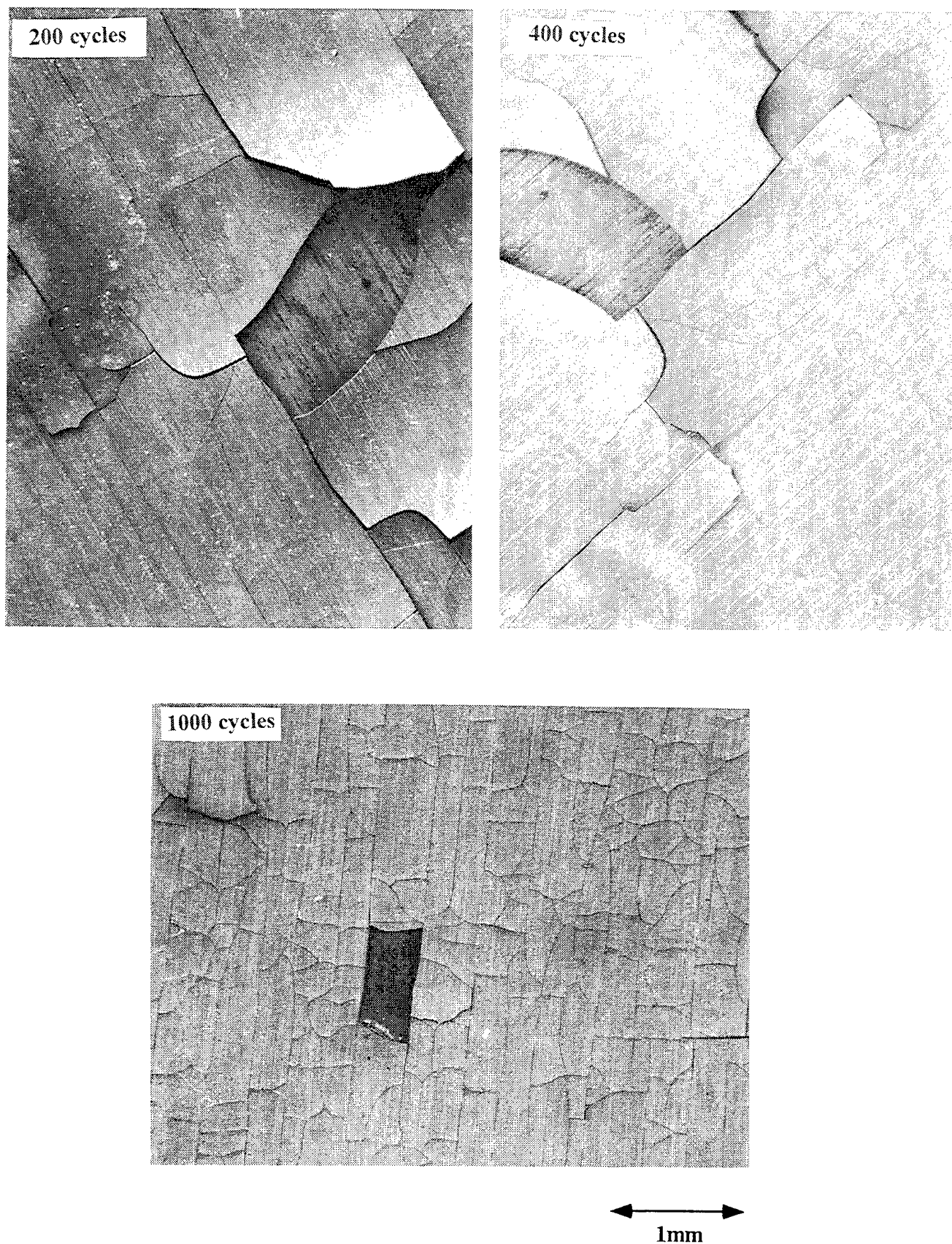


Figure 79. Surface optical micrographs of the sputtered Ti-55Al-9Cr gamma sample at various intervals throughout the 760°C (1400°F) cyclic oxidation test in air. Large thermal expansion mismatch cracks are observed along with coating spallation.

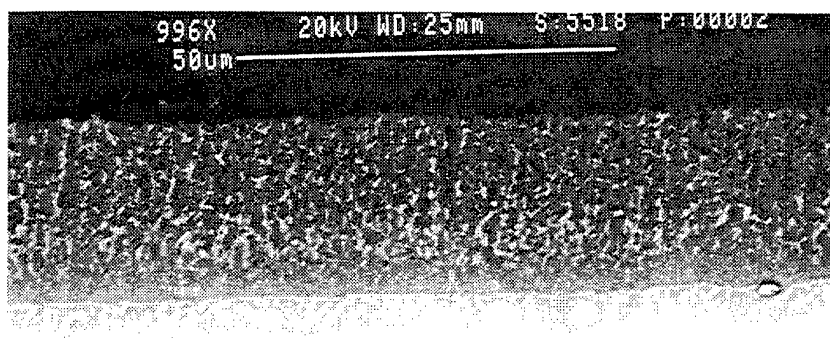


Figure 80. Backscattered electron micrograph from a cross section of the sputtered Ti-55Al-9Cr/alpha-2 sample after the 760°C (1400°F) cyclic oxidation test in air.

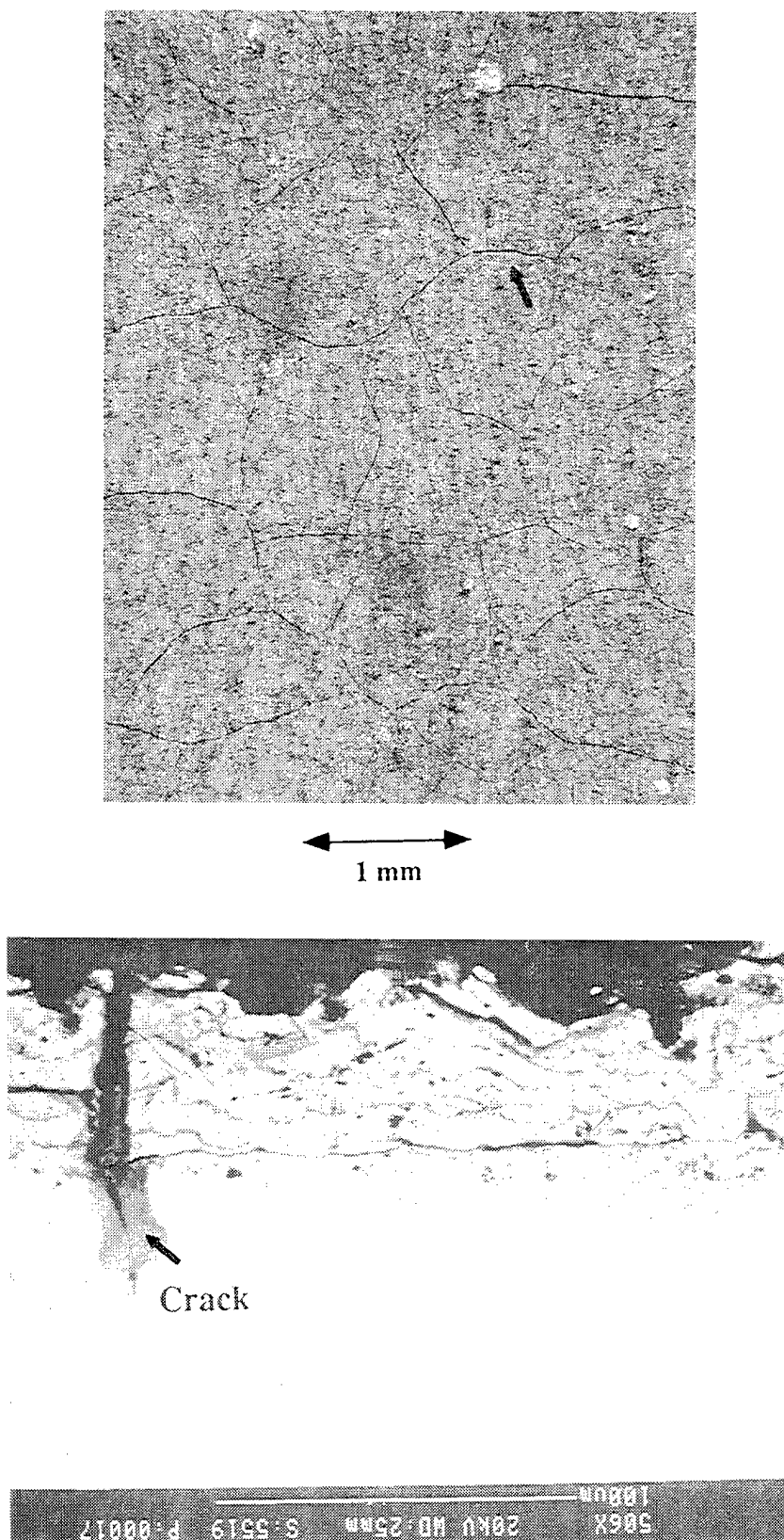
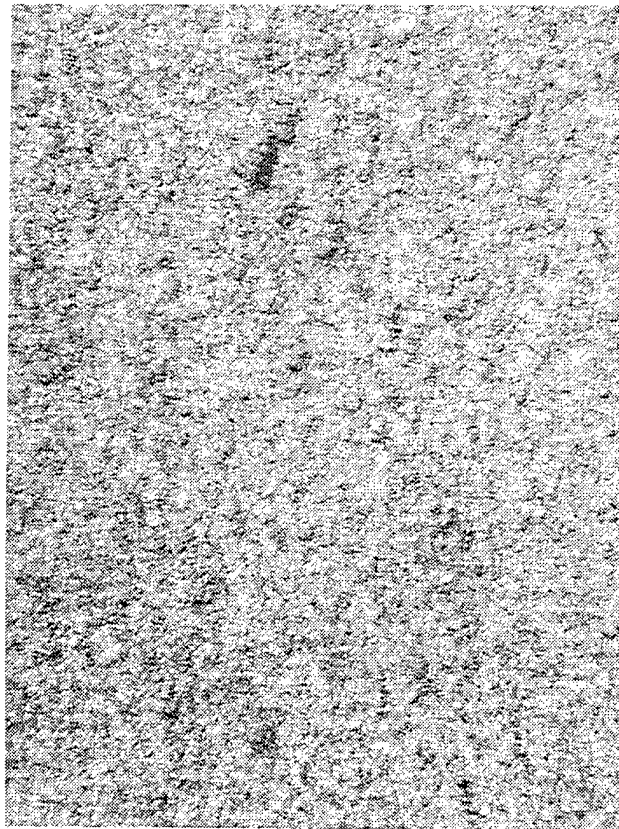


Figure 81. Surface and cross section micrographs of the LPPS Ti-44Al-28Cr coating on the alpha-2 sample after the 1000 hour 760°C cyclic oxidation test in air.



1 mm

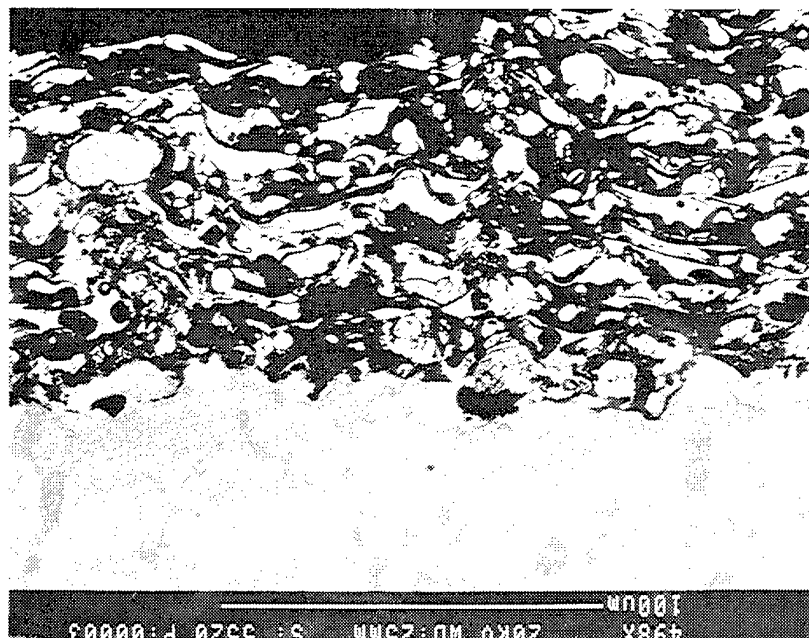
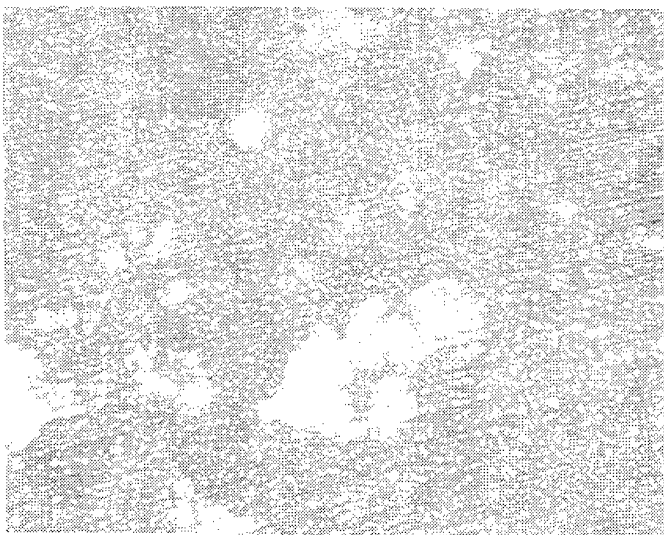
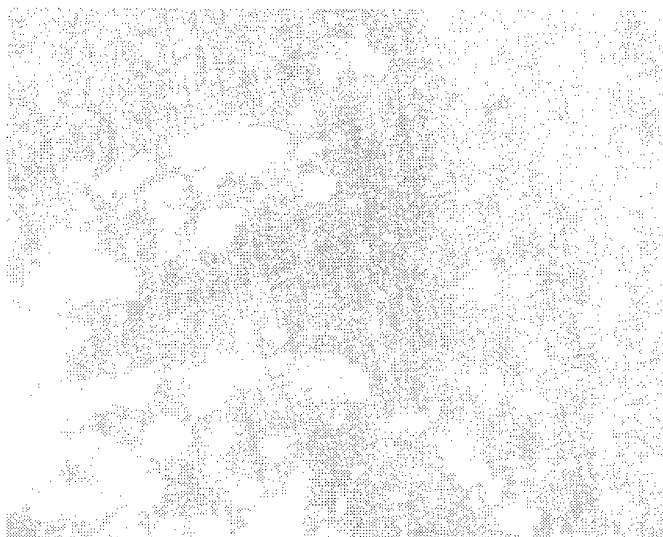


Figure 82. Surface and cross section micrographs of the M³ coating on the alpha-2 sample after the 1000 hour 760°C cyclic oxidation test in air.

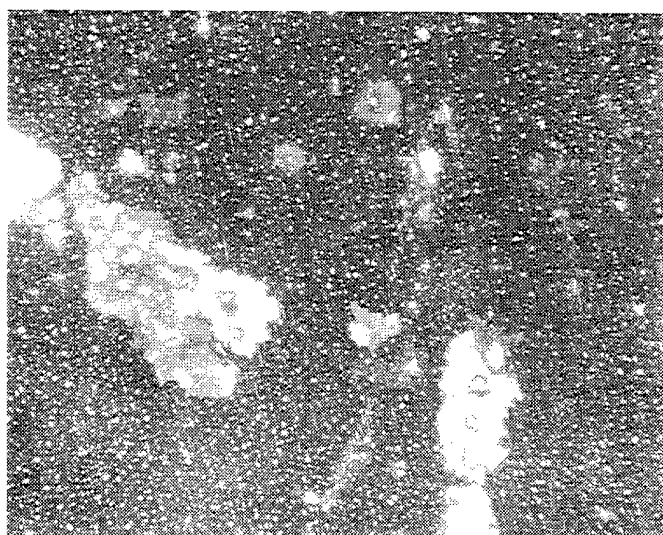
200 cycles



600 cycles



400 cycles



1000 cycles

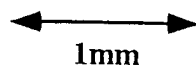
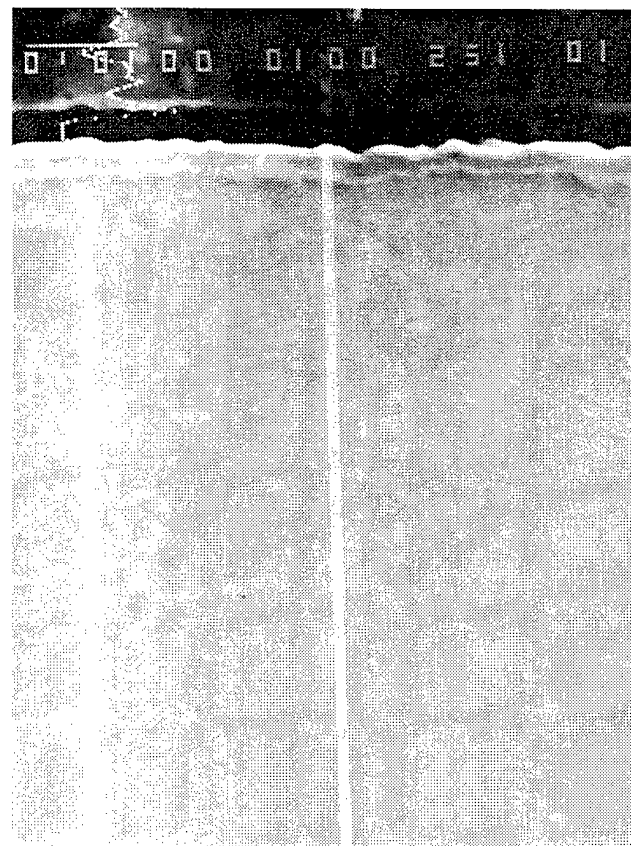
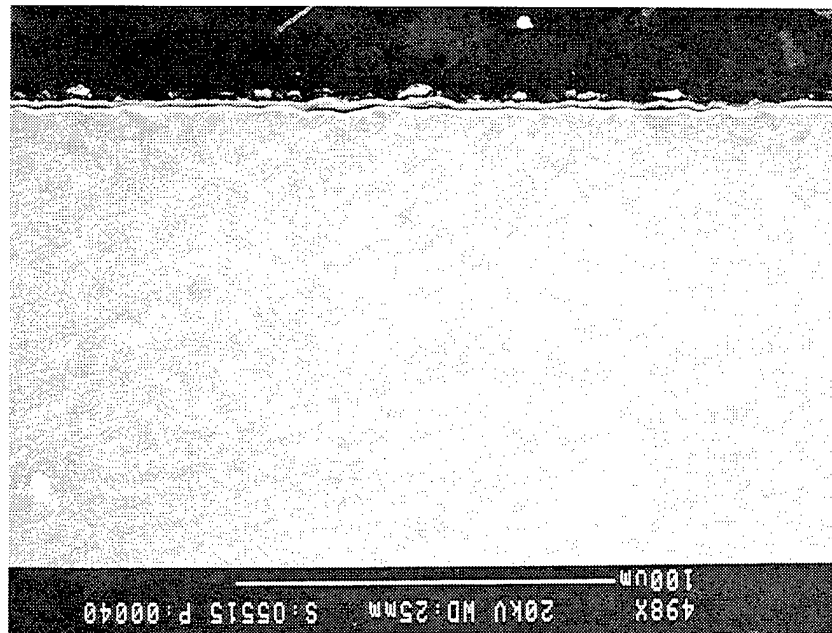


Figure 83. Surface optical micrographs of the uncoated Ti-24.5Al-12.5Nb-1.5Mo sample at various intervals throughout the 760°C (1400°F) cyclic oxidation test in air. Locally thick oxides that spalled are evident.



Oxygen →

Figure 84. Secondary electron micrographs of the uncoated Ti-24.5Al-12.5Nb-1.5Mo sample after the 760°C (1400°F) cyclic oxidation test in air. One micrograph shows a microprobe trace for oxygen.

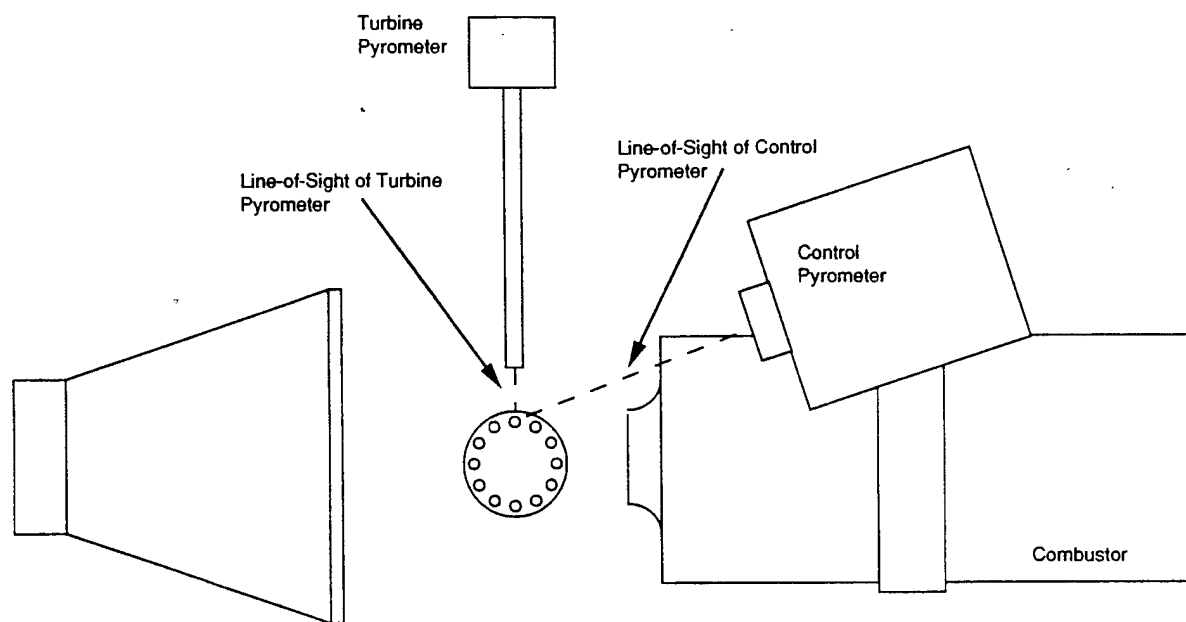


Figure 85. A schematic of the high velocity hot corrosion/oxidation rig used to test coated and uncoated Ti-aluminides in engine simulative environments. Photograph of the CHC/O rig in operation. The samples rotate on a carousel in front of a combustor.

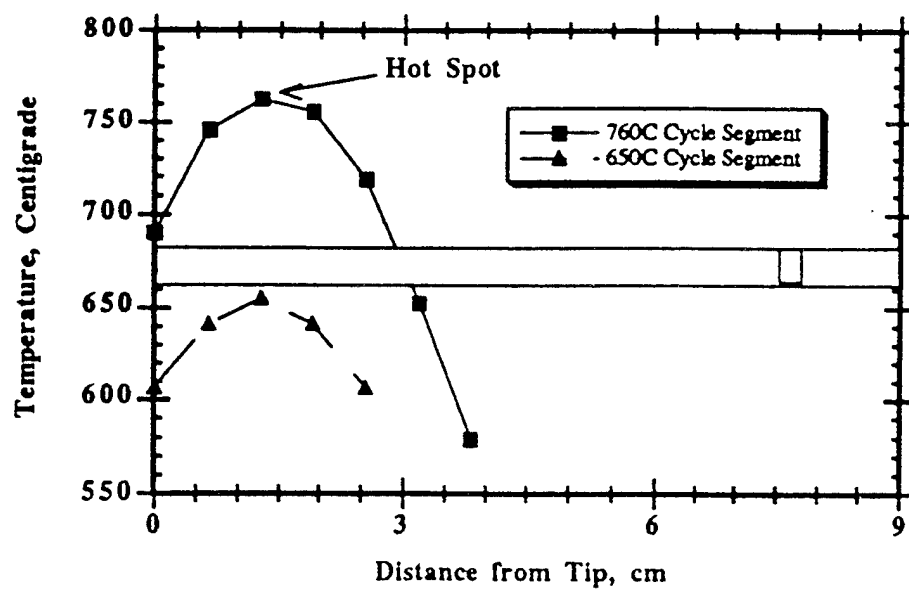


Figure 86. Graphs showing the temperature distribution of the environmental pins used to test the coated and uncoated Ti-aluminides in high pressure compressor conditions.

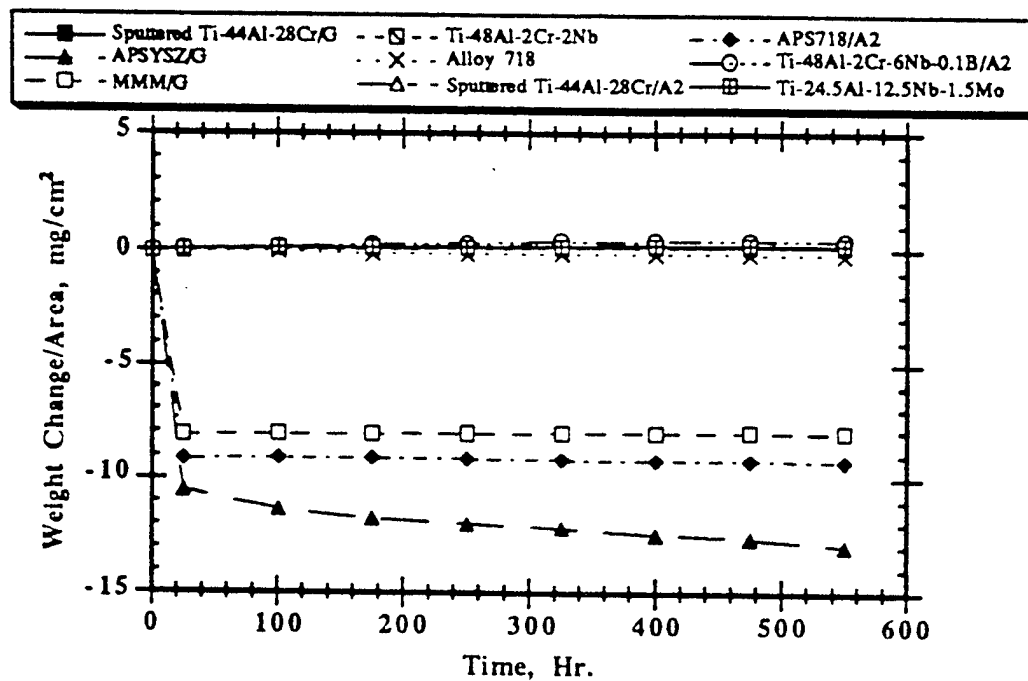


Figure 87. Weight change/area data for unrinsed coated and uncoated Ti-aluminides during the high pressure compressor burner rig test. Thermally sprayed coatings had large spallation events early in the test. The other coatings exhibited little weight change.

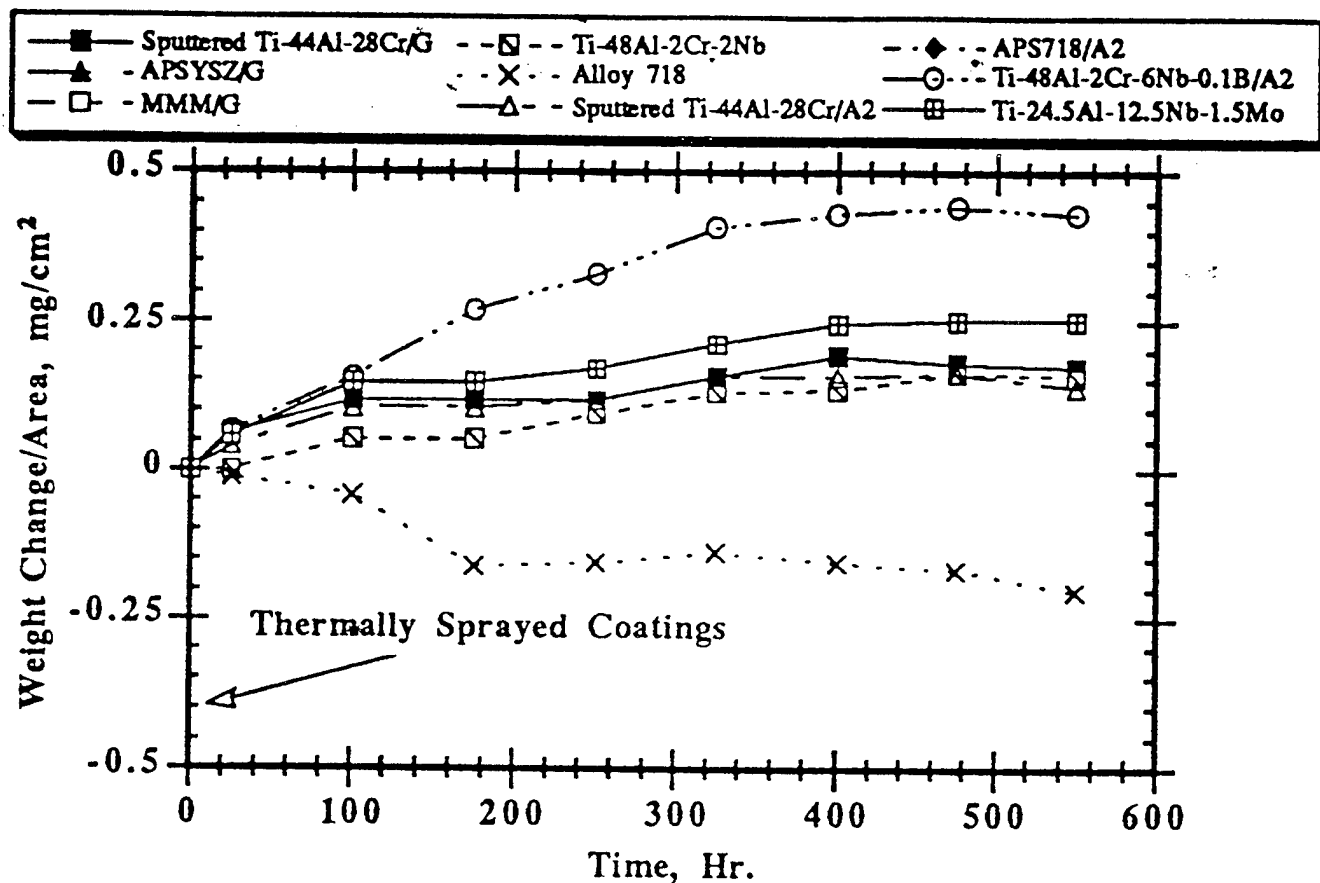


Figure 88. Weight change/area data for unrinsed coated and uncoated Ti-aluminides during the high pressure compressor burner rig test. The y-axis has been enlarged to differentiate the behavior of systems that showed little weight change.

Cyclic Oxidation/Corrosion Testing
Test #B17 Rinsed Coated Ti-Aluminides
1400°F-5min/1200°F-5min/0.25ppm Salt-1st 30sec.
3200 Cycles Total - 550Hr. at Temp.

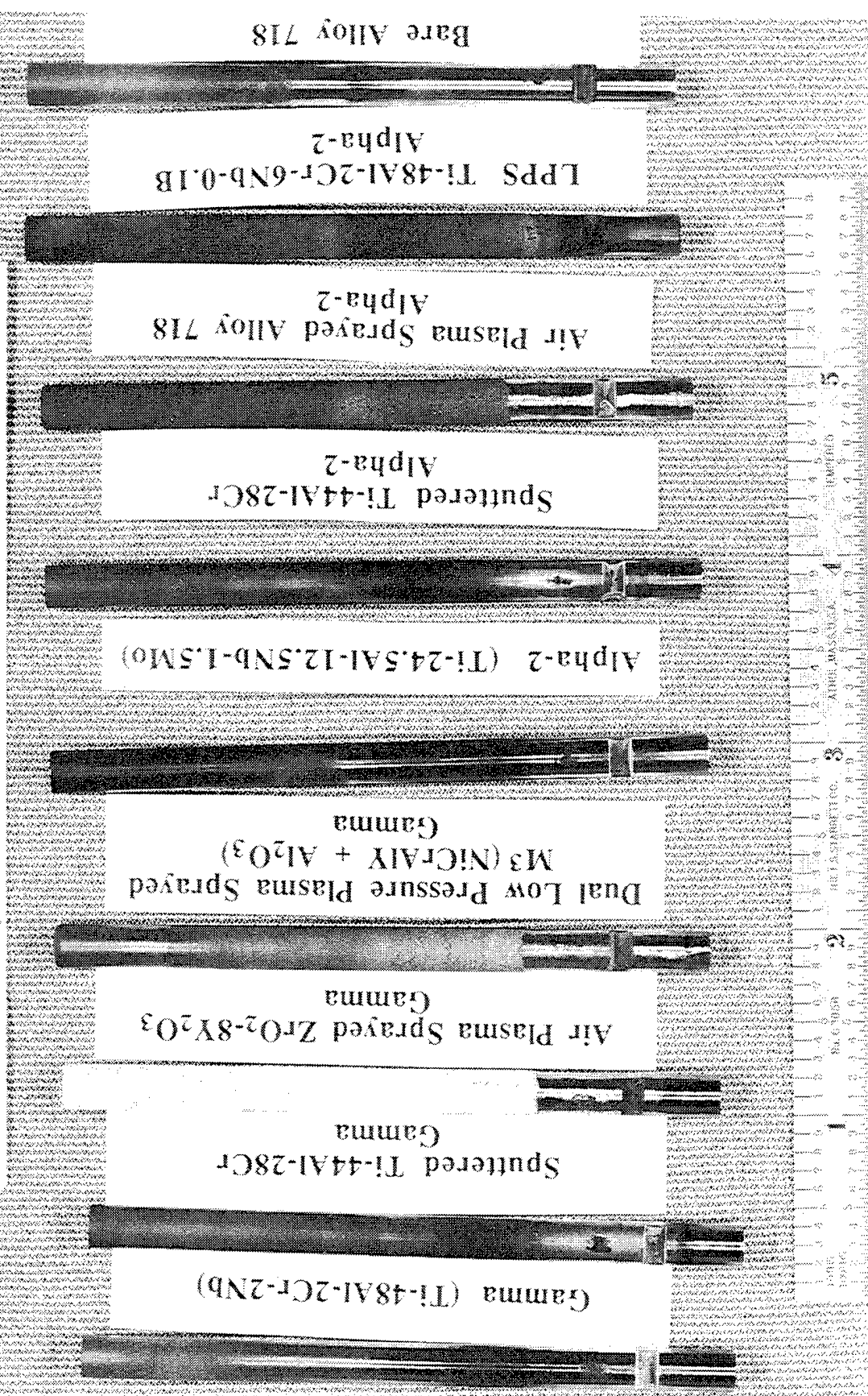


Figure 89. Color photograph shows the coated and uncoated Ti-aluminide samples after 3200cycles or 550Hr under high pressure compressor (CHC/O) environmental conditions. The notched side faced the combustor.

Cyclic Oxidation/Corrosion Testing
 Test #B17 Rinsed Coated Ti-Aluminides
 1400oF-5min/1200oF-5min/0.25ppm Salt-1 $\frac{1}{2}$ 30sec.
 3200 Cycles Total - 550Hr. at Temp.

Gamma (Ti-48Al-2Cr-2Nb)
 Sputtered Ti-44Al-28Cr
 Gamma
 Air Plasma Sprayed ZrO₂-8Y₂O₃
 Gamma
 Dual Low Pressure Plasma Sprayed
 M₃(NiCrAlY + Al₂O₃)
 Gamma
 Alpha-2 (Ti-24.5Al-12.5Nb-1.5Mo)
 Sputtered Ti-44Al-28Cr
 Alpha-2
 Air Plasma Sprayed Alloy 718
 Alpha-2
 LPPS Ti-48Al-2Cr-6Nb-0.1B
 Alpha-2
 Bare Alloy 718

Figure 90. Color photograph shows the coated and uncoated Ti-aluminide samples after 3200cycles or 550Hr under high pressure compressor (CHC/O) environmental conditions. This side of the pins faced away from the combustor.

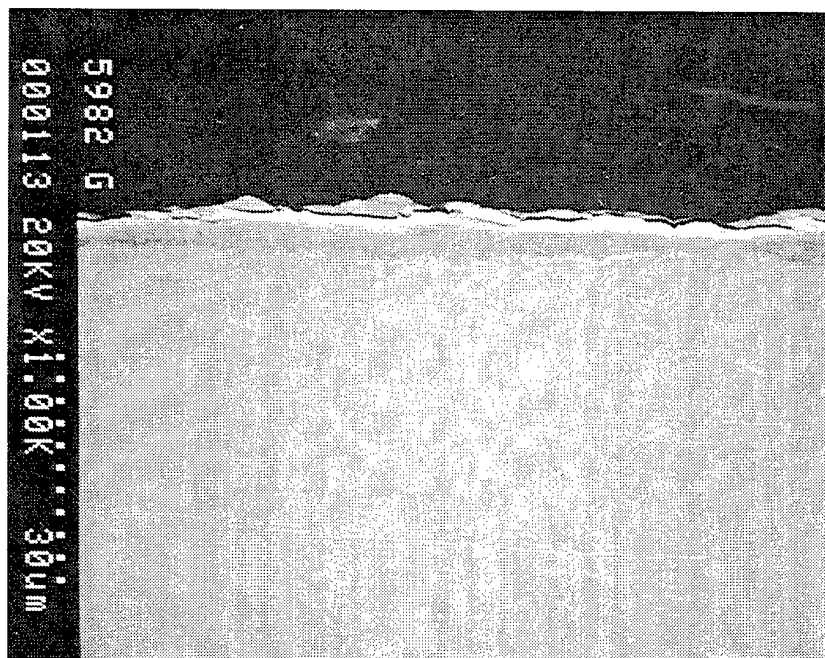


Figure 91. Cross sectional micrographs taken from the hot spot of the uncoated gamma alloy after the HPC environmental test.

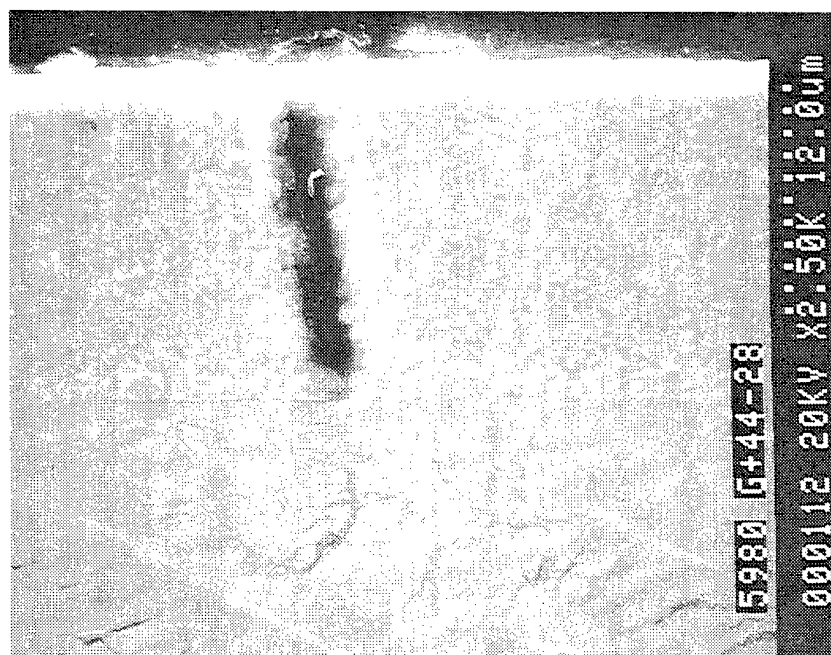
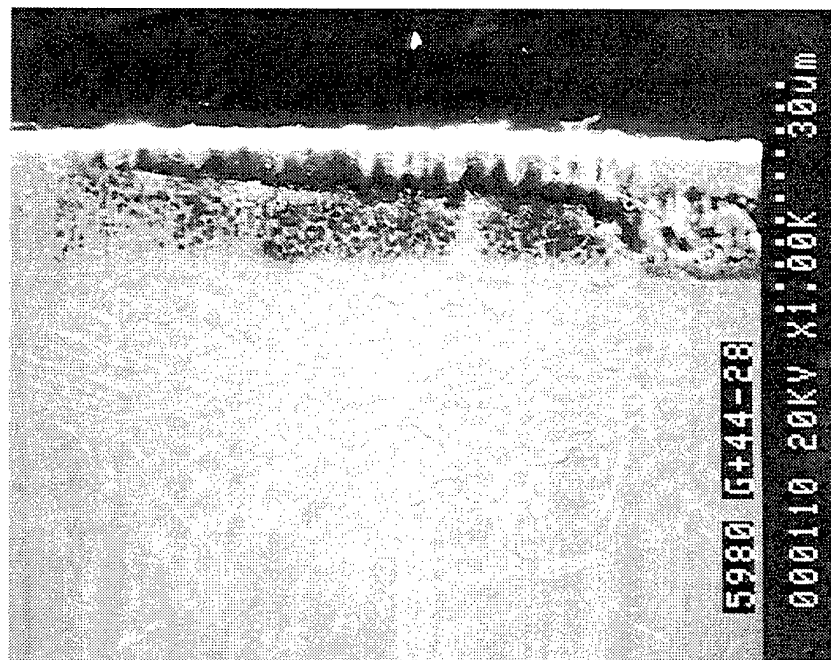


Figure 92. Cross sectional micrographs taken from the hot spot of the sputtered Ti-44Al-28Cr gamma alloy after the HPC environmental test. Through-thickness defects were observed in the coating, but did not penetrate the substrate.

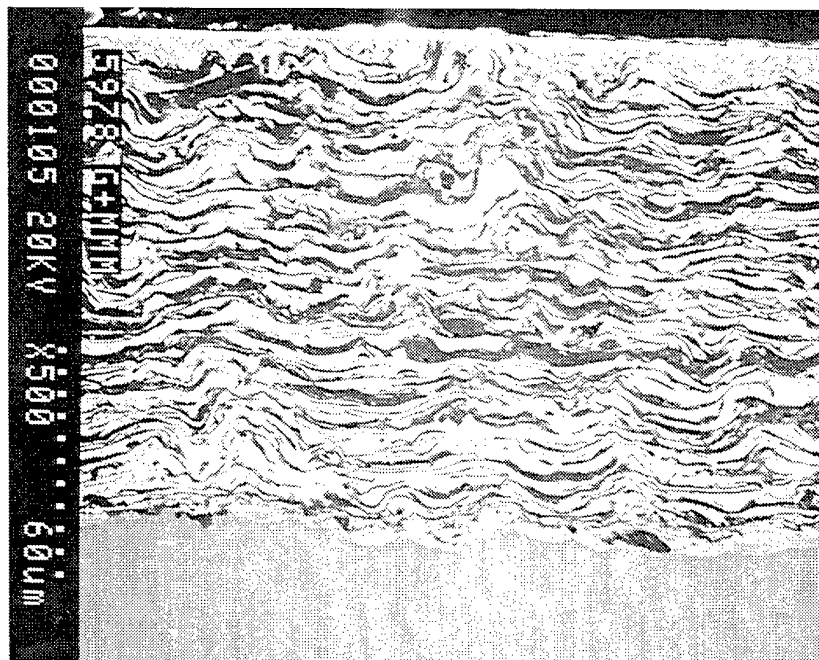


Figure 93. Cross sectional micrographs taken from the hot spot of the cermet (50%NiCrAlY +alumina) coating on the gamma alloy after the HPC environmental test. The coating shows no cracking, spalling or signs of degradation.

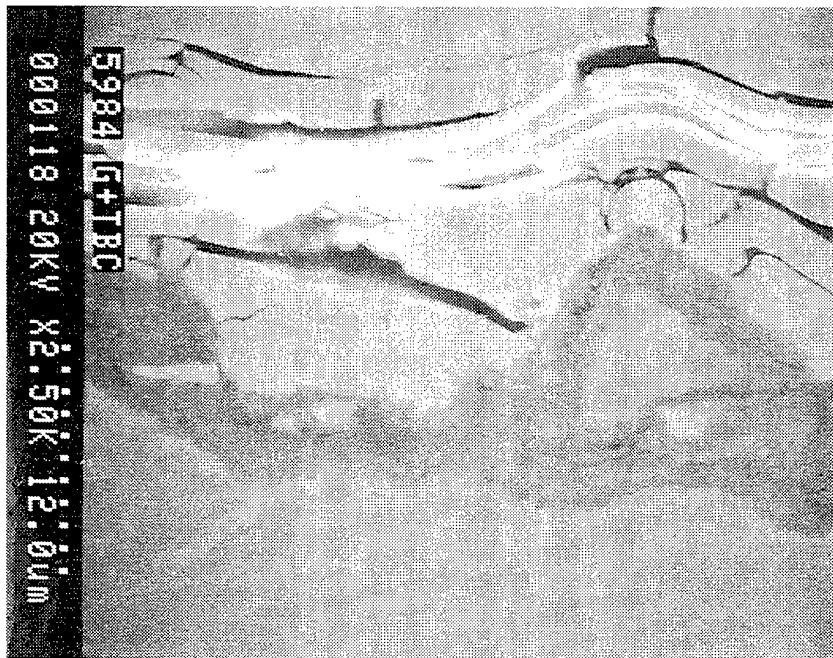
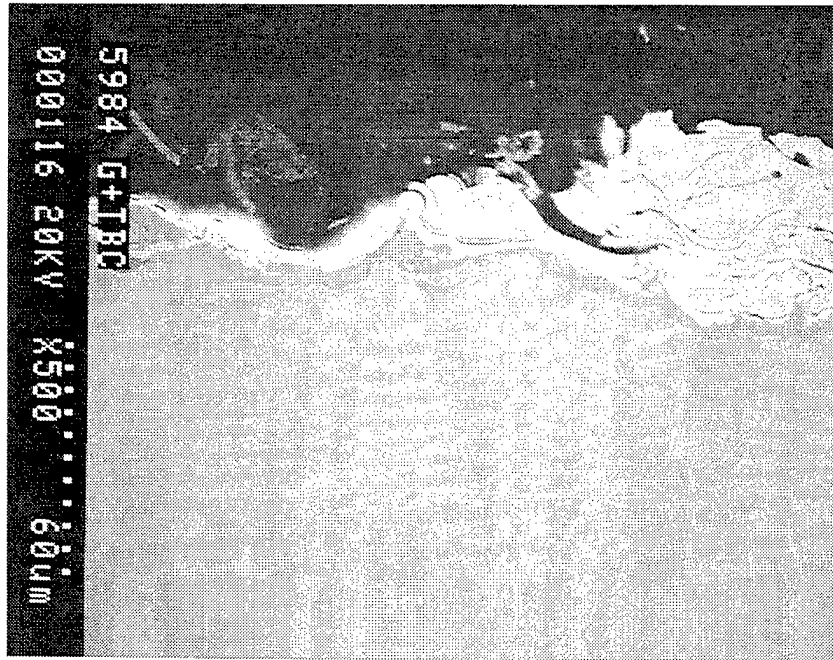


Figure 94. Micrographs of the APS YSZ coating on the gamma alloy at the hot spot after the HPC environmental test.

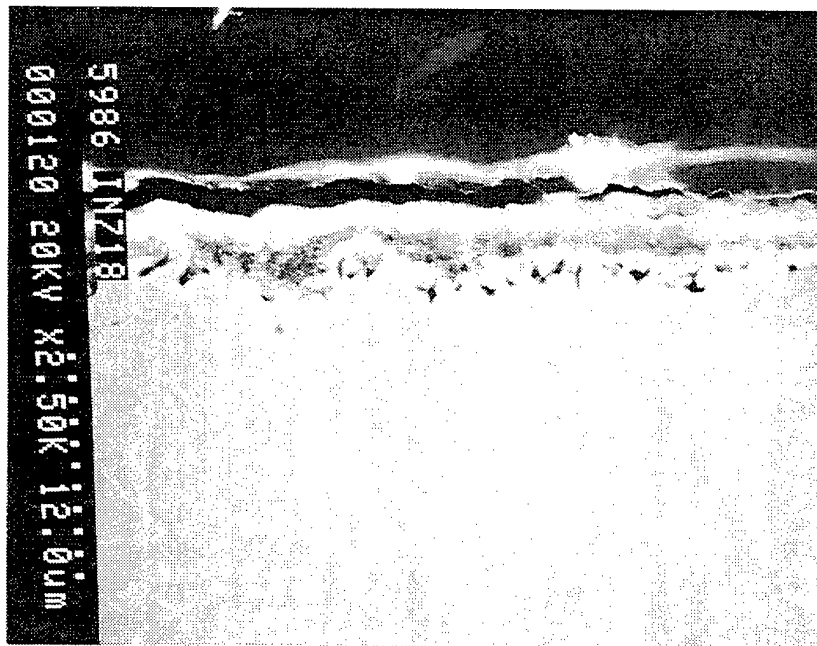
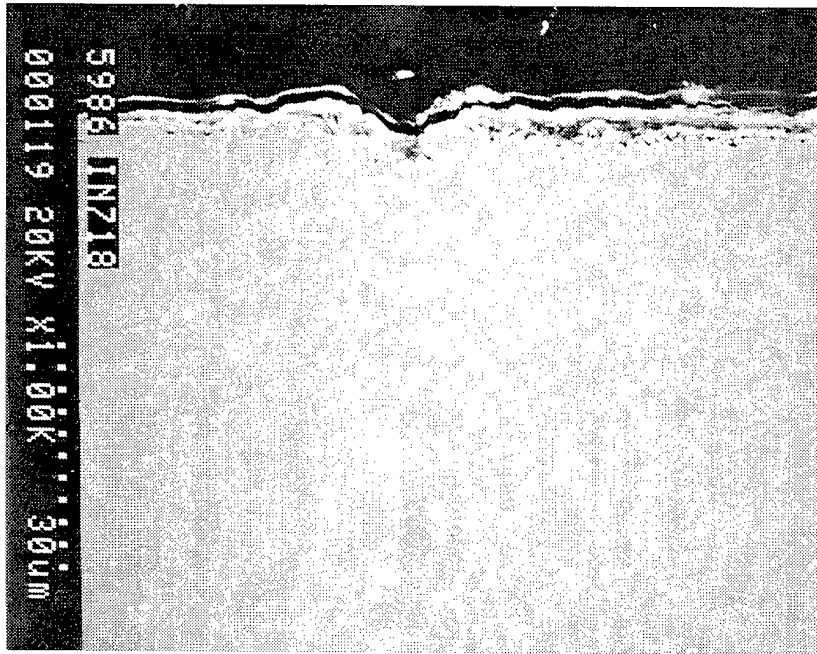


Figure 95. Cross sectional micrographs taken from the hot spot of the monolithic Alloy 718 after the HPC environmental test.

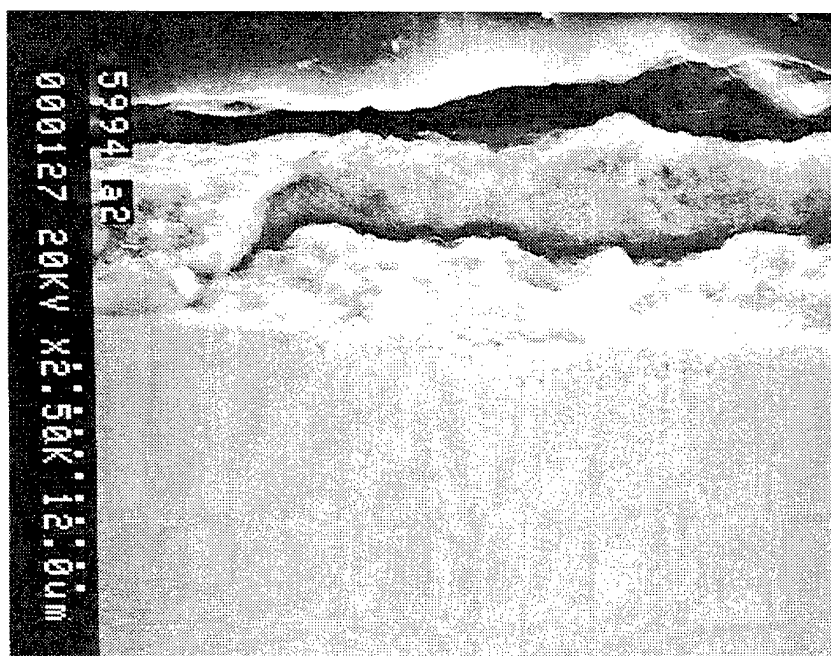
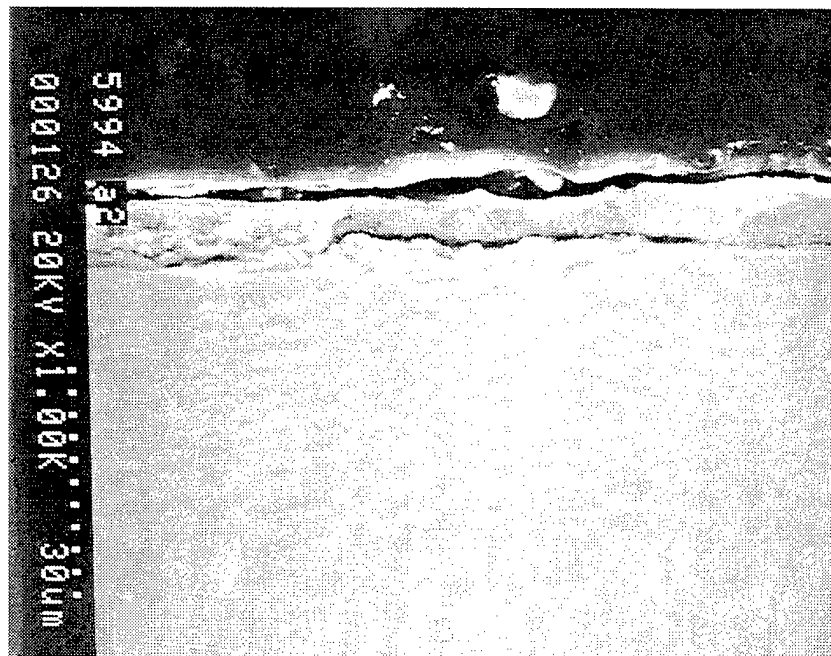


Figure 96. Cross sectional micrographs taken from the hot spot on the uncoated alpha-2 after the HPC environmental test. The alloy has a thick layered scale that might spall.

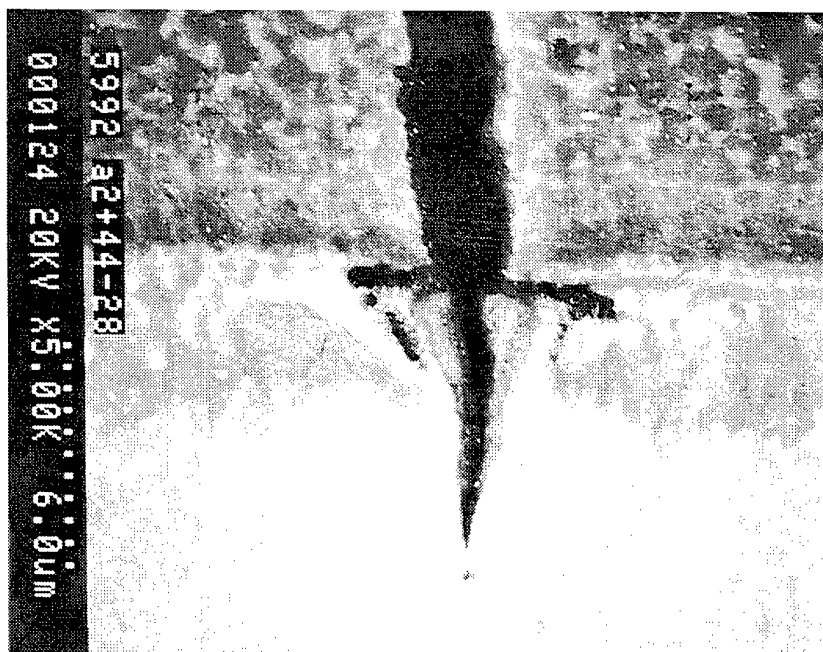
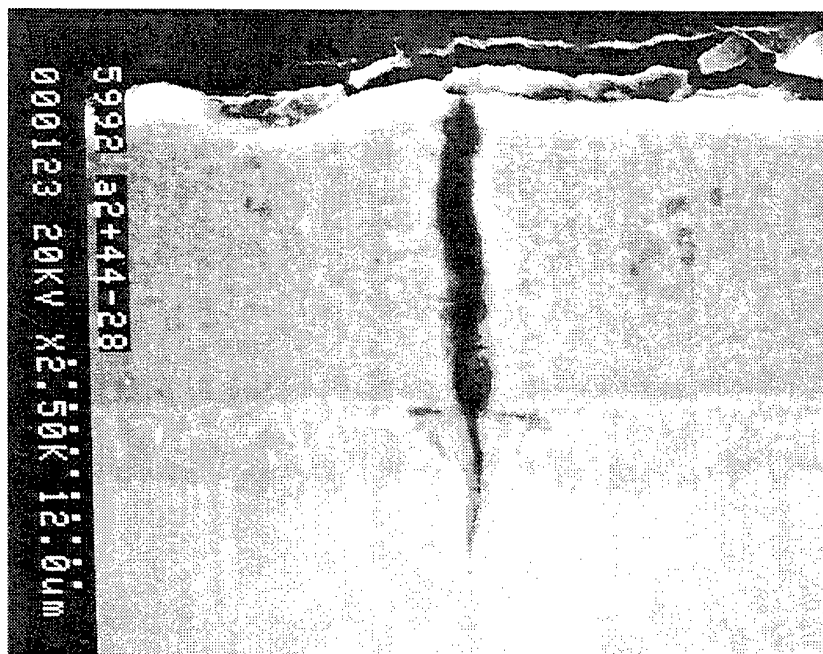


Figure 97. Micrographs of the cross section of the sputtered Ti-44Al-28Cr coating on alpha-2 after the HPC environmental test.

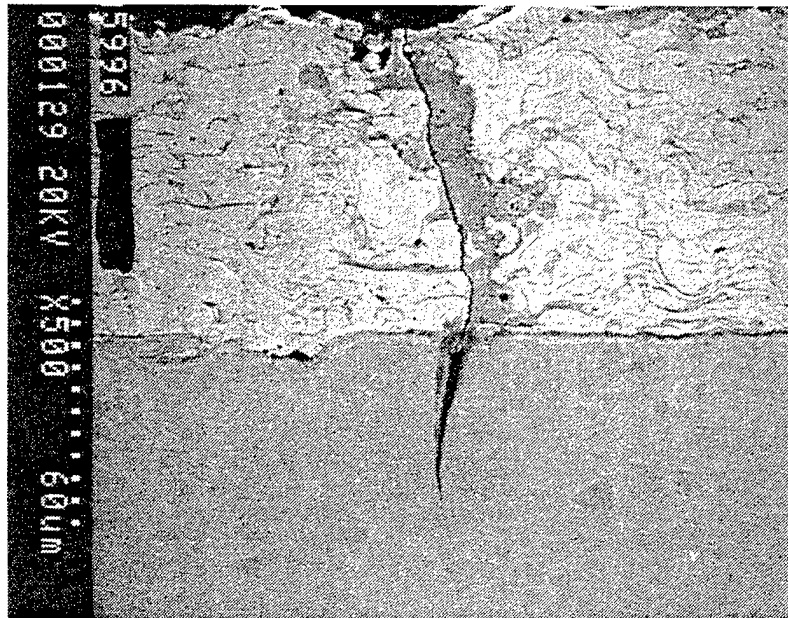


Figure 98. Micrographs of the cross section of the APS Alloy 718 coating on alpha-2 after the HPC environmental test.

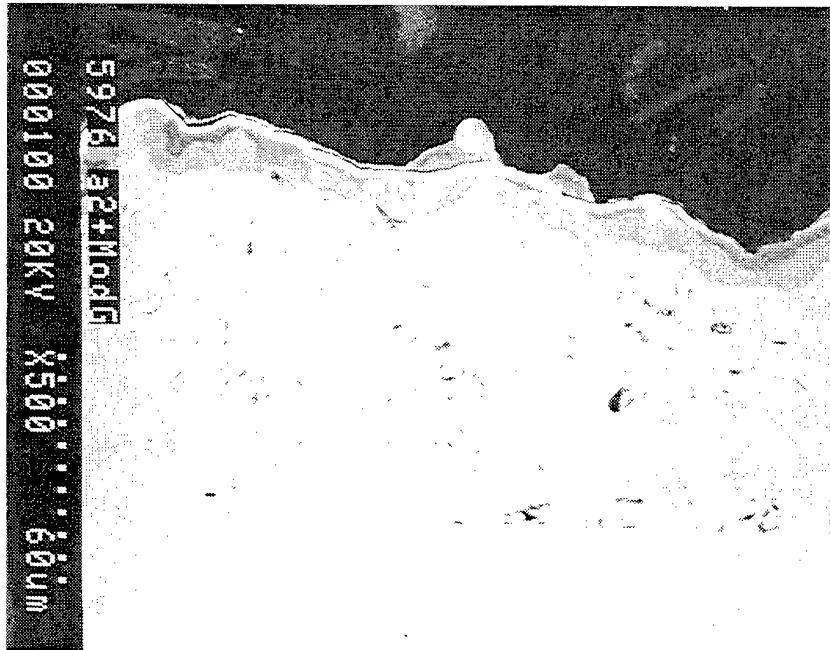


Figure 99. Micrographs of the cross section of the LPPS modified gamma coating on alpha-2 after the HPC environmental test. No thermal fatigue cracks were seen on the coating.

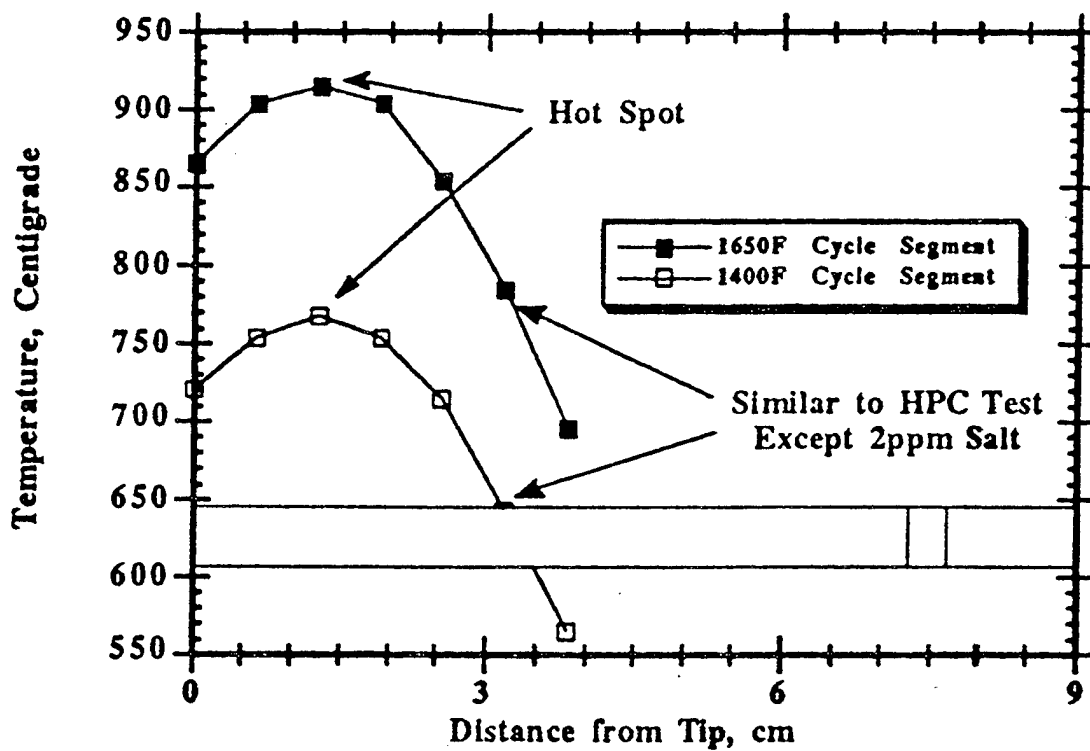


Figure 100. Temperature profile of the specimens in the low pressure turbine environmental test. The "hot" area is located 1cm from the top of the pin. A section of the pin 3.3cm from the tip provides the same cycle as the hot spot from the HPC test except with a high concentration of salt.

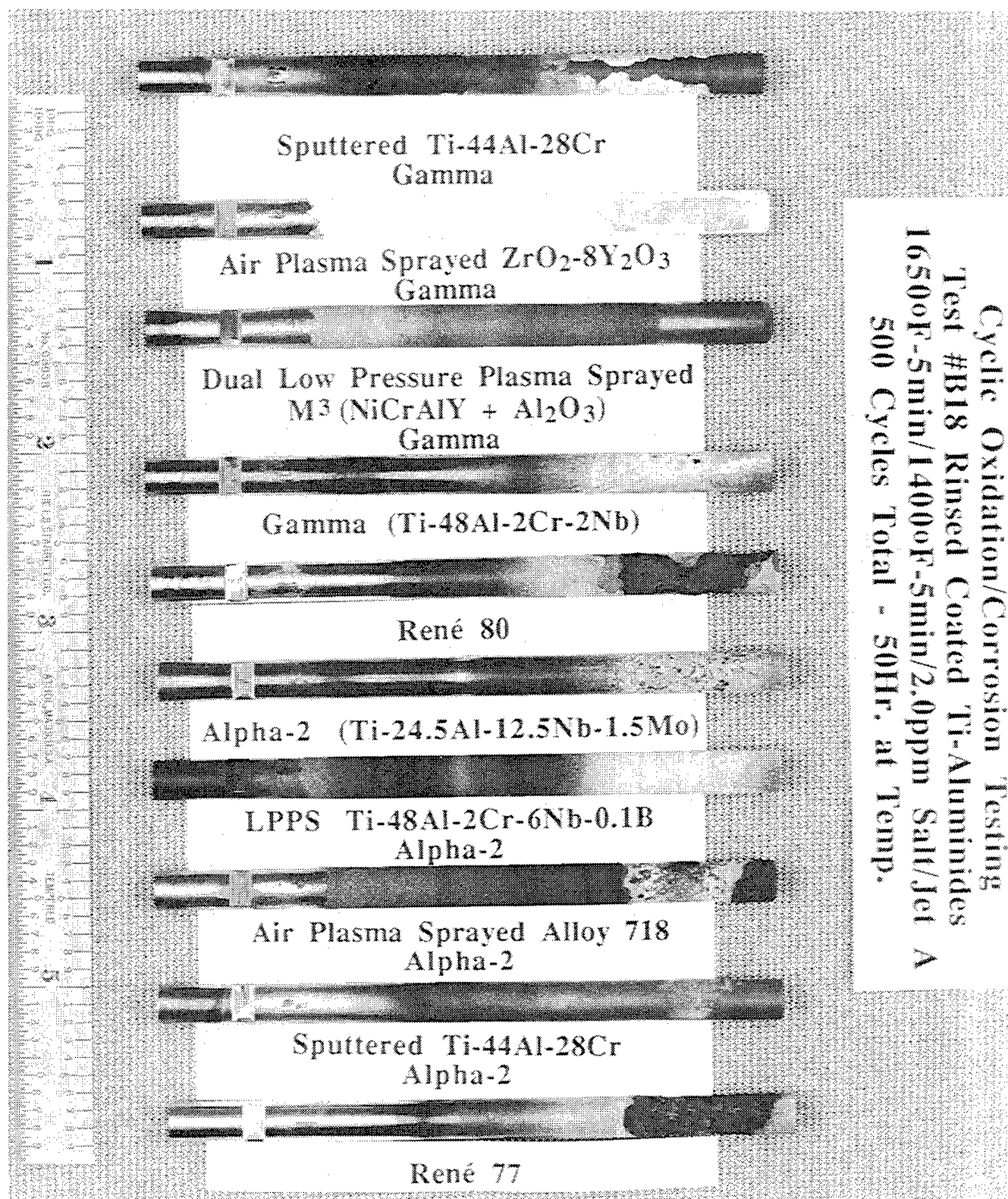


Figure 101. Color photograph shows the coated and uncoated Ti-aluminide samples after 498cycles or 50Hr under low pressure turbine (CHC/O) environmental conditions. The notched side faced the combustor. Note M^3 is the cermet coating.

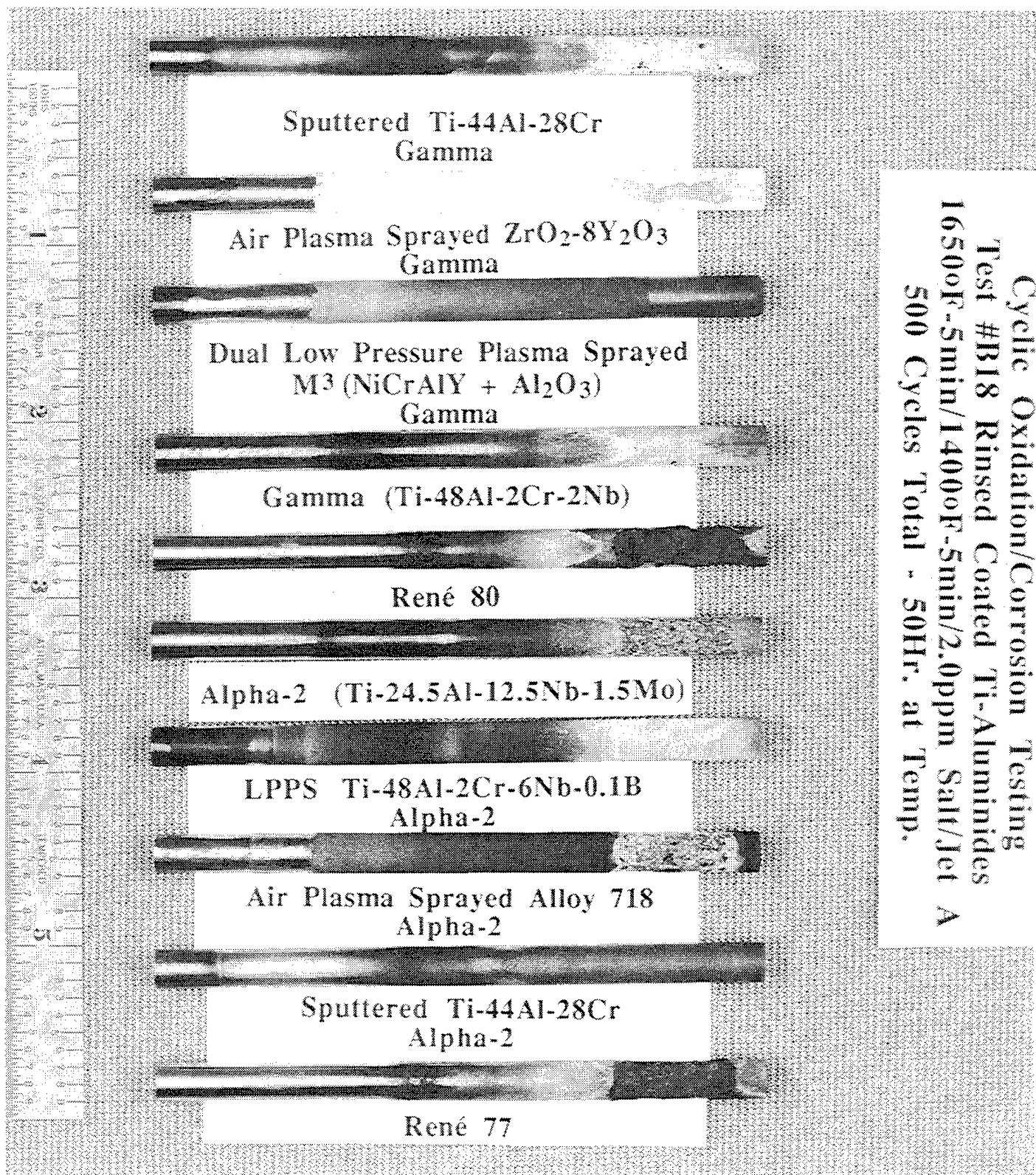
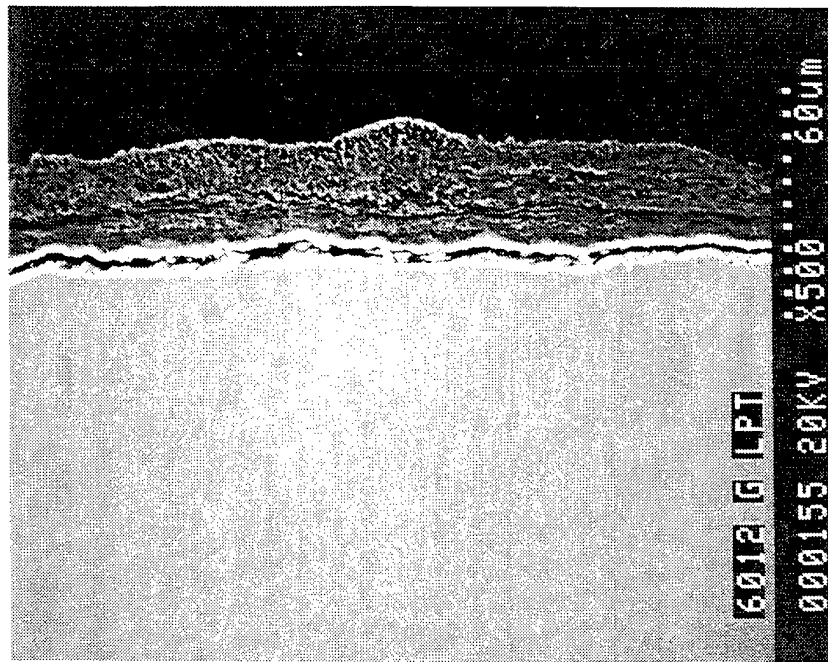
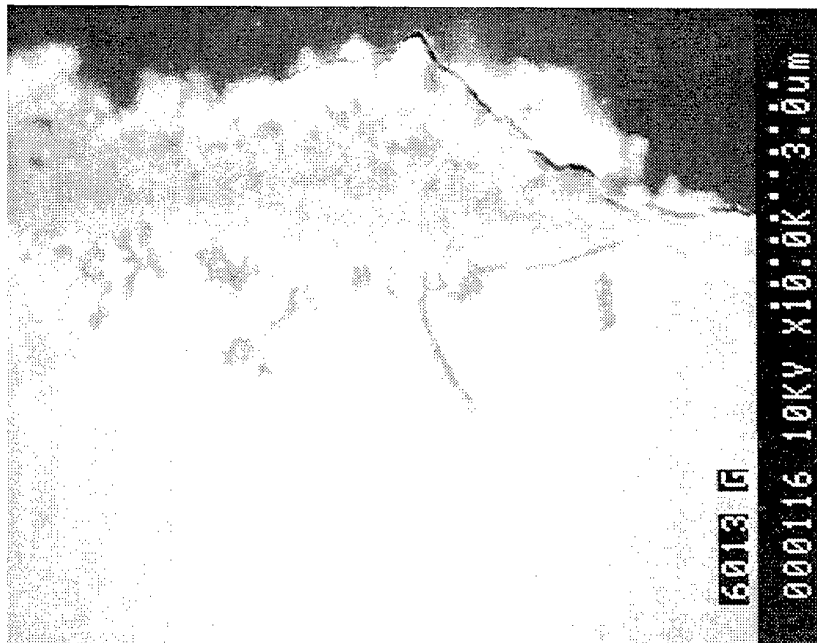


Figure 102. Color photograph shows the coated and uncoated Ti-aluminide samples after 498cycles or 50Hr under low pressure turbine (CHC/O) environmental conditions. This side of the pin faced away from the combustor. Note M^3 is the cermet coating.

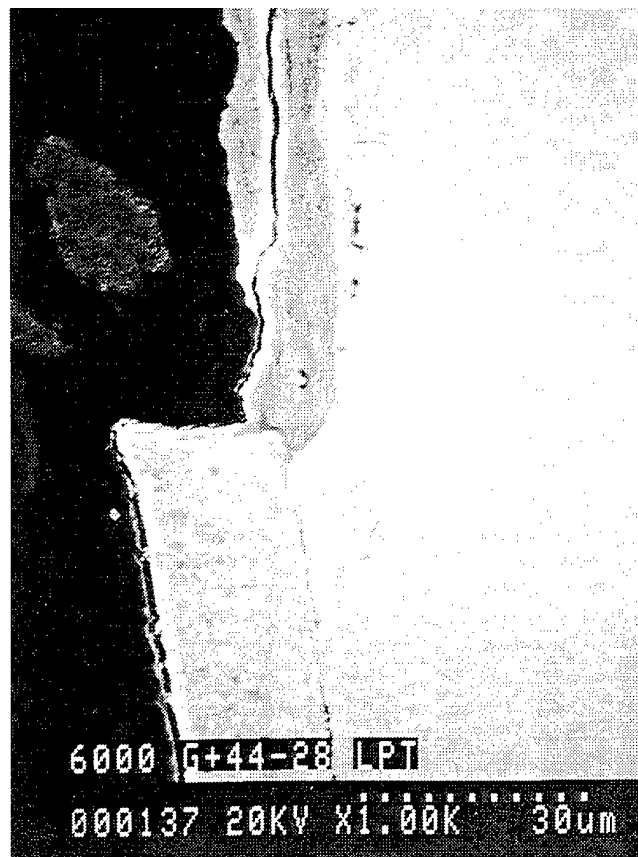


900°C
1652°F

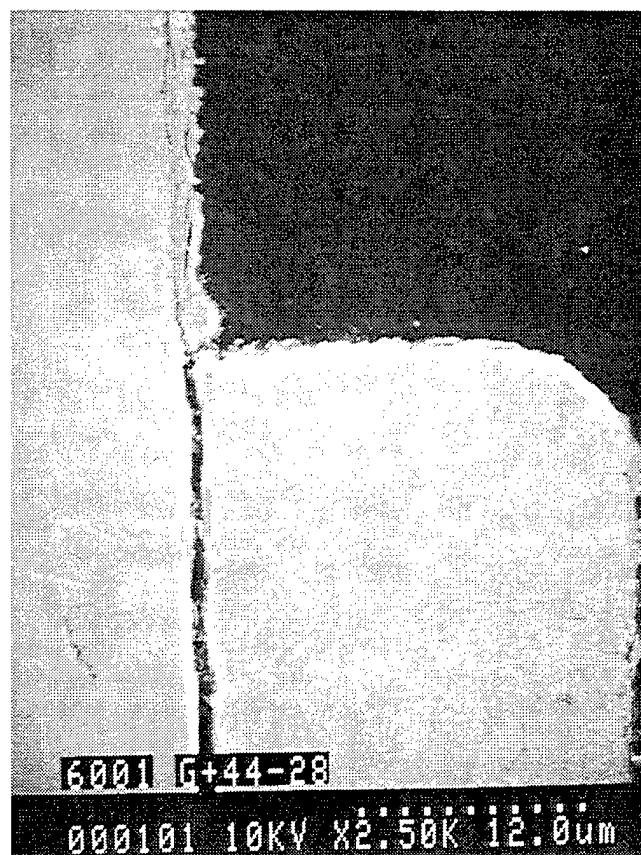


760°C
1400°F

Figure 103. Cross sectional micrographs taken from the hot spot (top) and the 3.3cm sections (bottom) of the uncoated gamma alloy after the LPT environmental test.

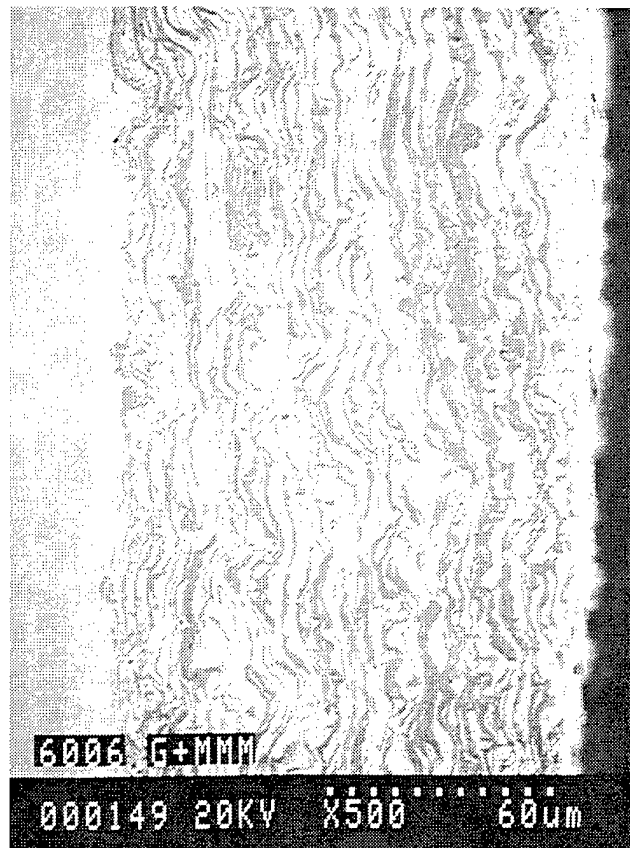


900°C



760°C

Figure 104. Cross sectional micrographs taken from the hot spot (top) and the 3.3cm sections (bottom) of the sputtered Ti-44Al-28Cr coating on the gamma alloy after the LPT environmental test.



900°C



760°C

Figure 105. Cross sectional micrographs taken from the hot spot (top) and the 3.3cm sections (bottom) of the cermet (M³) coating on the gamma alloy after the LPT environmental test. No significant degradation was observed.

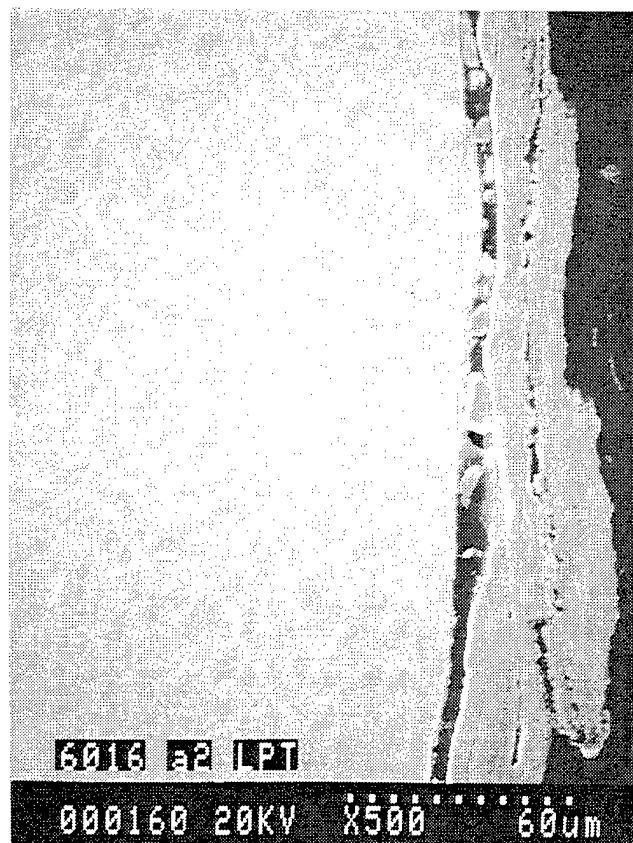


900°C

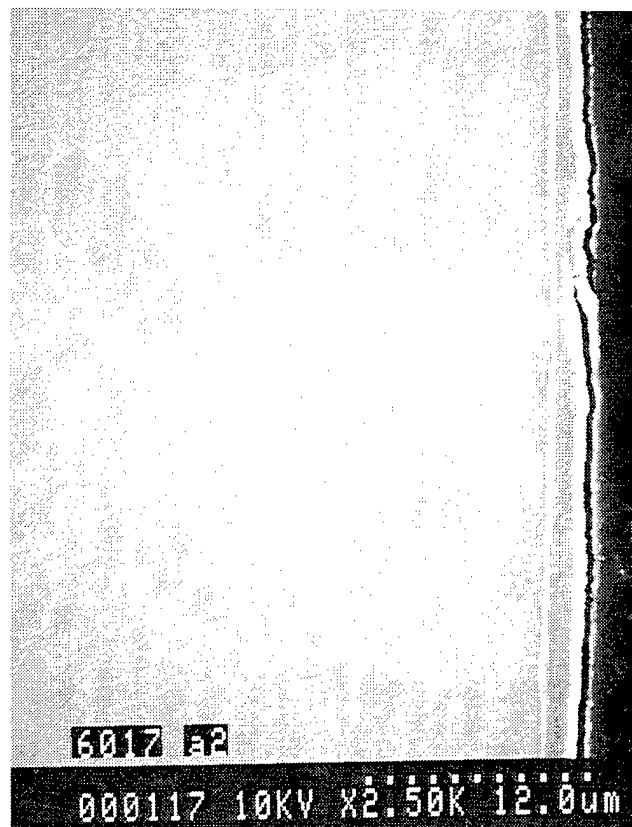


760°C

Figure 106. Cross sectional micrographs taken from the hot spot (top) and the 3.3cm sections (bottom) of the APS YSZ coating on the gamma alloy after the LPT environmental test. The coating spalled during the test.

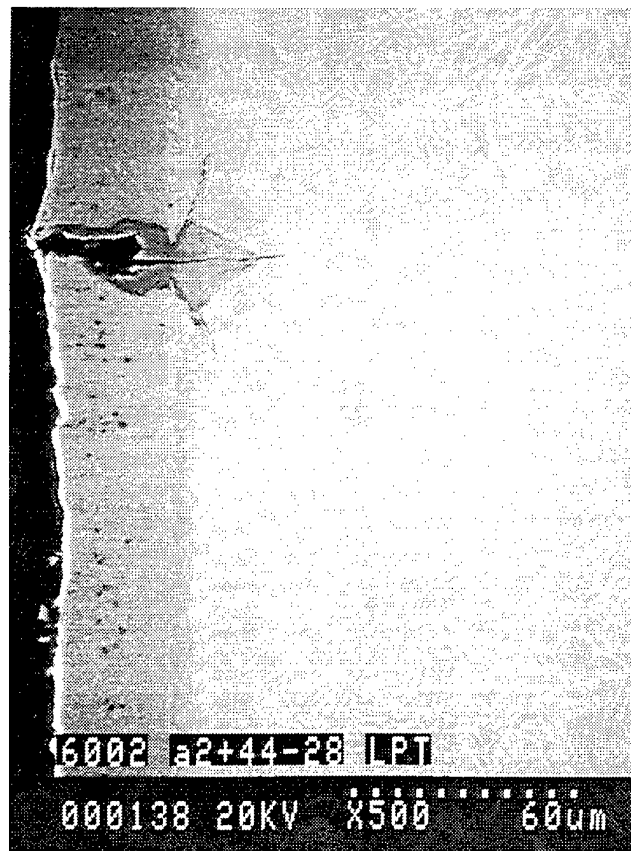


900°C

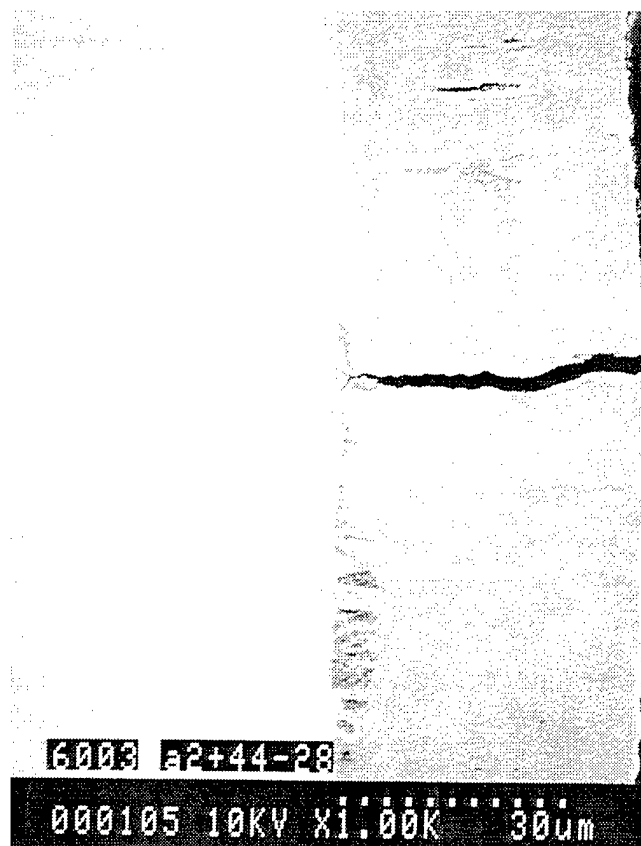


760°C

Figure 107. Cross sectional micrographs taken from the hot spot (top) and the 3.3cm sections (bottom) of uncoated alpha-2 after the LPT environmental test.



900°C



760°C

Figure 108. Cross sectional micrographs taken from the hot spot (top) and the 3.3cm sections (bottom) of sputtered Ti-44Al-28Cr coating on the alpha-2 alloy after the LPT environmental test.



900°C



760°C

Figure 109. Cross sectional micrographs taken from the hot spot (top) and the 3.3cm sections (bottom) of the APS Alloy 718 coating on the alpha-2 alloy after the LPT environmental test.

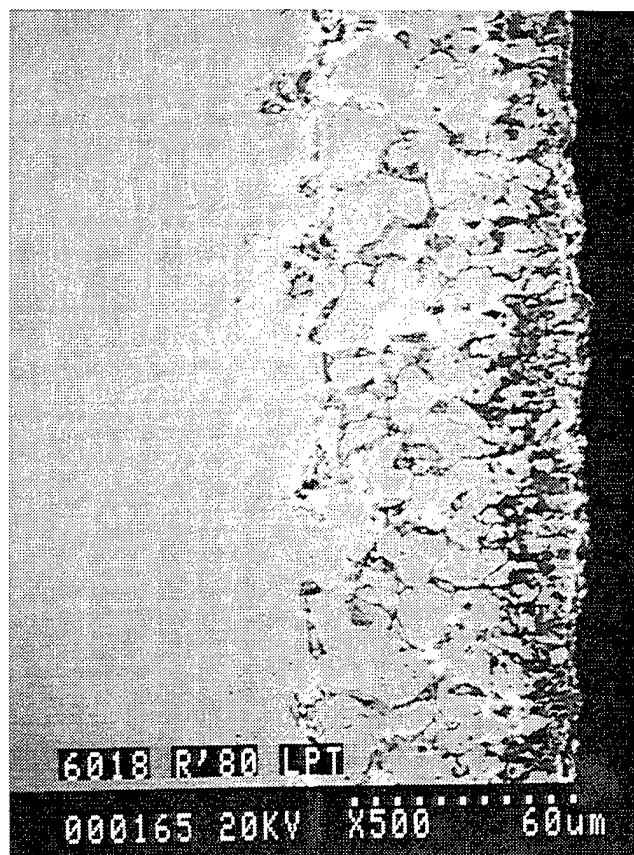


900°C

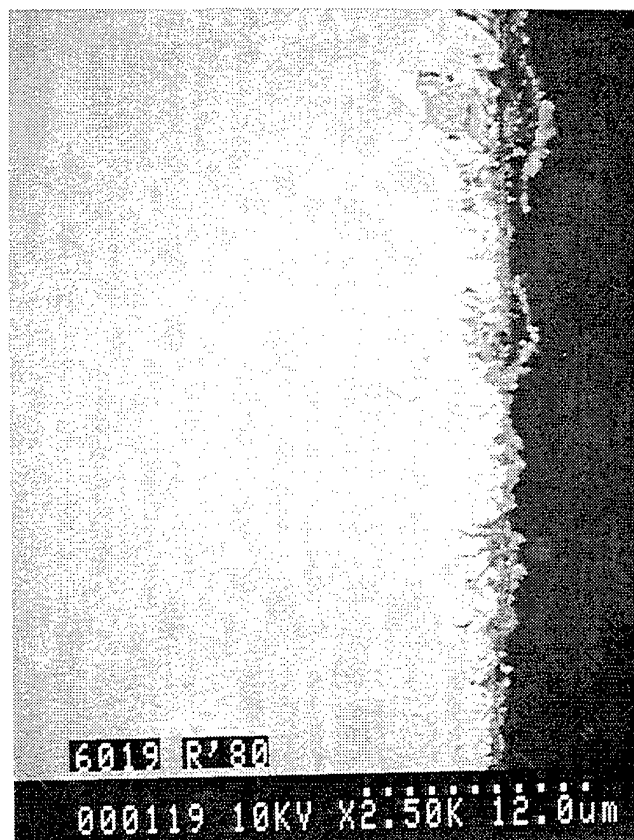


760°C

Figure 110. Cross sectional micrographs taken from the hot spot (top) and the 3.3cm sections (bottom) of the LPPS modified gamma coating on the alpha-2 alloy after the LPT environmental test.



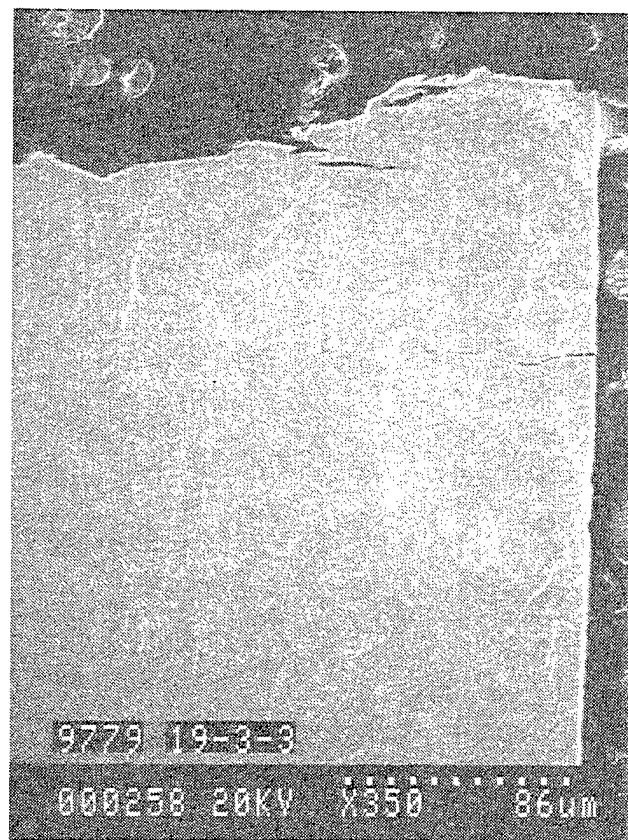
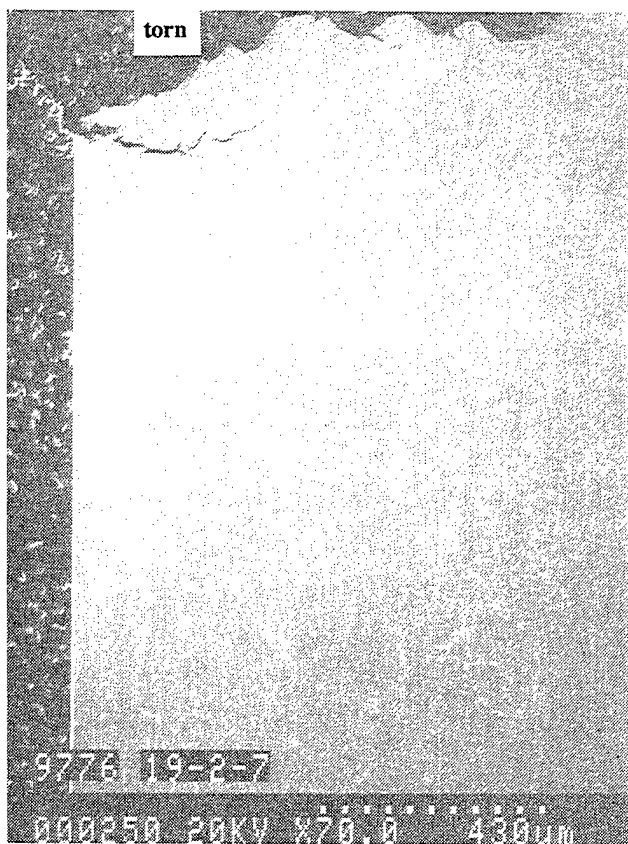
900°C



760°C

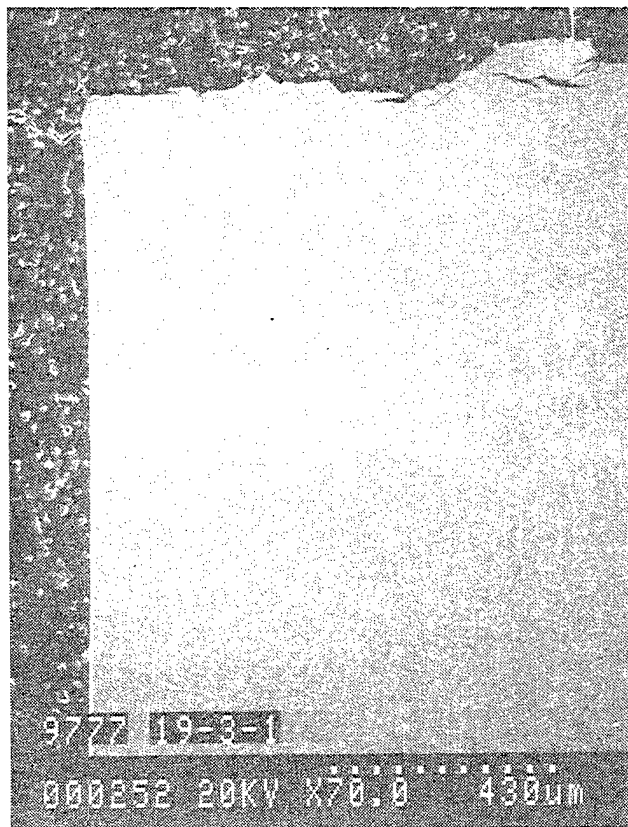
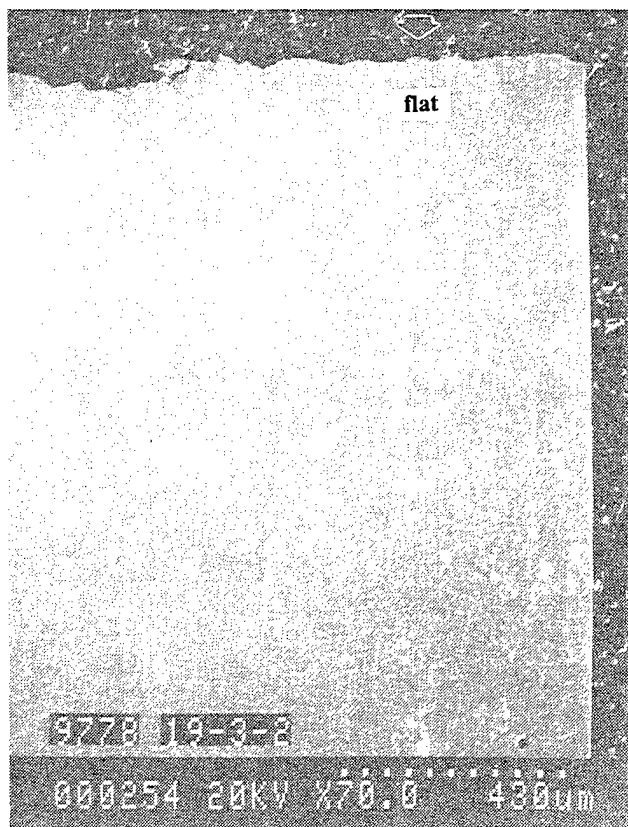
Figure 111. Cross sectional micrographs taken from the hot spot (top) and the 3.3cm sections (bottom) of the René 80 after the LPT environmental test.

RT Tensile



1050°F/40ksi/100h

750°F/50ksi/100h



1050°F/40ksi/750h

Figure 112. Low magnification cross sections of uncoated gamma (Ti-48Al-2Cr-2Nb) specimens showing the fracture path and little secondary tensile cracking after various salt free exposures.

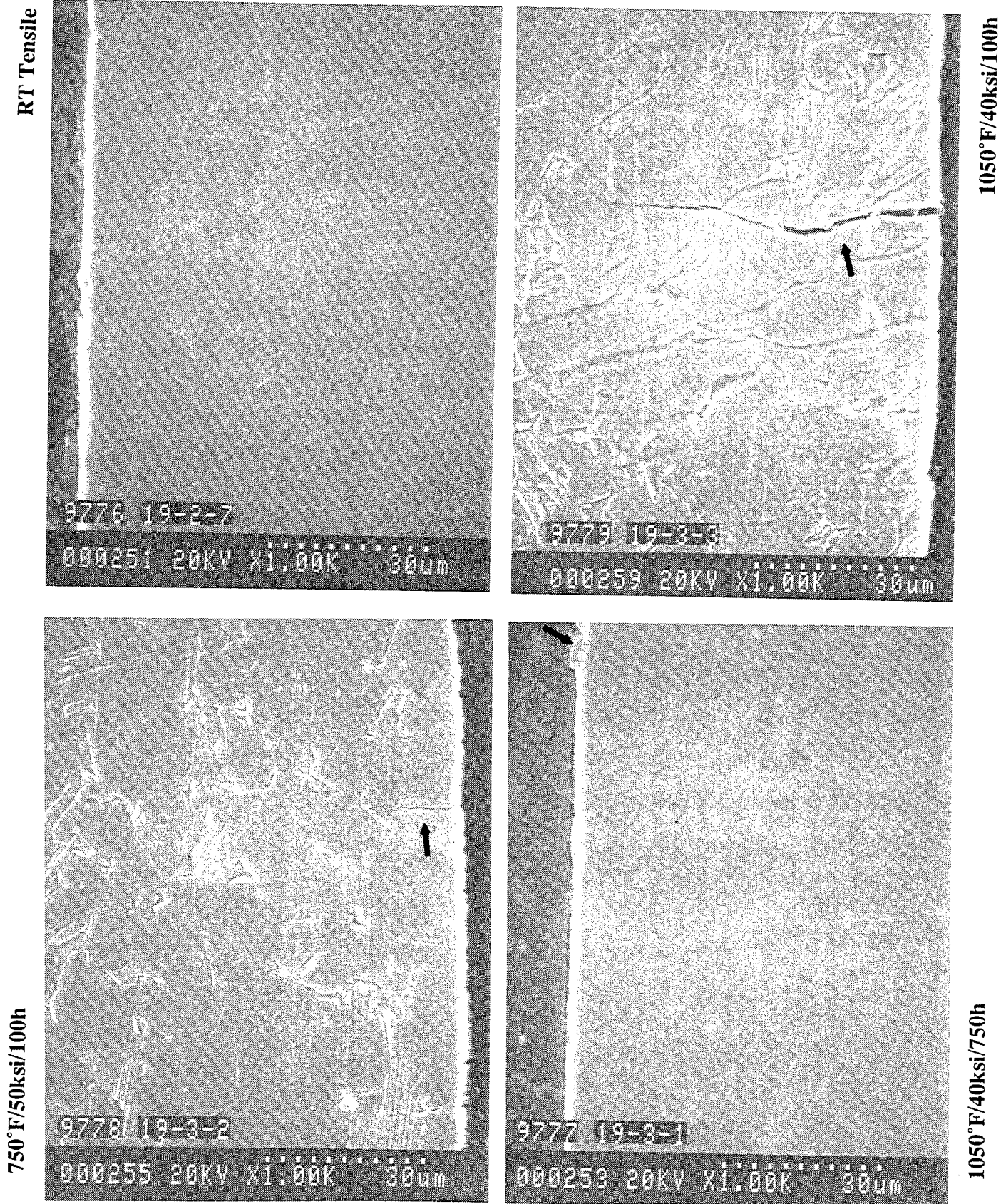


Figure 113. Higher magnification cross sections of uncoated gamma (Ti-48Al-2Cr-2Nb) specimens showing the a very thin external scale.

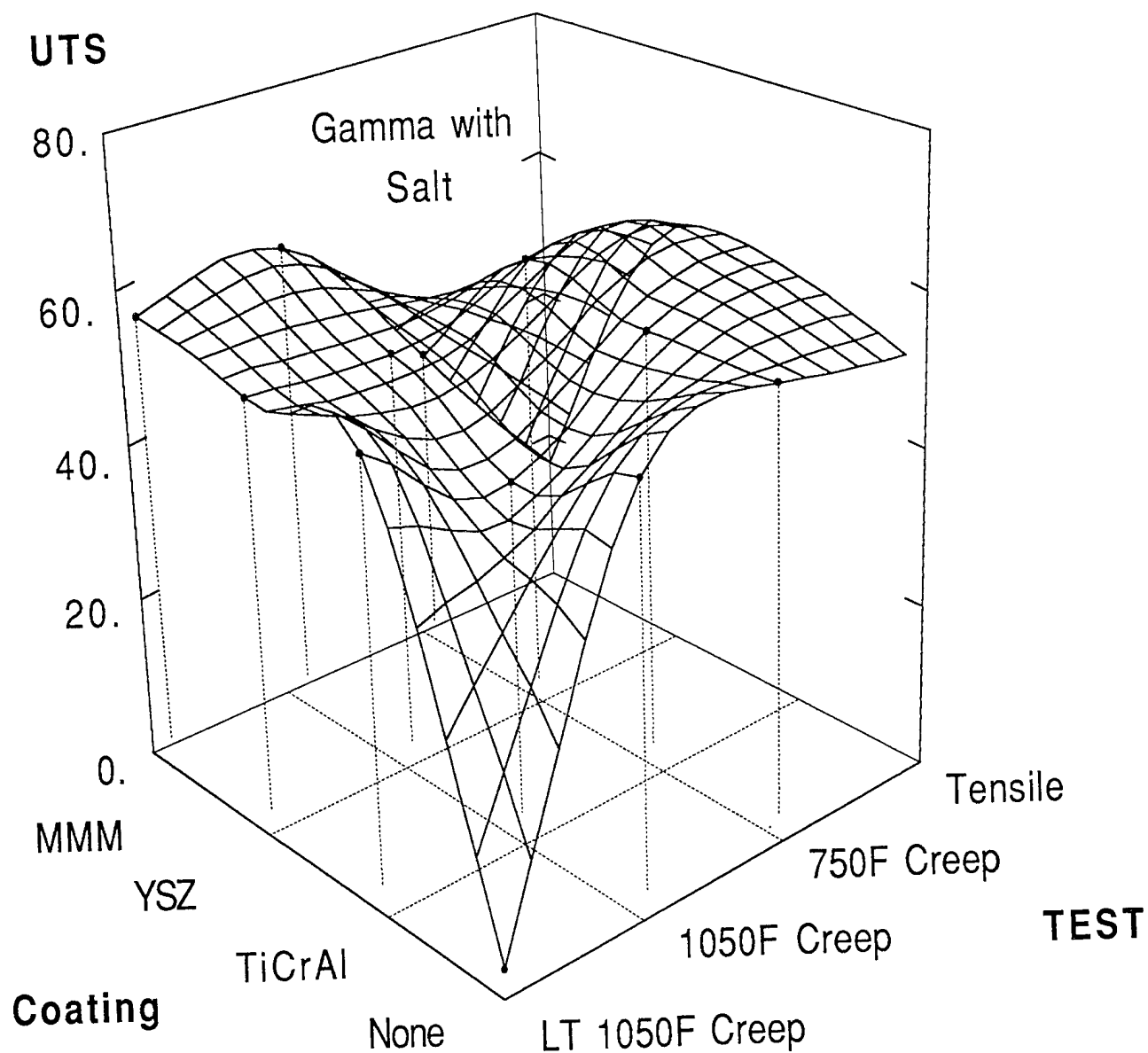


Figure 114. The UTS response surface is flat (~50-60ksi) for gamma samples as a function of coating and exposure. Only the 1050°F/40ksi/750h salt exposure of the bare gamma sample resulted in total embrittlement.

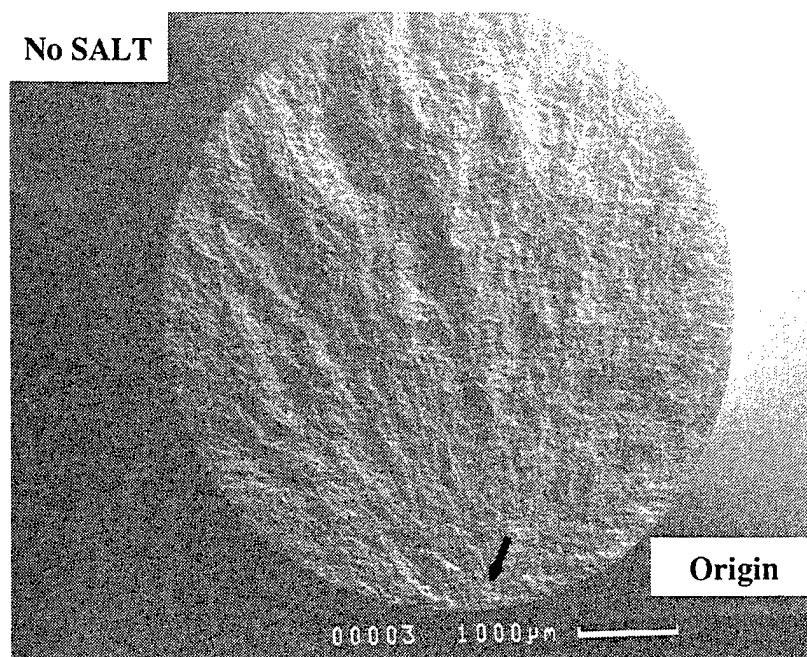
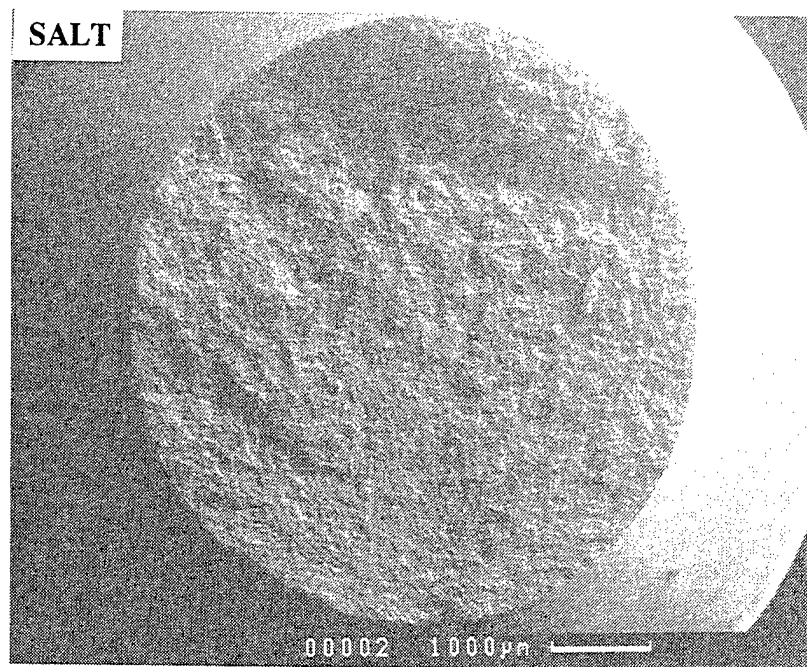
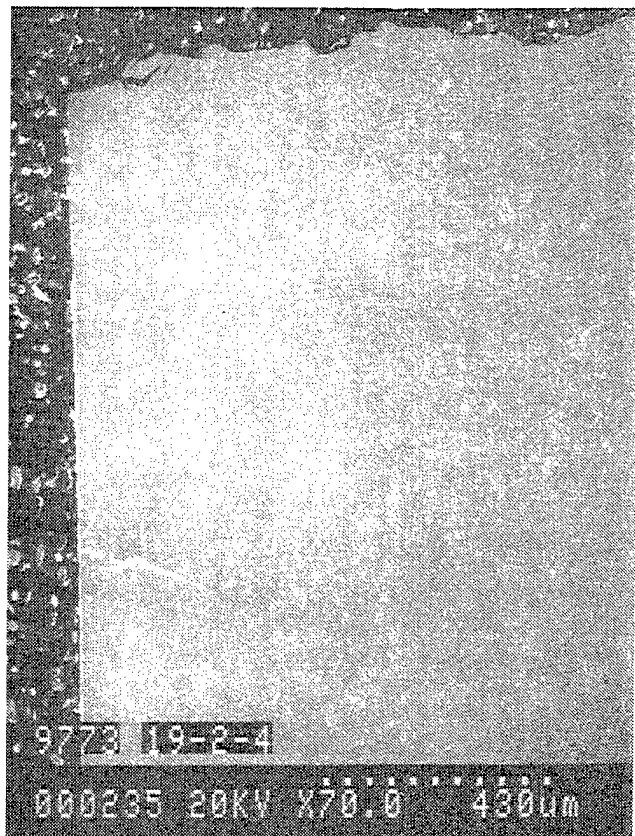
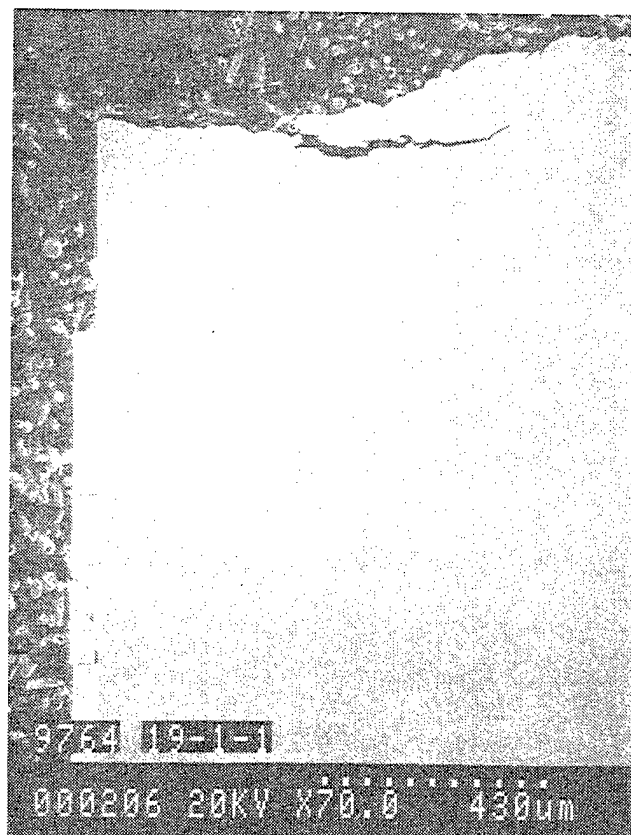


Figure 115. Post exposure low magnification fractographs of gamma samples after tensile testing showing a difference in crack initiation. The sample exposed without salt has a single origin, while the salt exposed sample has multiple origins.

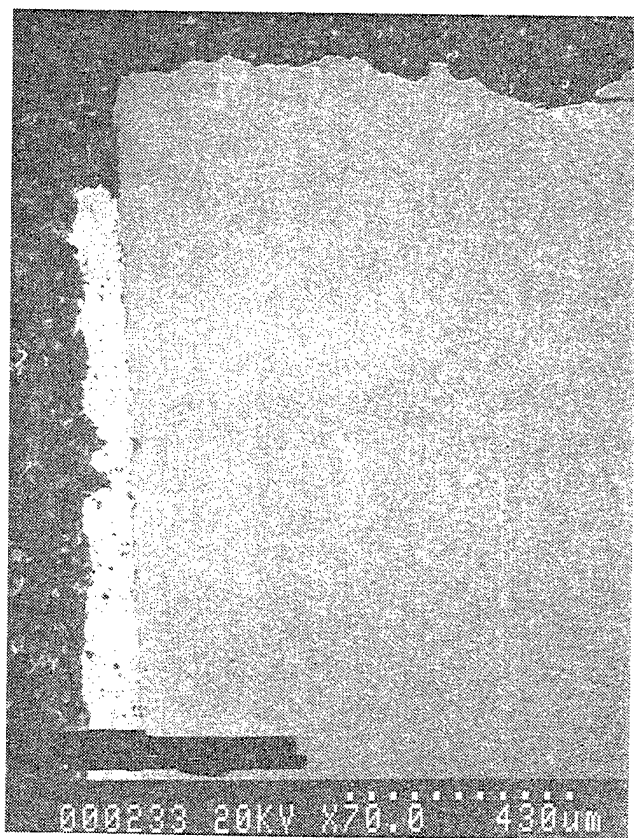
Uncoated 750°F/50ksi/100h



Sputtered TiCrAl 750°F/50ksi/100h



APS YSZ 750°F/50ksi/100h



NiCrAlY M³ 750°F/50ksi/100h

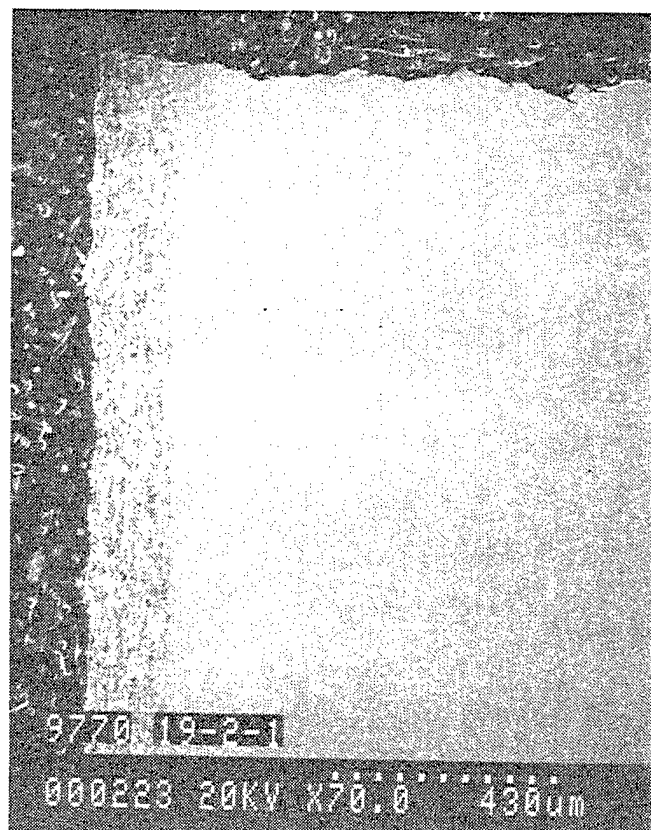
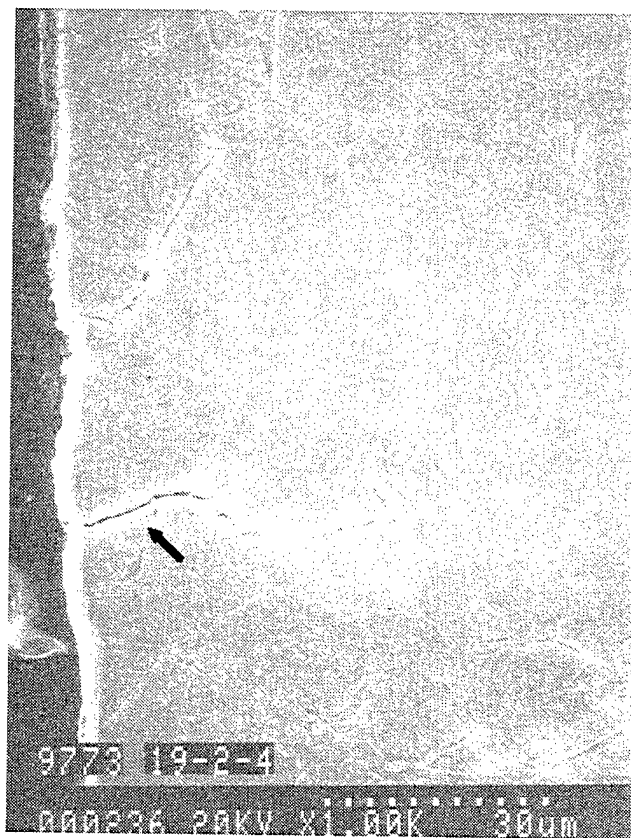
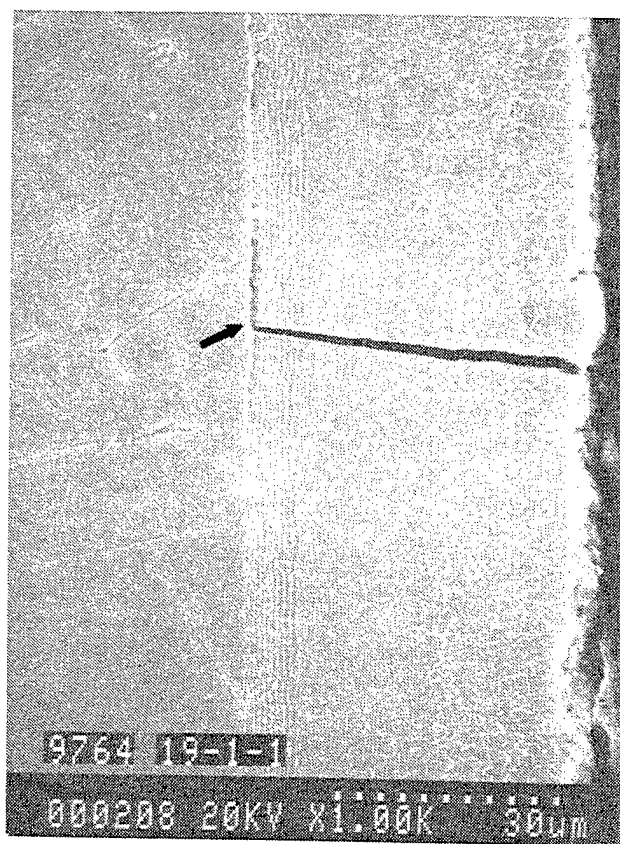


Figure 116. Low magnification cross sections of coated and uncoated gamma (Ti-48Al-2Cr-2Nb) specimens showing the fracture path and little HSSCC cracking after a 750°F/50ksi/100h exposure.

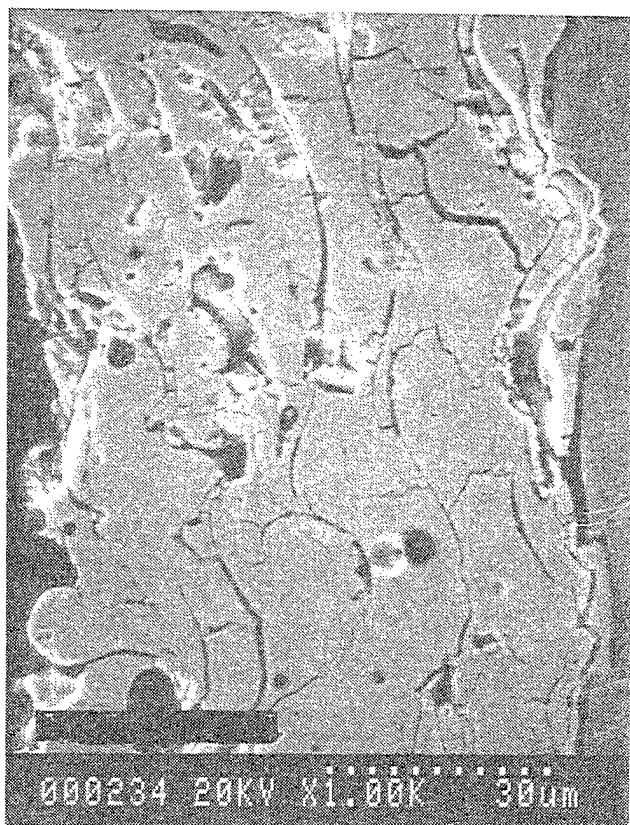
Uncoated 750°F/50ksi/100h



Sputtered TiCrAl 750°F/50ksi/100h



APS YSZ 750°F/50ksi/100h



NiCrAlY M³ 750°F/50ksi/100h

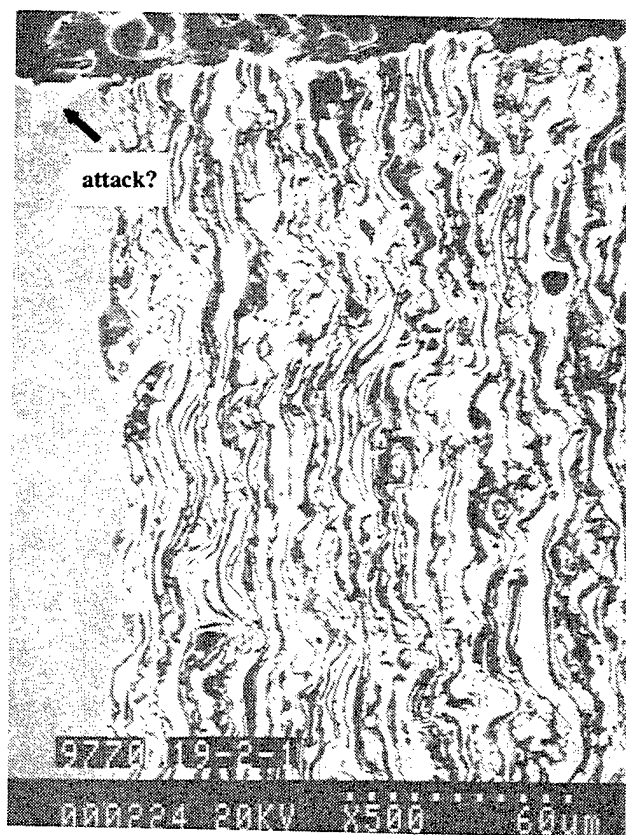
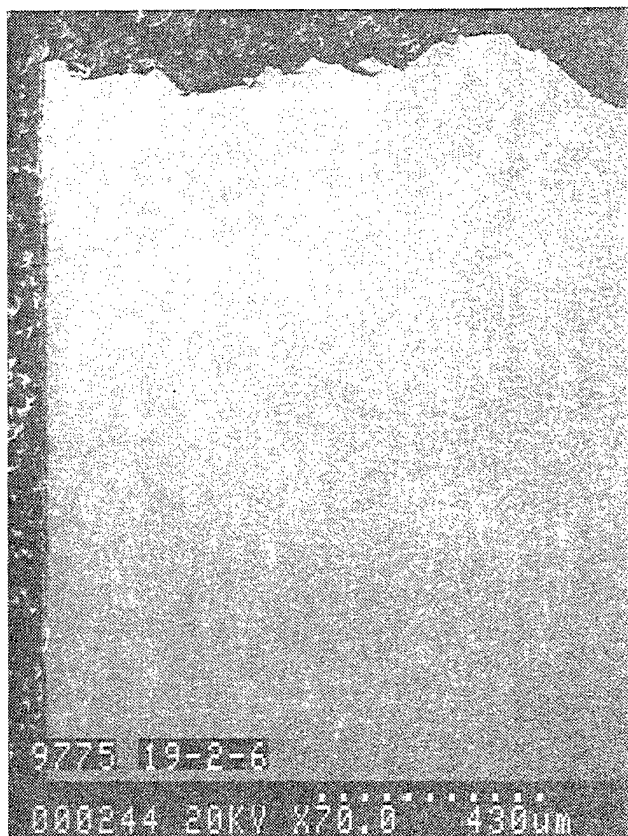


Figure 117. High magnification cross sections of coated and uncoated gamma (Ti-48Al-2Cr-2Nb) specimens showing coating attack, substrate attack and cracking after a HSSCC exposure for 750°F/50ksi/100h.

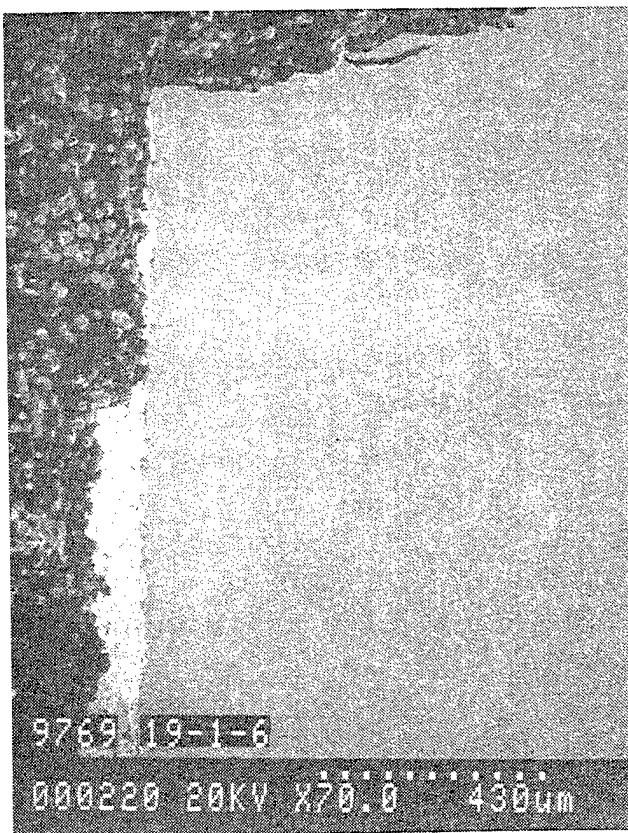
Uncoated 1050°F/40ksi/750h



Sputtered TiCrAl 1050°F/40ksi/750h



APS YSZ 1050°F/40ksi/750h



NiCrAlY M3 1050°F/40ksi/750h

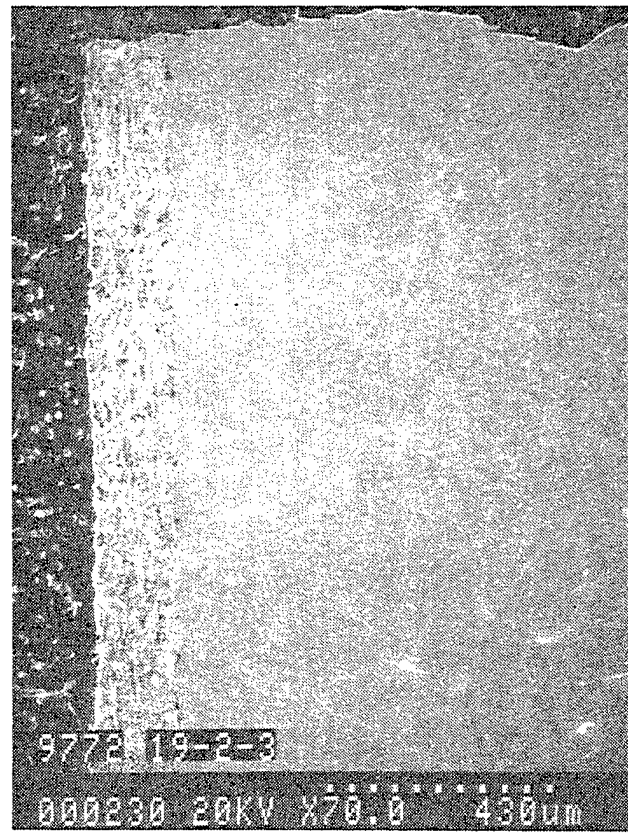
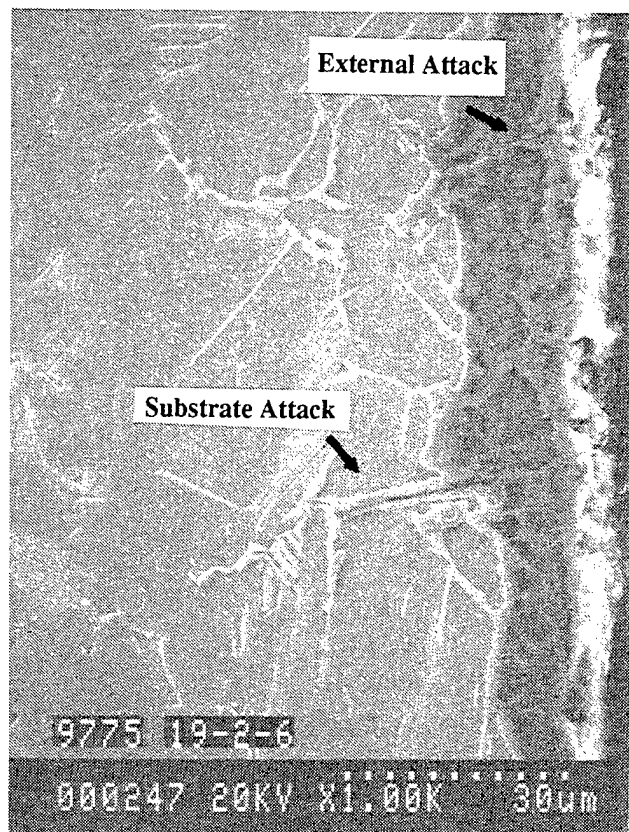
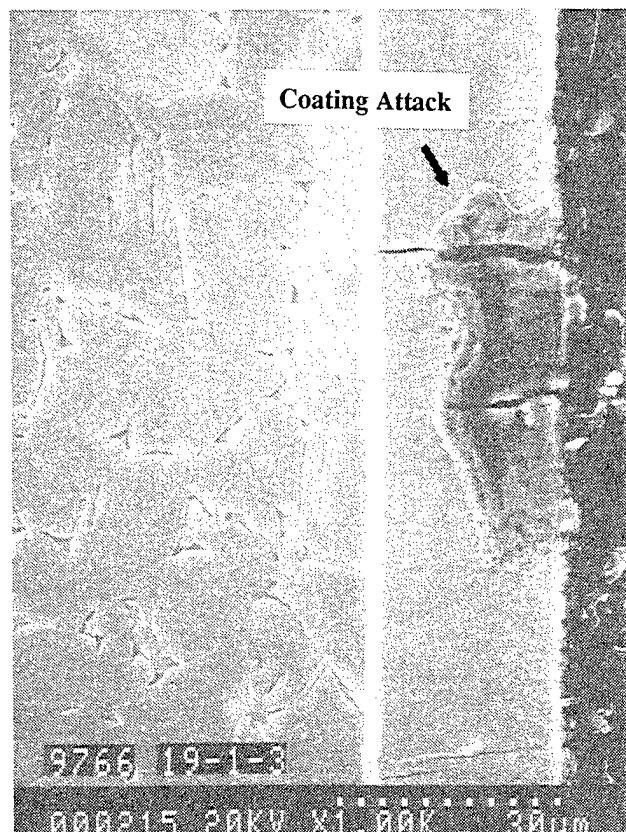


Figure 118. Low magnification cross sections of coated and uncoated gamma (Ti-48Al-2Cr-2Nb) specimens showing the morphology of the fracture path and cracking after a HSSCC exposure for 1050°F/40ksi and different times.

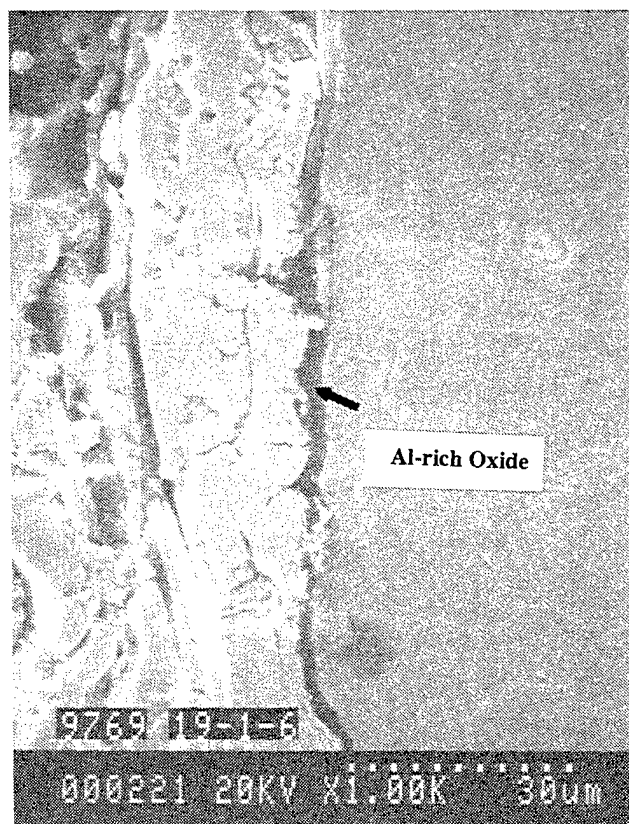
Uncoated 1050°F/40ksi/750h



Sputtered TiCrAl 1050°F/40ksi/750h



APS YSZ 1050°F/40ksi/750h



NiCrAlY M³ 1050°F/40ksi/750h

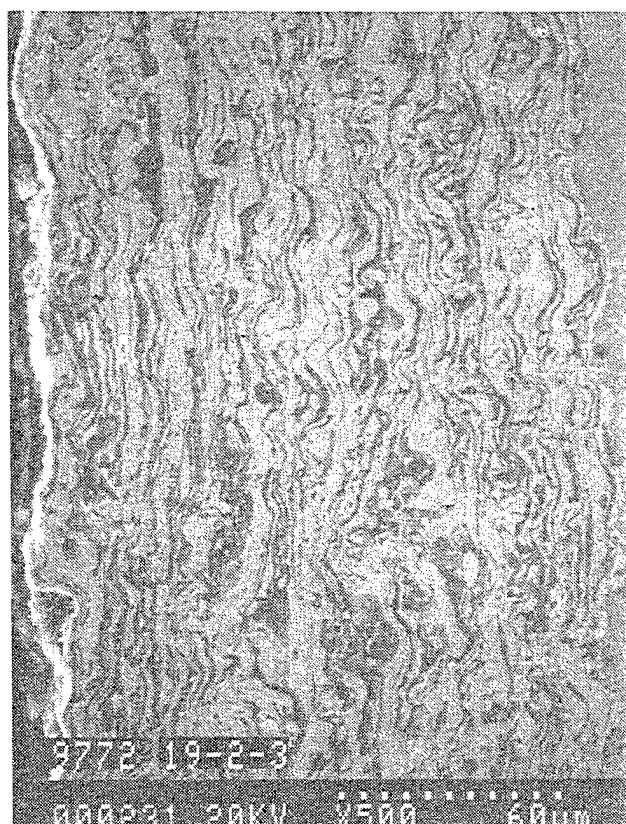


Figure 119. High magnification cross sections of coated and uncoated gamma (Ti-48Al-2Cr-2Nb) specimens showing the morphology of HSSCC attack in the substrate and on coatings after a 1050°F/40ksi exposure for different times. The attack is most notable on the uncoated gamma where a thick Cl-rich external scale and intergranular attack are observed.

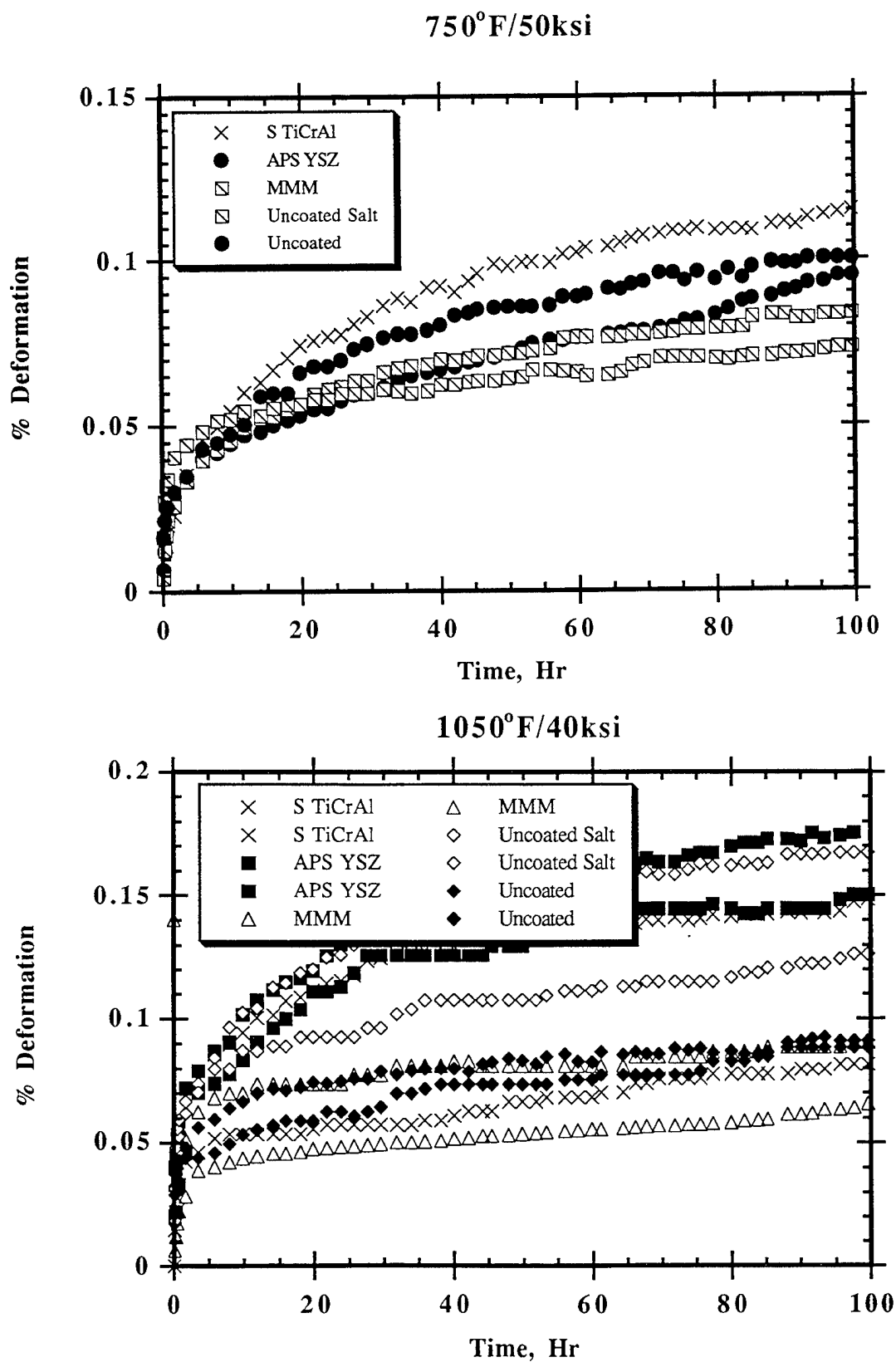
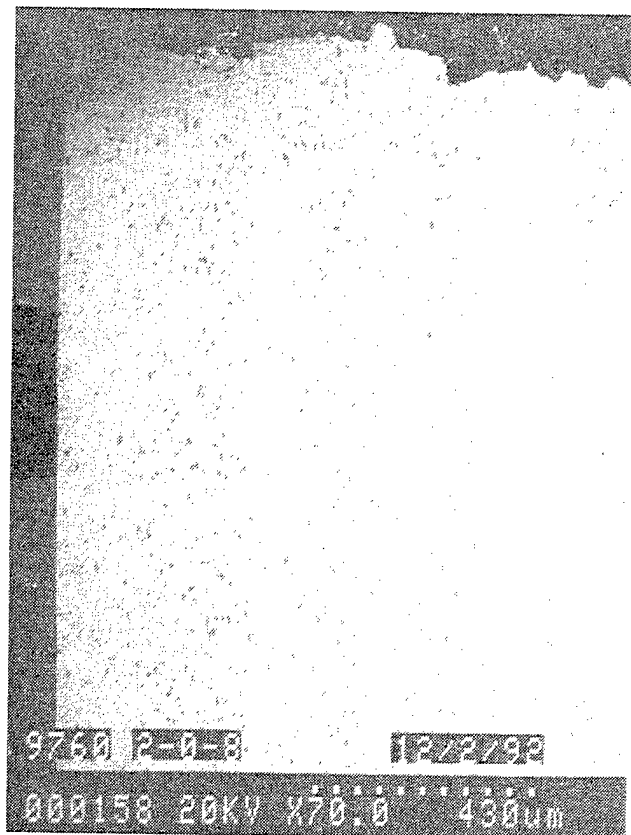


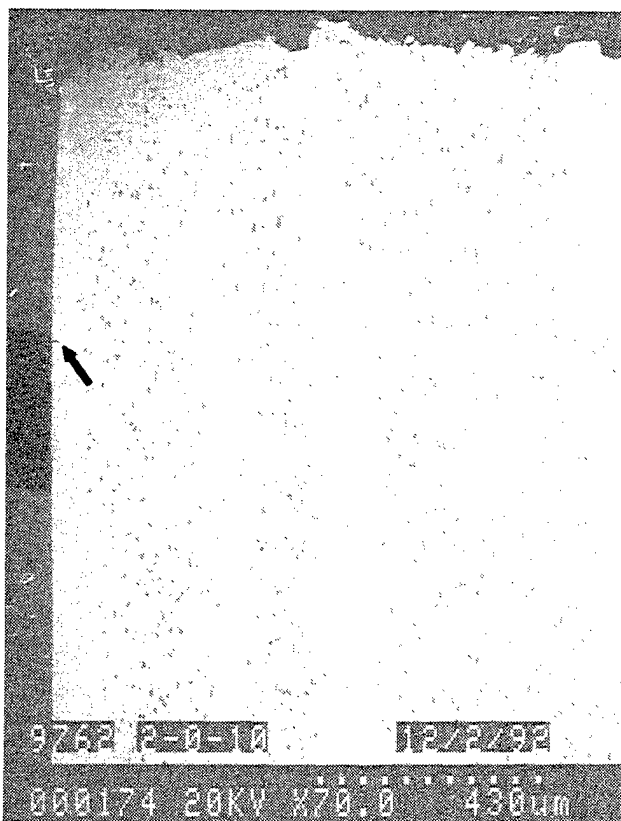
Figure 120. Curves showing the creep behavior of coated and uncoated gamma alloys during 100h exposures at 750°F/50ksi and 1050°F/40ksi. The gamma alloys crept at nearly the same rate for the two exposures.

RT Tensile



1050°F/40ksi/100h

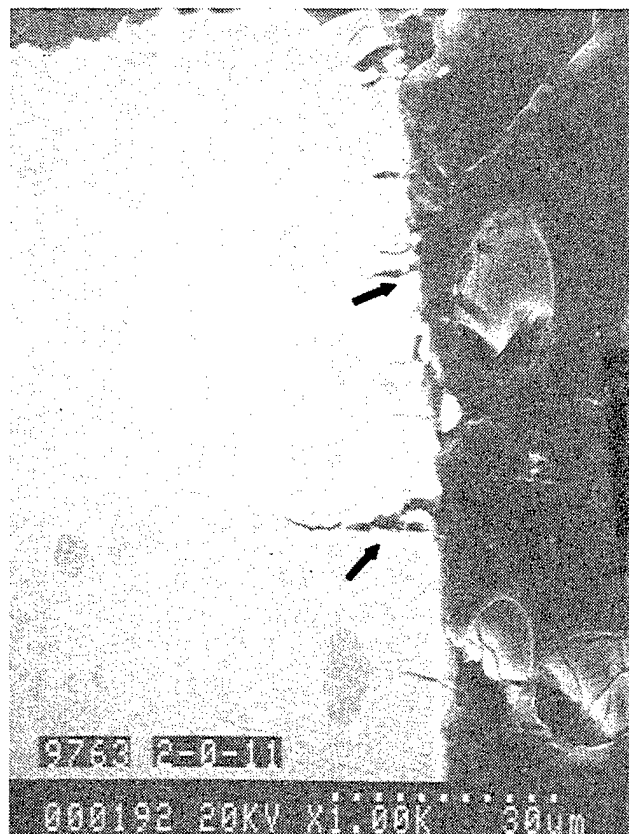
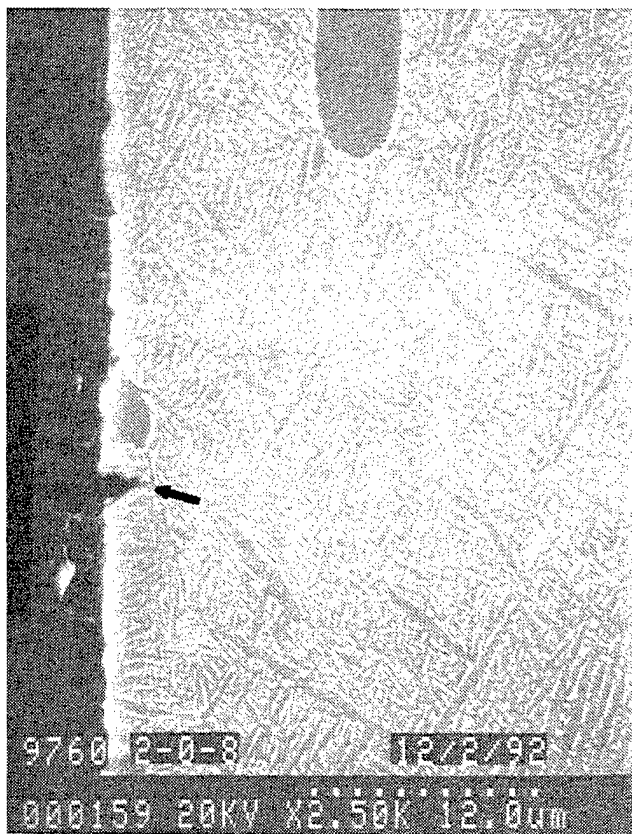
750°F/50ksi/100h



1050°F/40ksi/750h

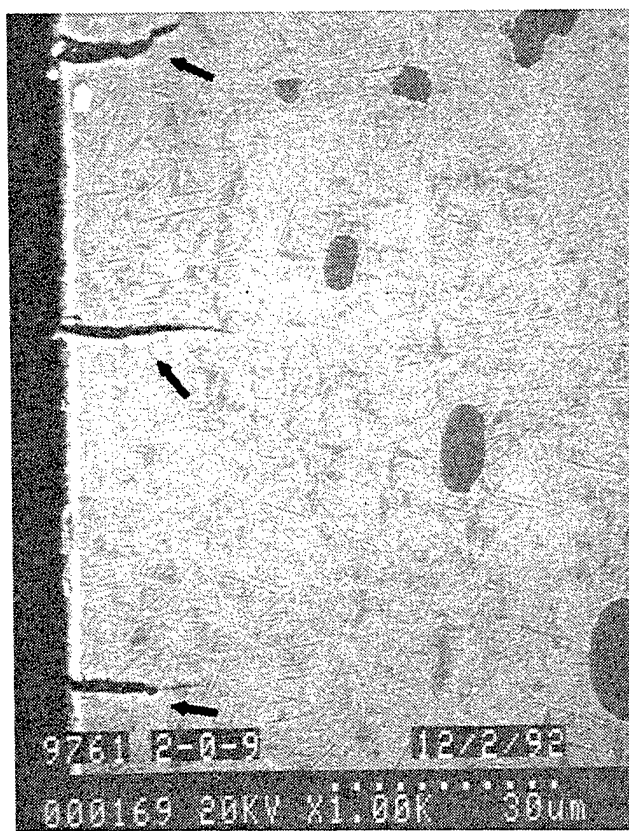
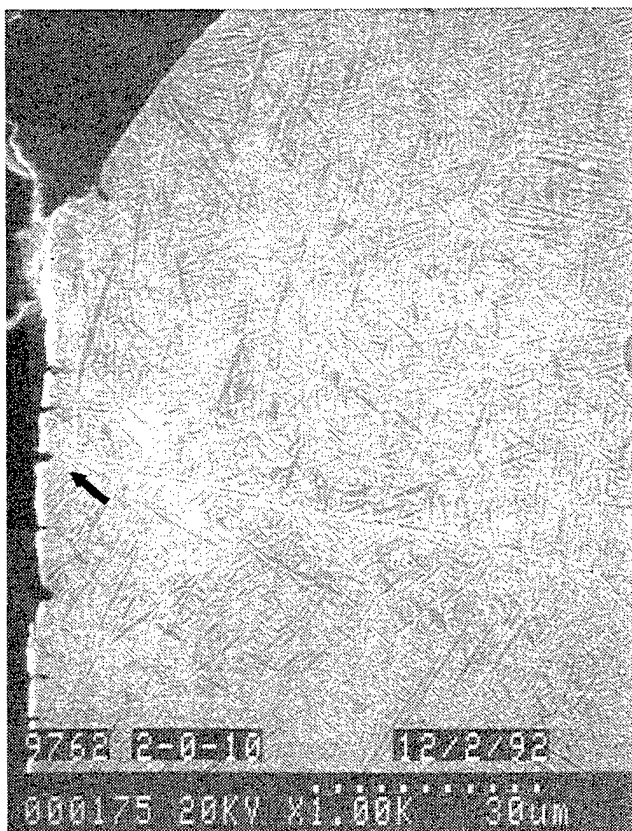
Figure 121. Low magnification cross sections of uncoated alpha-2 (Ti-24.5Al-12.5Nb-1.5Mo) specimens showing the fracture path and secondary tensile cracking after various exposures.

RT Tensile



1050°F/40ksi/100h

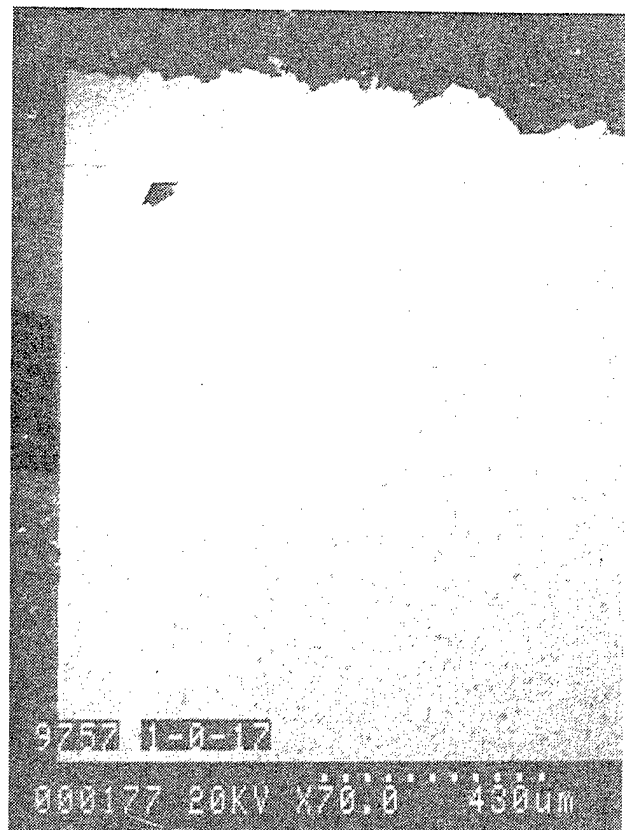
750°F/50ksi/100h



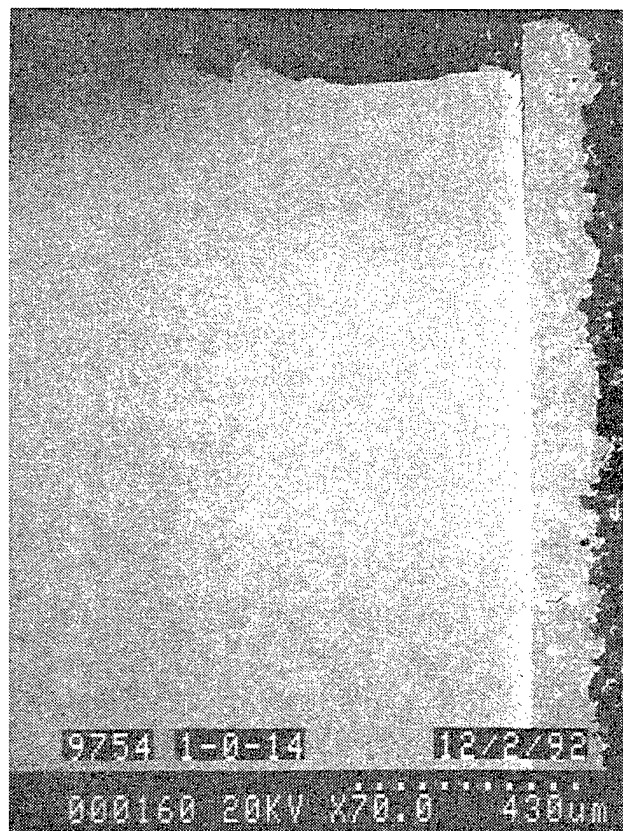
1050°F/40ksi/750h

Figure 122. High magnification cross sections of uncoated alpha-2 (Ti-24.5Al-12.5Nb-1.5Mo) specimens showing the thin external scale and secondary tensile cracking after various exposures. A regular distribution of secondary tensile cracks is observed (arrows).

Uncoated 750°F/50ksi/100h



LPPS Modified Gamma 750°F/50ksi/43.2h



Sputtered TiCrAl 750°F/50ksi/100h



APS Alloy 718 750°F/50ksi/100h

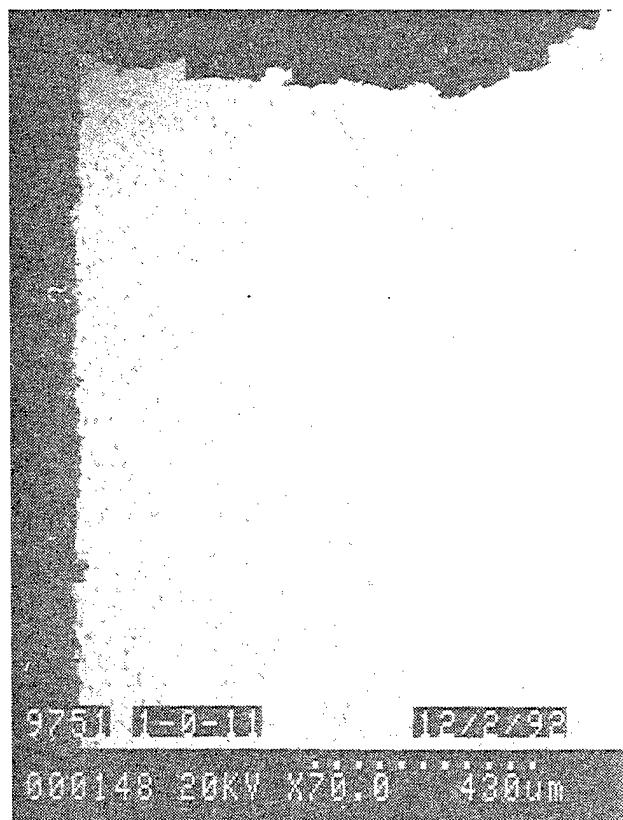
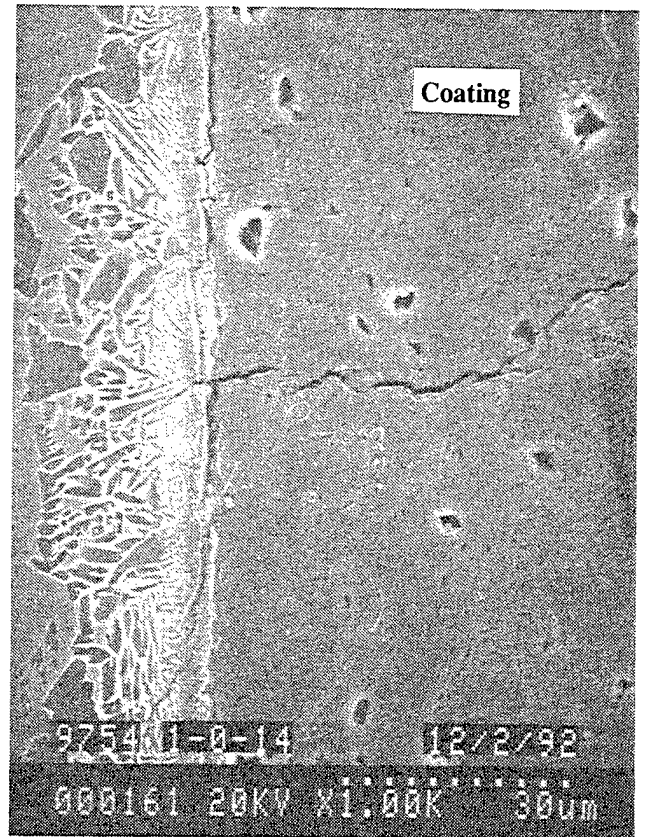
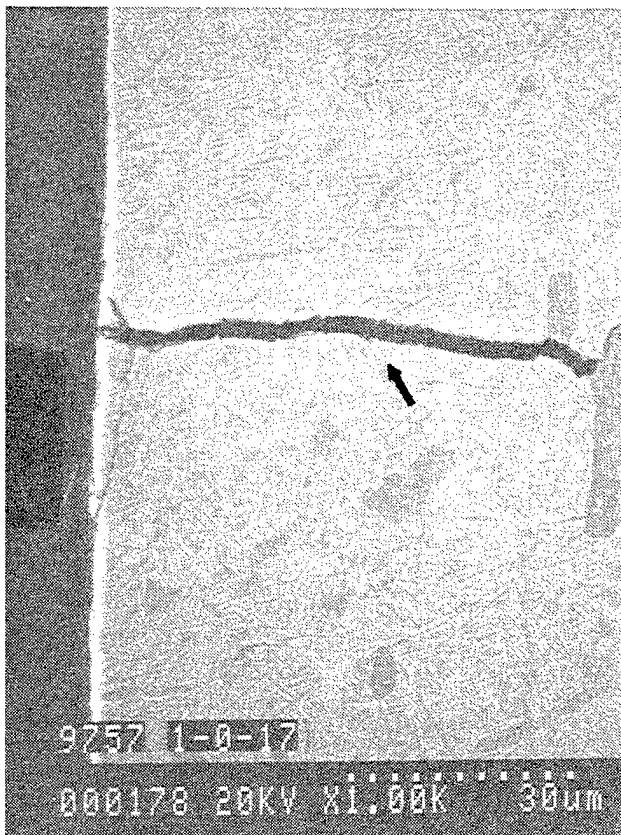


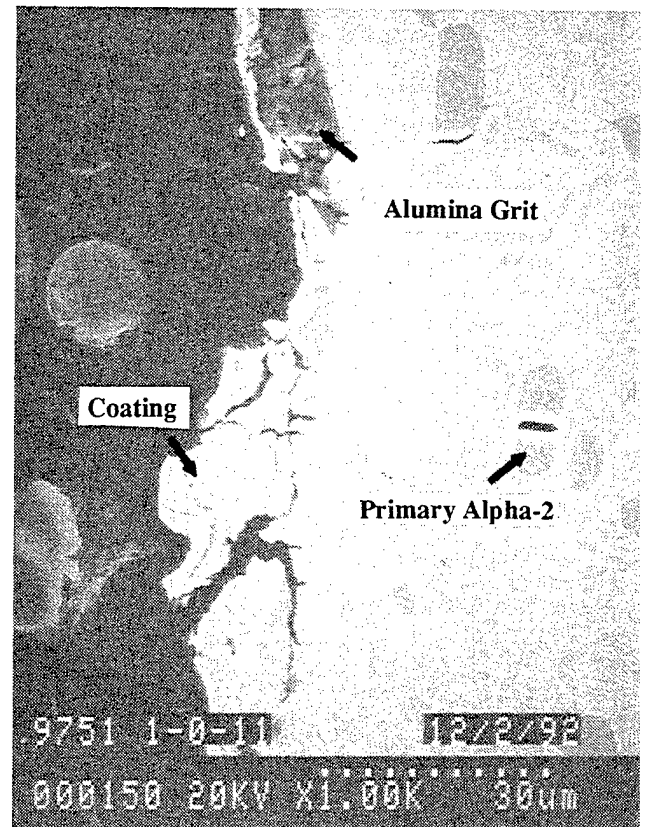
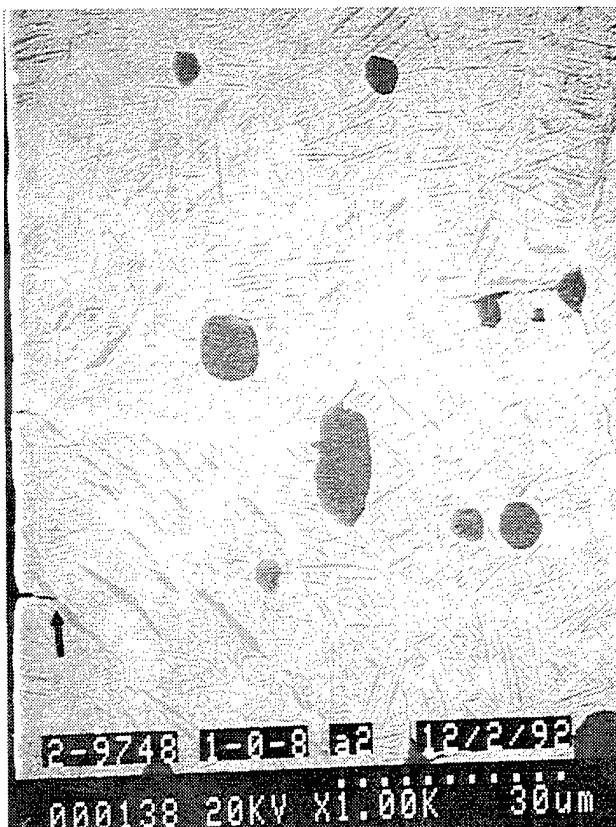
Figure 123. Low magnification cross sections of coated and uncoated alpha-2 (Ti-24.5Al-12.5Nb-1.5Mo) specimens showing a flatter fracture path and one large HSSCC crack after a salt exposure at 750°F/50ksi.

Uncoated 750°F/50ksi/100h



LPPS Modified Gamma 750°F/50ksi/43.2h

Sputtered TiCrAl 750°F/50ksi/100h



APS Alloy 718 750°F/50ksi/100h

Figure 124. Higher magnification cross sections of coated and uncoated alpha-2 (Ti-24.5Al-12.5Nb-1.5Mo) specimens showing the surfaces after a salt exposure at 750°F/50ksi.

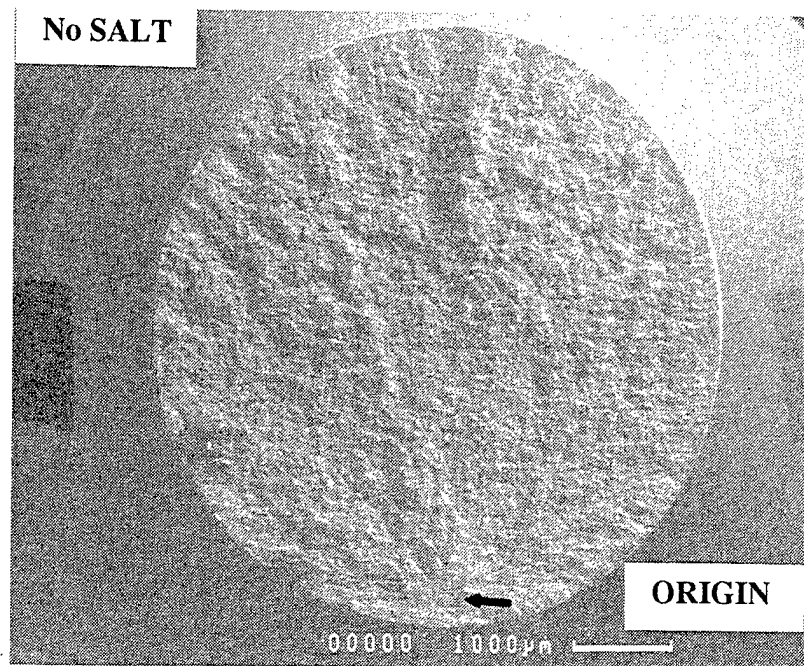
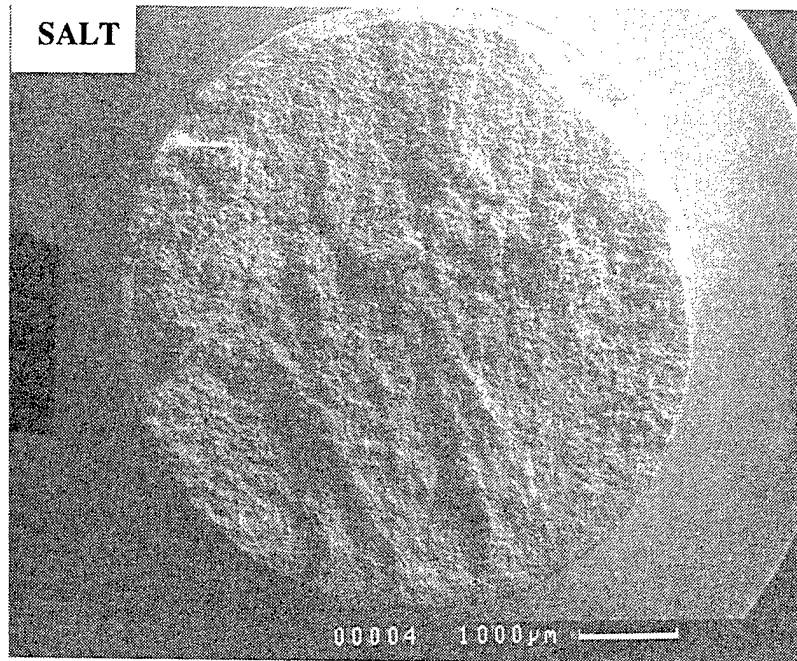


Figure 125. Low magnification fractographs of uncoated alpha-2 (Ti-24.5Al-12.5Nb-1.5Mo) specimens exposed with and without salt at 1050°F/40ksi/100h. The sample exposed with salt had multiple fracture origins.

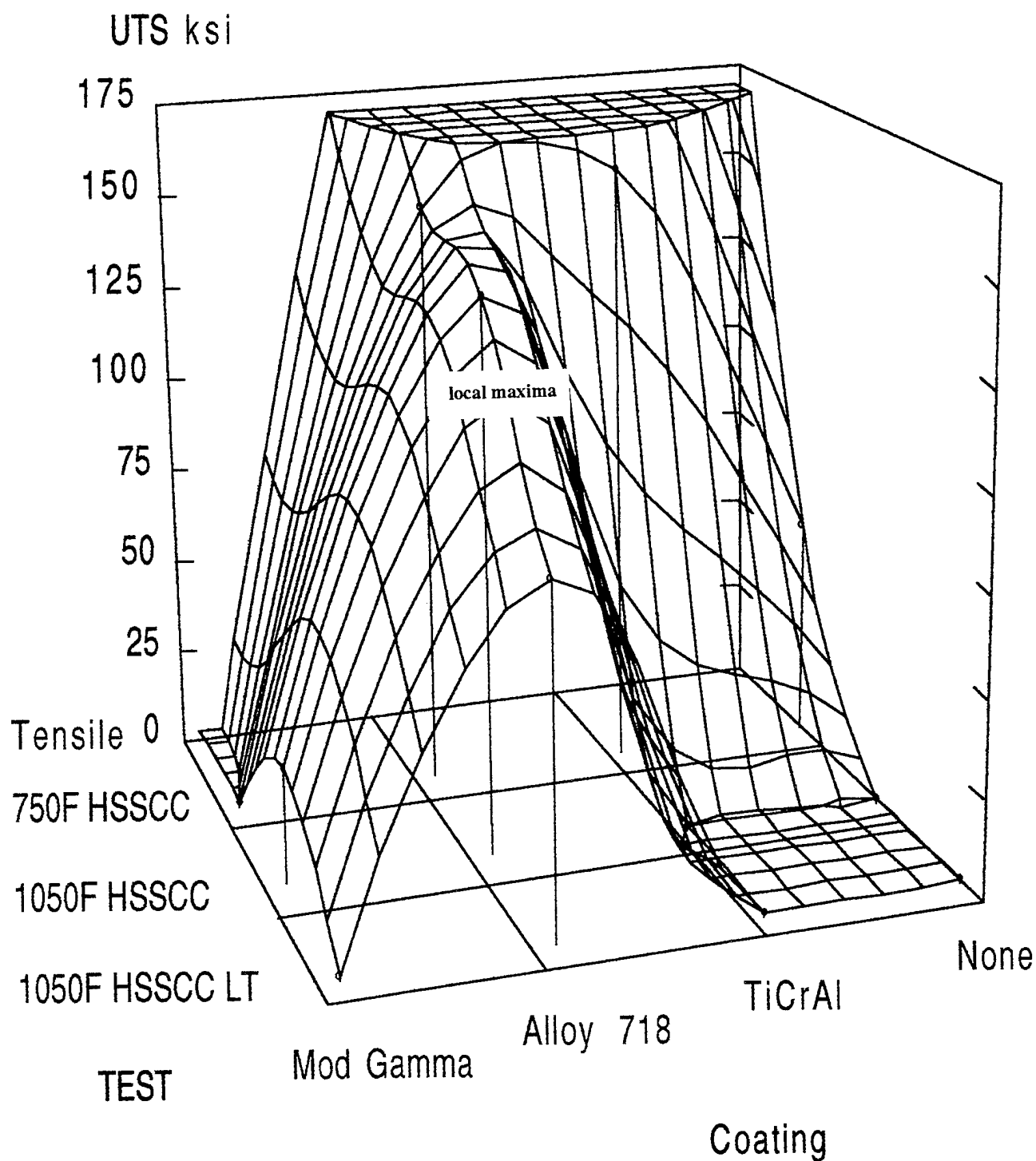
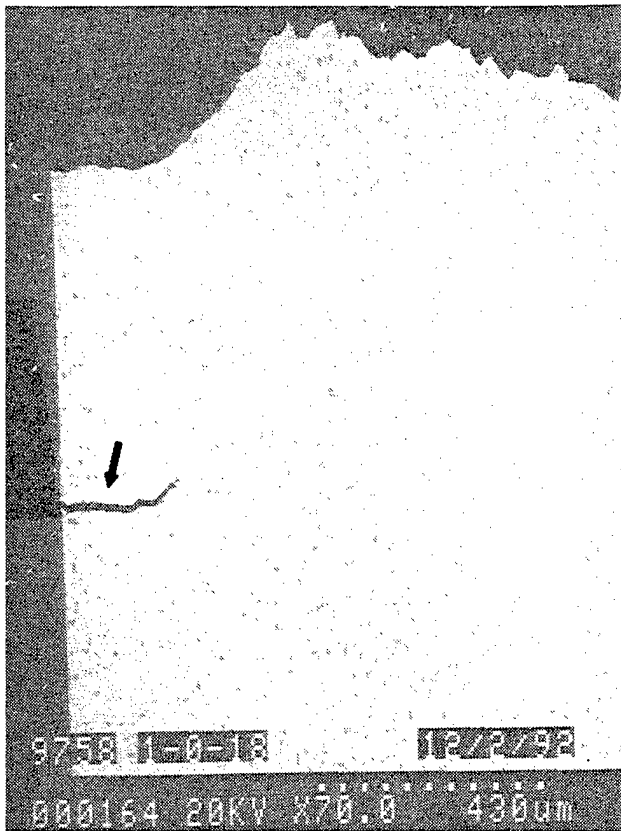
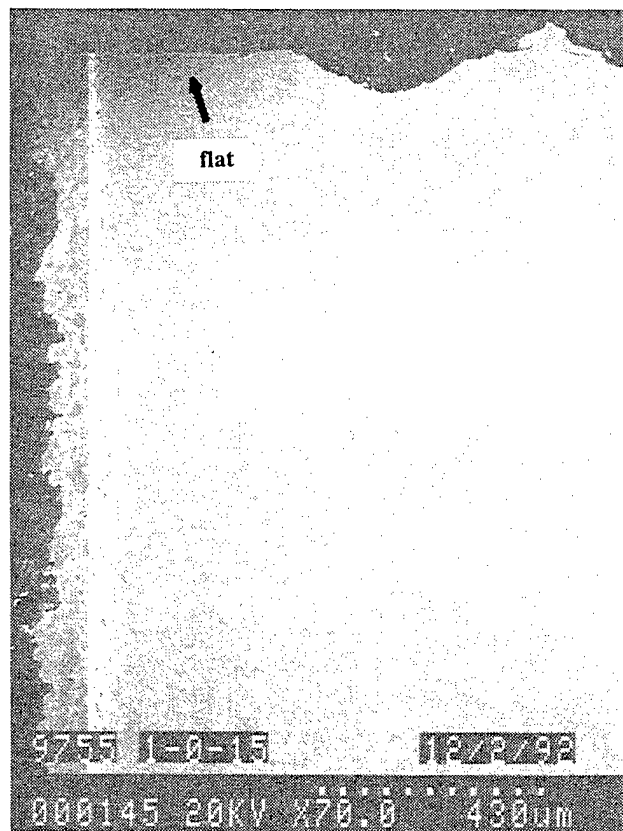


Figure 126. Plot showing the potency of the air plasma sprayed Alloy 718 as a coating for HSSCC resistance. The Alloy 718 coating achieves a local maxima on the UTS response surface of coating vs. test. "LT" means long time exposure.

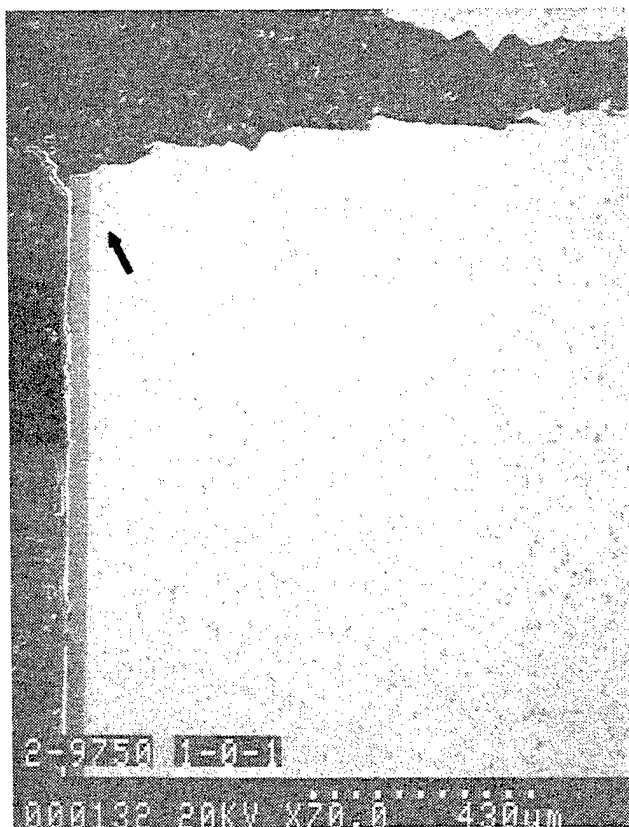
Uncoated 1050°F/40ksi/39.1h



LPPS Modified Gamma 1050°F/40ksi/10h



Sputtered TiCrAl 1050°F/40ksi/12.5h



APS Alloy 718 1050°F/40ksi/100h

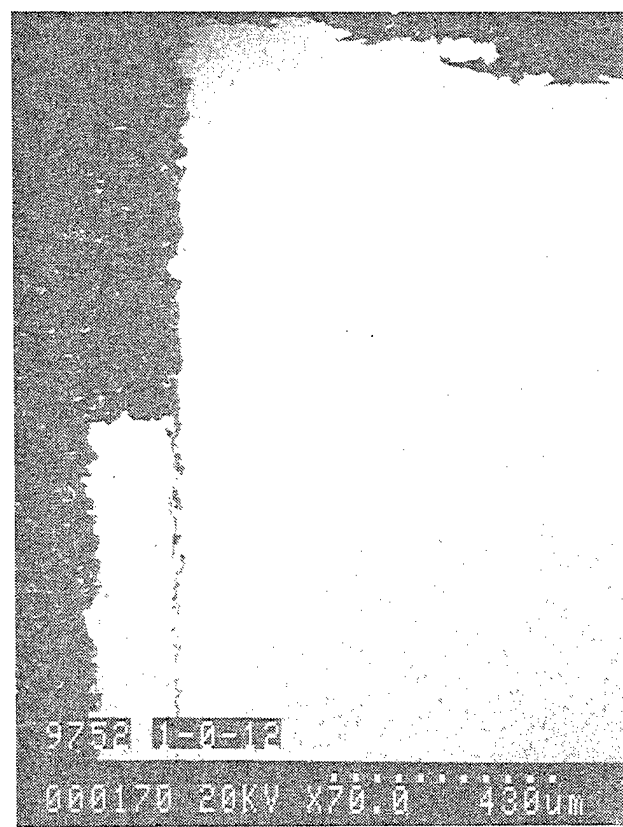
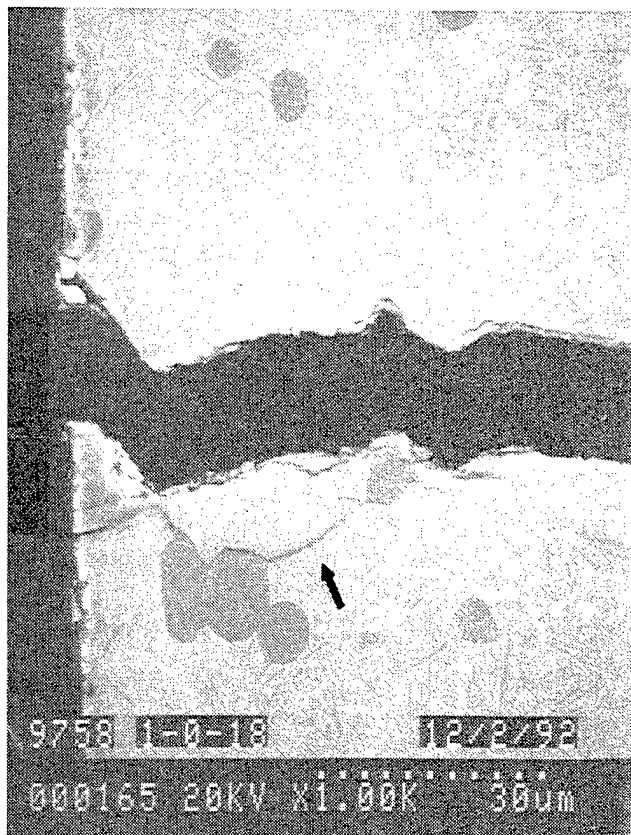


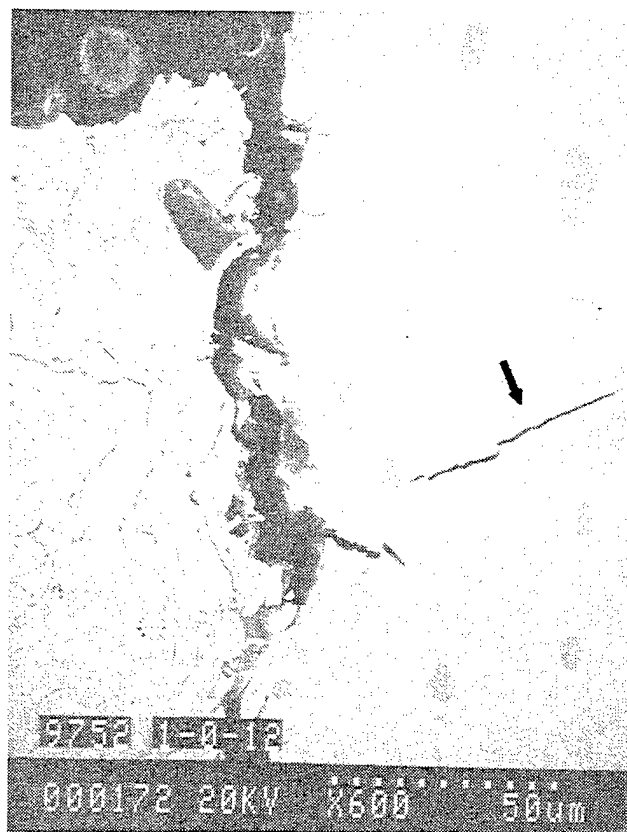
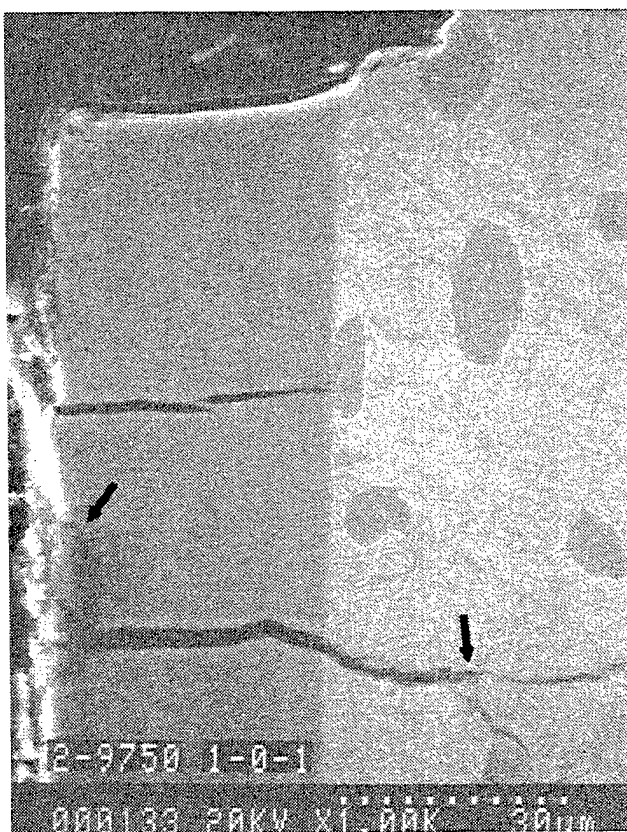
Figure 127. Low magnification cross sections of coated and uncoated alpha-2 (Ti-24.5Al-12.5Nb-1.5Mo) specimens showing a flatter fracture path and a large HSSCC crack in the bare sample after a salt exposure at 1050°F/40ksi.

Uncoated 1050°F/40ksi/39.1h



LPPS Modified Gamma 1050°F/40ksi/10h

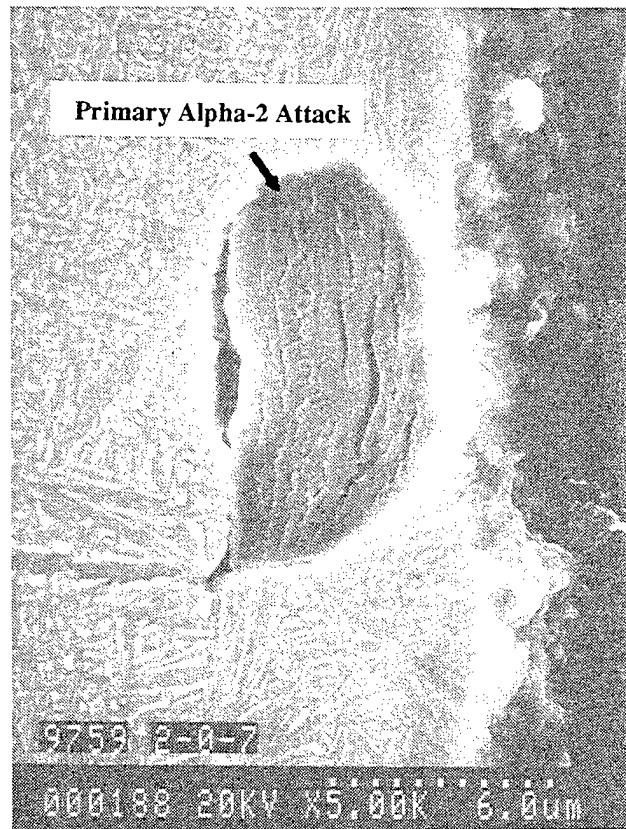
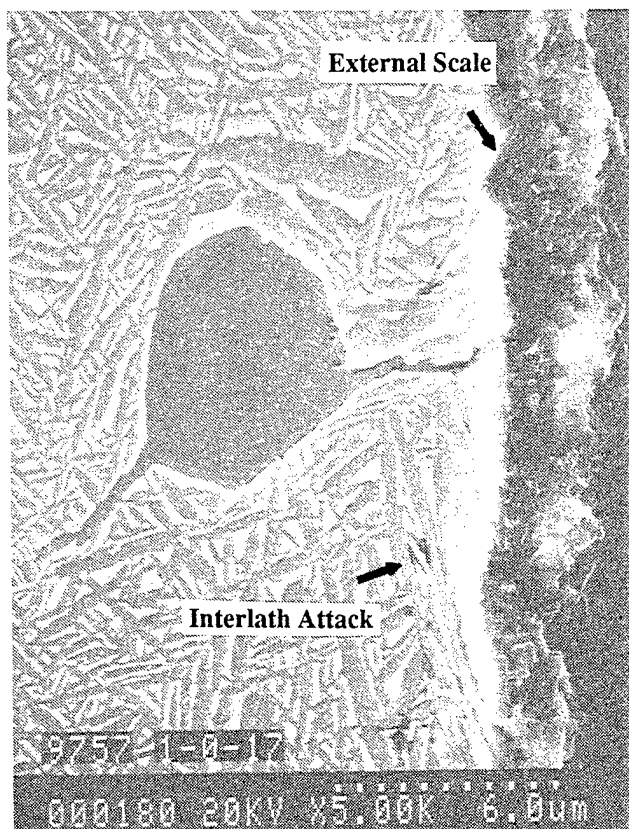
Sputtered TiCrAl 1050°F/40ksi/12.5h



APS Alloy 718 1050°F/40ksi/100h

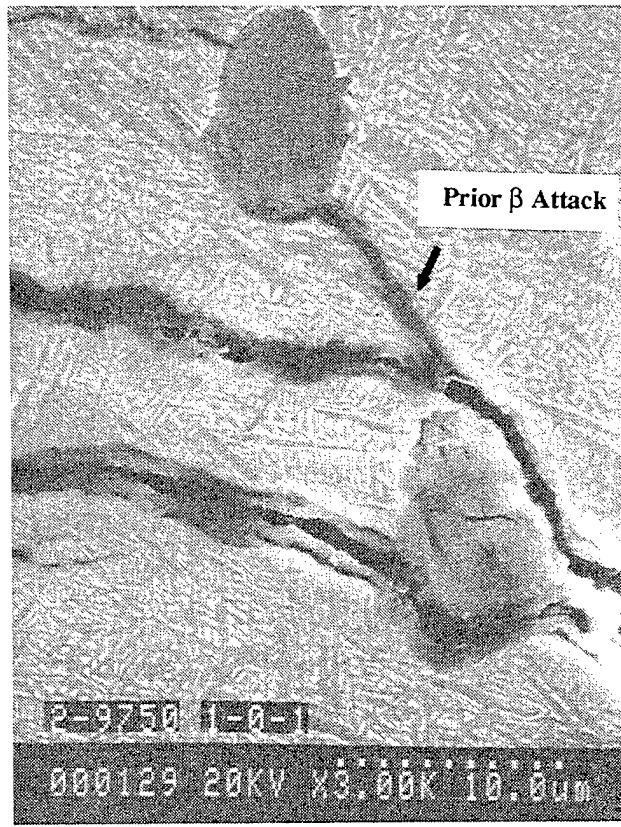
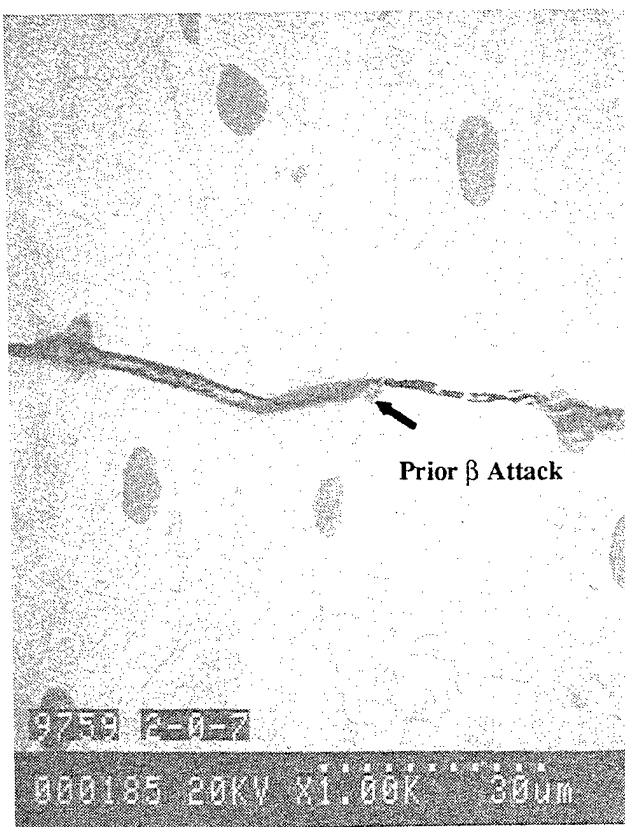
Figure 128. Higher magnification cross sections of coated and uncoated alpha-2 (Ti-24.5Al-12.5Nb-1.5Mo) specimens showing cracking at the surface after various salt exposures at 1050°F/40ksi.

Uncoated 750°F/50ksi/100h



Uncoated 1050°F/40ksi/28.5h

Uncoated 1050°F/40ksi/28.5h



Sputtered TiCrAl 1050°F/40ksi/12.5h

Figure 129. Higher magnification cross sections of alpha-2 (Ti-24.5Al-12.5Nb-1.5Mo) specimens showing attack at primary α_2 islands and prior β grain boundaries after a salt exposure at 1050°F/40ksi.

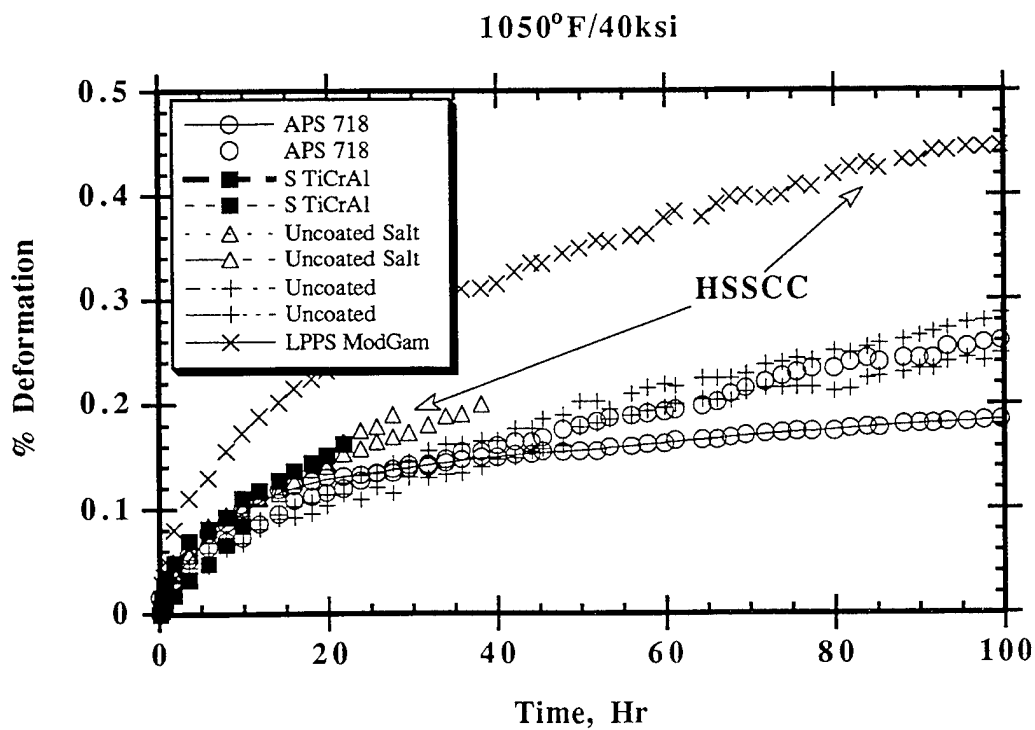
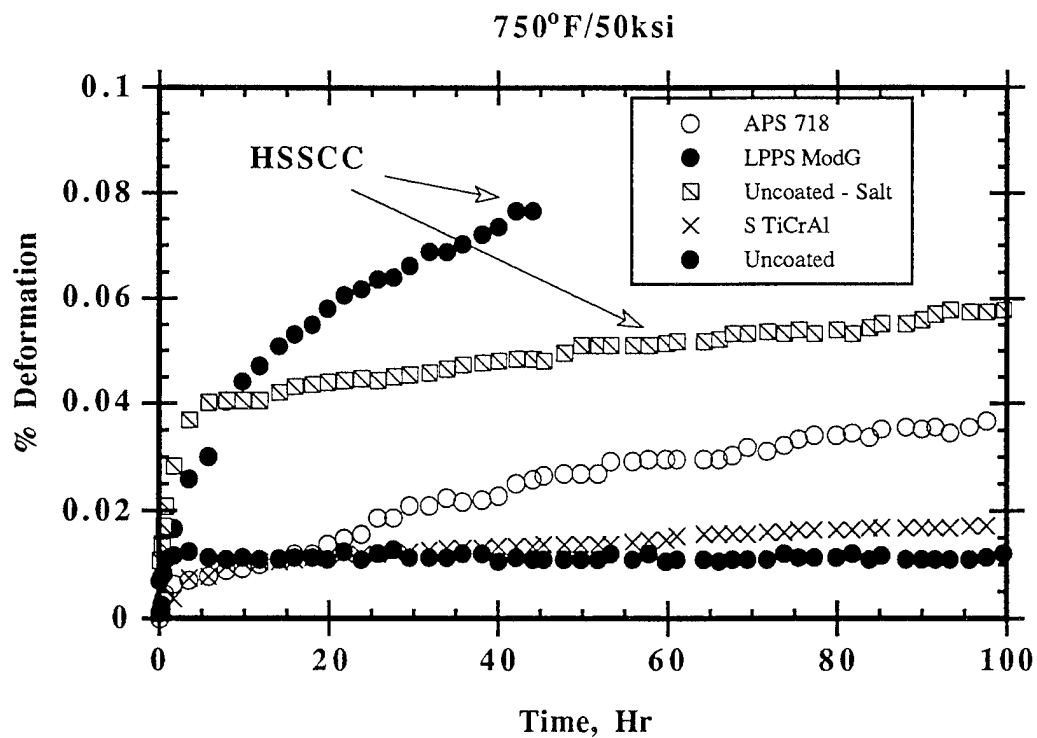


Figure 130. Creep curves for 100h exposures at 750°F/50ksi and 1050°F/40ksi of coated and uncoated alpha-2 showing greater deformation for samples undergoing HSSCC damage.

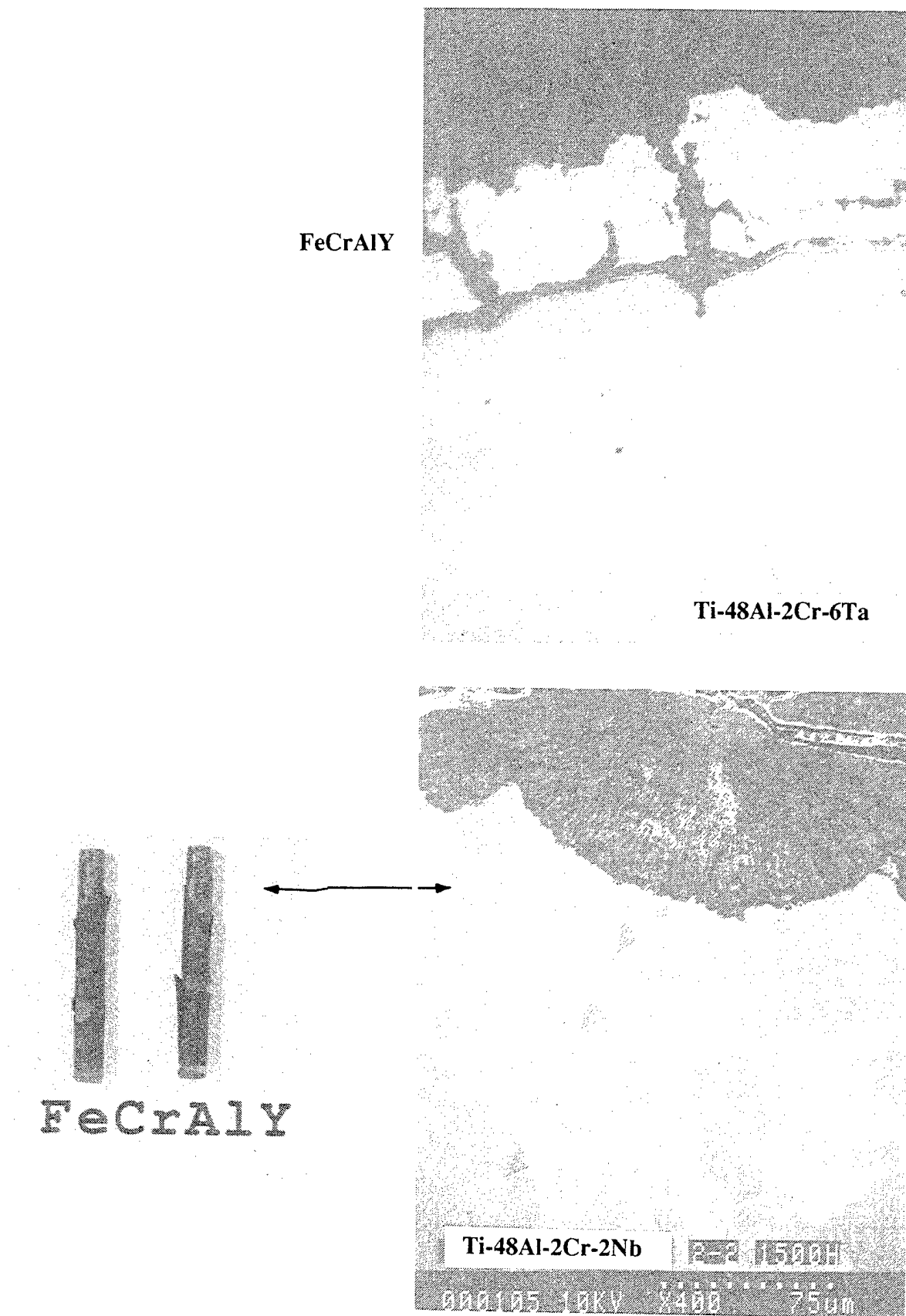


Figure 131. Micrographs of low pressure plasma sprayed FeCrAlY on cast and forged gamma alloys after 1500Hr of cyclic oxidation at 900°C (1652°F). Thermal fatigue cracks and coating spallation were observed.

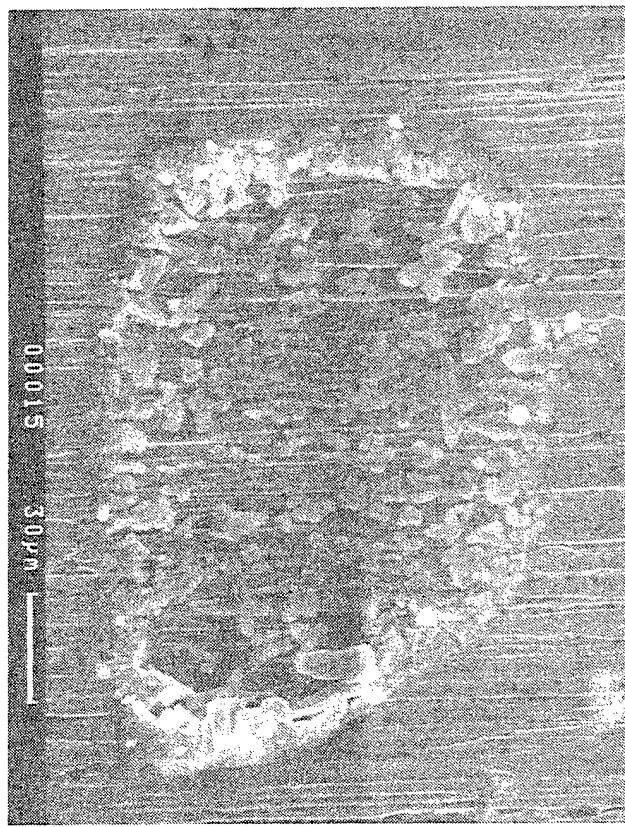
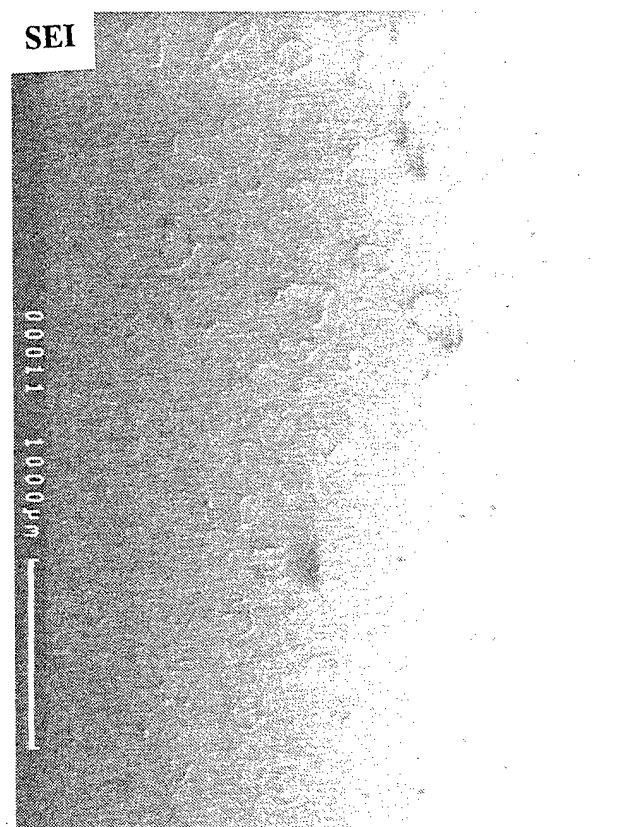
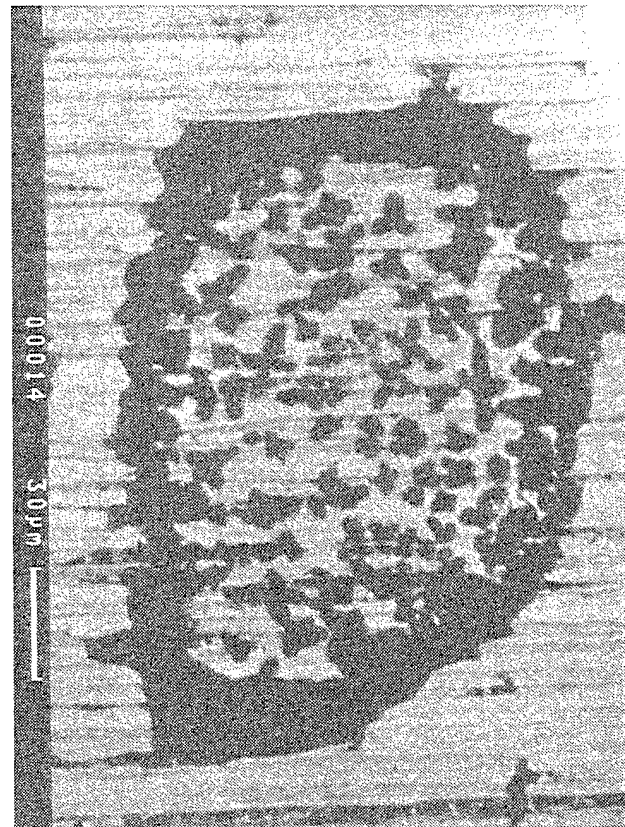
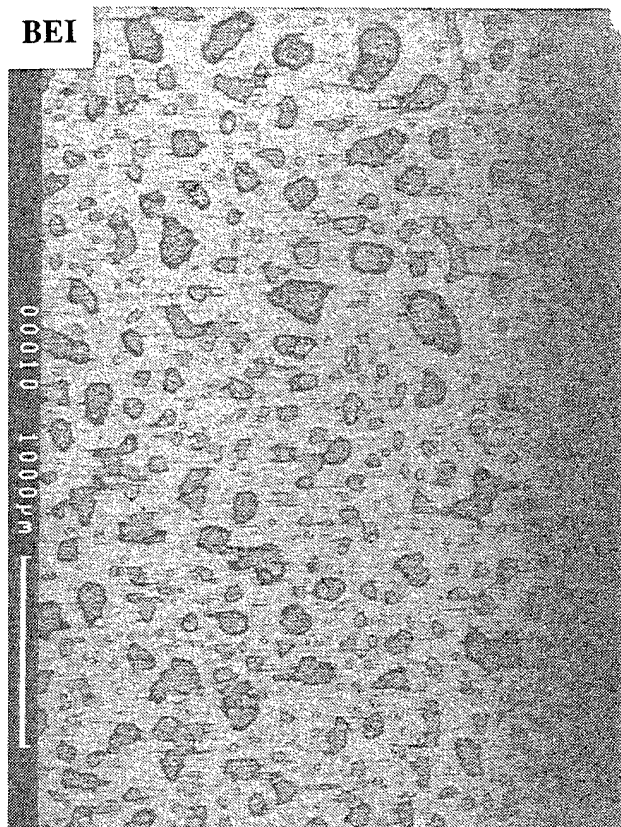


Figure 132. Backscattered and secondary micrographs showing the morphology of the sea salt after application on a steel tensile bar.

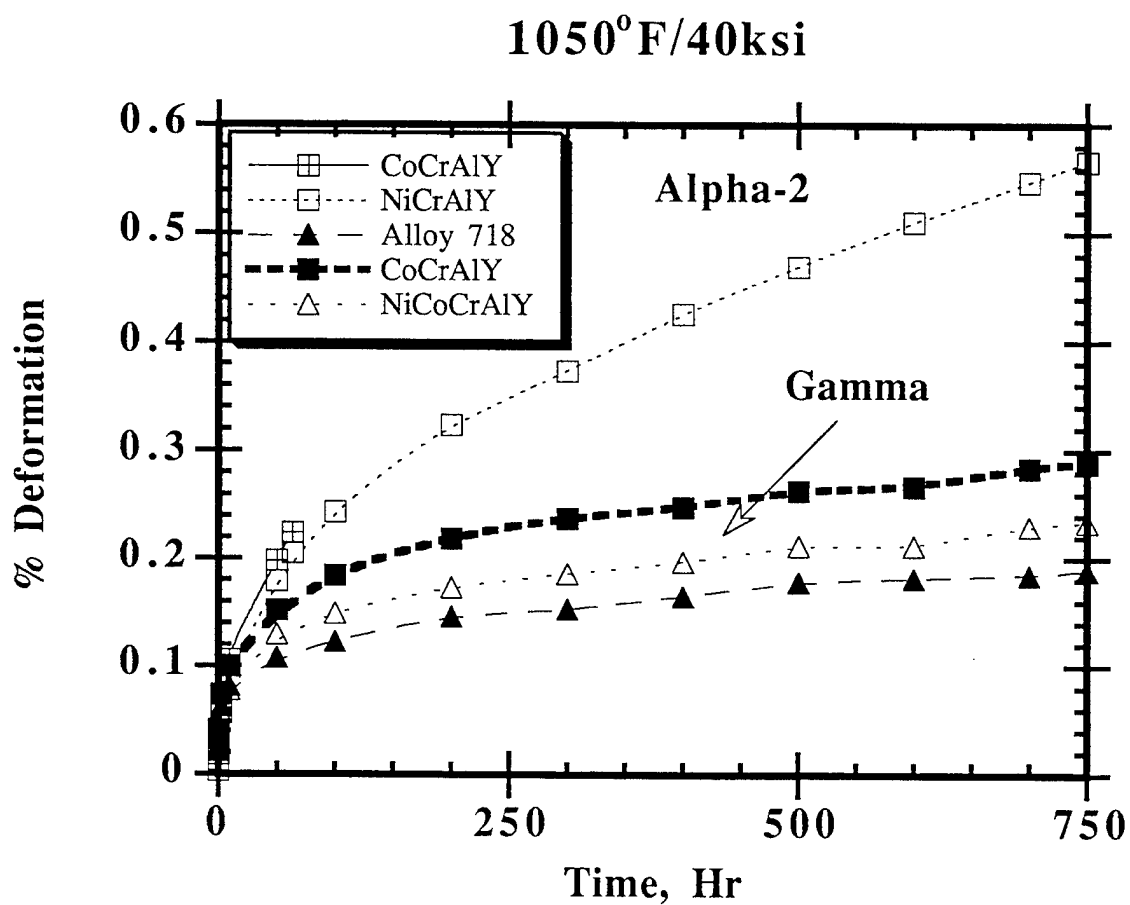


Figure 133. Curves showing the 750h creep behavior of cermet (M^3)coated gamma and alpha-2 alloys at 1050°F/40ksi. Only one of the coated alpha-2 alloys survived the exposure.

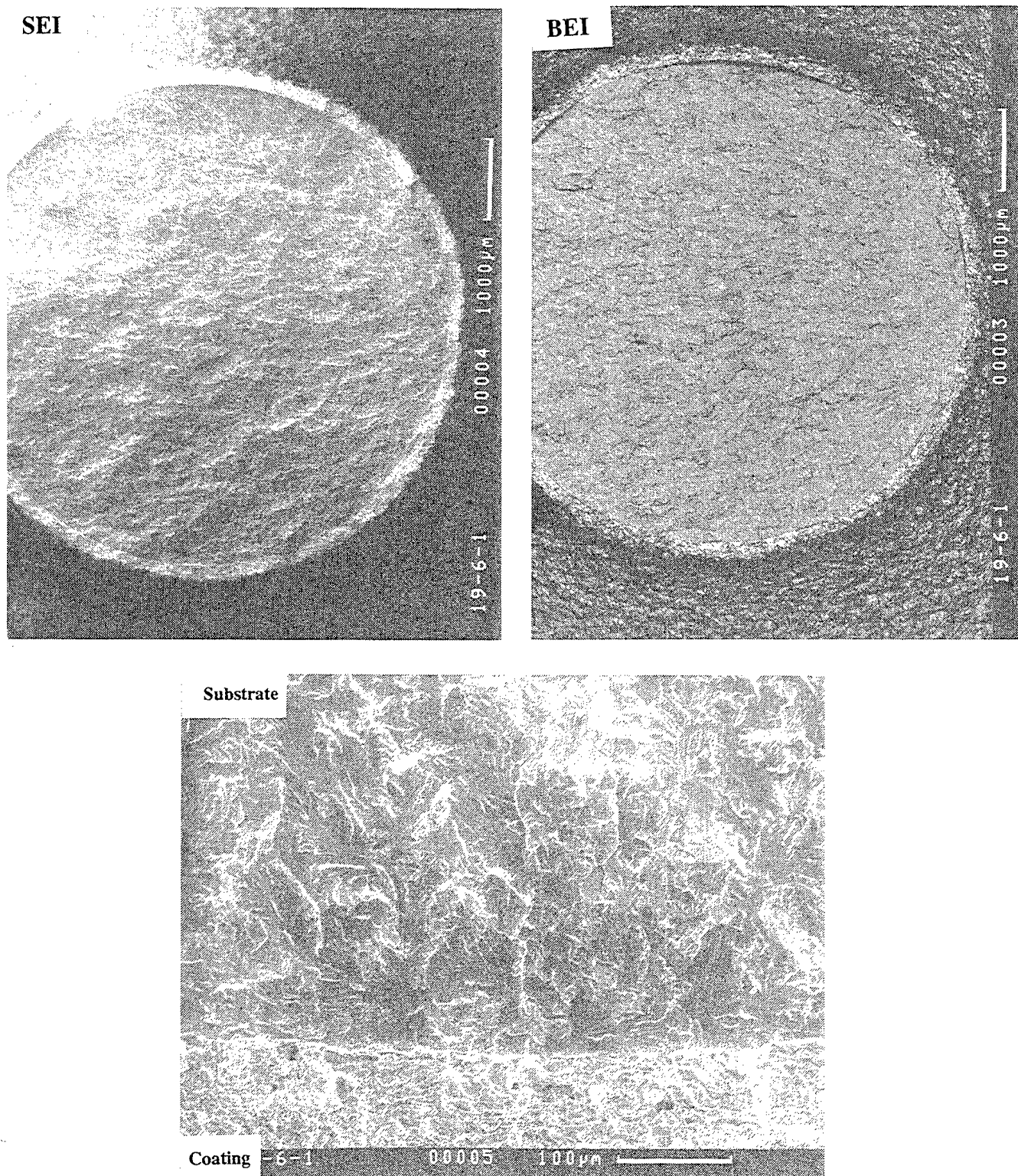


Figure 134. Micrographs showing the Alloy 718 cermet (M^3) specimen on gamma after a 750h HSSCC exposure at 1050°F/40ksi. The sample failed in the radius during the post exposure tensile test.

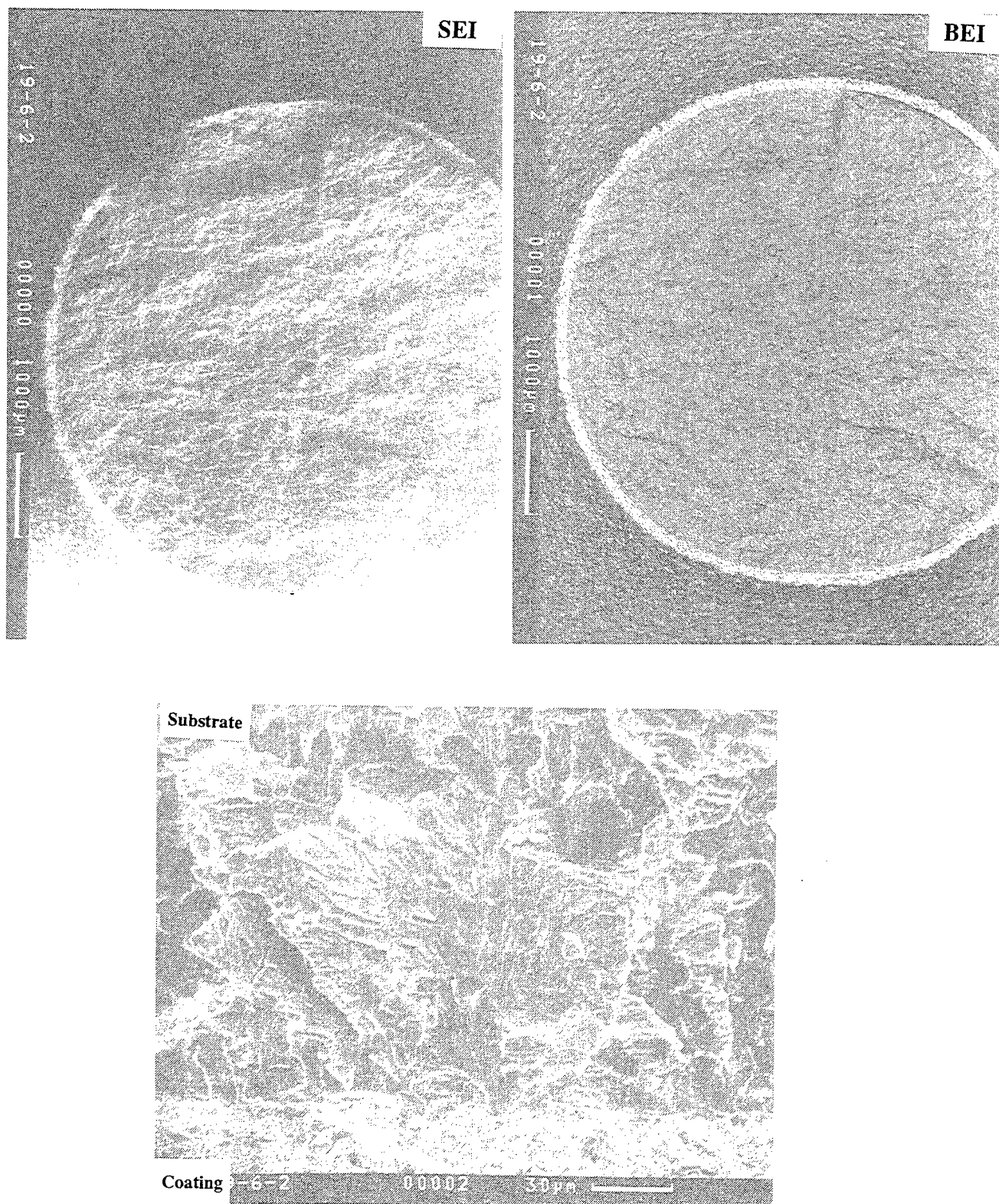


Figure 135. Micrographs showing the CoCrAlY cermet (M³) specimen on gamma after a 750h HSSCC exposure at 1050°F/40ksi. The sample failed in the radius during the post exposure tensile test.

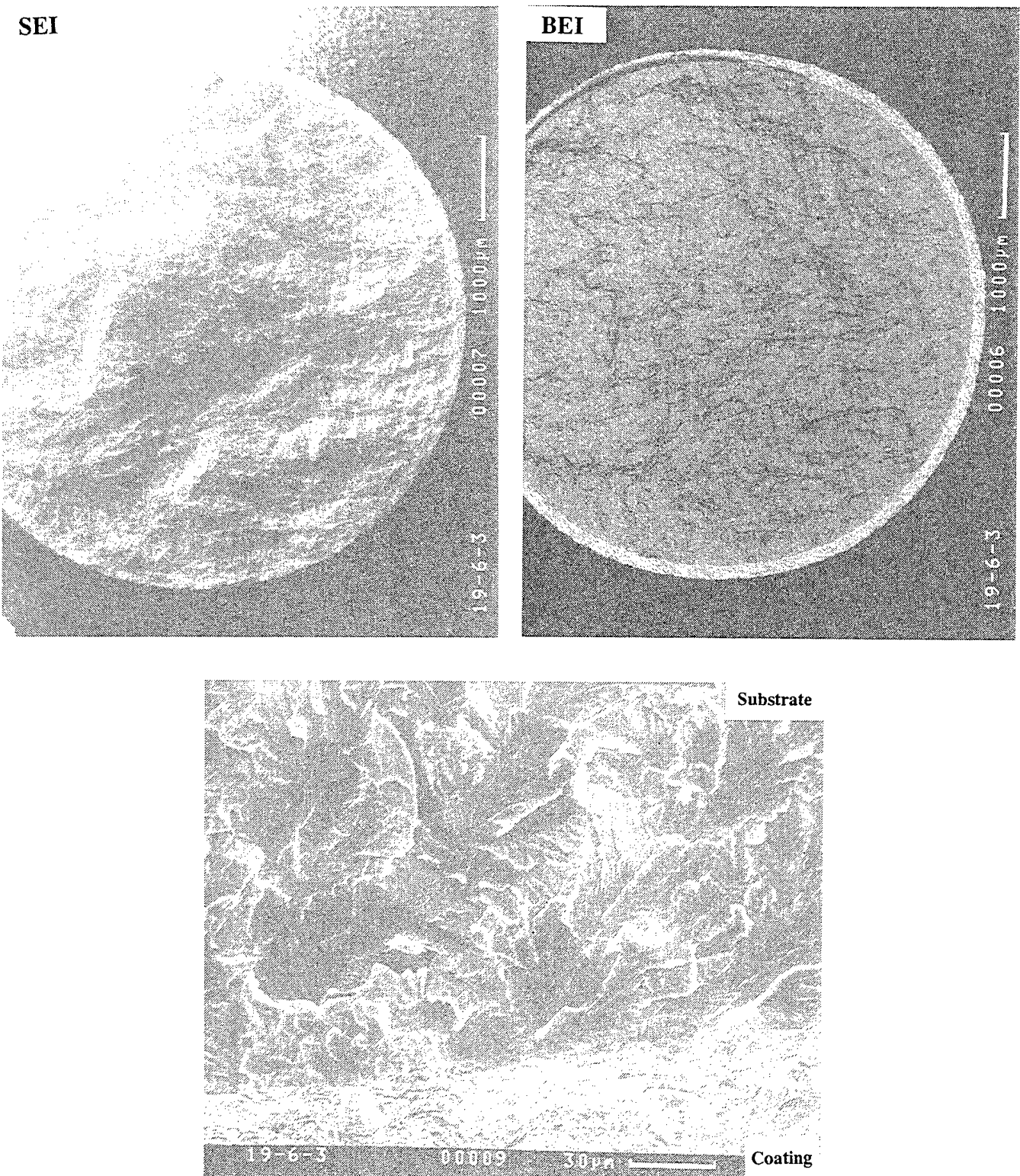


Figure 136. Micrographs showing the NiCoCrAlY cermet (M^3) specimen on gamma after a 750h HSSCC exposure at 1050°F/40ksi. The sample failed in the radius during the post exposure tensile test.

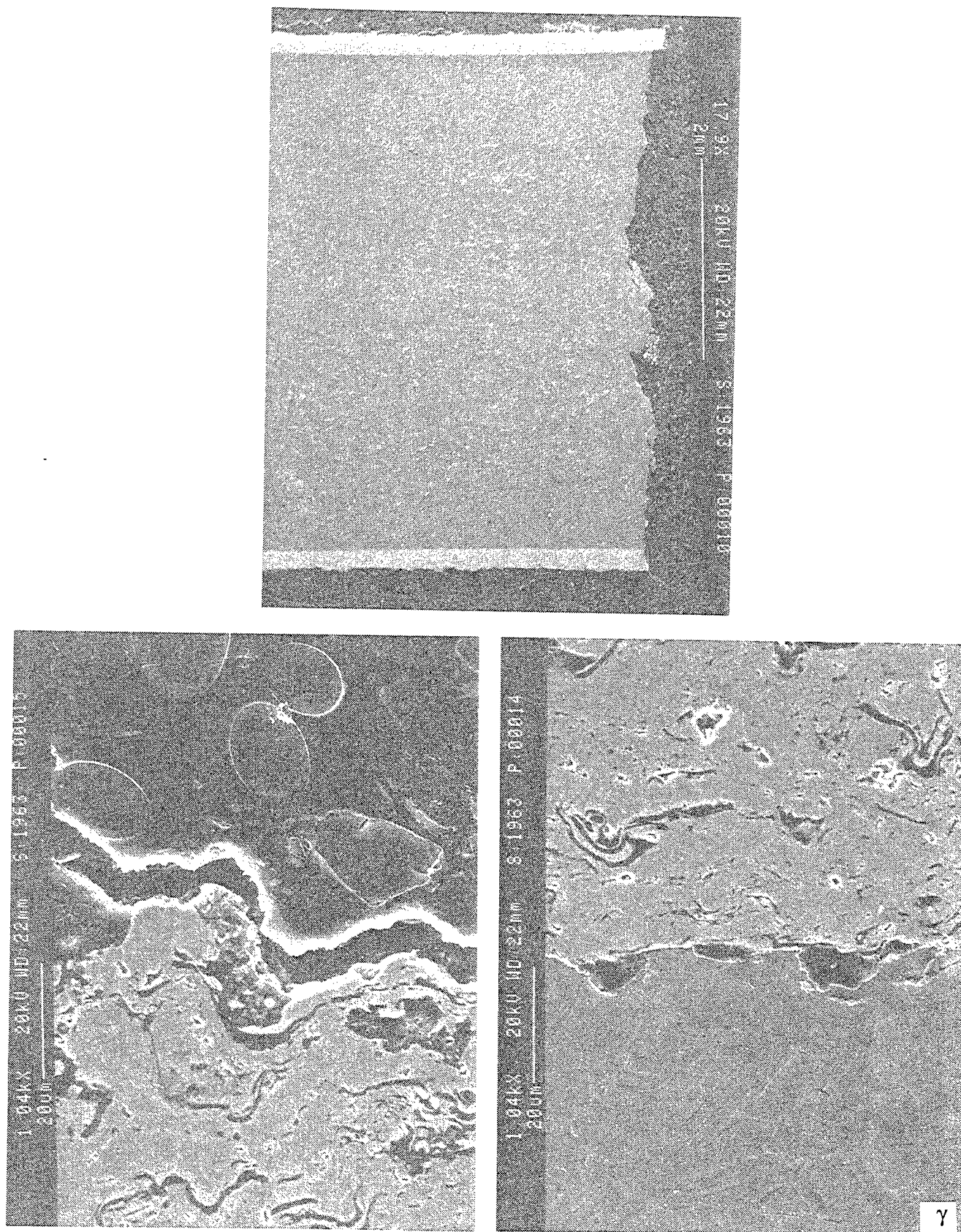


Figure 137. Micrographs showing the fractured cross section of the NiCoCrAlY composite coating on the gamma Ti-48Al-2Cr-2Nb alloy after a 1050°F/40ksi exposure with salt followed by a room temperature tensile test. The coating was adherent.

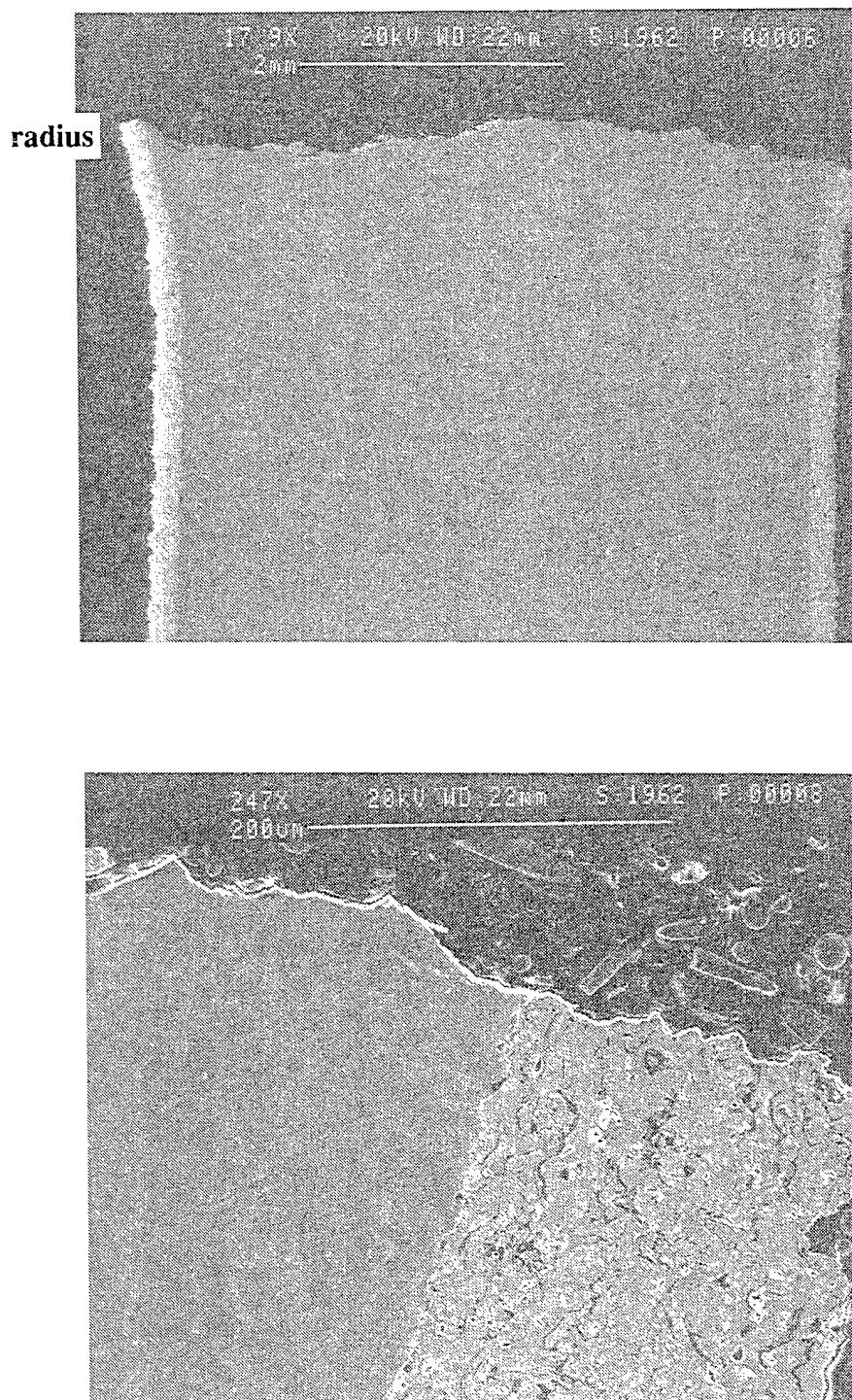


Figure 138. Micrographs showing the fractured cross section of the CoCrAlY composite coating on the gamma Ti-48Al-2Cr-2Nb alloy after a 1050°F/40ksi exposure with salt followed by a room temperature tensile test. The coating was adherent.

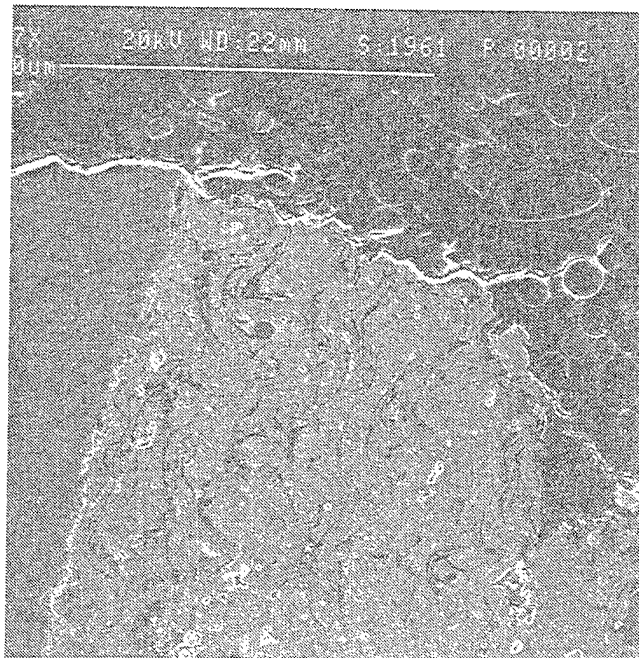
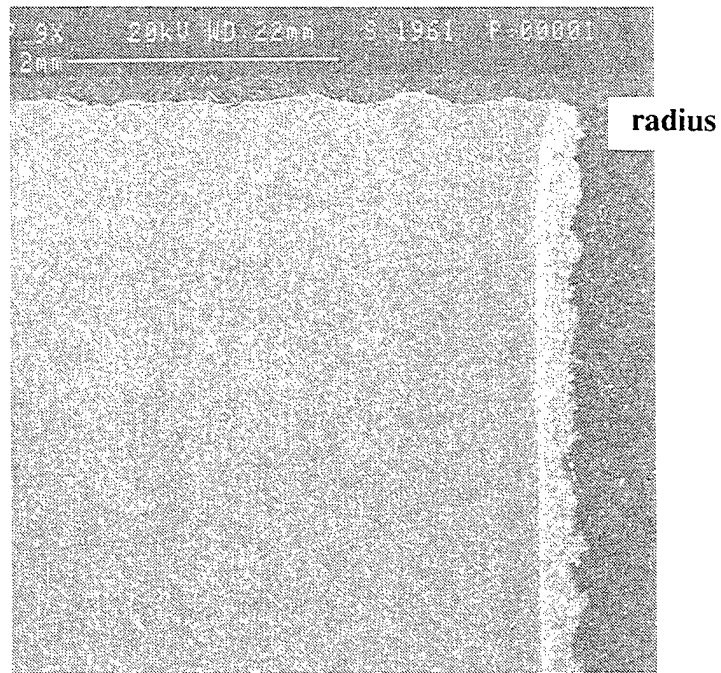
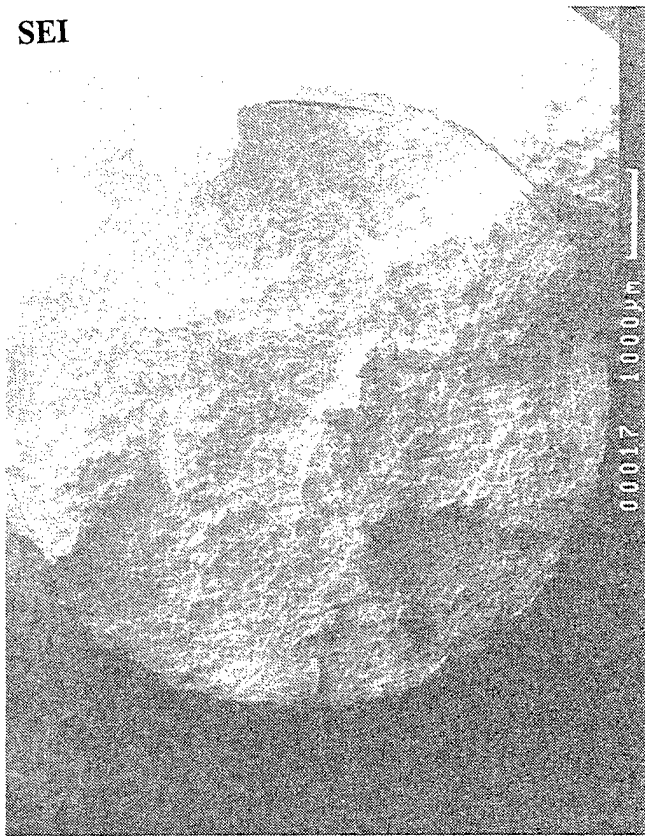


Figure 139. Micrographs showing the fractured cross section of the Alloy 718 cermet (M^3) coating on the gamma Ti-48Al-2Cr-2Nb alloy after a 1050°F/40ksi exposure with salt followed by a room temperature tensile test. The coating was adherent.

SEI



BEI

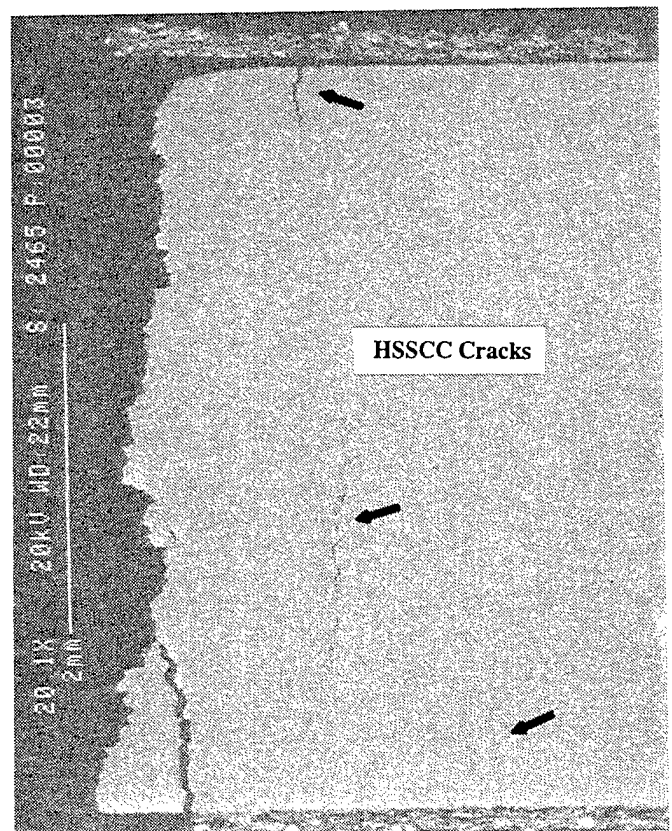
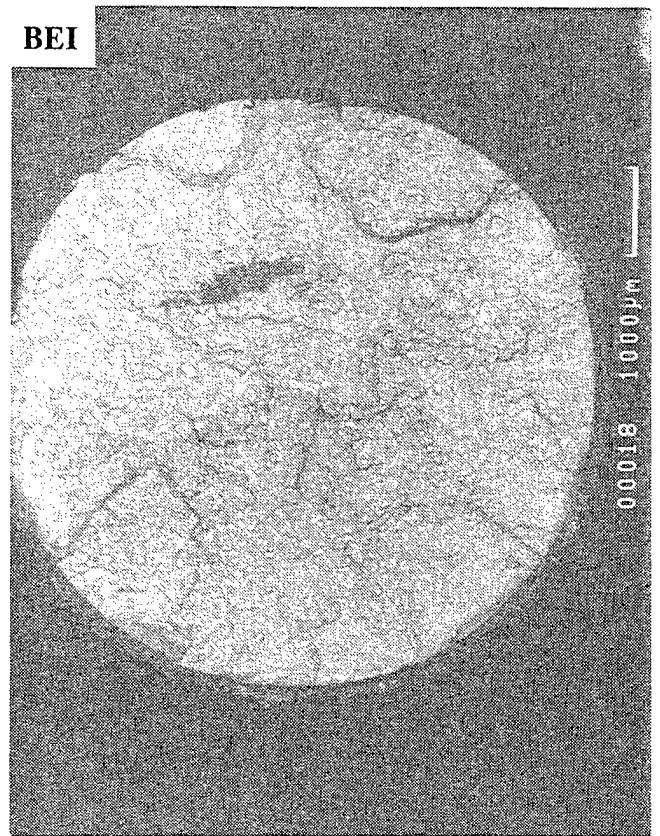


Figure 140. Micrographs of the Alloy 718 cermet (M^3)/alpha-2 specimen after 1.1h of HSSCC exposure. Large HSSCC cracks are observed throughout the cross section. The intergranular nature of the fracture cannot be overlooked.

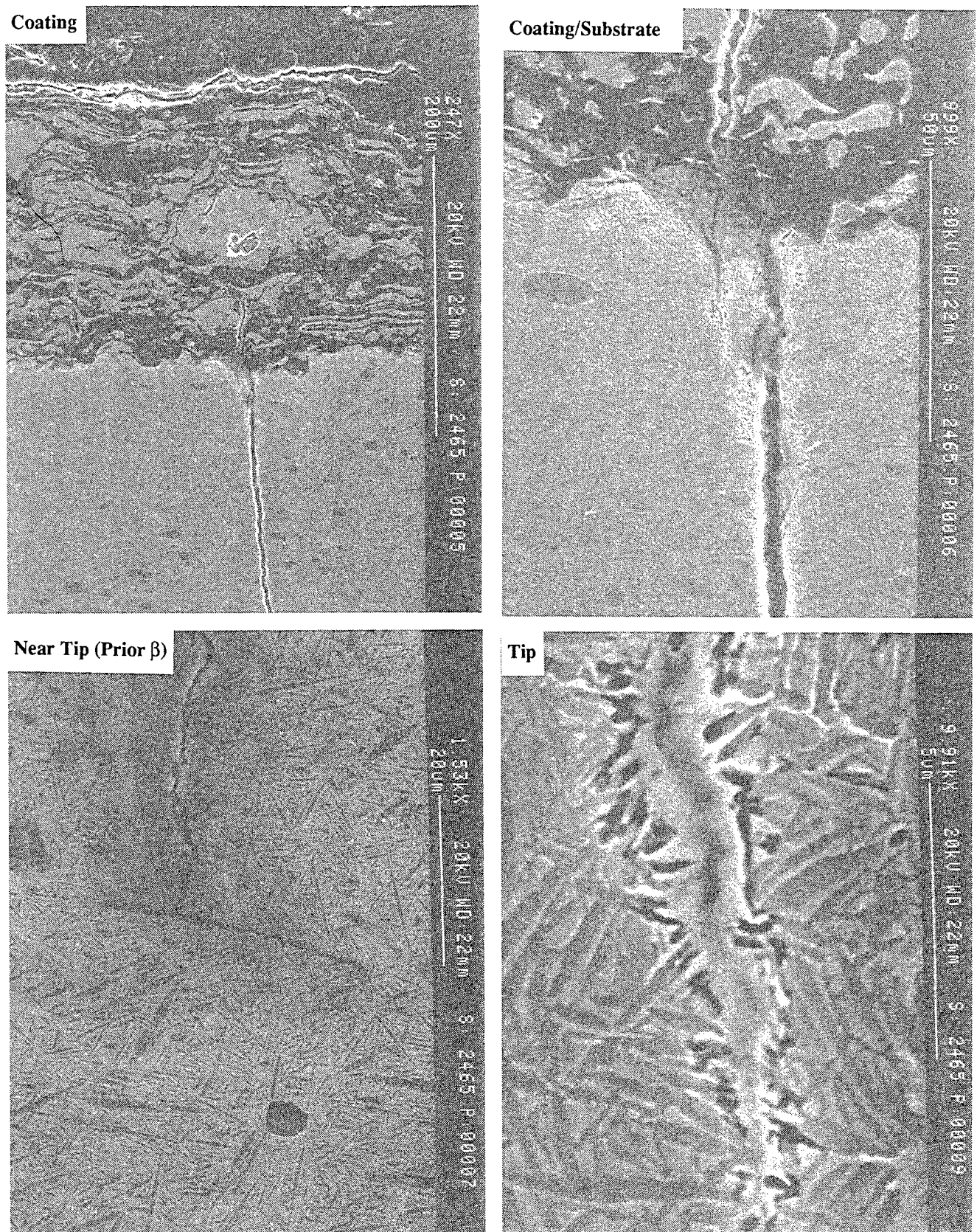


Figure 141. Micrographs of the Alloy 718 cermet (M³)/alpha-2 specimen after 1.1h of HSSCC exposure showing the morphology of the crack in the coating, at the coating/substrate interface and at the crack tip in the substrate. The crack tends to propagate down prior β grain boundaries.

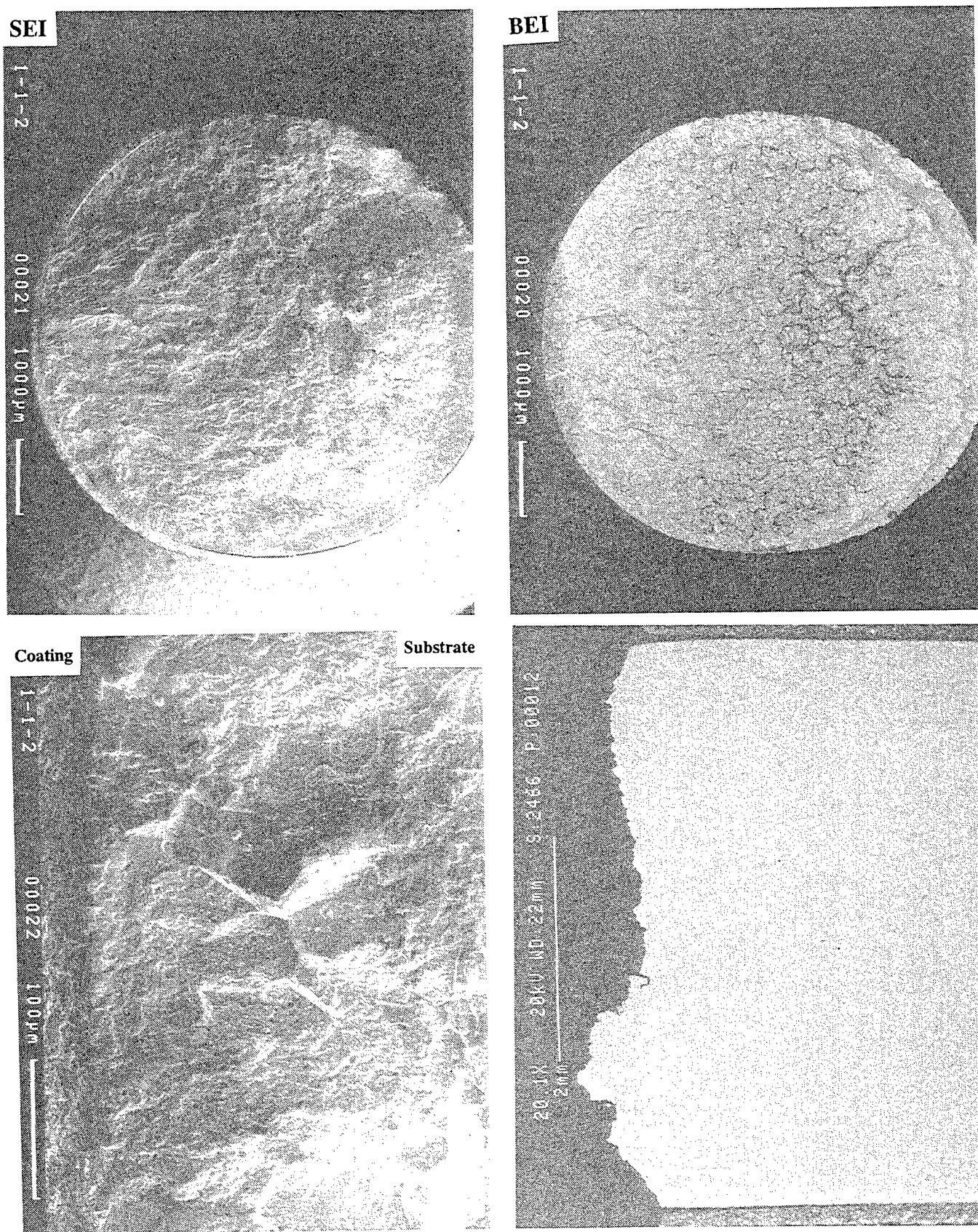


Figure 142. Micrographs showing the fracture surface of the CoCrAlY cermet (M^3)/alpha-2 coating after 62h of HSSCC exposure. The sample had a large origin that was associated with Cl.

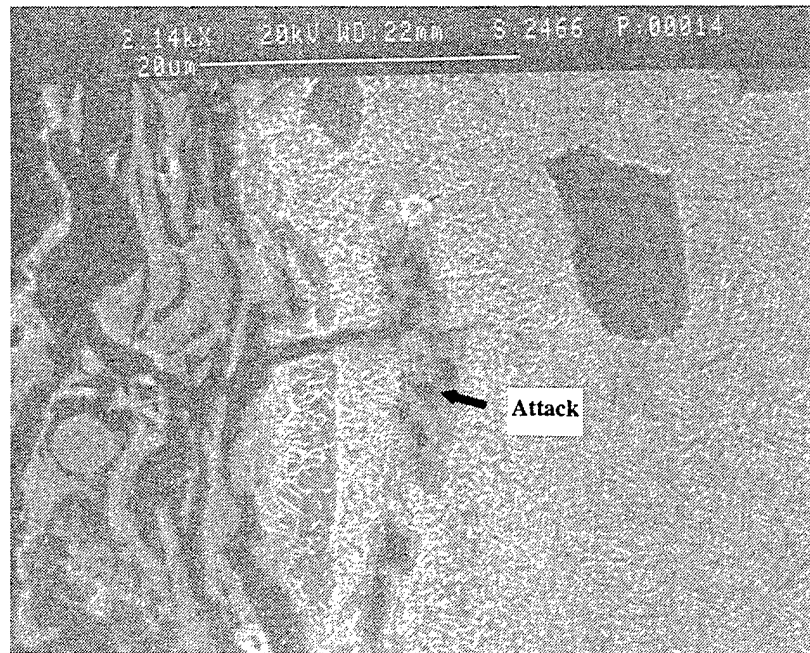
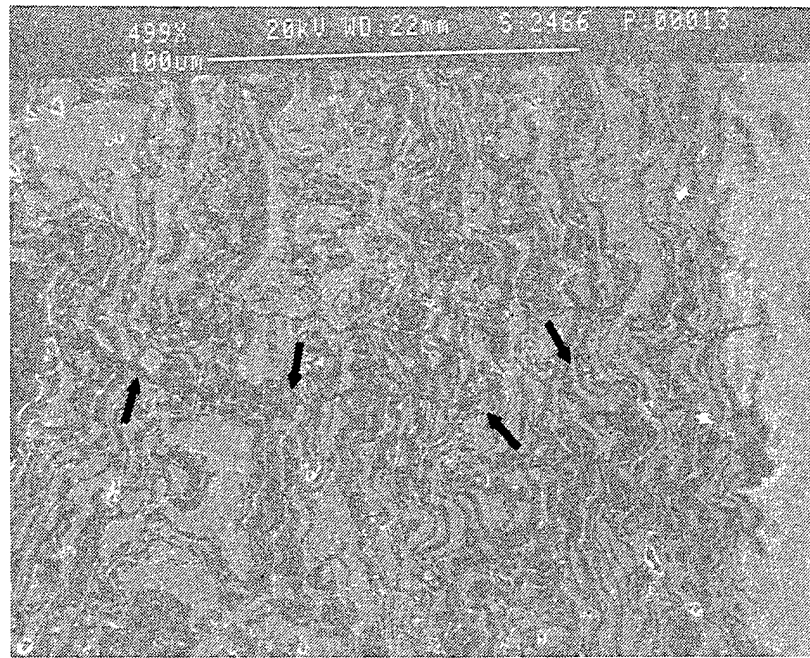


Figure 143. Micrographs of the CoCrAlY cermet (M^3)/ α -2 specimen after 62h of HSSCC exposure at 1050°F/40ksi. Cracks are observed to penetrate in regions of the coating where alumina is concentrated. Internal attack is noted in the substrate (arrow).

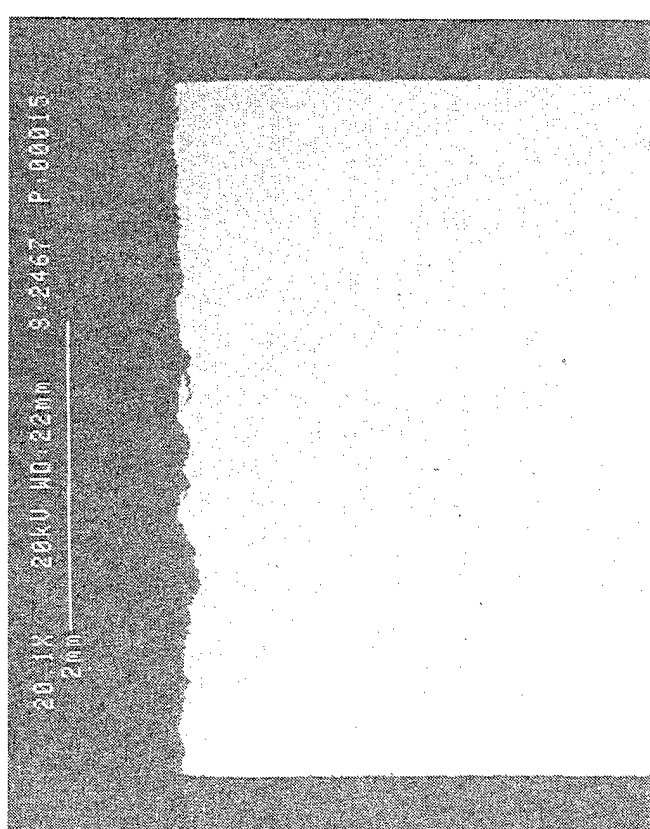
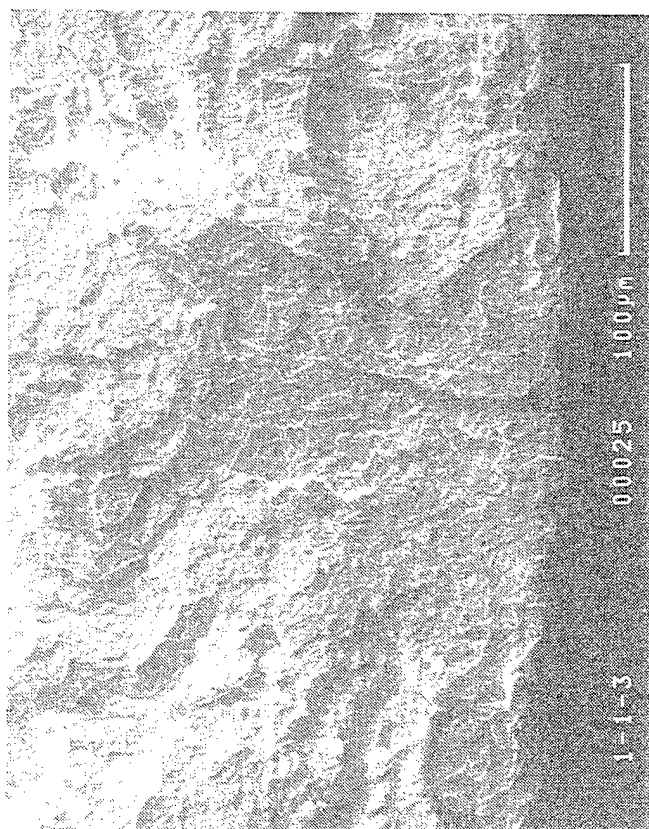
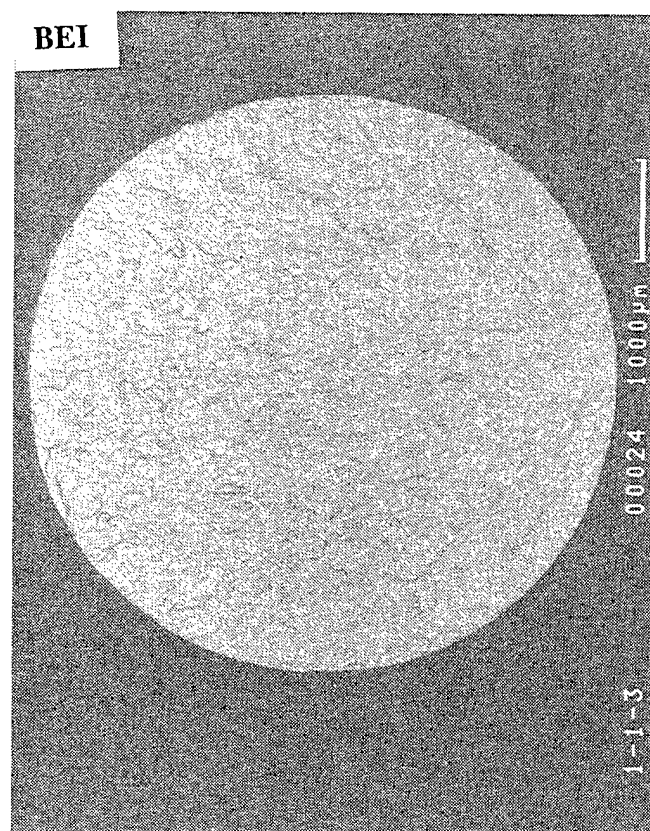
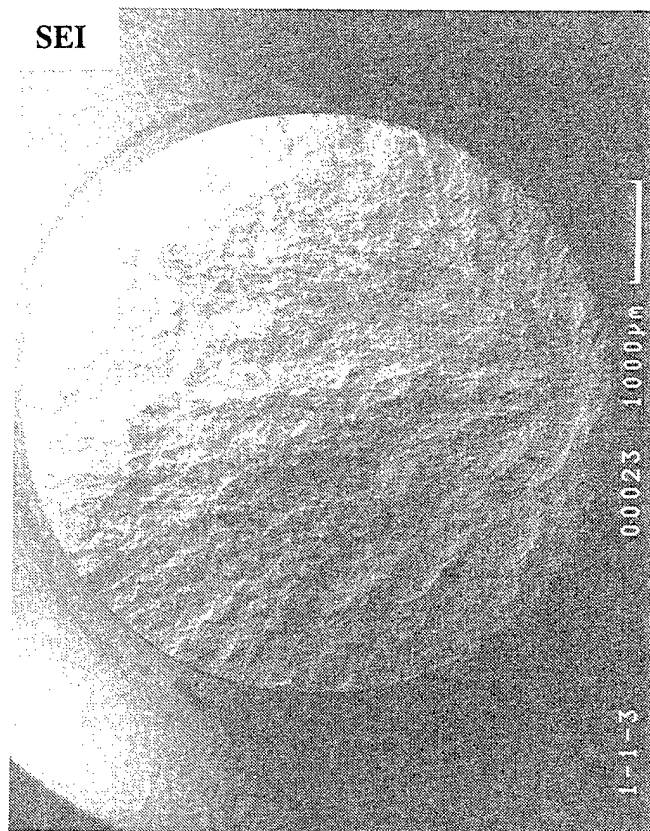


Figure 144. Micrographs showing the NiCrAlY cermet (M^3) specimen on alpha-2 after a 750h HSSCC exposure at 1050°F/40ksi. No HSSCC attack was observed in the substrate.

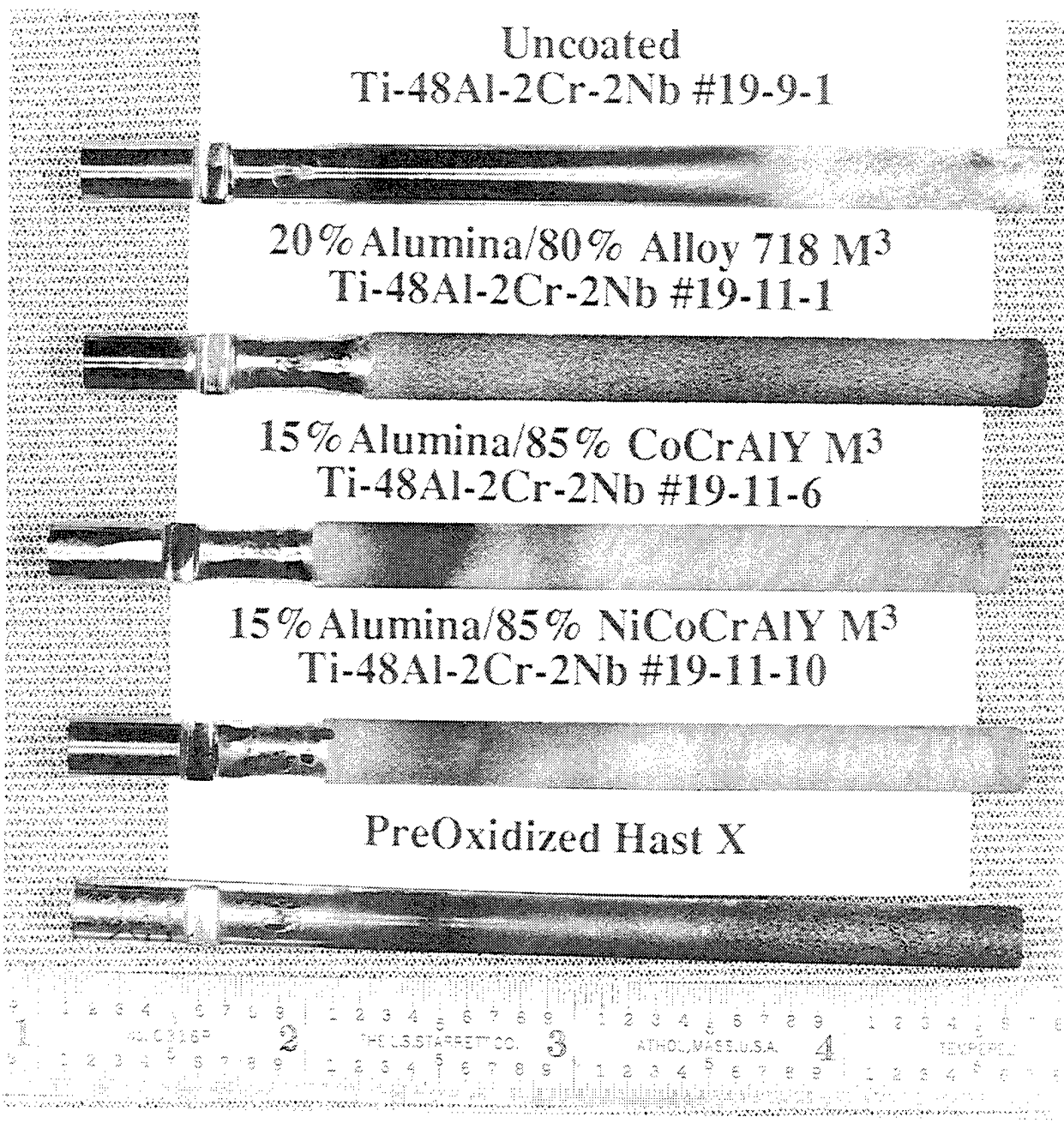


Figure 145. Color photographs showing the flame-side of coated and uncoated Ti-48Al-2Cr-2Nb gamma after 3749 cycles (625 hr) of burner rig testing using a 760°C/648°C cycle with 1ppm sea salt.

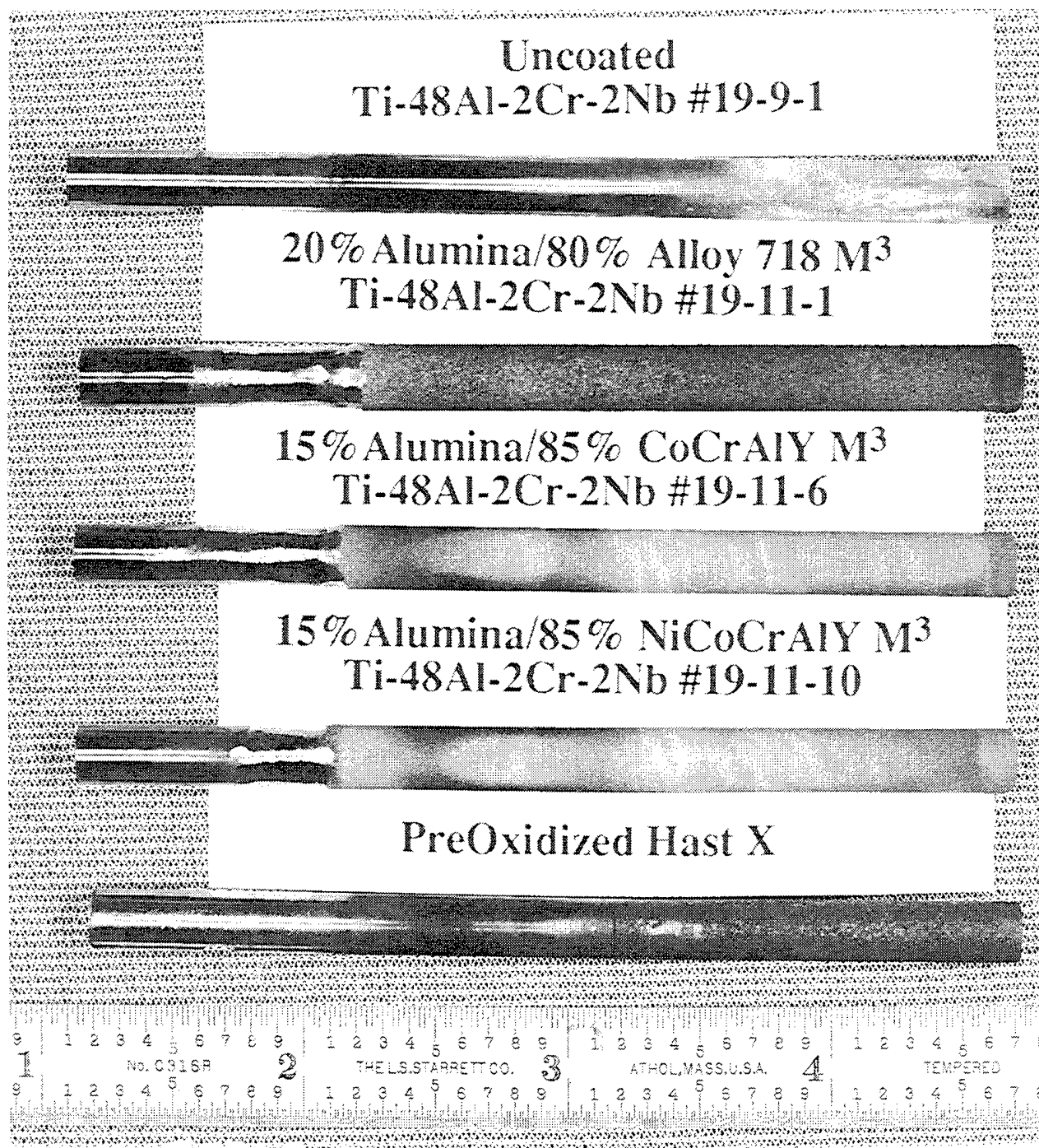


Figure 146. Color photographs showing the back-side of coated and uncoated Ti-48Al-2Cr-2Nb gamma after 3749 cycles (625 hr) of burner rig testing using a 760°C/648°C cycle with 1ppm sea salt.

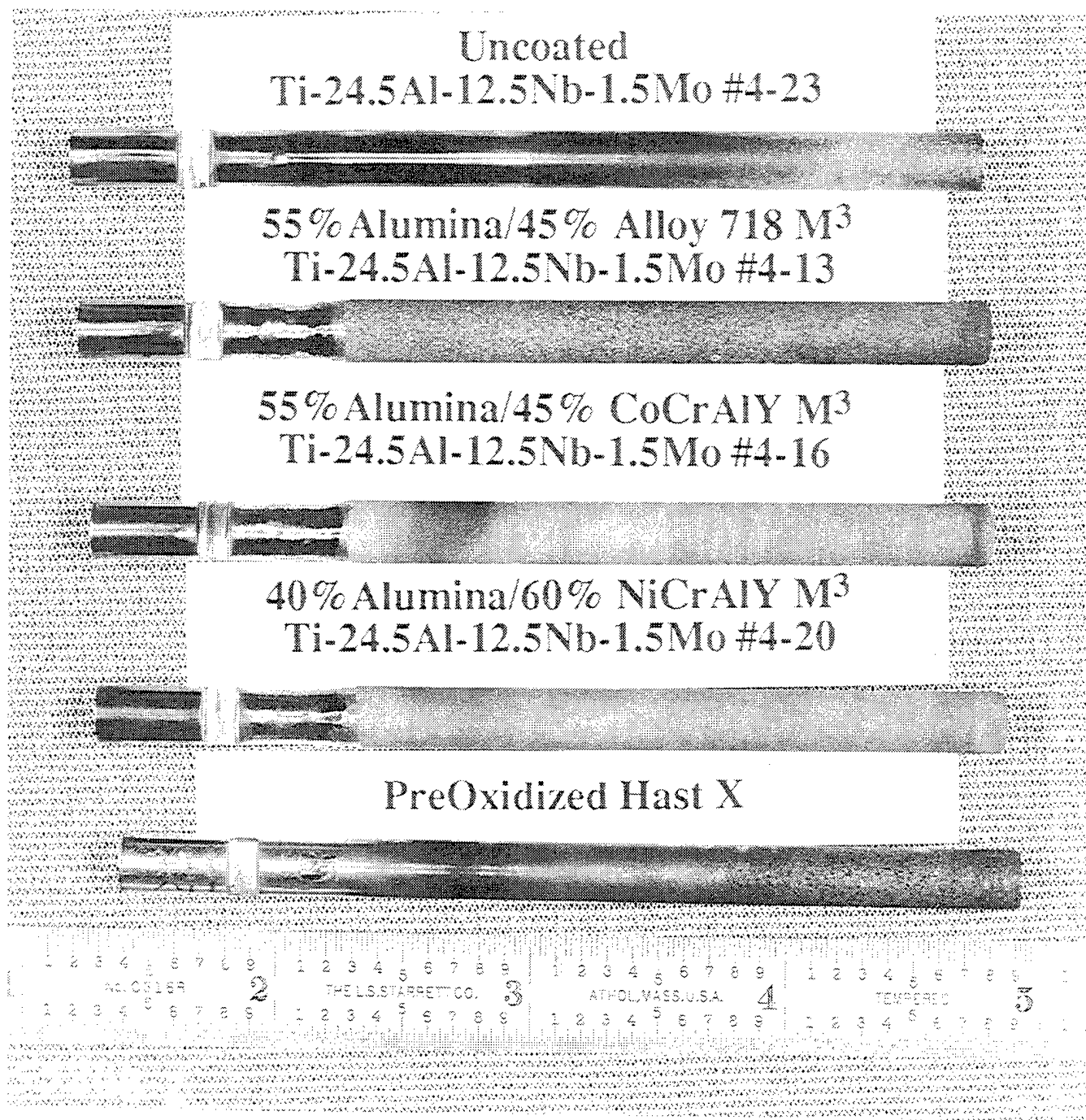


Figure 147. Color photographs showing the flame-side of coated and uncoated Ti-24.5Al-12.5Nb-1.5Mo alpha-2 after 3749 cycles (625 hr) of burner rig testing using a 760°C/648°C cycle with 1ppm sea salt.

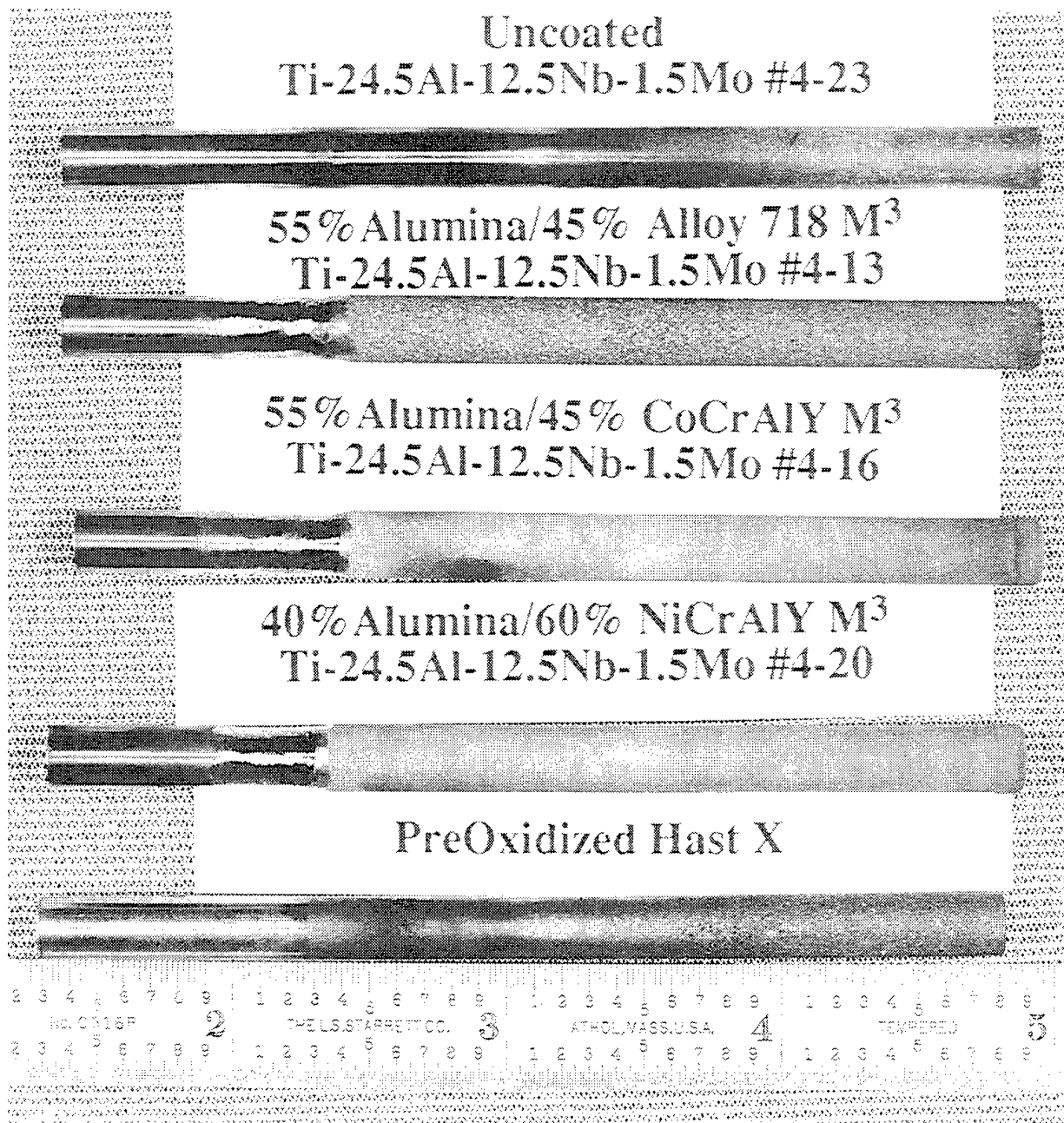
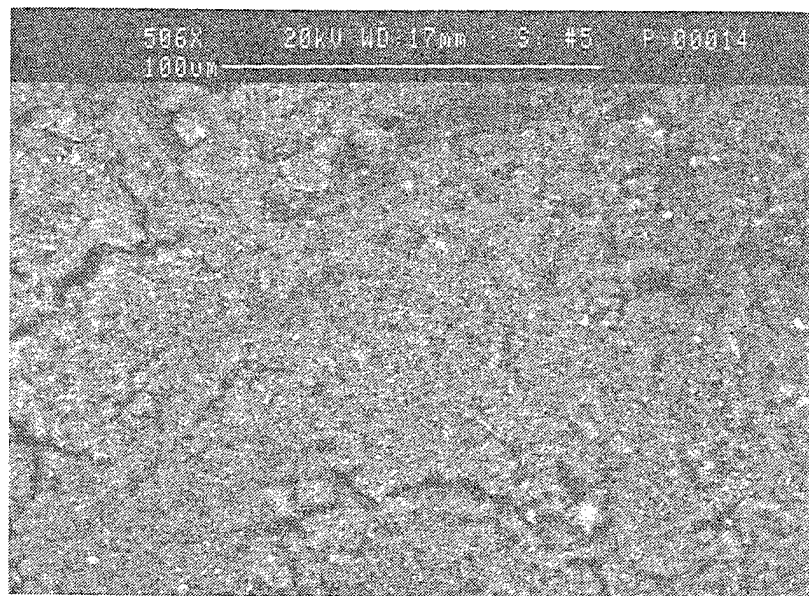
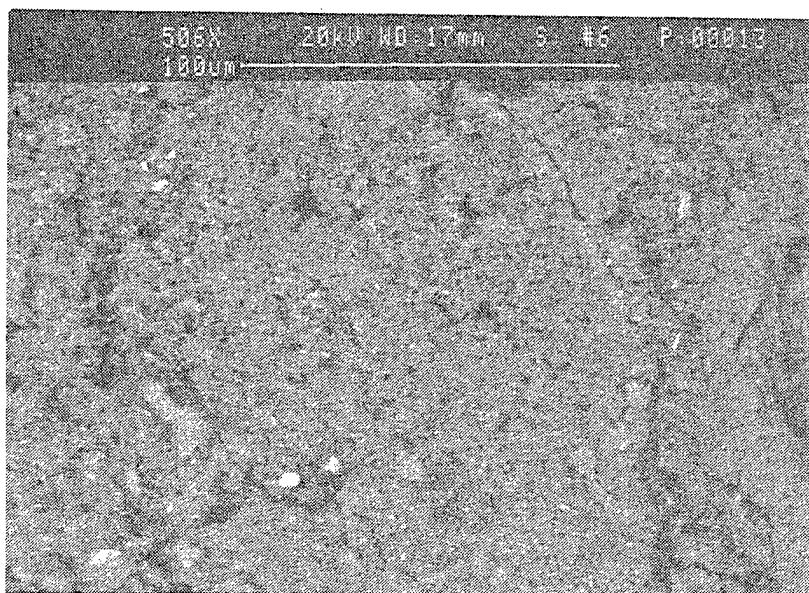


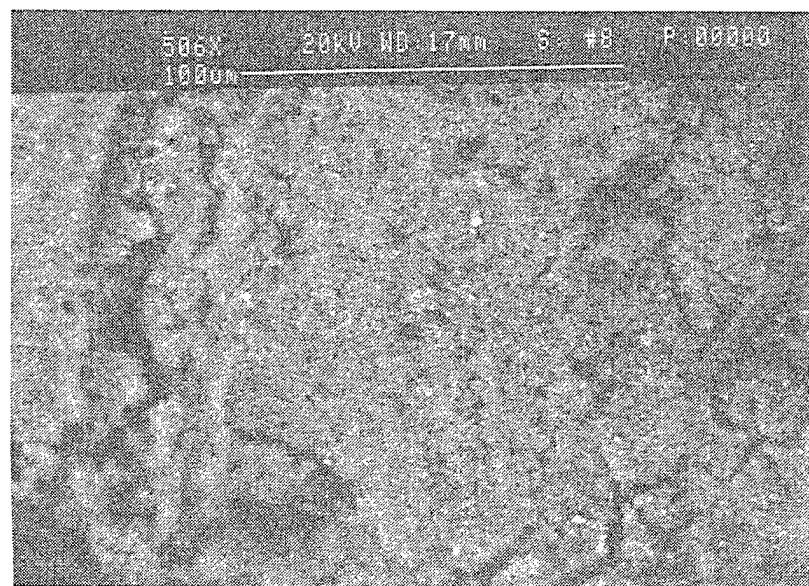
Figure 148. Color photographs showing the back-side of coated and uncoated Ti-24.5Al-12.5Nb-1.5Mo alpha-2 after 3749 cycles (625 hr) of burner rig testing using a 760°C/648°C cycle with 1ppm sea salt.



tan



gray



clear

Figure 149. Micrographs showing particulate found on filter paper after rinsing. The particles were mainly MgO.

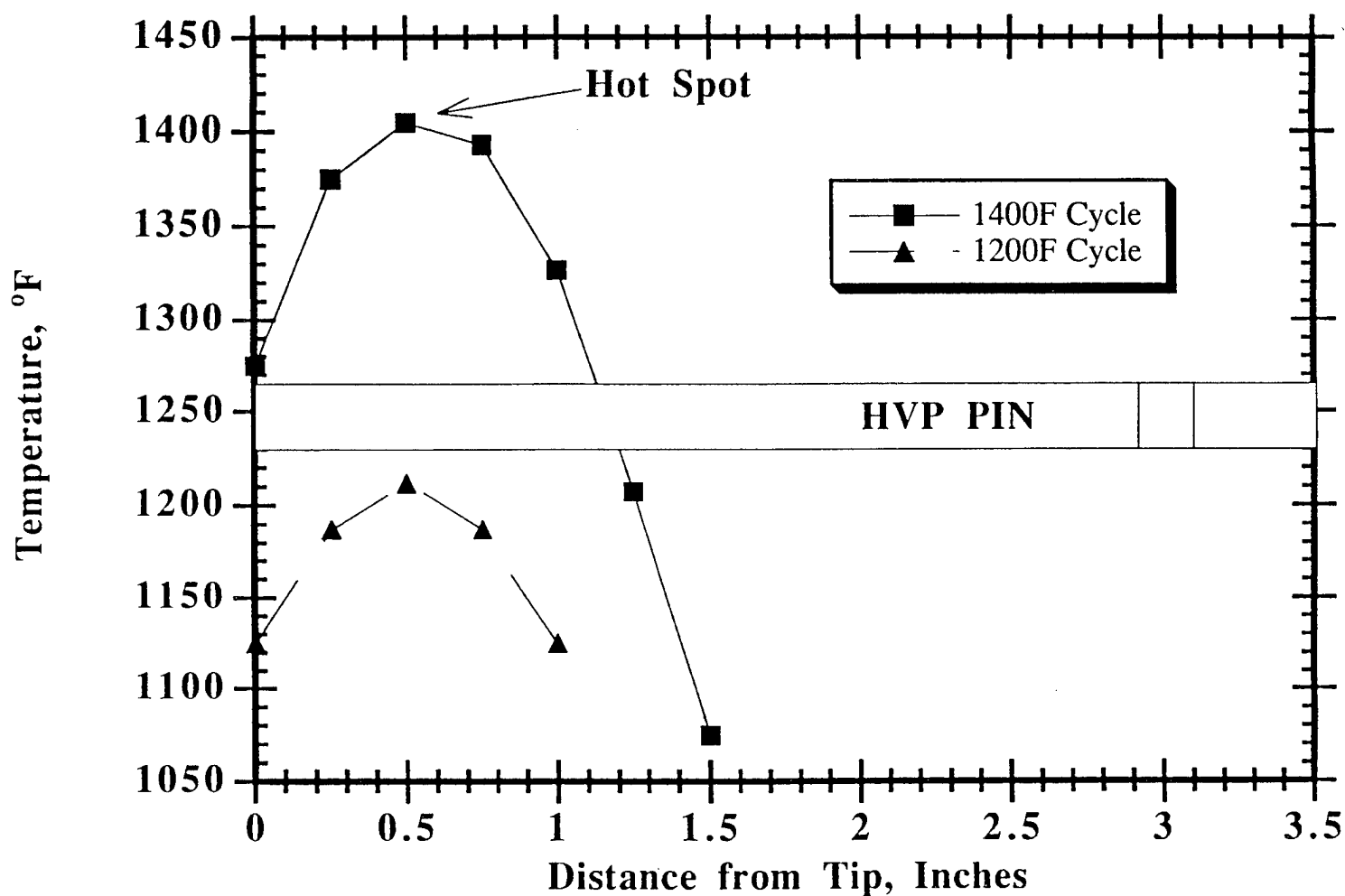
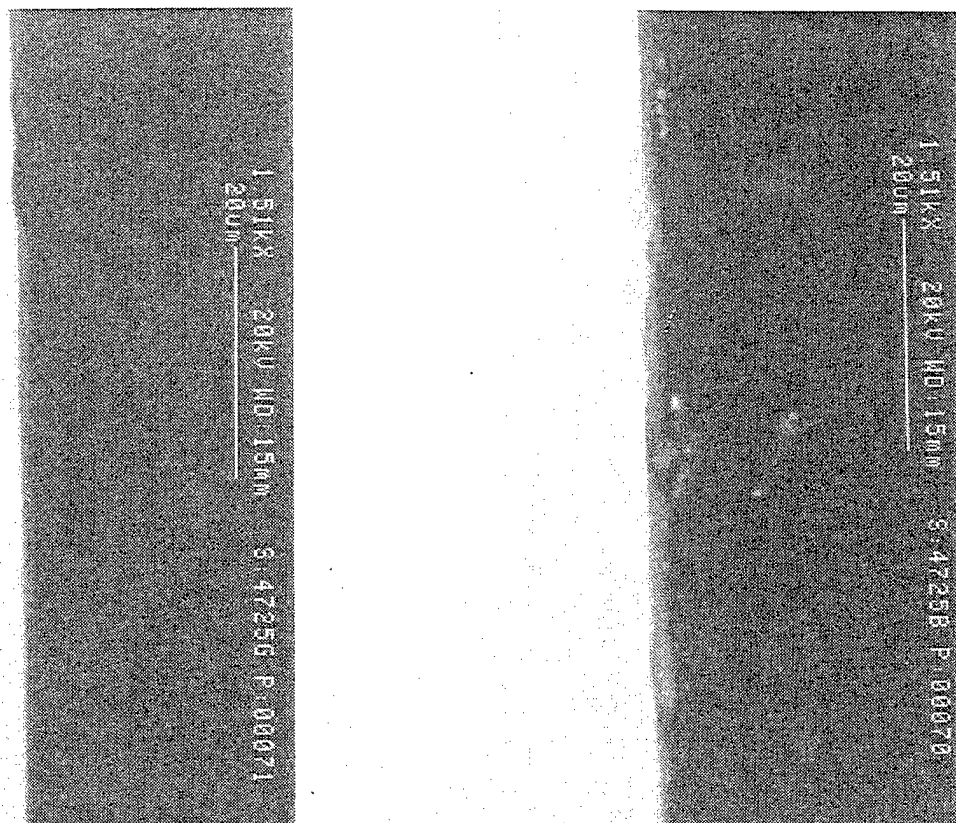
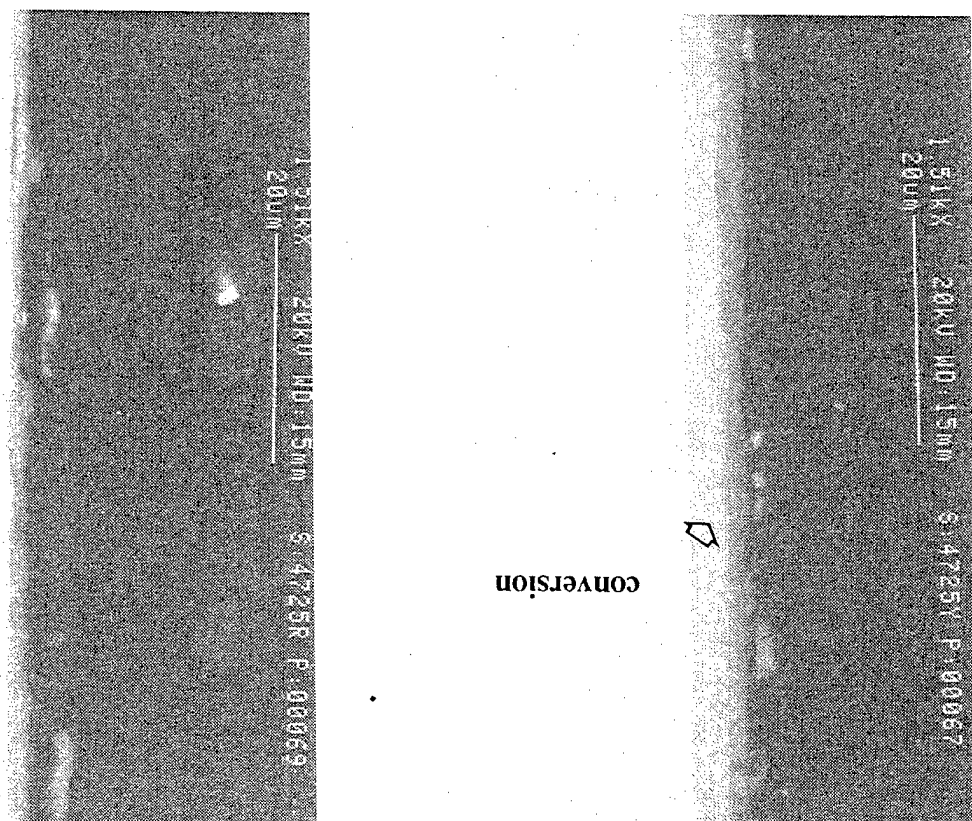


Figure 150. Graph showing the temperature profile of the pins during the 760/648°C burner rig test. Careful cross sectioning allows different conditions to be analyzed on the same pin.

648°C (1200°F) Peak Temperature



760°C (1400°F) Peak Temperature



398°C (750°F) < T

704°C (1300°F) Peak Temperature

Figure 151. Micrographs showing cross sections of the Ti-24.5Al-12.5Nb-1.5Mo alpha-2 as a function of peak temperature attained during burner rig testing.

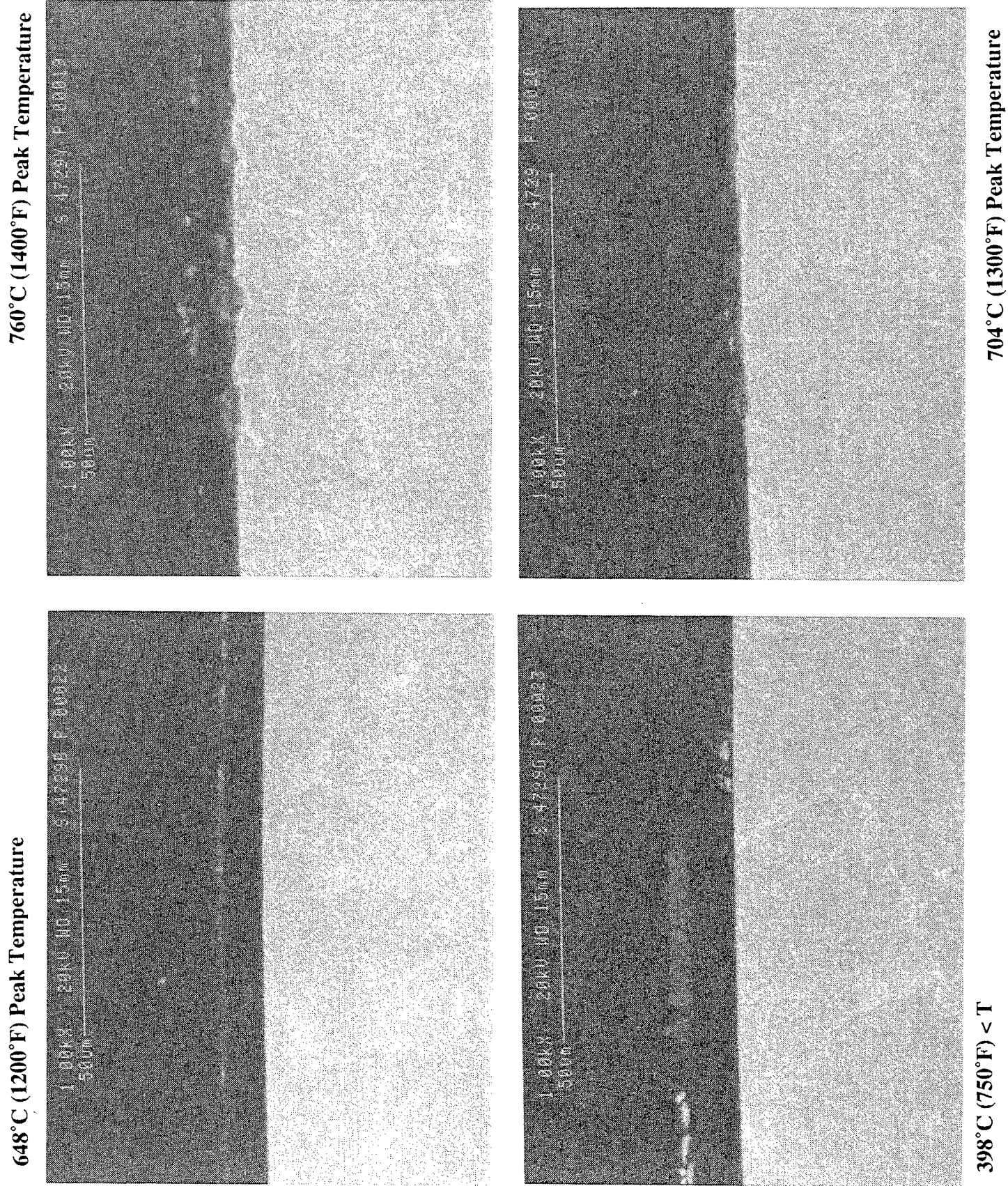
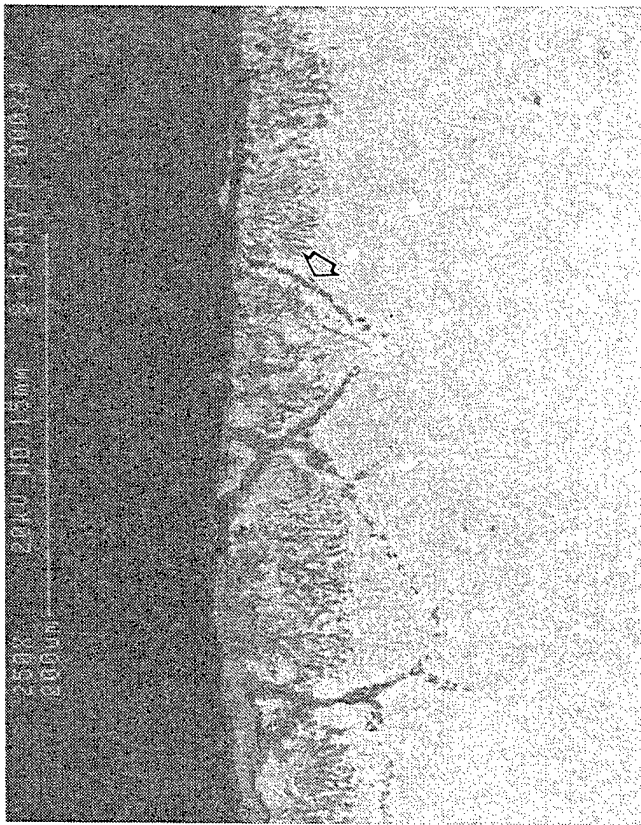


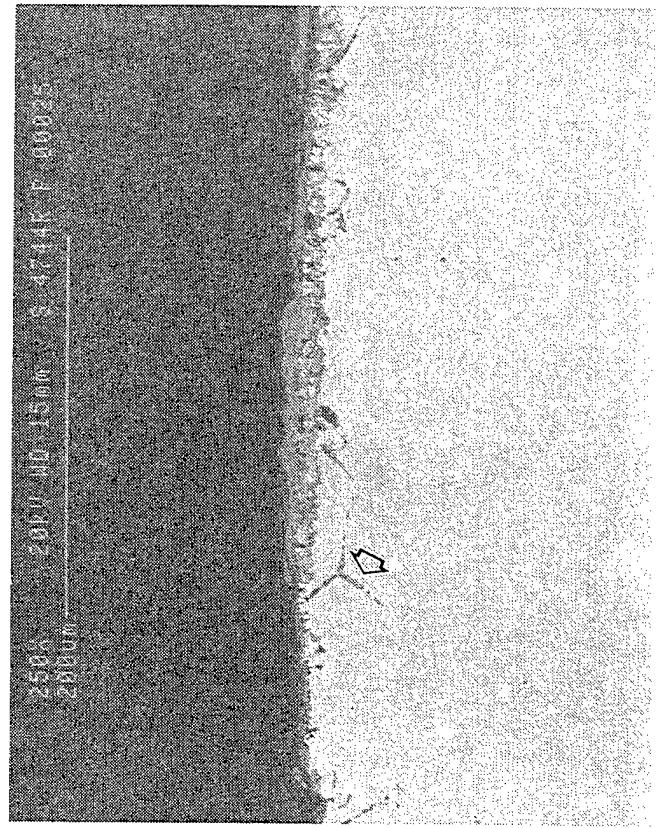
Figure 152. Micrographs showing cross sections of the Ti-48Al-2Cr-2Nb gamma alloy as a function of peak temperature attained during burner rig testing.

intergranular oxidation

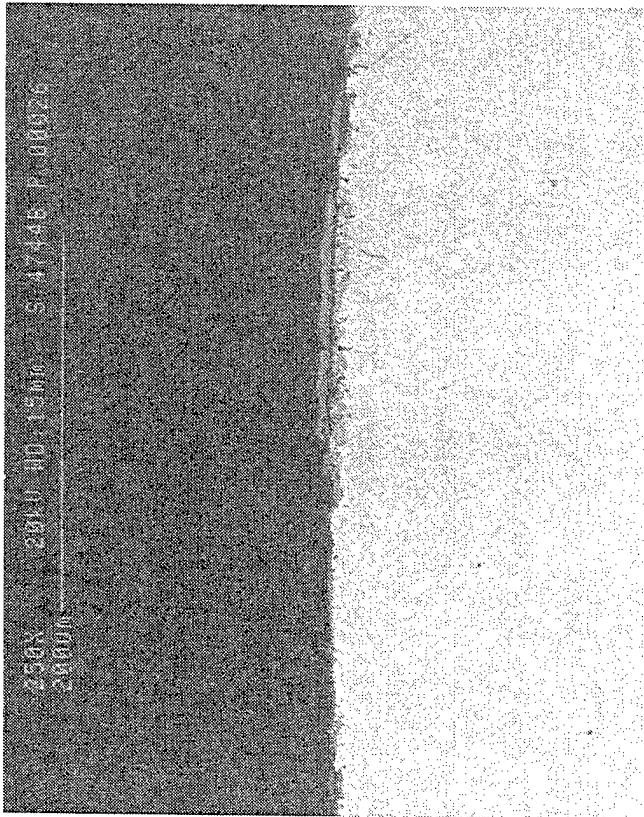
760°C (1400°F) Peak Temperature



704°C (1300°F) Peak Temperature



648°C (1200°F) Peak Temperature



398°C (750°F) < T

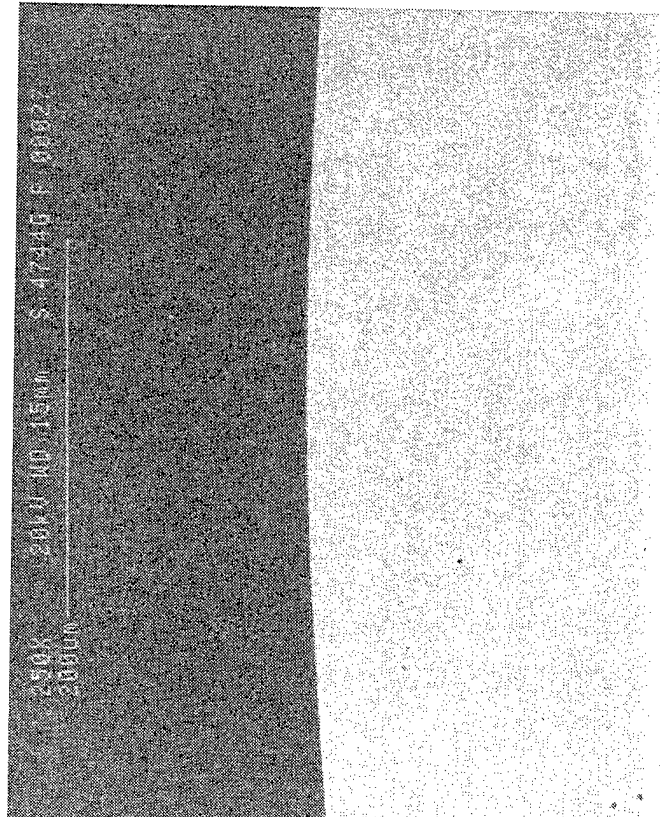
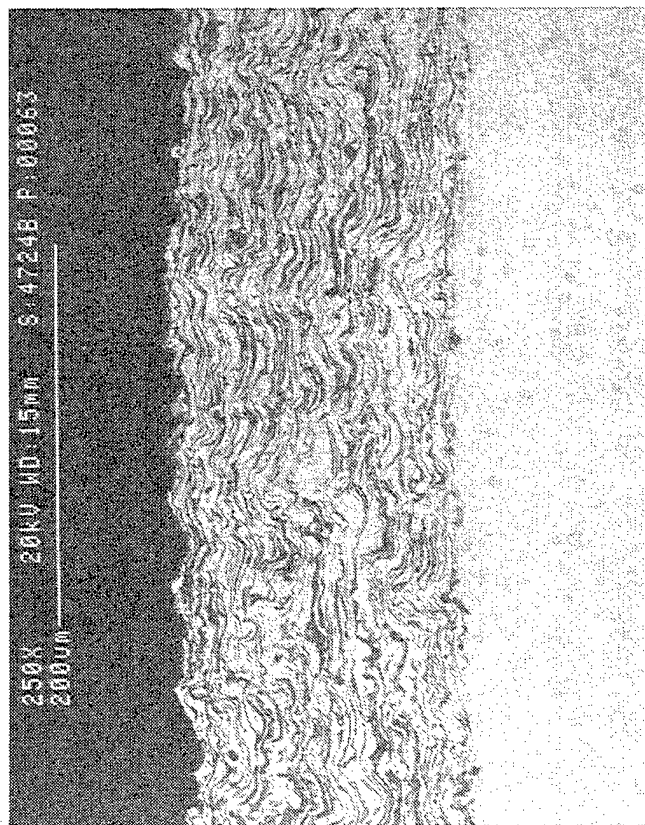
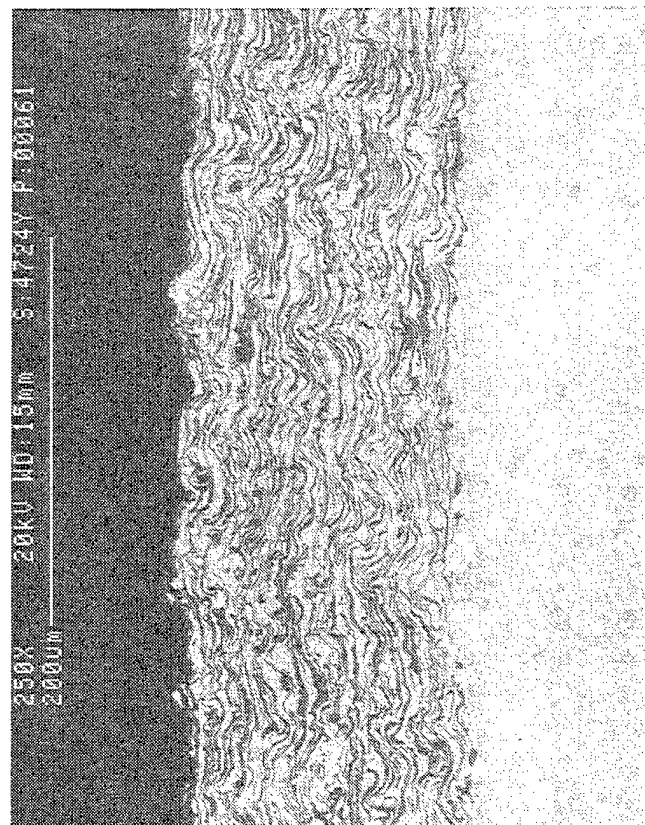


Figure 153. Micrographs showing cross sections of the Hastelloy X as a function of peak temperature attained during burner rig testing.

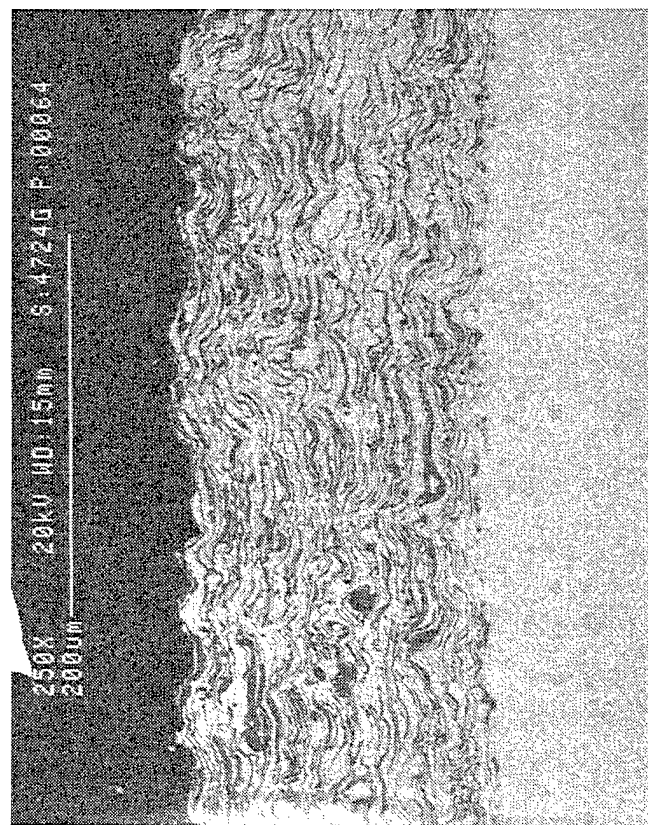
648°C (1200°F) Peak Temperature



760°C (1400°F) Peak Temperature



398°C (750°F) < T



704°C (1300°F) Peak Temperature

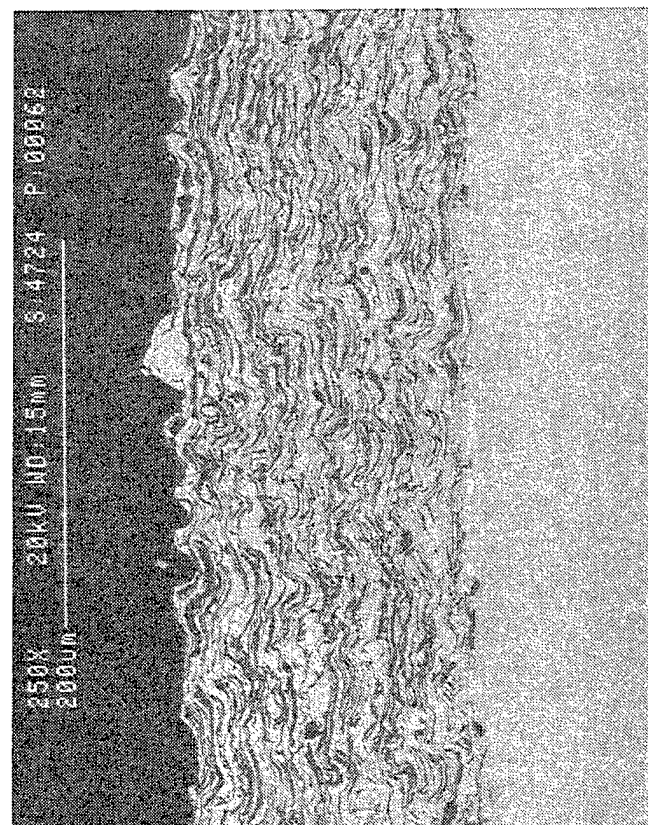
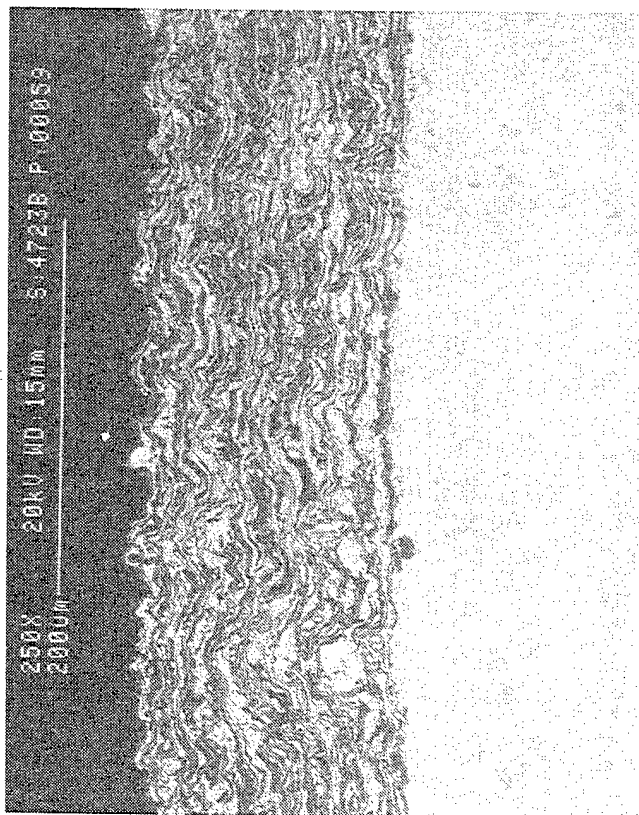
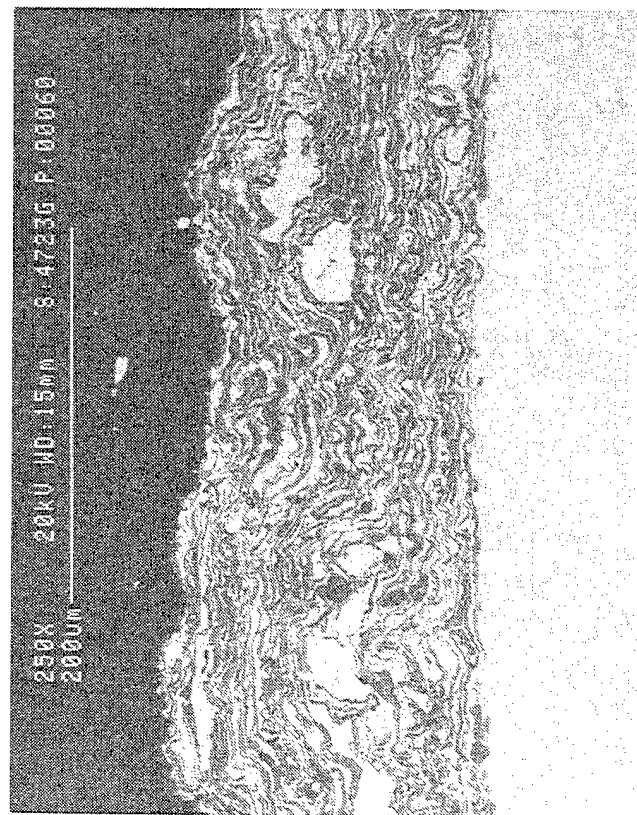
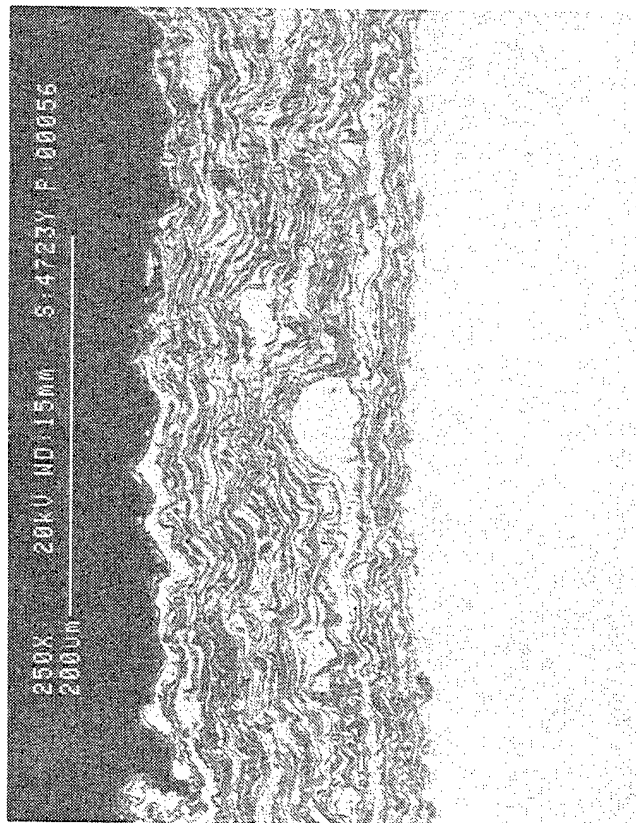


Figure 154. Micrographs showing cross sections of the NiCrAlY cermet (M^3) coated alpha-2 as a function of peak temperature attained during burner rig testing.

648°C (1200°F) Peak Temperature



760°C (1400°F) Peak Temperature



398°C (750°F) < T

704°C (1300°F) Peak Temperature

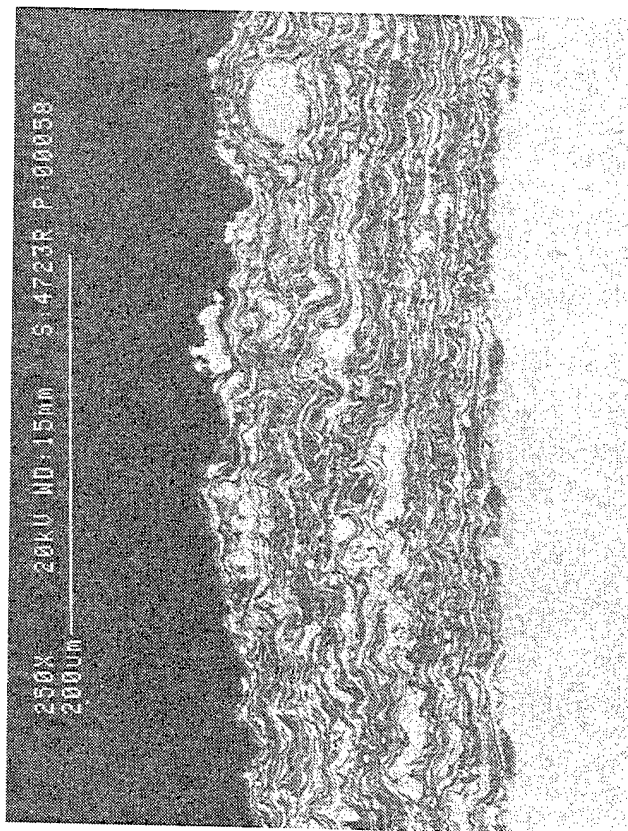
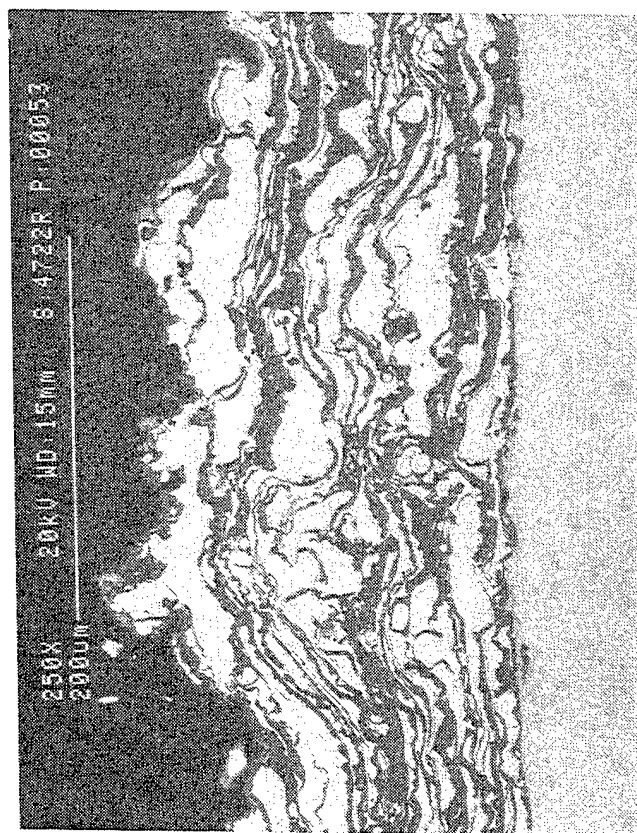
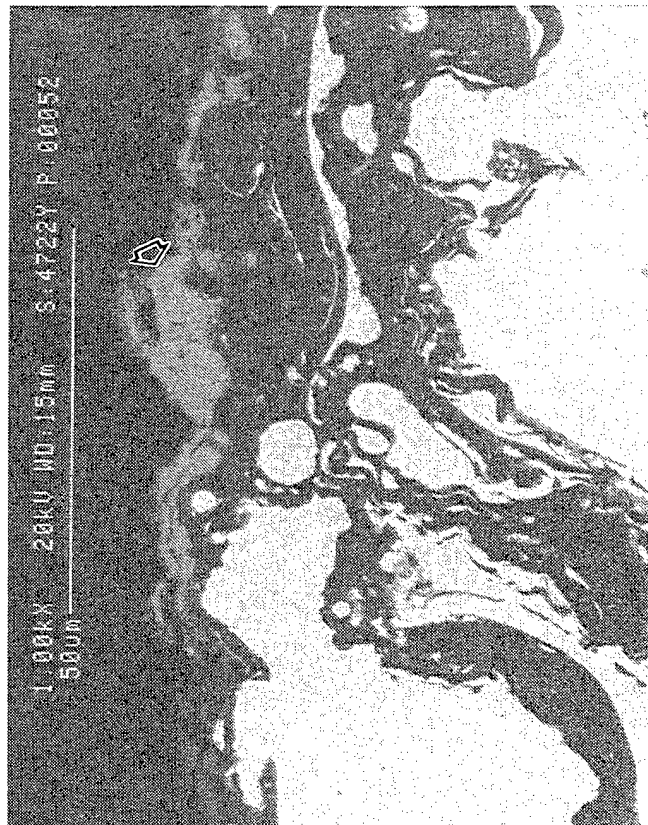


Figure 155. Micrographs showing cross sections of the CoCrAlY cermet (M³) coated alpha-2 as a function of peak temperature attained during burner rig testing.

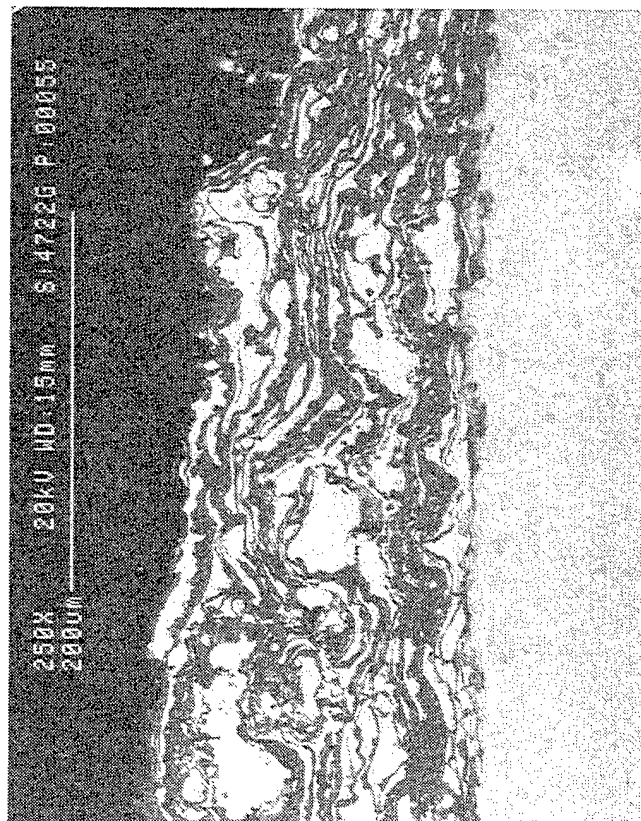
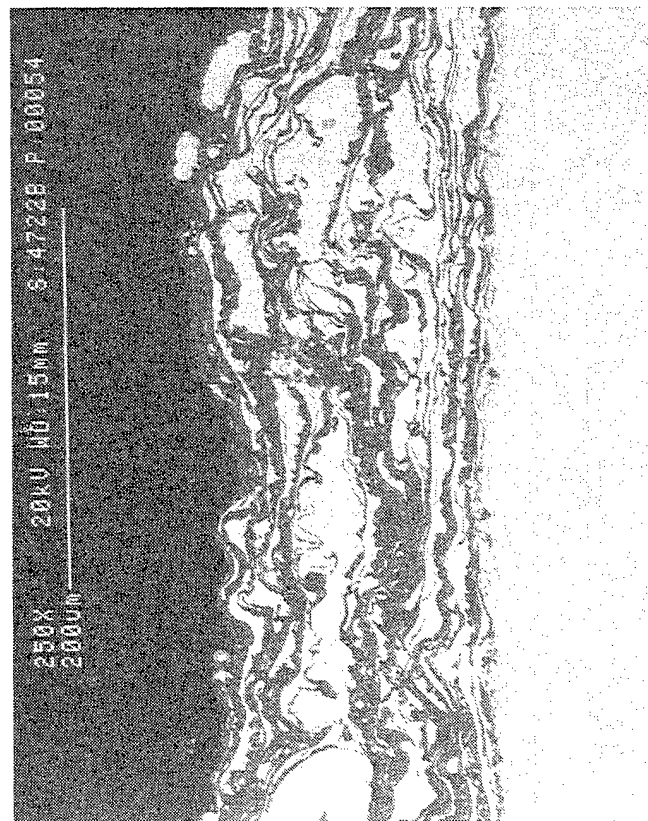
external attack

760°C (1400°F) Peak Temperature



704°C (1300°F) Peak Temperature

648°C (1200°F) Peak Temperature

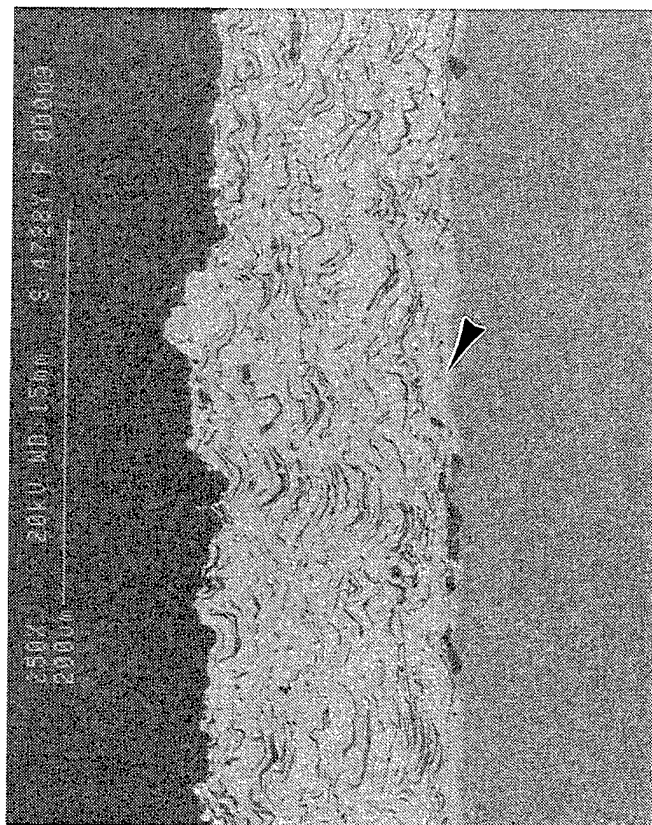


398°C (750°F) < T

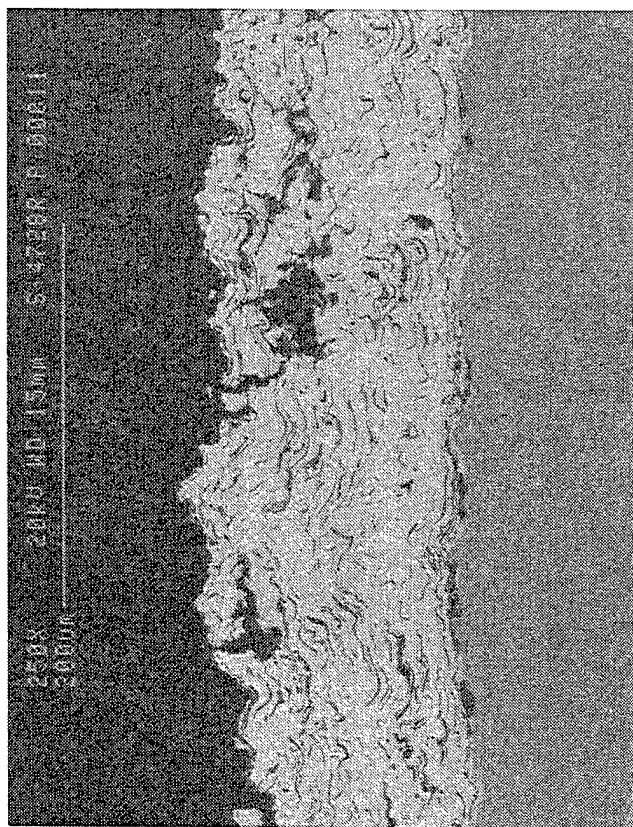
Figure 156. Micrographs showing cross sections of the Alloy 718 cermet (M^3) coated alpha-2 as a function of peak temperature attained during burner rig testing.

reaction zone

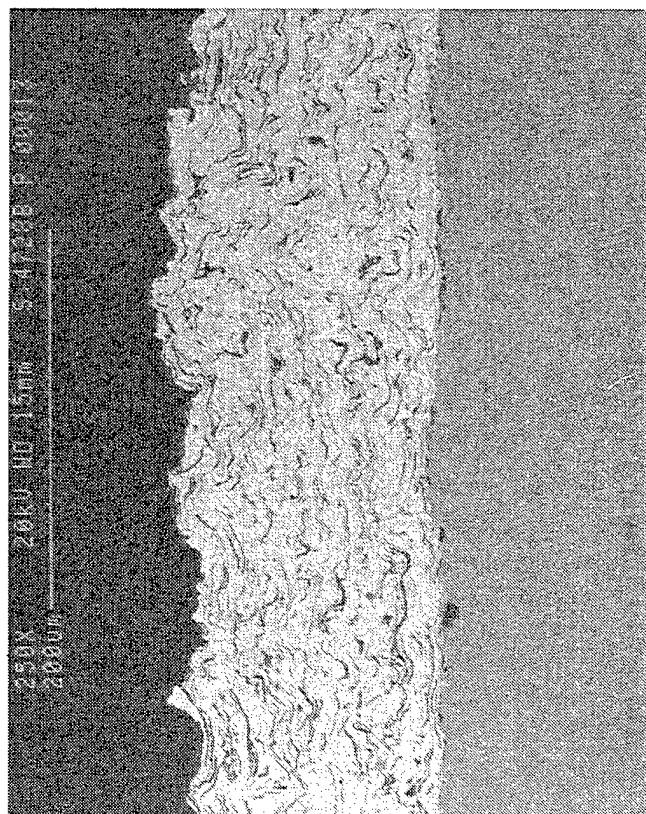
760°C (1400°F) Peak Temperature



704°C (1300°F) Peak Temperature



648°C (1200°F) Peak Temperature



398°C (750°F) < T

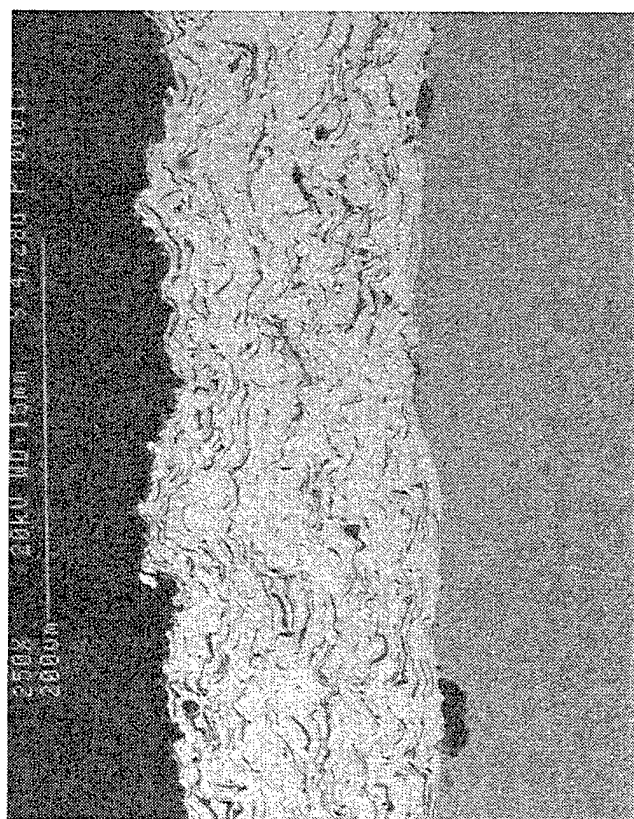
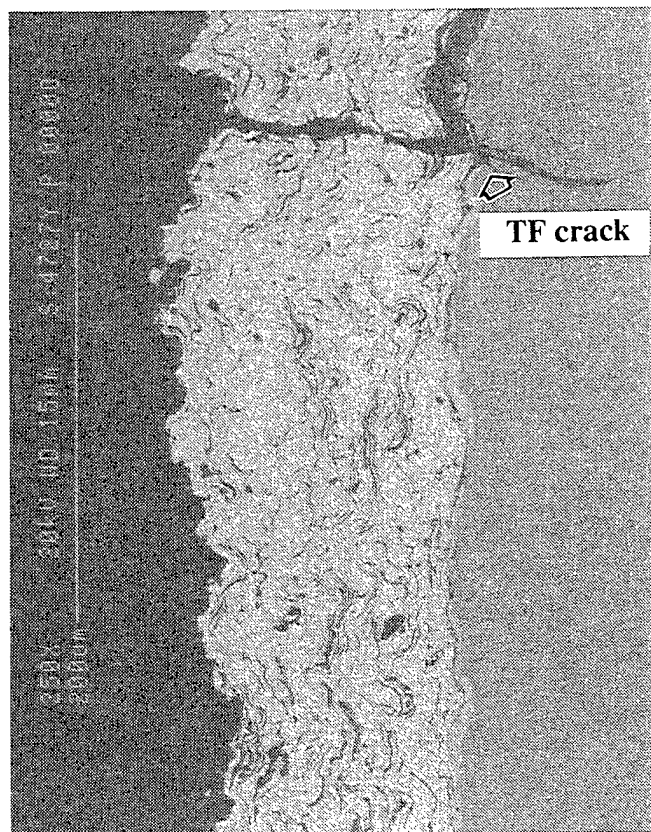
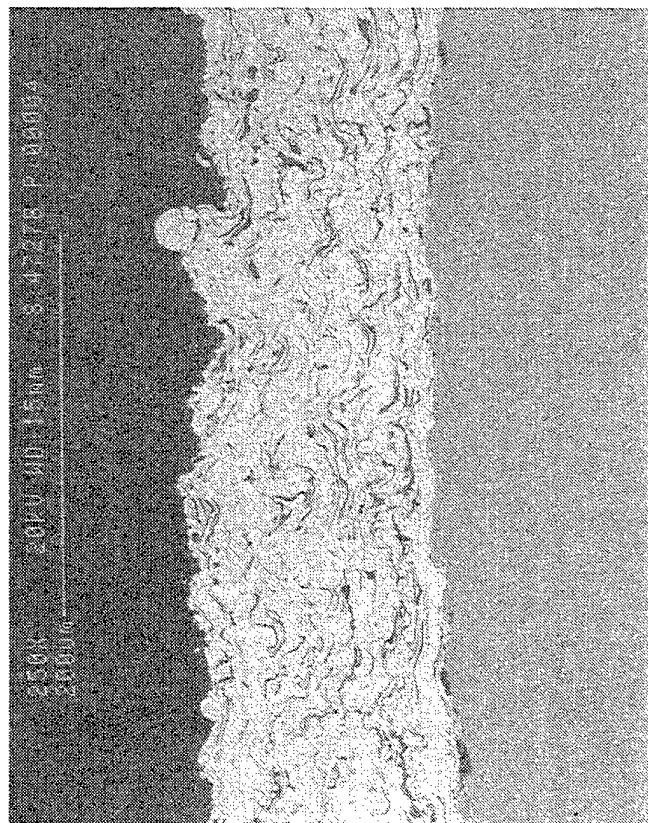


Figure 157. Micrographs showing cross sections of the NiCoCrAlY cermet (M³) coated alpha-2 as a function of peak temperature attained during burner rig testing.

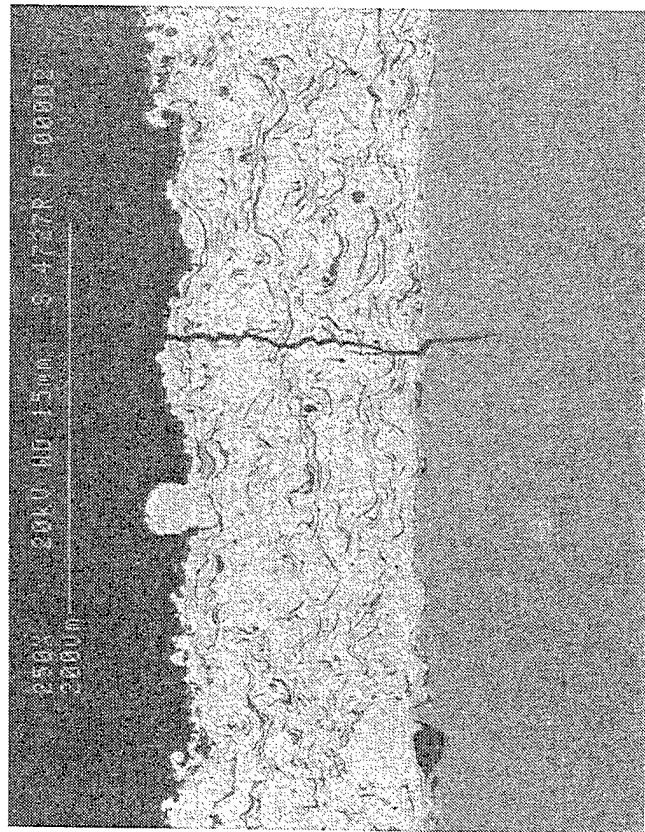
760°C (1400°F) Peak Temperature



648°C (1200°F) Peak Temperature



704°C (1300°F) Peak Temperature



398°C (750°F) < T

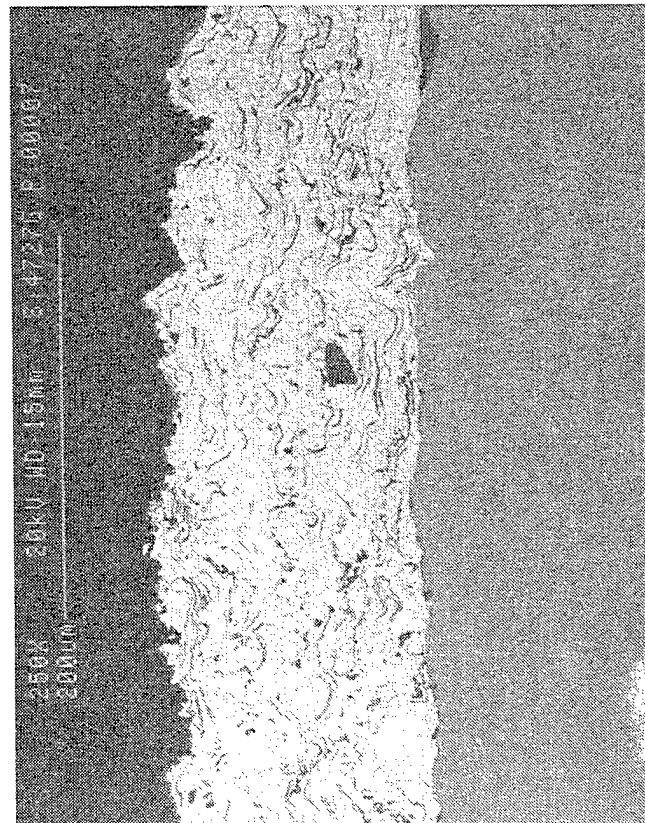
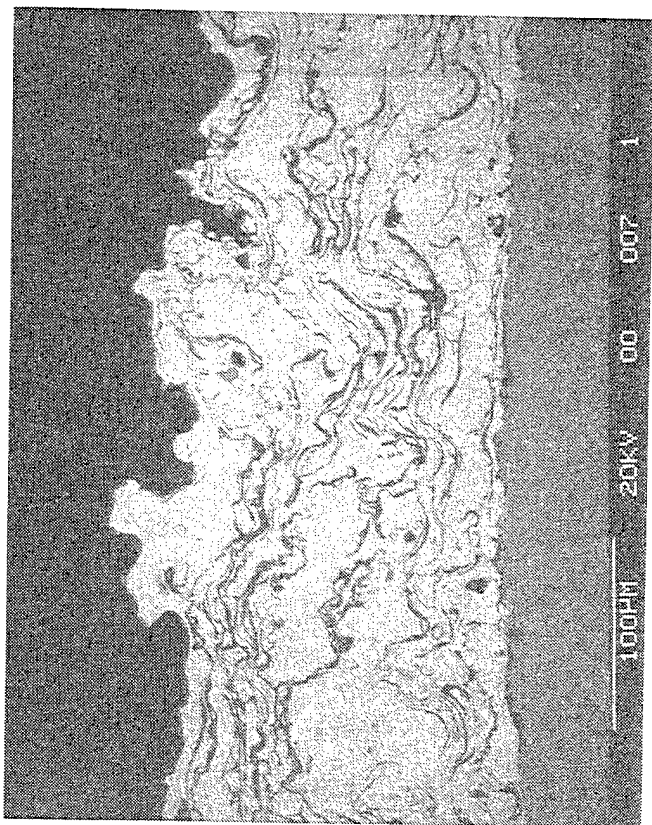
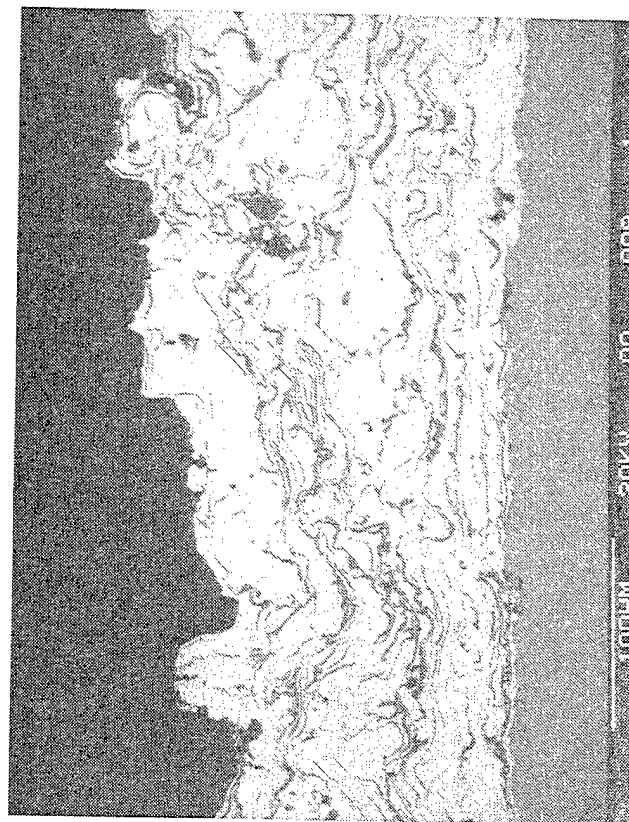
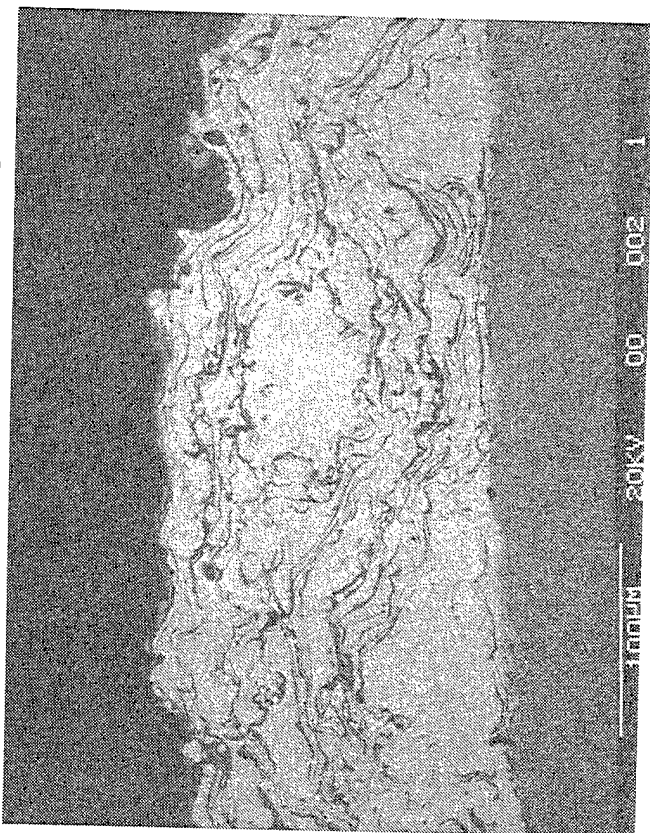


Figure 158. Micrographs showing cross sections of the CoCrAlY cermet (M^3) coated gamma as a function of peak temperature attained during burner rig testing.

648°C (1200°F) Peak Temperature



760°C (1400°F) Peak Temperature



704°C (1300°F) Peak Temperature

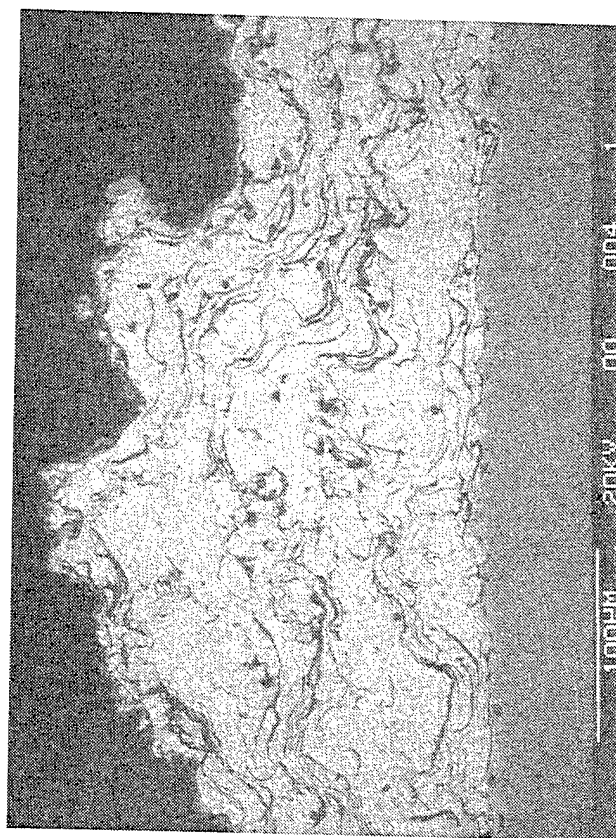


Figure 159. Micrographs showing cross sections of the Alloy 718 cermet (M³) coated gamma as a function of peak temperature attained during burner rig testing.

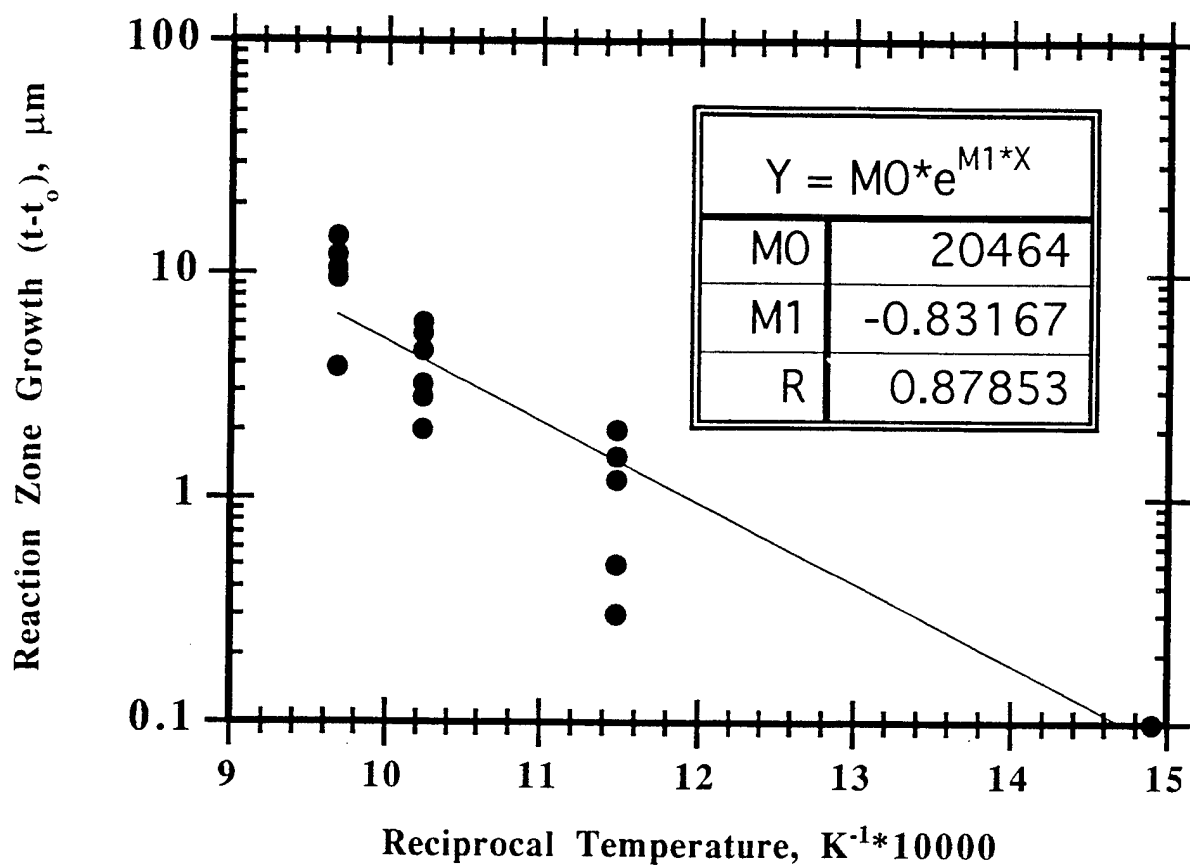


Figure 160. Graph summarizing reaction zone thickness as a function of peak exposure temperature. An equation that fits the line drawn through the data is shown in the figure.

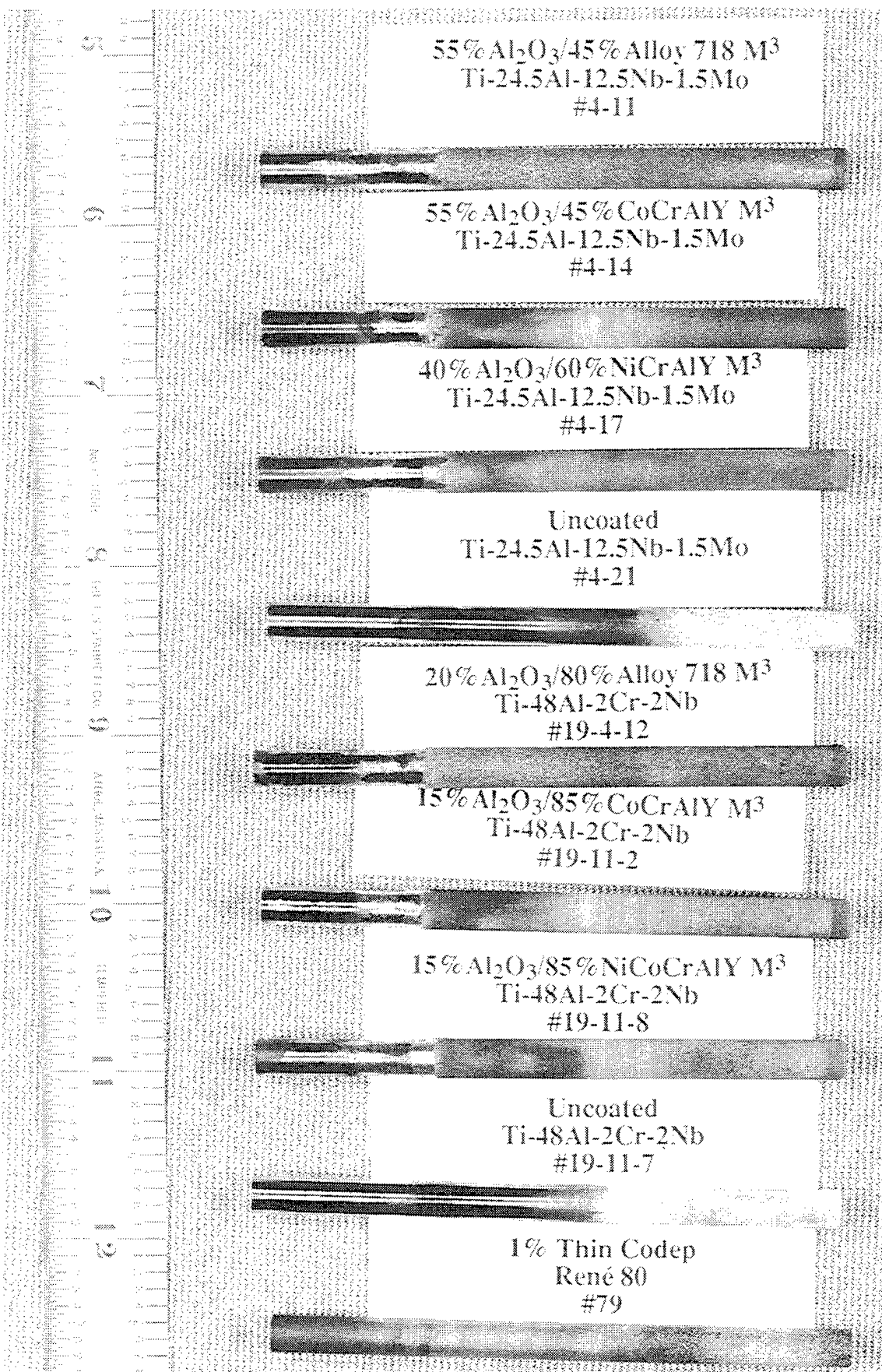


Figure 161. Color photograph of the back-side all of the pins after rinsing and 516 hours of burner rig testing at 871/760°C in 1-2ppm of sea salt. The figure allows comparisons between alpha-2 and gamma systems.

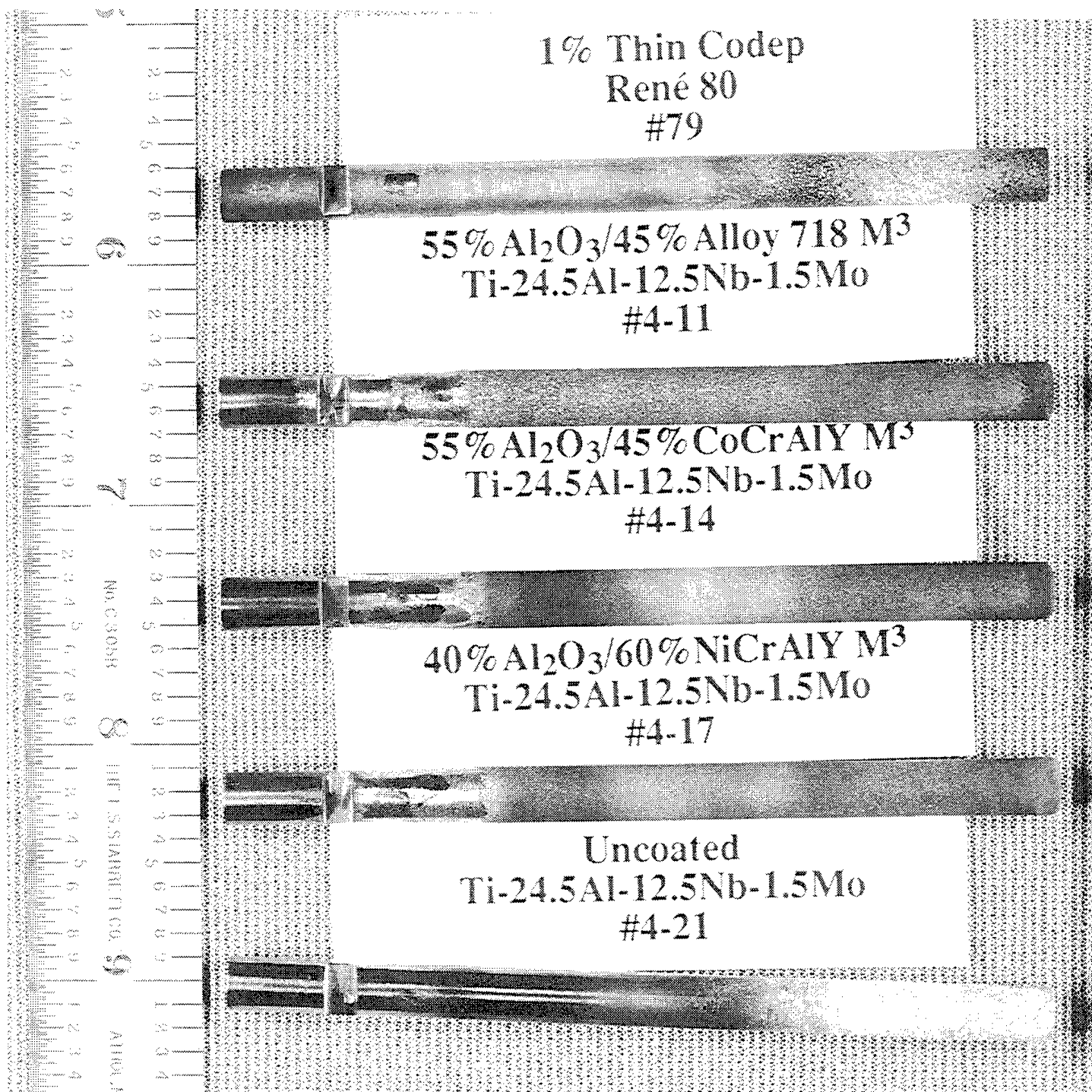


Figure 162. Color photograph of the flame-side of rinsed coated and uncoated alpha-2 after 516 hours of burner rig testing at 871/760°C in 1-2ppm of sea salt.

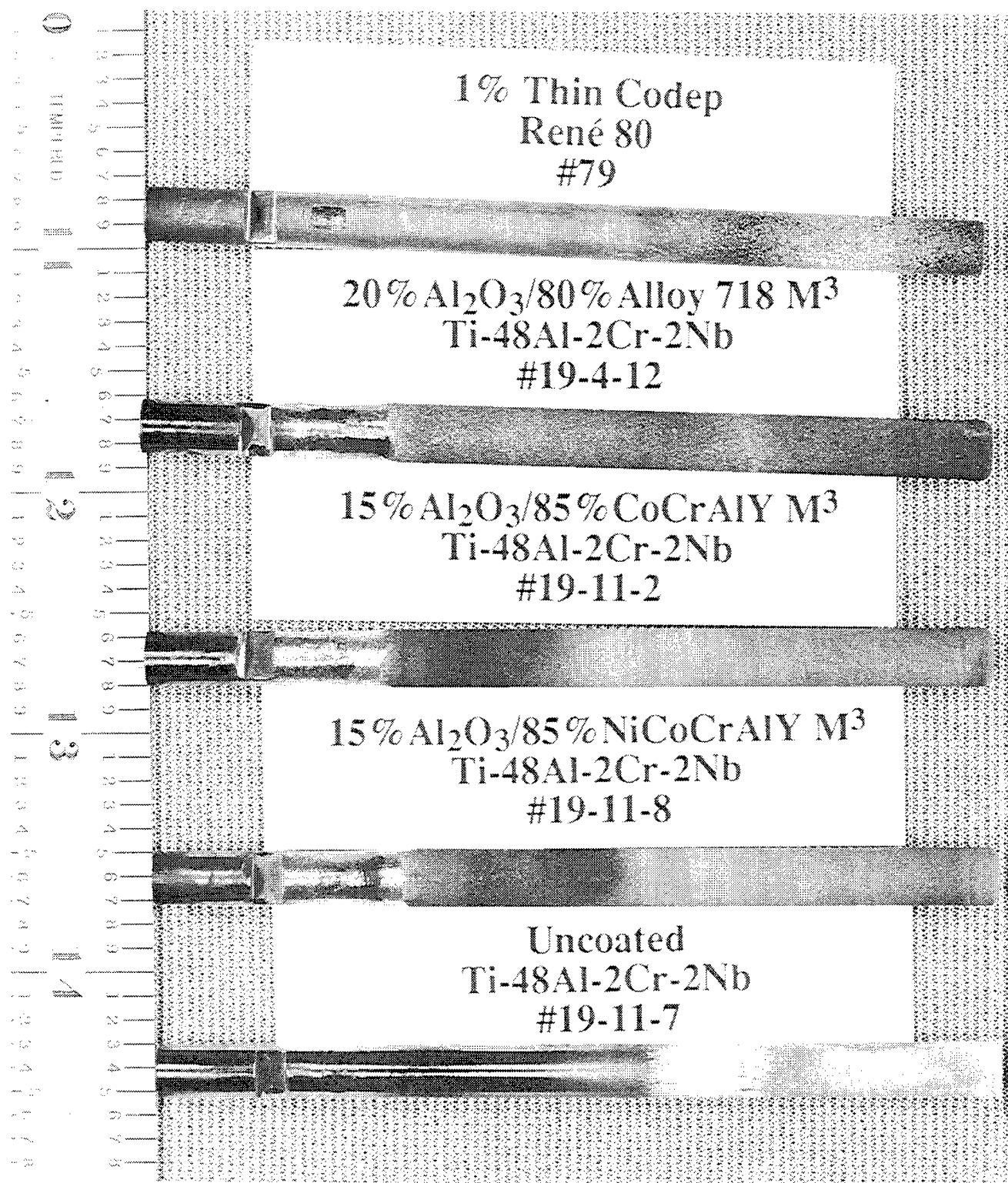


Figure 163. Color photograph of the flame-side of rinsed coated and uncoated gamma after 516 hours of burner rig testing at 871/760°C in 1-2ppm of sea salt.

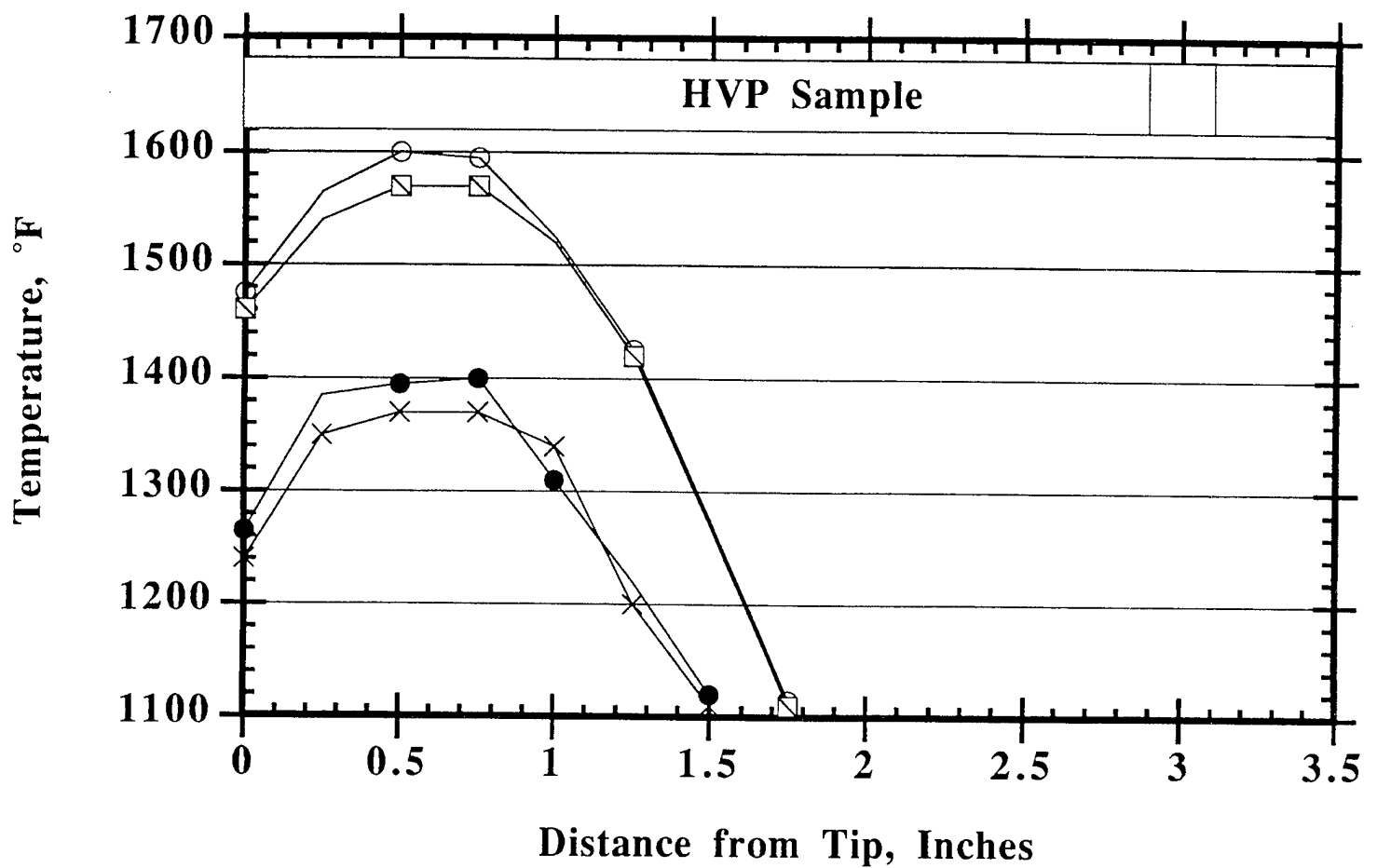


Figure 164. Graph showing the temperature distribution along the length of the pin for the 871/760°C burner rig test.

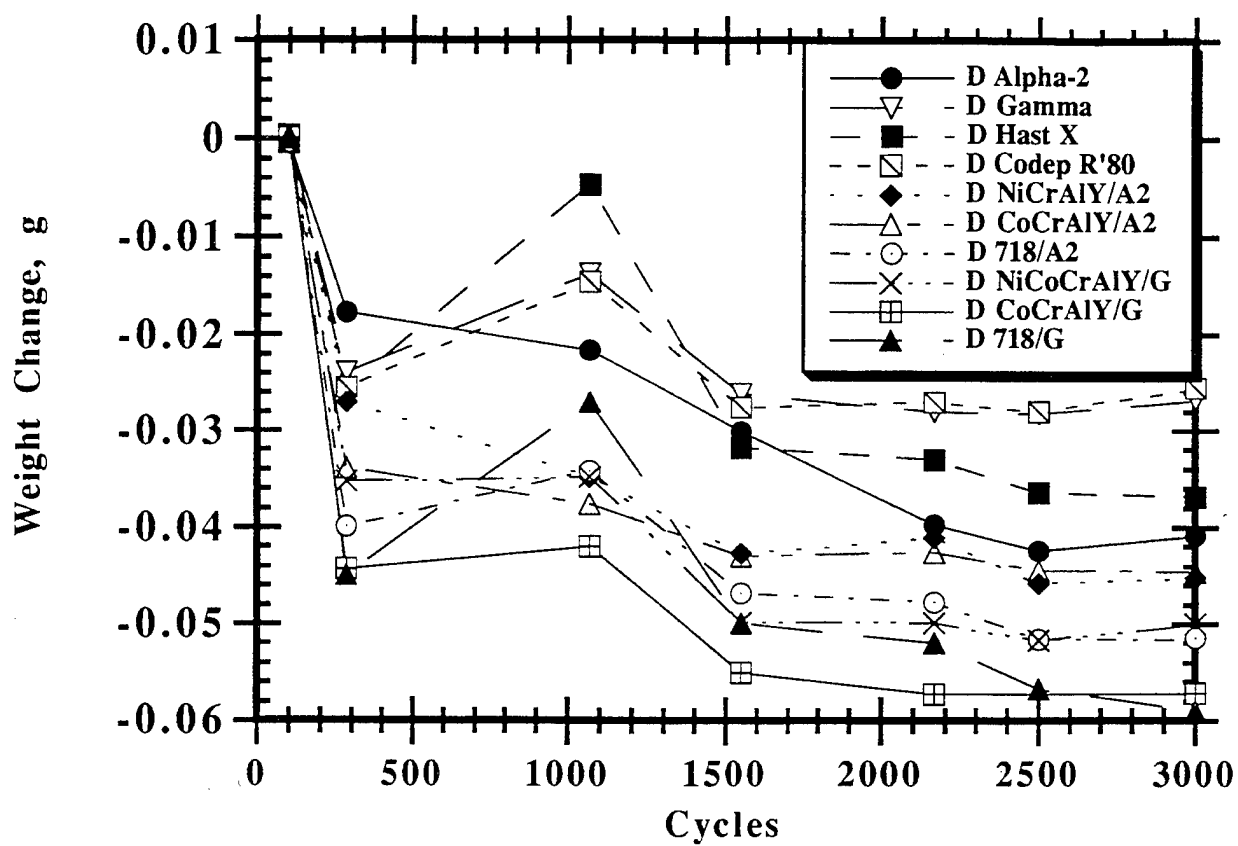
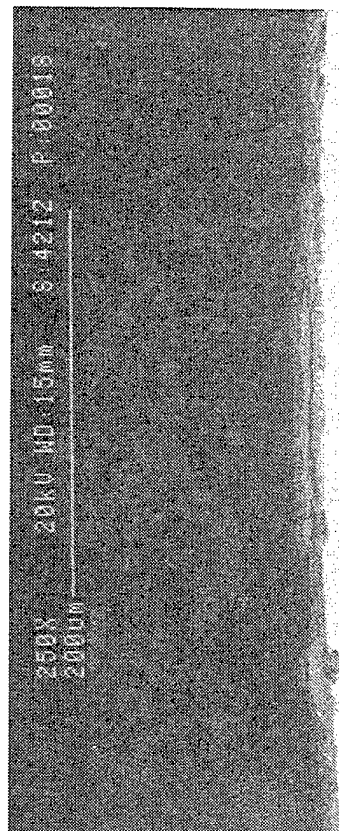
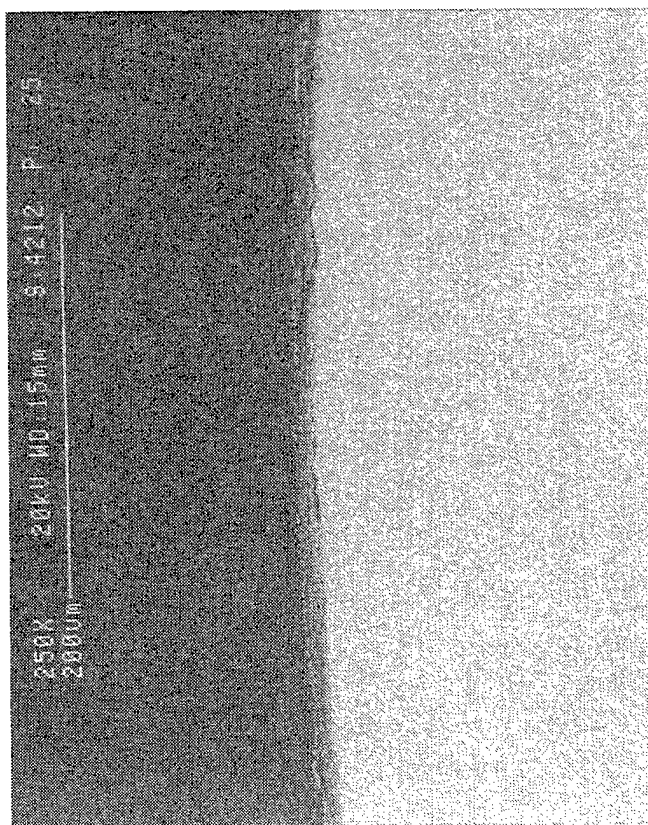


Figure 165. Graph showing the weight change after rinsing for coated and uncoated samples during the 871/760°C burner rig test.

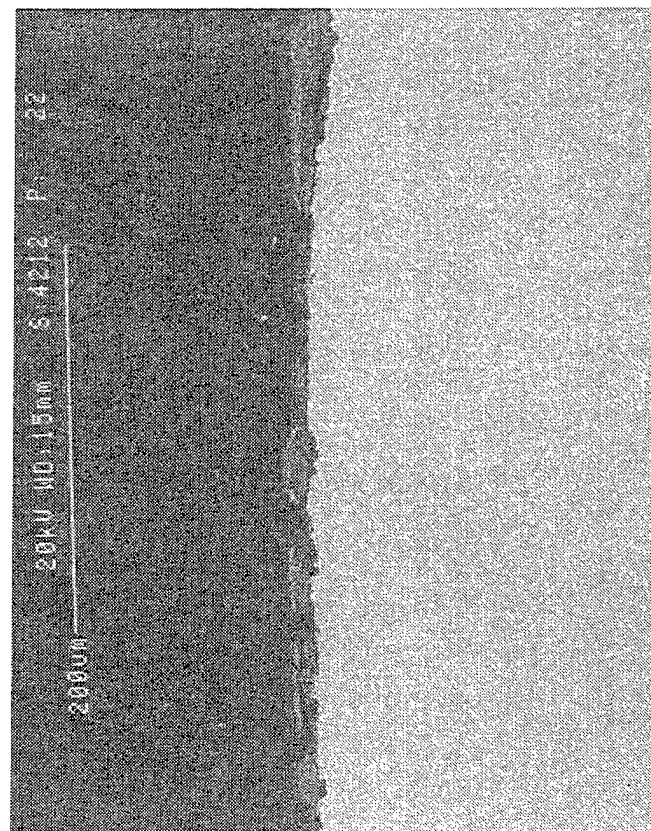
871C (1600°F) Peak Temperature



760°C (1400°F) Peak Temperature



820°C (1510°F) Peak Temperature



510°C (950°F) < T

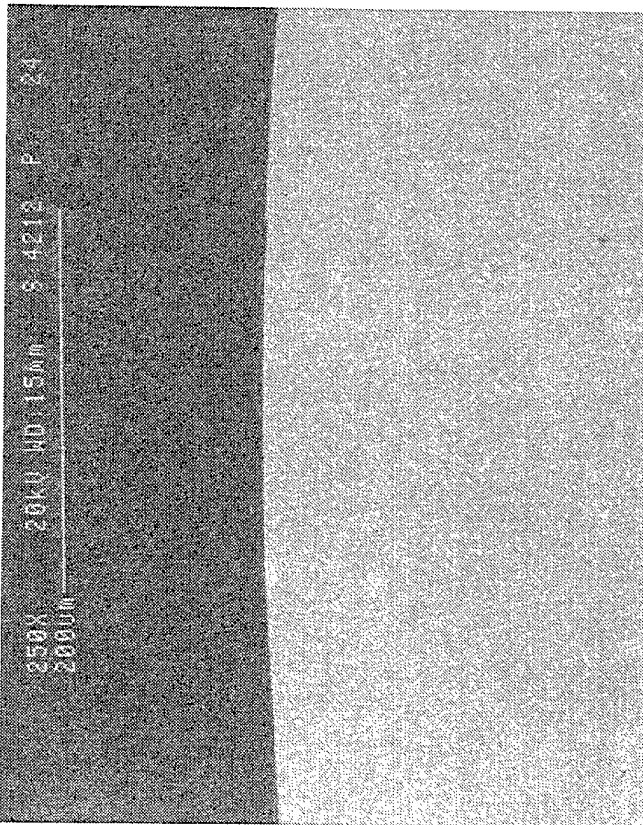


Figure 166. Micrographs showing cross sections of uncoated gamma after the 871/760°C burner rig test.

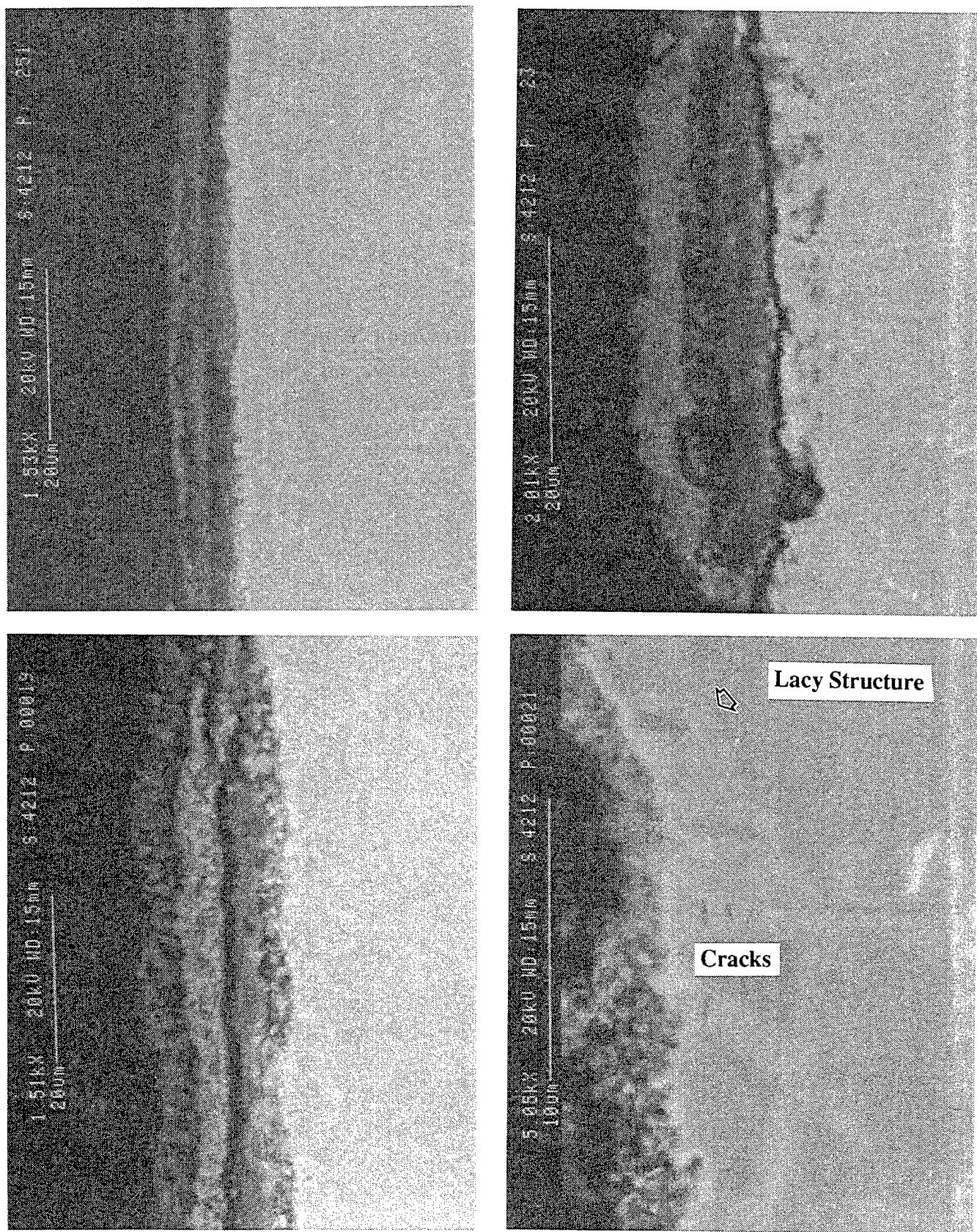
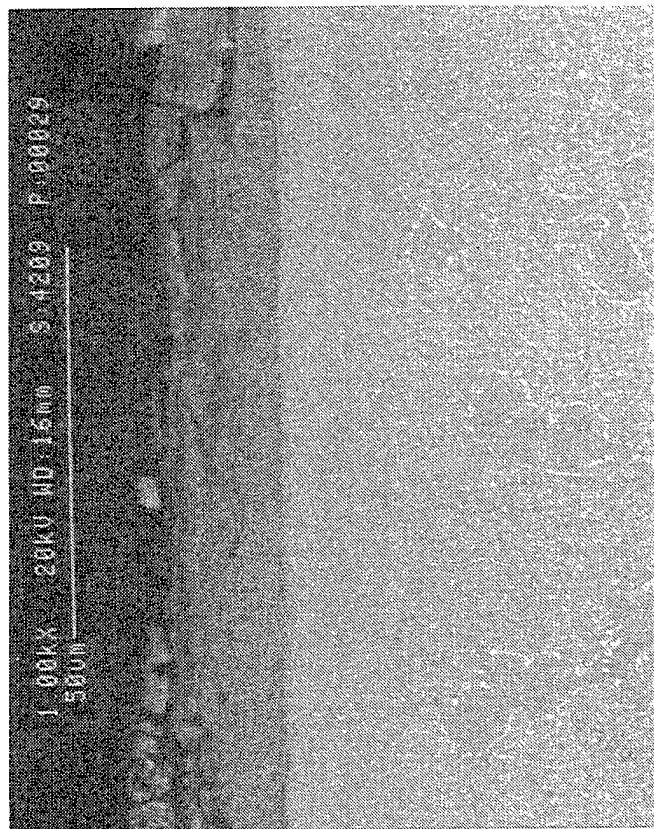
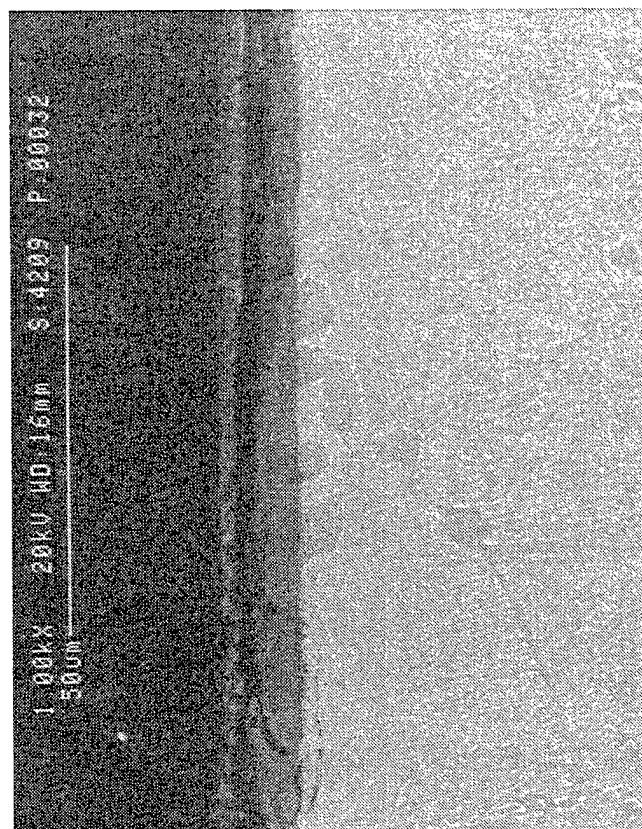


Figure 167. Micrographs showing the attack of uncoated gamma in the 871°C section. Thick oxide scales formed as well as a lacy microstructure in the gamma substrate that was prone to cracking.

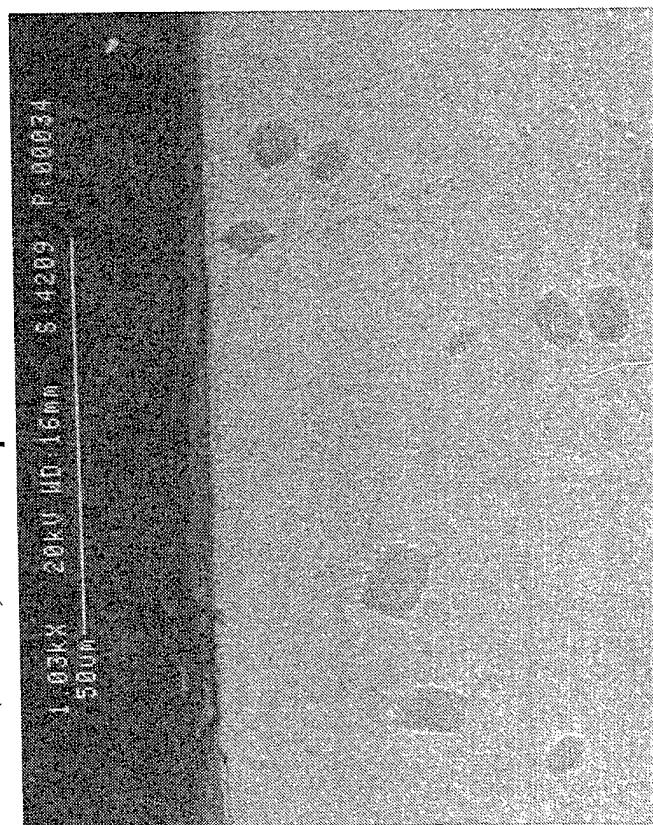
871°C (1600°F) Peak Temperature



820°C (1510°F) Peak Temperature



760°C (1400°F) Peak Temperature



510°C (950°F) < T

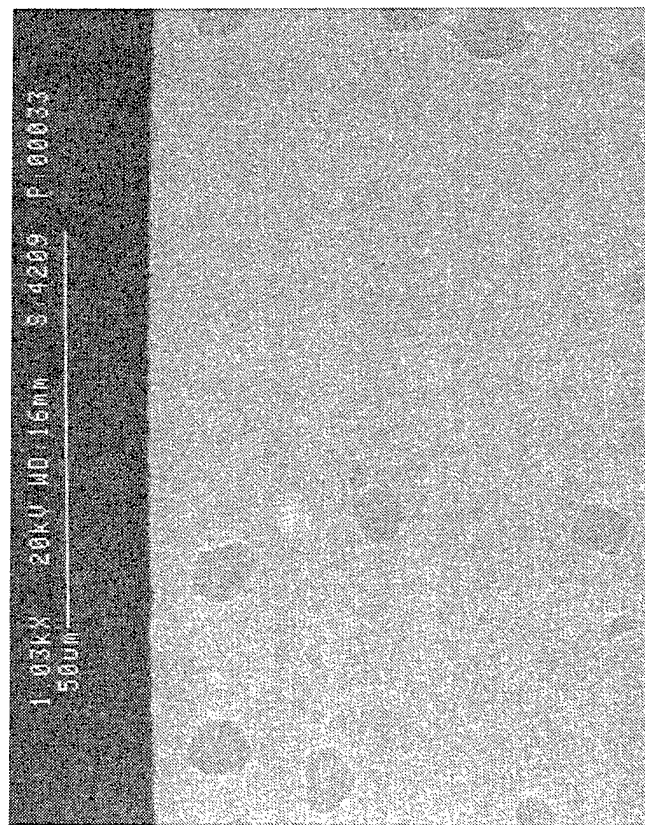
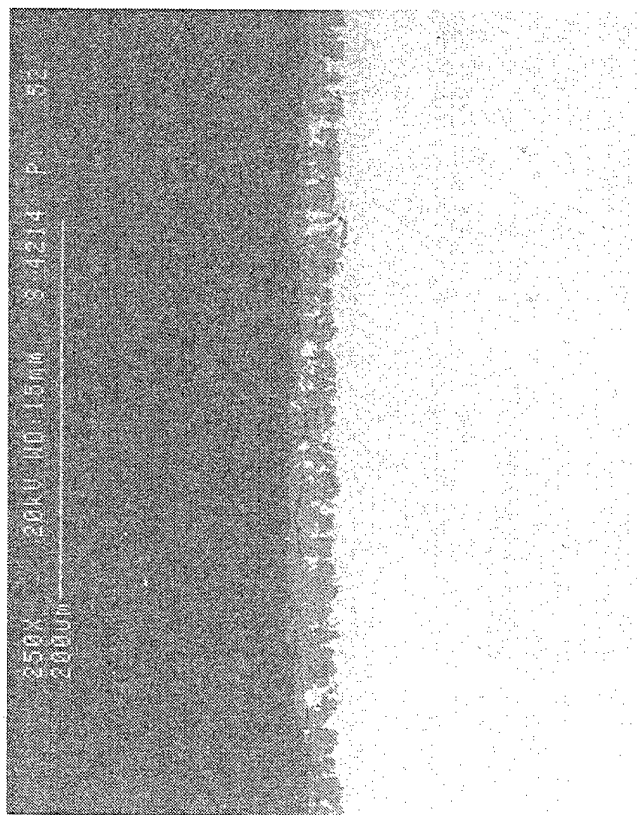
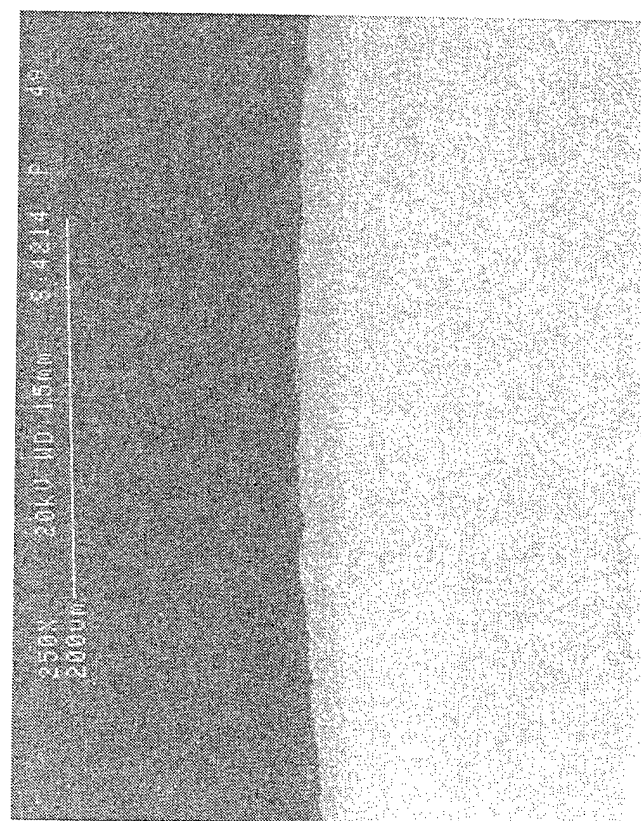
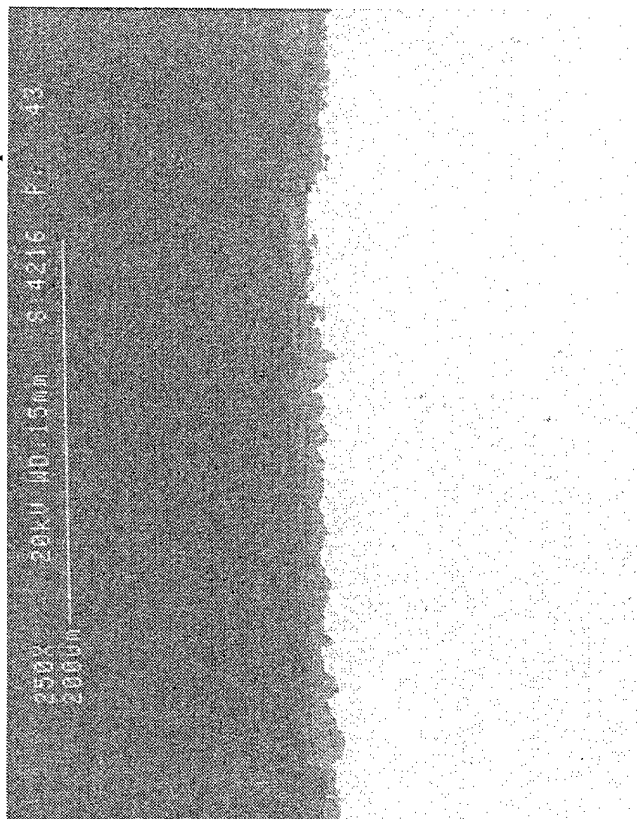


Figure 168. Micrographs showing cross sections of uncoated alpha-2 after the 871/760°C burner rig test.

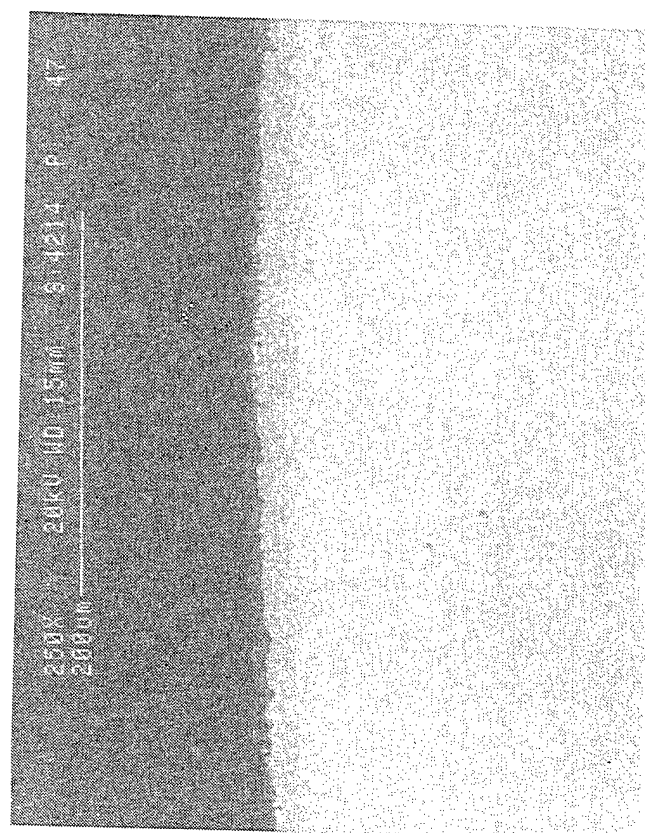
760°C (1400°F) Peak Temperature



871°C (1600°F) Peak Temperature

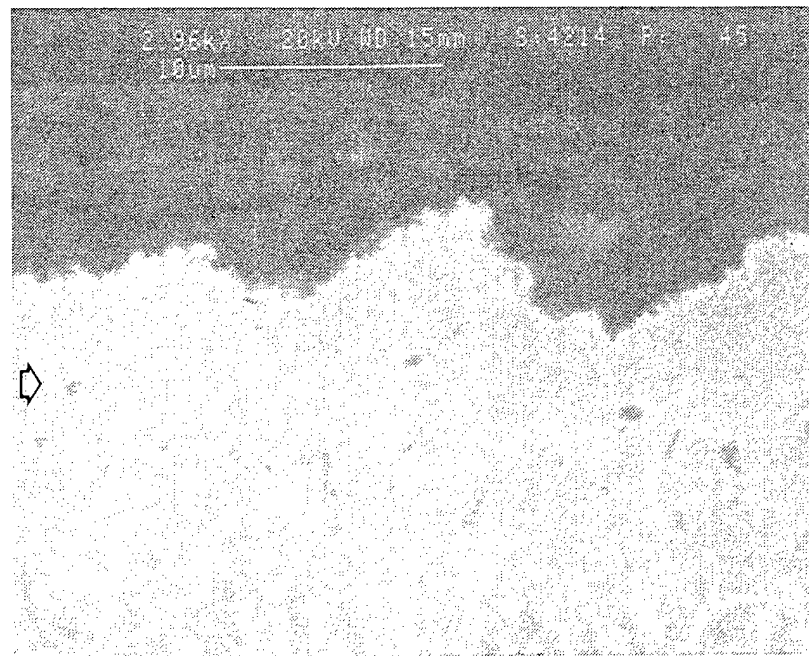
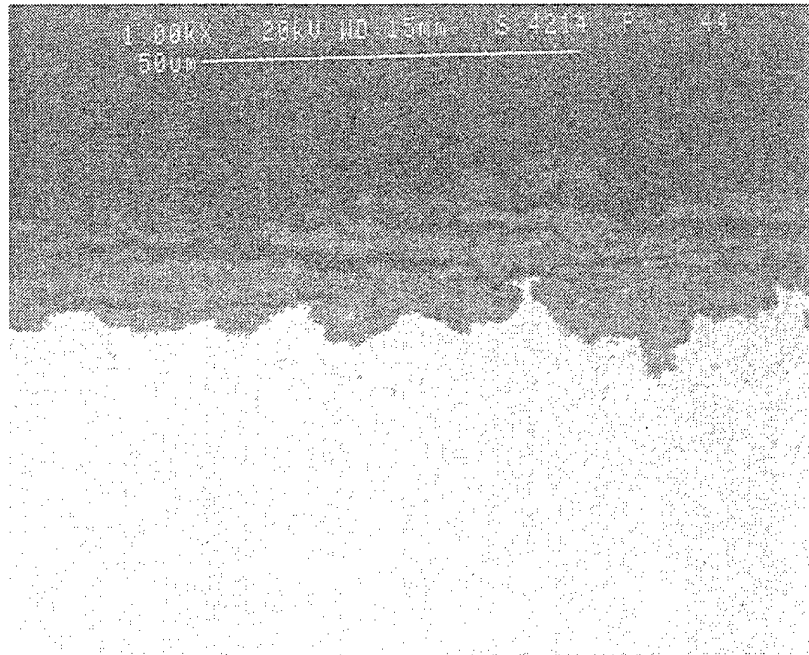


510°C (950°F) < T



820°C (1510°F) Peak Temperature

Figure 169. Micrographs showing cross sections of Codep coated R'80 after the 871/760°C burner rig test.



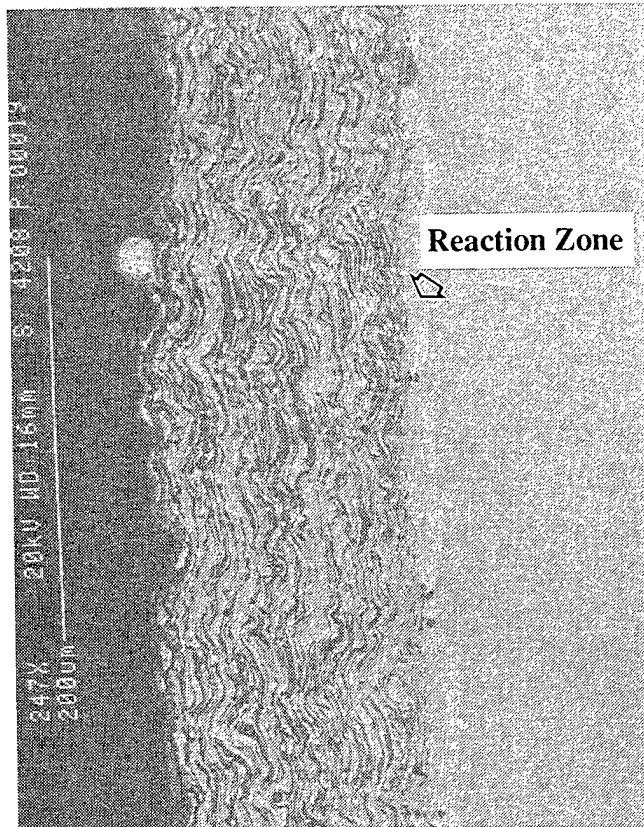
Lacy Structure



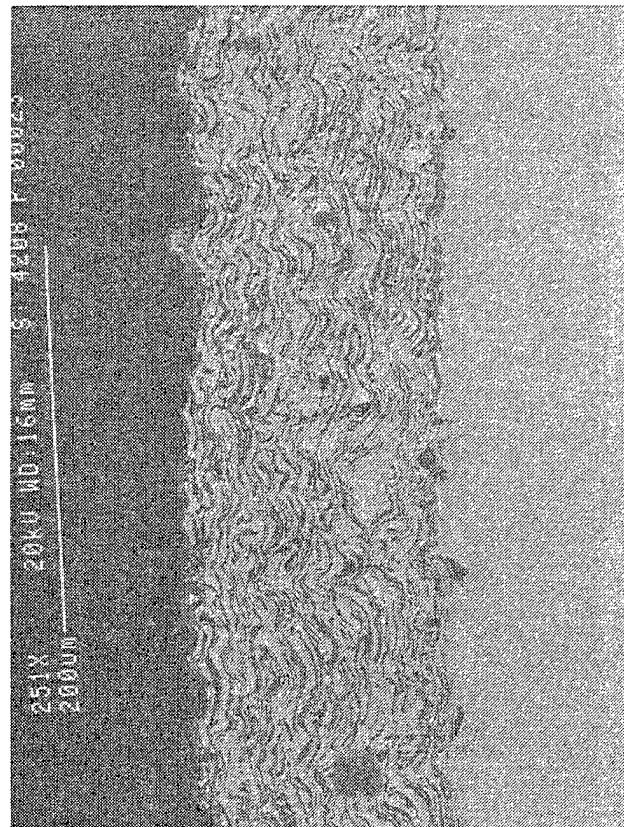
Oxidation/sulfidation

Figure 170. Micrographs showing the detail of the attack on Codep coated R'80 in the 871°C section. A lacy microstructure has formed similar to the uncoated gamma.

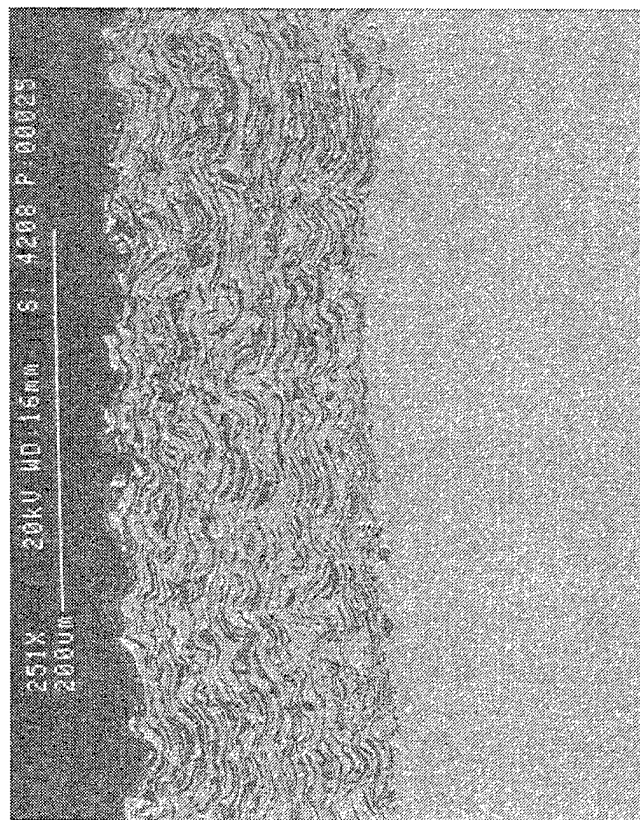
871°C (1600°F) Peak Temperature



820°C (1510°F) Peak Temperature



760°C (1400°F) Peak Temperature



510°C (950°F) < T

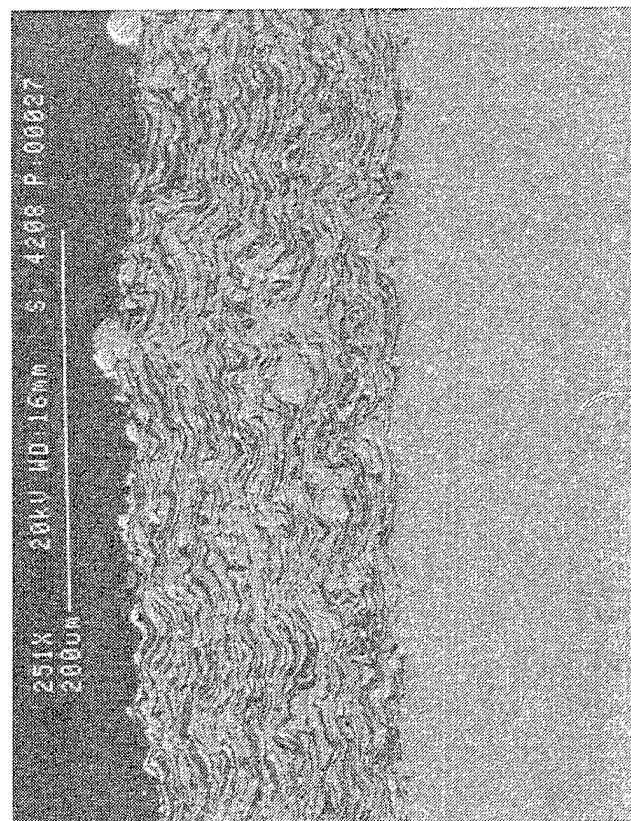
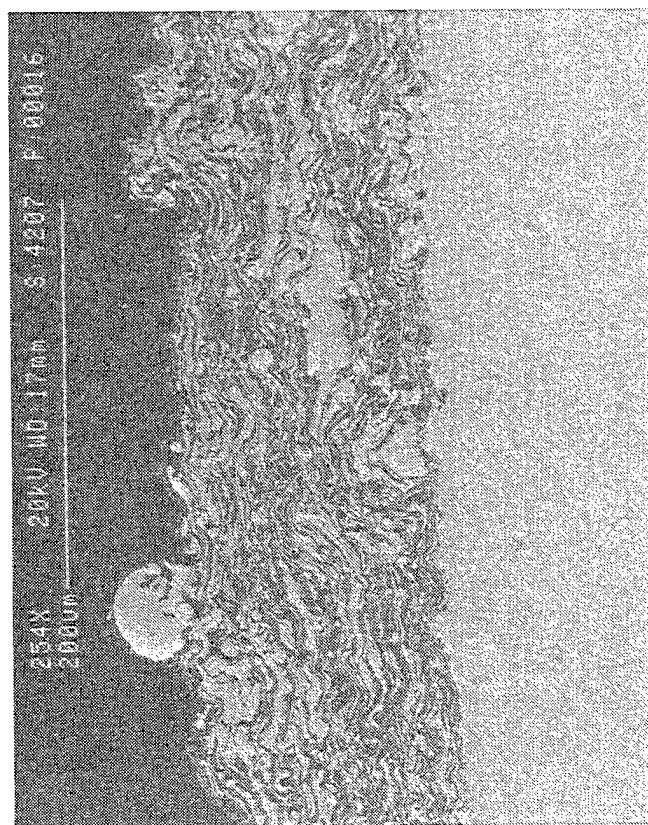


Figure 171. Micrographs showing cross sections of the NiCoCrAlY cermet (M³) coated gamma after the 871/760°C burner rig test.

760°C (1400°F) Peak Temperature



871°C (1600°F) Peak Temperature

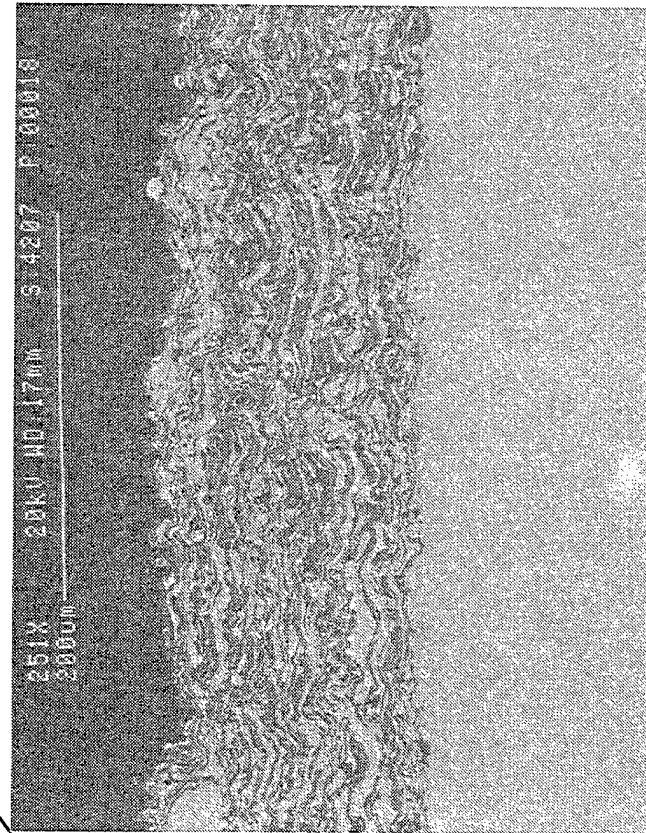
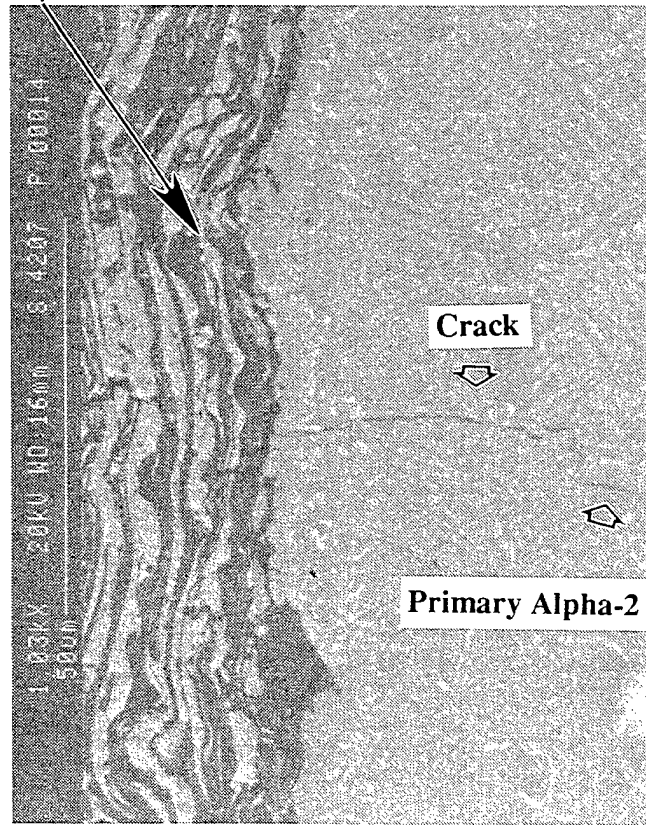
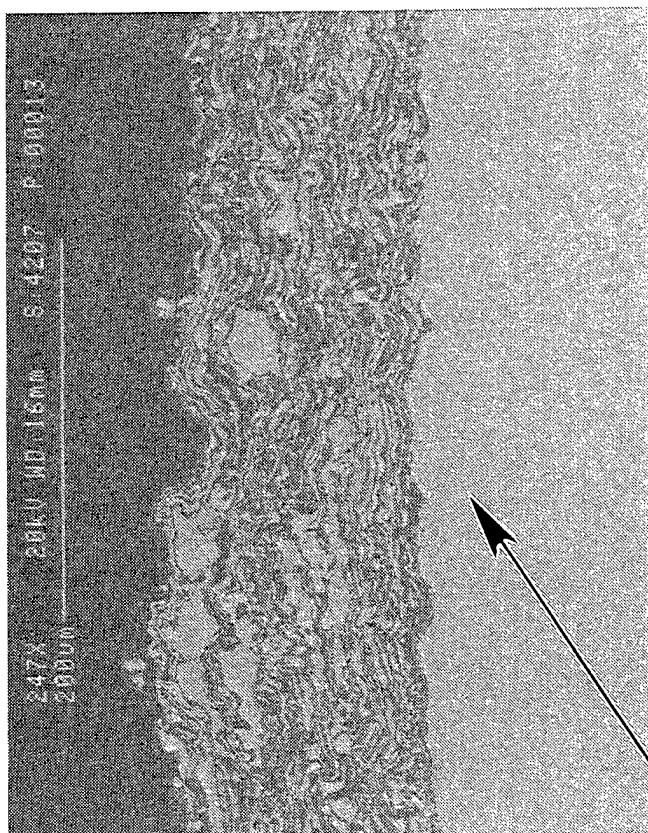
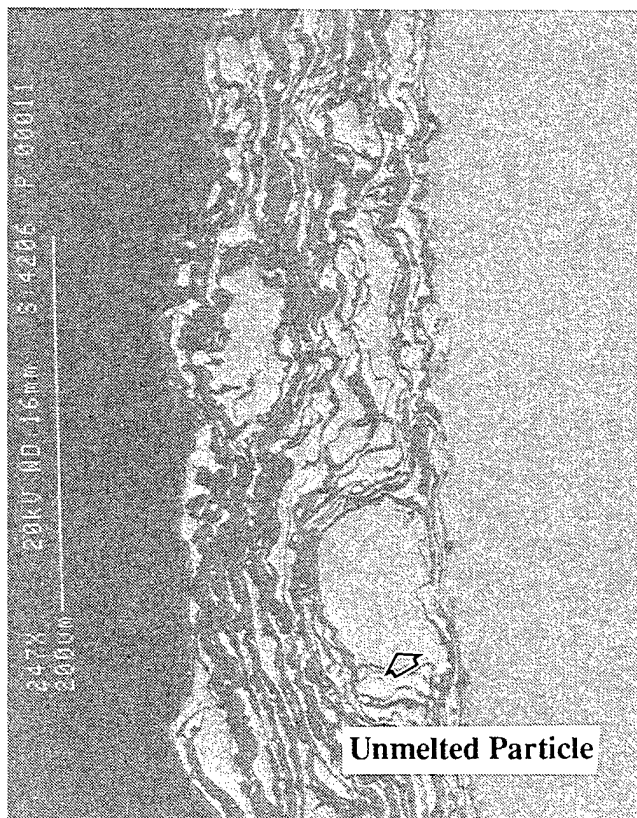
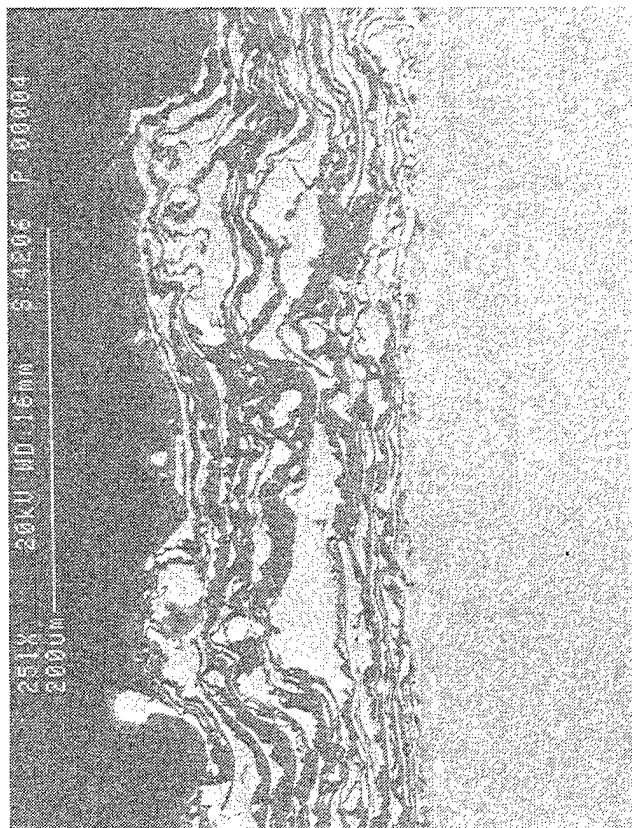


Figure 172. Micrographs showing cross sections of the CoCrAlY cermet (M^3) coated gamma after the 871/760°C burner rig test.

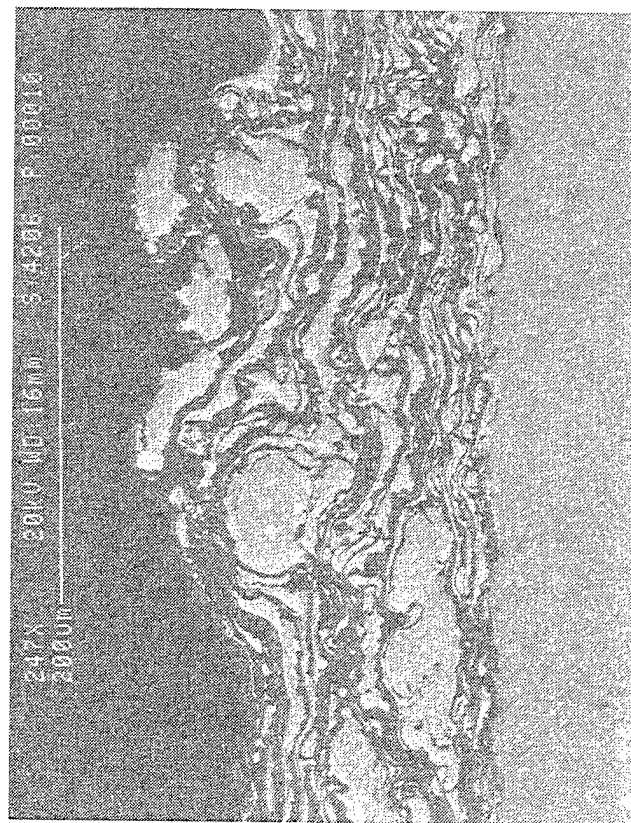
760°C (1400°F) Peak Temperature



871°C (1600°F) Peak Temperature



510°C (950°F) < T



820°C (1510°F) Peak Temperature

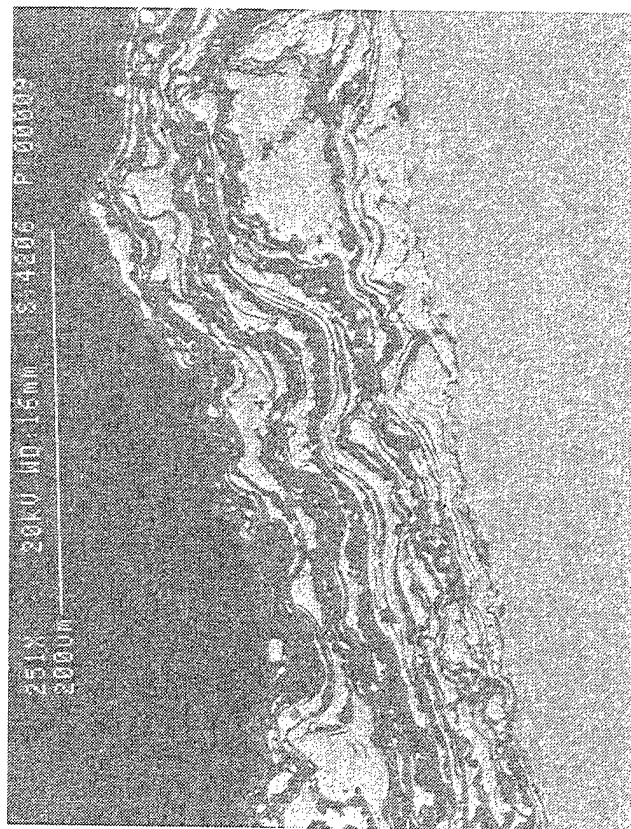
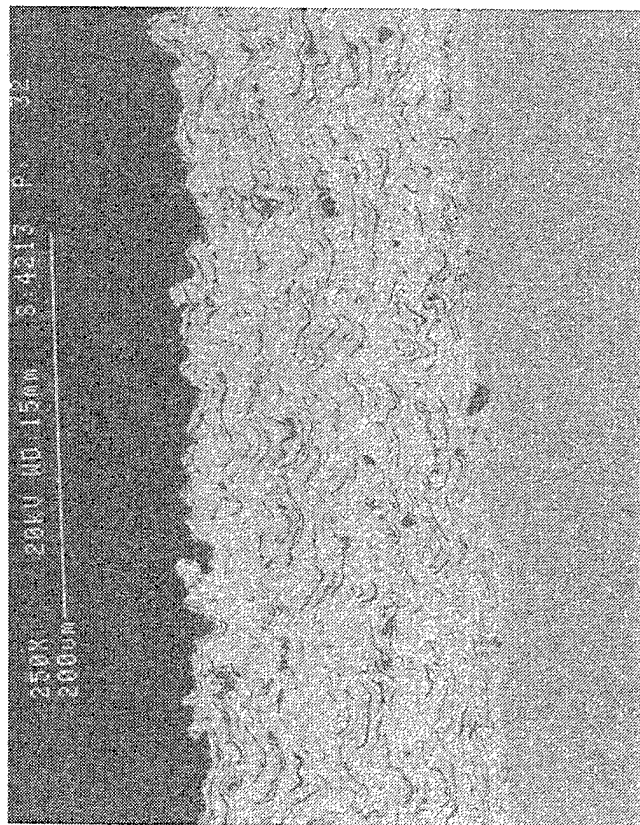
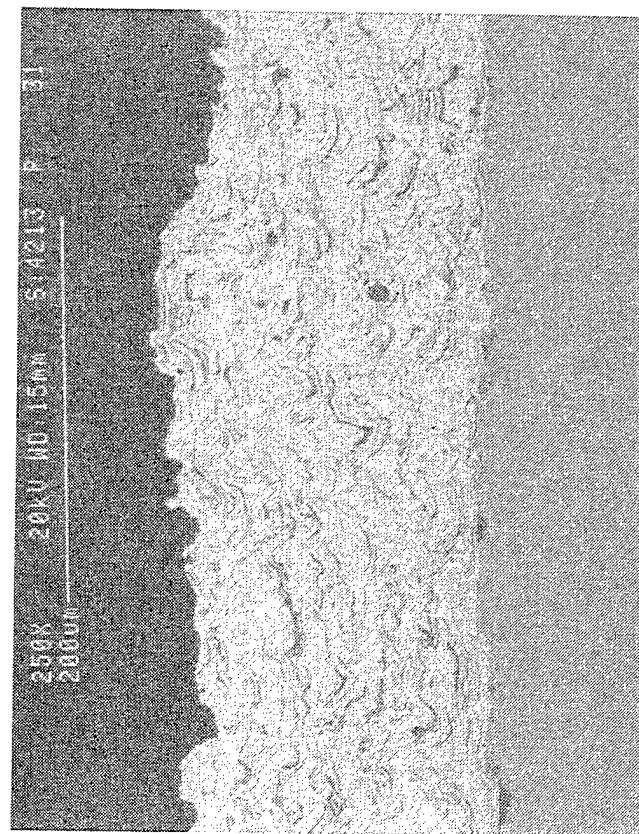
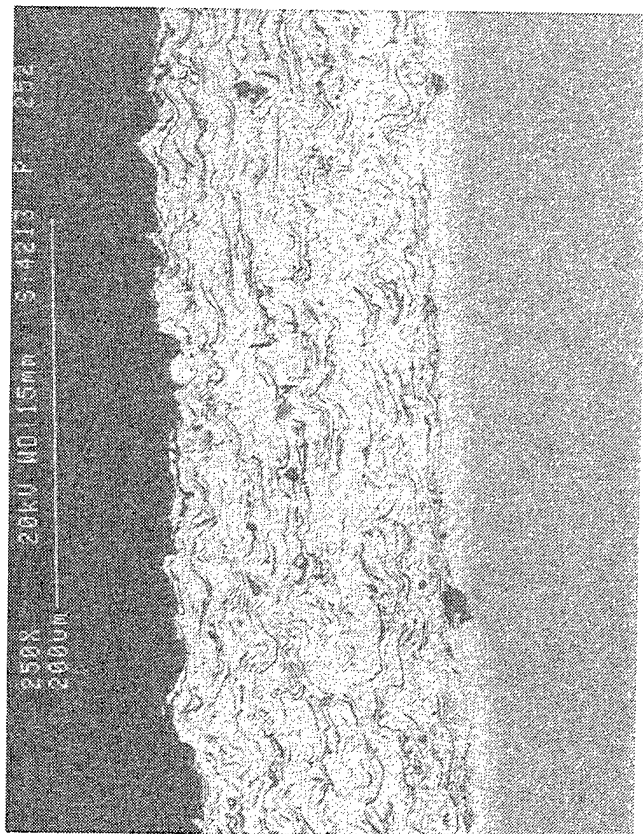


Figure 173. Micrographs showing cross sections of the Alloy 718 cermet (M³) coated gamma after the 871/760°C burner rig test.

760°C (1400°F) Peak Temperature



871°C (1600°F) Peak Temperature



510°C (950°F) < T

820°C (1510°F) Peak Temperature

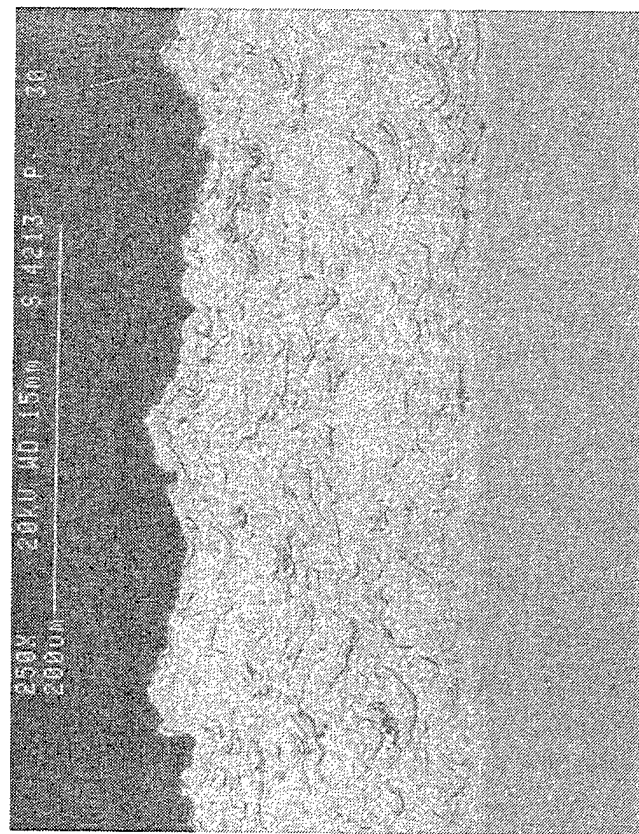
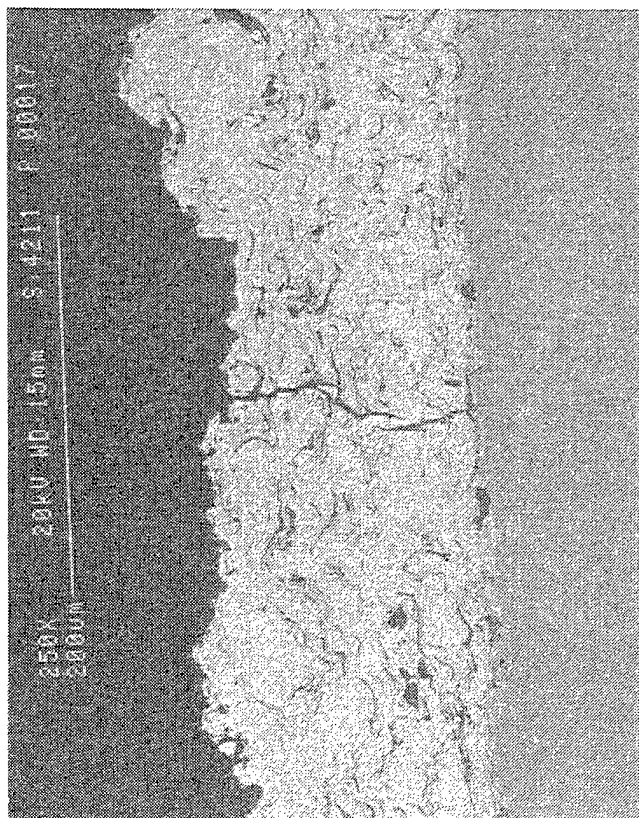
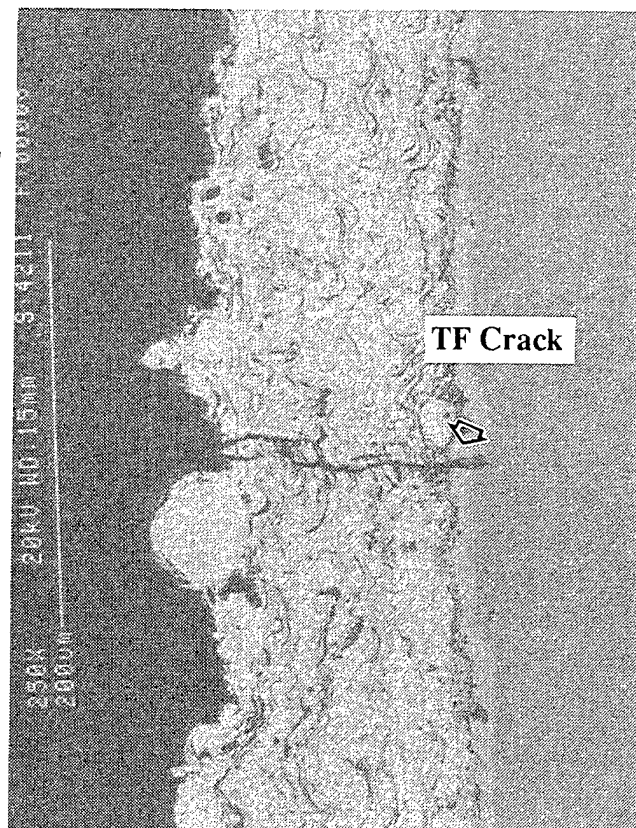


Figure 174. Micrographs showing cross sections of the NiCrAlY cermet (M^3) coated alpha-2 after the 871/760°C burner rig test.

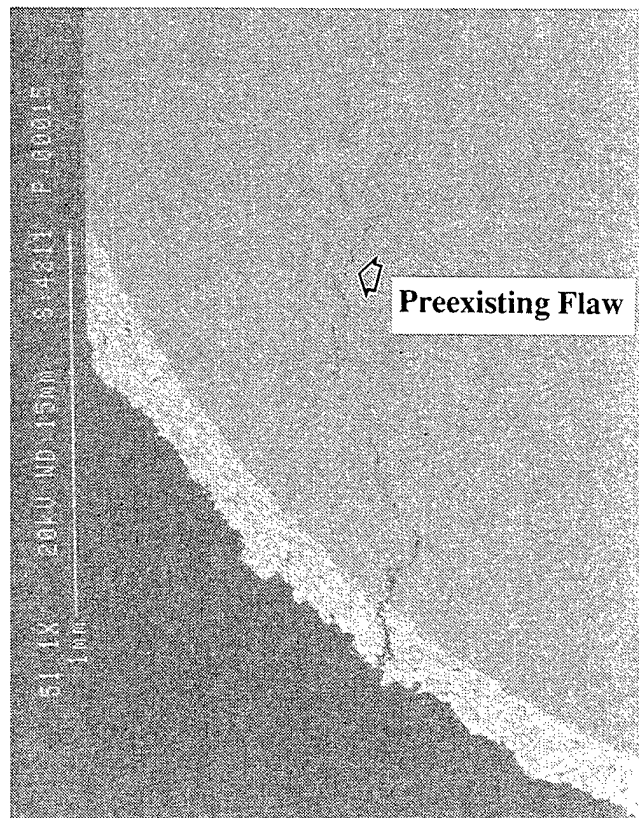
760°C (1400°F) Peak Temperature



871°C (1600°F) Peak Temperature



510°C (950°F) < T



820°C (1510°F) Peak Temperature

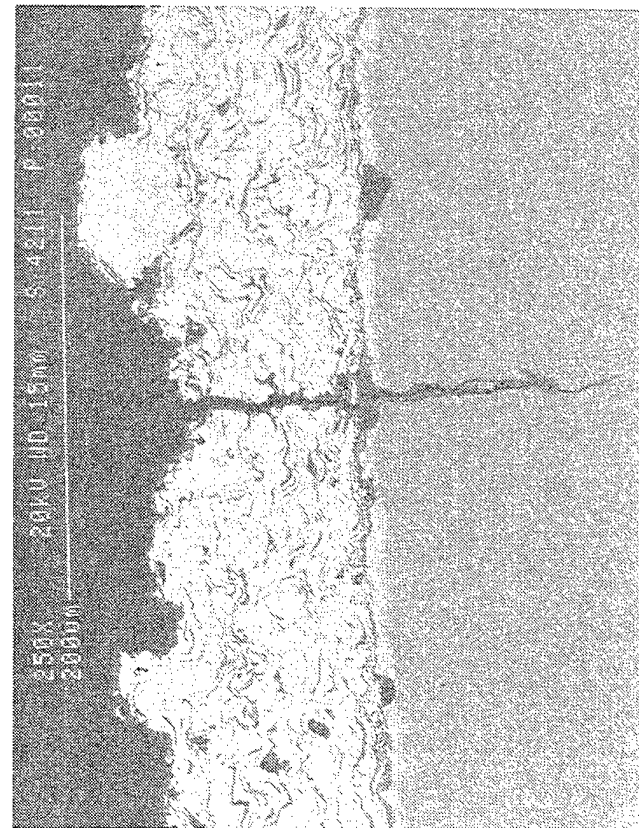
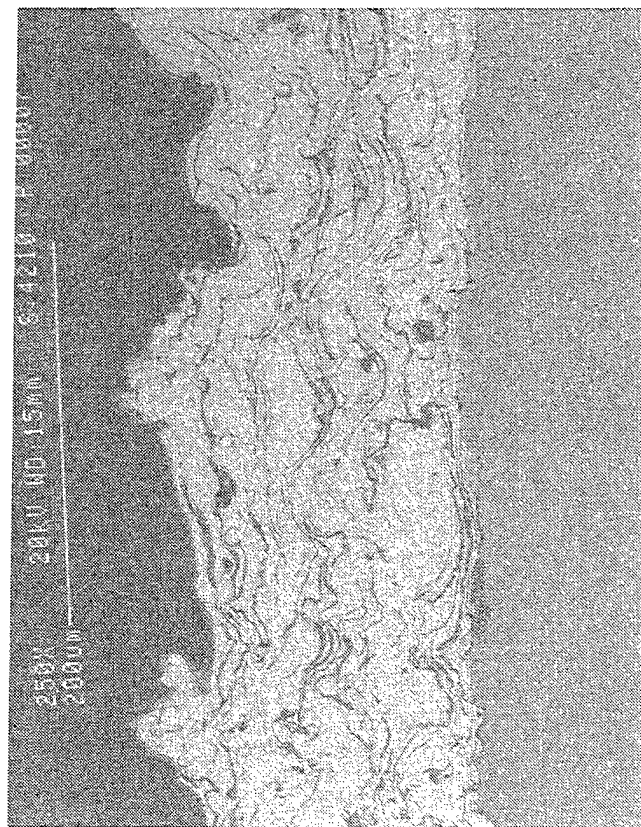
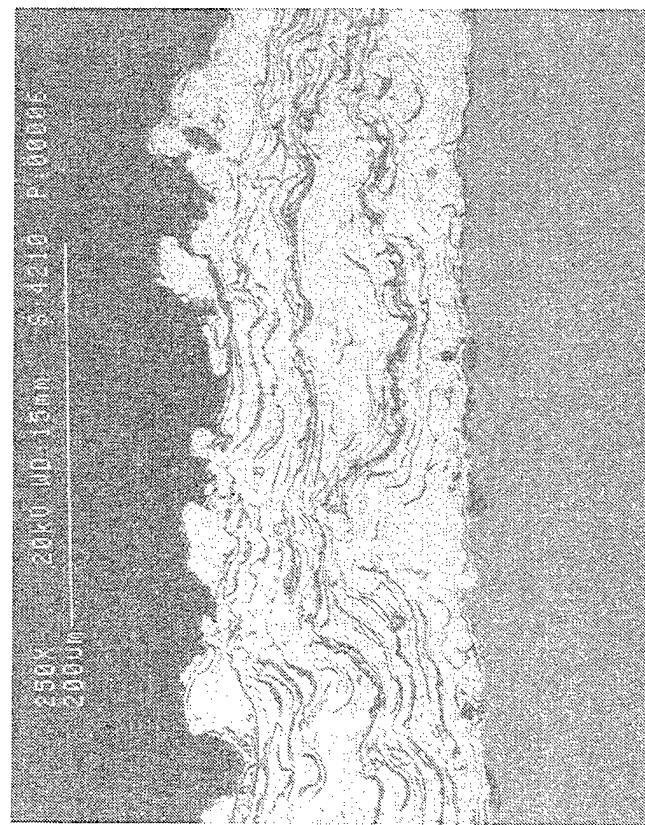
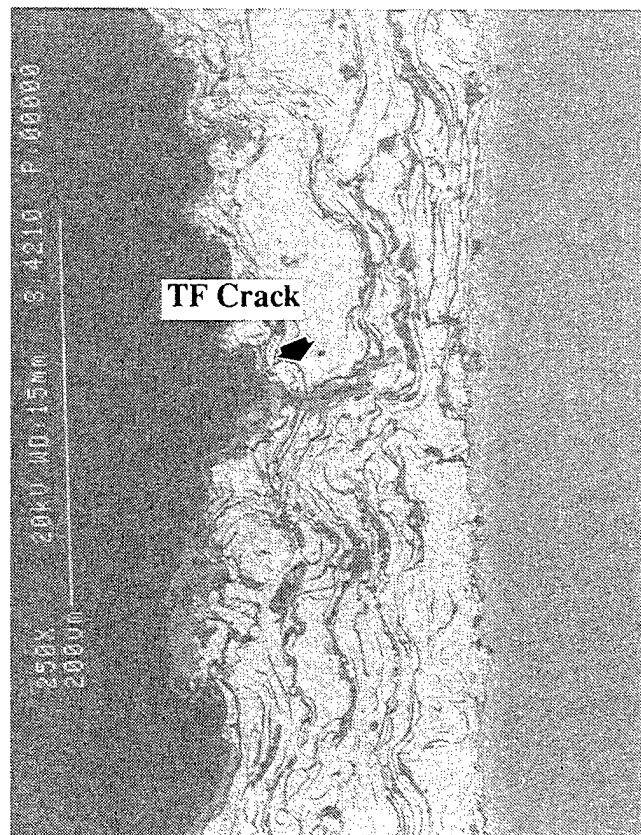


Figure 175. Micrographs showing cross sections of the CoCrAlY cermet (M³) coated alpha-2 after the 871/760°C burner rig test.

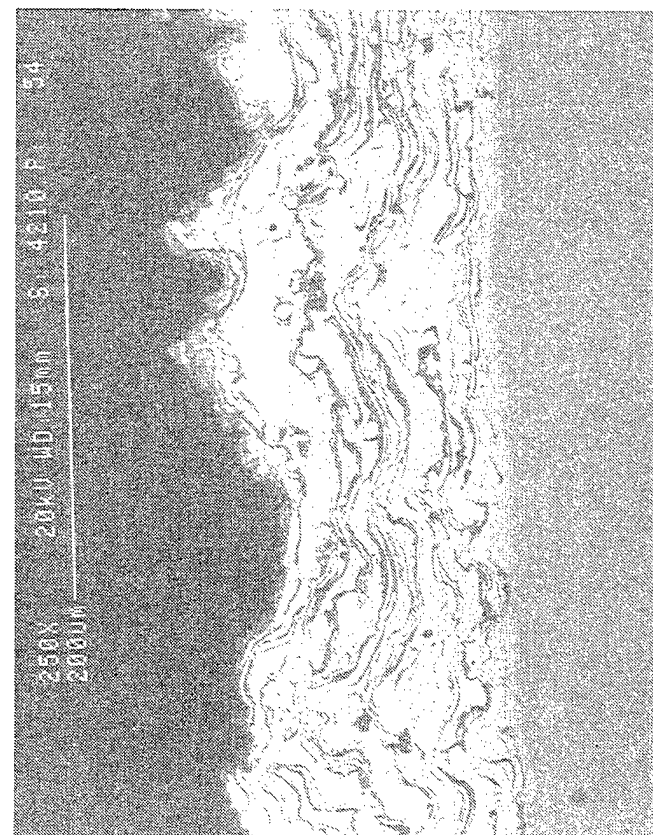
760°C (1400°F) Peak Temperature



871C (1600°F) Peak Temperature



510°C (950°F) < T



820°C (1510°F) Peak Temperature

Figure 176. Micrographs showing cross sections of the Alloy 718 cermet (M³) coated alpha-2 after the 871/760°C burner rig test.

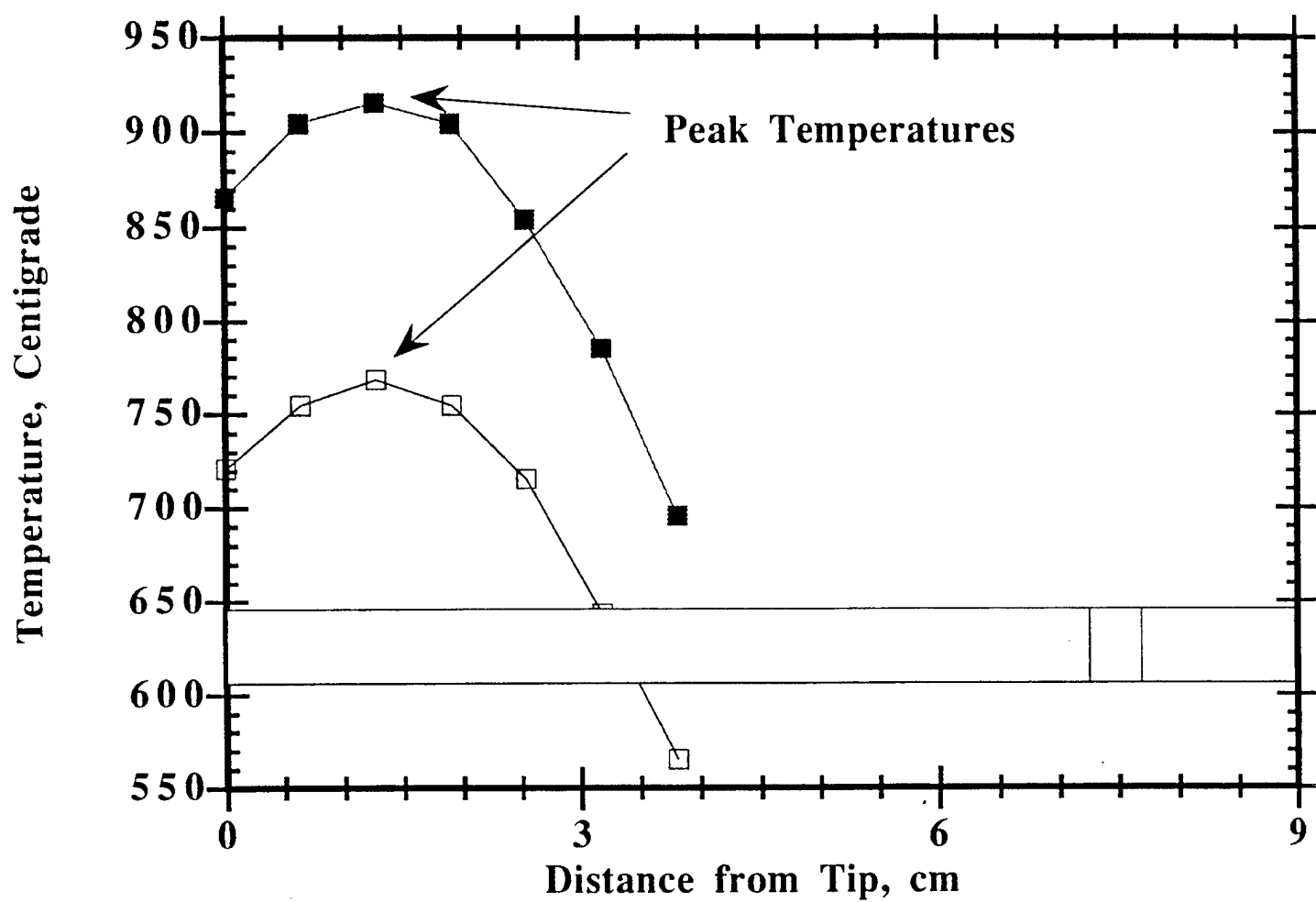


Figure 177. Graph showing the temperature distribution in pins tested in the 900/760°C burner rig test without salt.

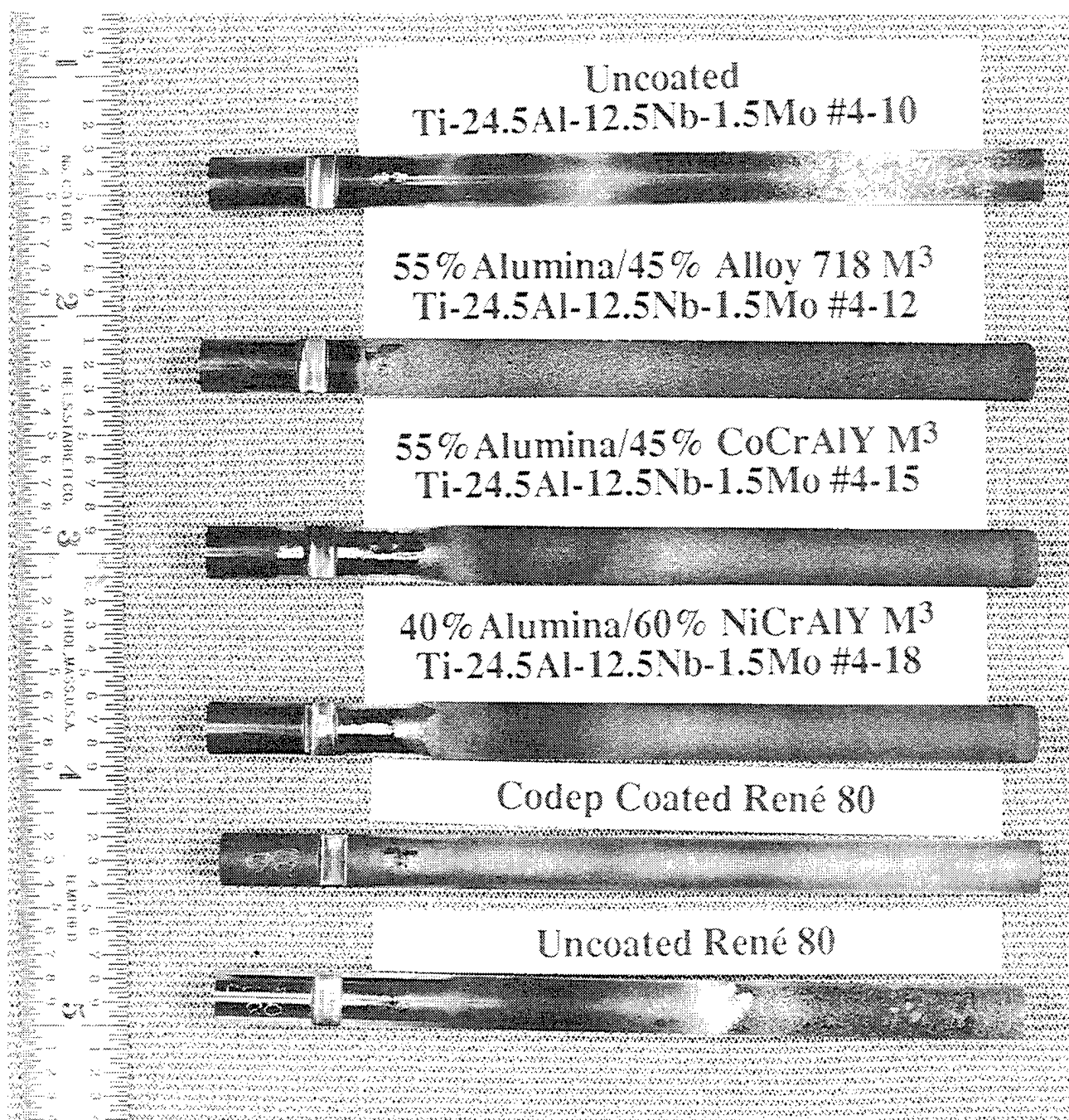


Figure 178. Color photograph showing the alpha-2 systems after the 900/760°C burner rig test with no salt.

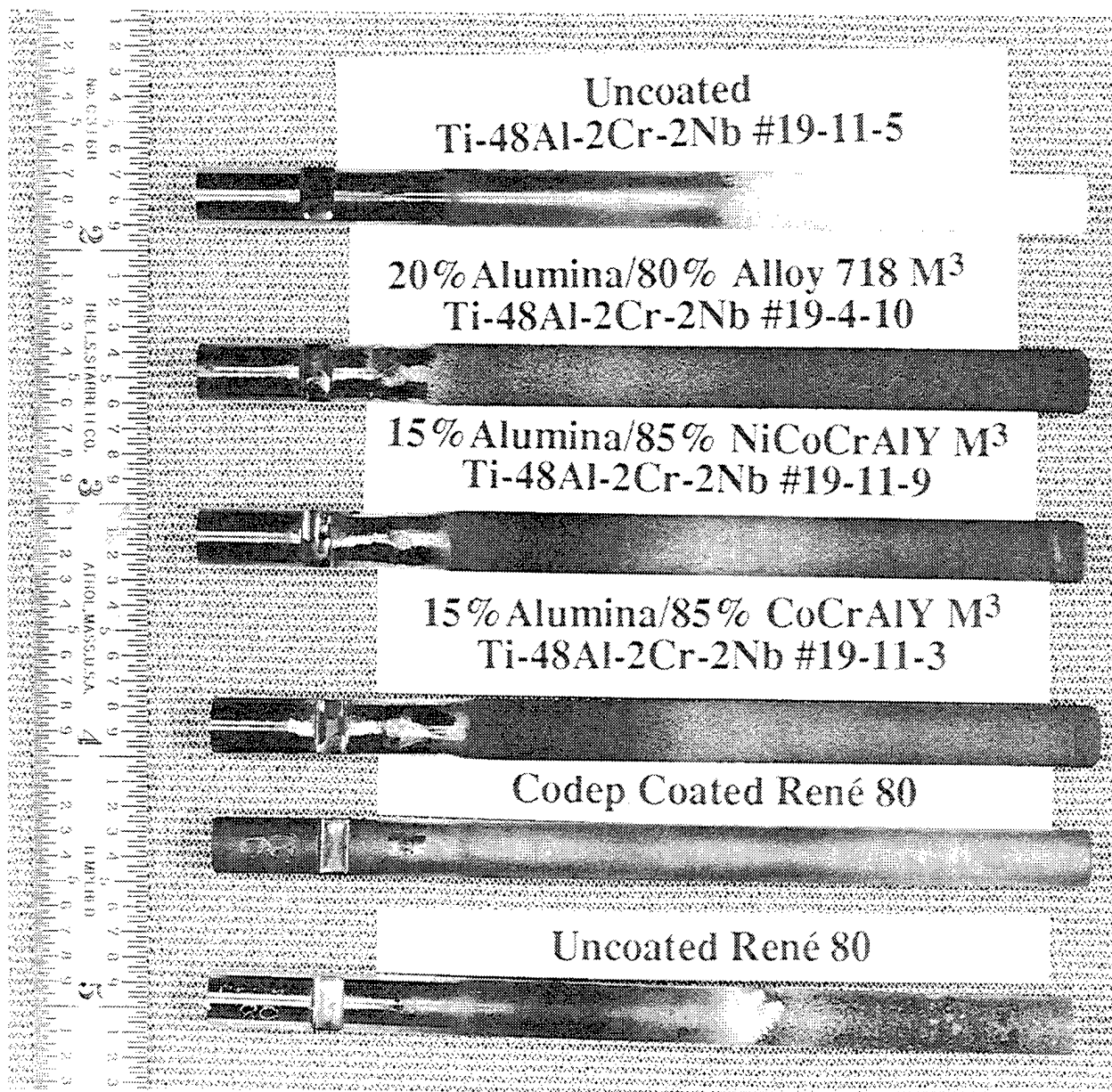


Figure 179. Color photograph showing the gamma systems after the 900/760°C burner rig test with no salt.

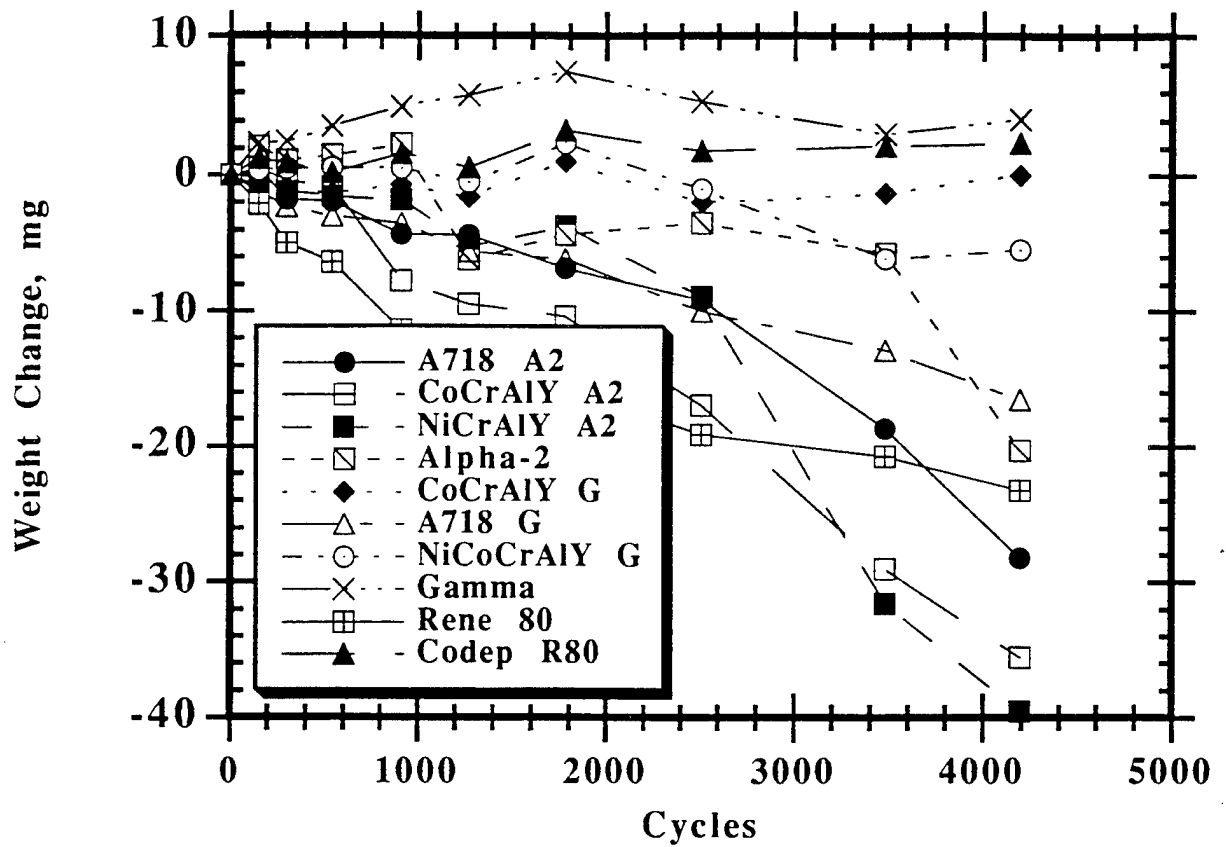
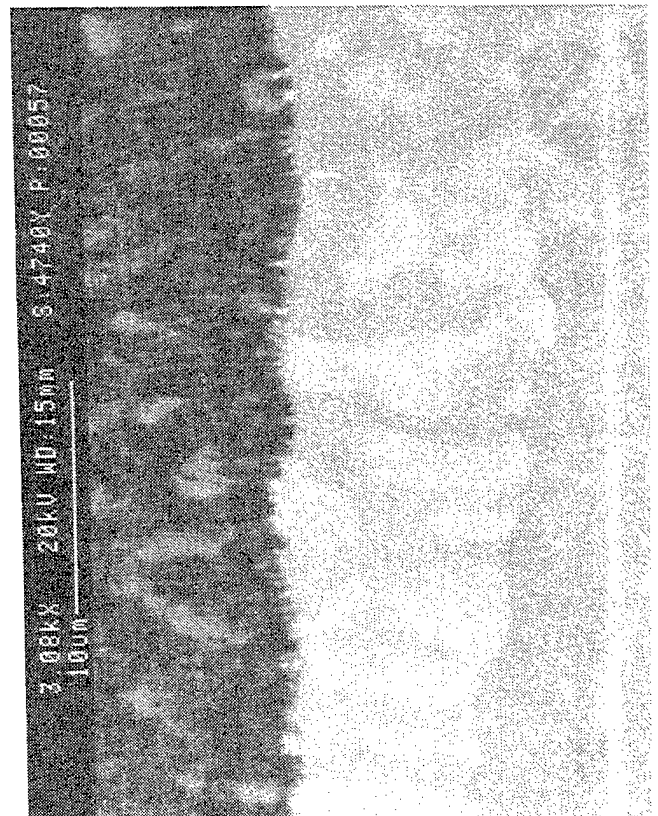
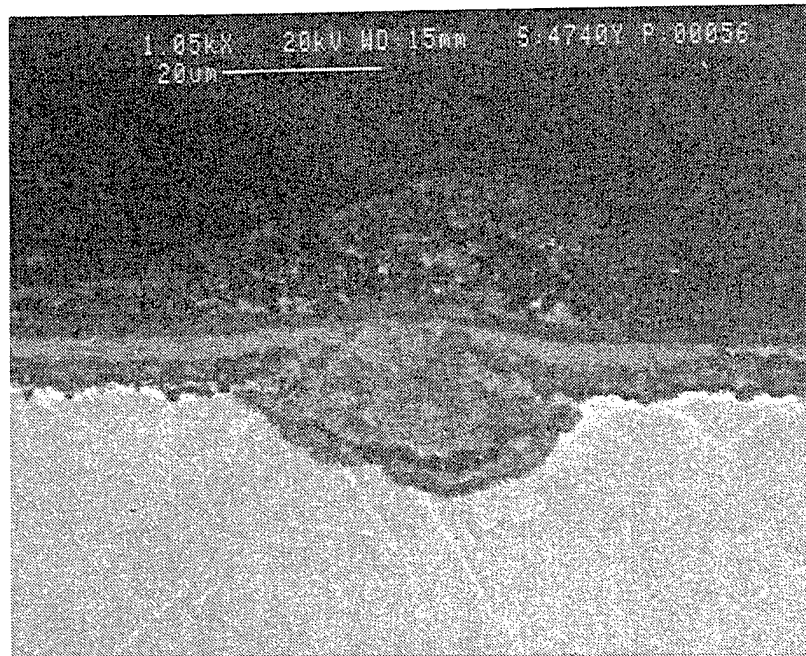


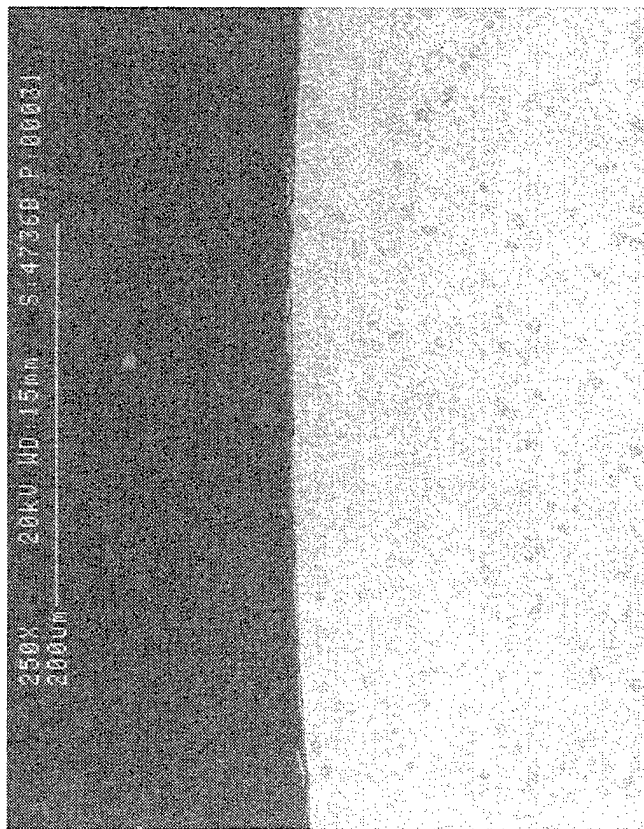
Figure 180. Graph showing the weight change of all the samples during the 900/760°C burner rig test with no salt.



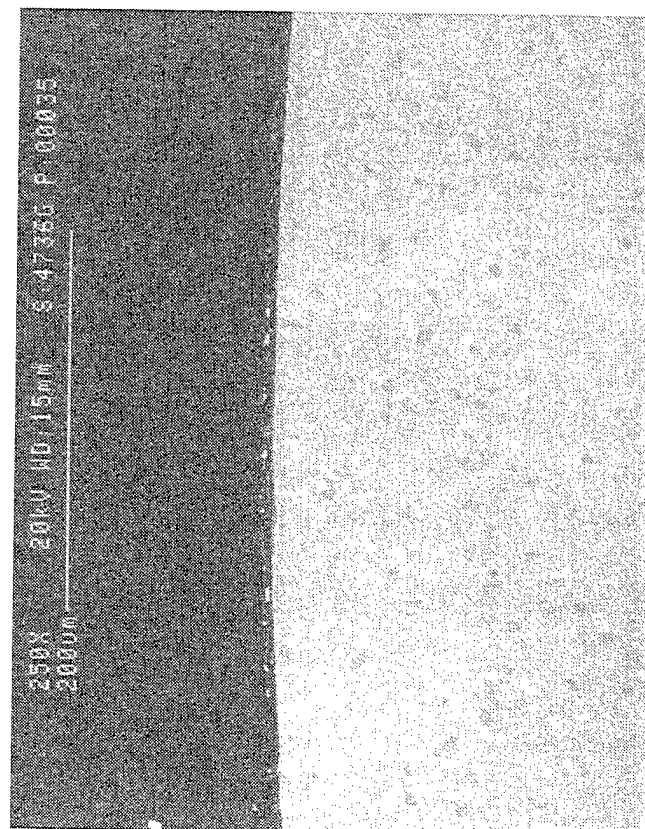
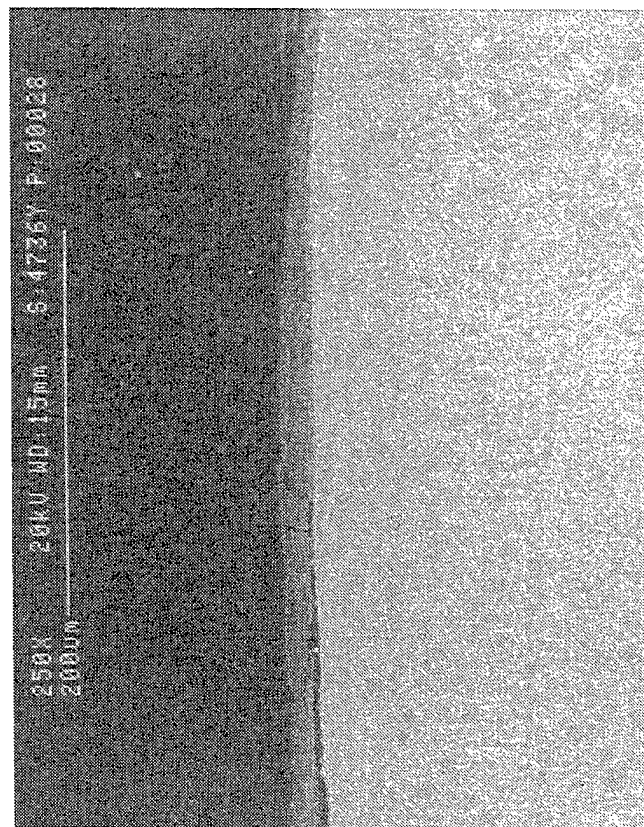
⌆
Cellular Morphology

Figure 181. Micrographs showing the 900°C section of the uncoated gamma after 900/760°C burner rig testing with no salt. The lacy or cellular morphology develops under the scale.

760°C (1400°F) Peak Temperature



900C (1650°F) Peak Temperature



510°C (950°F) < T

830°C (1520°F) Peak Temperature

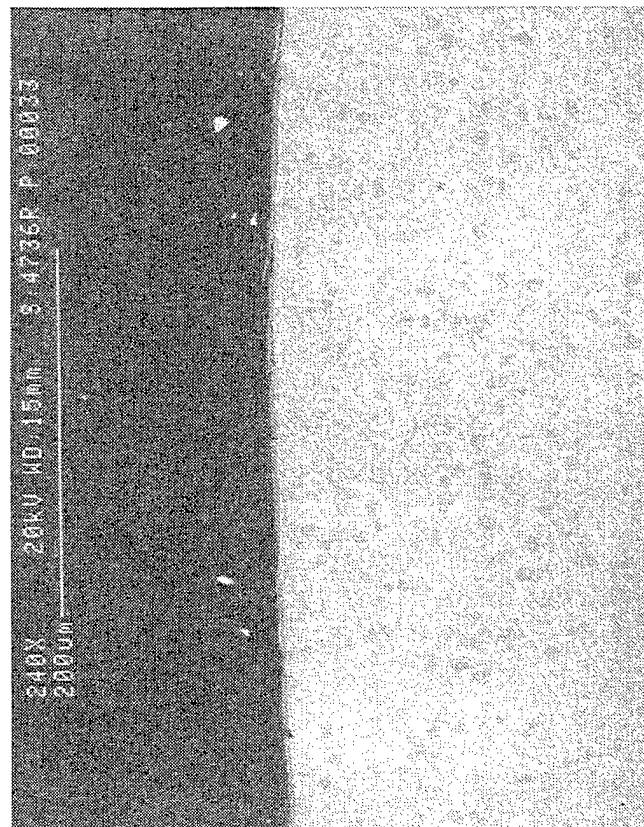
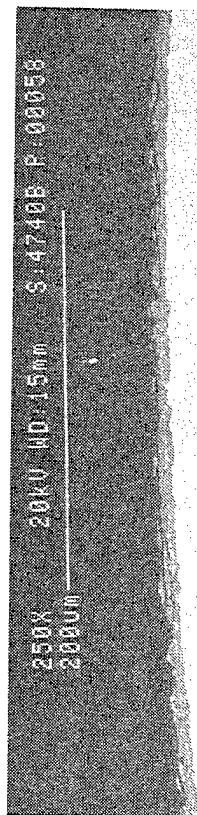
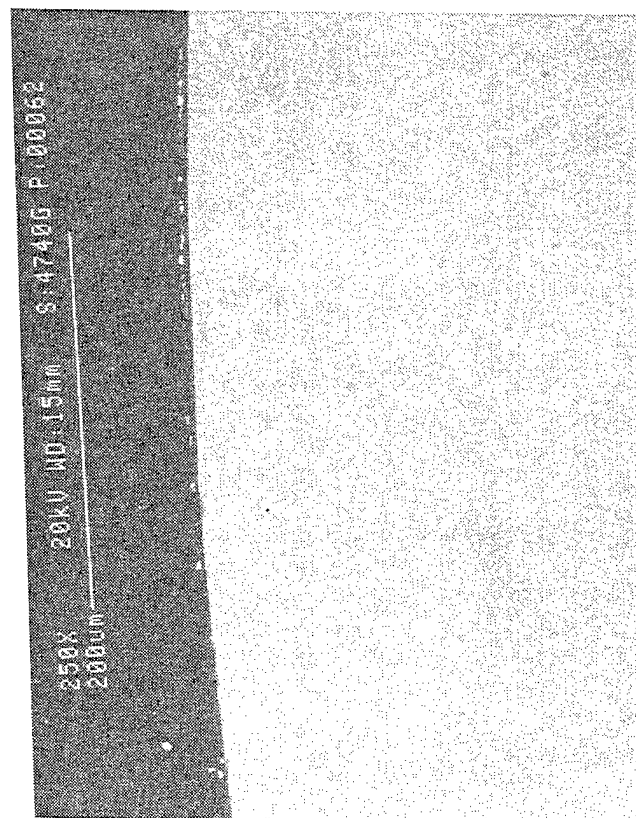
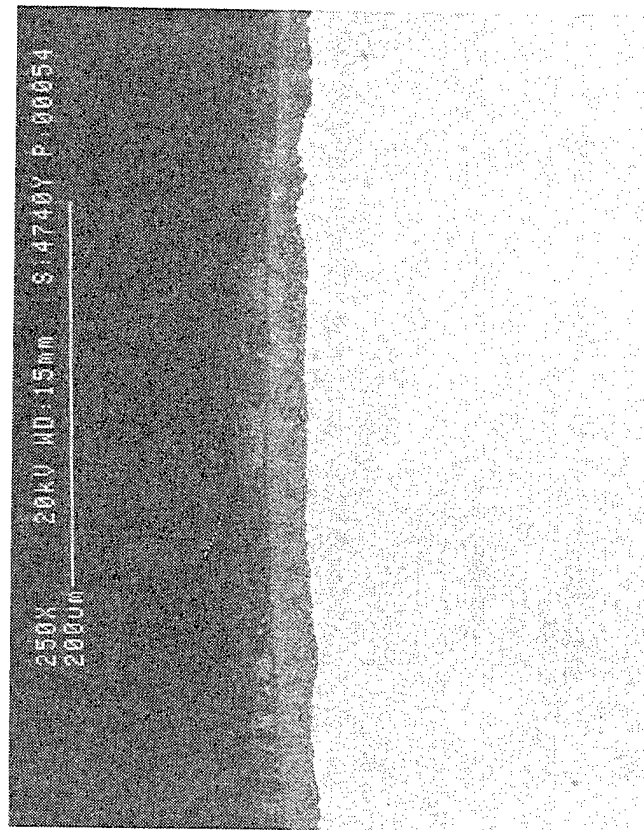


Figure 182. Micrographs showing cross sections of the uncoated alpha-2 as a function of peak temperature attained during 900/760°C burner rig testing with no salt.

760°C (1400°F) Peak Temperature



900°C (1650°F) Peak Temperature



510°C (950°F) < T

830°C (1520°F) Peak Temperature

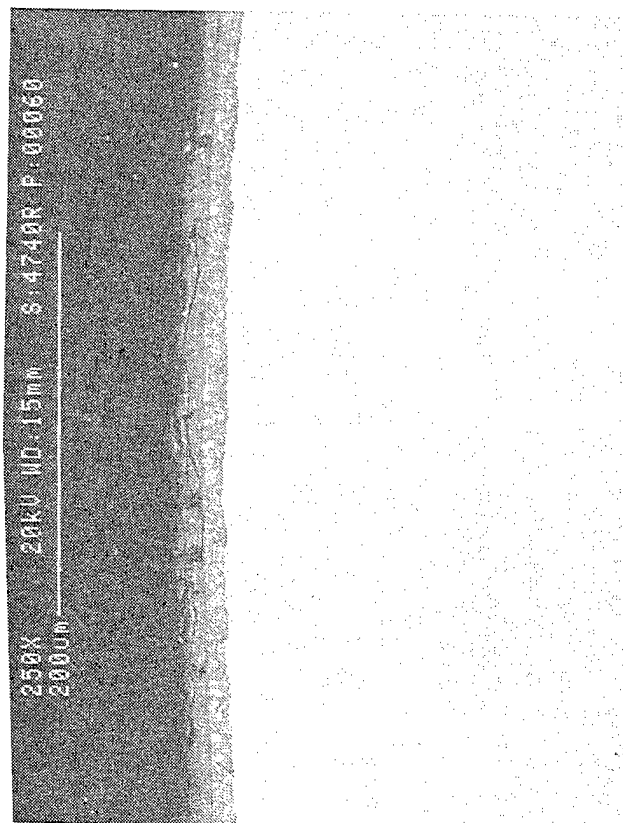
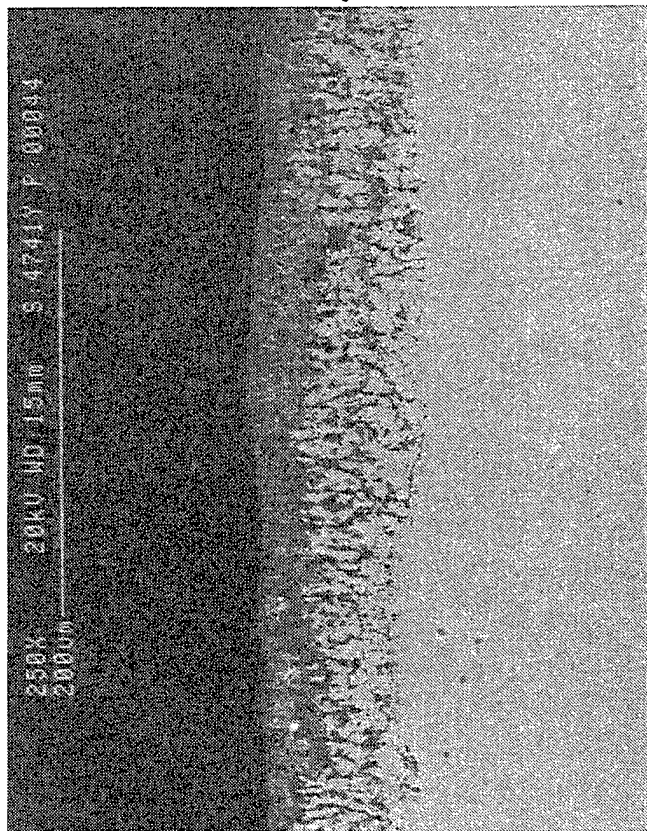


Figure 183. Micrographs showing cross sections of the uncoated alpha-2 as a function of peak temperature attained during 900/760°C burner rig testing with no salt.

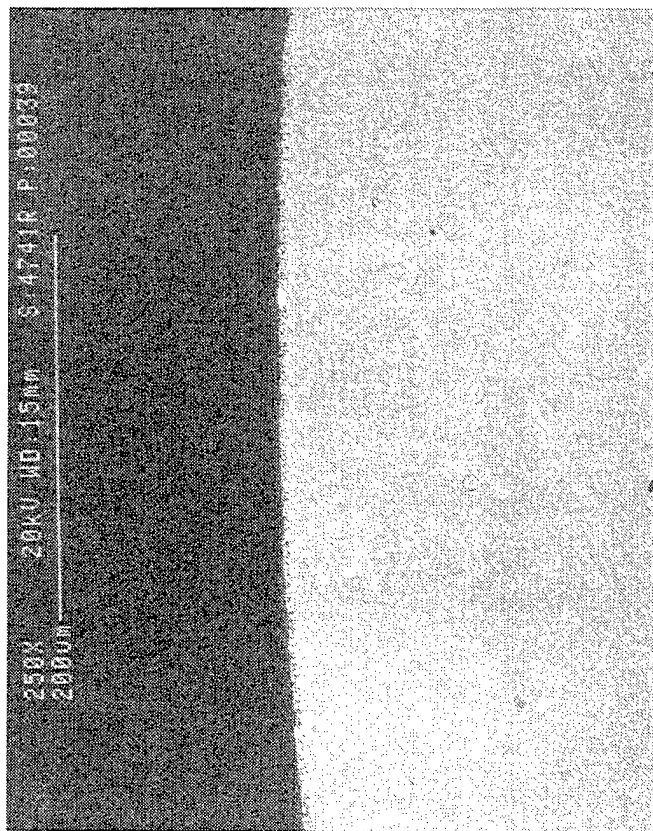
Internal Oxidation



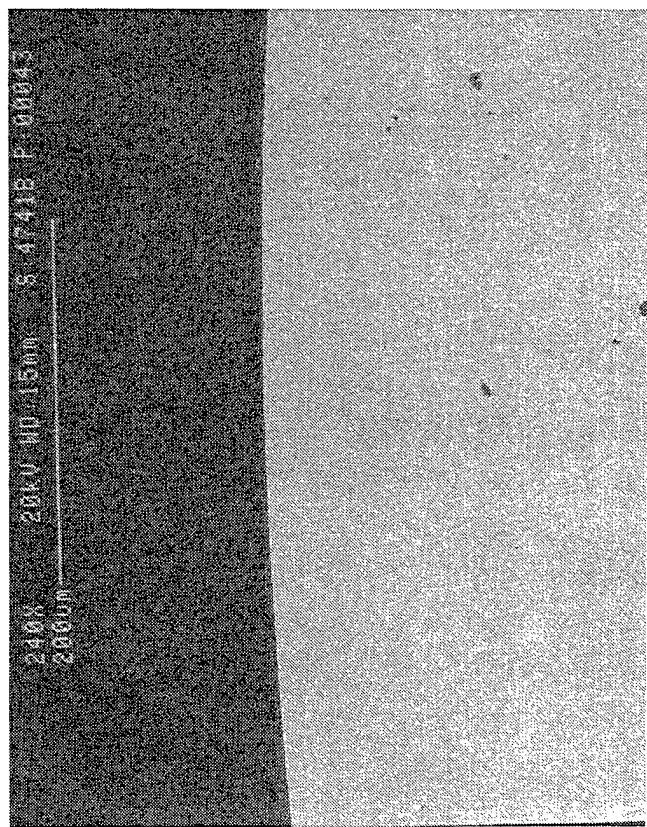
900°C (1650°F) Peak Temperature



830°C (1520°F) Peak Temperature



760°C (1400°F) Peak Temperature



510°C (950°F) < T

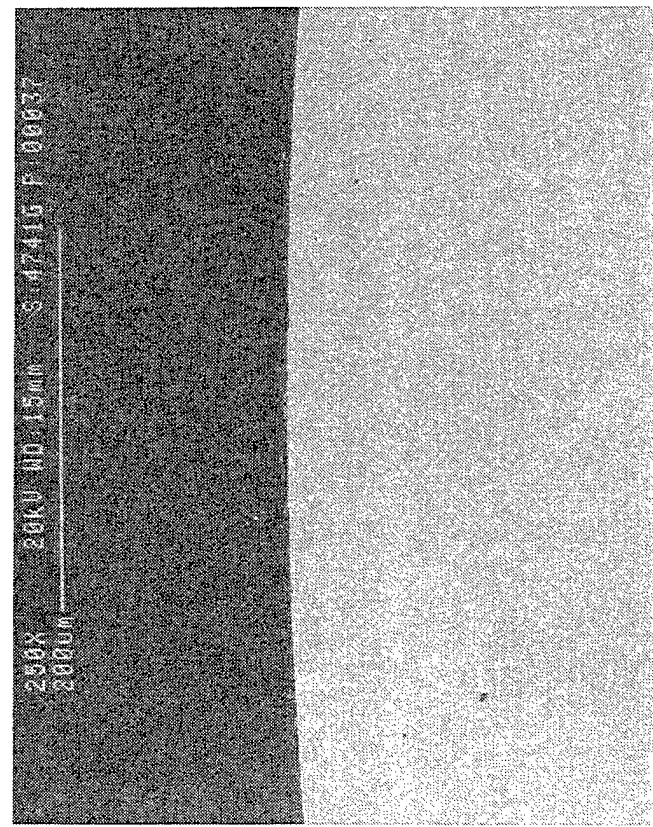
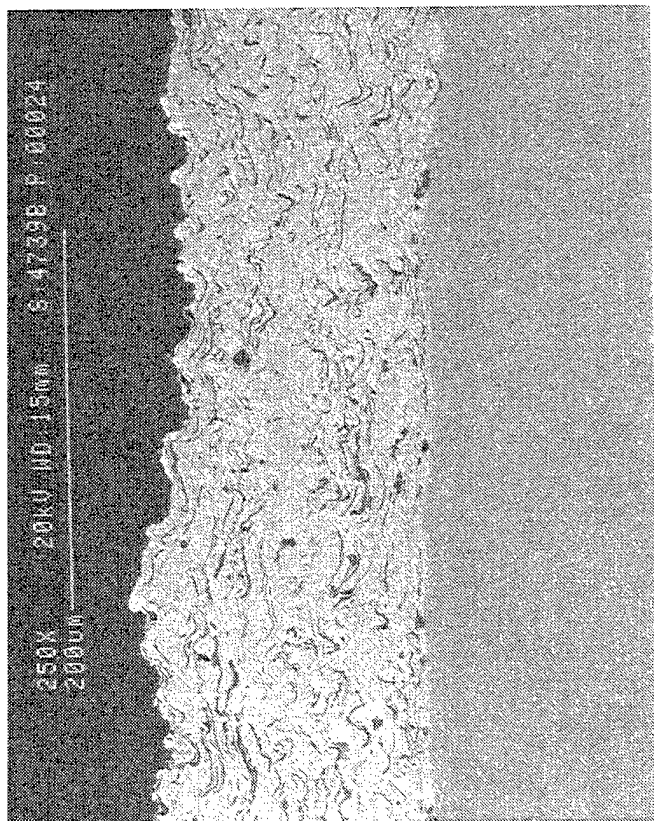
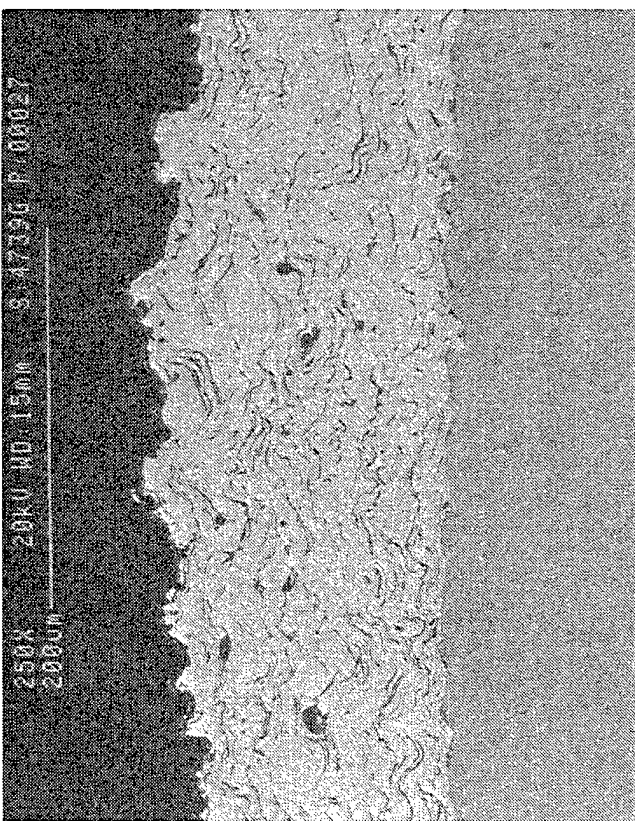
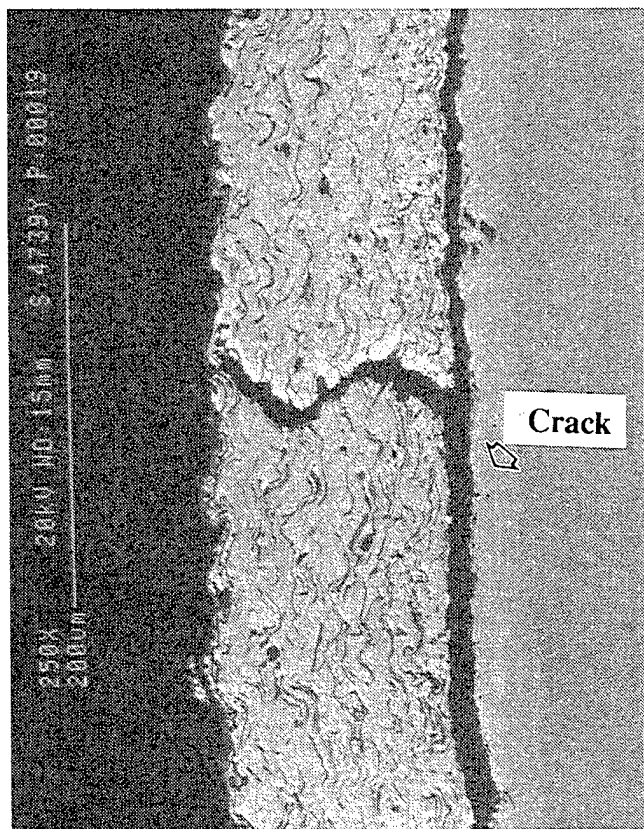


Figure 184. Micrographs showing cross sections of the uncoated R'80 as a function of peak temperature attained during 900/760°C burner rig testing with no salt.

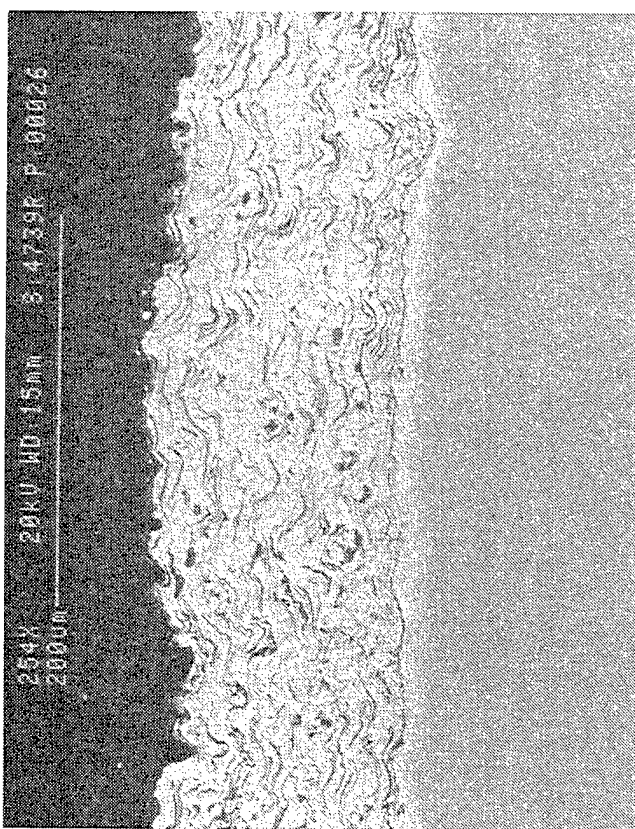
760°C (1400°F) Peak Temperature



900°C (1650°F) Peak Temperature



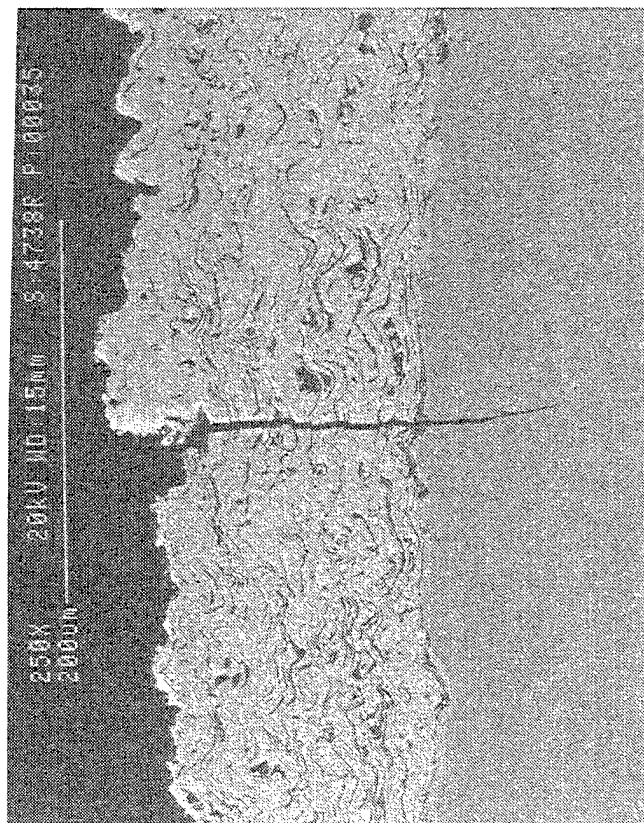
510°C (950°F) < T



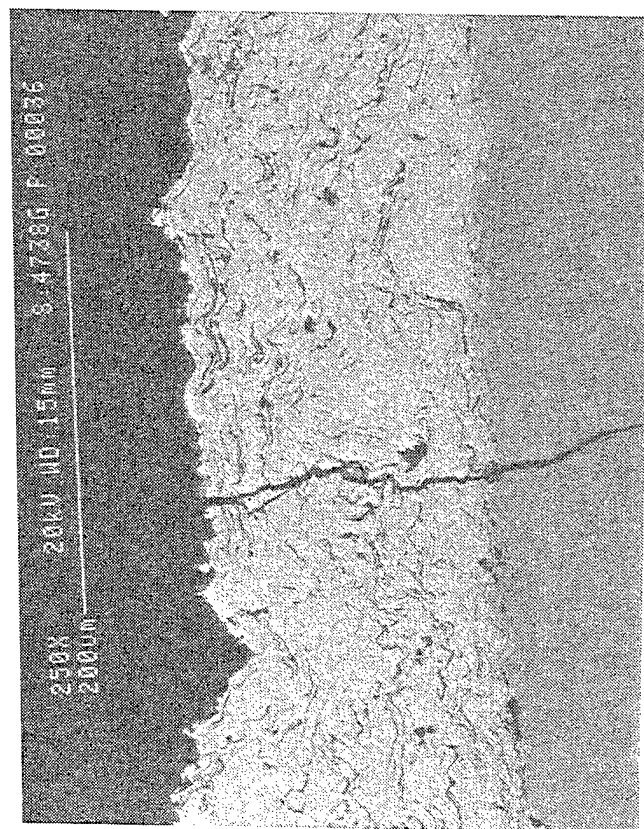
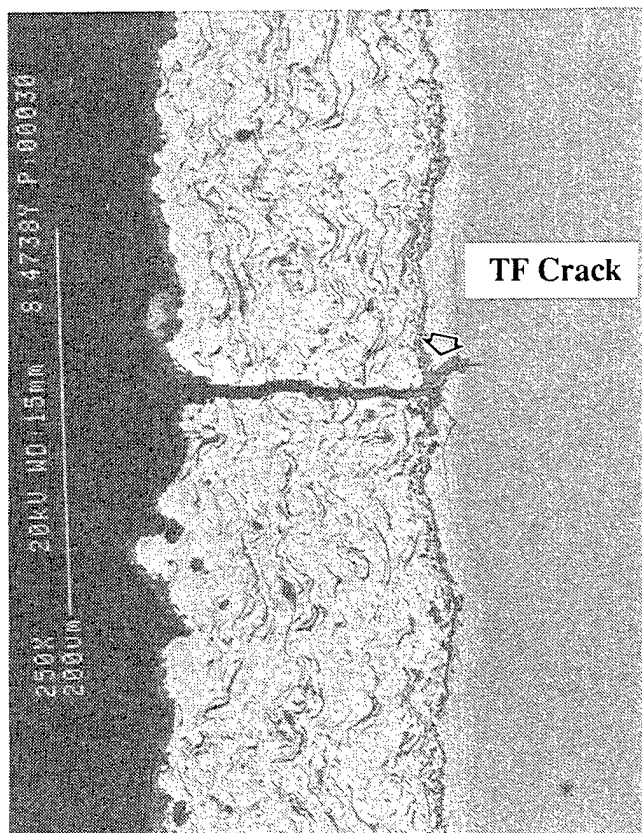
830°C (1520°F) Peak Temperature

Figure 185. Micrographs showing cross sections of the NiCoCrAlY cermet (M³) coated gamma as a function of peak temperature attained during 900/760°C burner rig testing with no salt.

760°C (1400°F) Peak Temperature



900°C (1650°F) Peak Temperature



510°C (950°F) < T

830°C (1520°F) Peak Temperature

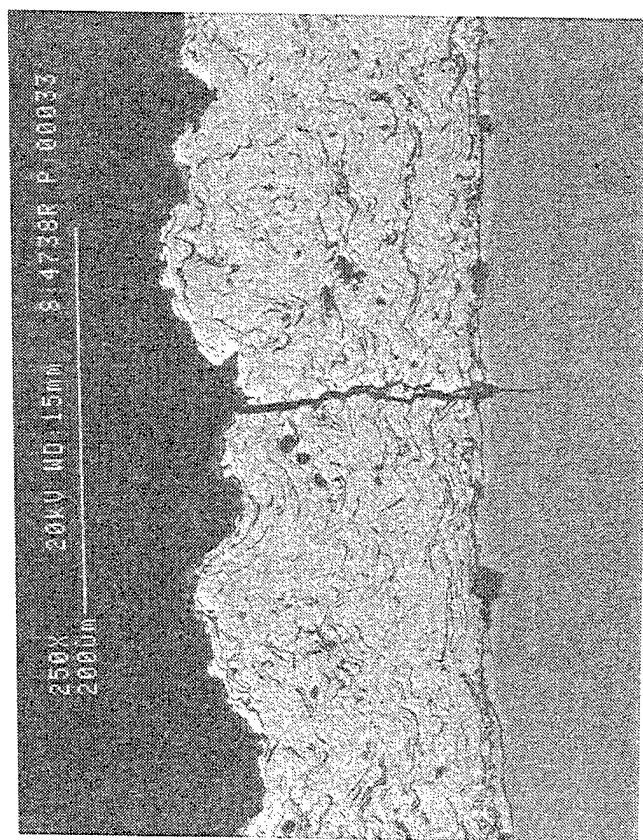
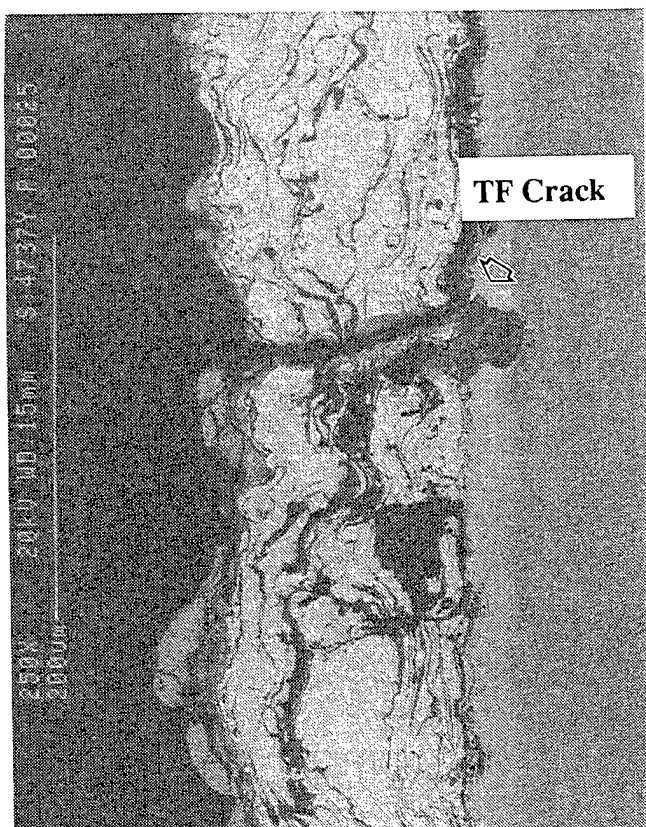
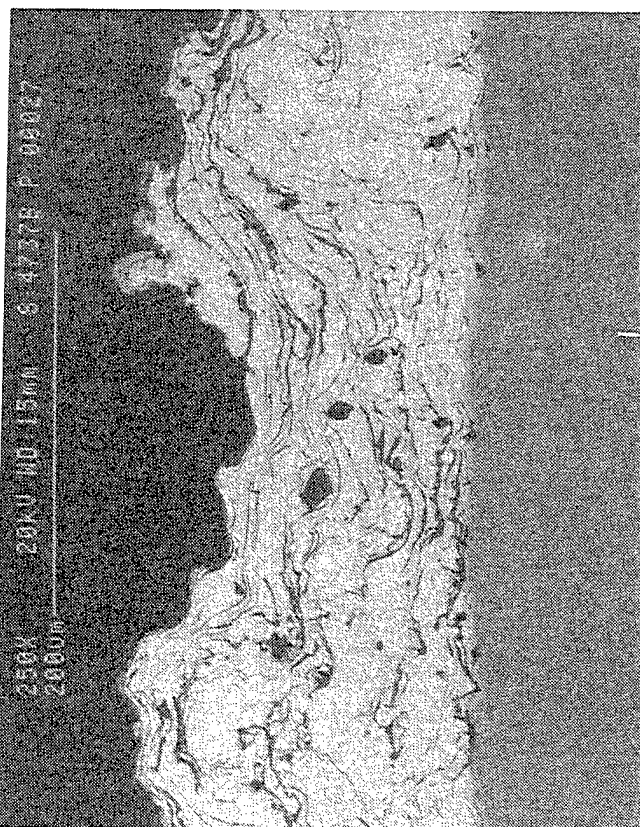
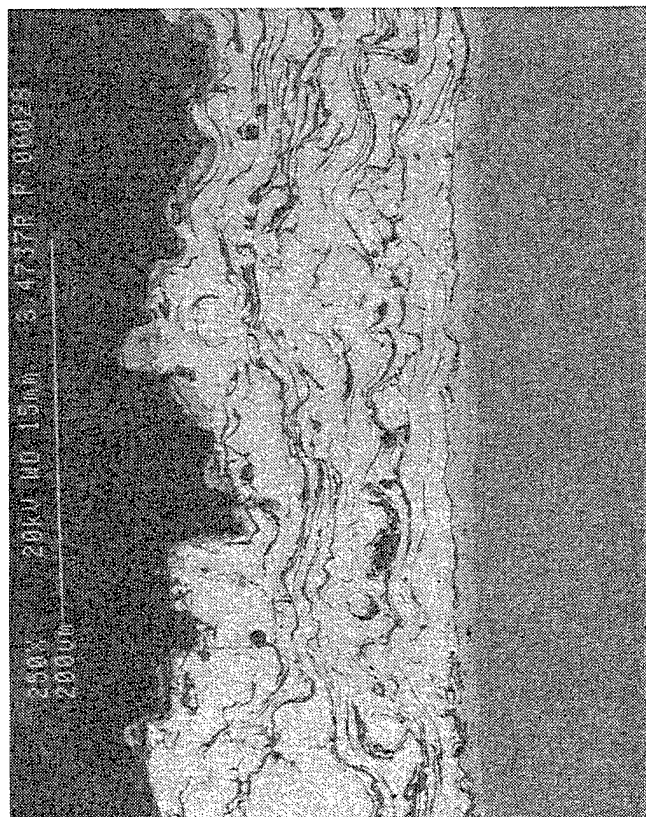


Figure 186. Micrographs showing cross sections of the CoCrAlY cermet (M^3) coated gamma as a function of peak temperature attained during 900/760°C burner rig testing with no salt.

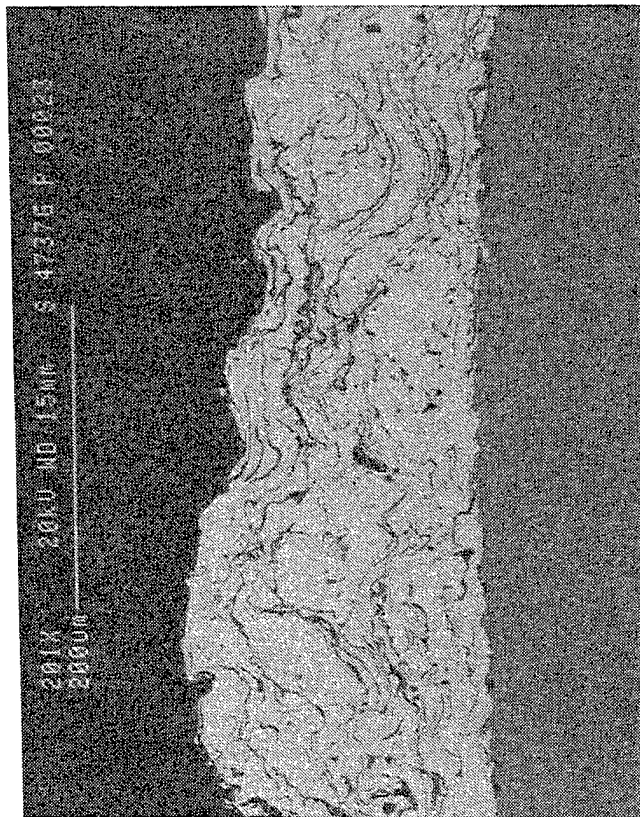
900°C (1650°F) Peak Temperature



760°C (1400°F) Peak Temperature



830°C (1520°F) Peak Temperature



510°C (950°F) < T

Figure 187. Micrographs showing cross sections of the Alloy 718 cermet (M^3) coated gamma as a function of peak temperature attained during 900/760°C burner rig testing with no salt.

Reaction Zone

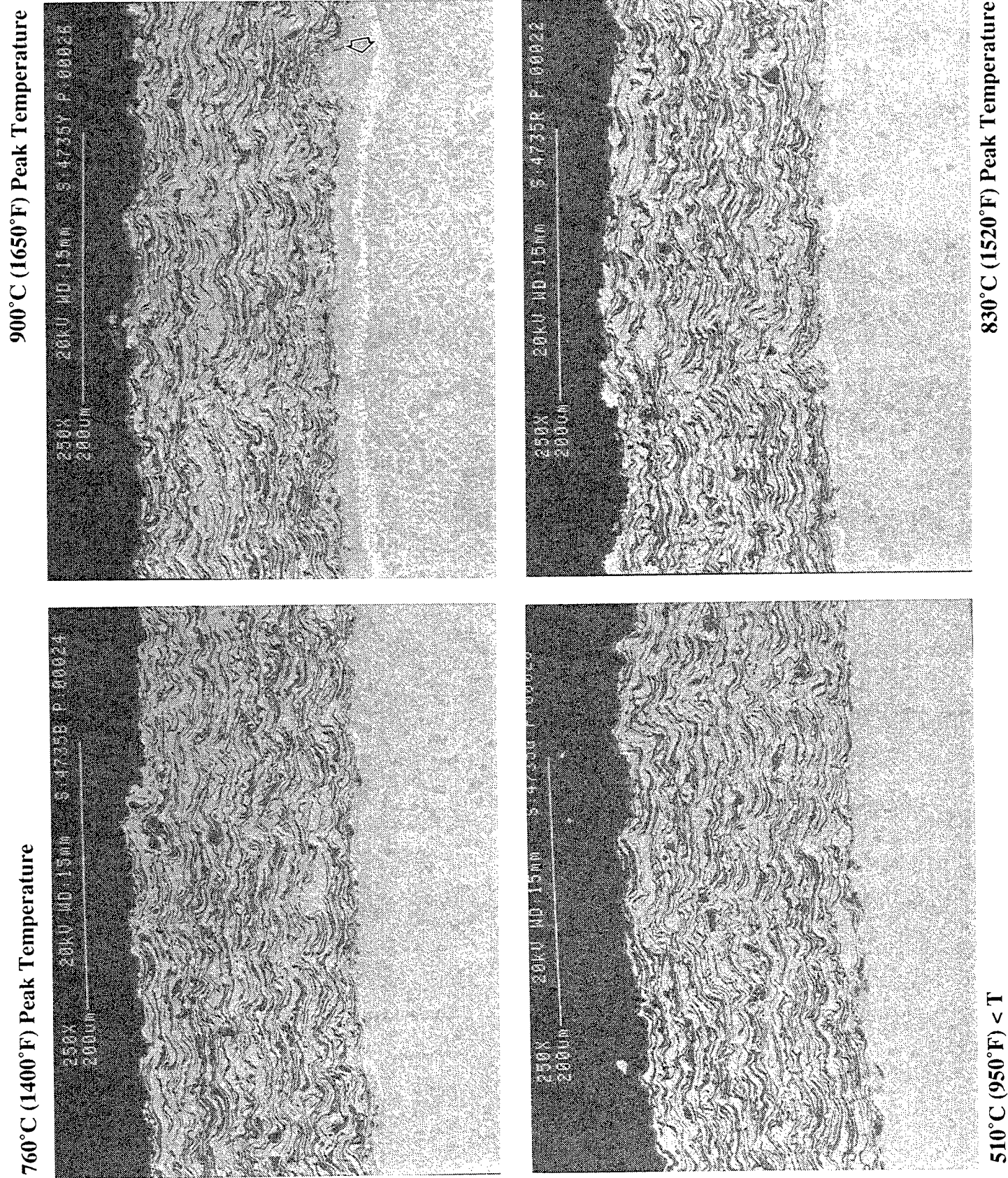
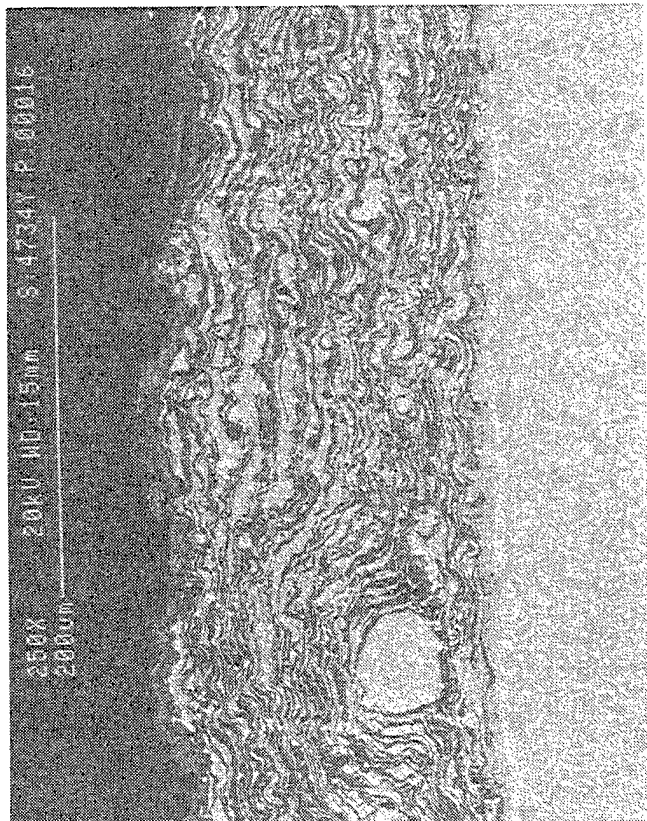
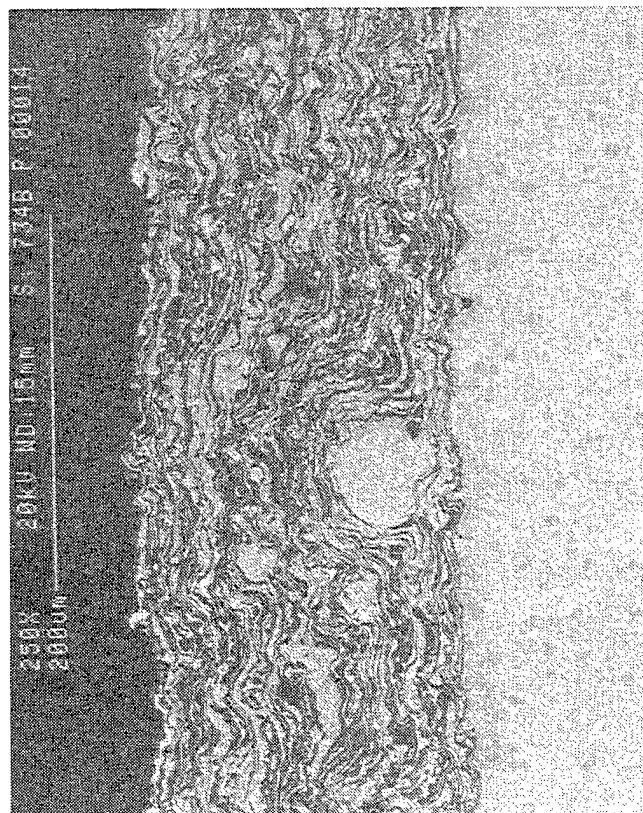


Figure 188. Micrographs showing cross sections of the NiCrAlY cermet (M³) coated alpha-2 as a function of peak temperature attained during 900/760°C burner rig testing with no salt.

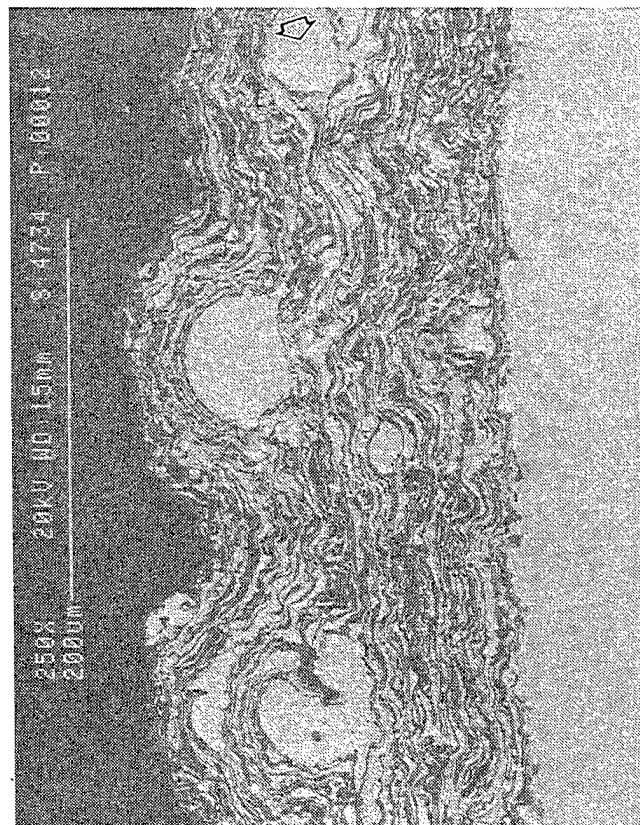
900°C (1650°F) Peak Temperature



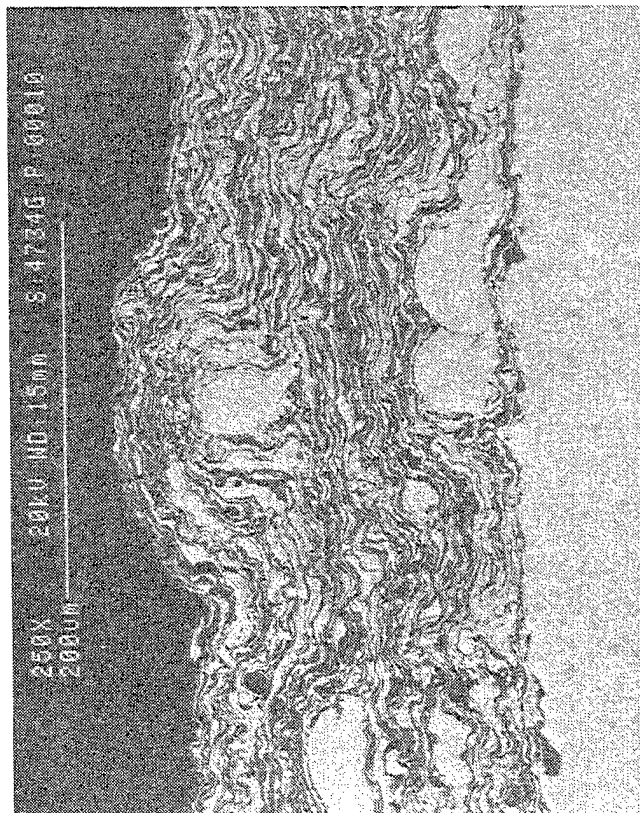
760°C (1400°F) Peak Temperature



Unmelted Particles



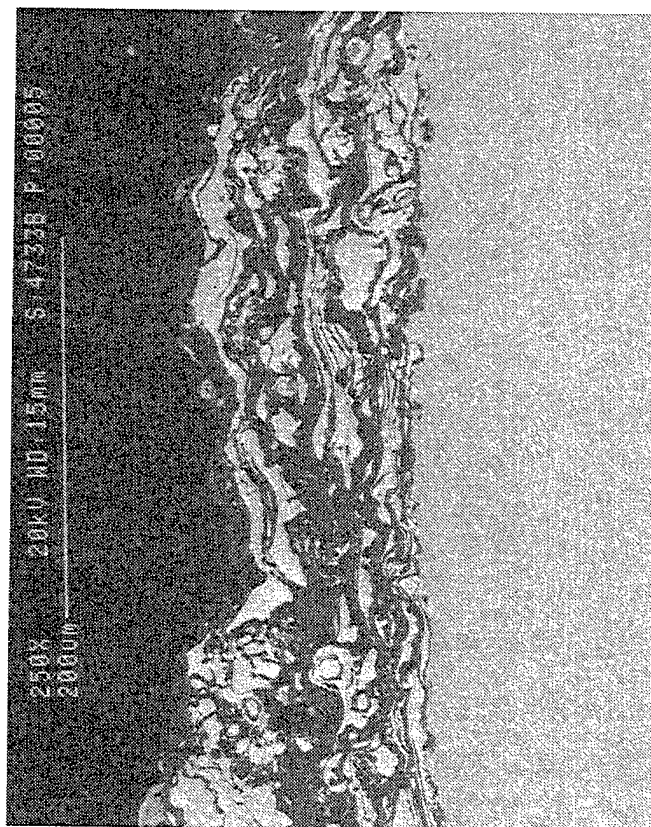
830°C (1520°F) Peak Temperature



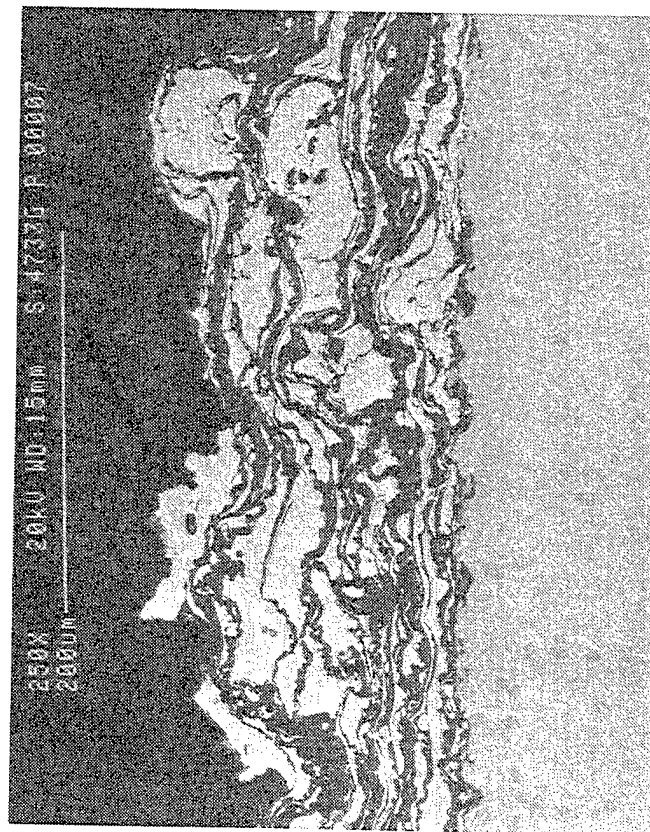
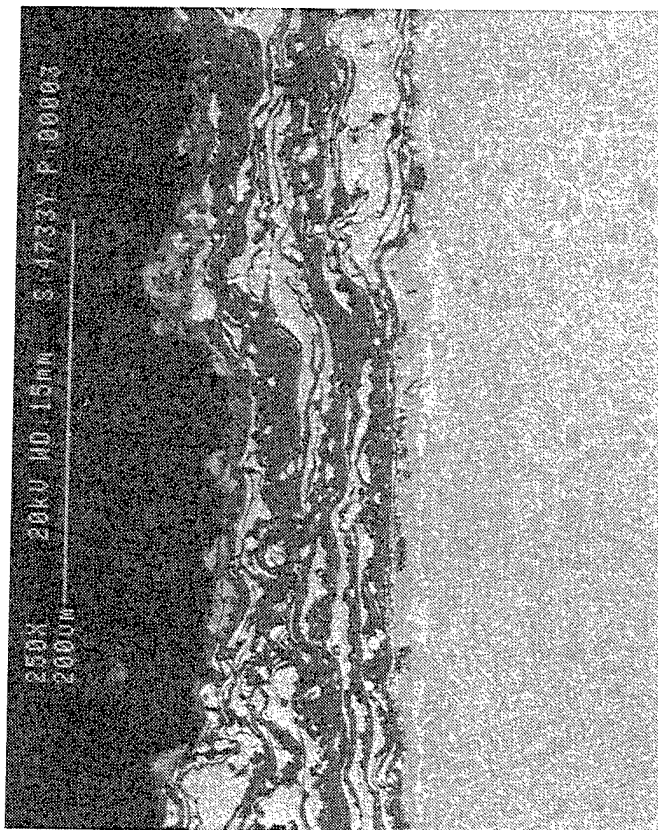
510°C (950°F) < T

Figure 189. Micrographs showing cross sections of the CoCrAlY cermet (M³) coated alpha-2 as a function of peak temperature attained during 900/760°C burner rig testing with no salt.

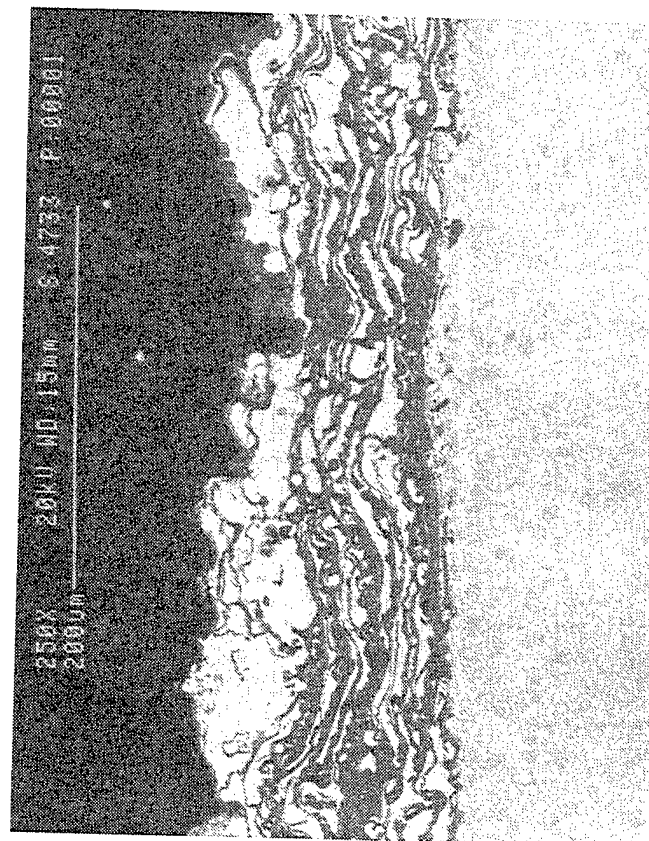
760°C (1400°F) Peak Temperature



900°C (1650°F) Peak Temperature



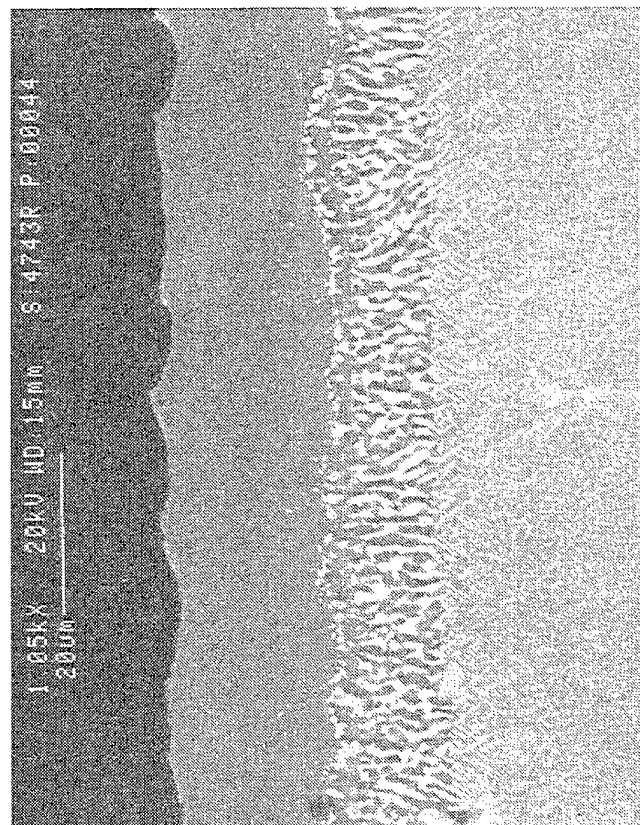
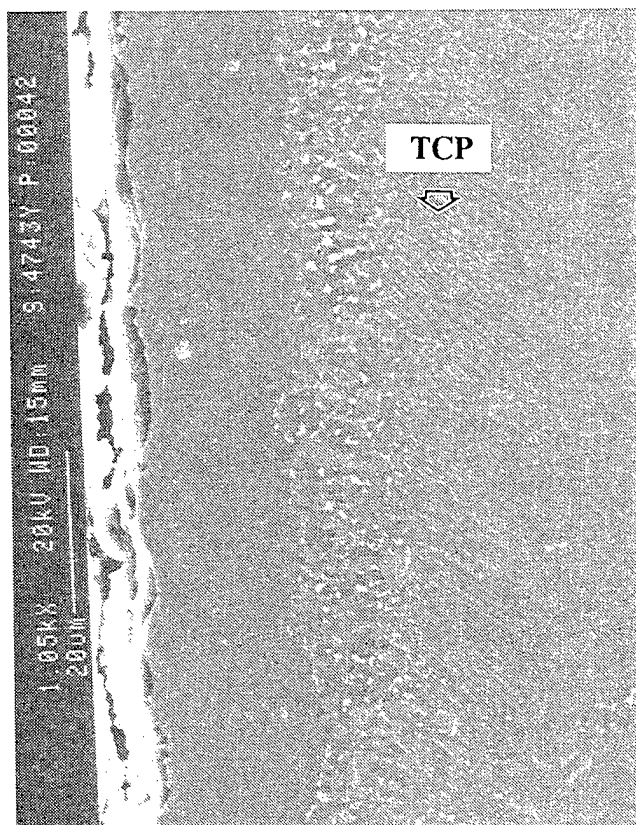
510°C (950°F) < T



830°C (1520°F) Peak Temperature

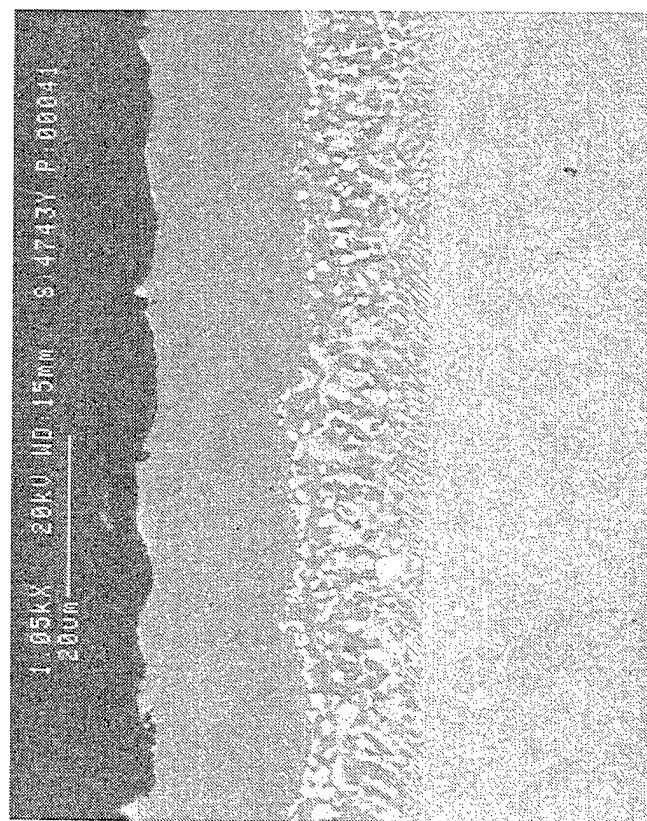
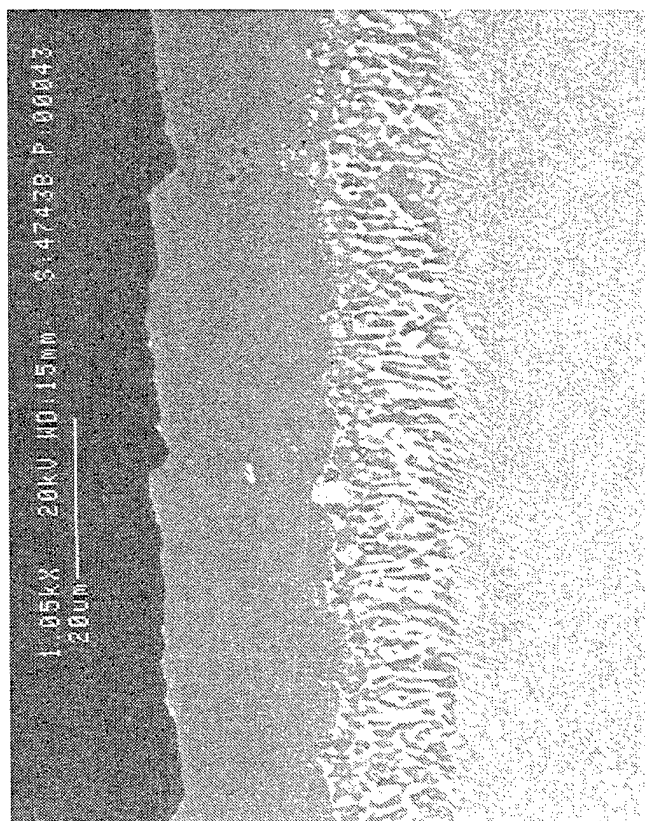
Figure 190. Micrographs showing cross sections of the Alloy 718 cermet (M^3) coated alpha-2 as a function of peak temperature attained during 900/760°C burner rig testing with no salt.

900°C (1650°F) Peak Temperature



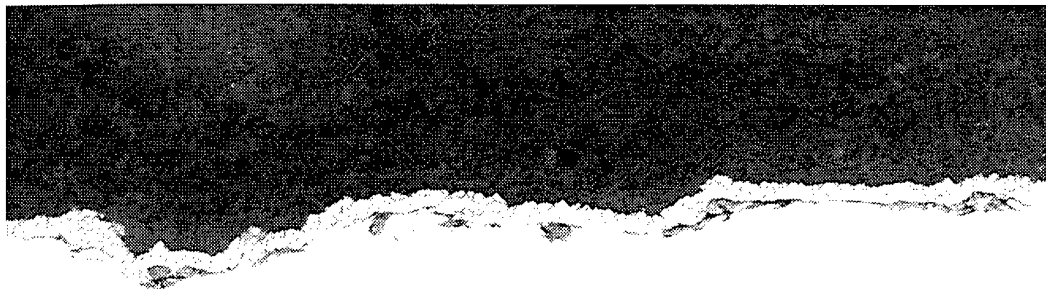
830°C (1520°F) Peak Temperature

760°C (1400°F) Peak Temperature



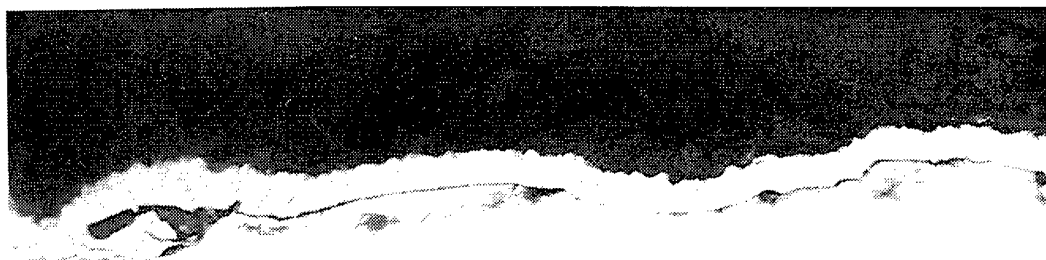
510°C (950°F) < T

Figure 191. Micrographs showing cross sections of the Codep coated R'80 as a function of peak temperature attained during 900/760°C burner rig testing with no salt.



20 μm

74996A1E 500x

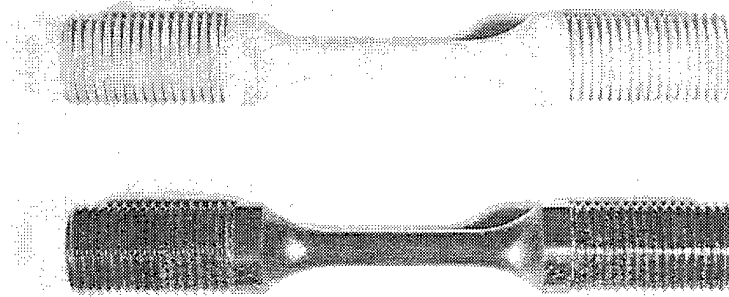


10 μm

74996A1F 1000x

Figure 192. Optical micrograph of W diffusion barrier deposited by CVD.

**Uncoated
Gamma**



**Uncoated
Alpha-2**

Figure 193. Photograph of alpha-2 and gamma tensile samples after the cyclic exposure at 760°C for 100 hours.

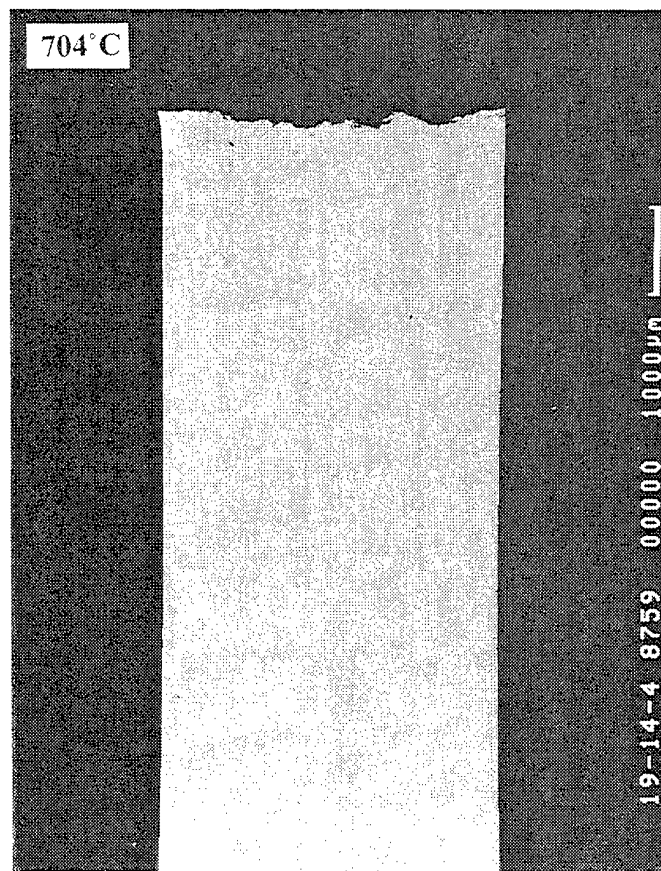
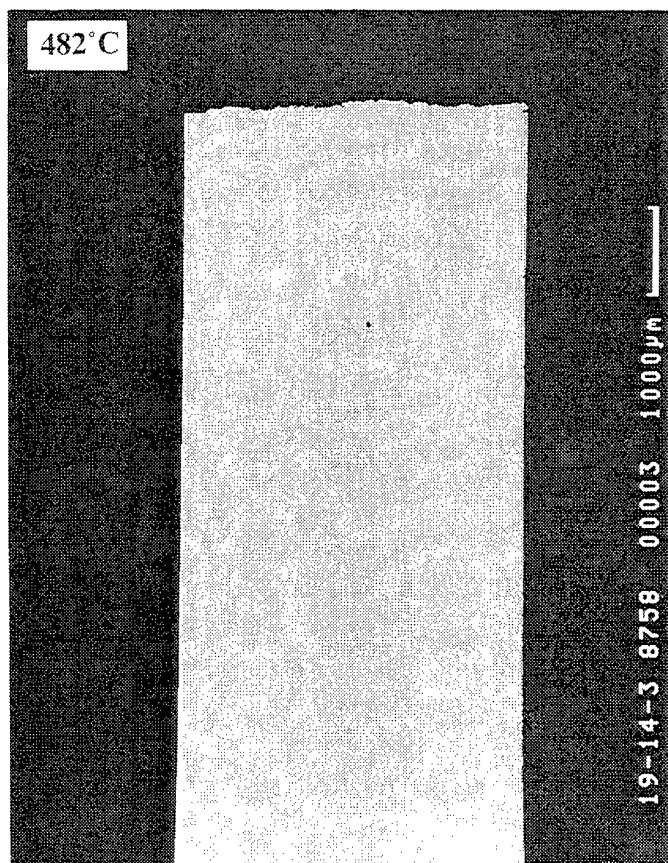
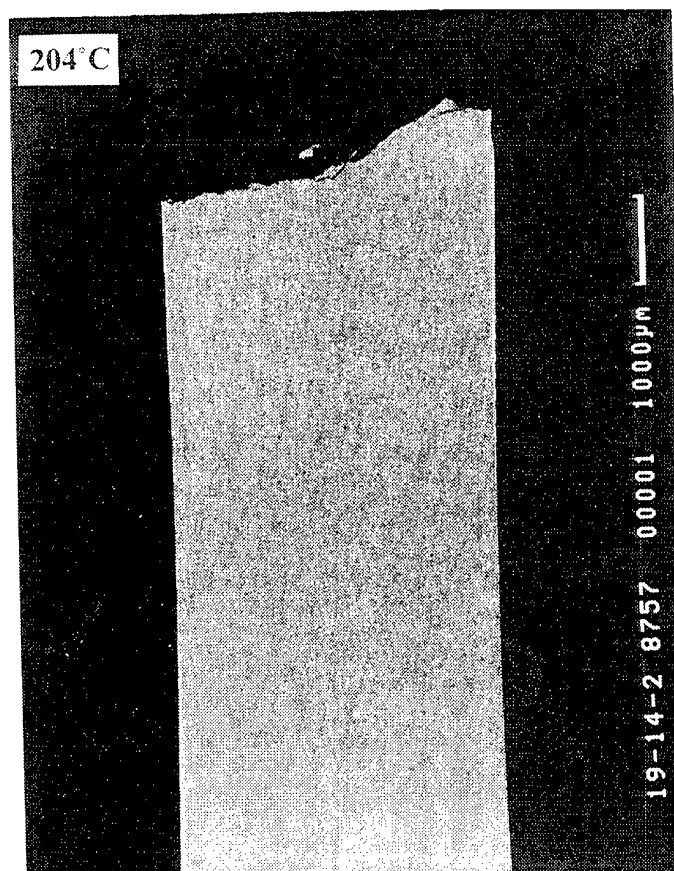
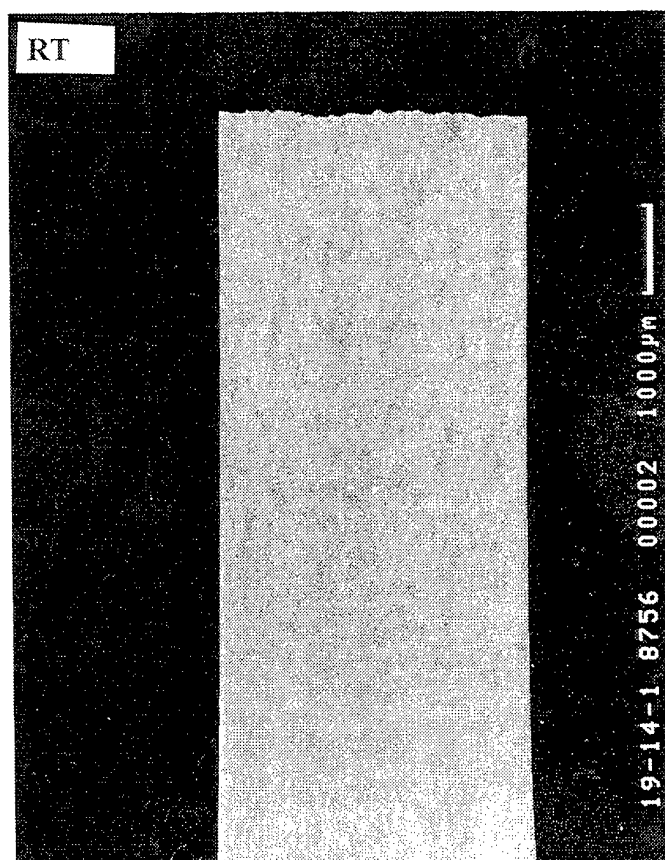


Figure 194. Cross sections of uncoated unexposed gamma tensile samples as a function of temperature.

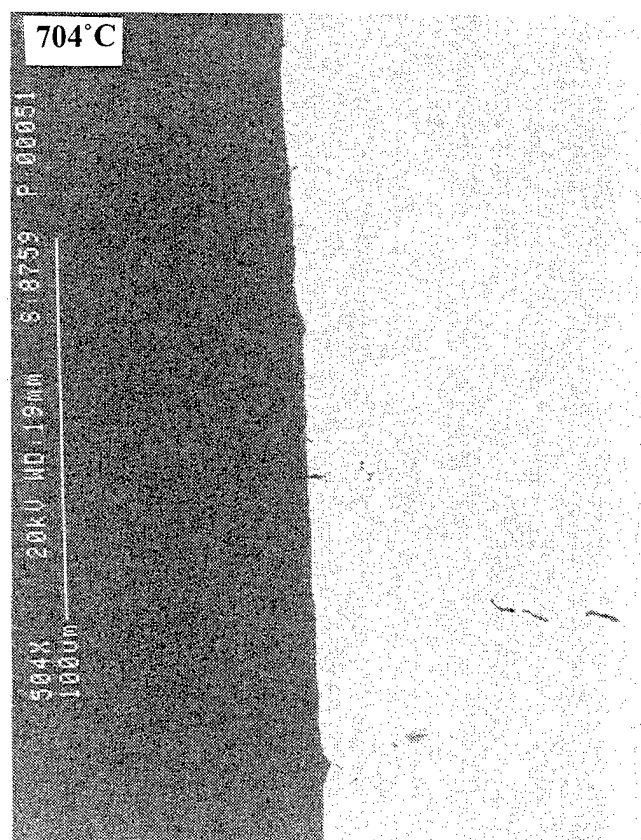
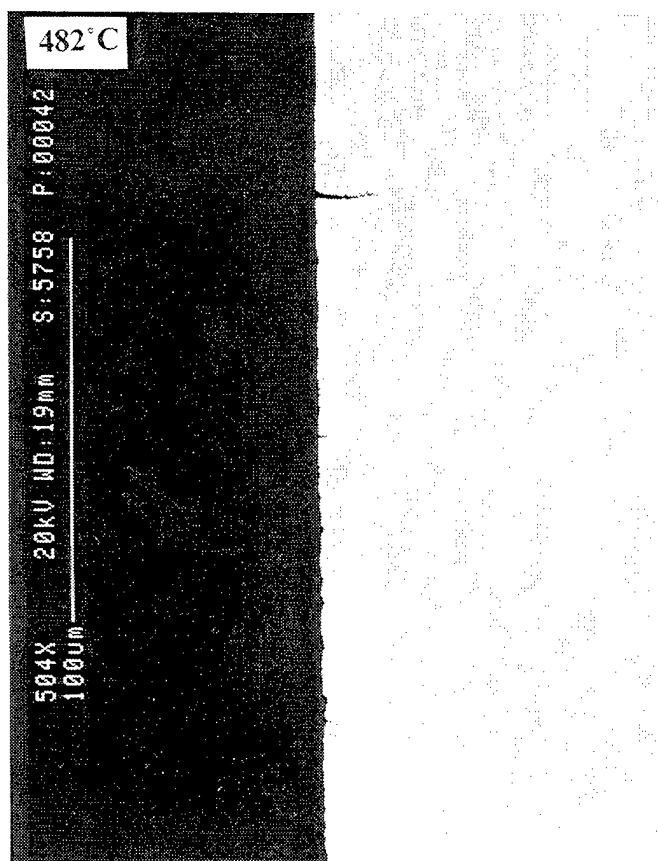
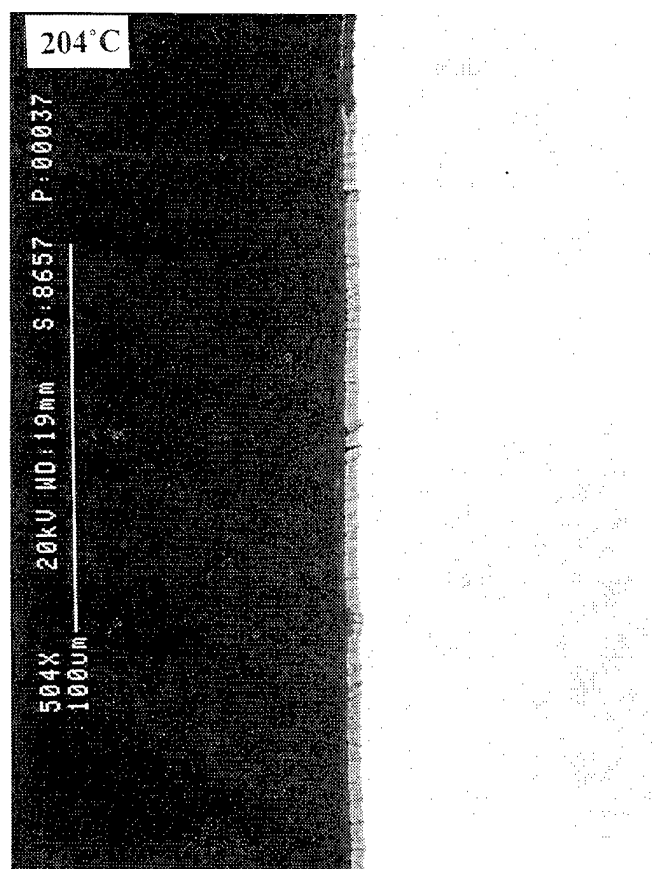
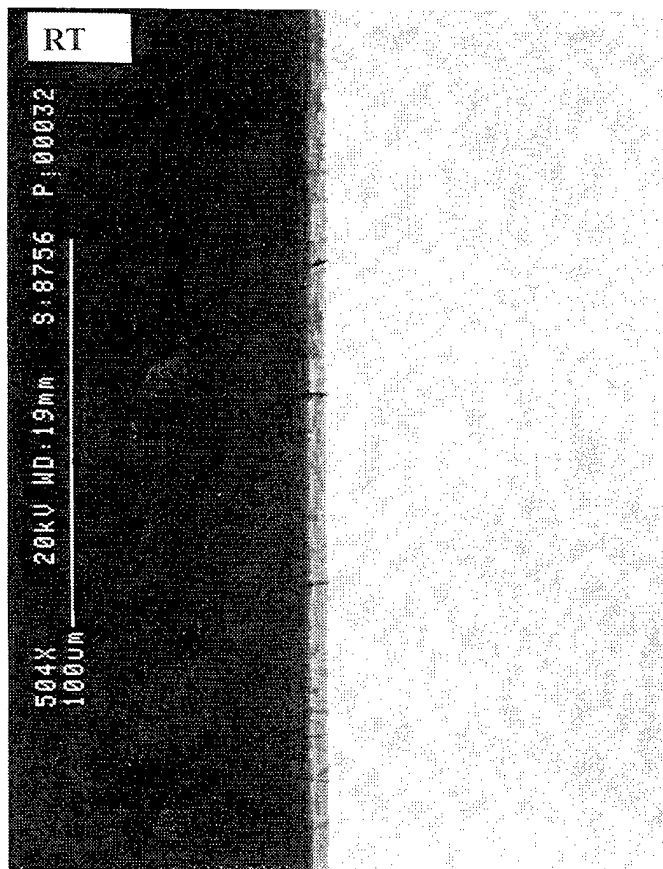


Figure 195. Cross sections of uncoated unexposed gamma tensile samples as a function of temperature.

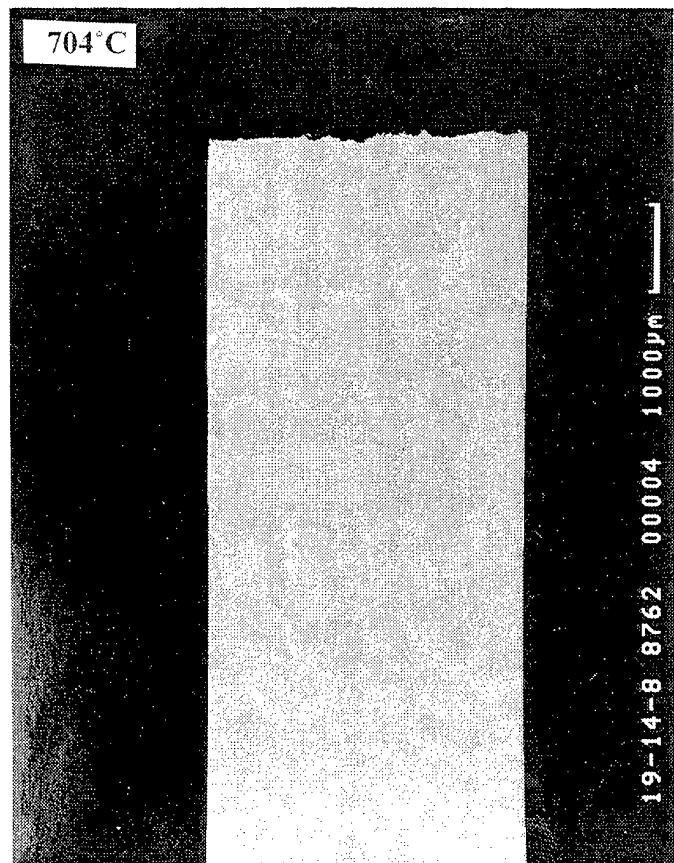
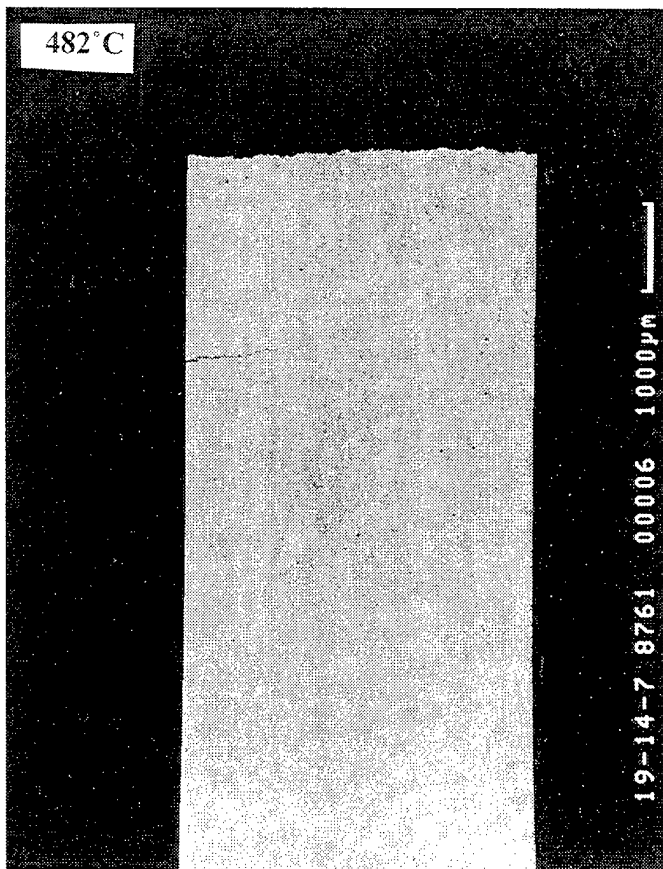
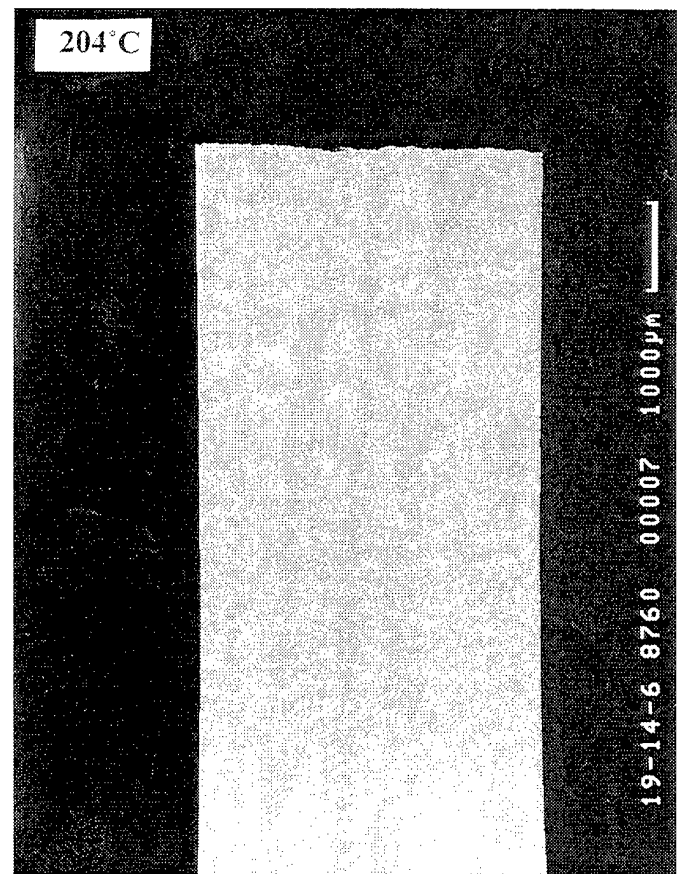


Figure 196. Cross sections of uncoated gamma tensile samples cyclically exposed at 760°C/100hr as a function of temperature.

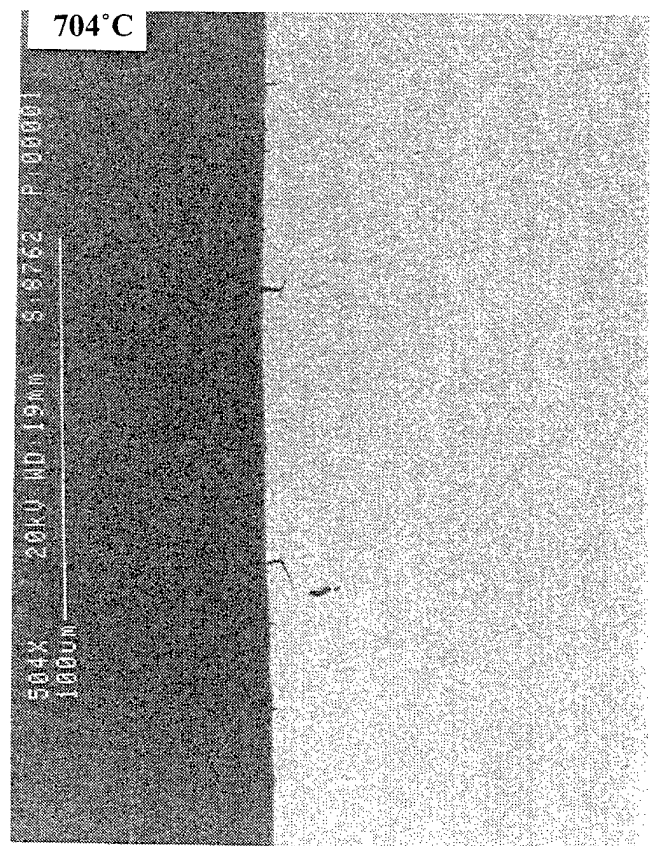
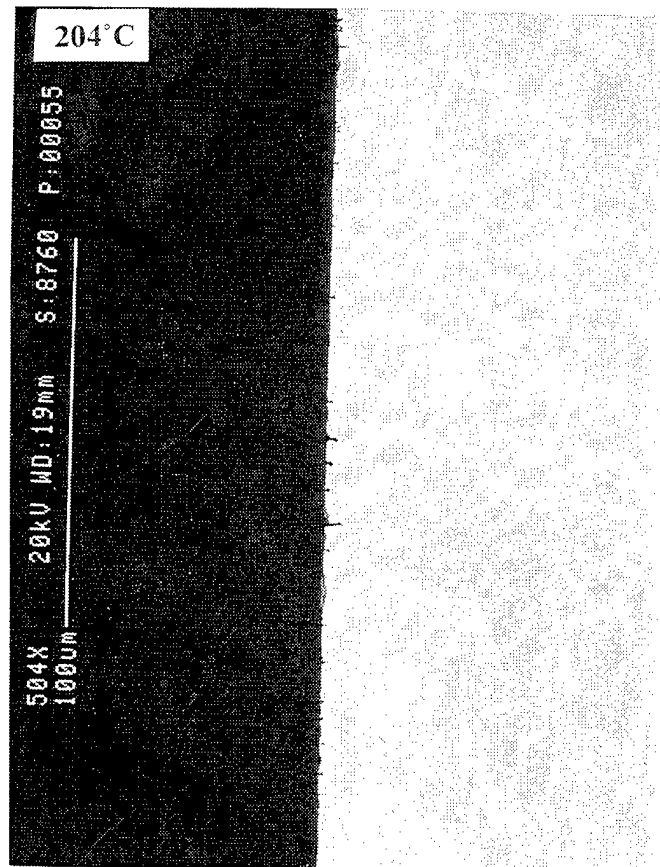
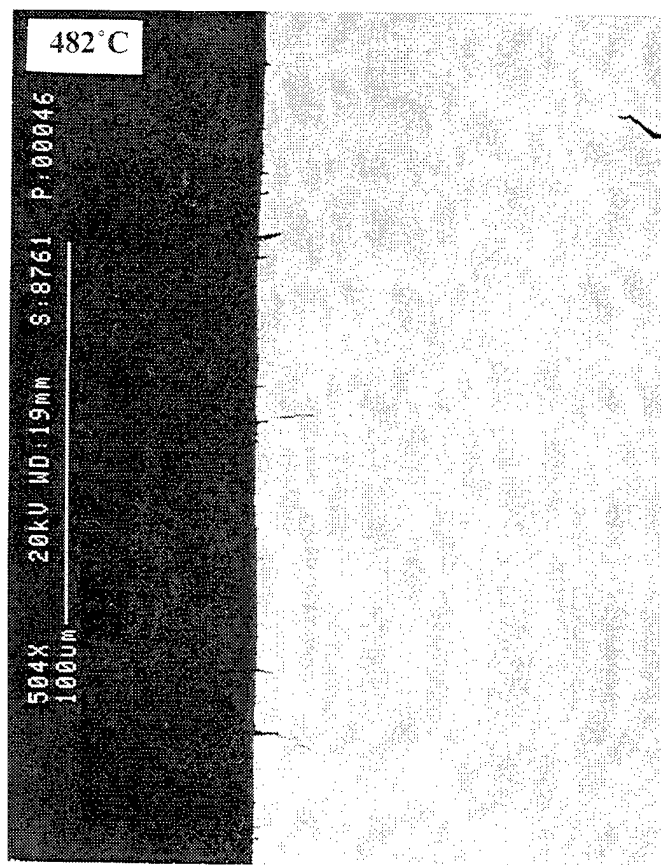


Figure 197. Cross sections of uncoated gamma tensile samples cyclically exposed at 760°C/100hr as a function of temperature.

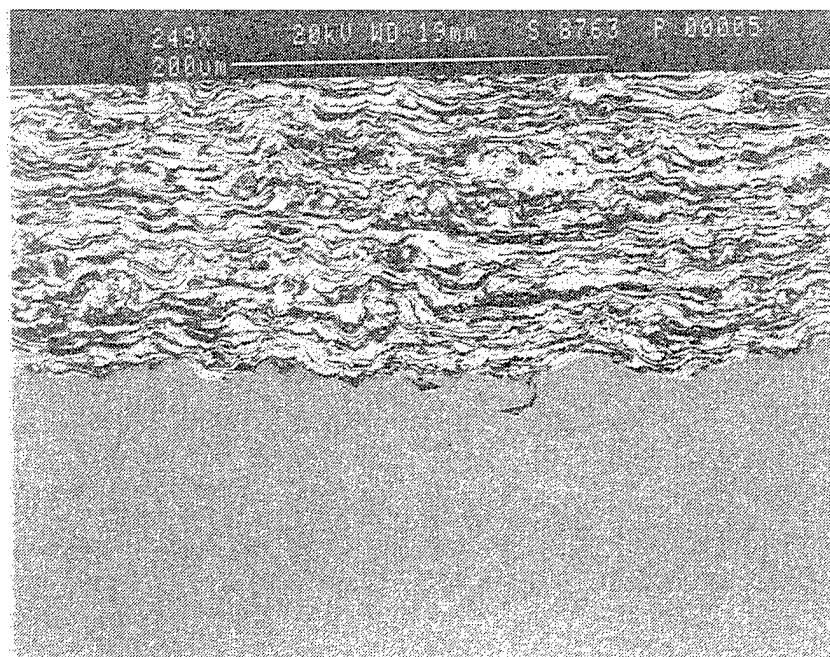
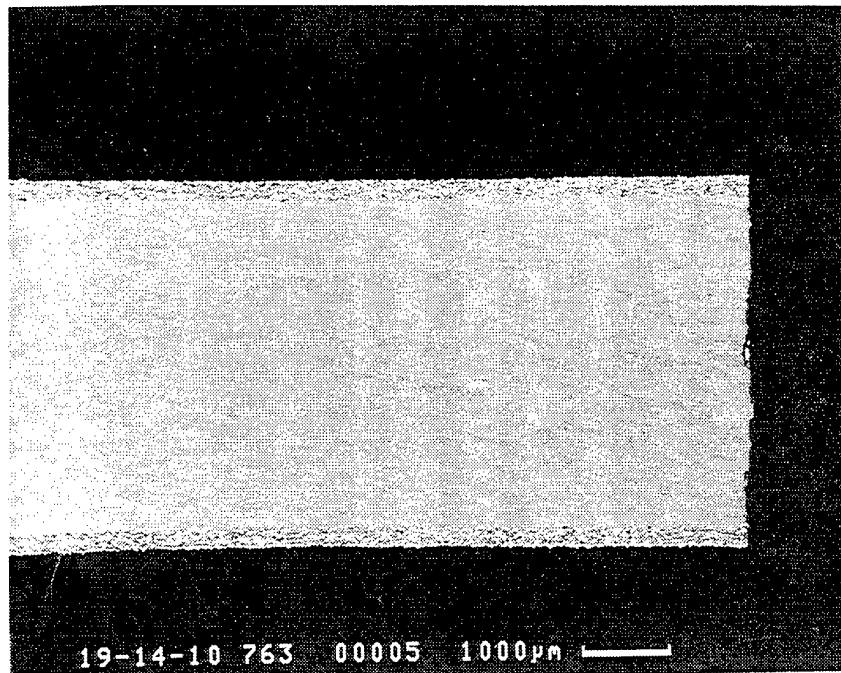


Figure 198. Cross sections of cermet coated gamma tensile samples tested at 704°C.

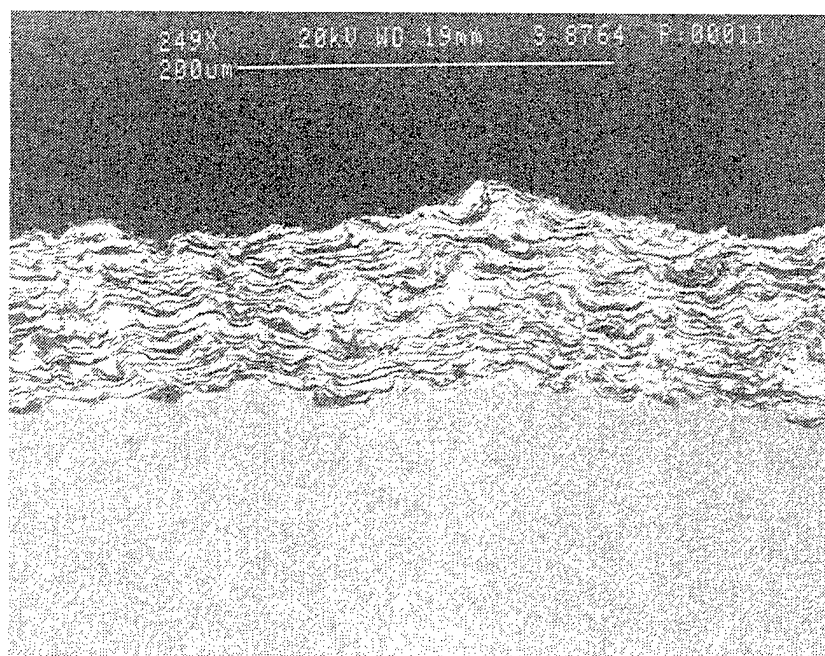
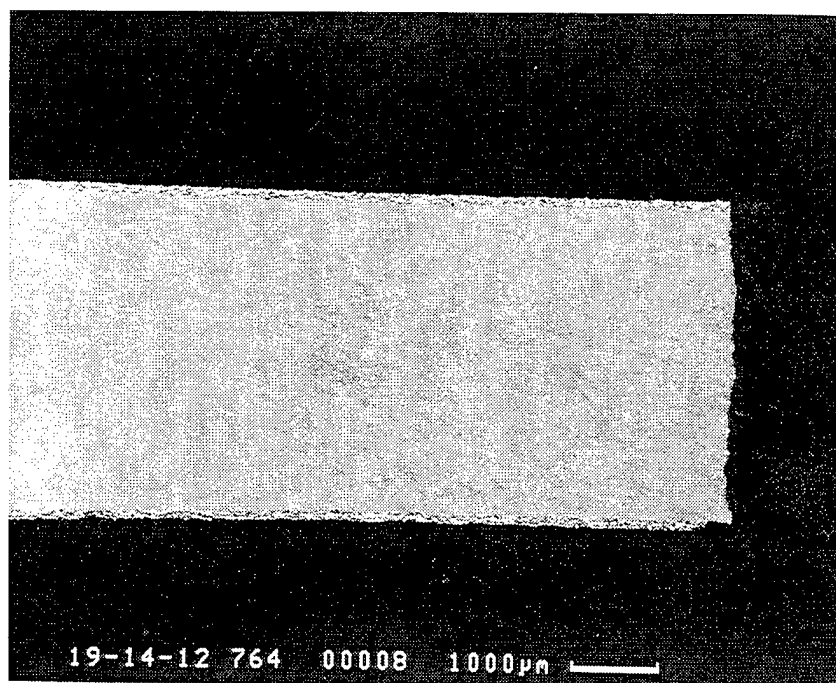


Figure 199. Cross sections of cermet coated gamma tensile sample cyclically exposed at 760°C/100hr tested at 704°C.

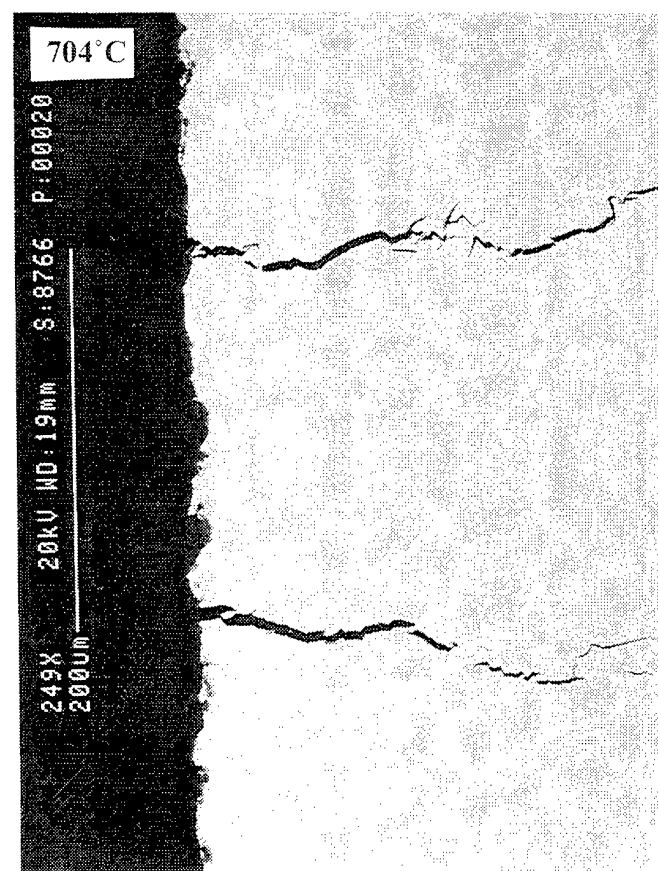
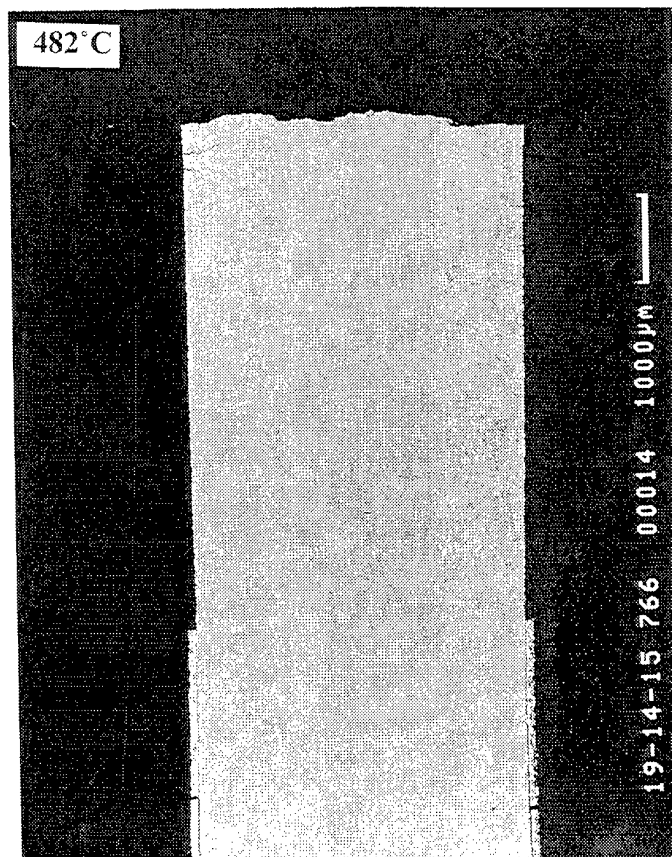
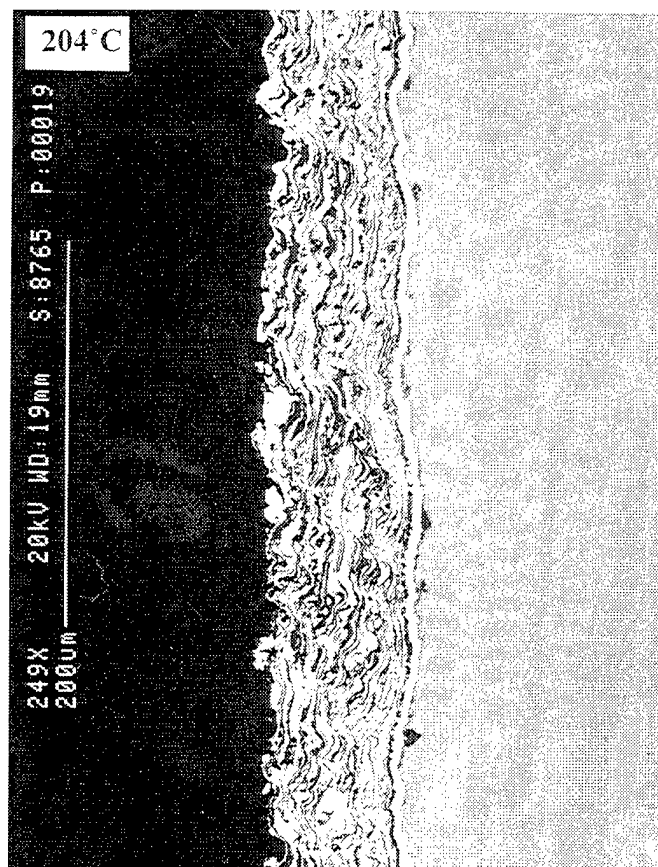
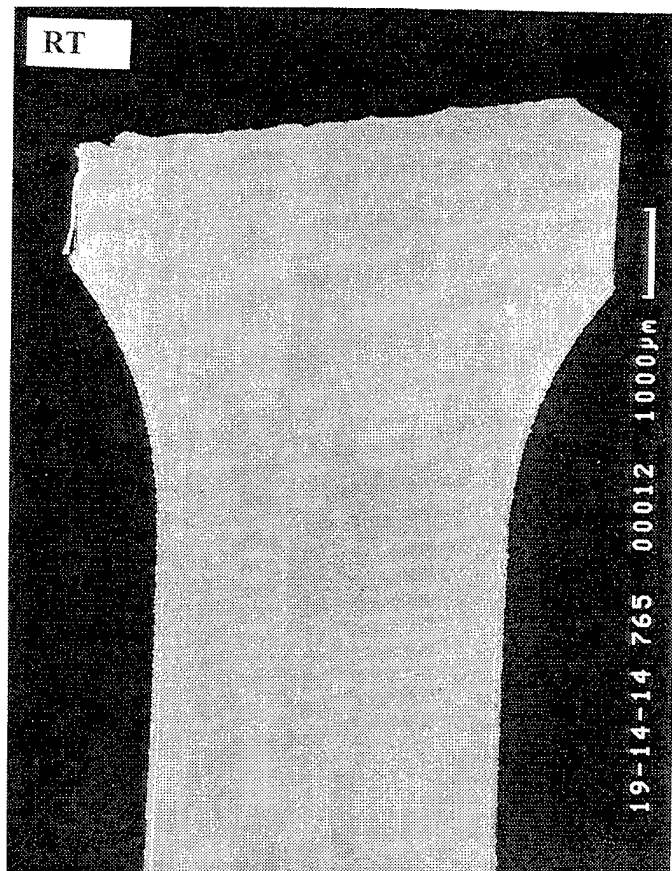


Figure 200. Cross sections of unexposed cermet W CVD coated gamma tensile sample after tensile testing.

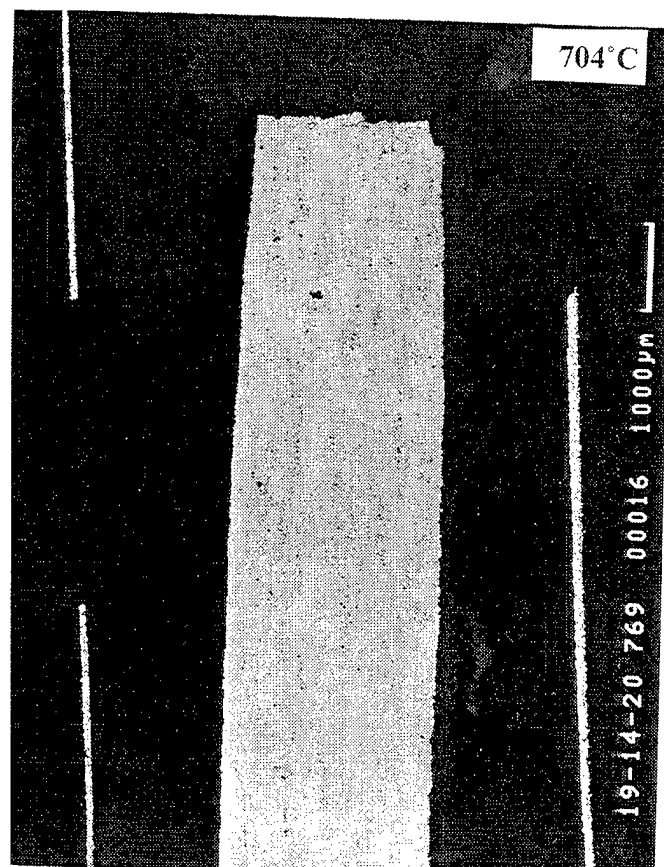
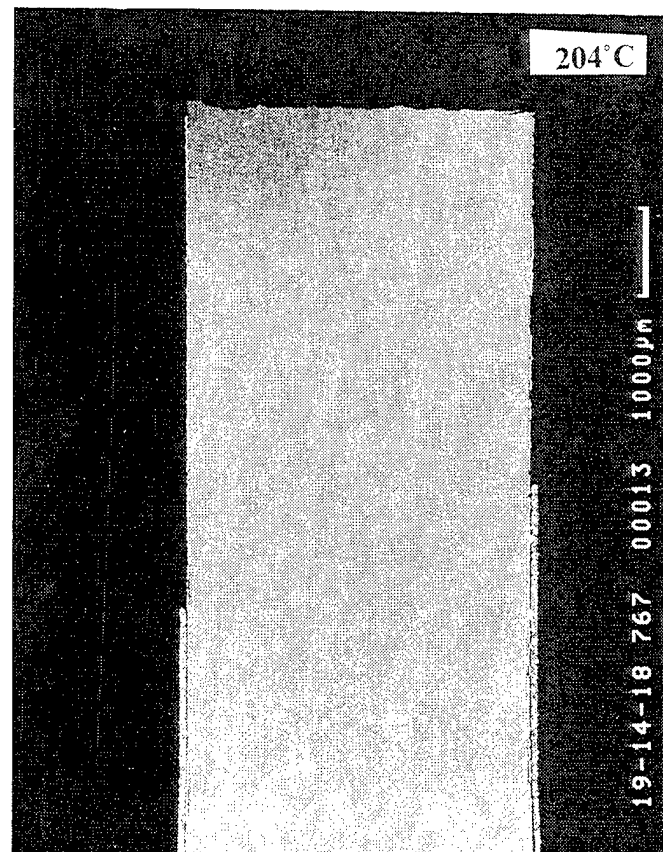
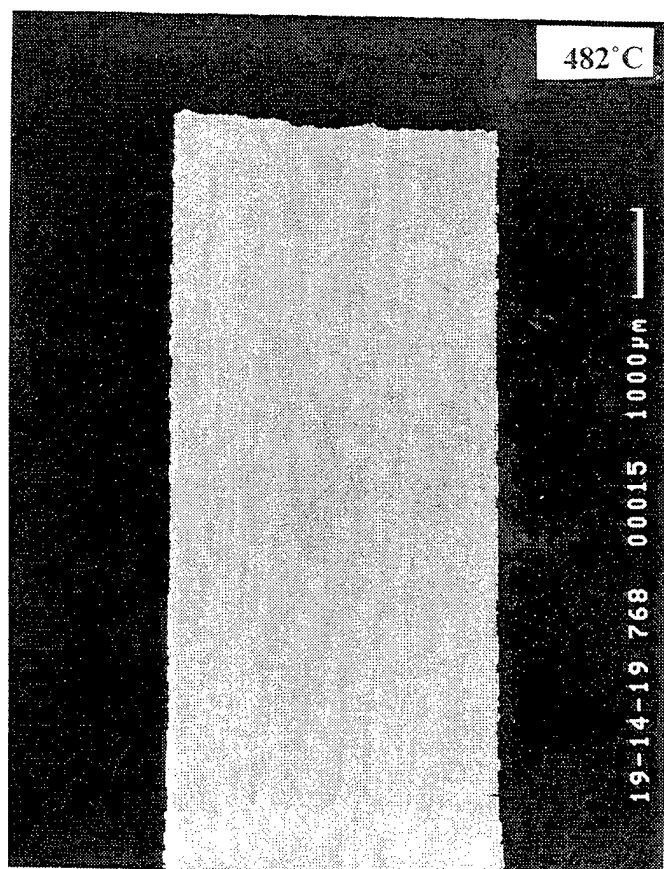


Figure 201. Cross sections of unexposed cermet W CVD coated gamma tensile sample cyclically exposed at 760°C/100hr tested at 704°C after tensile testing.

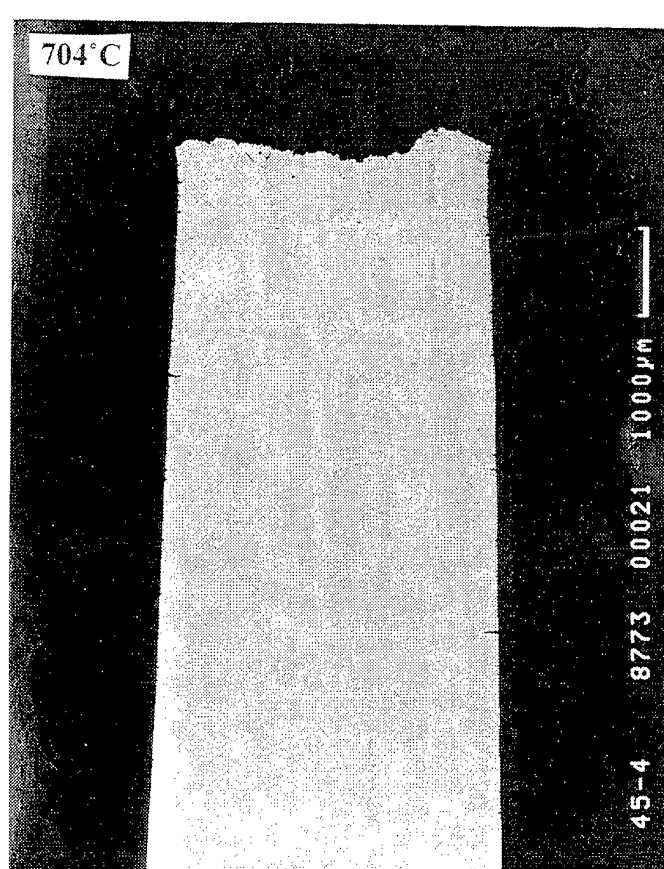
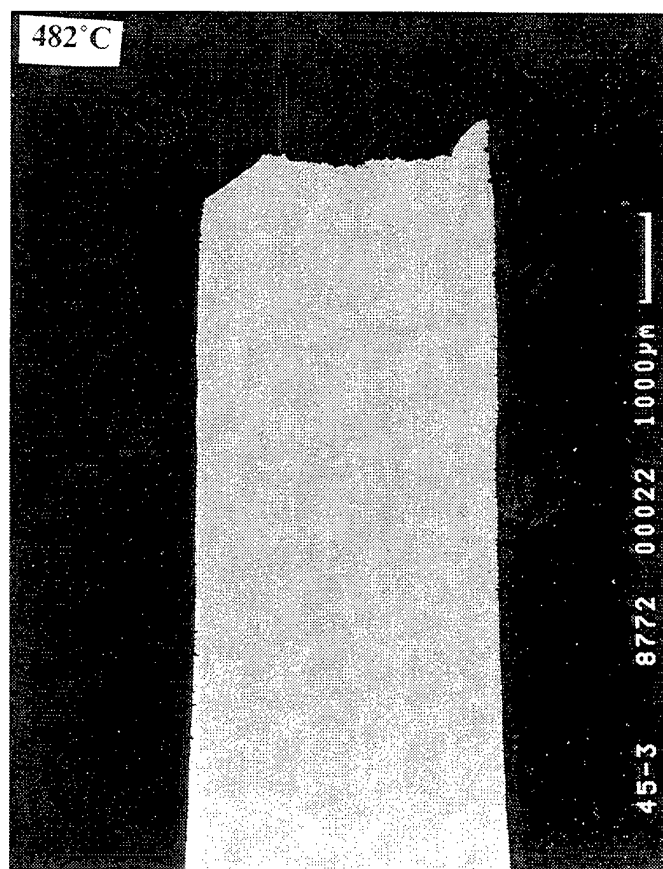
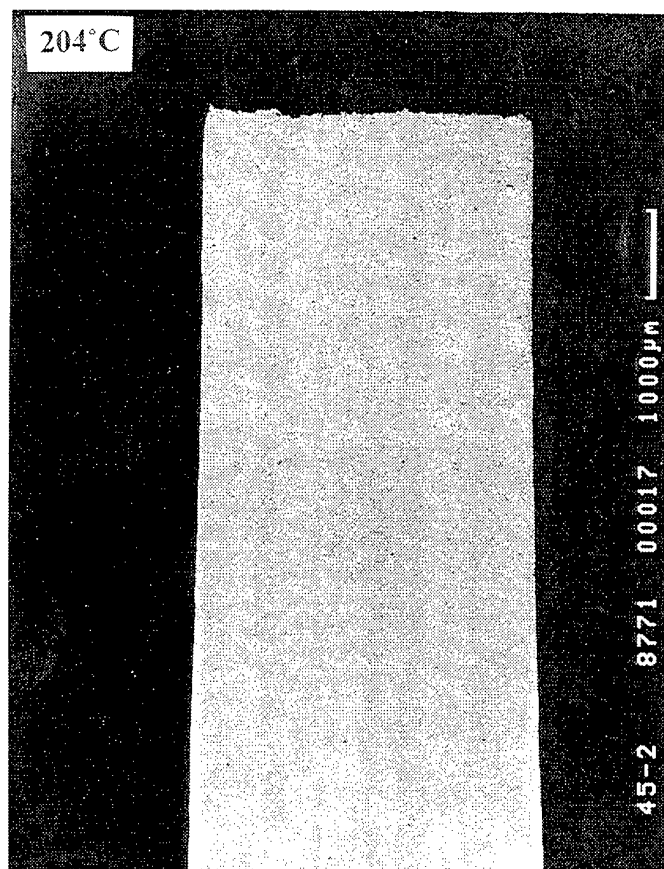
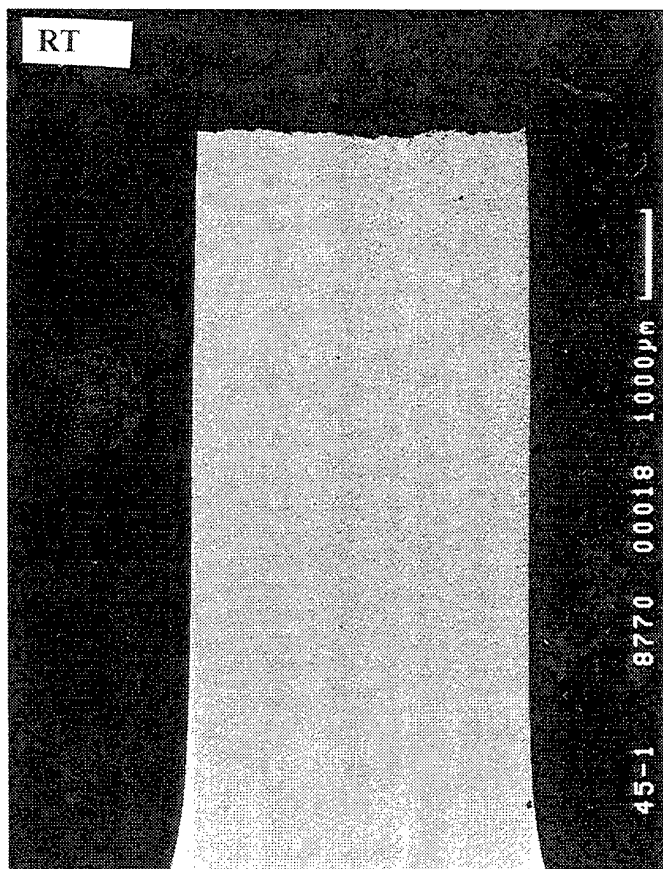


Figure 202. Cross sections of uncoated alpha-2 tensile samples as a function of temperature.

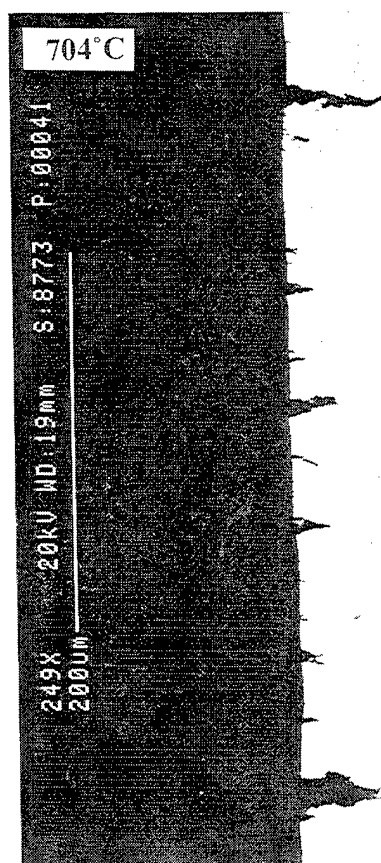
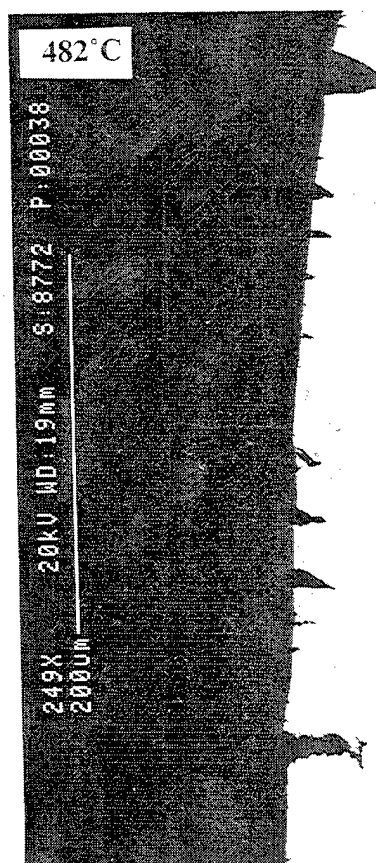
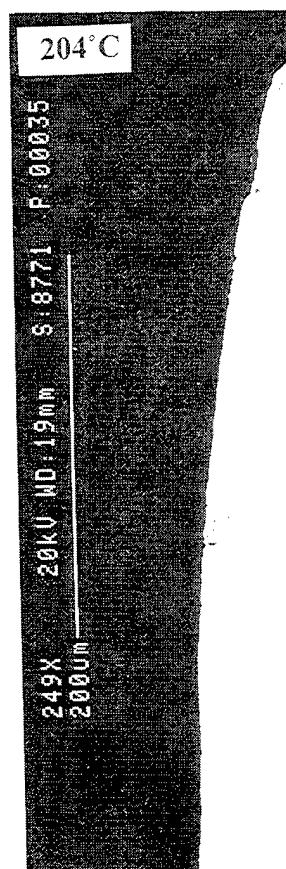
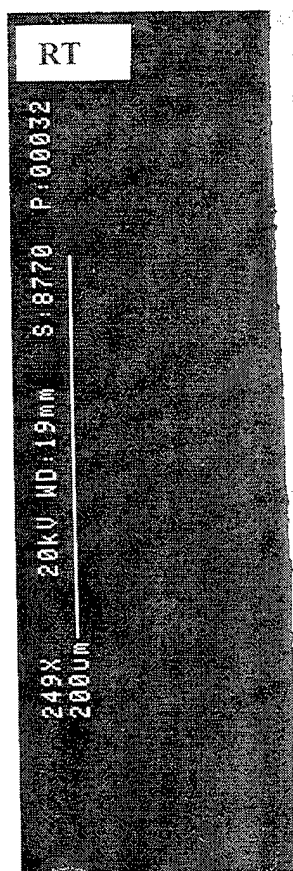


Figure 203. Cross sections of uncoated unexposed alpha-2 tensile samples as a function of temperature.

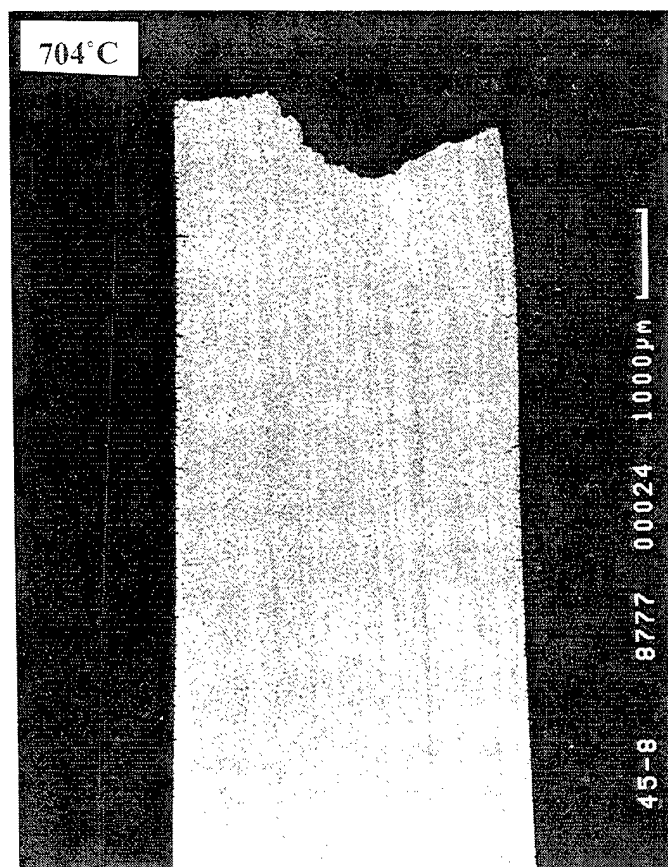
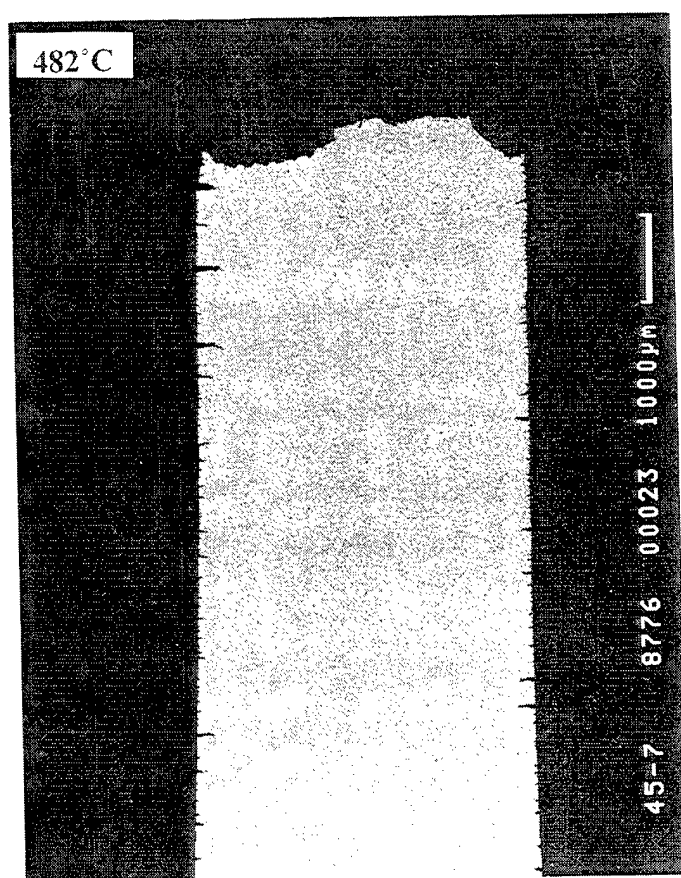
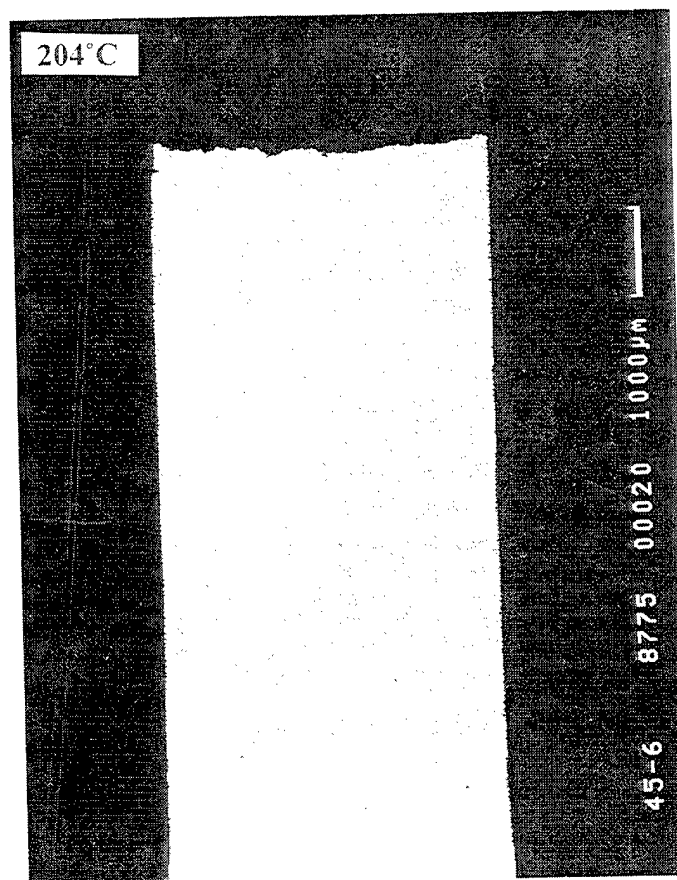
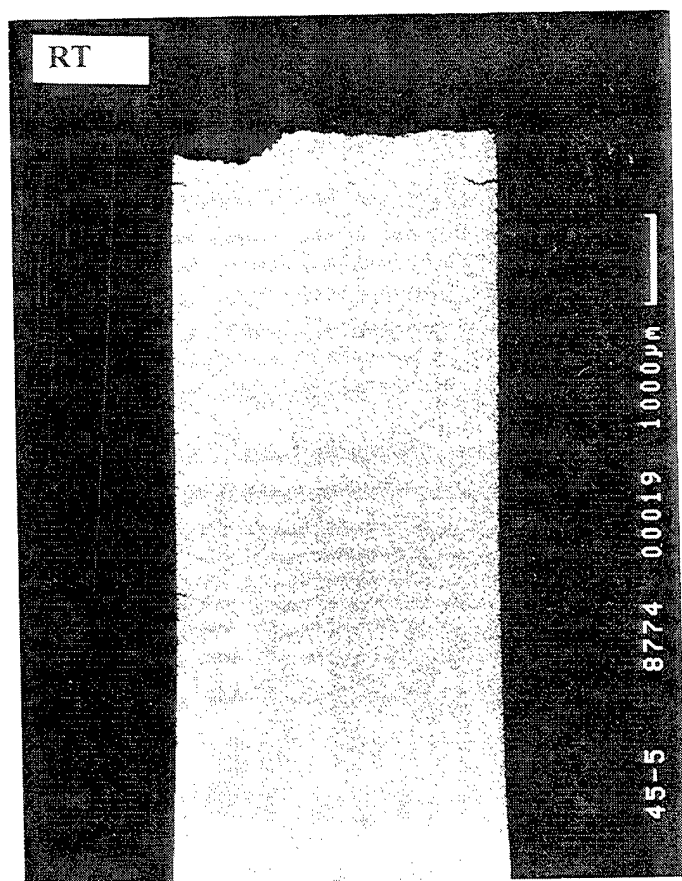


Figure 204. Cross sections of uncoated alpha-2 tensile samples cyclically exposed at 760°C/100hr as a function of temperature.

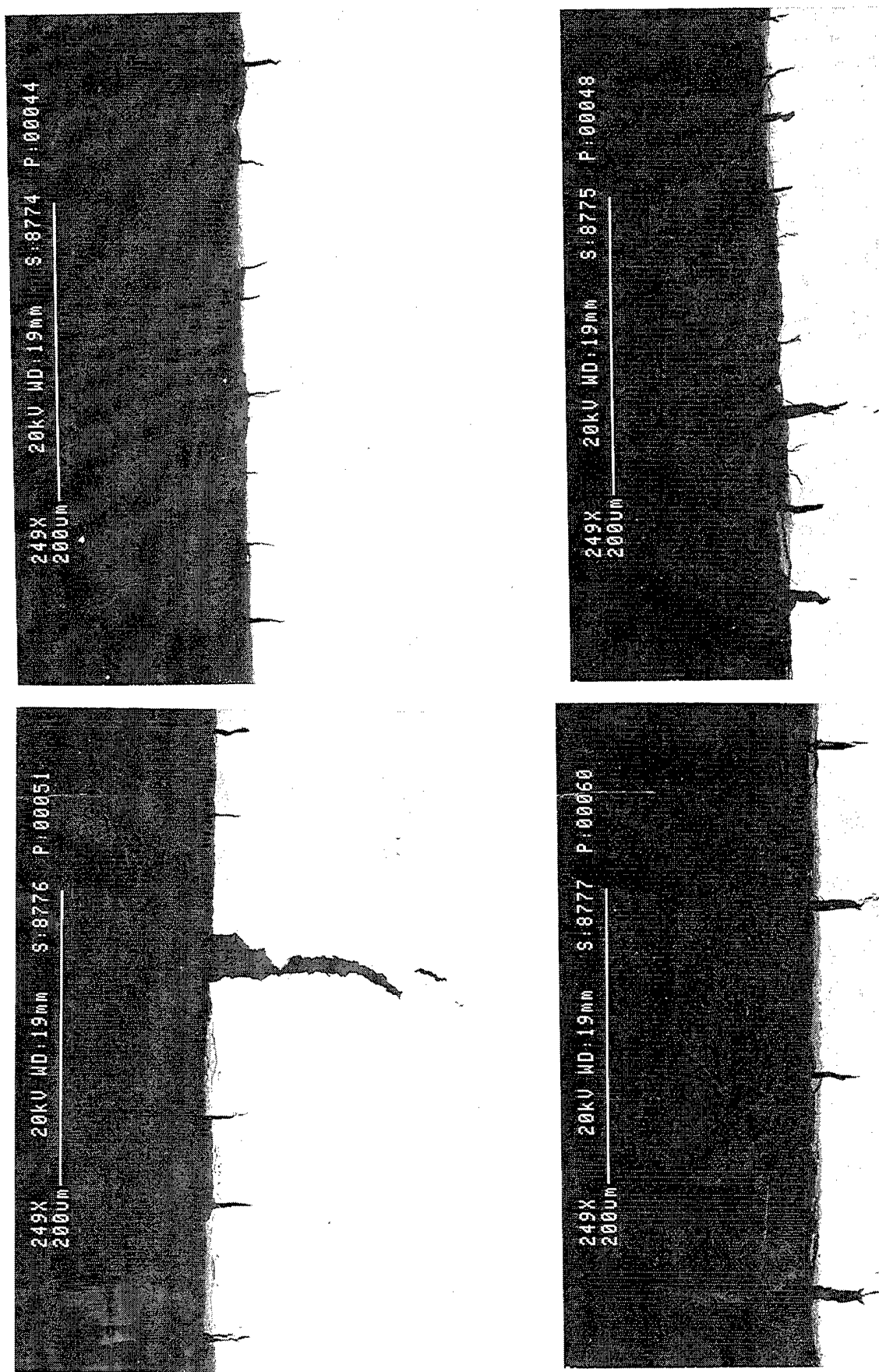
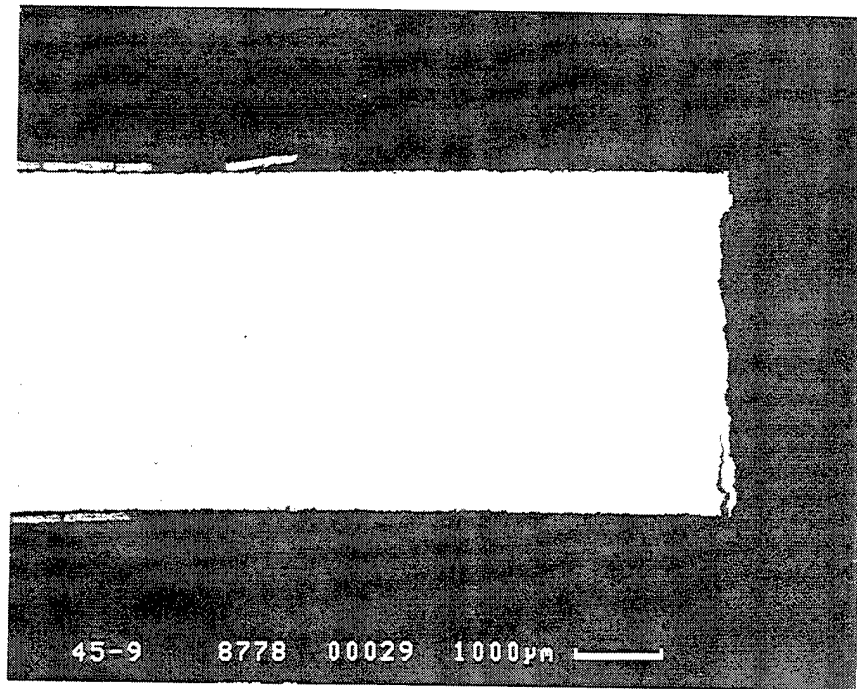
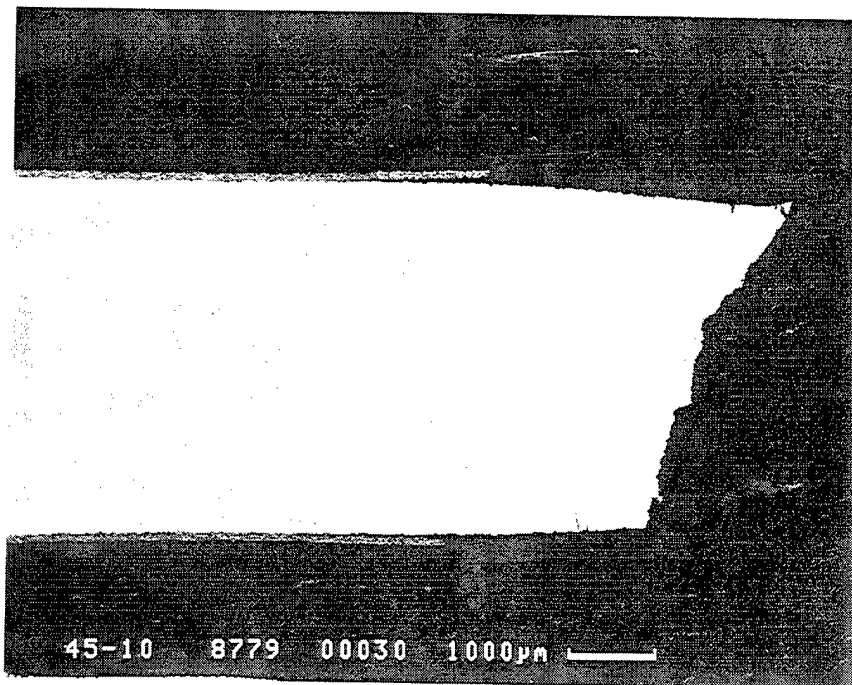


Figure 205. Cross sections of uncoated alpha-2 tensile samples cyclically exposed at 760°C/100hr as a function of temperature.

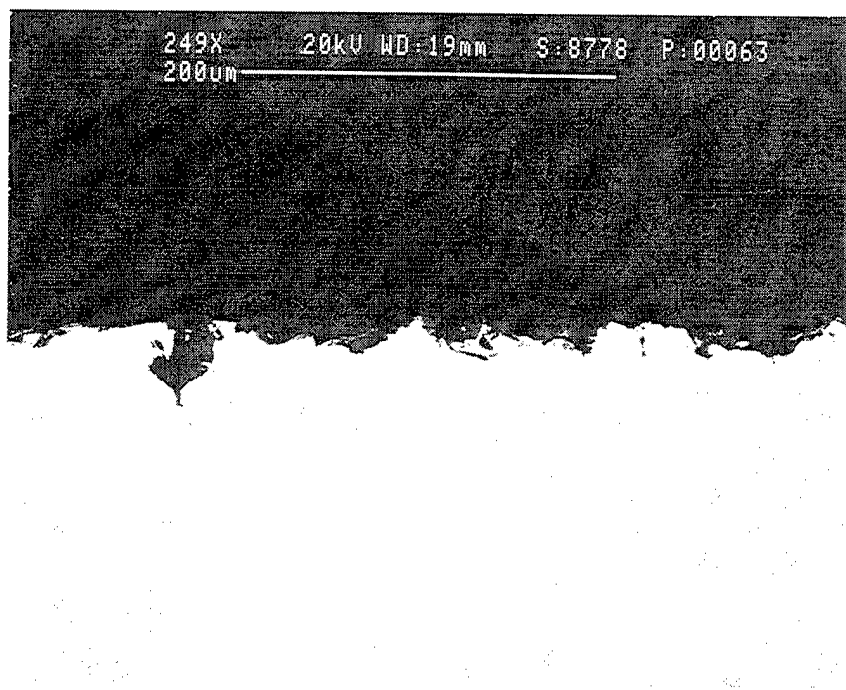


RT

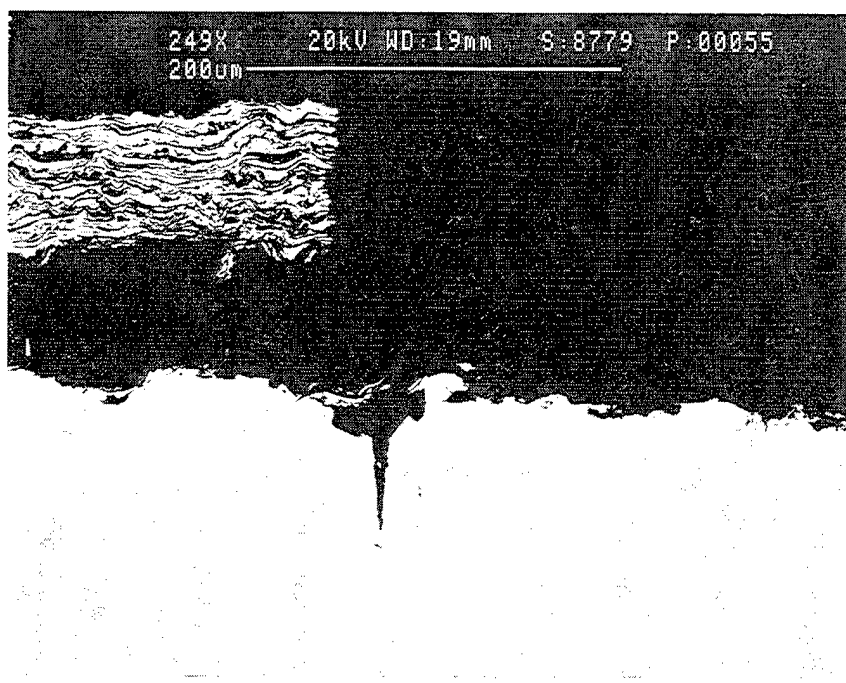


704°C

Figure 206. Cross sections of unexposed cermet coated alpha-2 tensile sample after testing.

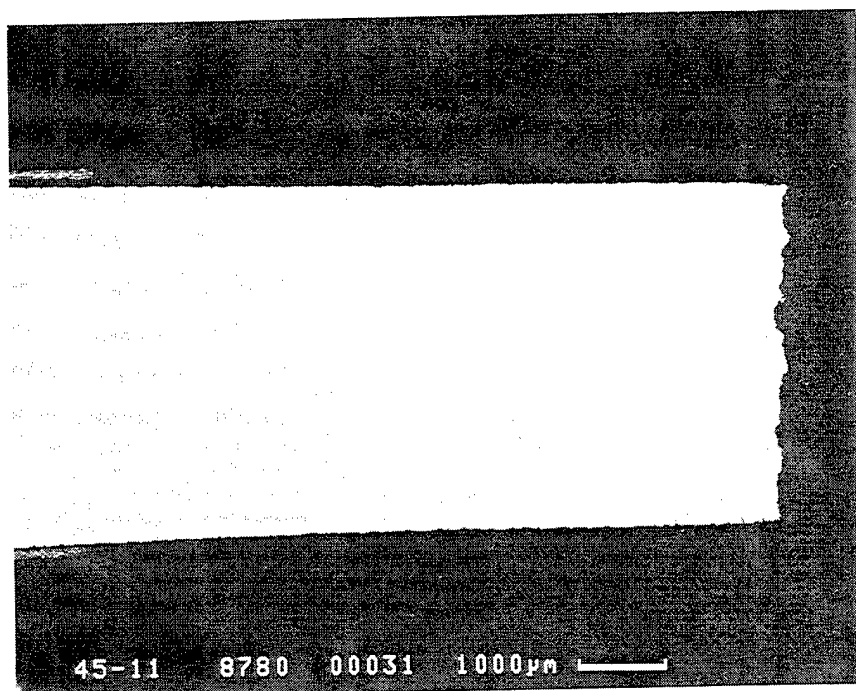


RT

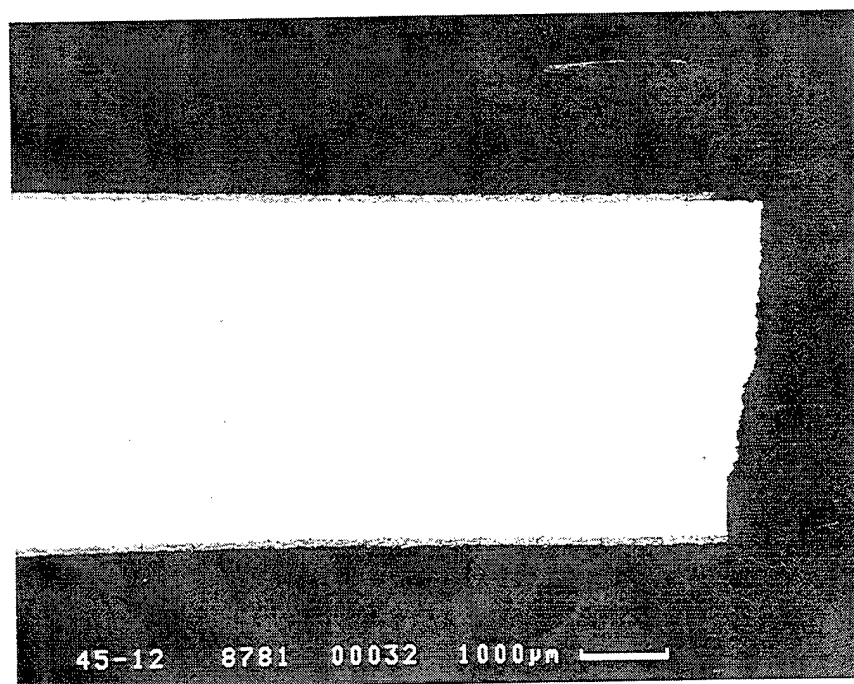


704°C

Figure 207. Cross sections of unexposed cermet coated alpha-2 tensile sample after testing.

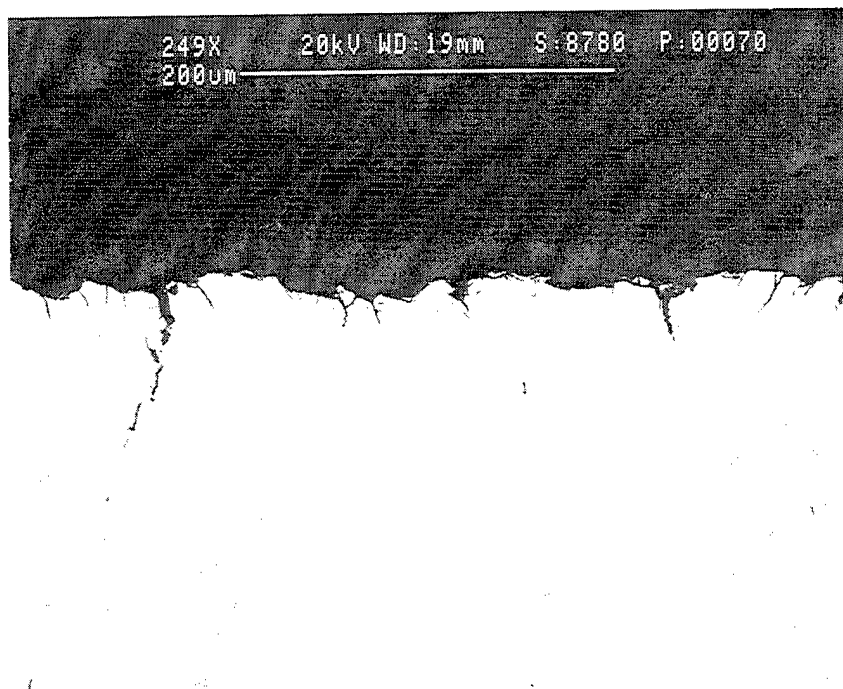


RT

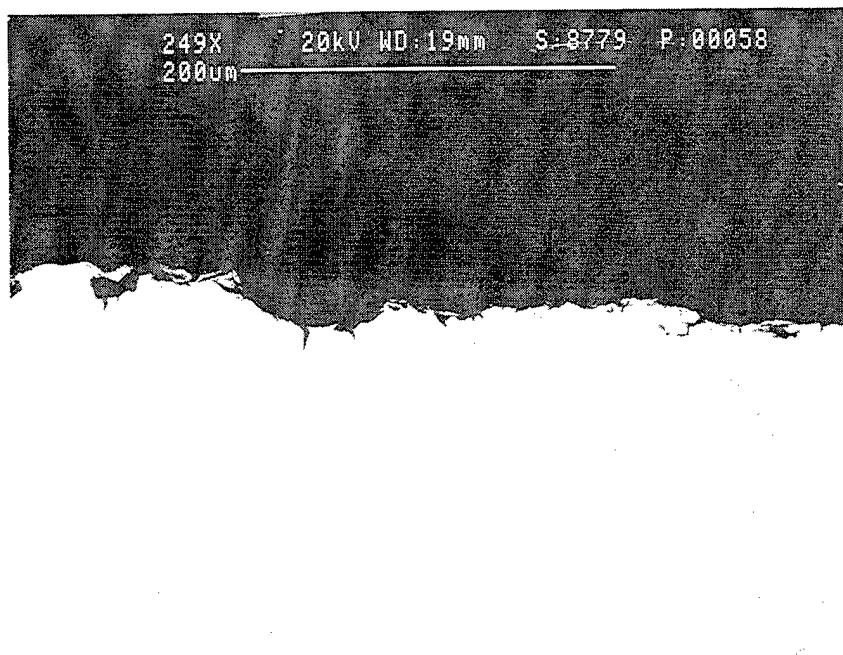


704°C

Figure 208. Cross sections of cermet coated alpha-2 tensile sample cyclically exposed at 760°C/100Hr before testing.



RT



704°C

Figure 209. Cross sections of cermet coated alpha-2 tensile sample cyclically exposed at 760°C/100Hr before testing.

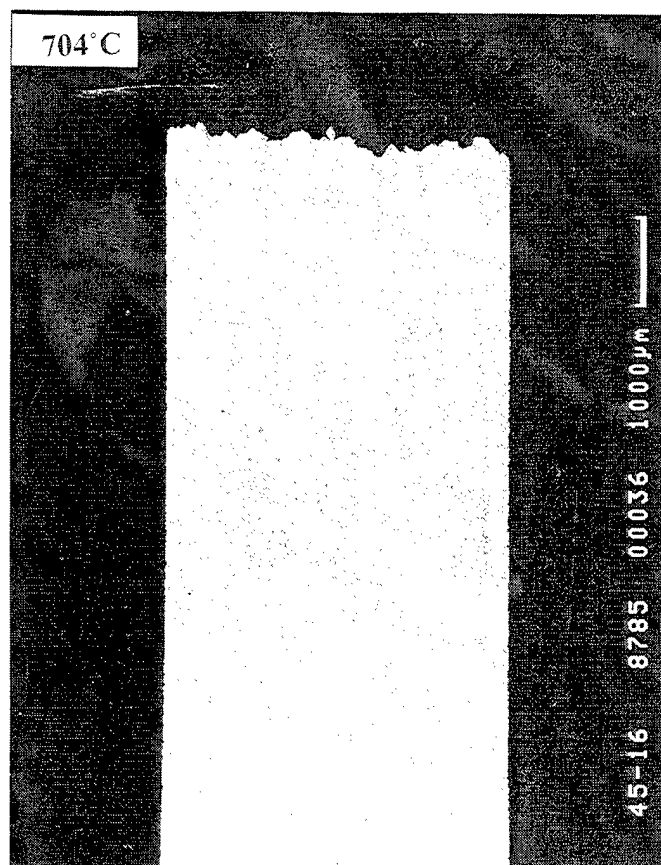
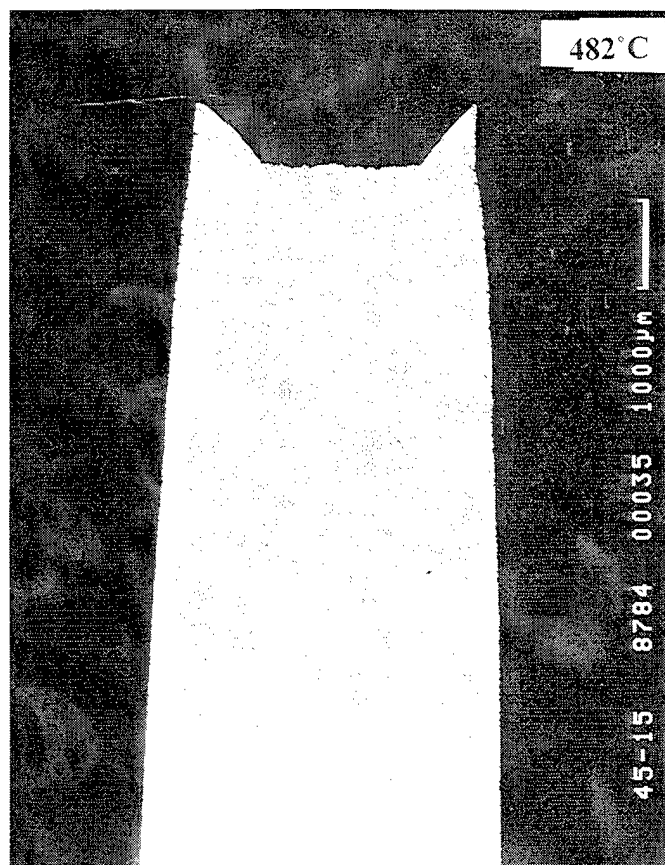
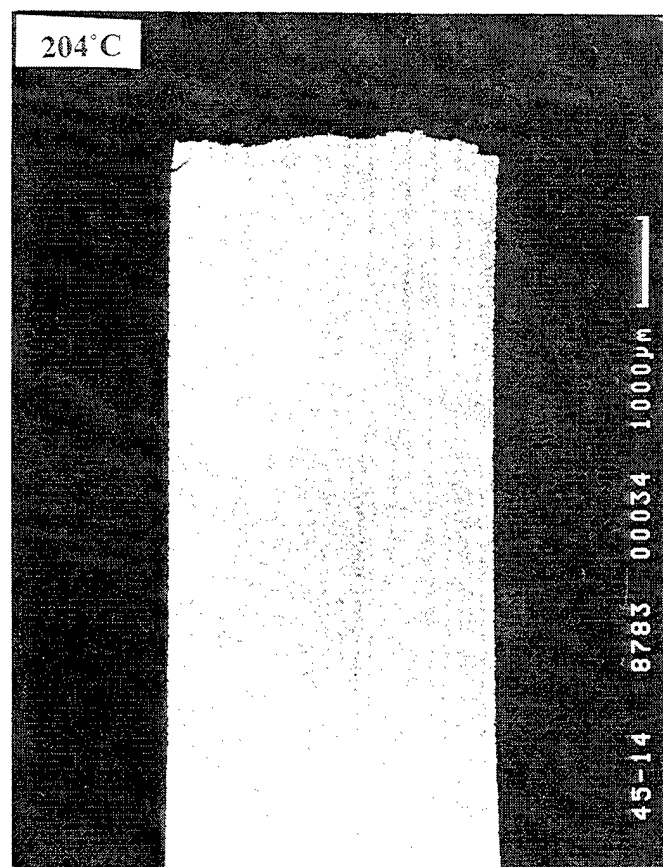
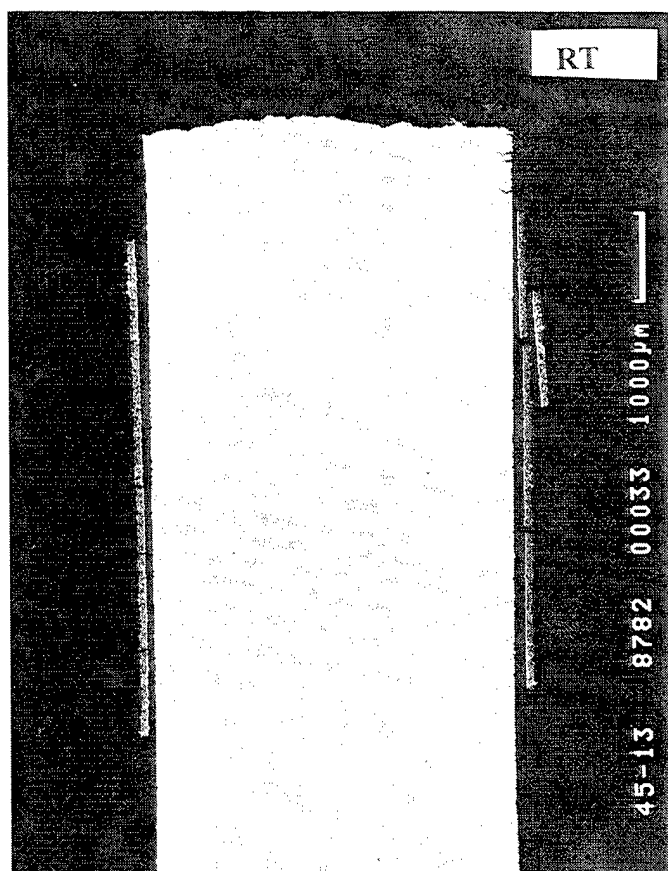


Figure 210. Cross sections of unexposed cermet coated CVD W alpha-2 tensile sample after testing.

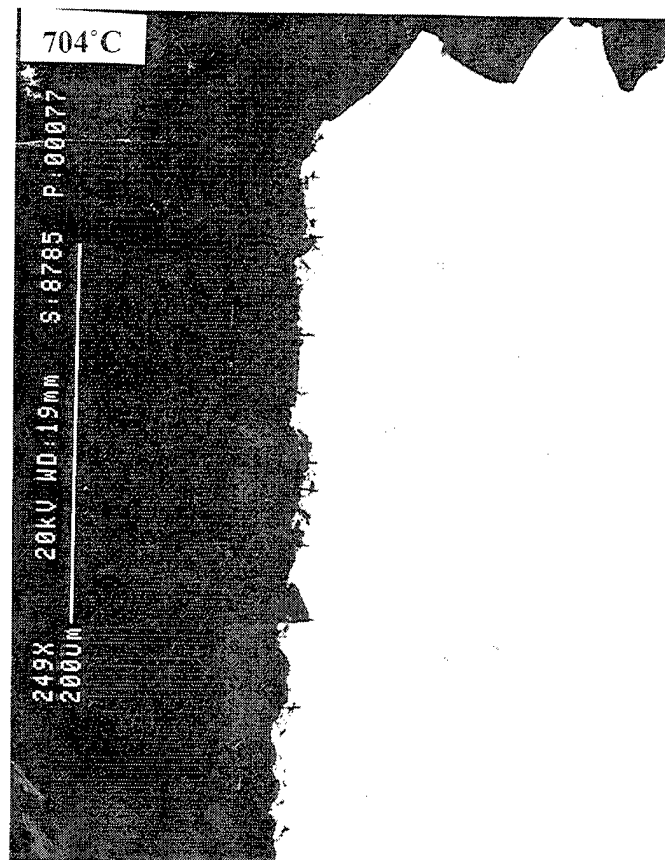
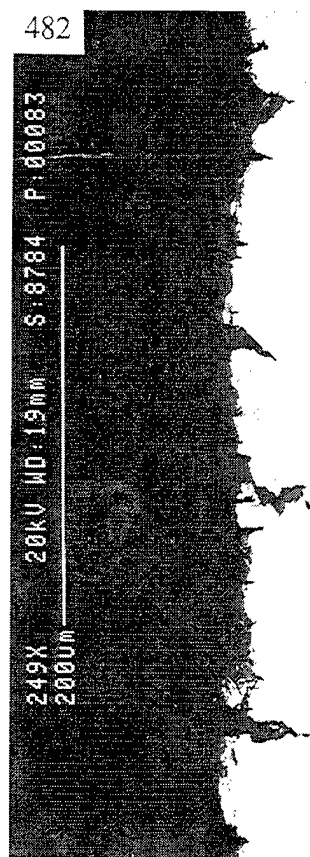
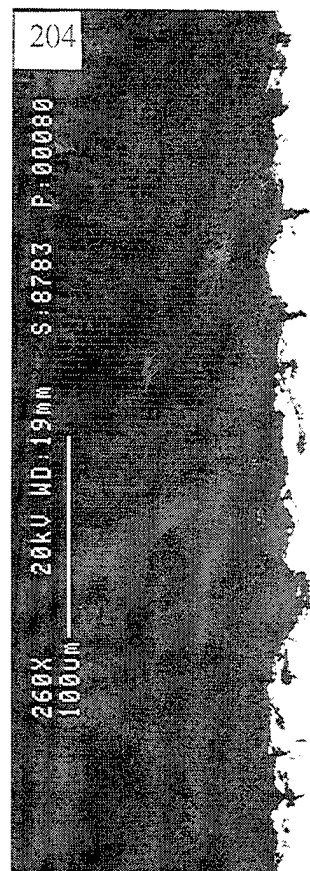
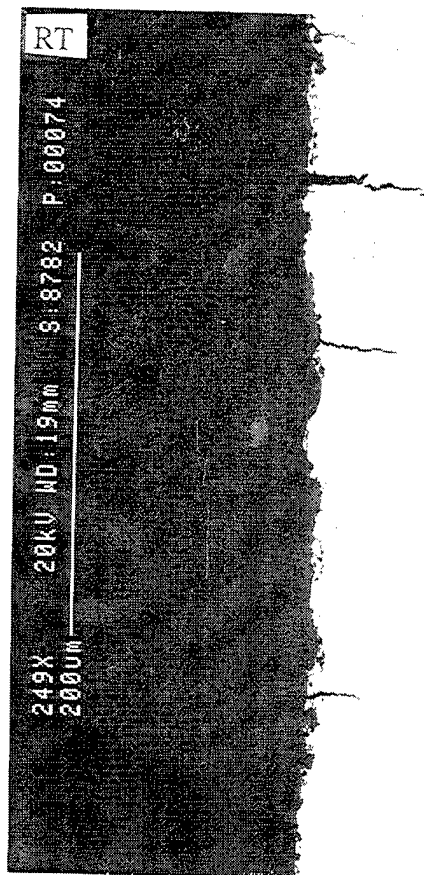


Figure 211. Cross sections of unexposed cermet coated CVD W alpha-2 tensile sample after testing.

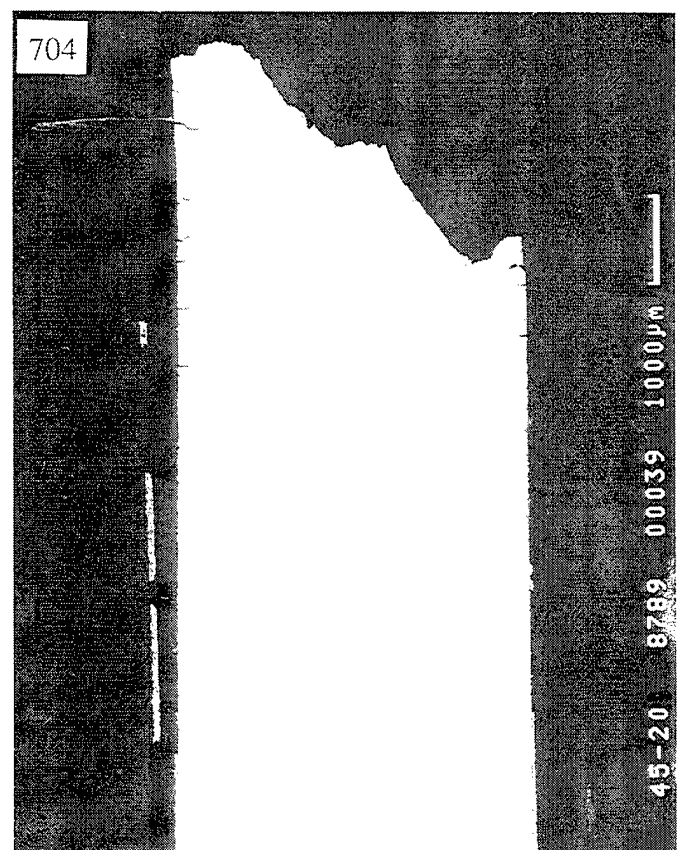
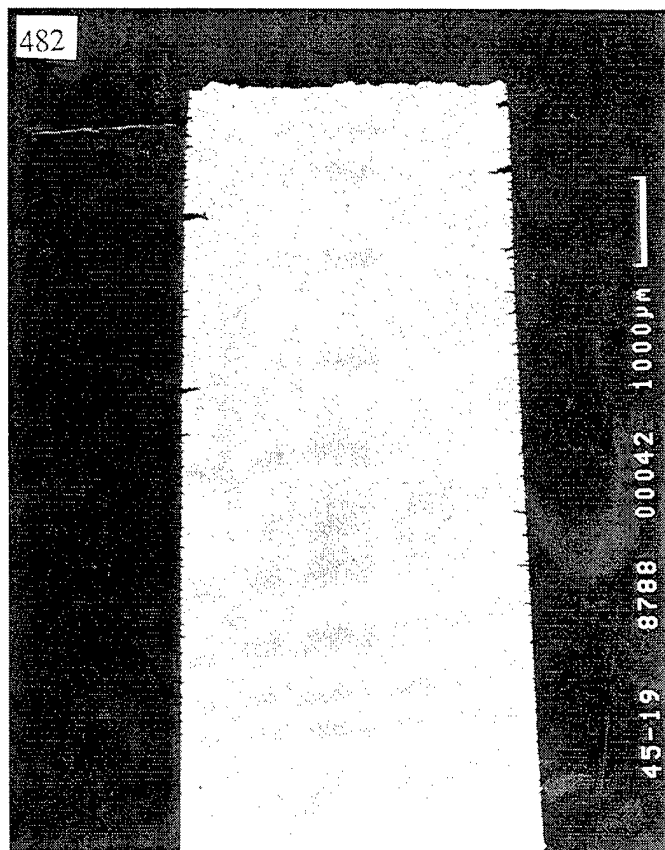
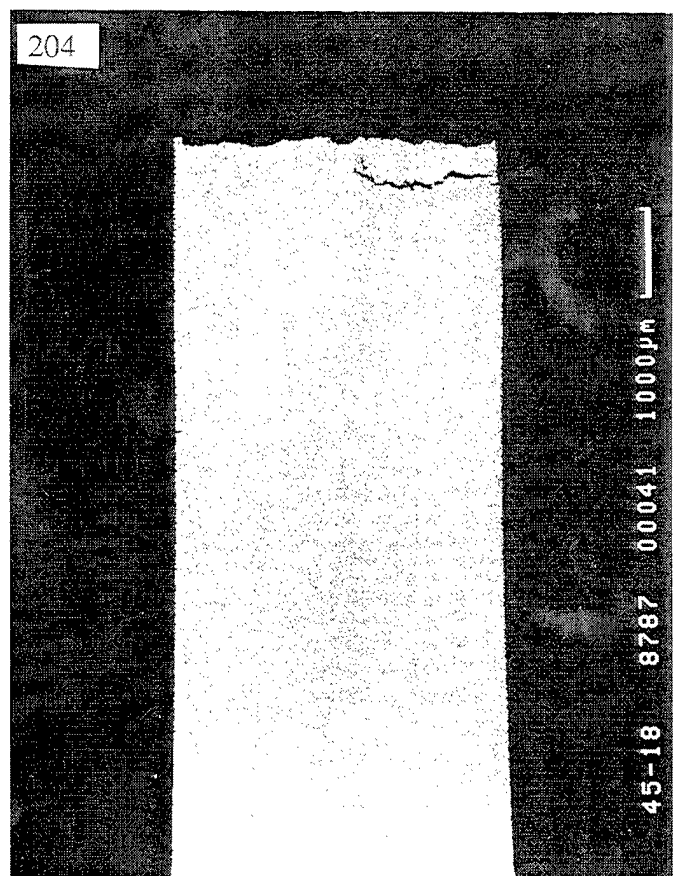
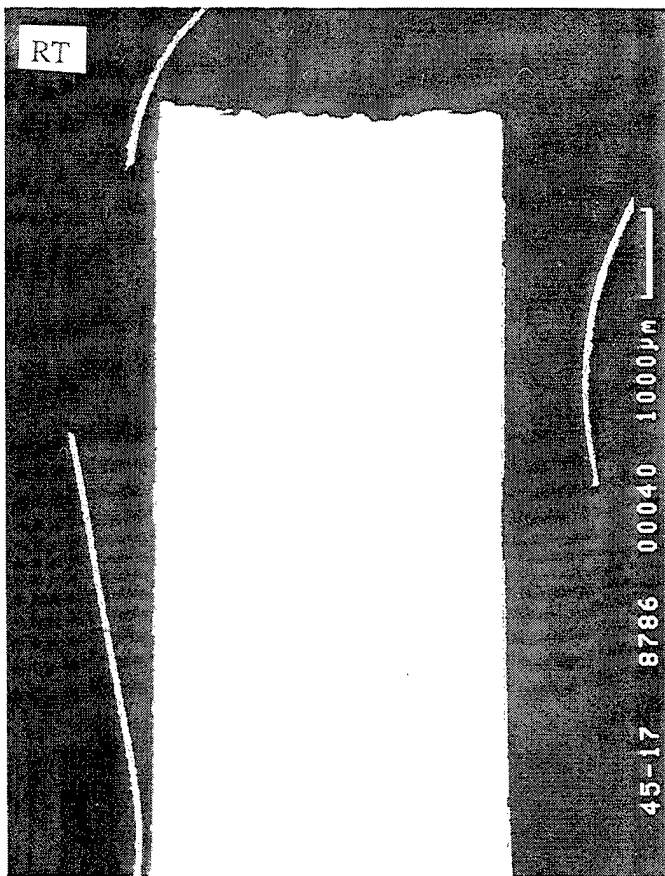


Figure 212. Cross sections of cermet coated CVD W alpha-2 tensile sample cyclically exposed at 760°C/100Hr before testing.

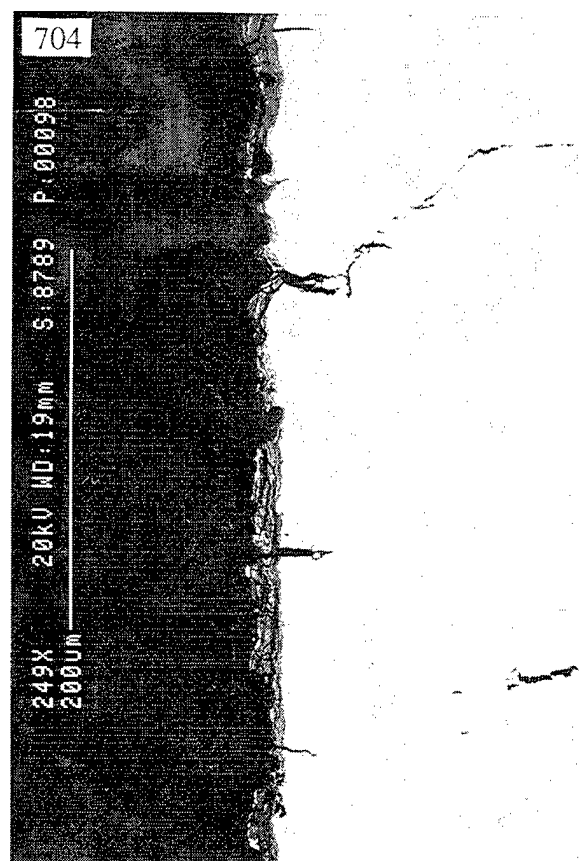
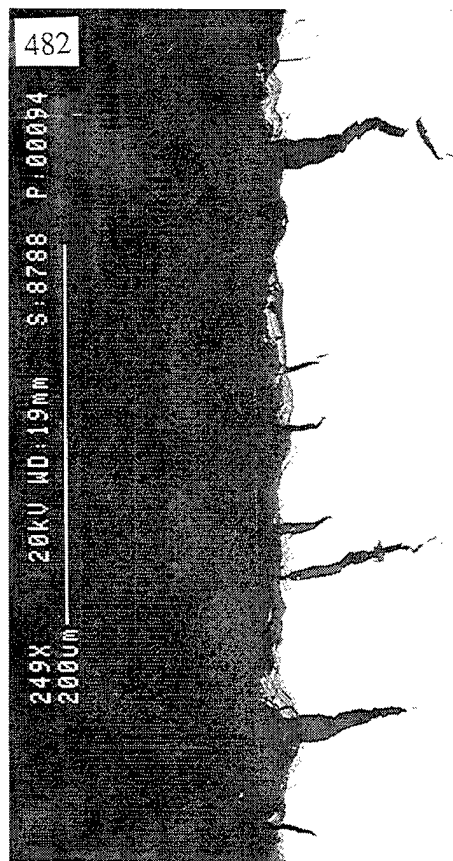
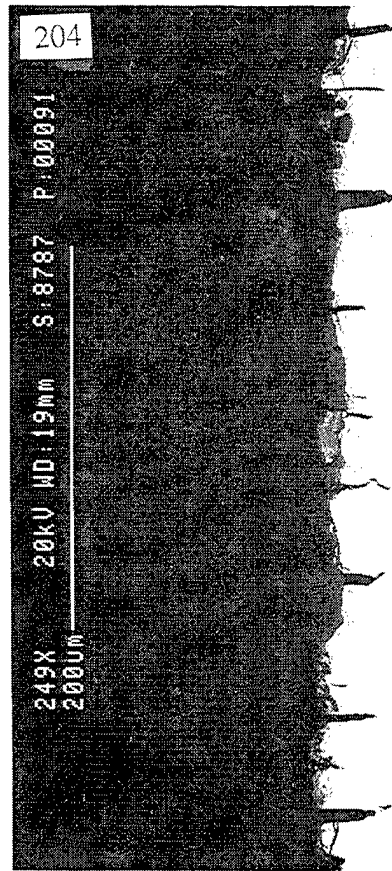
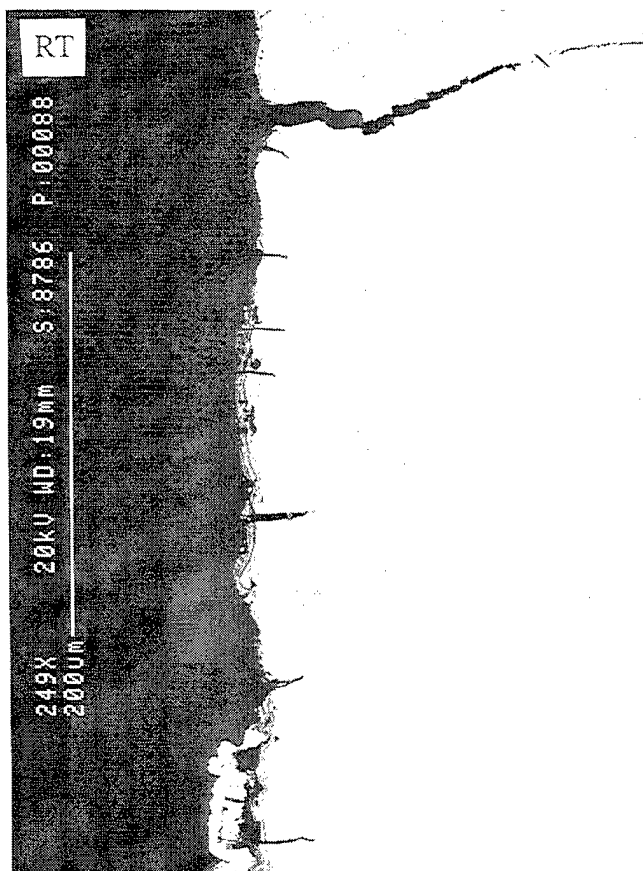


Figure 213. Cross sections of cermet coated CVD W alpha-2 tensile sample cyclically exposed at 760°C/100Hr before testing.

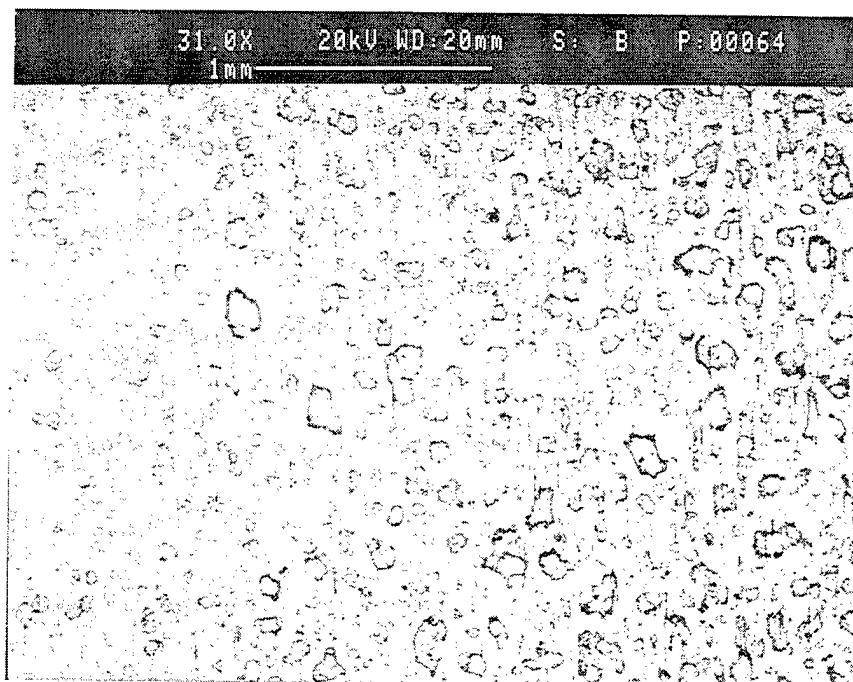
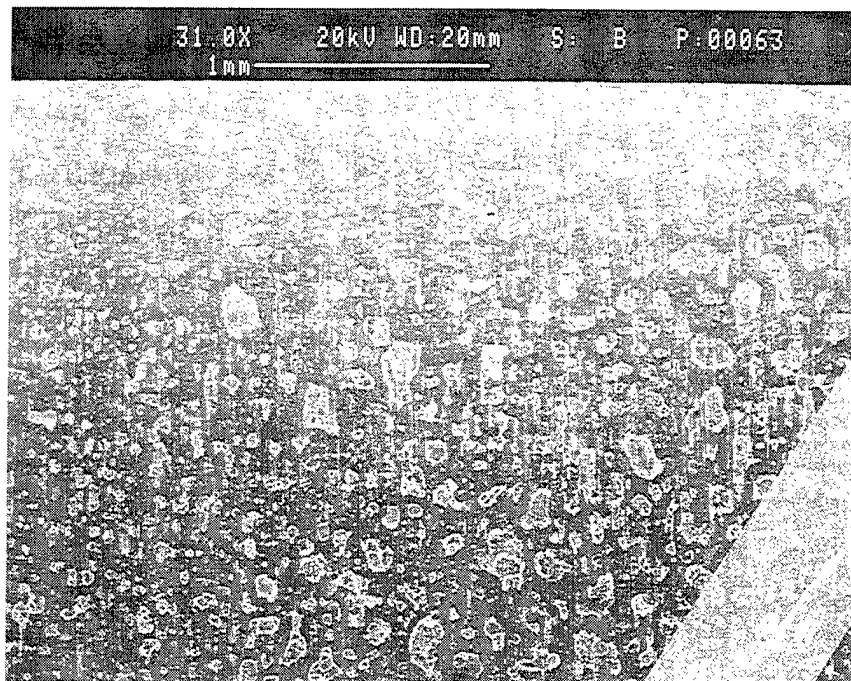


Figure 214. Micrograph of salt distribution on a steel tensile sample.

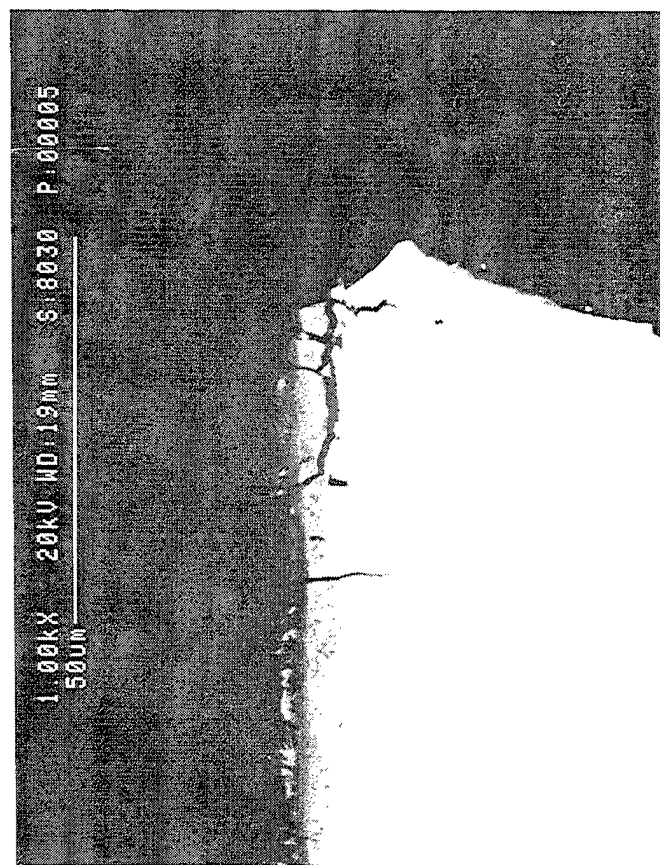
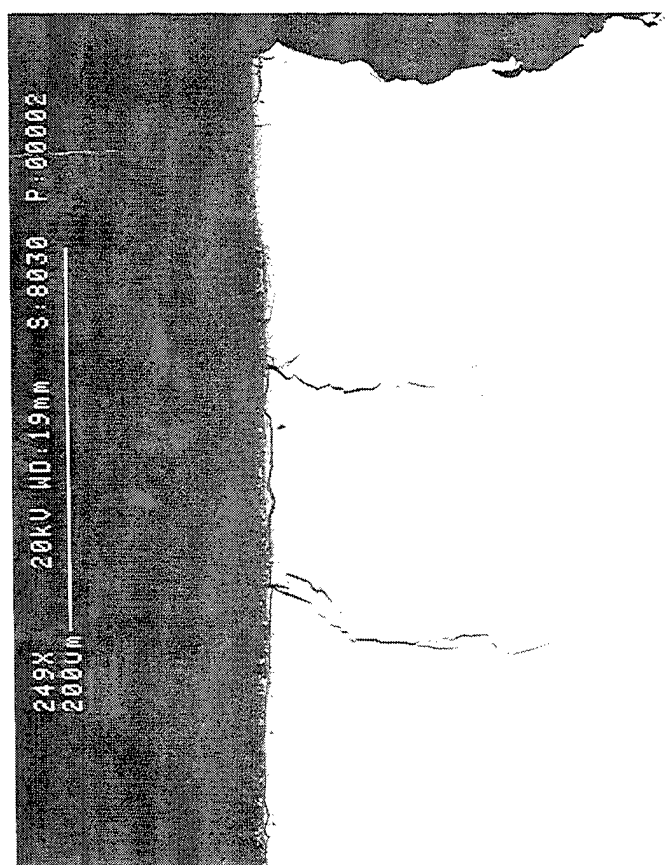
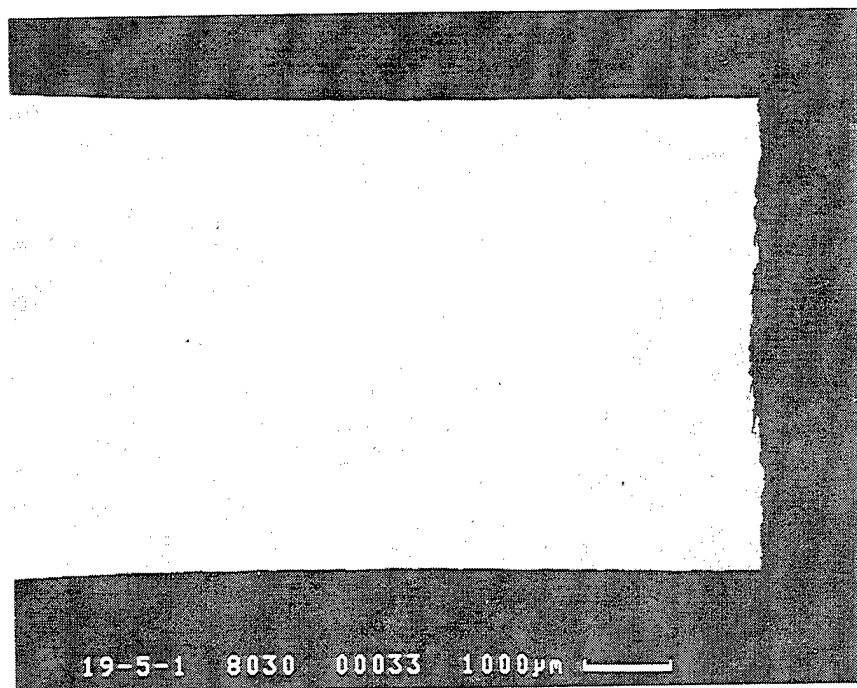


Figure 215. Cross sections of uncoated unexposed gamma samples after HSSCC testing. This exposure had no salt.

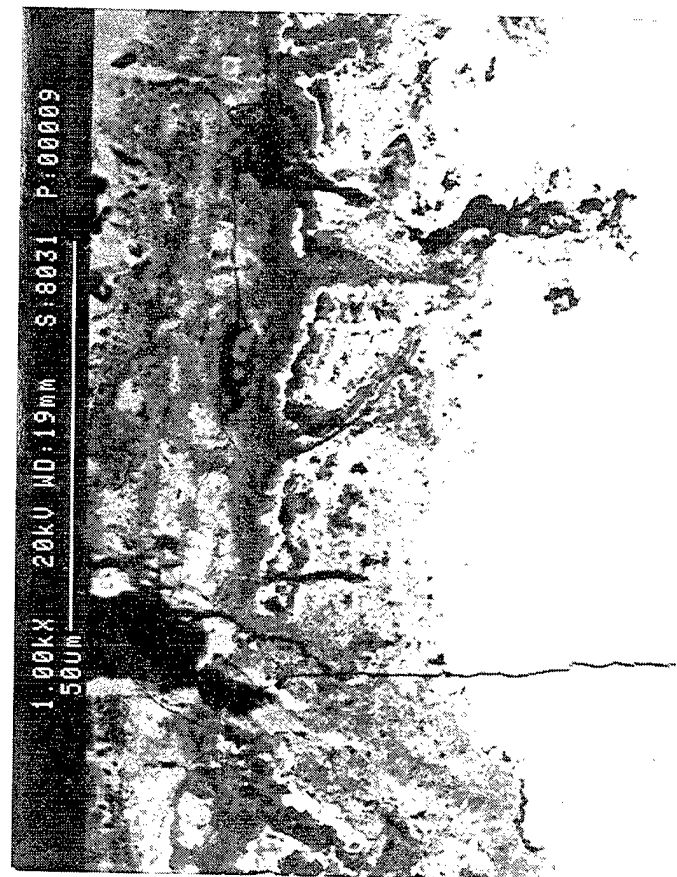
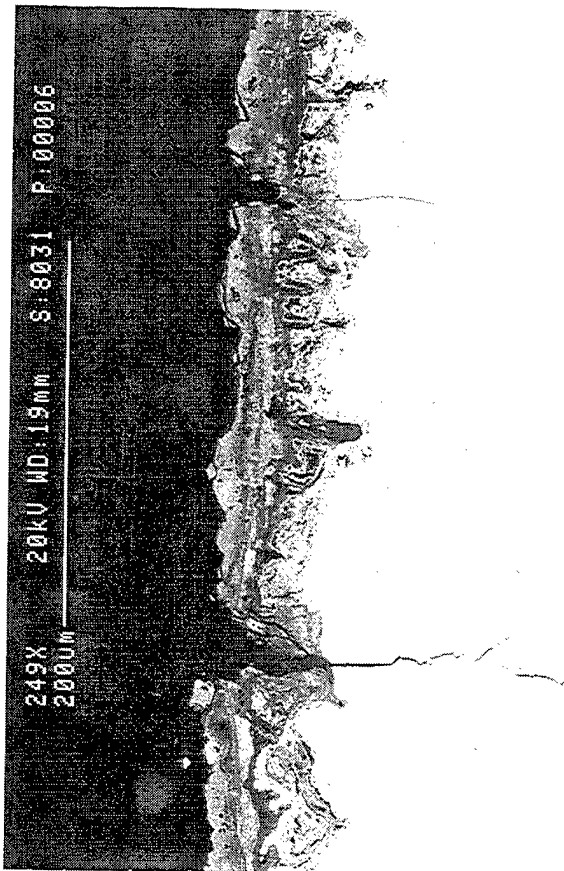
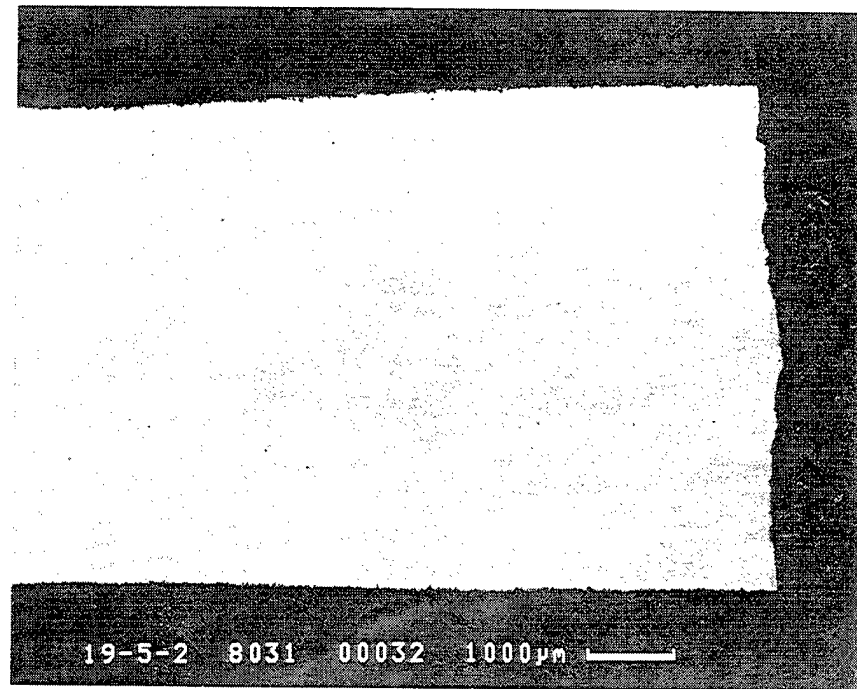


Figure 216. Cross sections of uncoated unexposed gamma tensile samples after HSSCC testing. This exposure had salt.

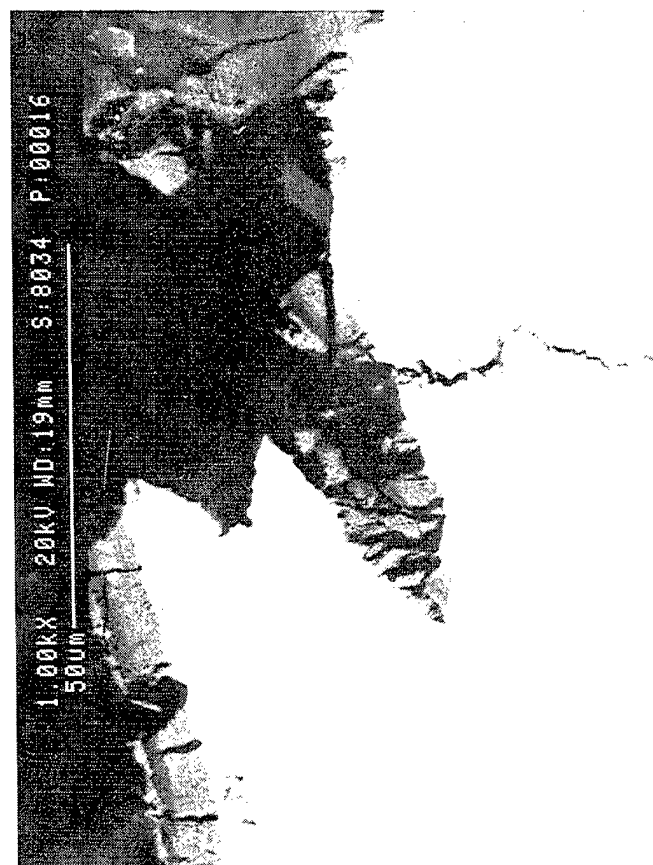
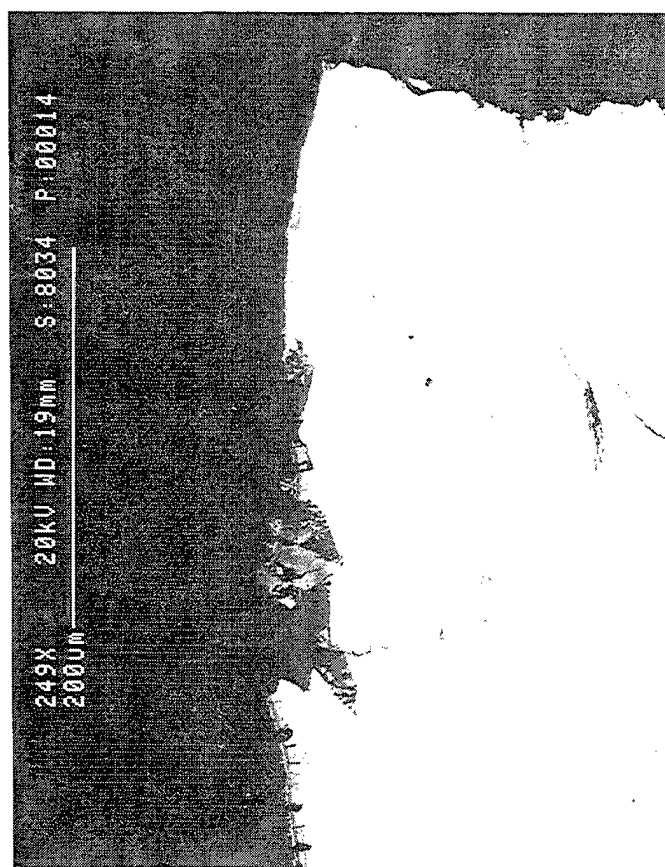
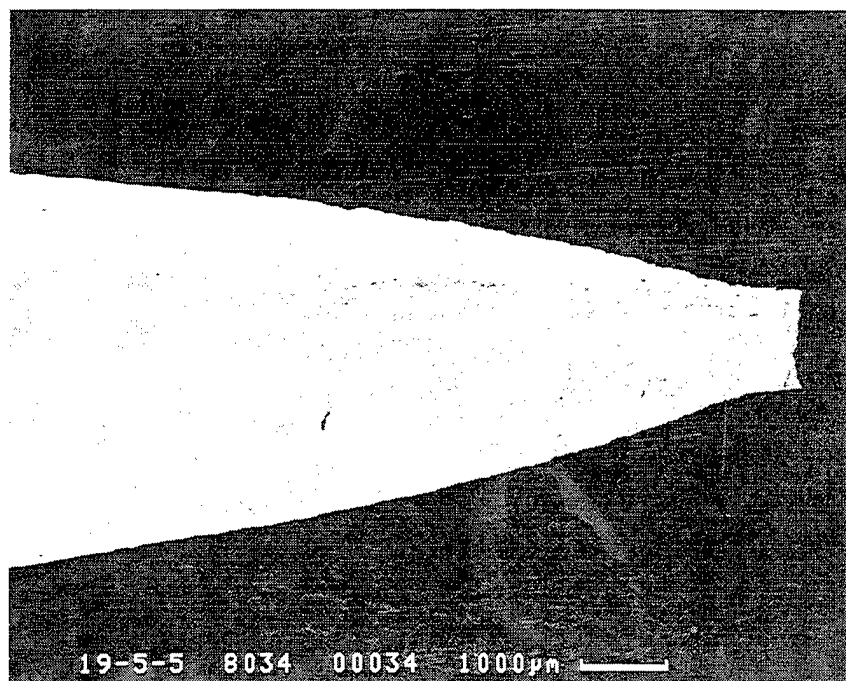


Figure 217. Cross sections of uncoated gamma samples cyclically exposed at 760°C/100Hr after HSSCC testing. This exposure had no salt.

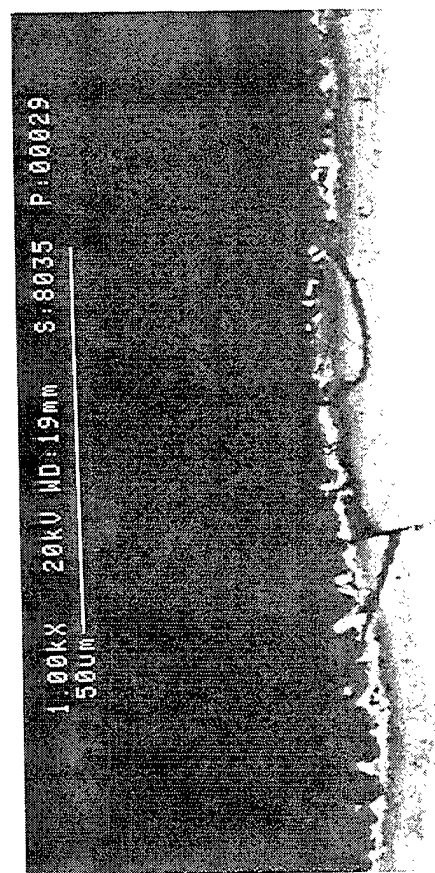
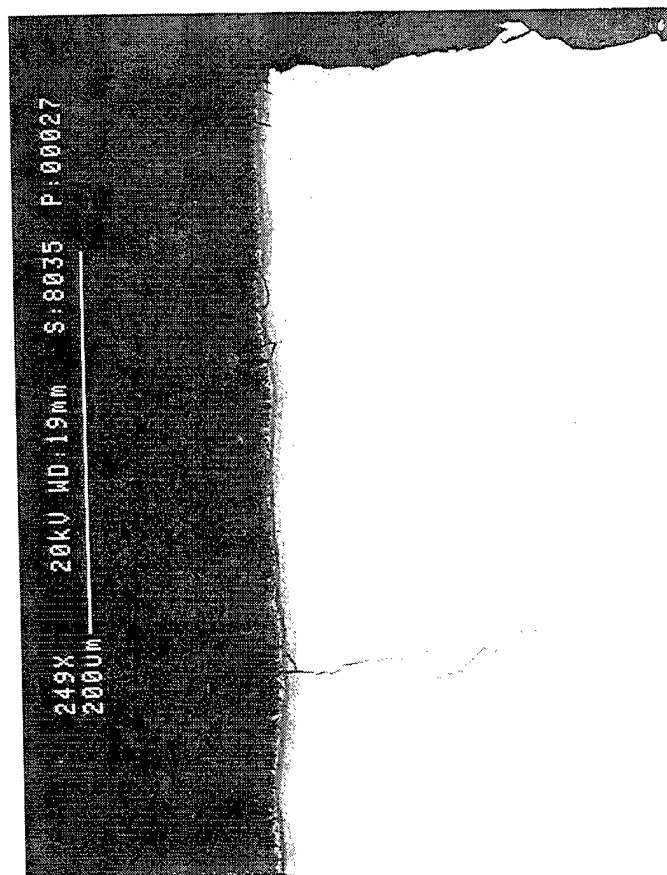
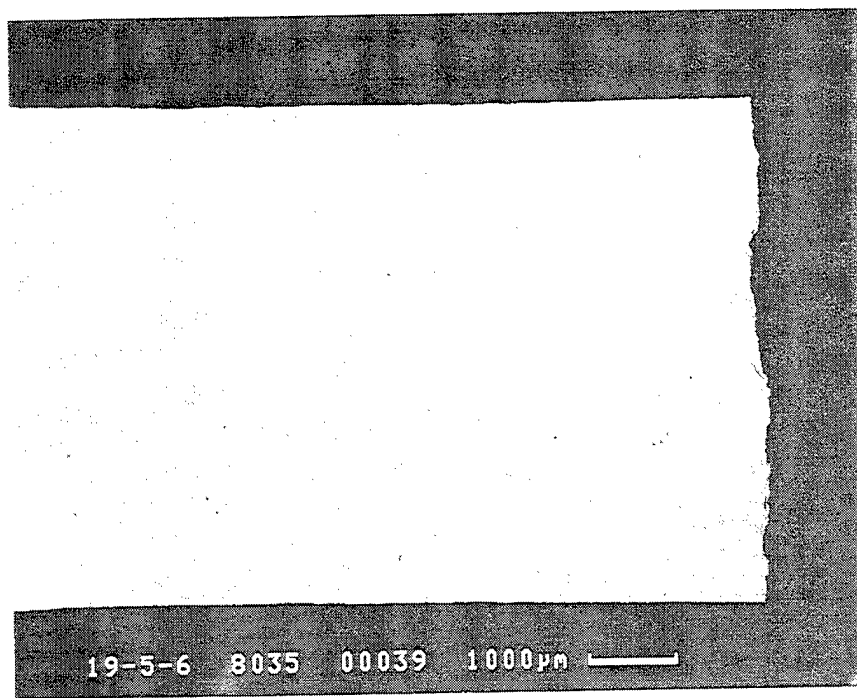


Figure 218. Cross sections of uncoated gamma samples cyclically exposed at 760°C/100Hr after HSSCC testing. This exposure had salt.

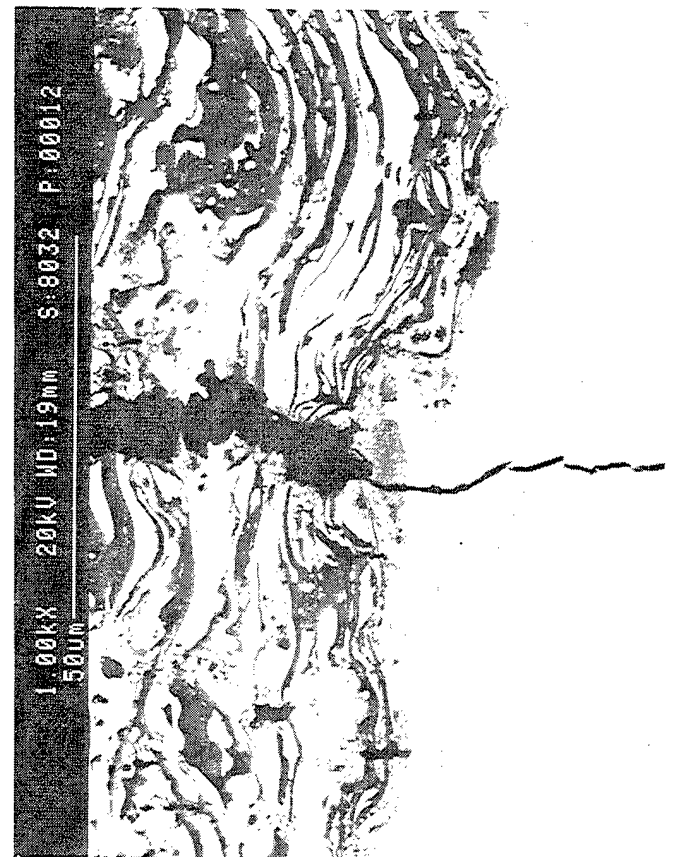
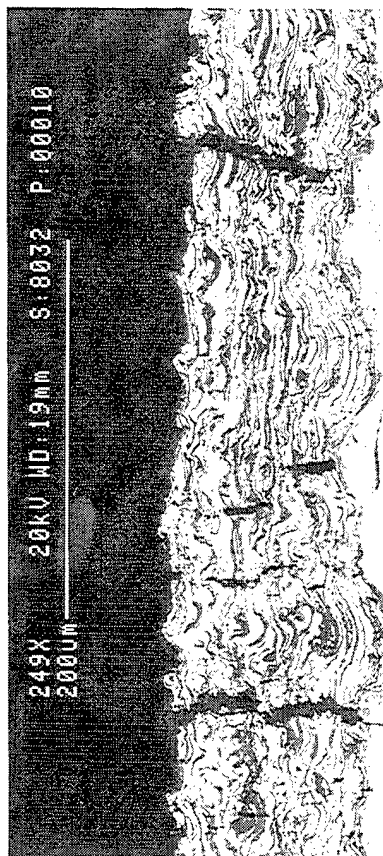
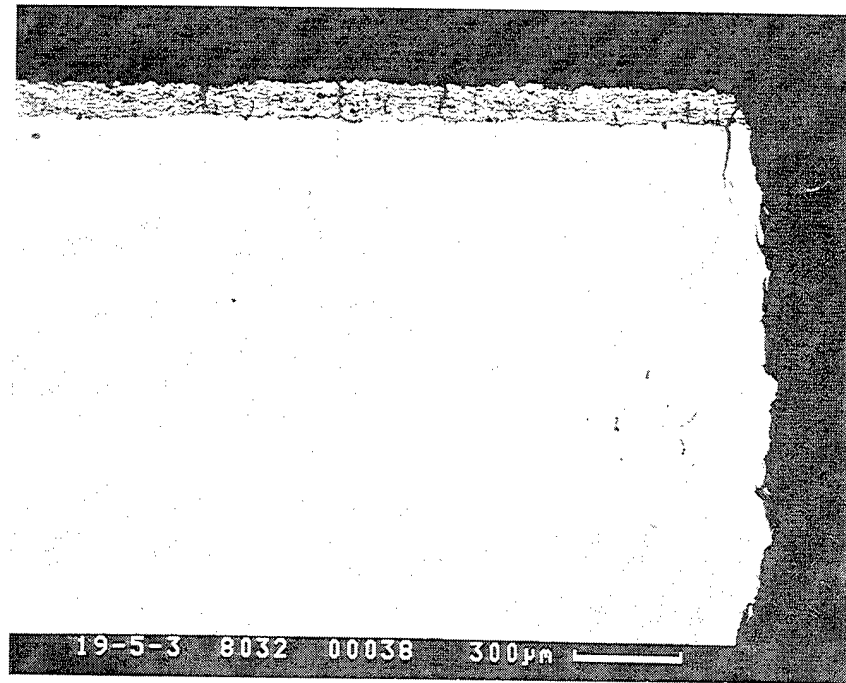


Figure 219. Cross sections of unexposed cermet coated gamma tensile samples after HSSCC testing. This exposure had salt.

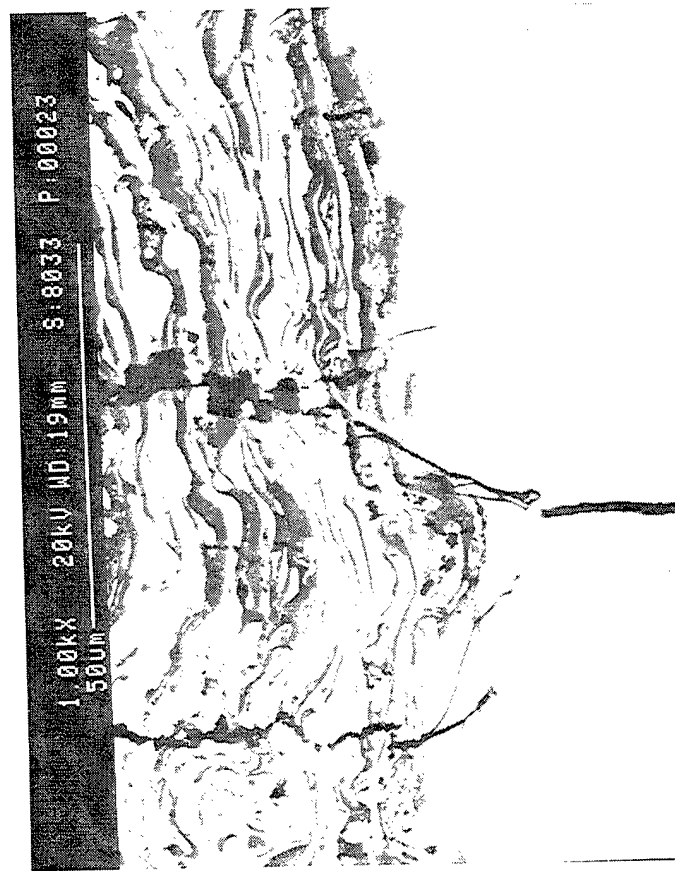
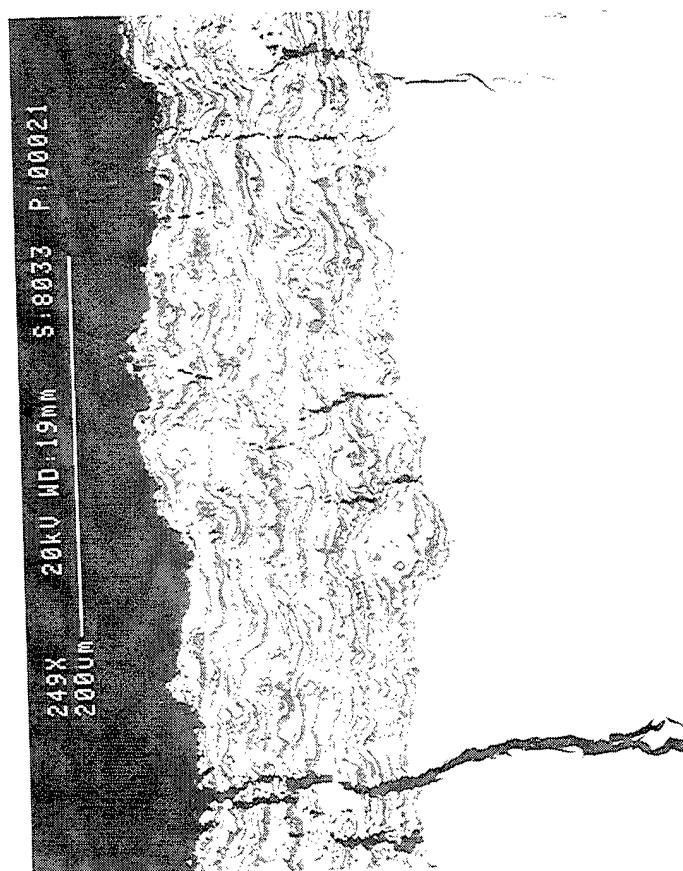
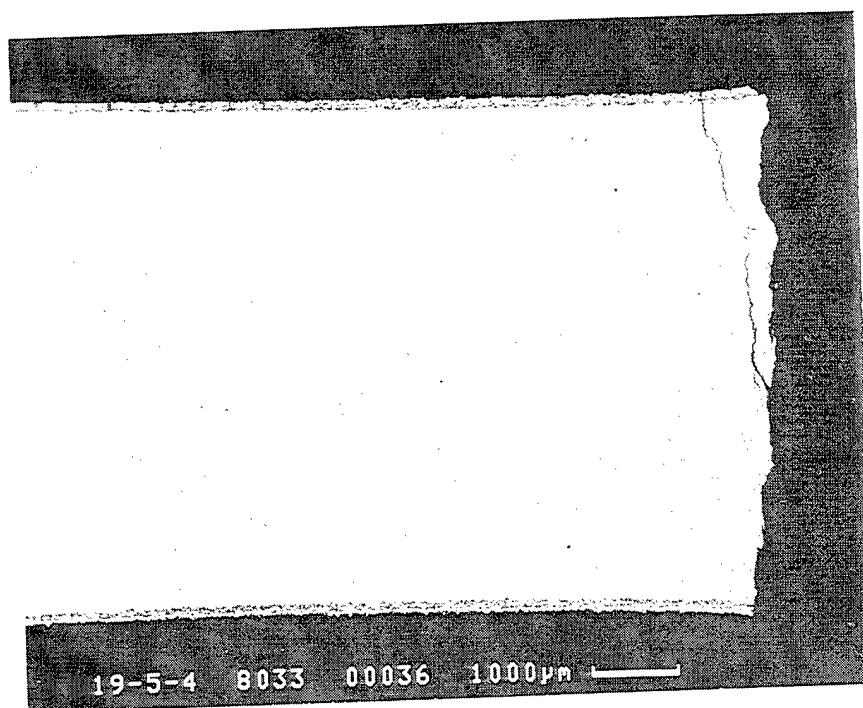


Figure 220. Cross sections of unexposed cermet coated gamma tensile samples after HSSCC testing. This exposure had salt.

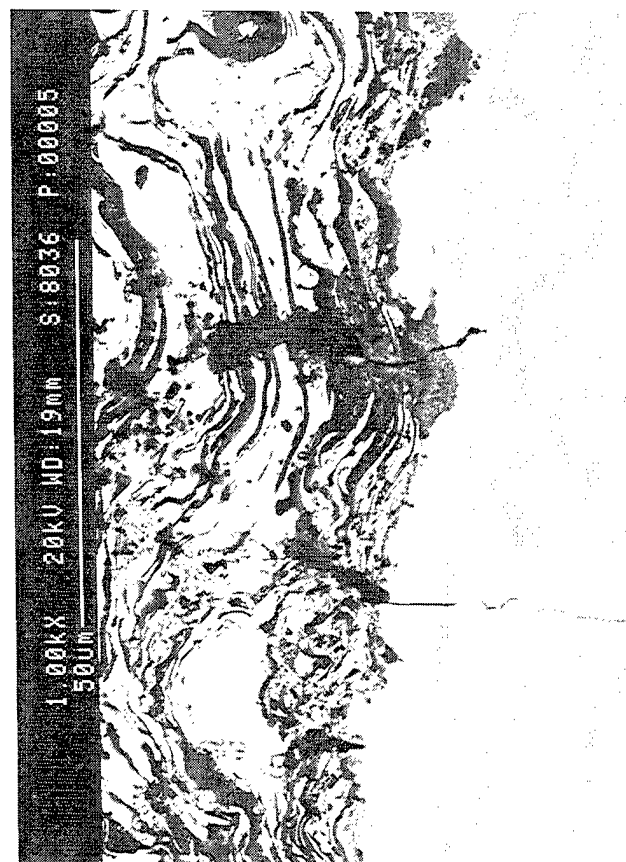
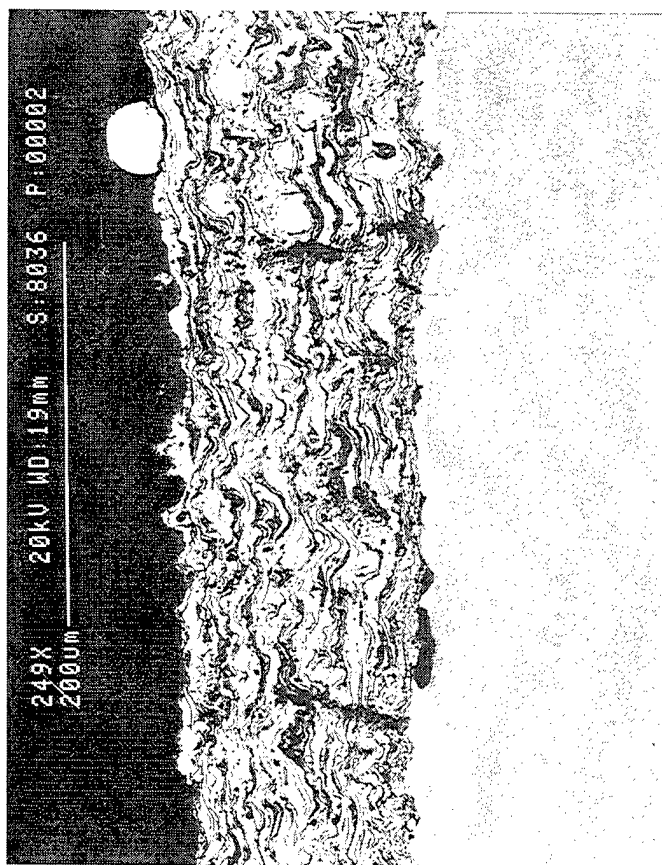
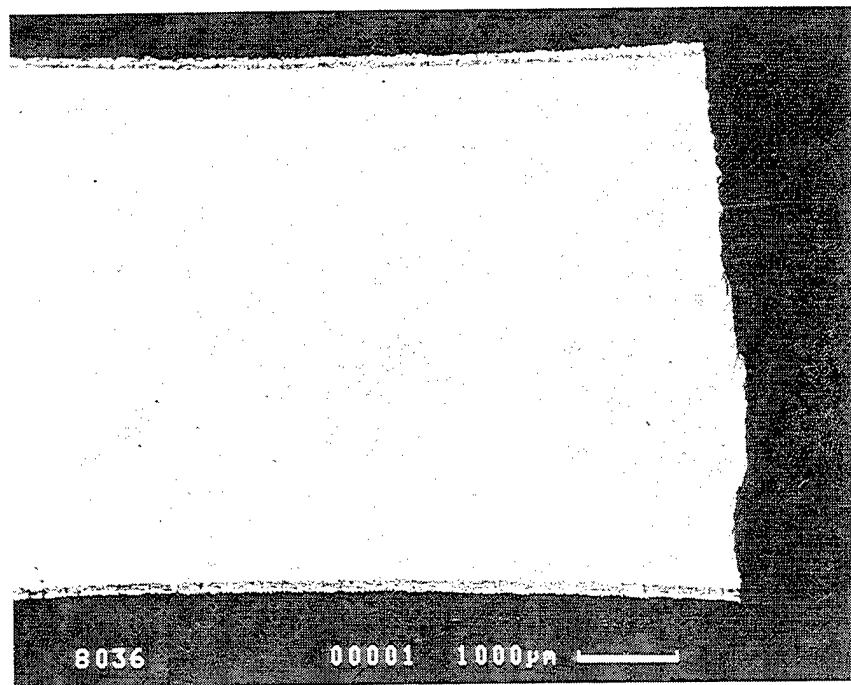


Figure 221. Cross sections of cermet coated gamma tensile sample cyclically exposed at 760°C/100Hr after HSSCC testing. This exposure had no salt.

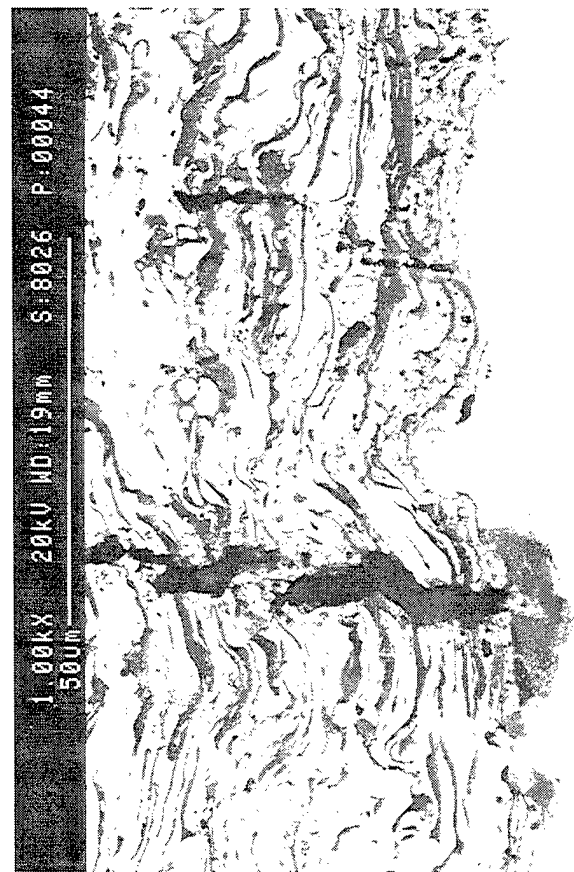
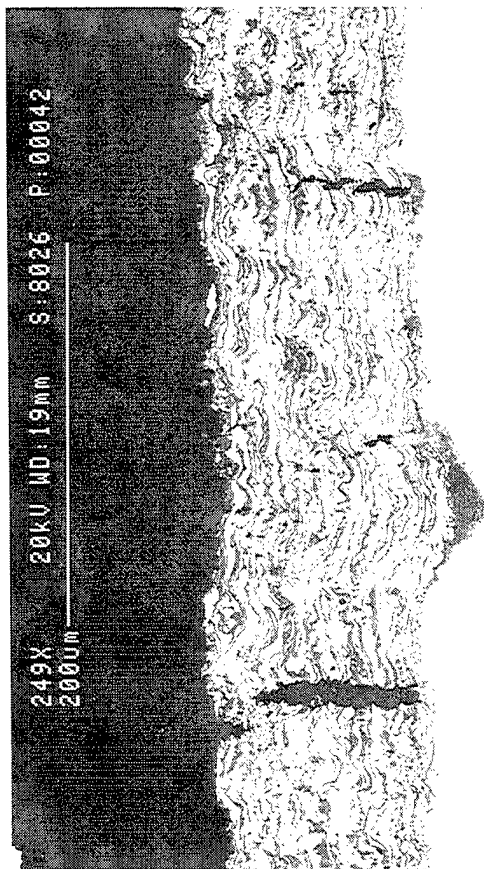
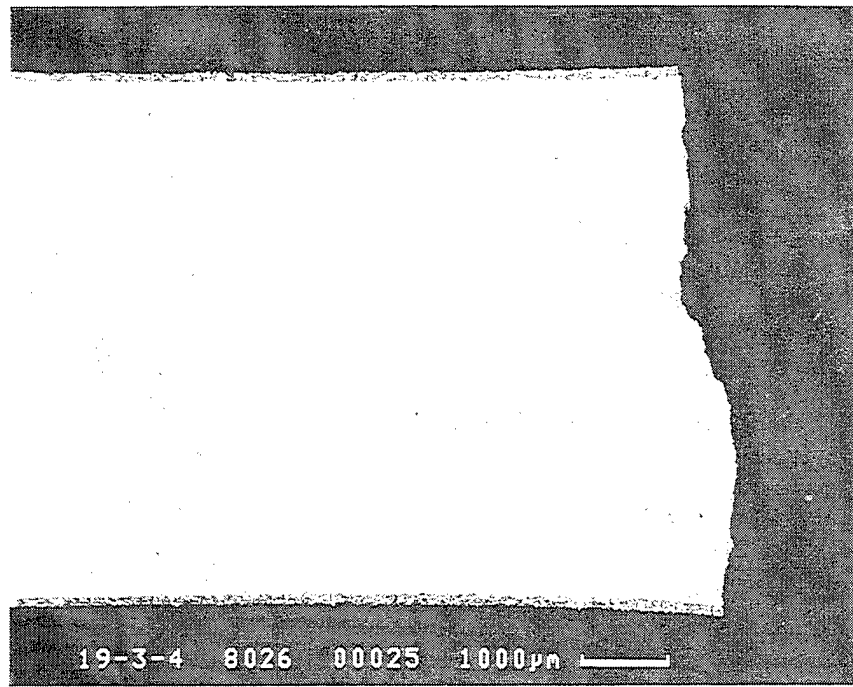


Figure 222. Cross sections of cermet coated gamma tensile sample cyclically exposed at 760°C/100Hr after HSSCC testing. This exposure had salt.

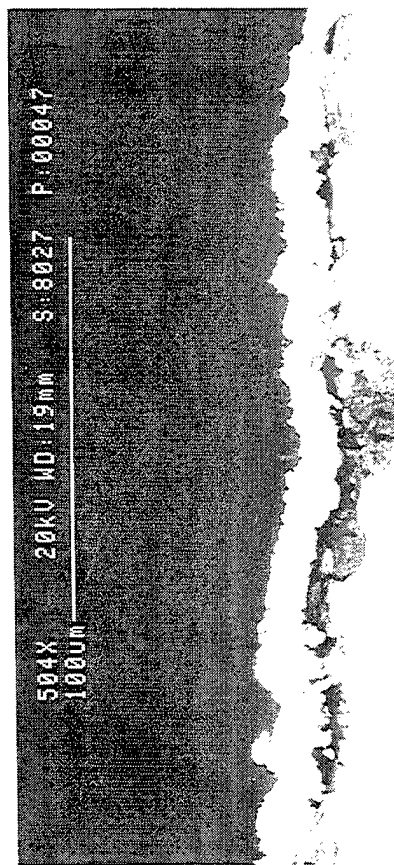
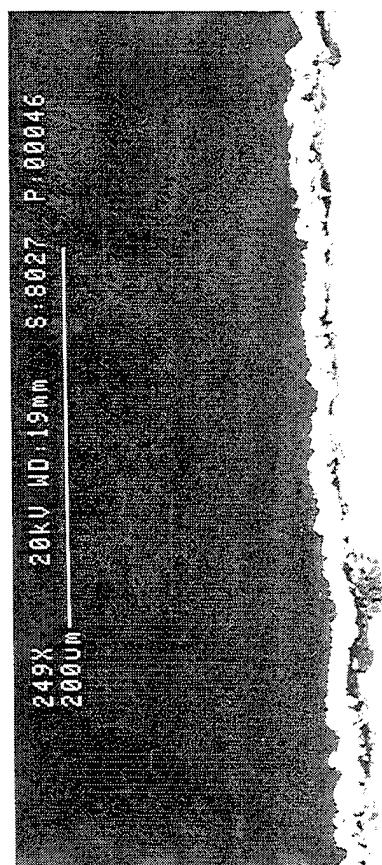
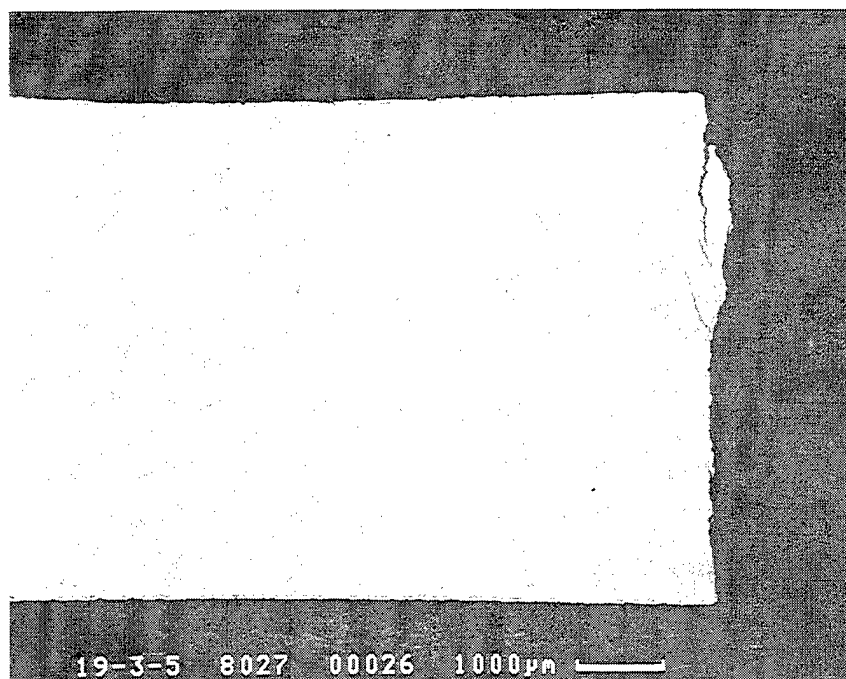


Figure 223. Cross sections of unexposed cermet W CVD coated gamma tensile sample after HSSCC testing. This exposure had no salt.

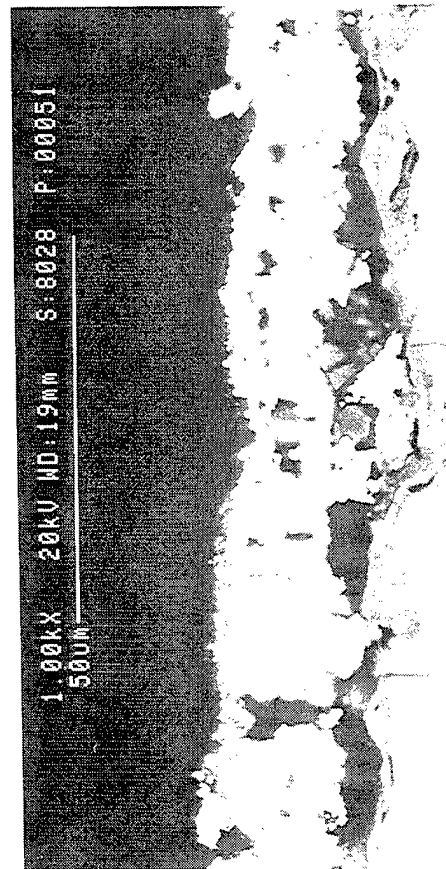
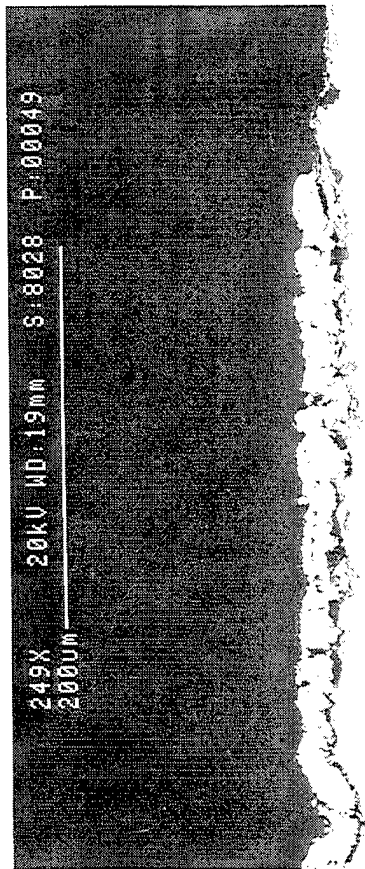
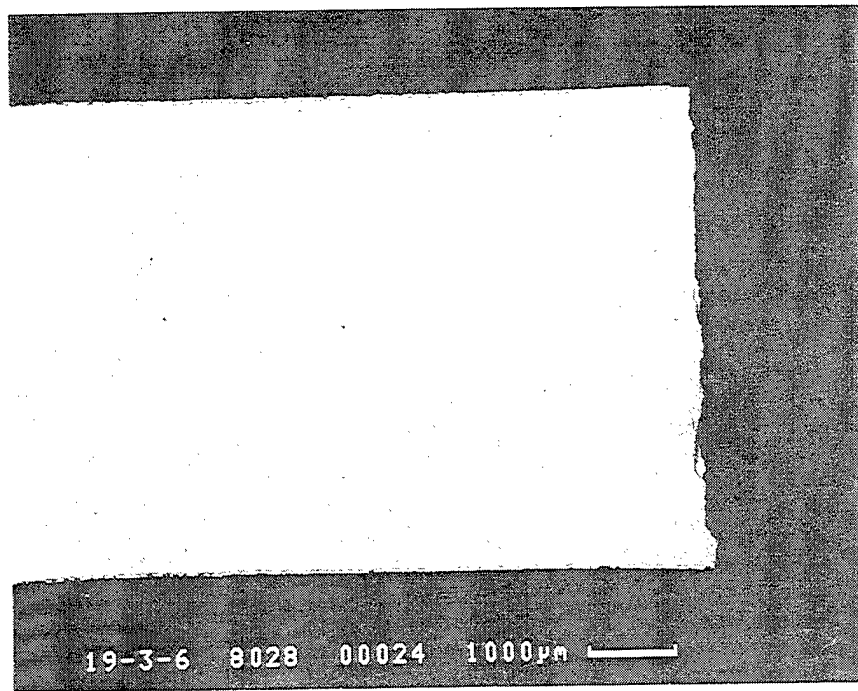


Figure 224. Cross sections of unexposed cermet W CVD coated gamma tensile sample after HSSCC testing. this exposure had salt.

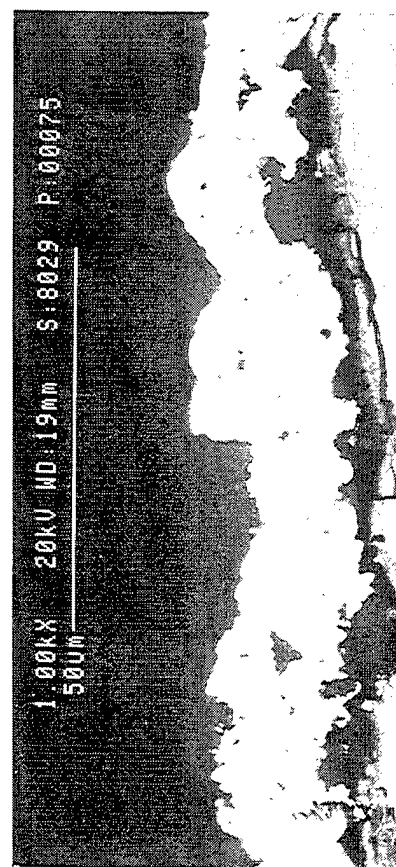
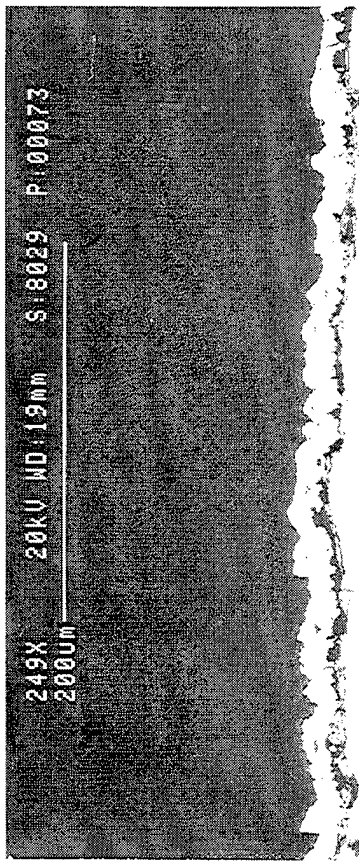
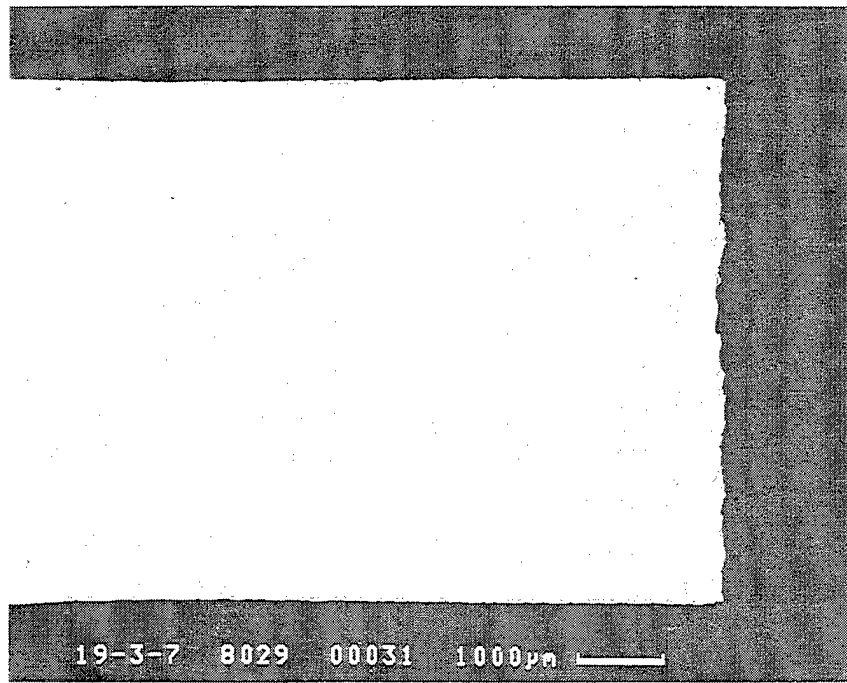


Figure 225. Cross sections of cermet W CVD coated gamma tensile sample cyclically exposed at 760°C/100Hr after HSSCC testing. This exposure had no salt.

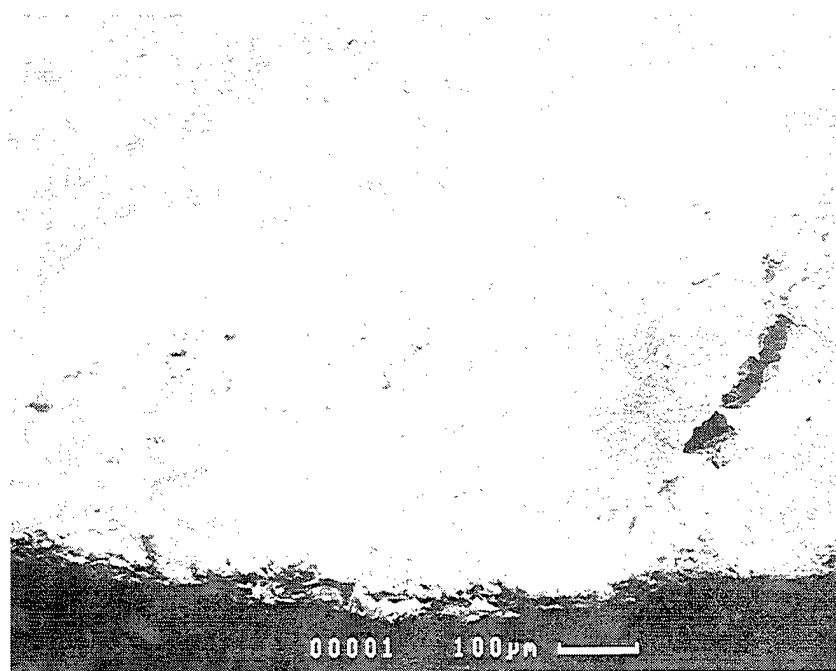
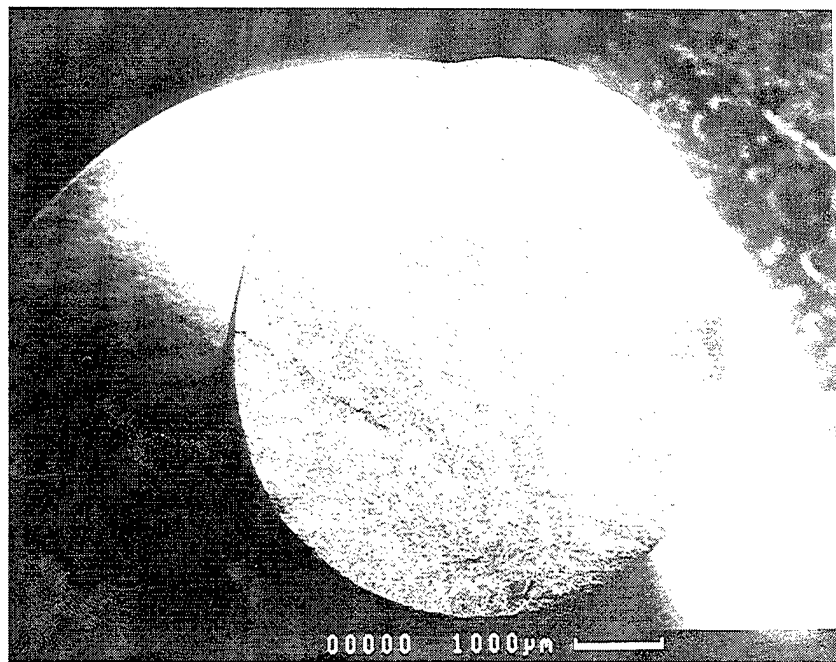


Figure 226. Cross sections of cermet W CVD coated gamma tensile sample cyclically exposed at 760°C/100hr after HSSCC testing. This exposure had no salt.

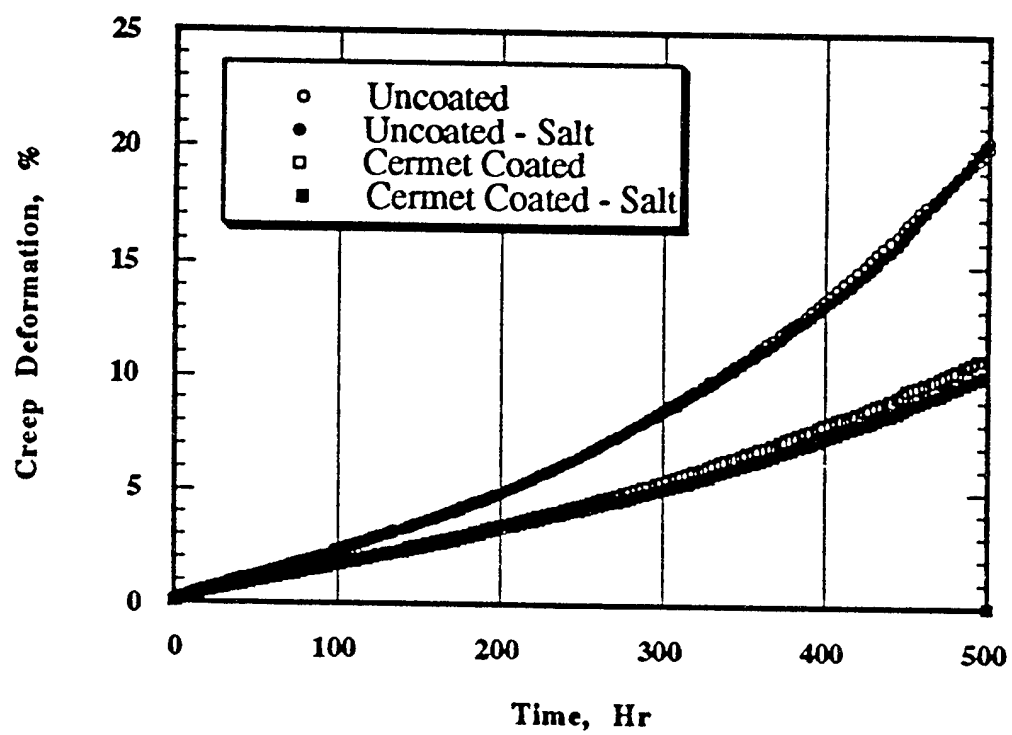


Figure 227. Graph showing creep behavior of unexposed coated and uncoated gamma samples.

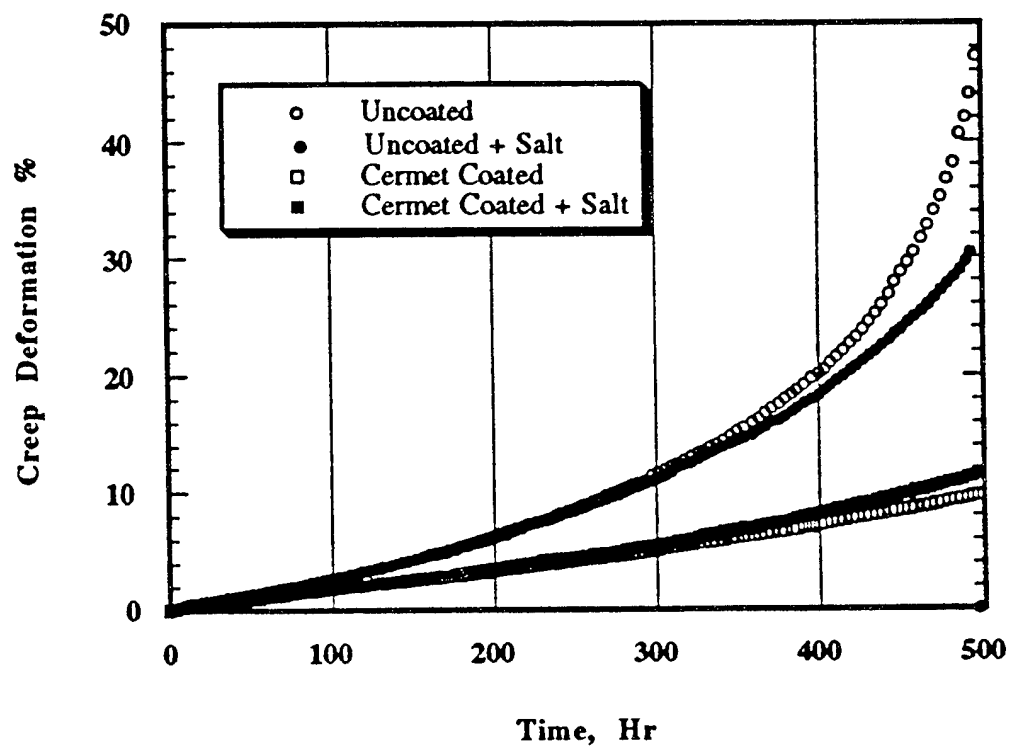


Figure 228. Graph showing creep behavior of cyclically exposed coated and uncoated gamma samples.

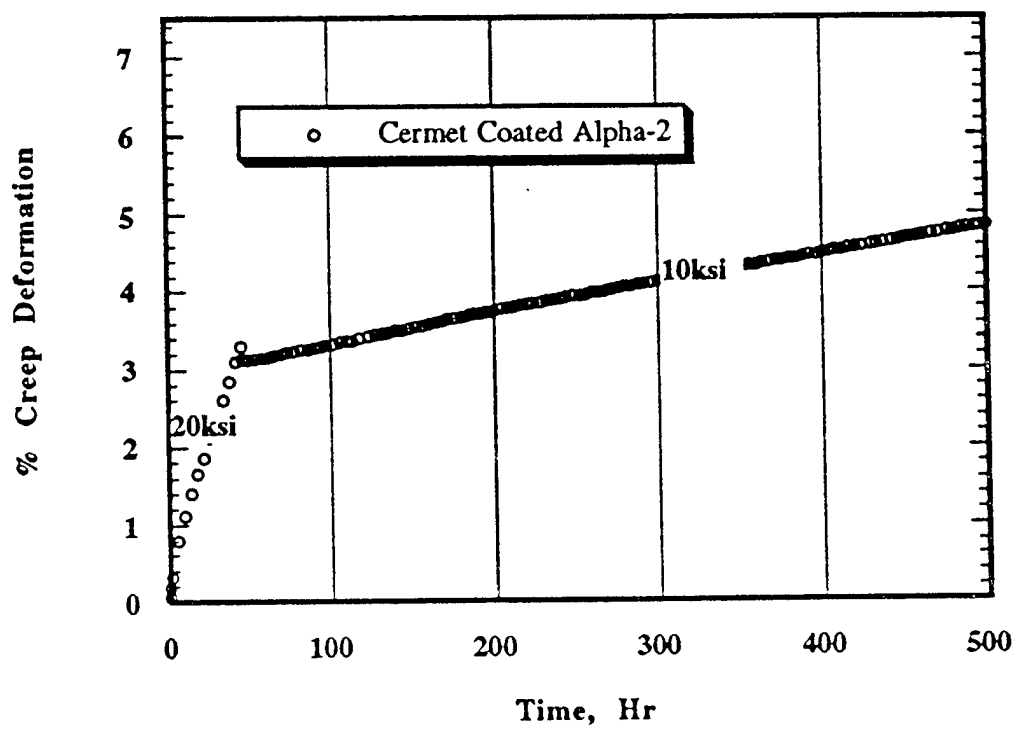


Figure 229. Graph showing the change in creep behavior of alpha-2 when stress was reduced from 20 to 10ksi at 760°C.

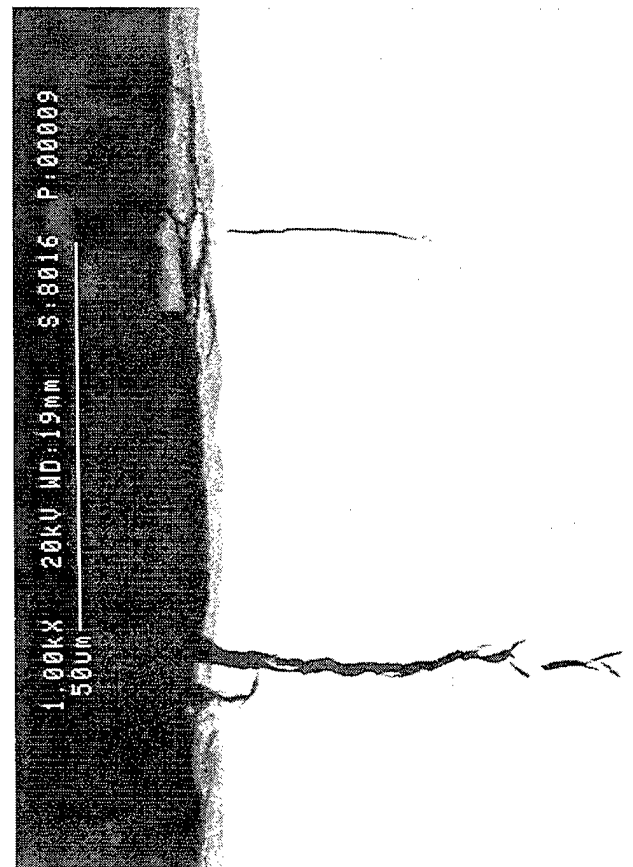
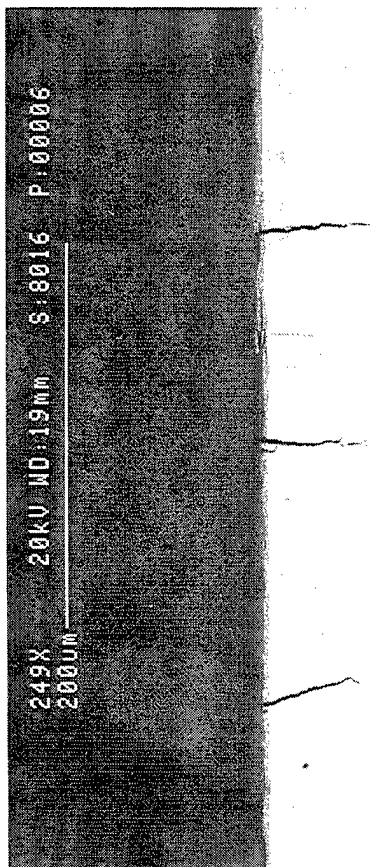
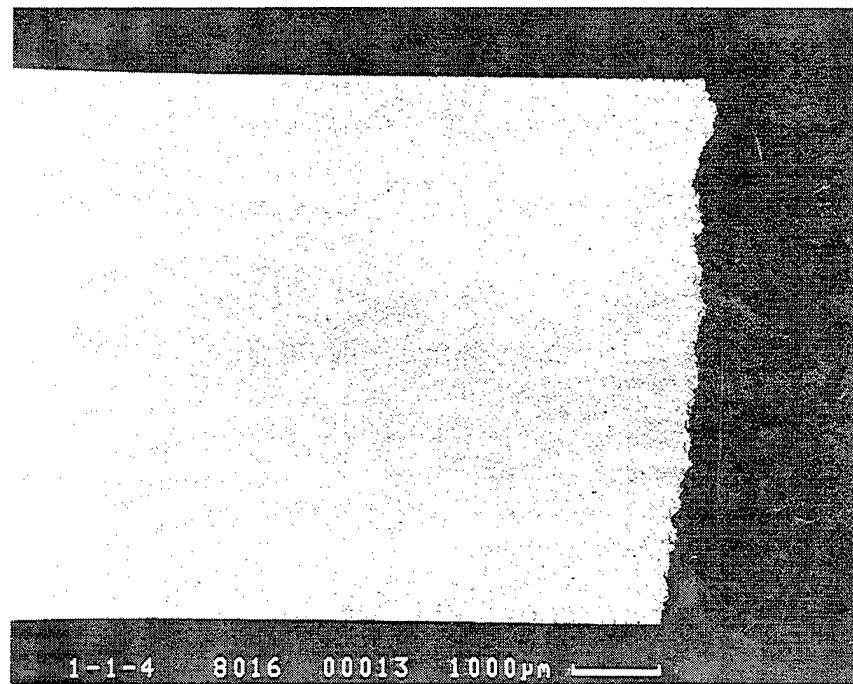


Figure 230. Cross sections of uncoated unexposed alpha-2 samples after HSSCC testing. This exposure had no salt.

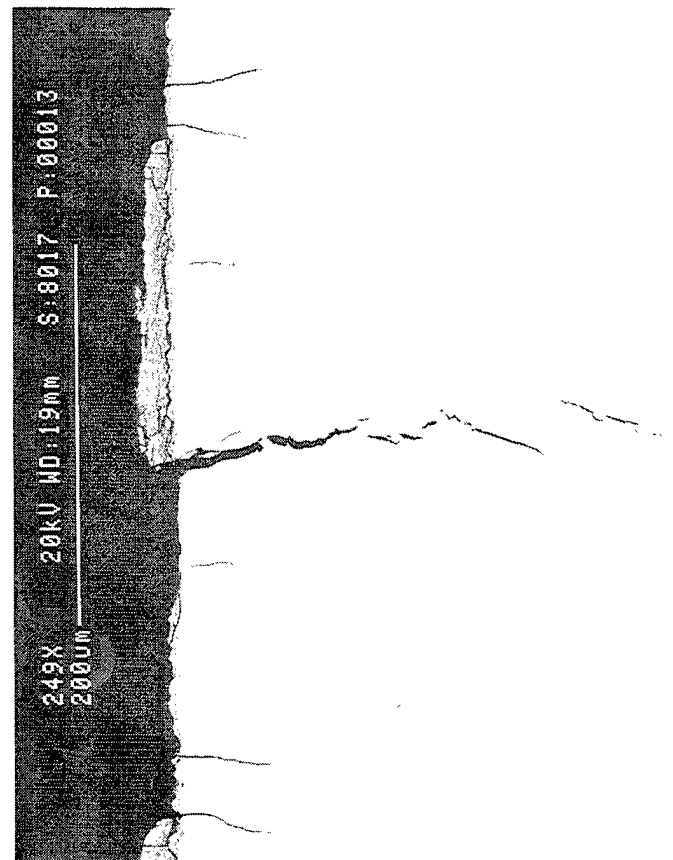
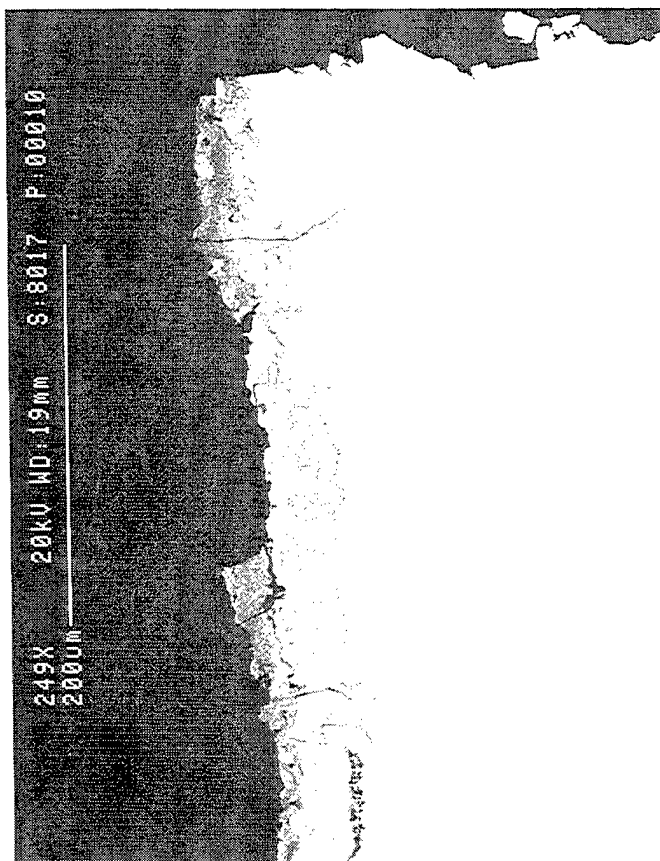
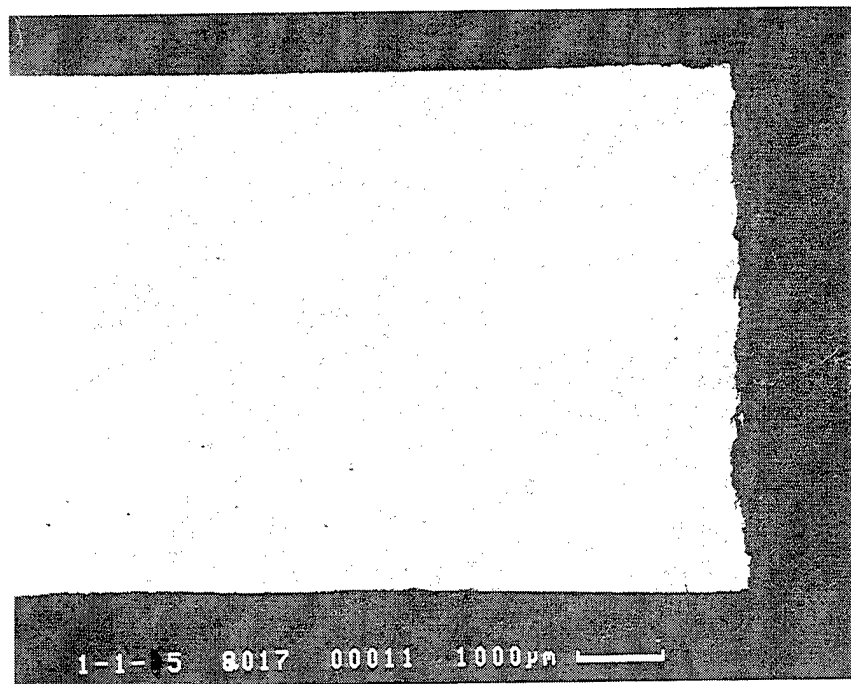


Figure 231. Cross sections of uncoated unexposed alpha-2 tensile samples after HSSCC testing. This exposure had salt.

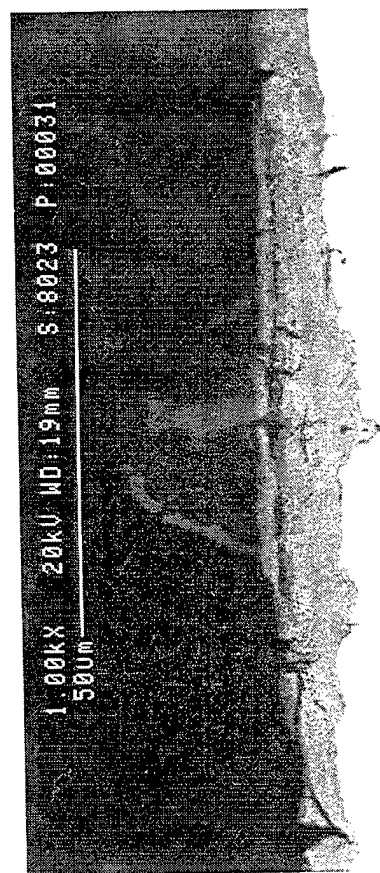
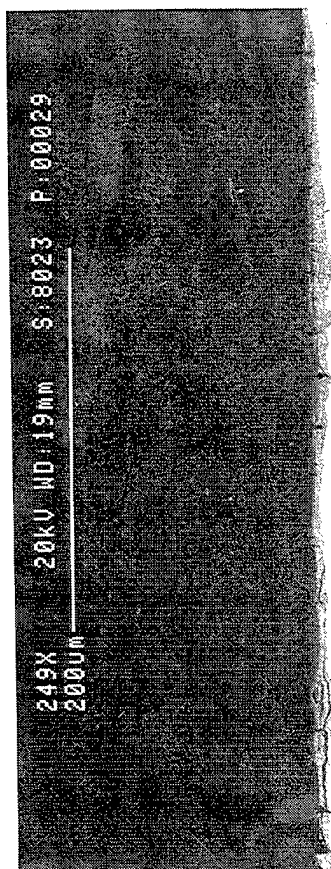
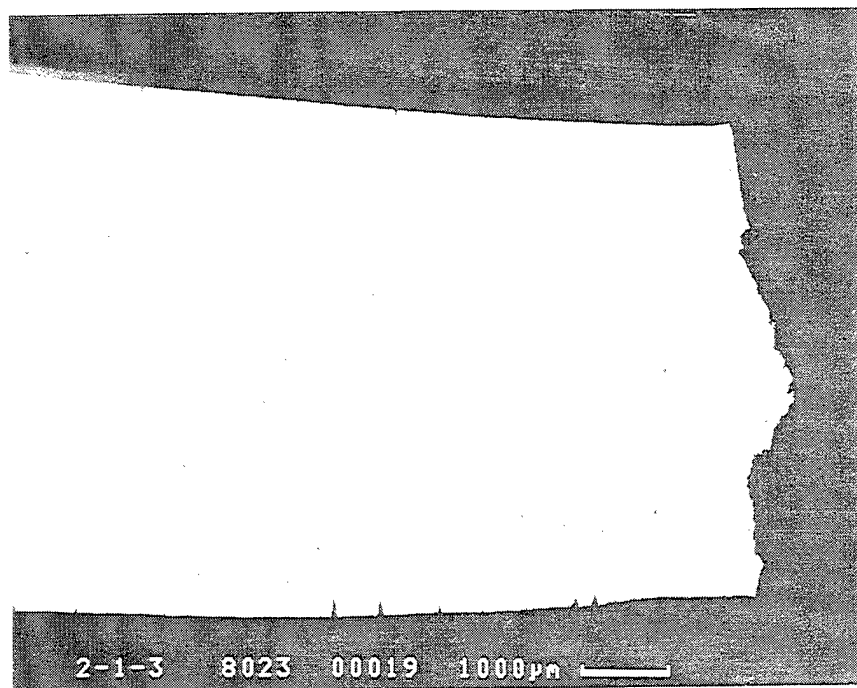


Figure 232. Cross sections of uncoated alpha-2 samples cyclically exposed at 760°C/100Hr after rupture during HSSCC testing. This exposure had no salt.

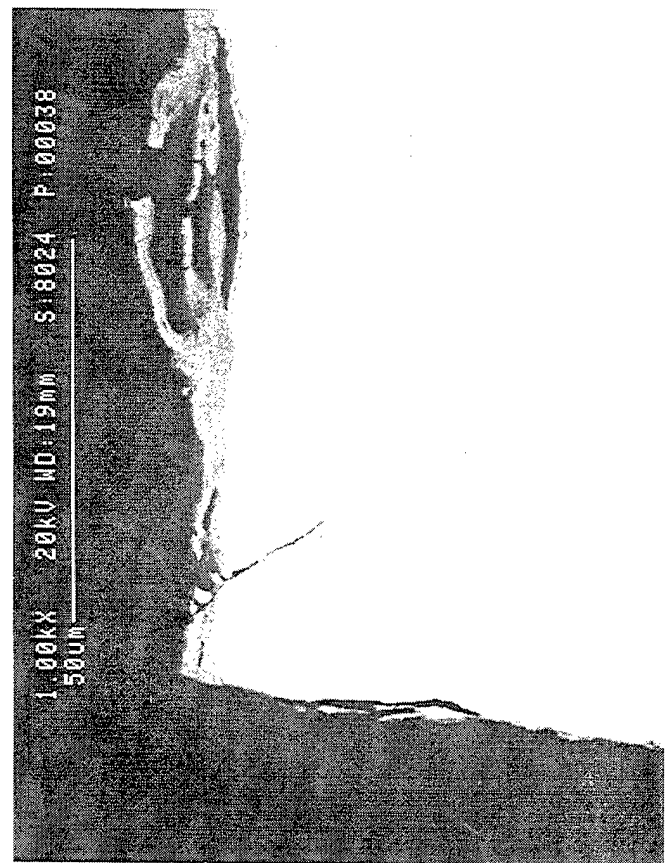
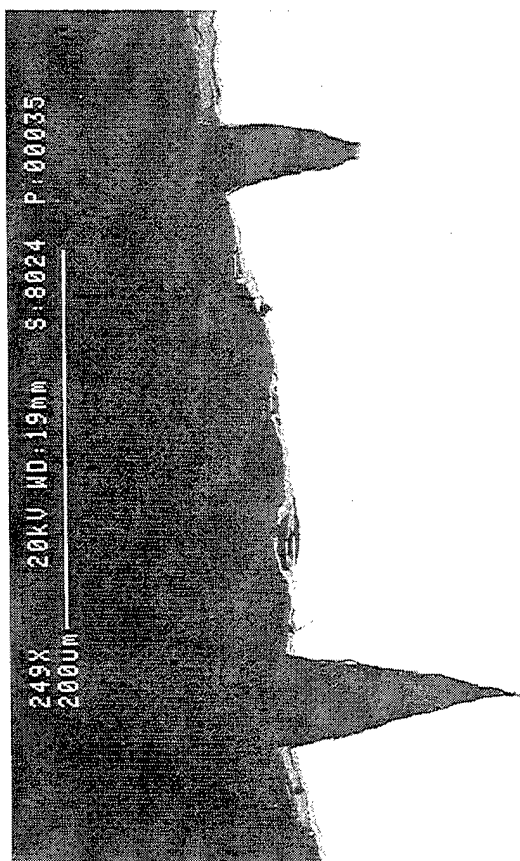
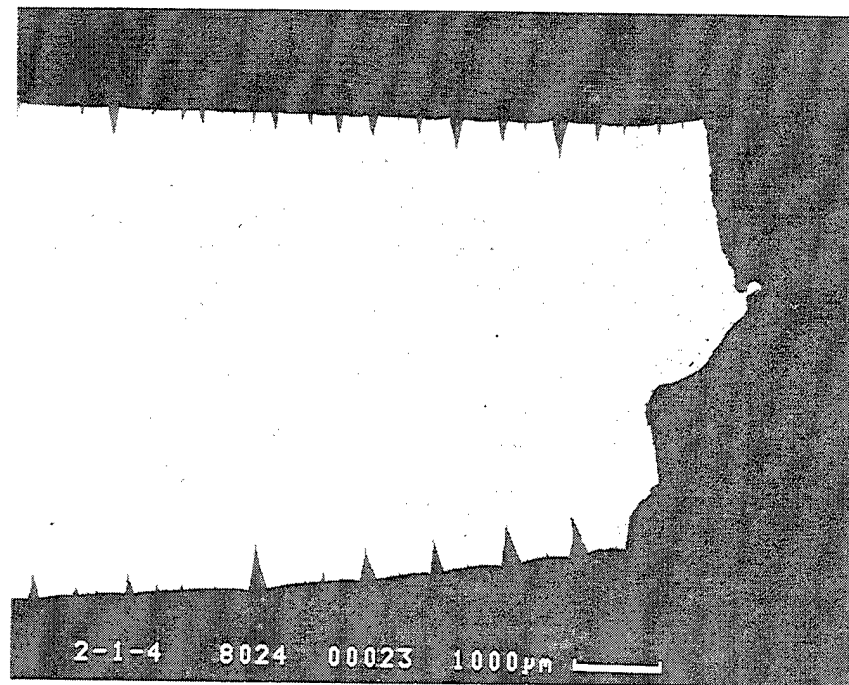


Figure 233. Cross sections of uncoated alpha-2 samples cyclically exposed at 760°C/100Hr after rupture during HSSCC testing. This exposure had salt.

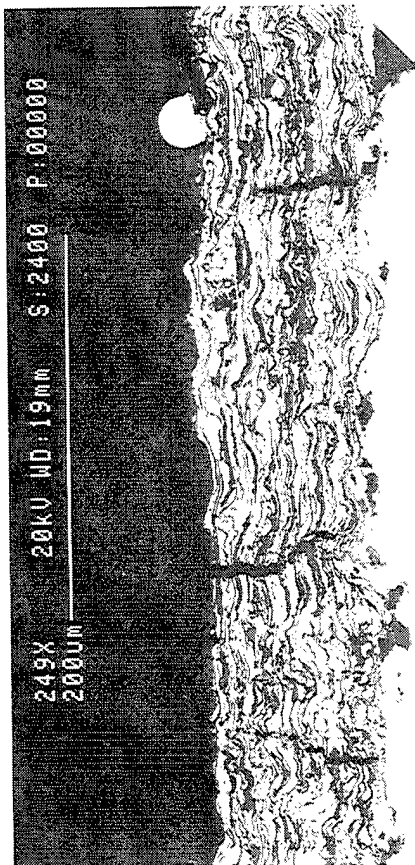
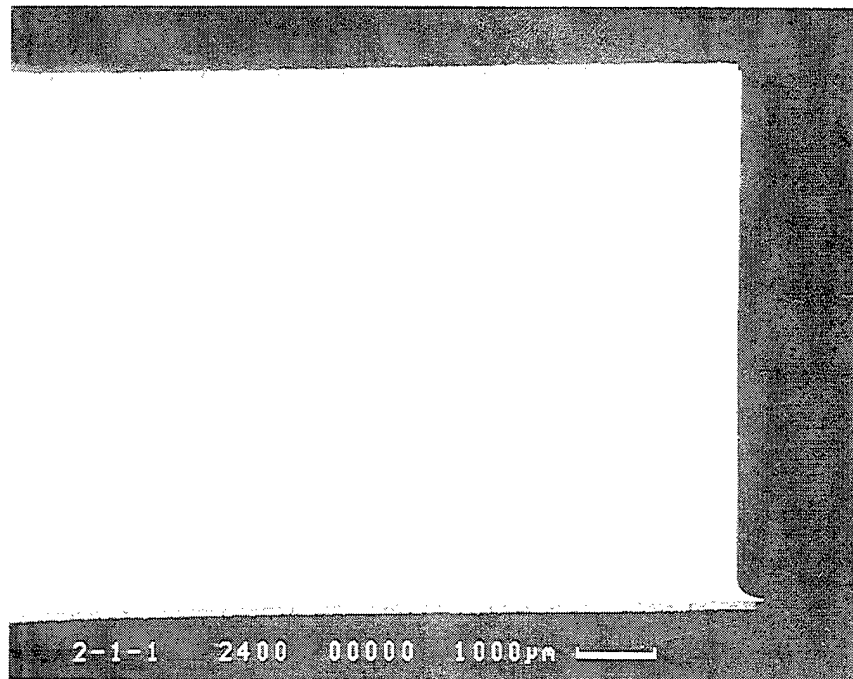


Figure 234. Cross sections of unexposed cermet coated alpha-2 tensile samples after HSSCC testing. This exposure had no salt.

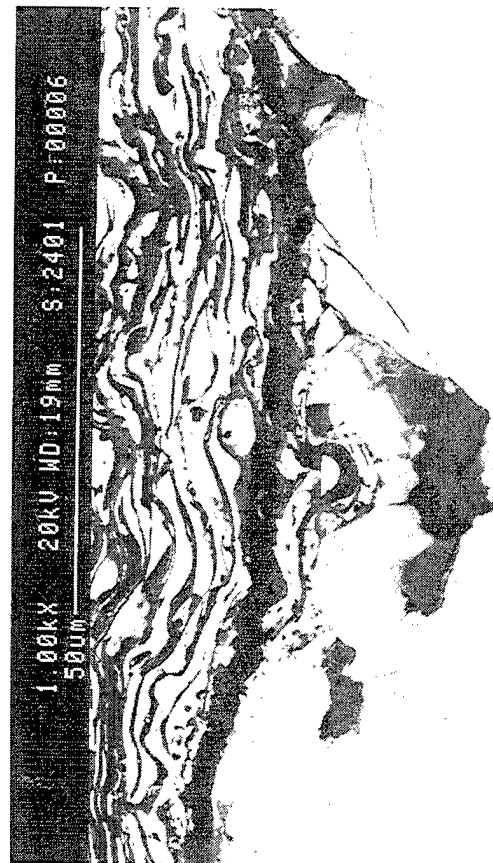
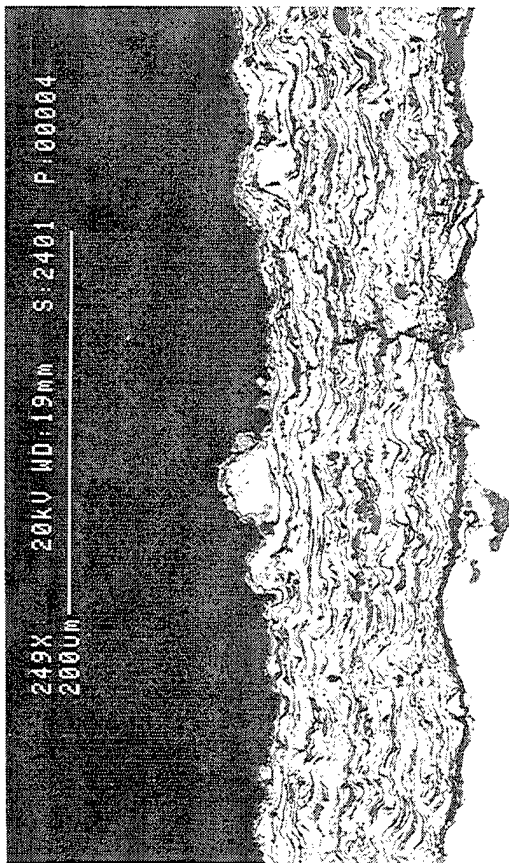
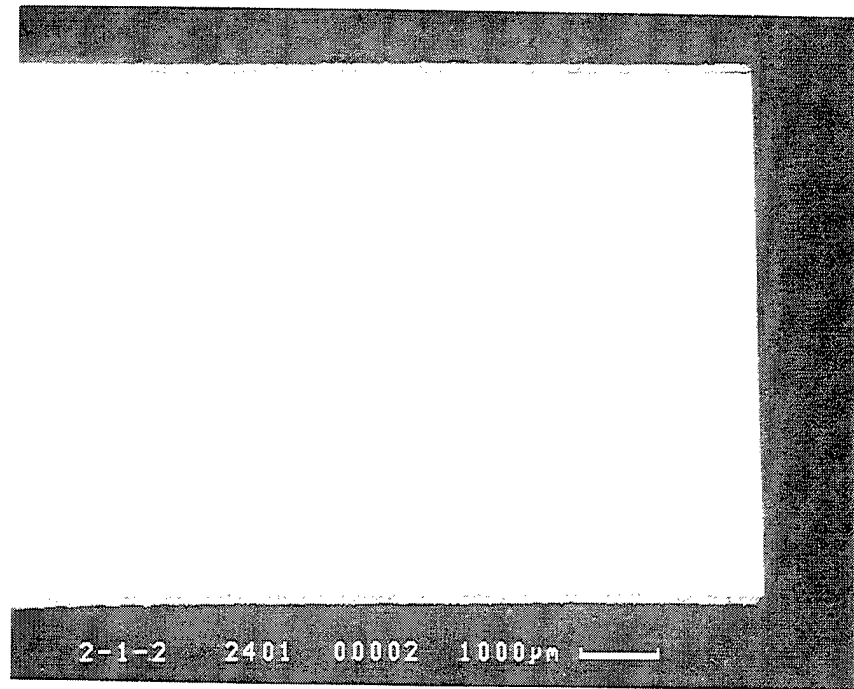


Figure 235. Cross sections of unexposed cermet coated alpha-2 tensile samples after HSSCC testing. This exposure had salt.

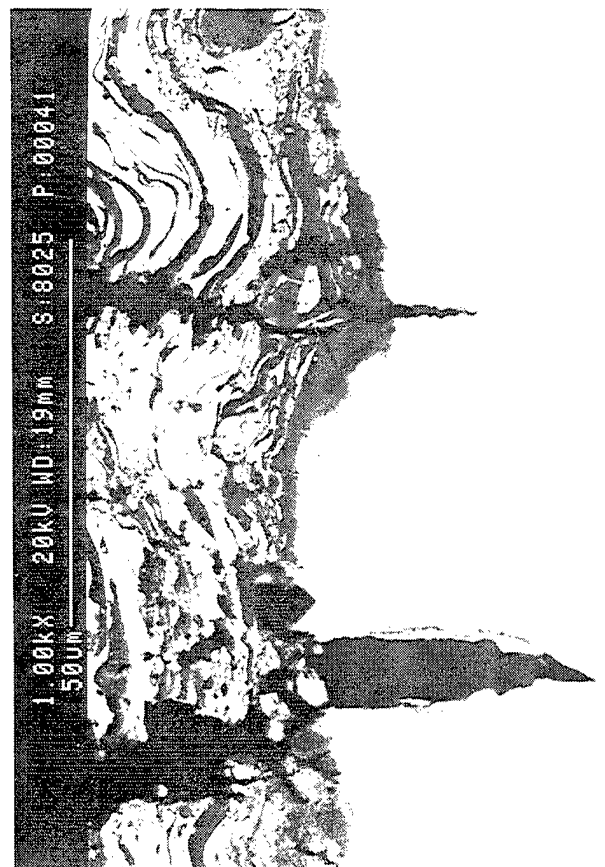
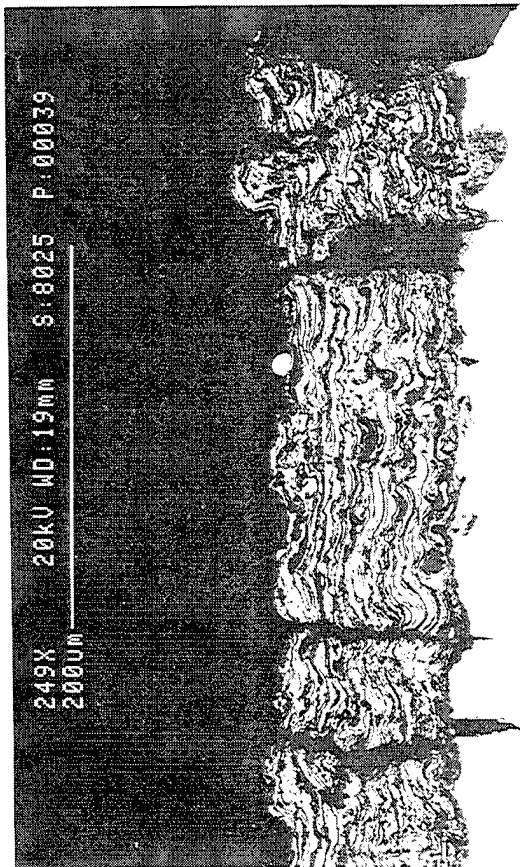
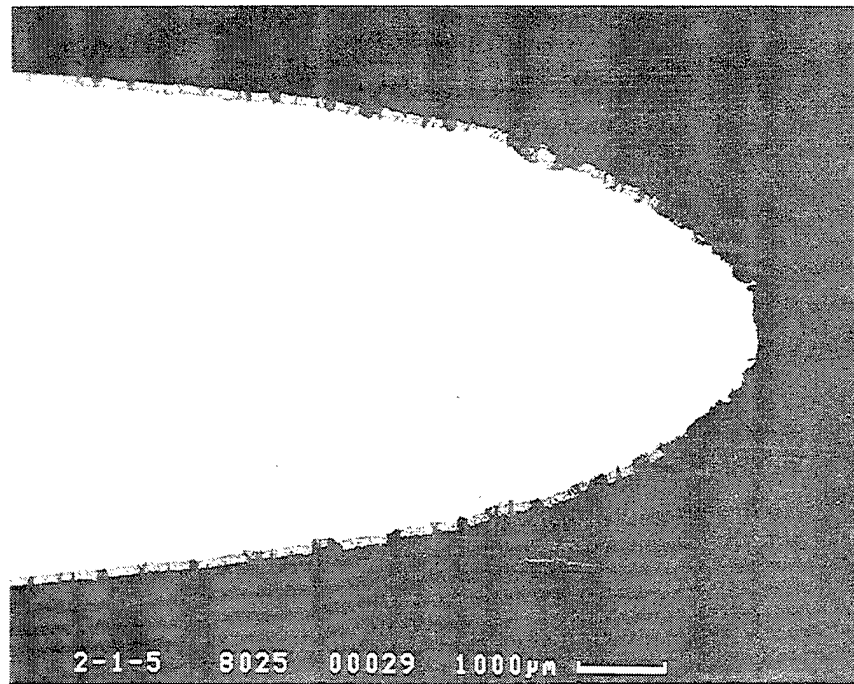


Figure 236. Cross sections of cermet coated alpha-2 tensile sample cyclically exposed at 760°C/100Hr after rupture during HSSCC testing. This exposure had no salt.

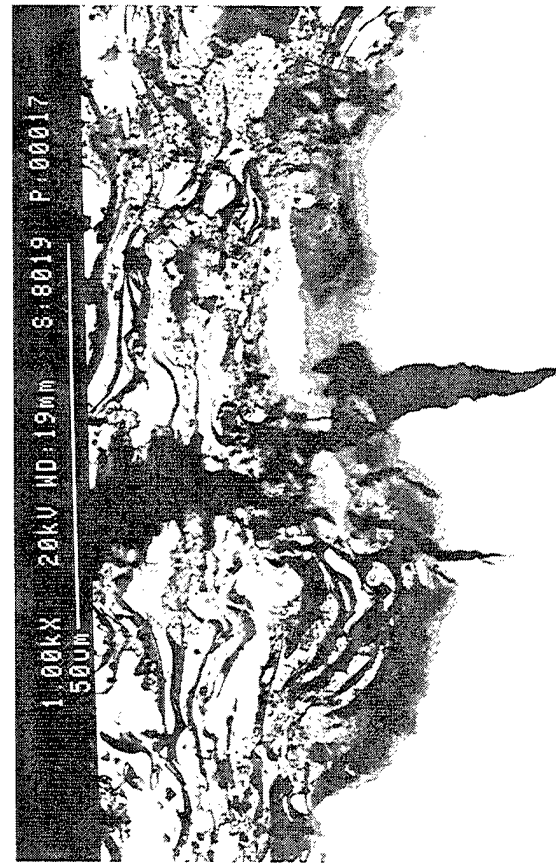
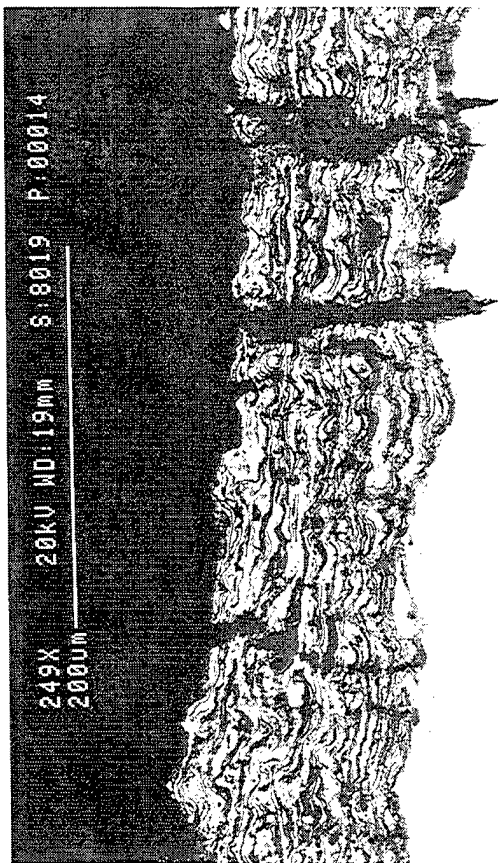
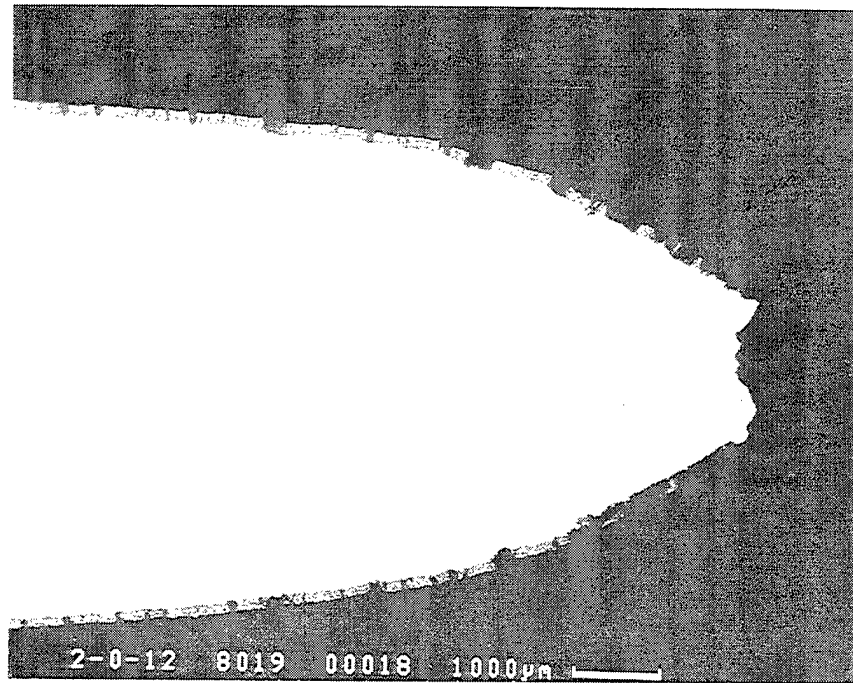


Figure 237. Cross sections of cermet coated alpha-2 tensile sample cyclically exposed at 760°C/100hr after rupture during HSSCC testing.

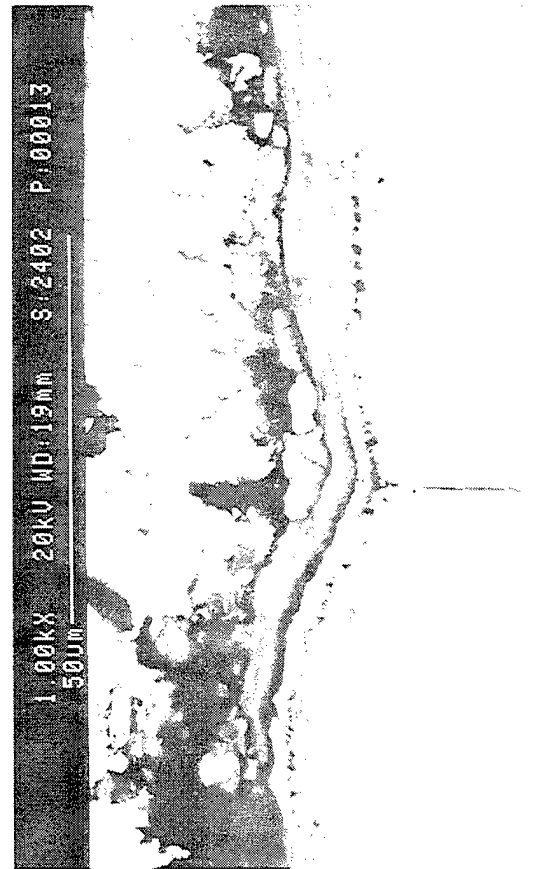
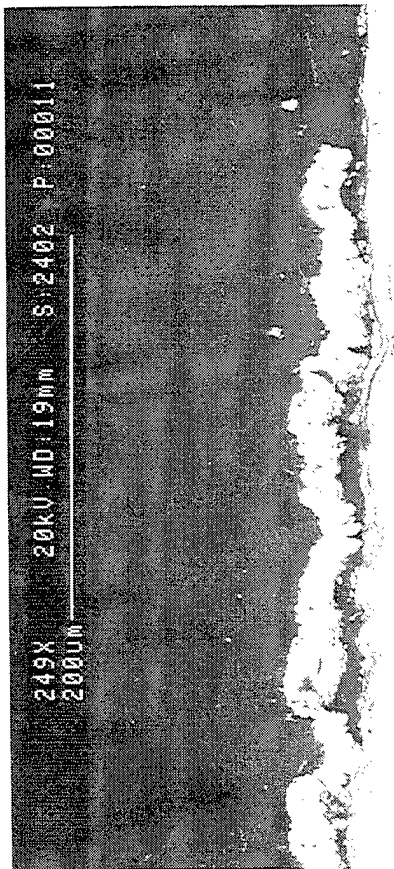
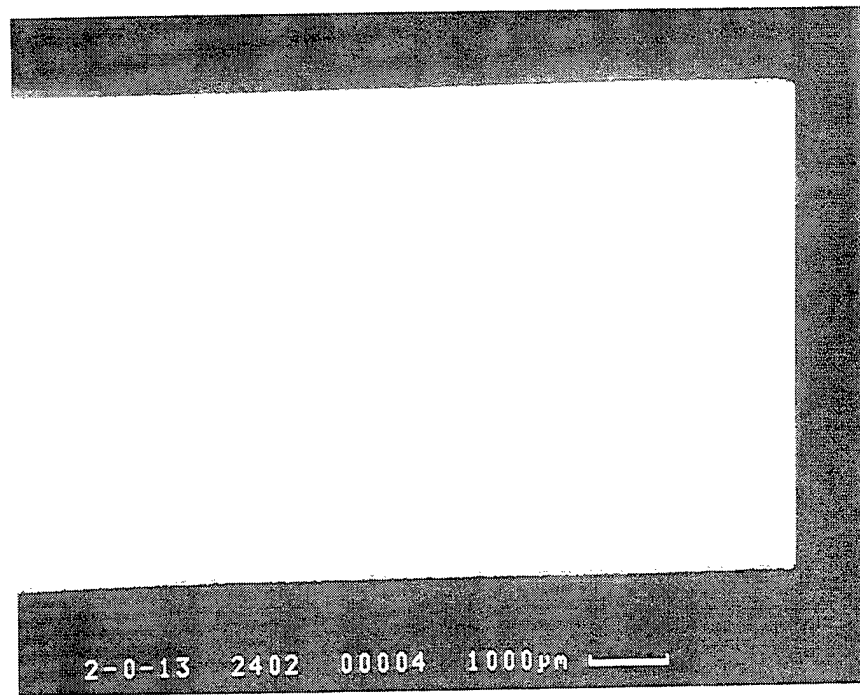


Figure 238. Cross sections of unexposed cermet W CVD coated alpha-2 tensile sample after HSSCC testing. This exposure had no salt.

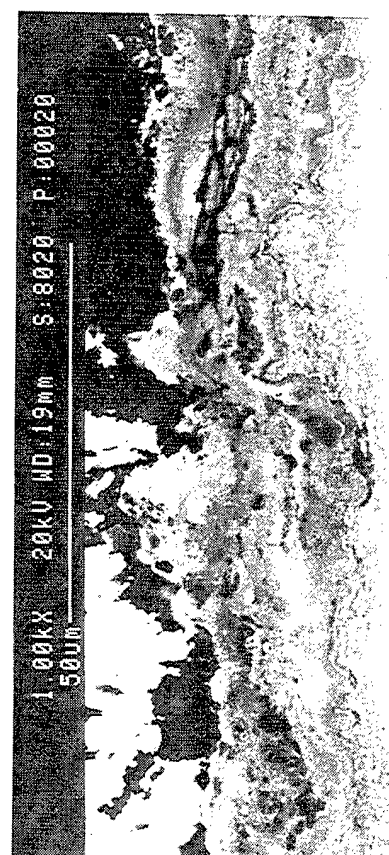
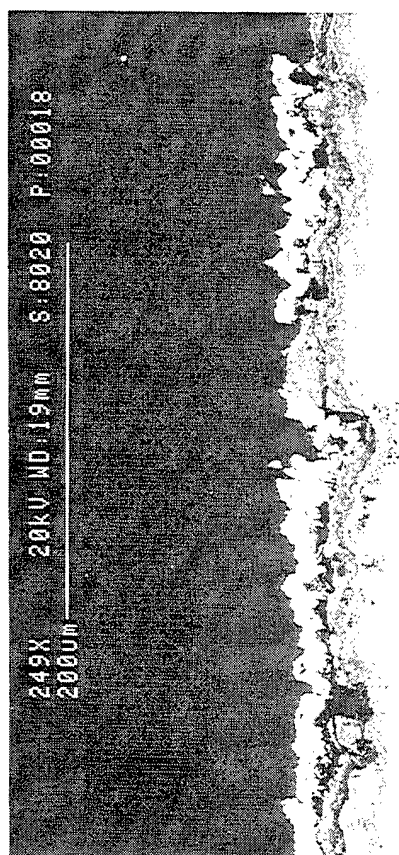
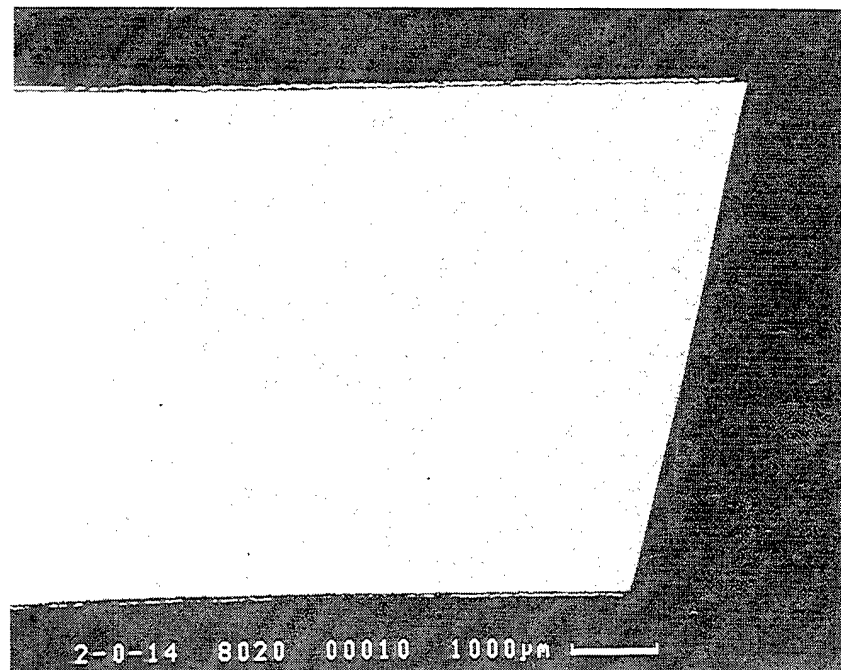


Figure 239. Cross sections of unexposed cermet W CVD coated alpha-2 tensile sample after HSSCC testing. This exposure had salt.

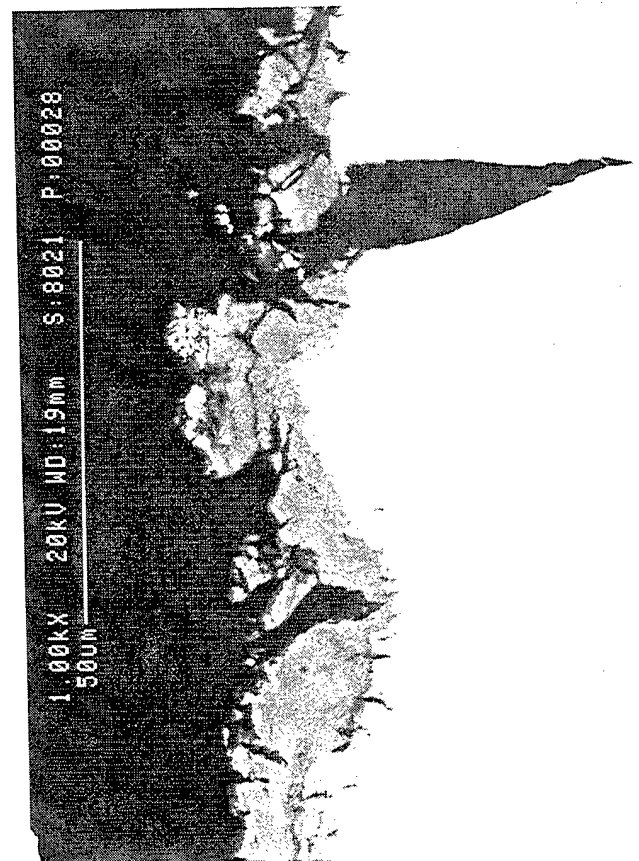
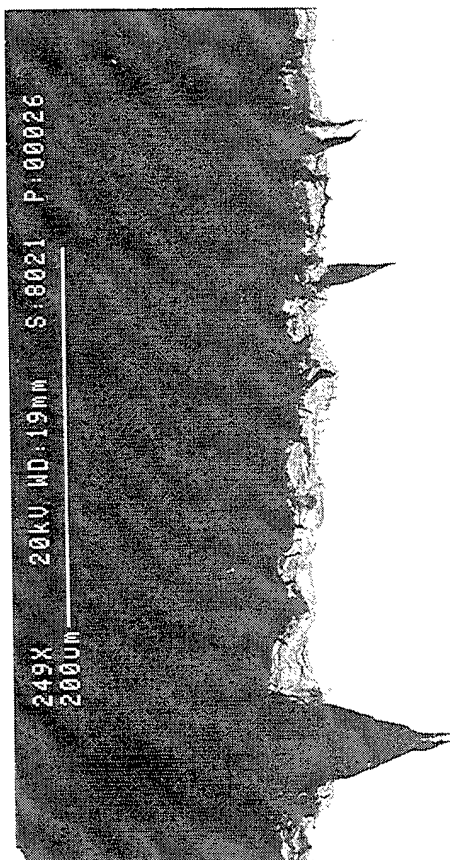
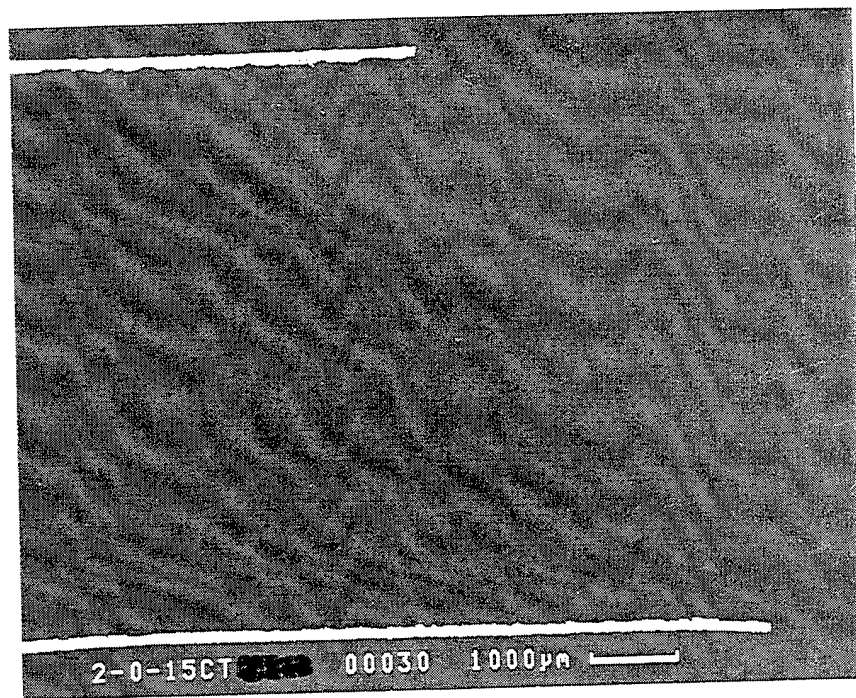


Figure 240. Cross sections of cermet W CVD coated alpha-2 tensile sample cyclically exposed at 760°C/100Hr after rupture during HSSCC testing. This exposure had no salt.

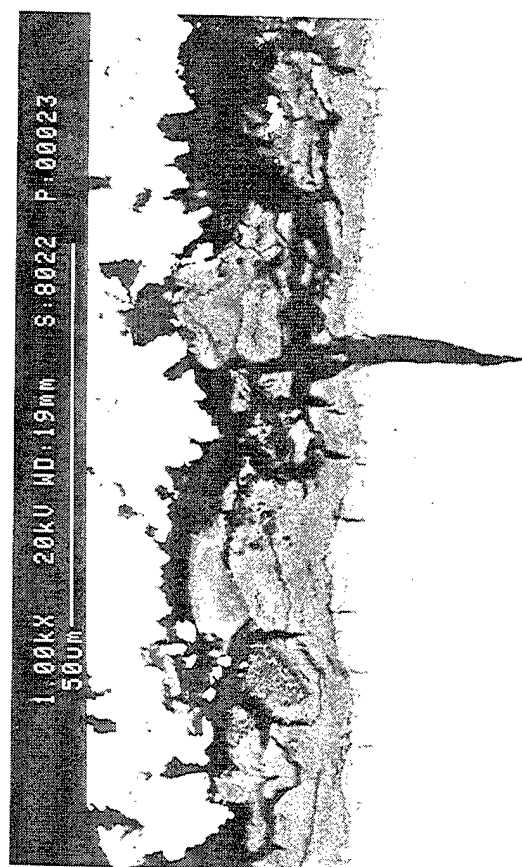
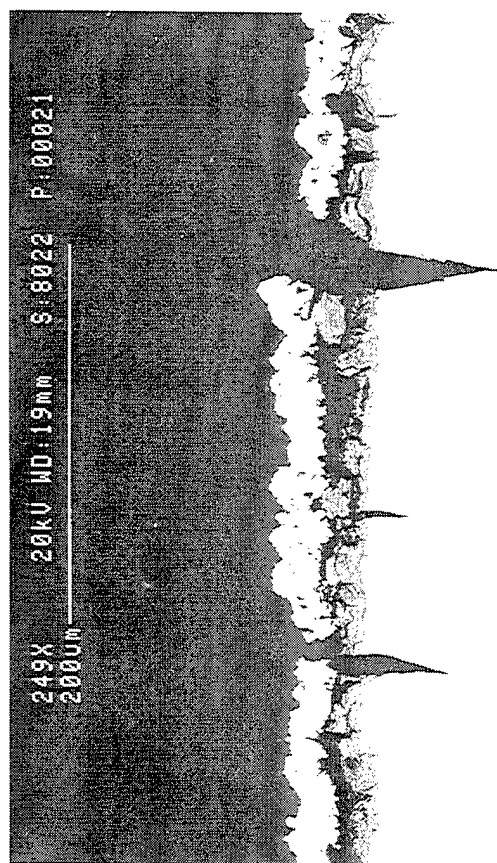
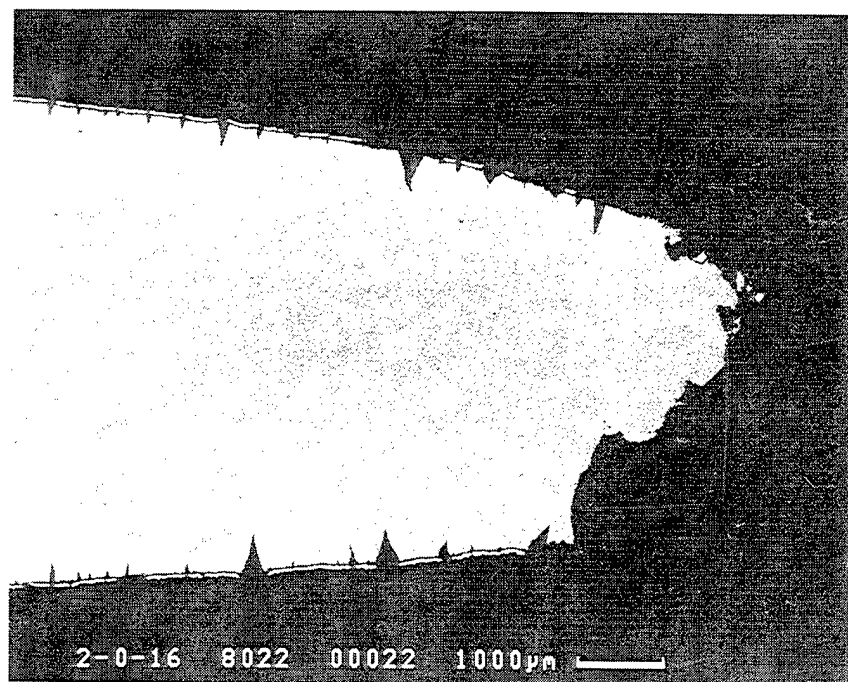


Figure 241. Cross sections of cermet W CVD coated alpha-2 tensile sample cyclically exposed at 760°C/100Hr after rupture during HSSCC testing.

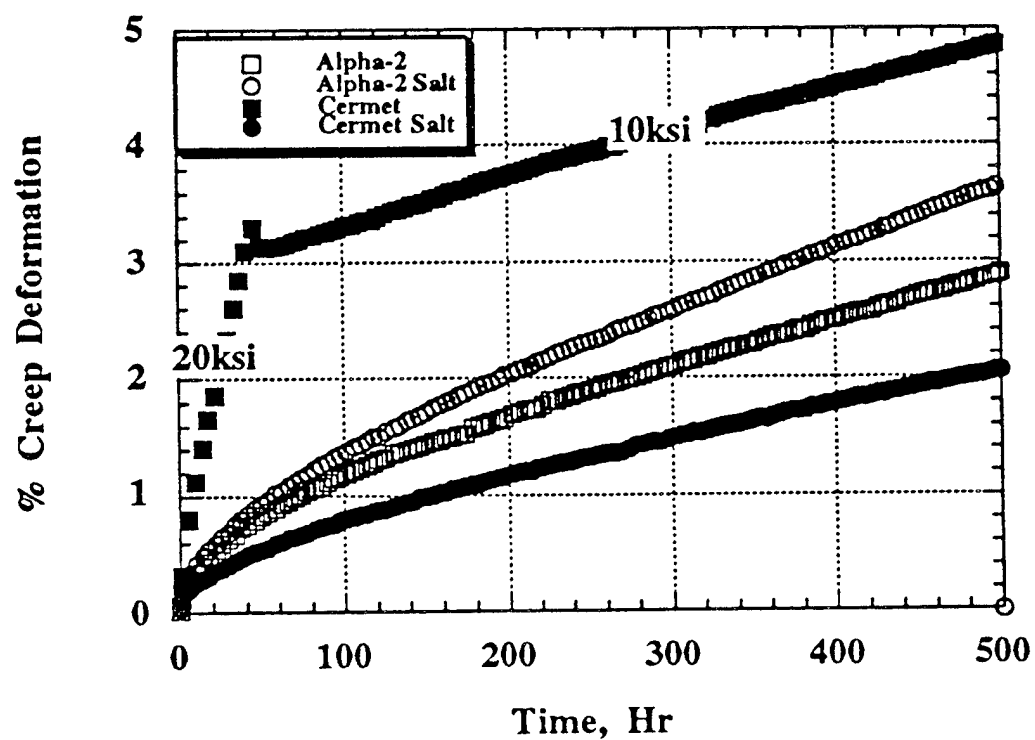


Figure 242. Graph showing creep behavior of unexposed coated and uncoated alpha-2 samples without salt.

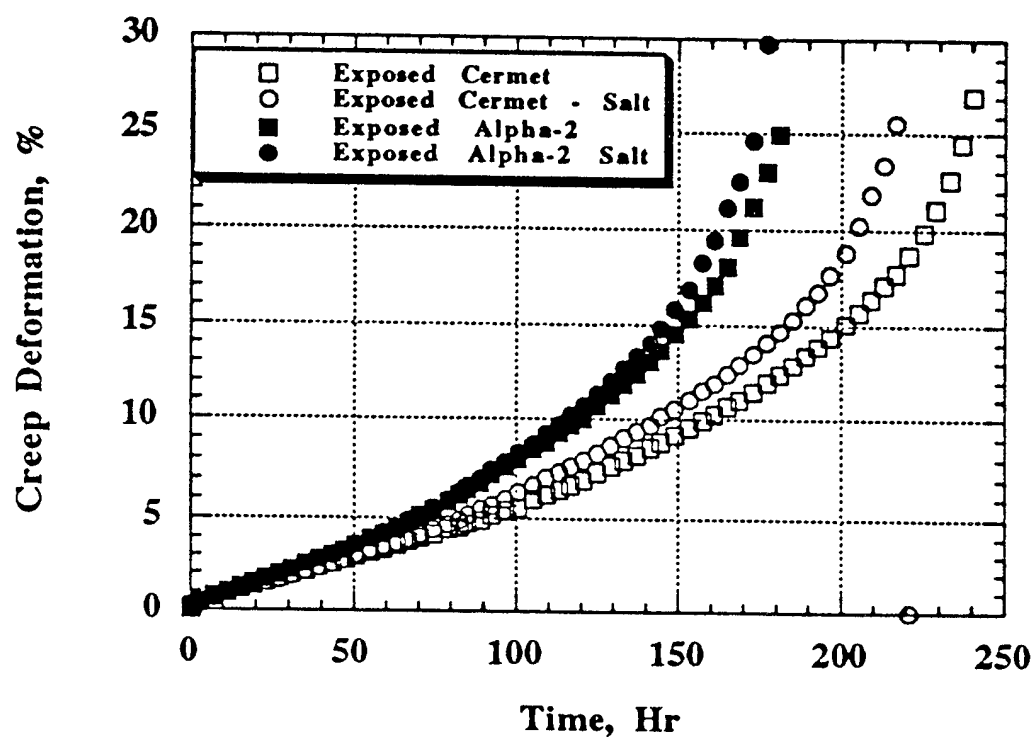


Figure 243. Graph showing creep behavior of cyclically exposed coated and uncoated alpha-2 samples with salt.

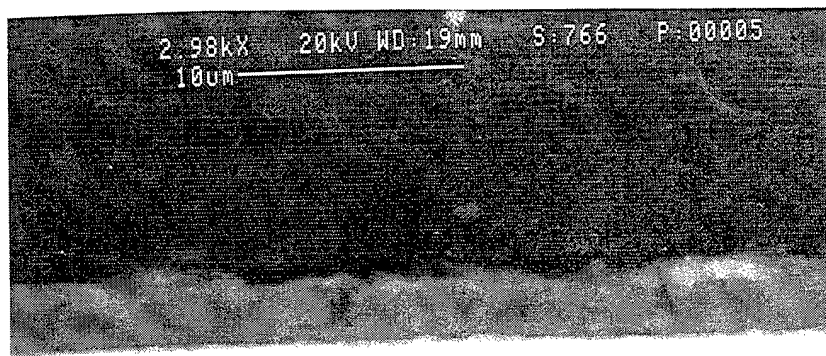
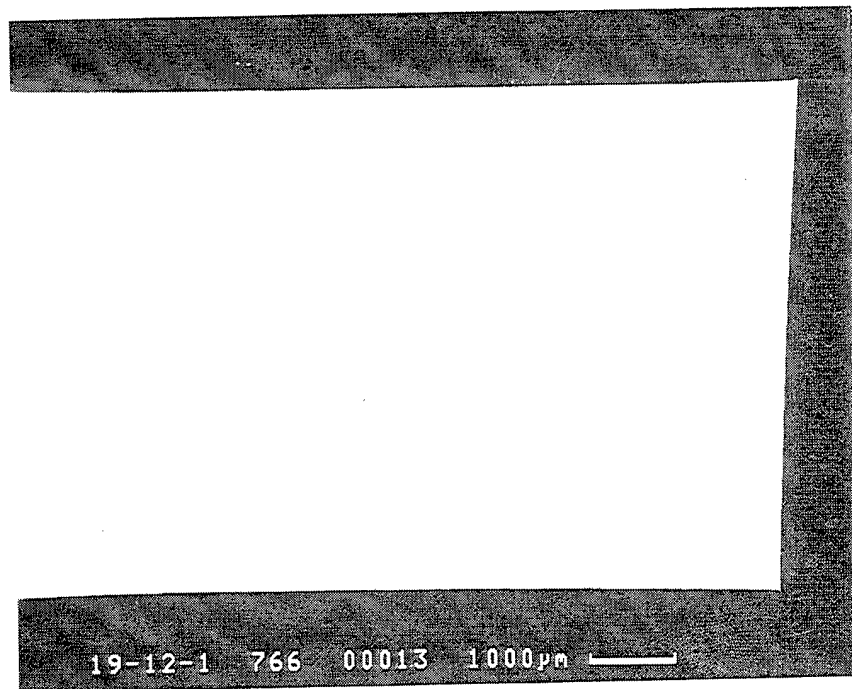


Figure 244. Cross sections of cyclically exposed and uncoated gamma tested at RT and 0.4% strain for 200,000 cycles.

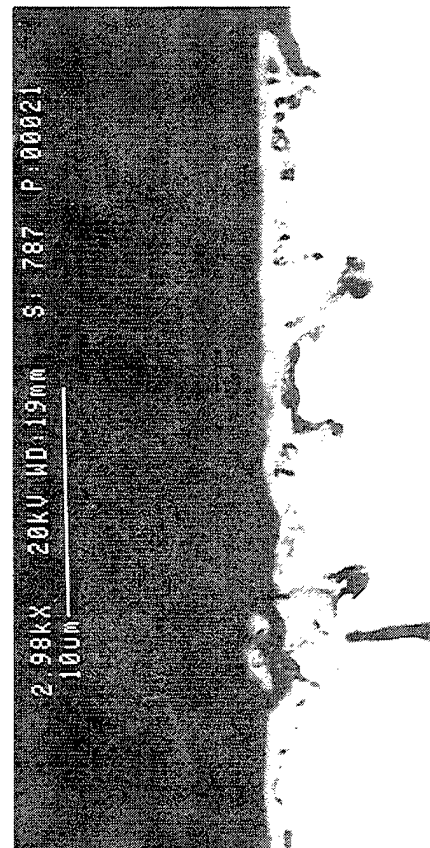
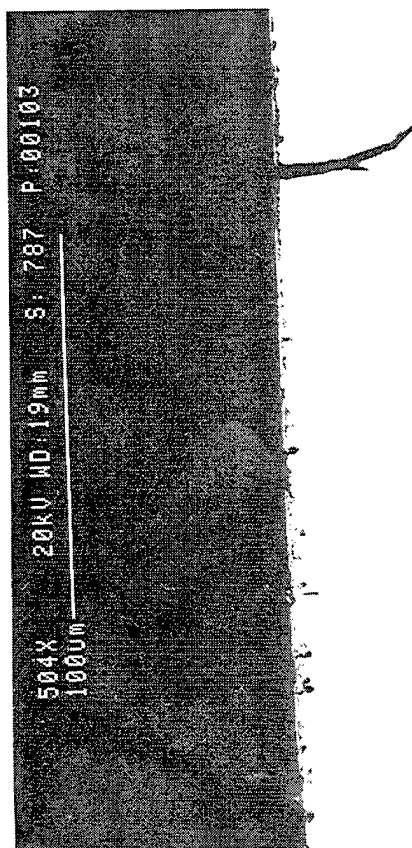
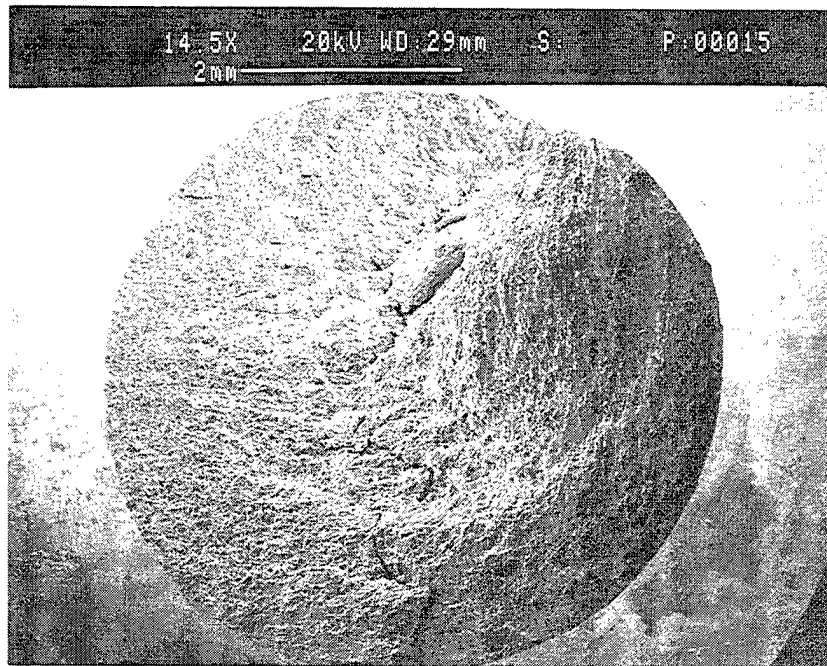


Figure 245. Cross sections of cyclically exposed and uncoated gamma tested at 760°C (1400°F) and 0.4% strain for 282641 cycles.

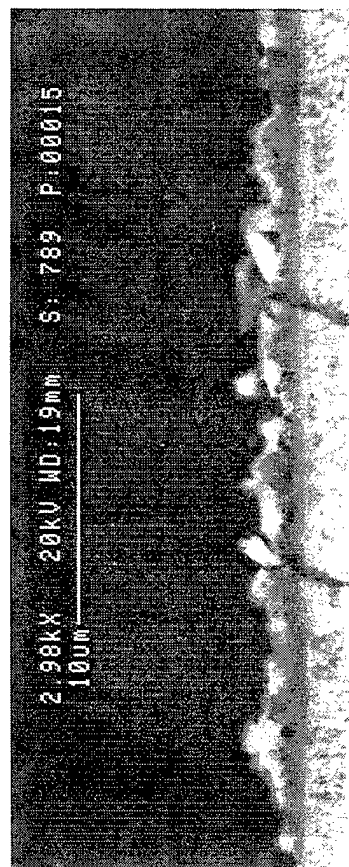
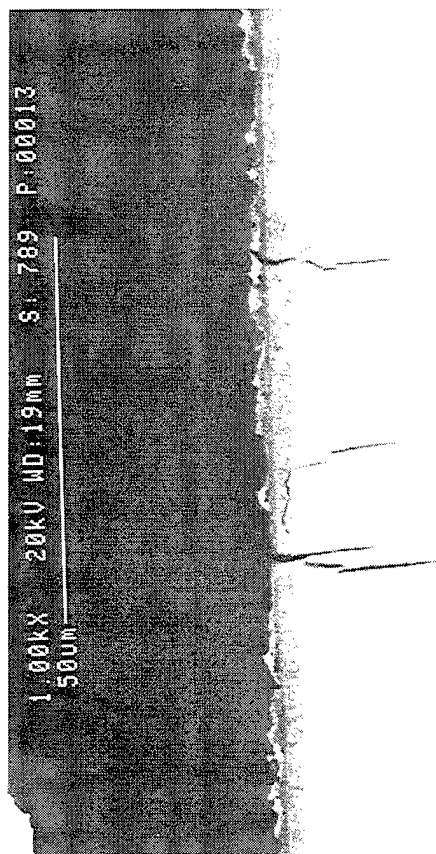
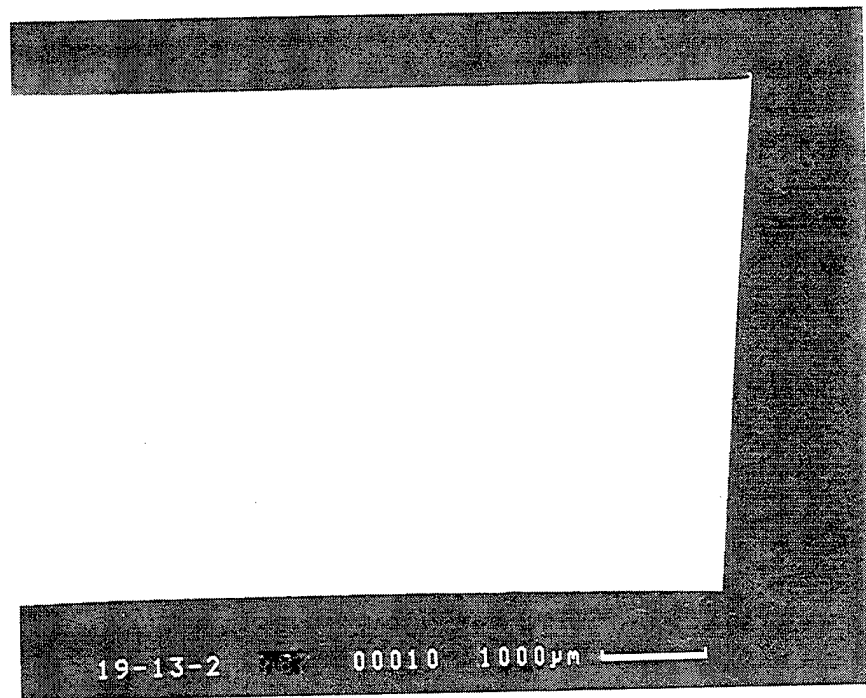


Figure 246. Cross sections of cyclically exposed and uncoated gamma sample tested at 760°C (1400°F) and 0.4% strain for 200,000 cycles.

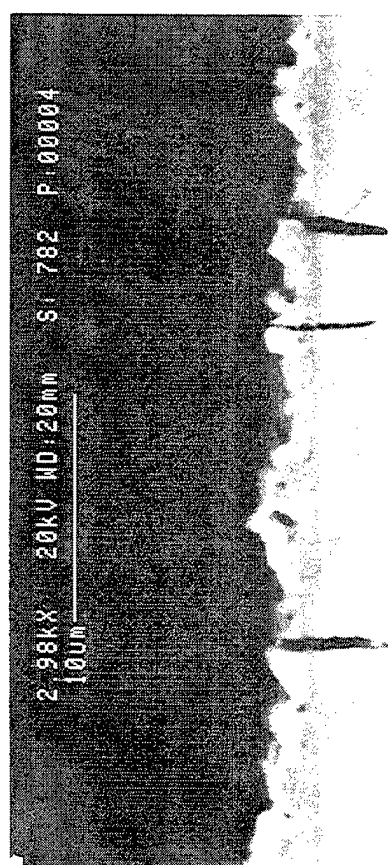
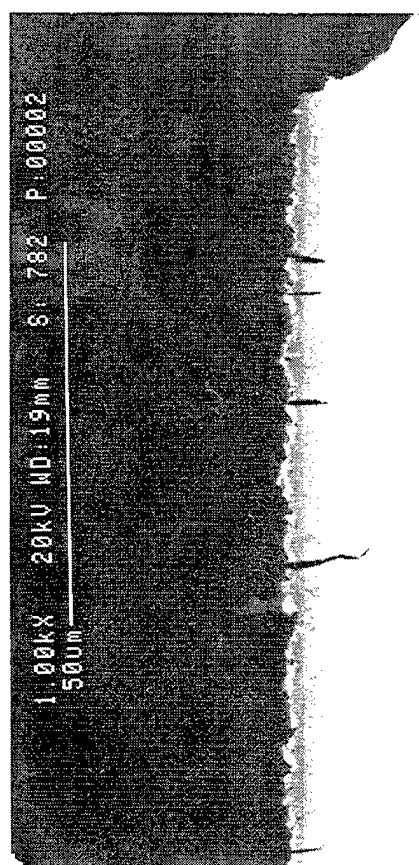
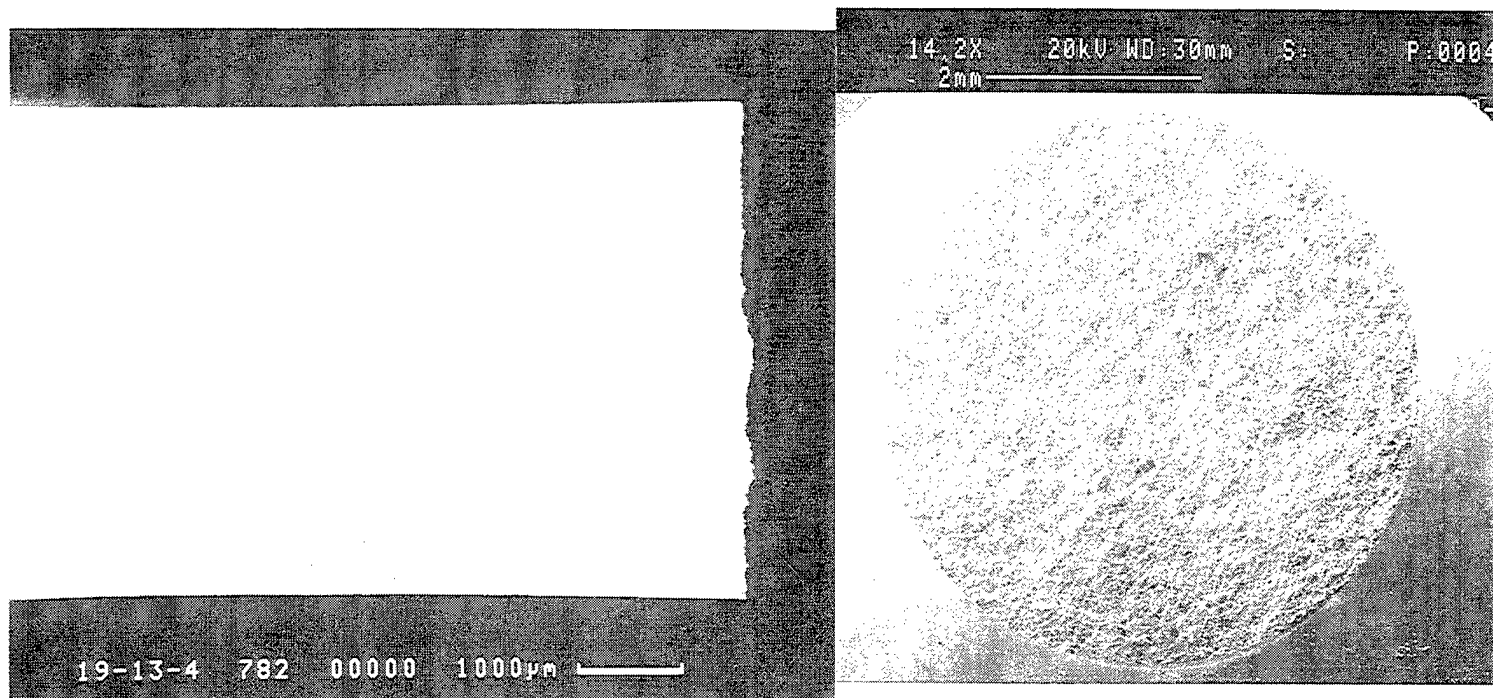


Figure 247. Cross section of the cyclically exposed, uncoated gamma sample tested at 648°C and 0.4% strain for 1549 cycles.

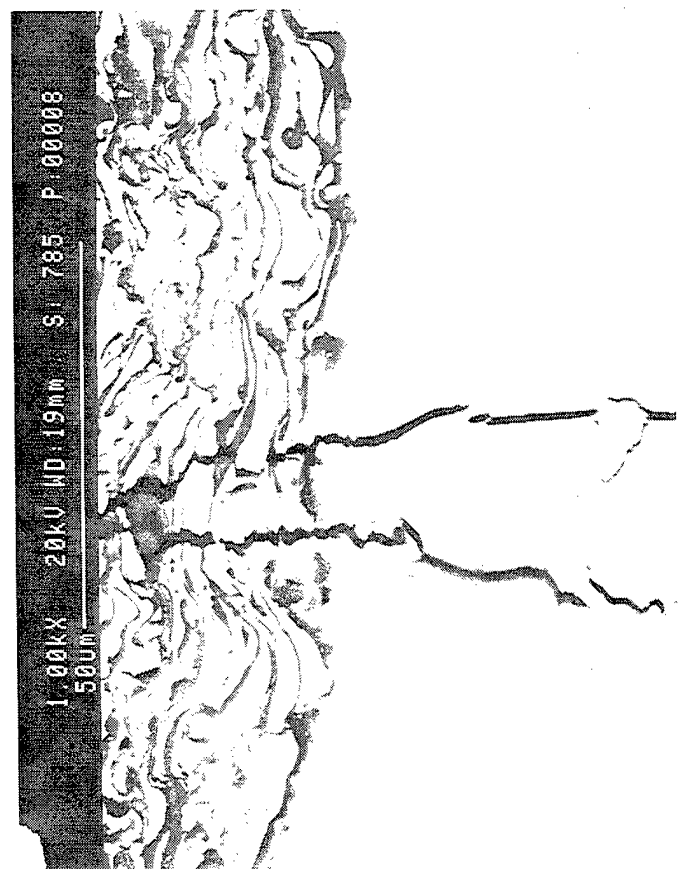
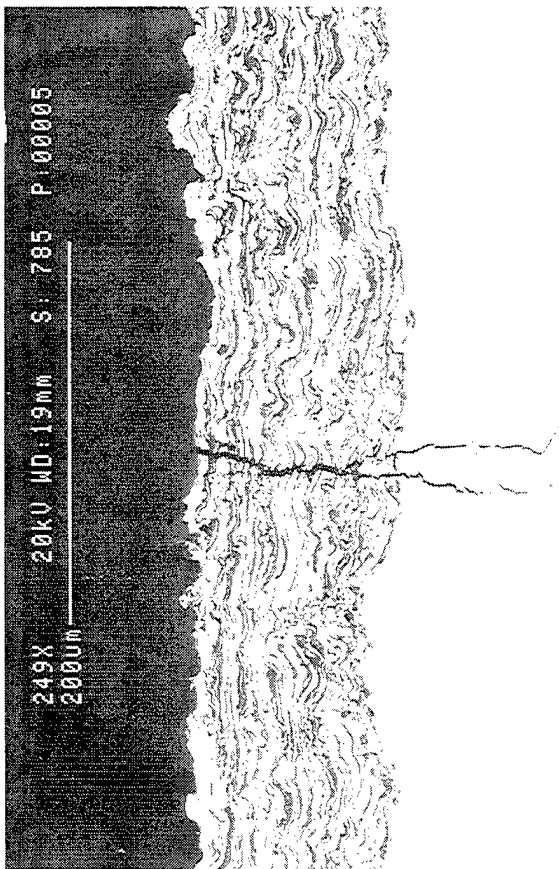
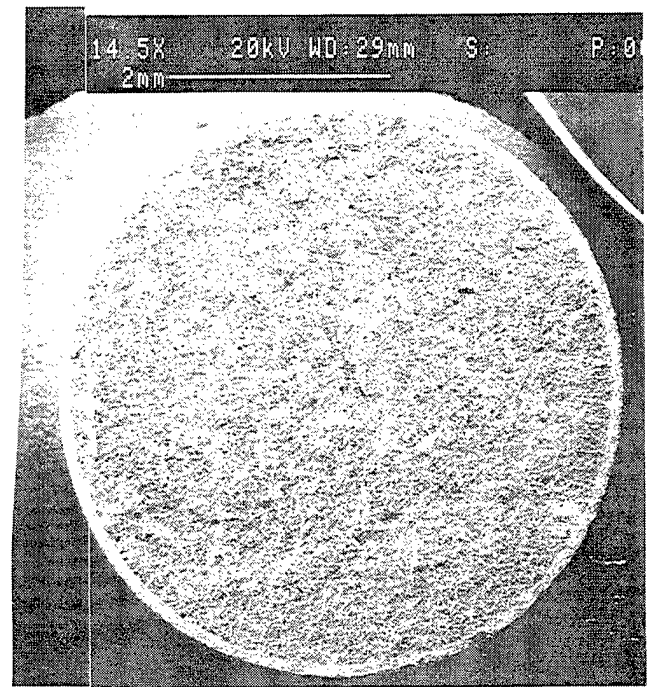
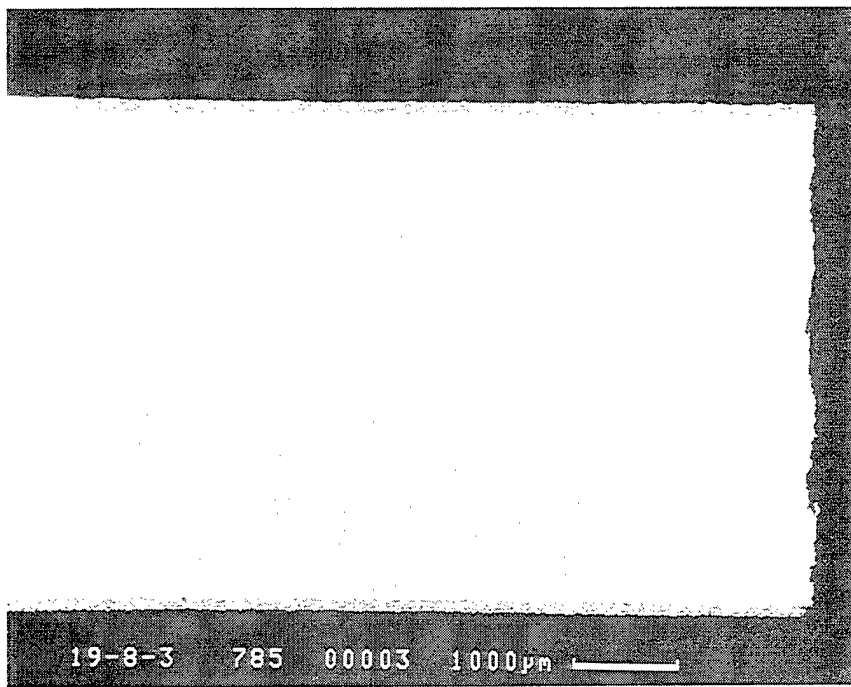


Figure 248. Cross sections of unexposed cermet coated gamma samples fatigue tested at 760°C and 0.4% strain for 345 cycles.

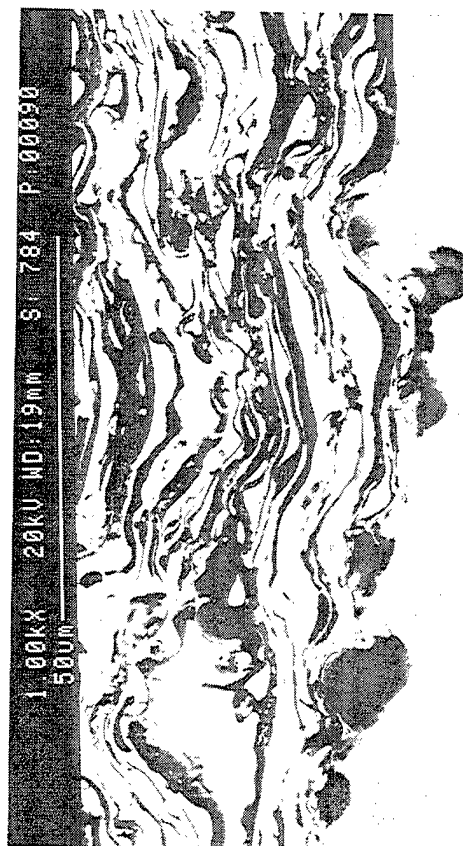
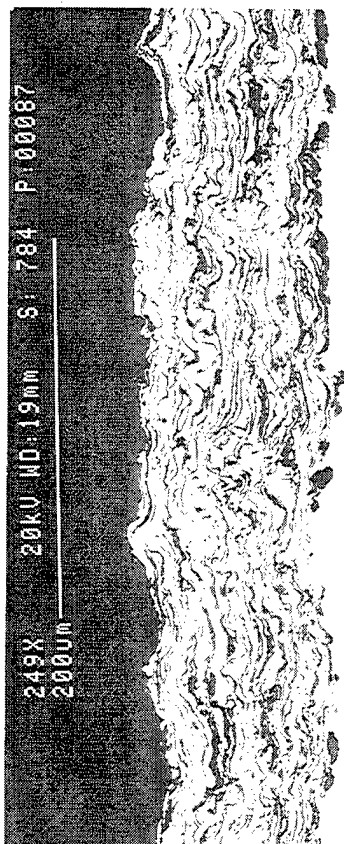
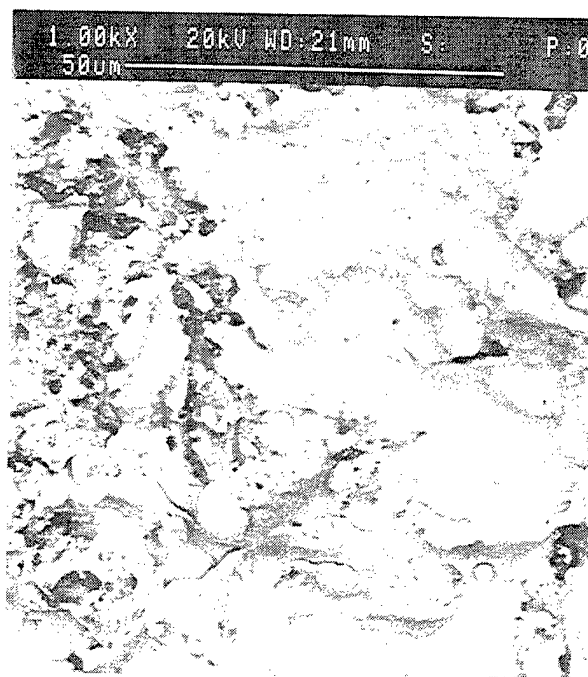
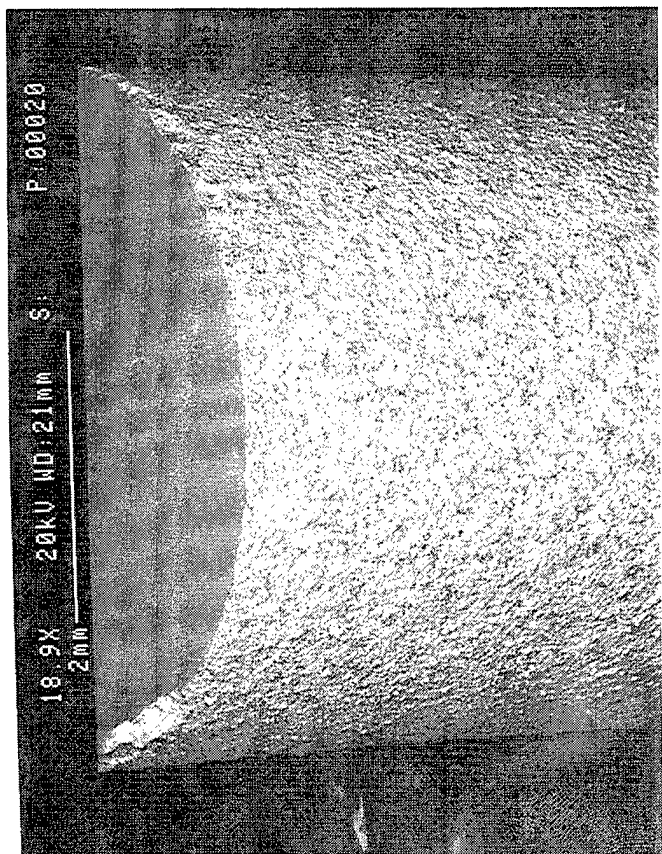


Figure 249. Cross sections of unexposed cermet coated gamma samples fatigue tested at 760°C and 0.25% strain for 248746 cycles.

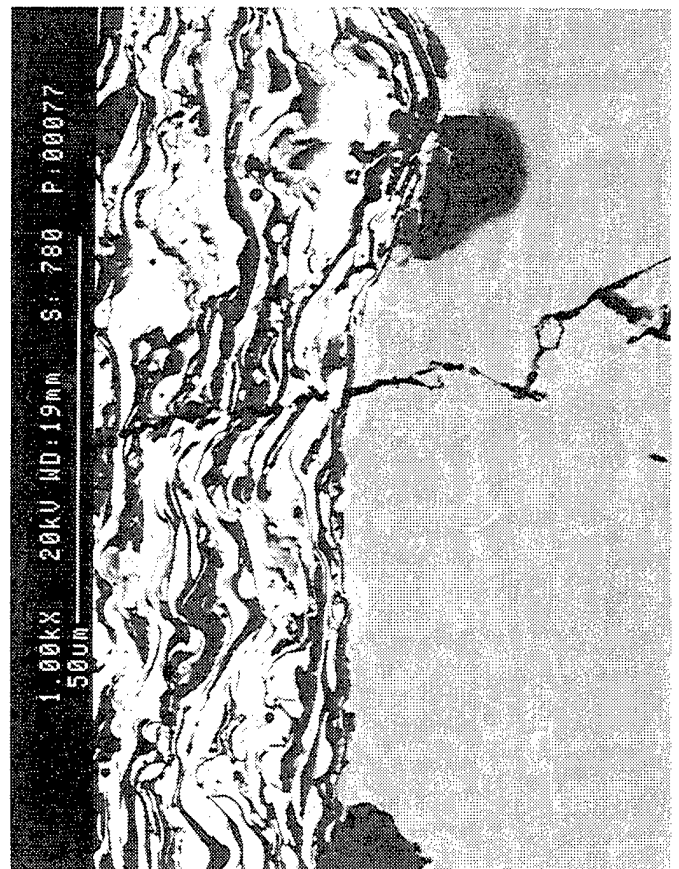
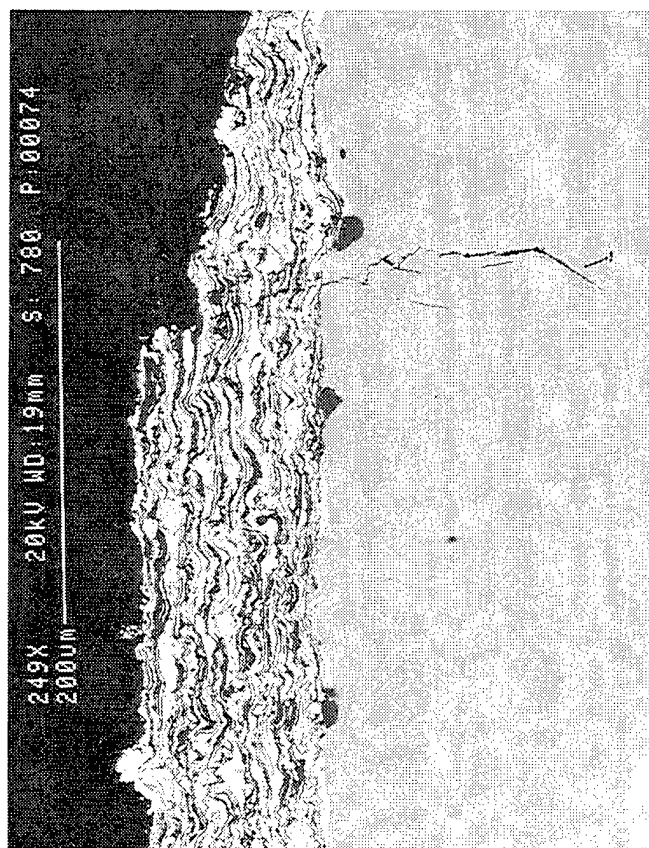
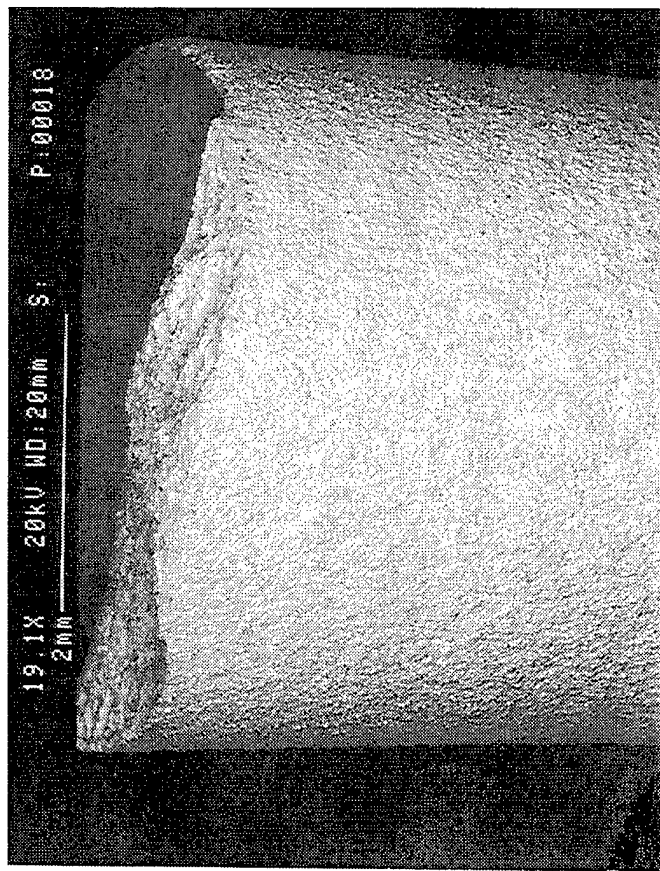


Figure 250. Cross sections of cyclically exposed cermet coated samples fatigue tested at 648°C at 0.25% strain for 43825 cycles.

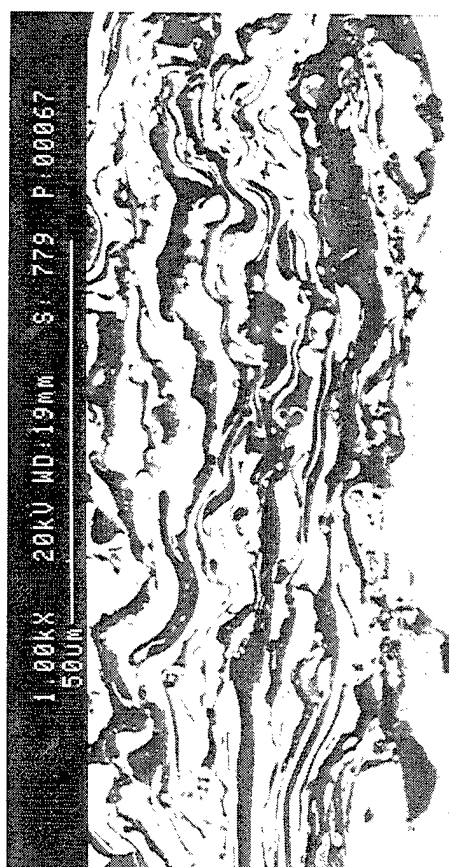
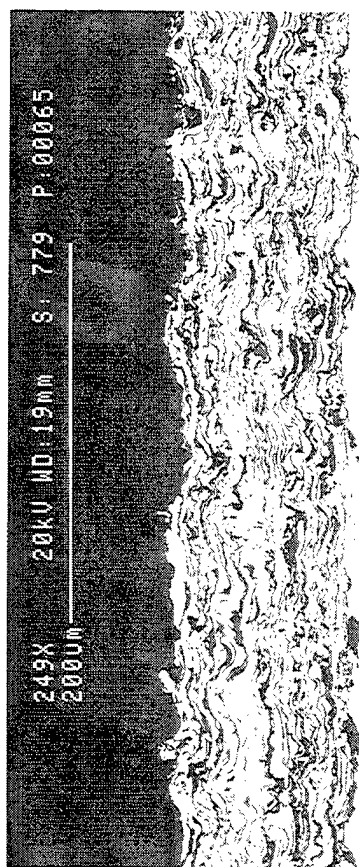
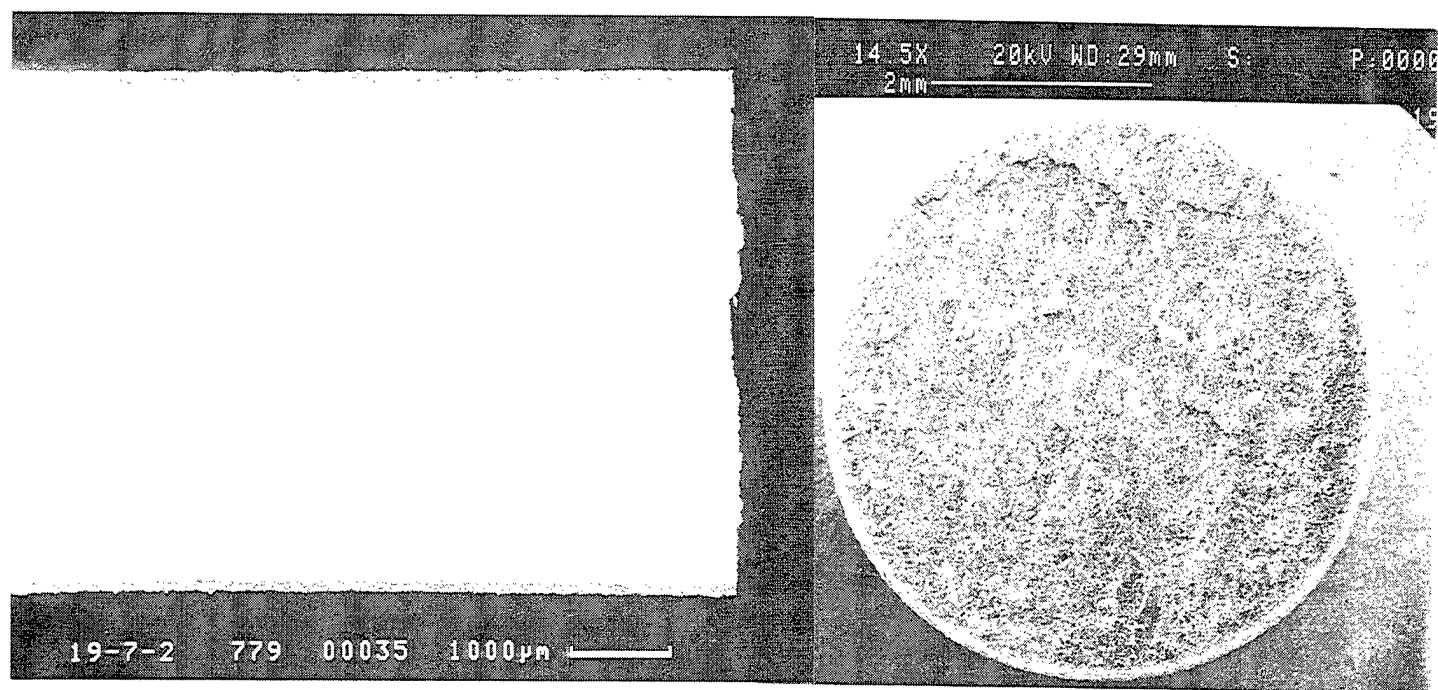


Figure 251. Cross sections of cyclically exposed cermet coated gamma sample fatigue tested at 648°C and 0.4% strain for 1 cycle.

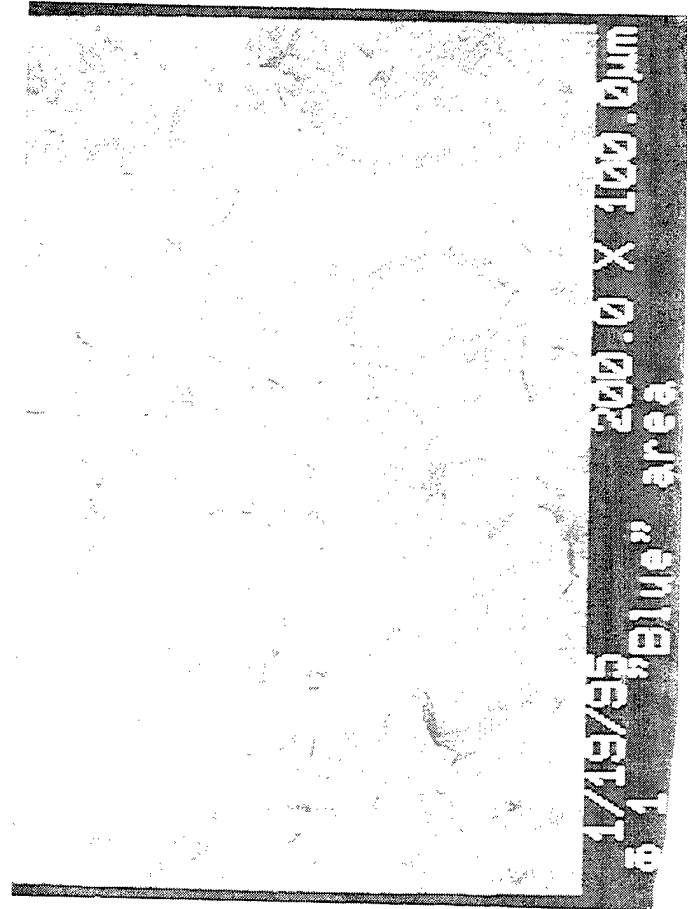
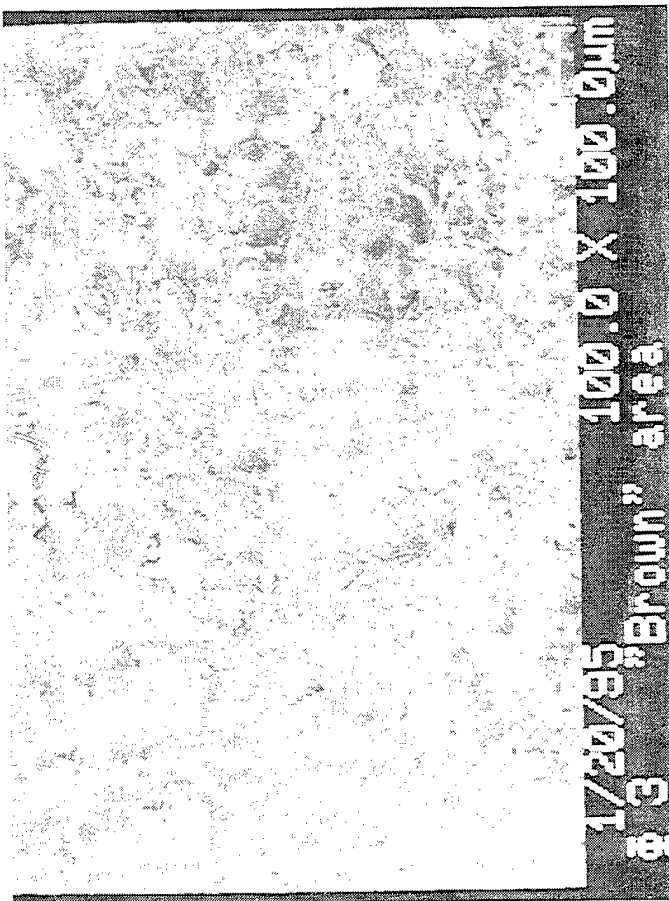
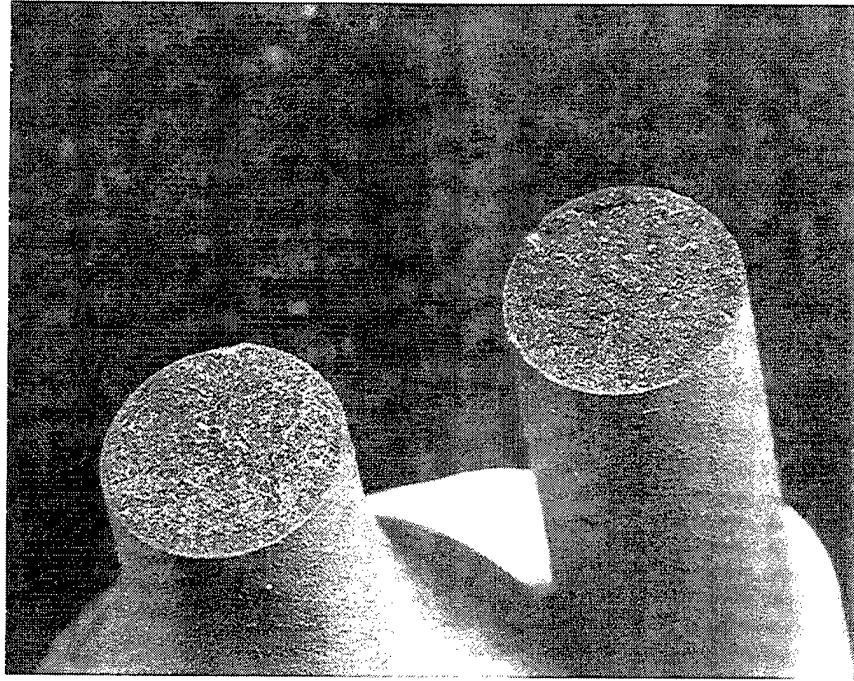


Figure 252. Color photograph of failed gamma bar (19-7-1) tested at 760°C and 0.4% strain for 3 cycles. Auger micrographs of the brown and blue tinted surfaces are shown.

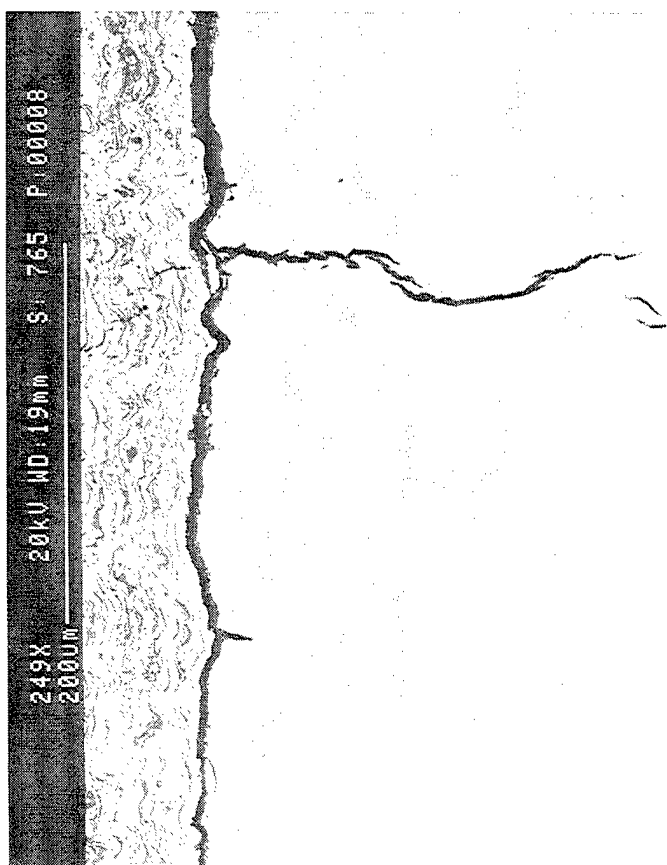
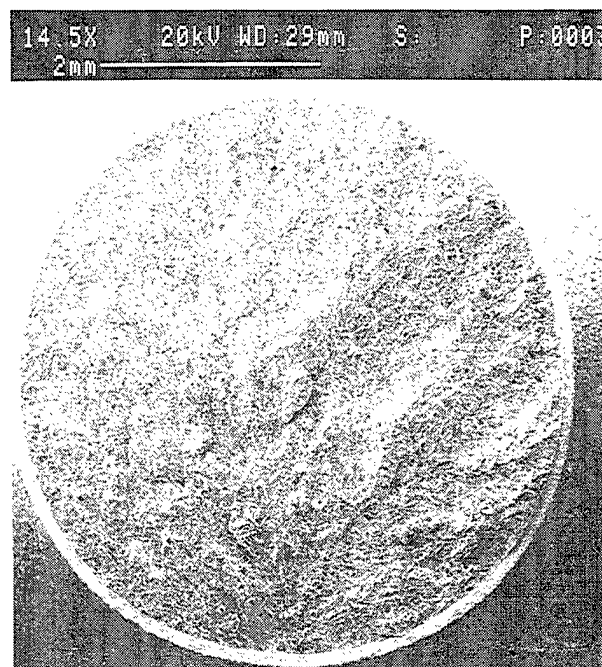
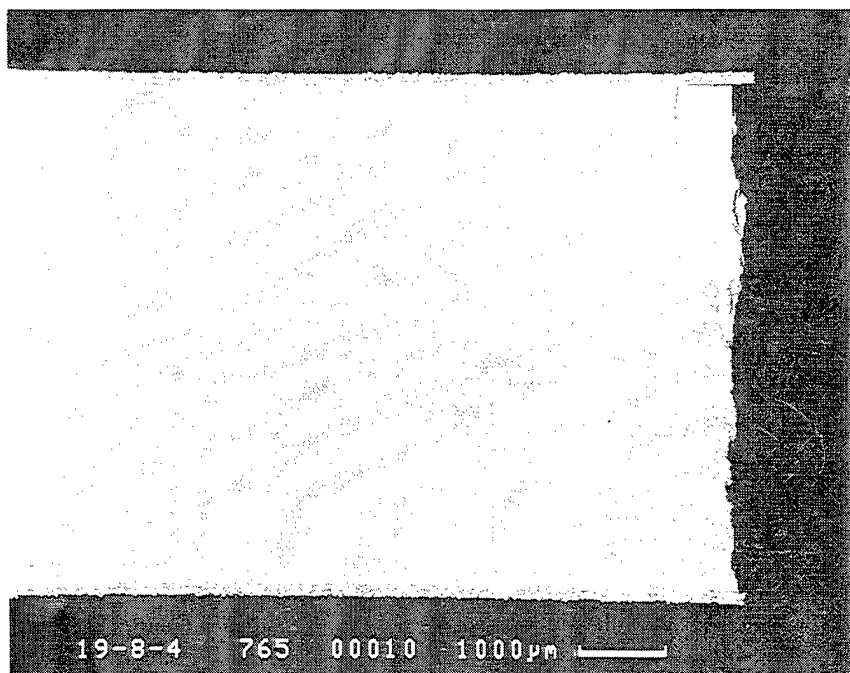


Figure 253. Cross section of CVD W + cermet coated gamma sample fatigue tested at RT and 0.3% strain for 3 cycles.

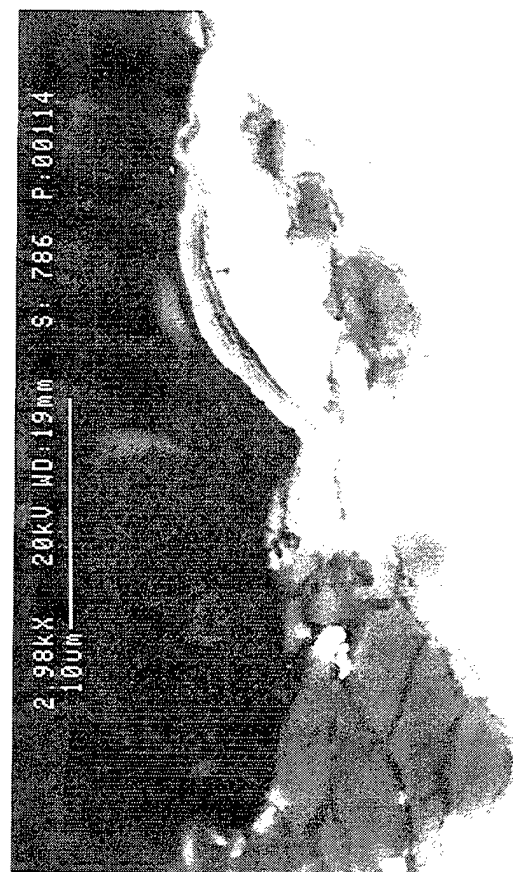
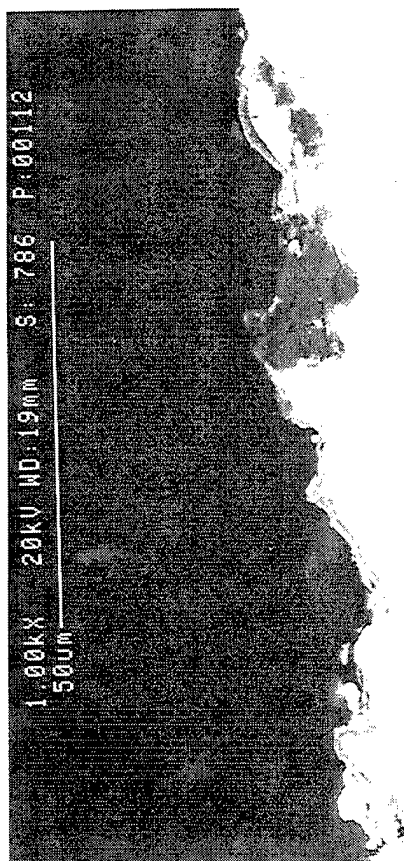
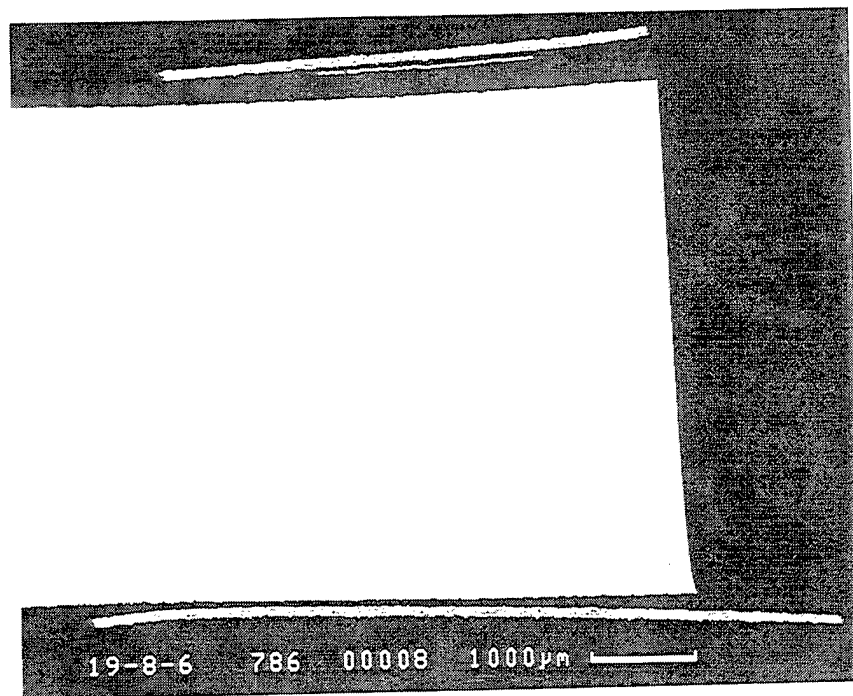


Figure 254. Cross section of cyclically exposed CVD W + cermet coated gamma sample fatigue tested at 760°C and 0.3% strain for 5168 cycles.

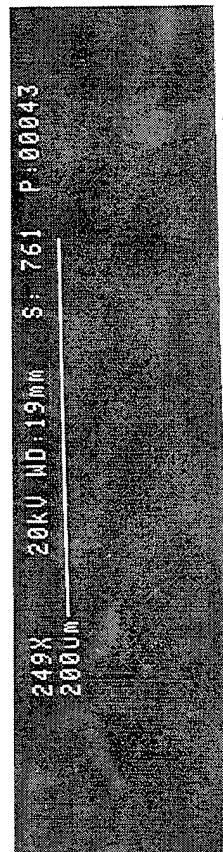
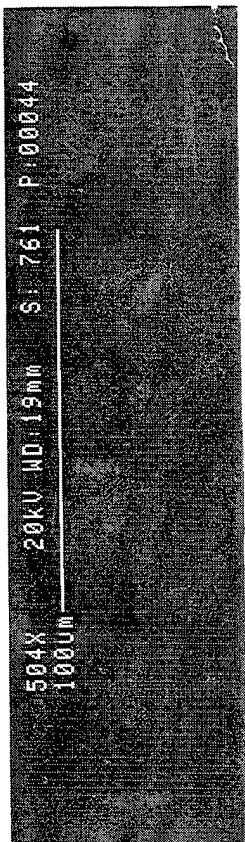
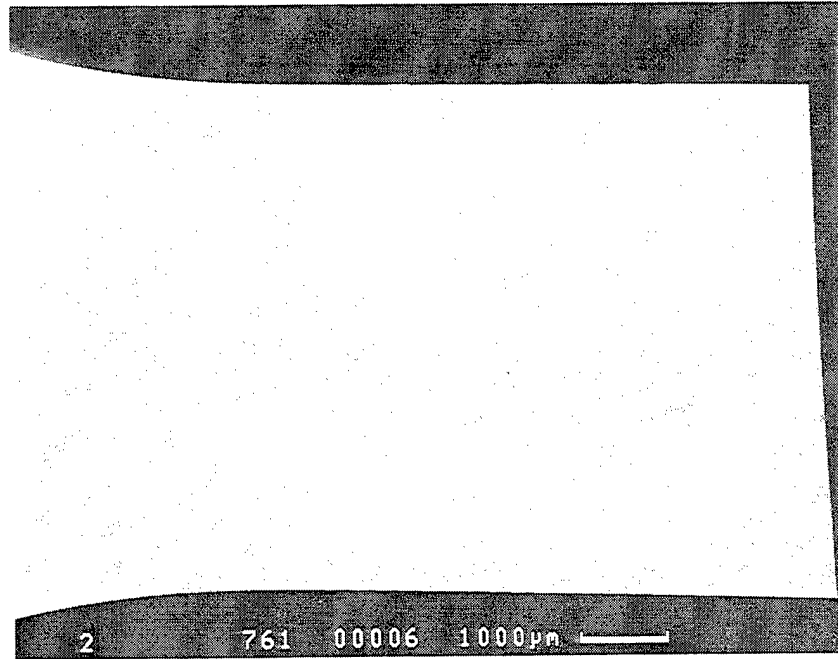


Figure 255. Cross section of uncoated unexposed alpha-2 fatigue tested at RT and 0.8% strain for 200,000 cycles.

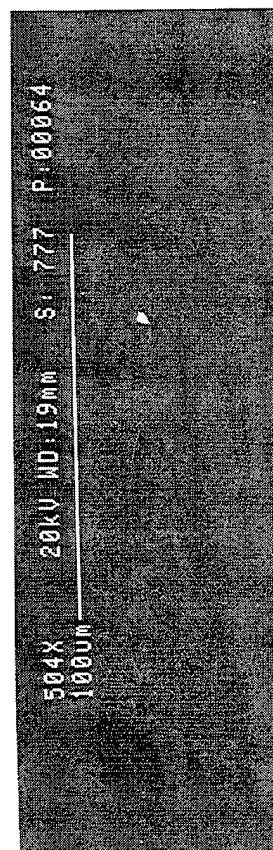
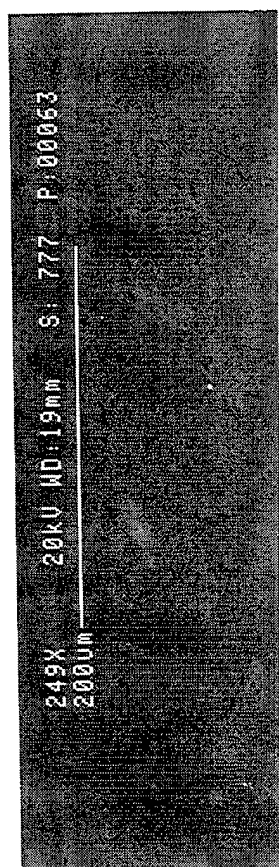
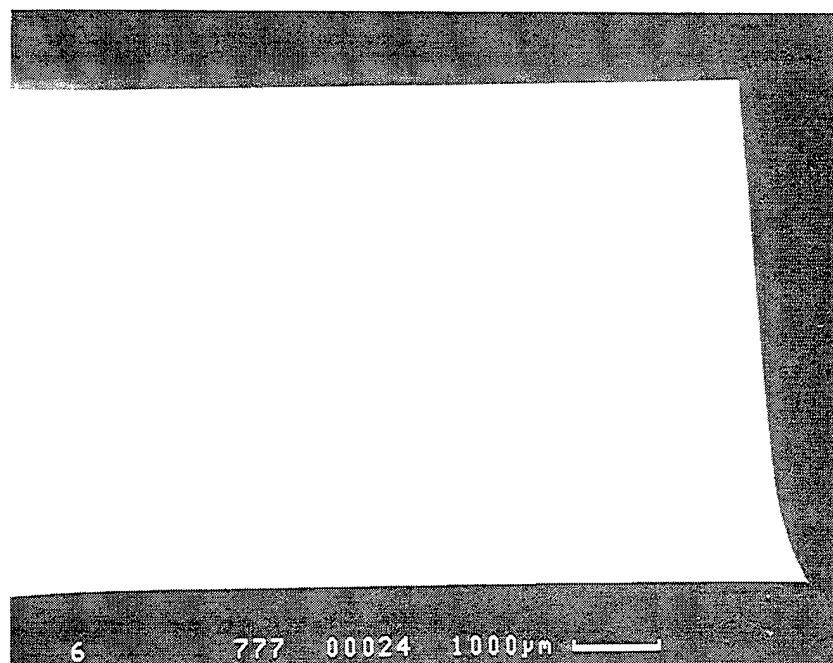


Figure 256. Cross section of uncoated unexposed alpha-2 fatigue tested at 648°C and 0.8% strain for 200,000 cycles.

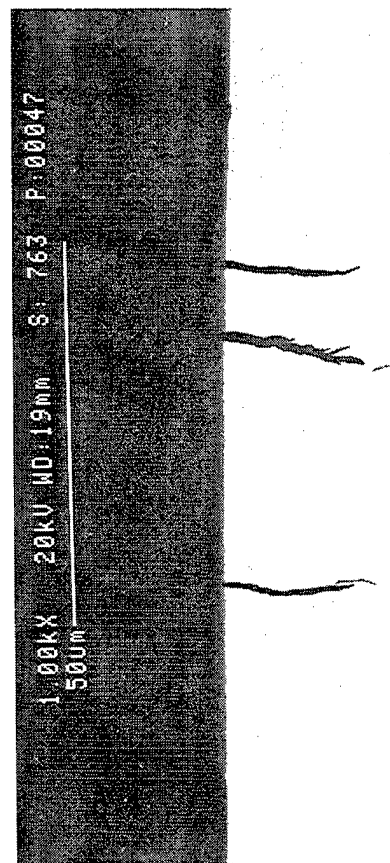
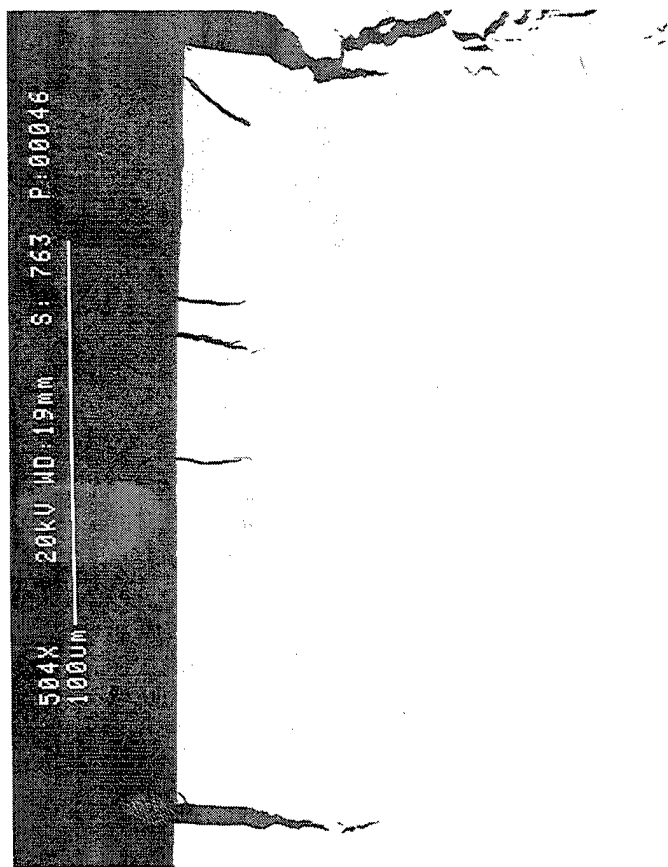
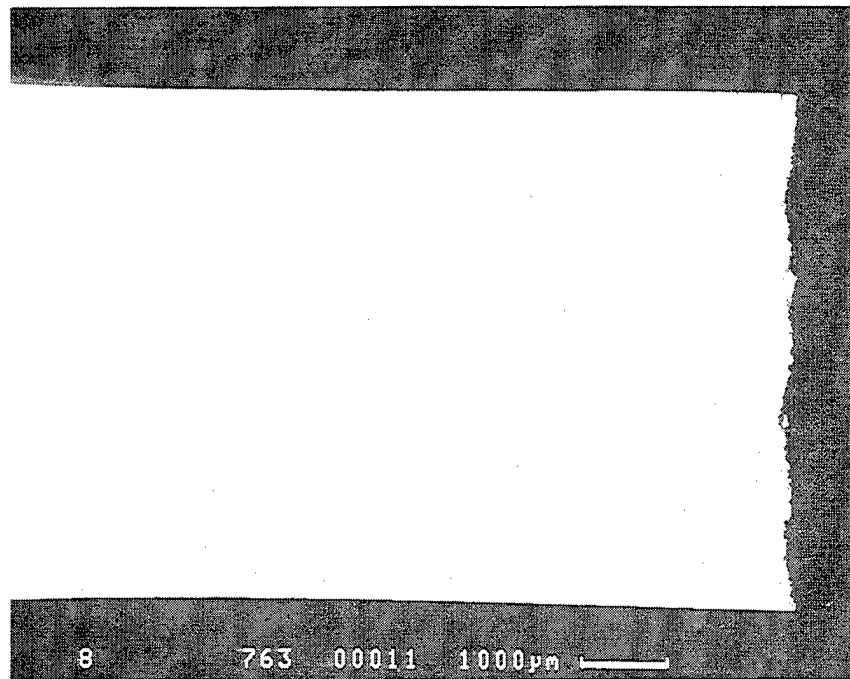


Figure 257. Cross section of uncoated cyclically exposed alpha-2 fatigue tested at RT and 0.8% strain for 323 cycles.

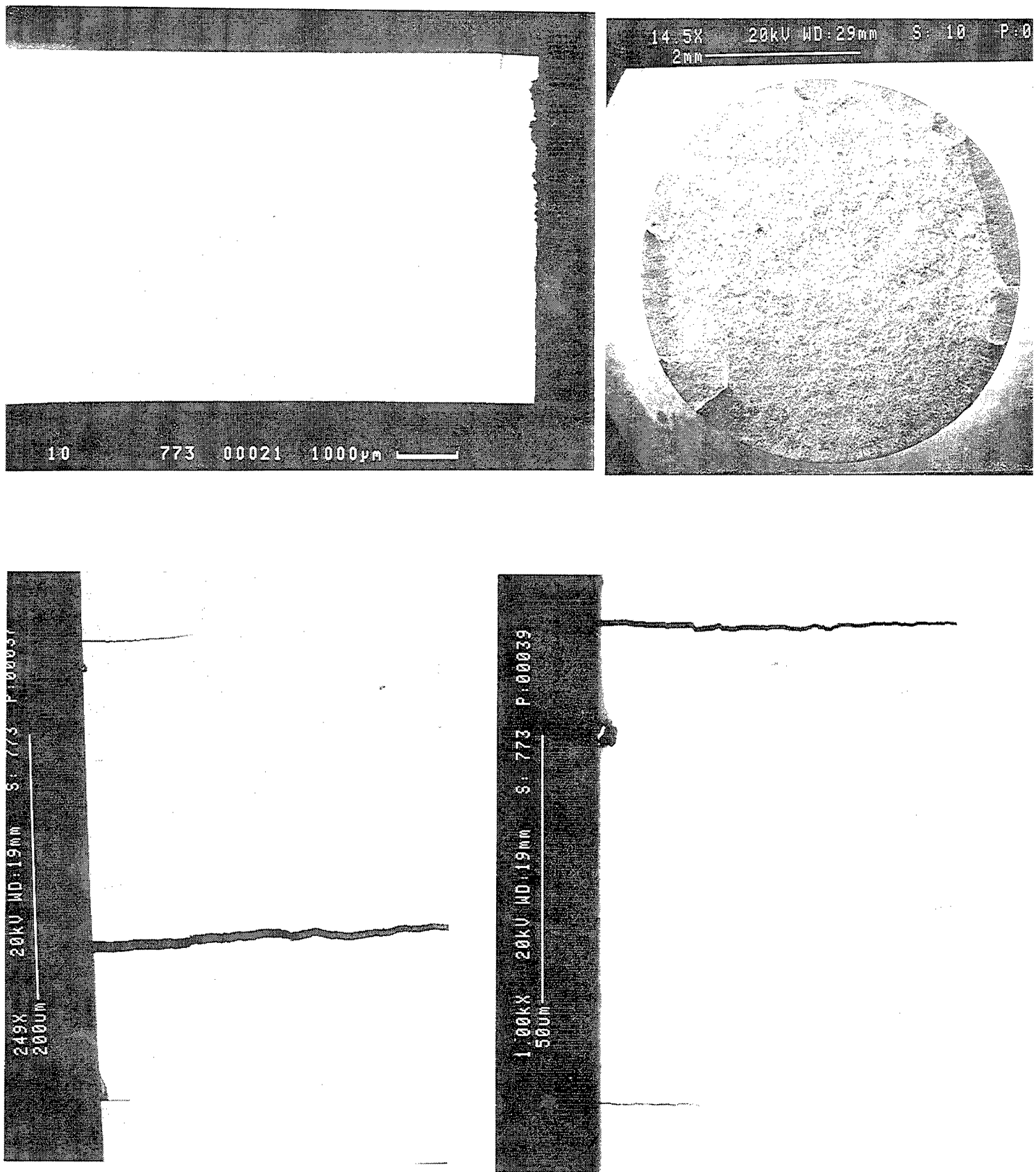


Figure 258. Cross section of uncoated cyclically exposed alpha-2 fatigue tested at 648°C (1200°F) and 0.8% strain for 3608 cycles.

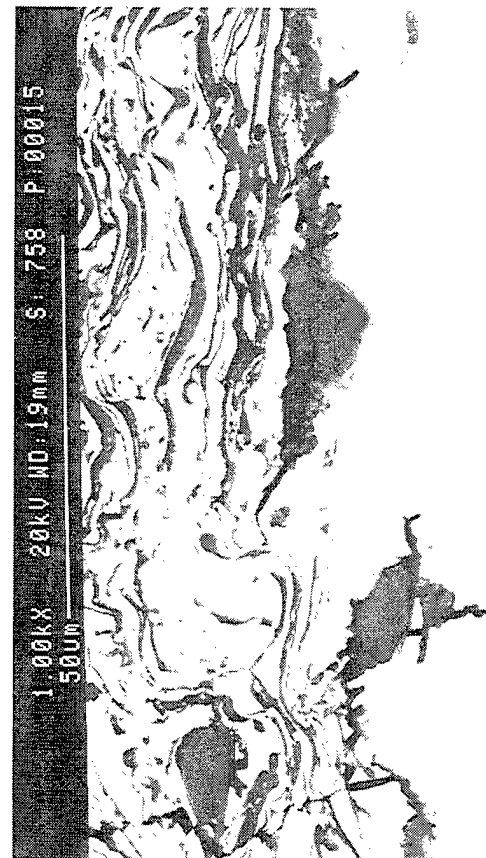
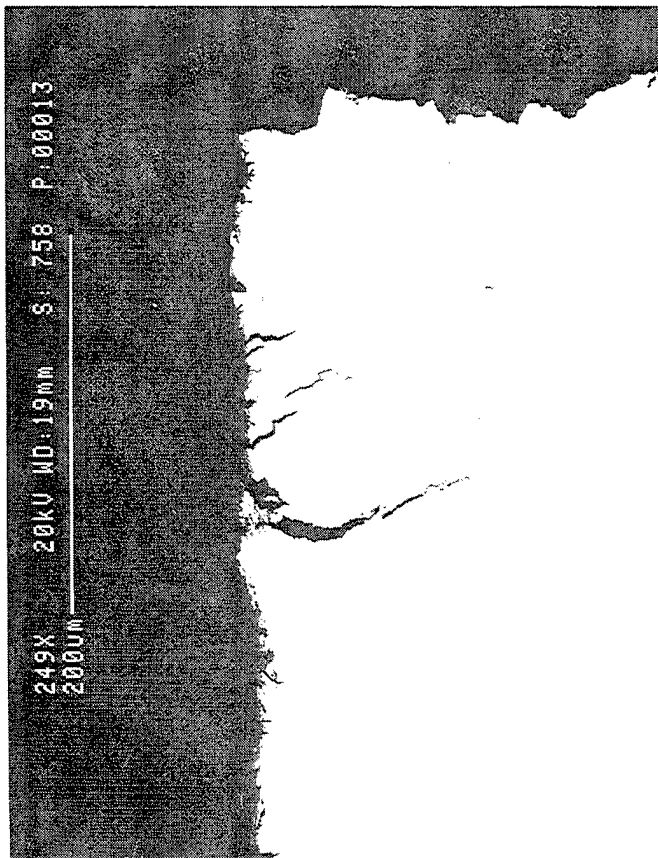
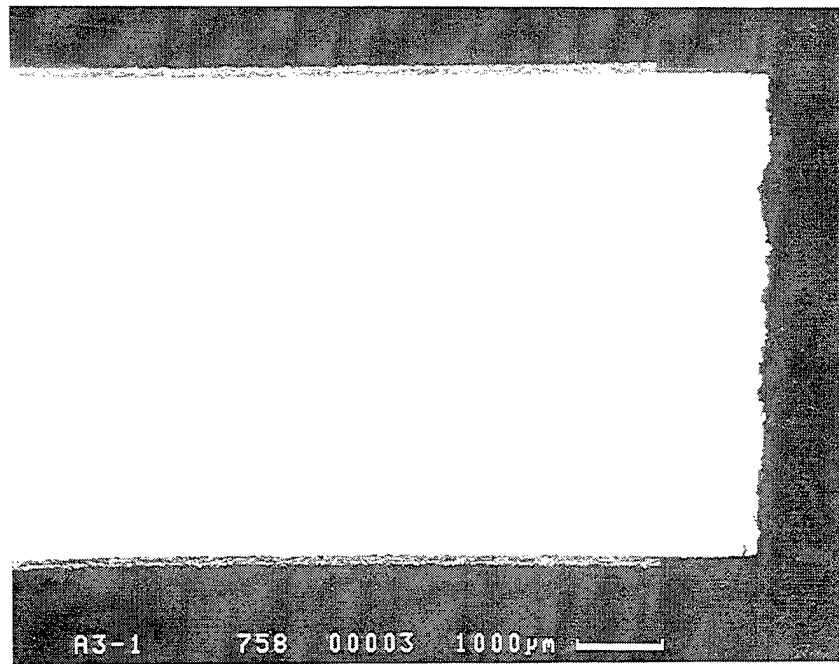


Figure 259. Cermet coated unexposed alpha-2 sample cross sections tested at RT and 0.8% strain for 378 cycles.

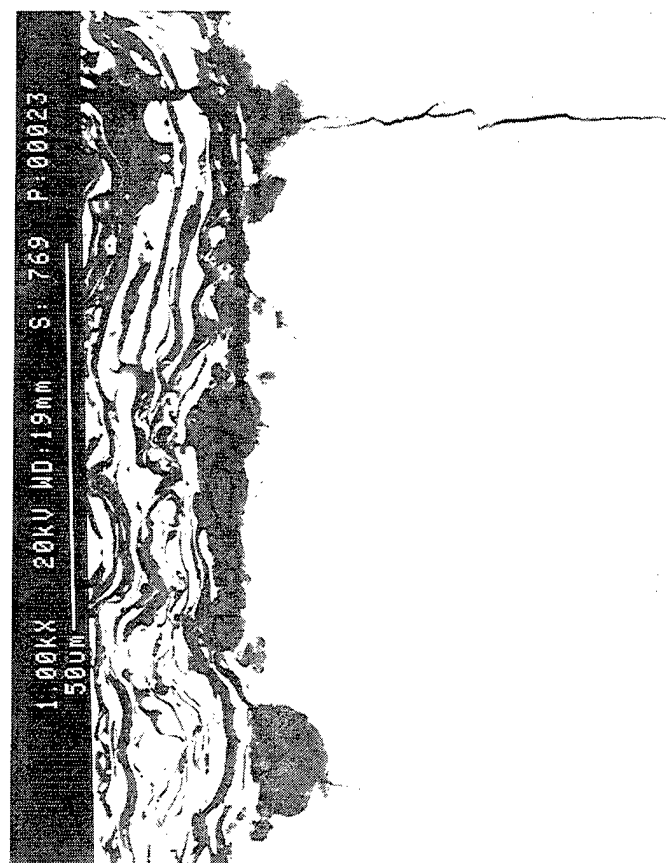
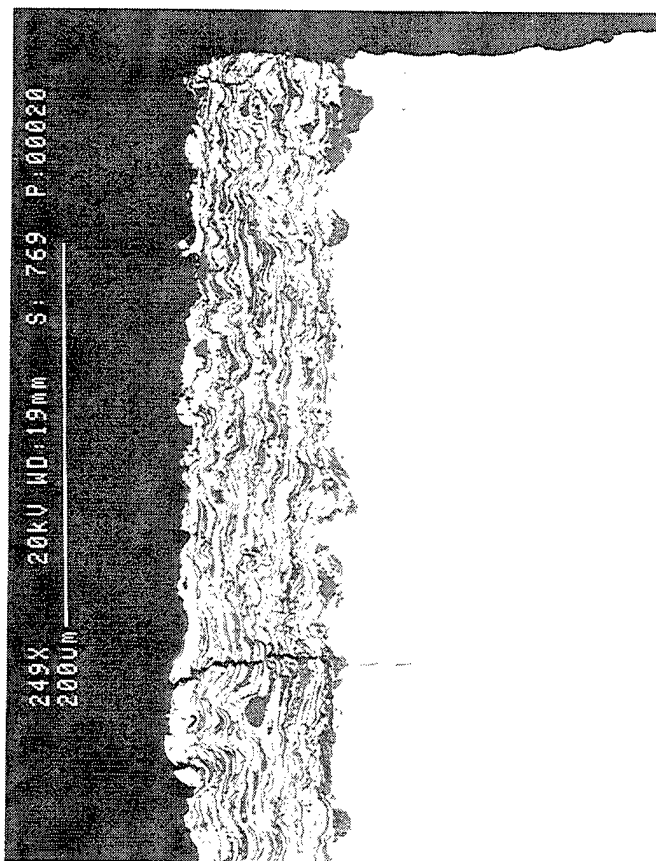
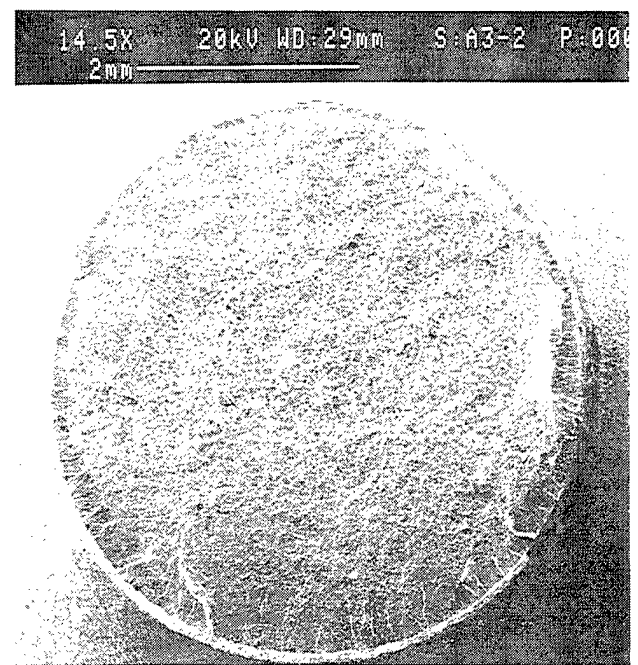
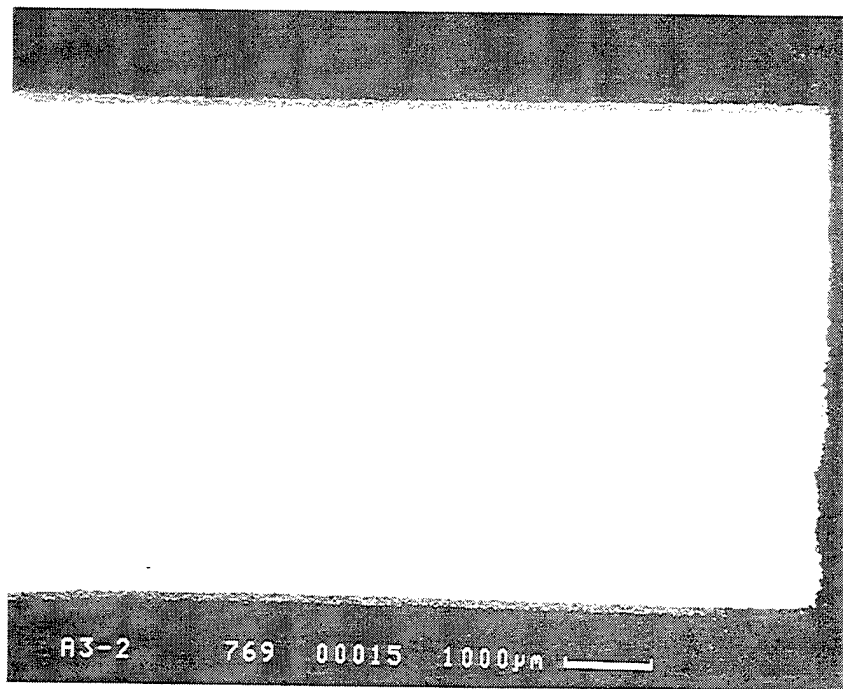


Figure 260. Cermet coated unexposed alpha-2 sample cross sections tested at 426°C and 0.8% strain for 3608 cycles.

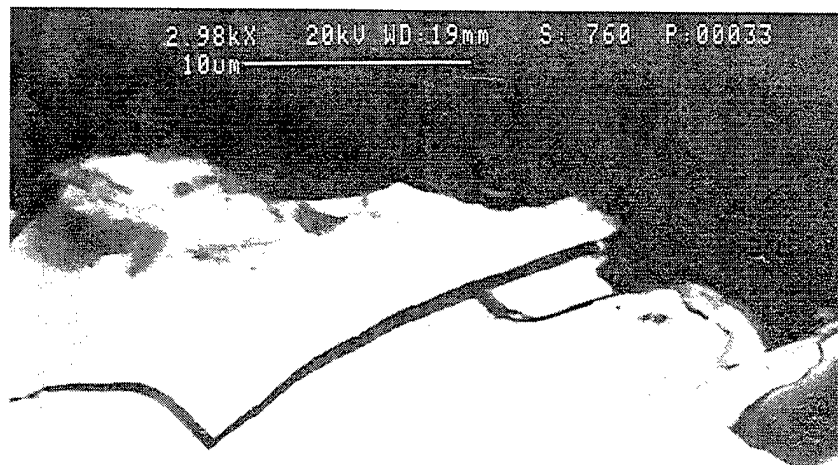
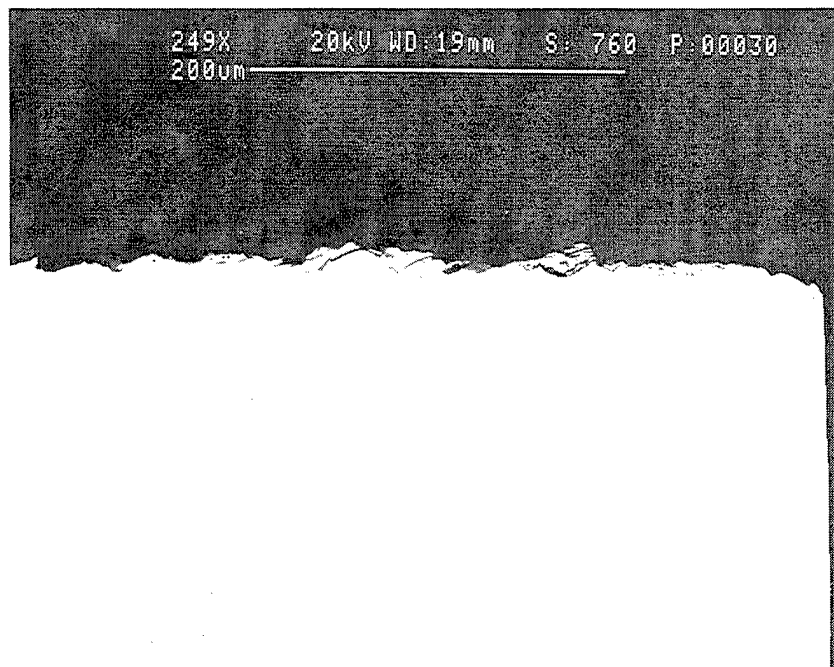


Figure 261. Cermet coated cyclically exposed alpha-2 samples tested at RT and 0.8% strain for 172 cycles. The coating spalled.

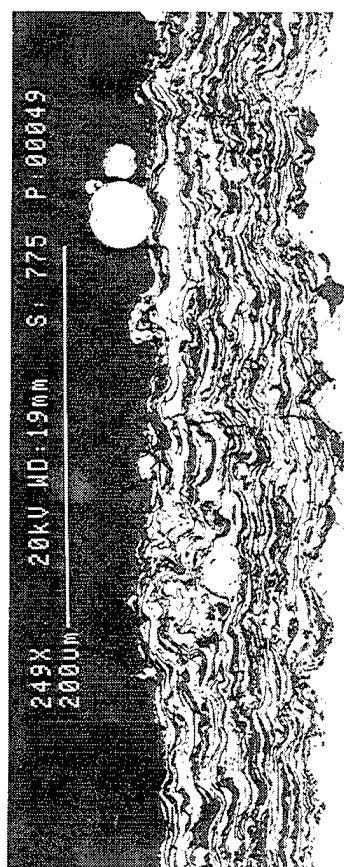
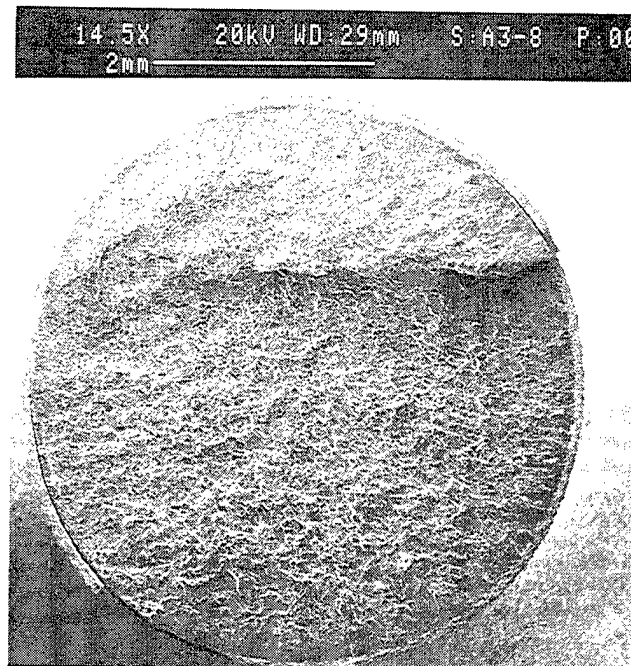
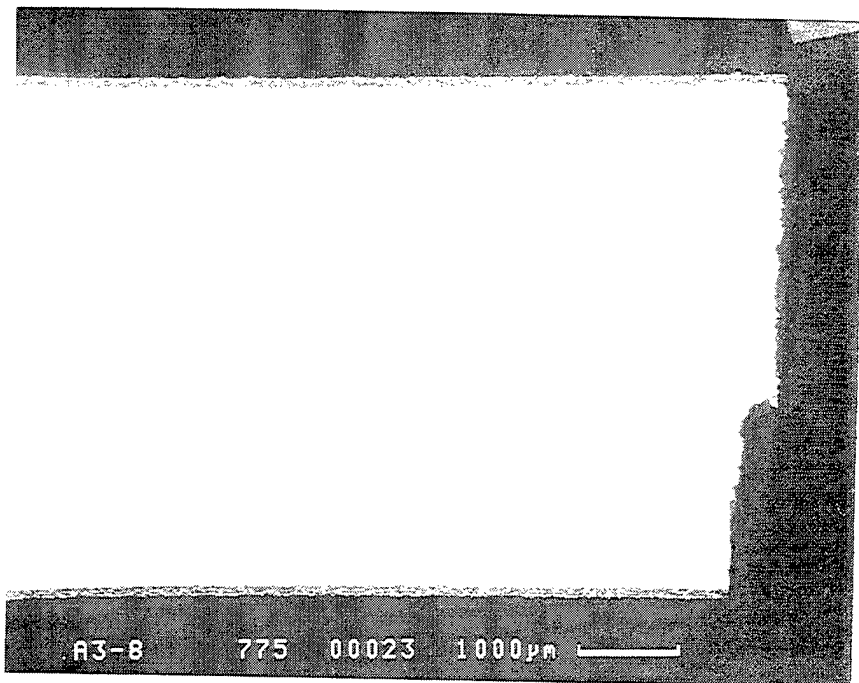


Figure 262. Cermet coated cyclically exposed alpha-2 samples tested at 648°C and 0.8% strain for 530 cycles.

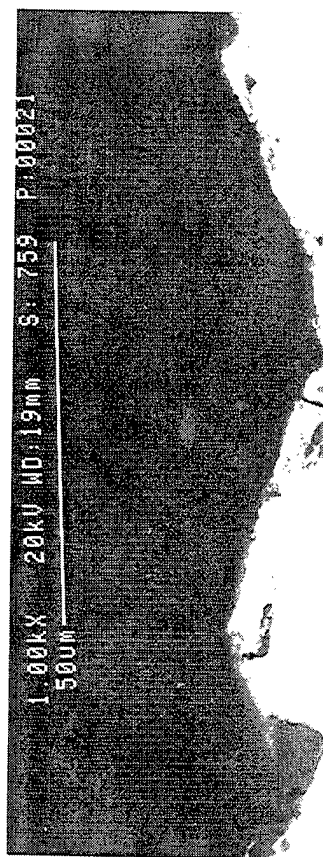
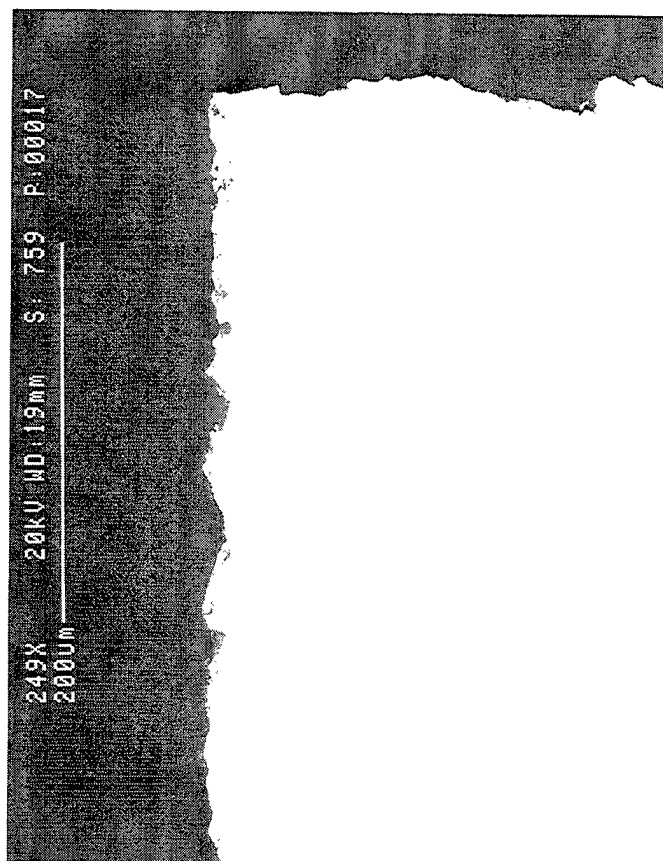
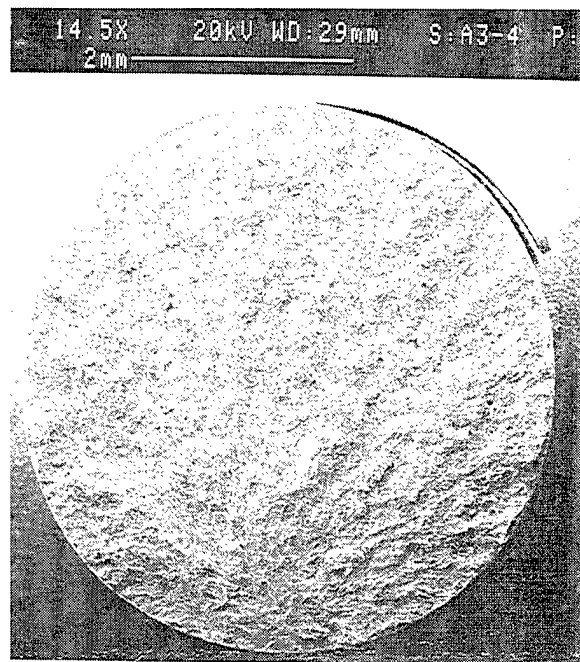
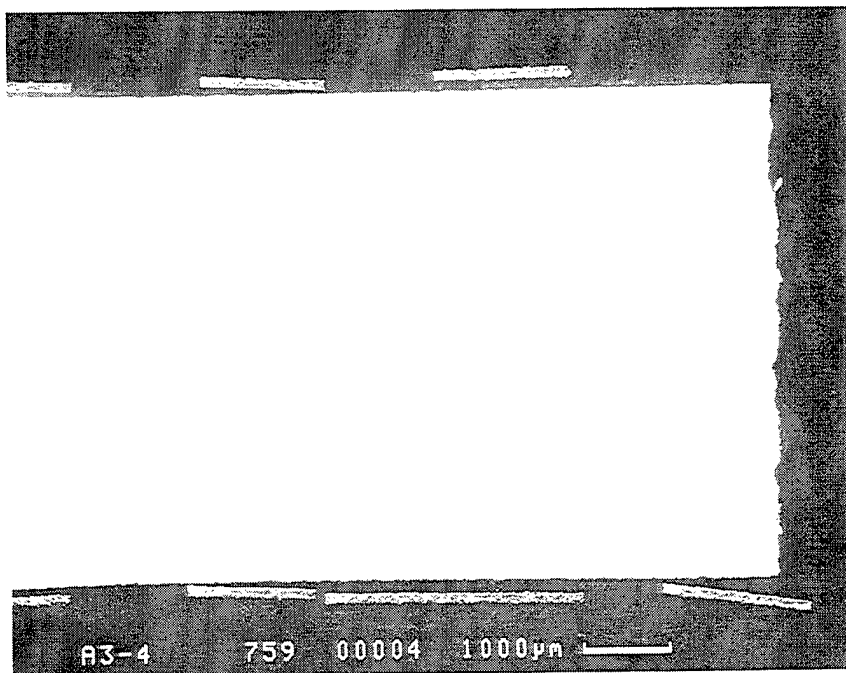


Figure 263. Cermet coating with W CVD diffusion barrier fatigue tested at RT at a strain of 0.8% for 523 cycles.

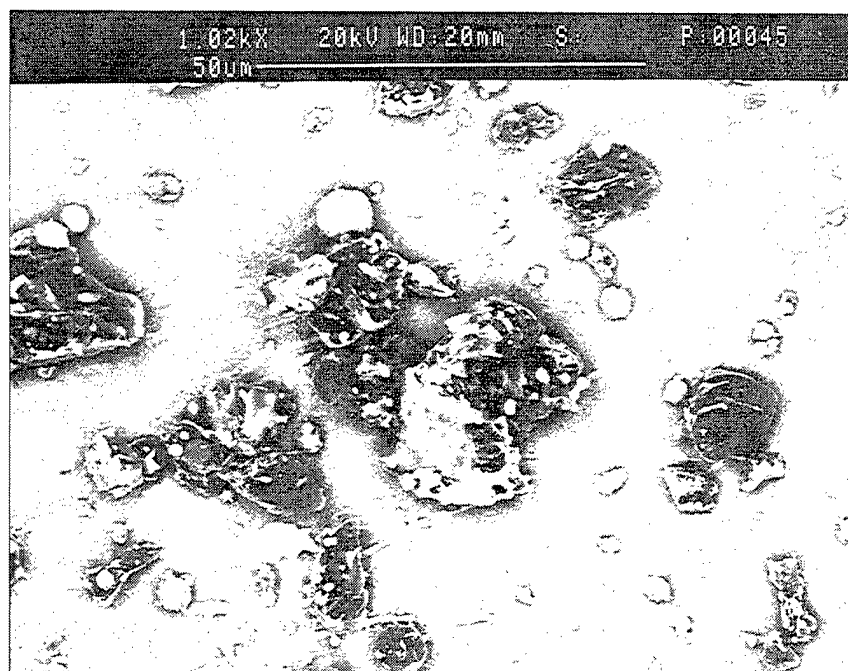
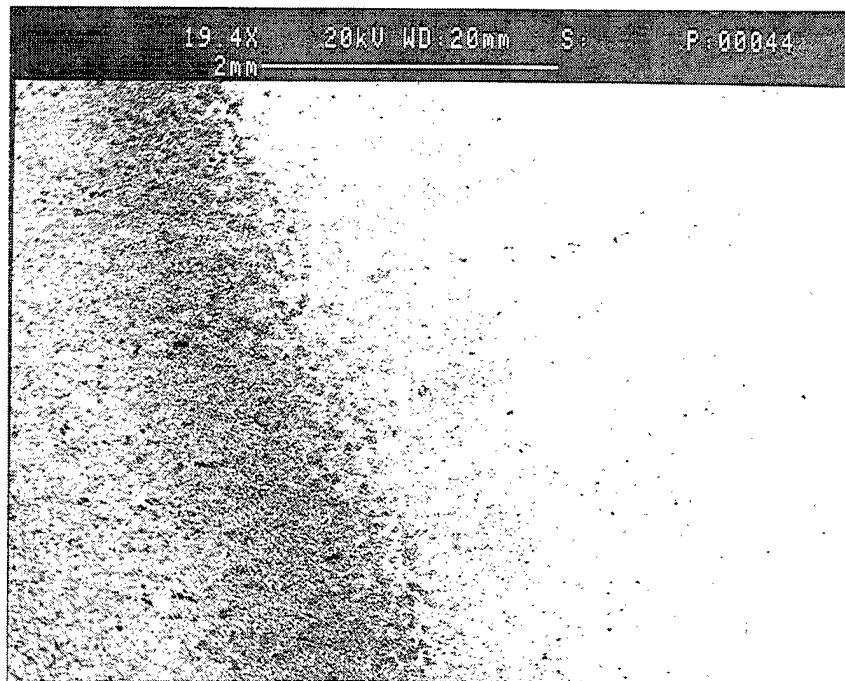
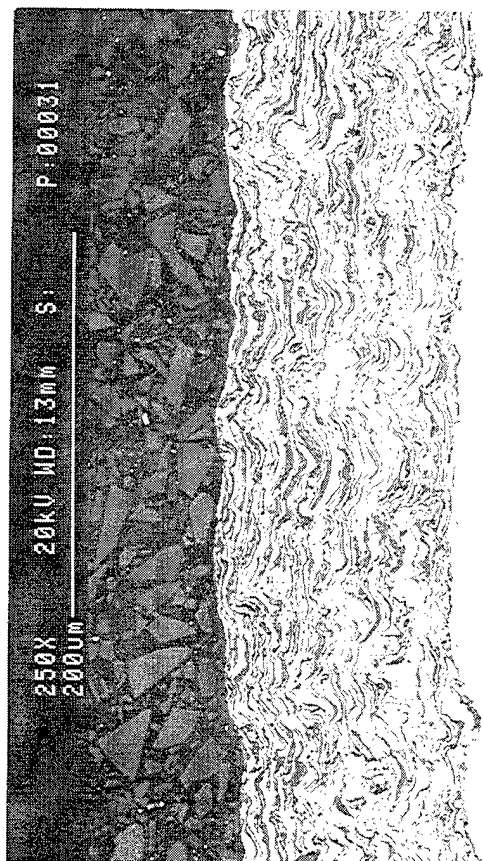
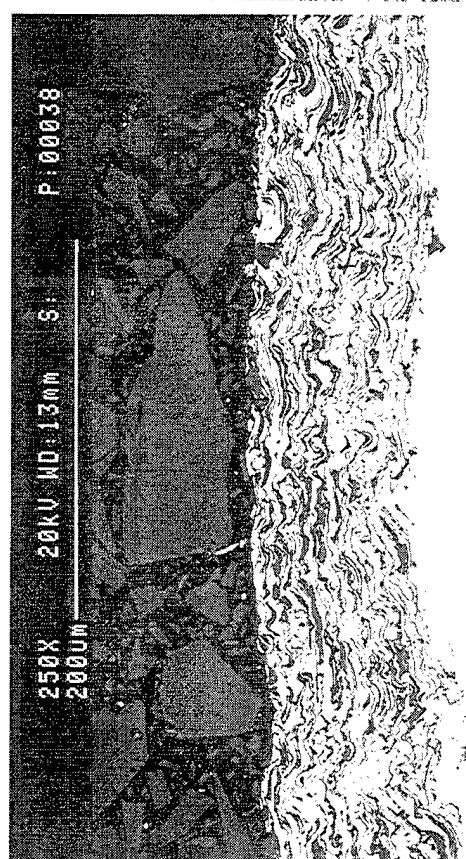
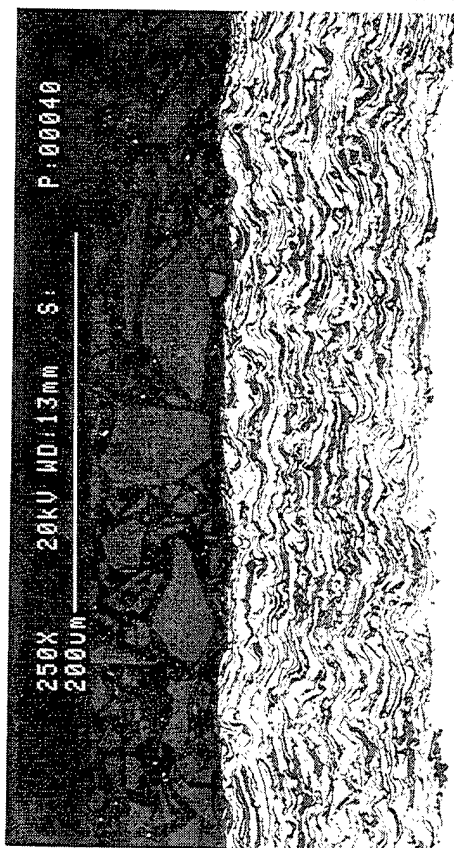
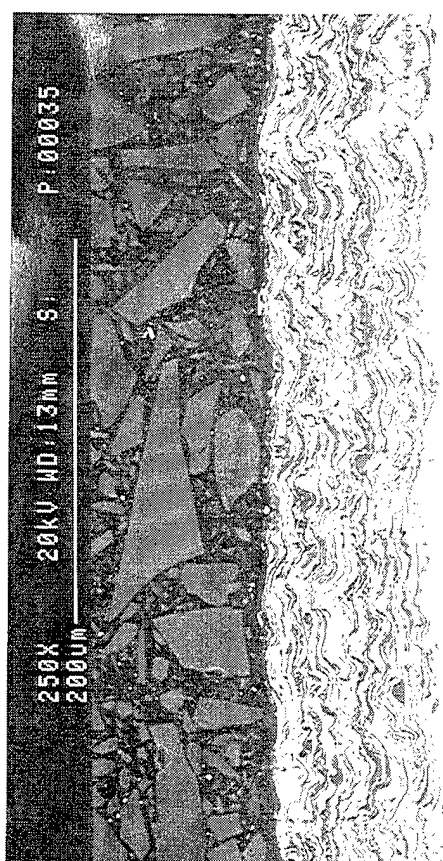


Figure 264. Micrograph of steel tape used to masked cermet coated samples used in Task 3.

0 Preheat



5 Preheat



15 Preheat Short Stroke

15 Preheat Long Stroke

Figure 265. Micrographs of microstructures obtained using various preheat cycles.

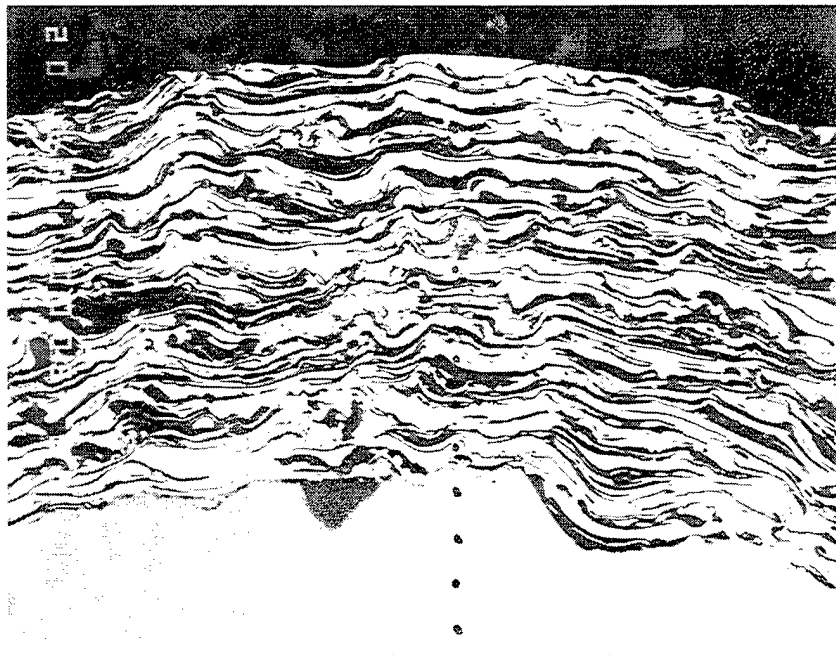


Figure 266. Micrographs of cermet coated Low Pressure Turbine Blade.

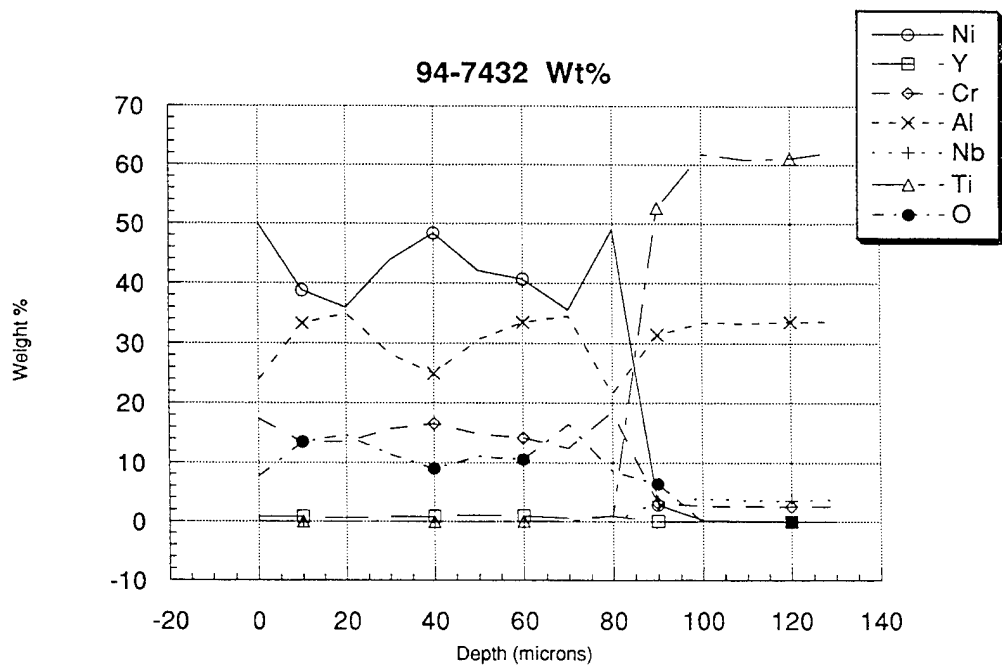
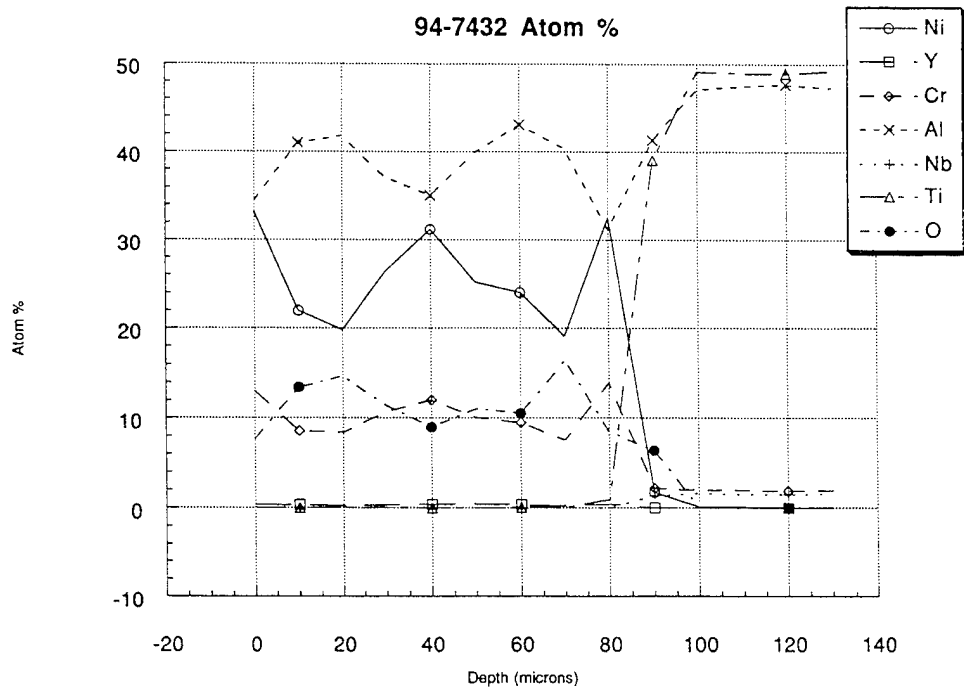


Figure 267. Microprobe results are shown for the cermet coating on a cast gamma LPT blade.

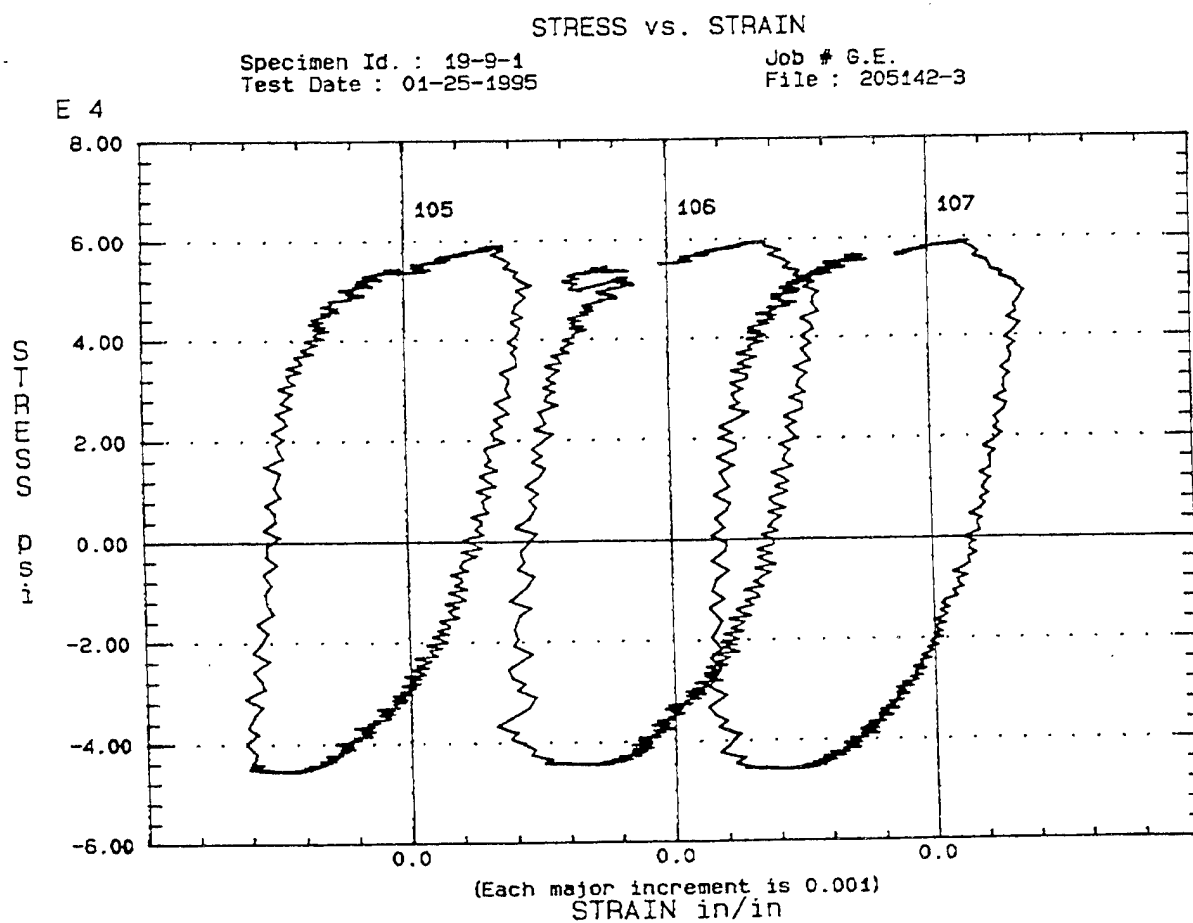


Figure 268. Plots showing loading profile for the uncoated gamma alloy tested in TMF.

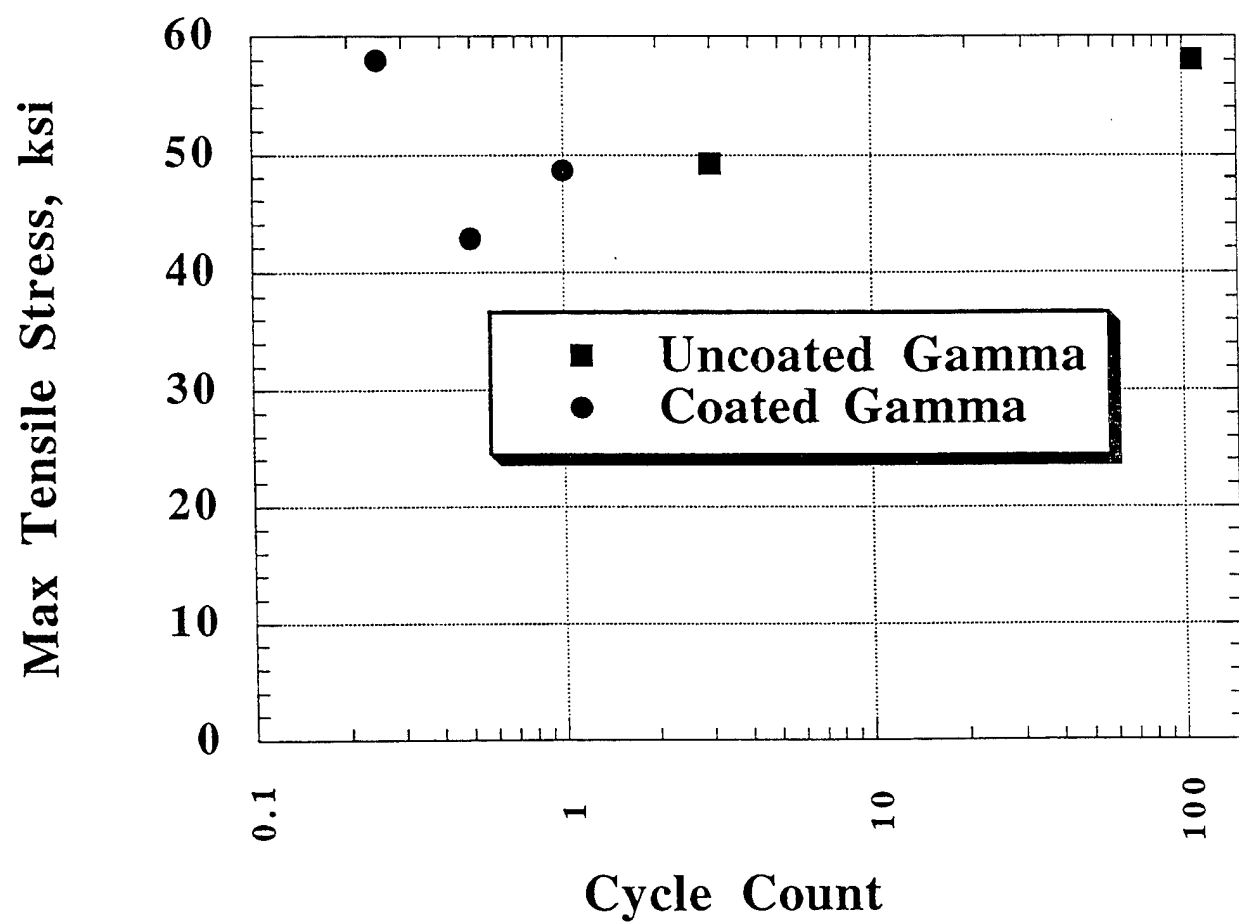


Figure 269. Plot of TMF results for coated and uncoated gamma.

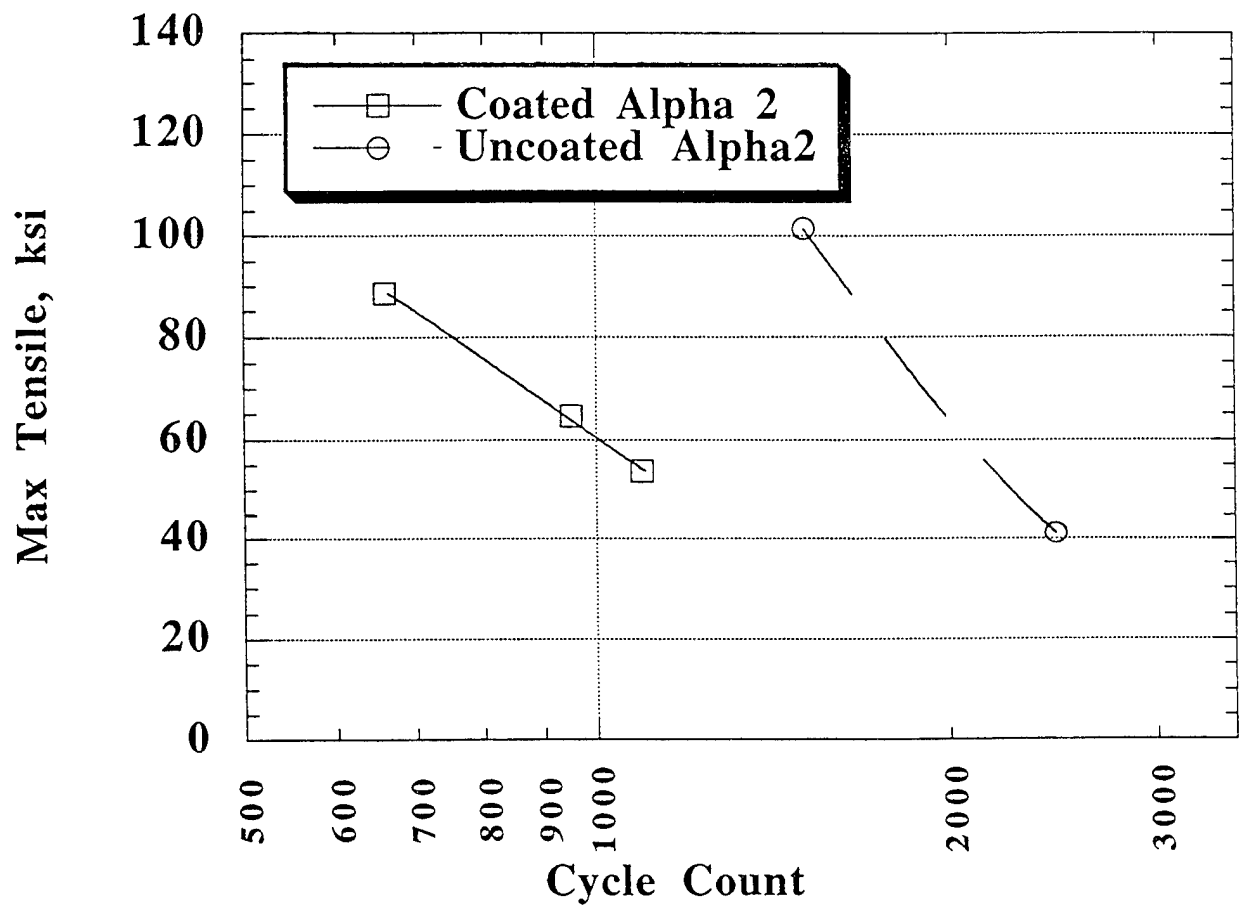


Figure 270. Plot of TMF results for coated and uncoated alpha-2.

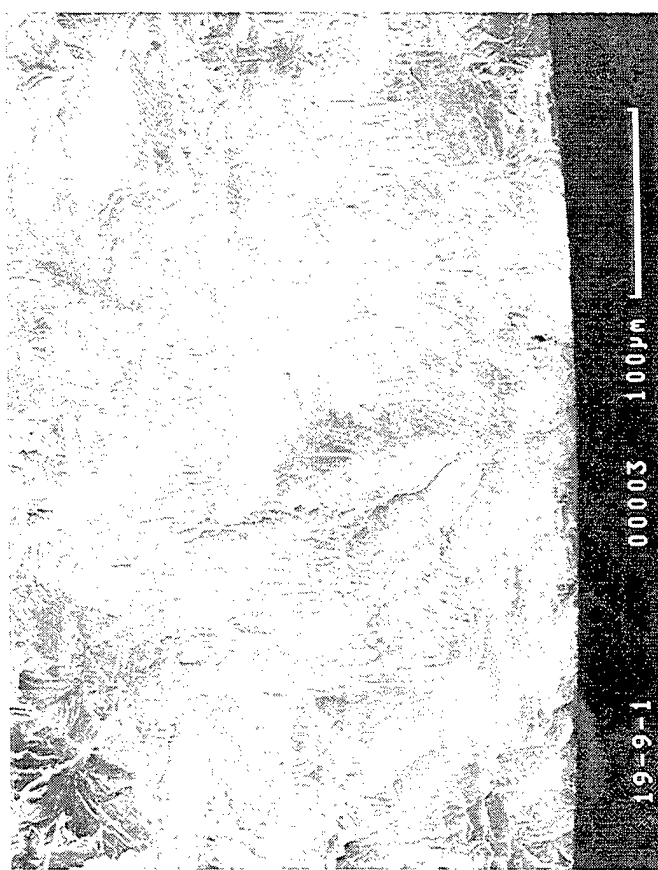
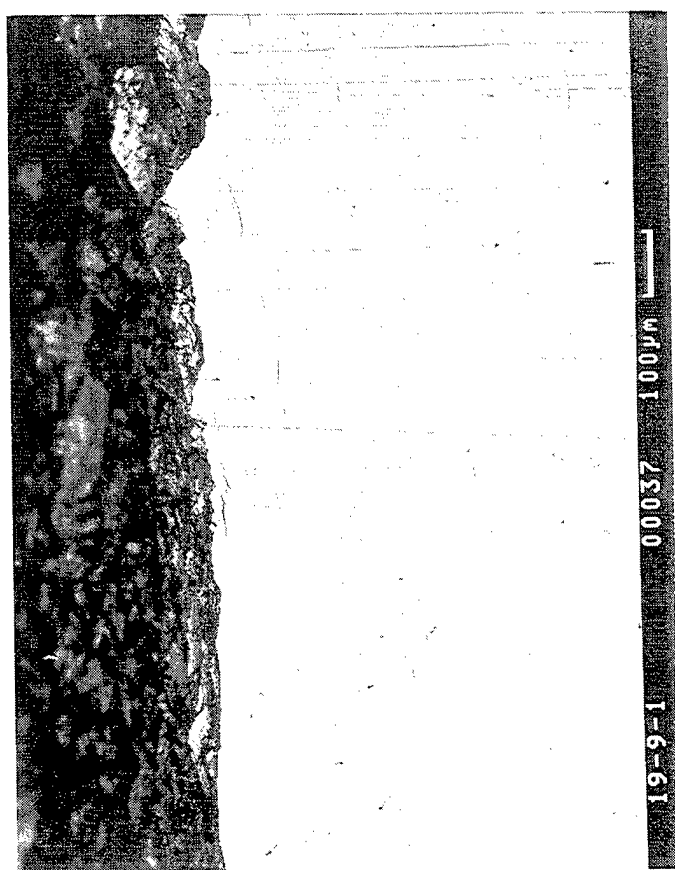
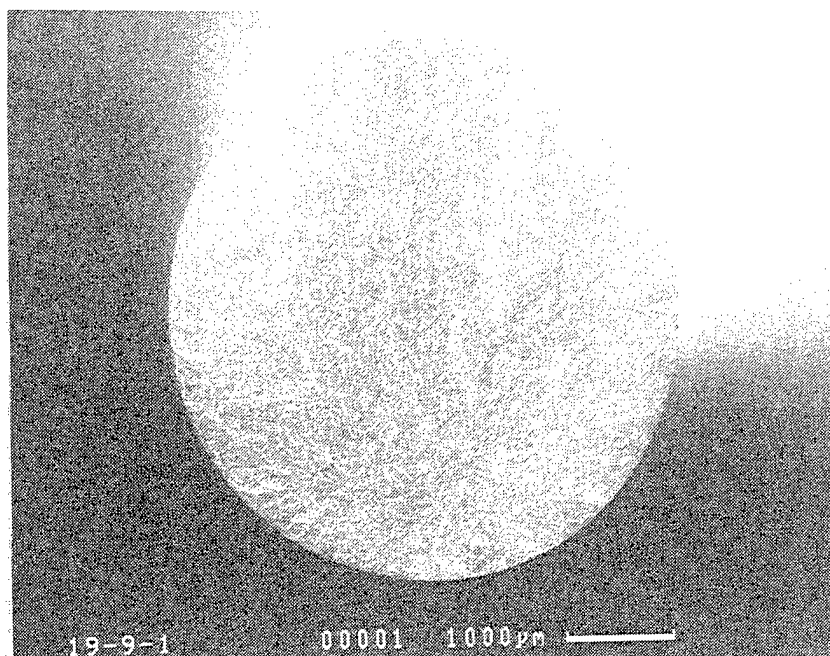


Figure 271. Fractography of the uncoated gamma sample that failed after 108 TMF cycles.

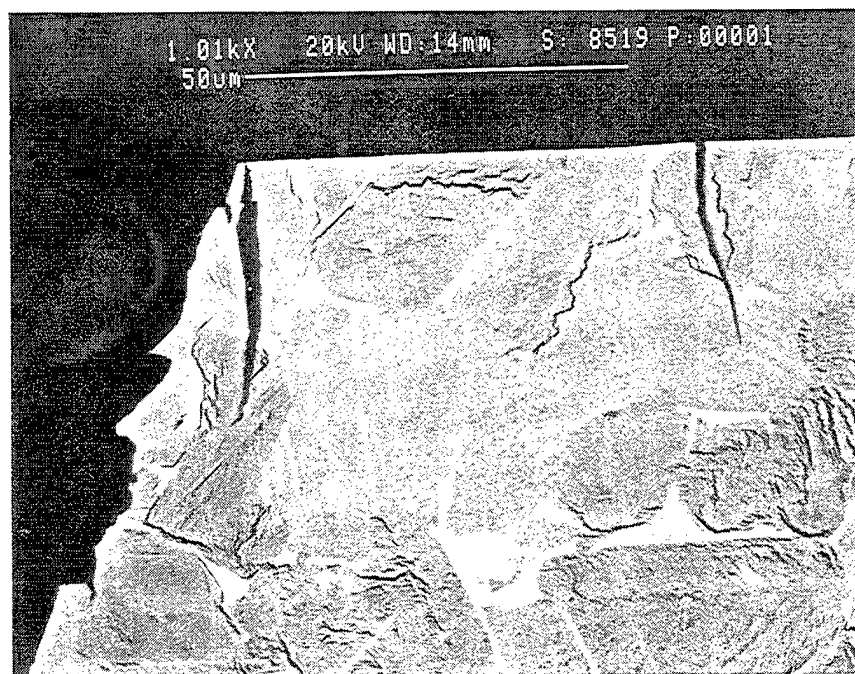
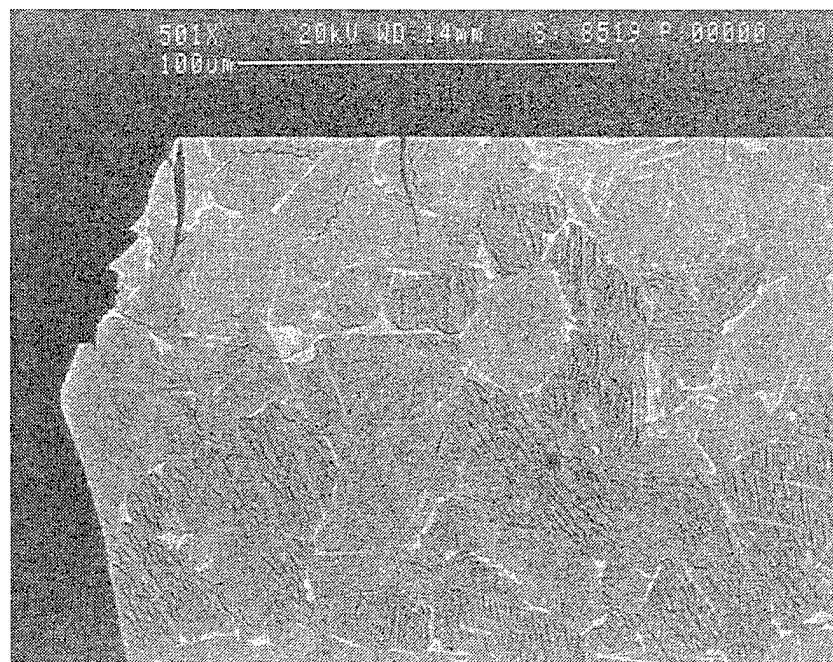


Figure 272. Cross section of the uncoated gamma sample that failed after 108 TMF cycles.

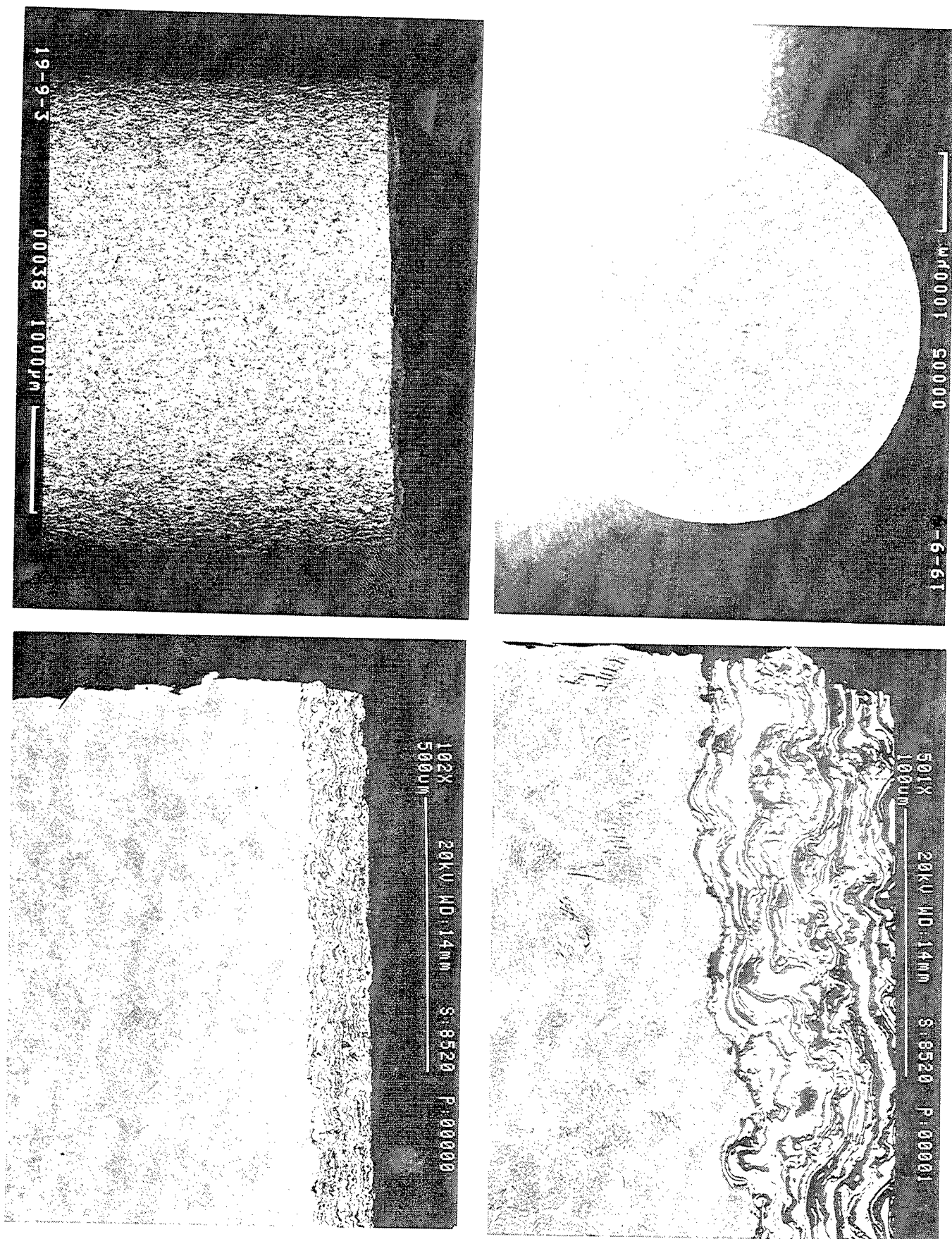


Figure 273. Surface and cross section of a cermet coated gamma sample that failed during the first TMF cycle.

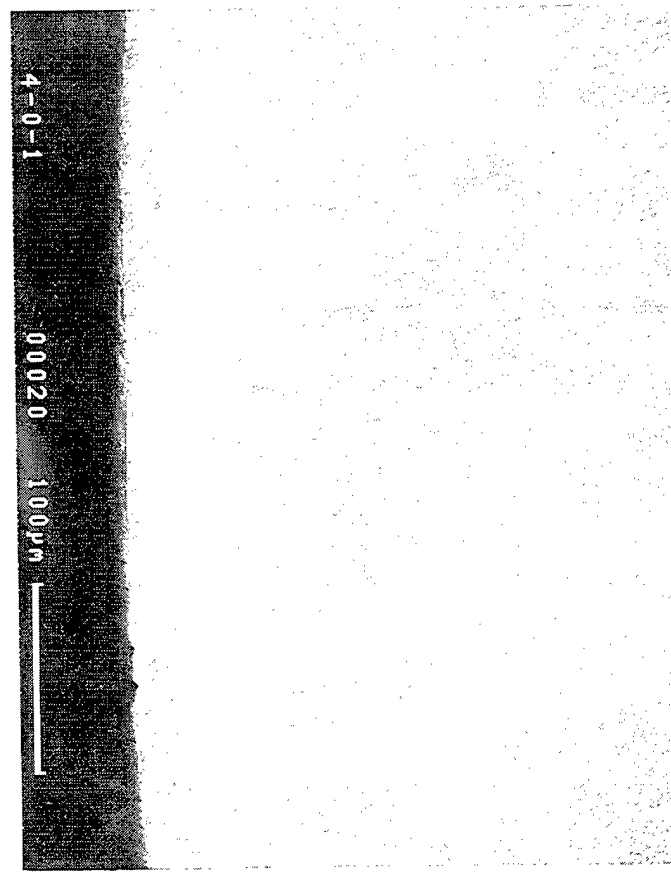
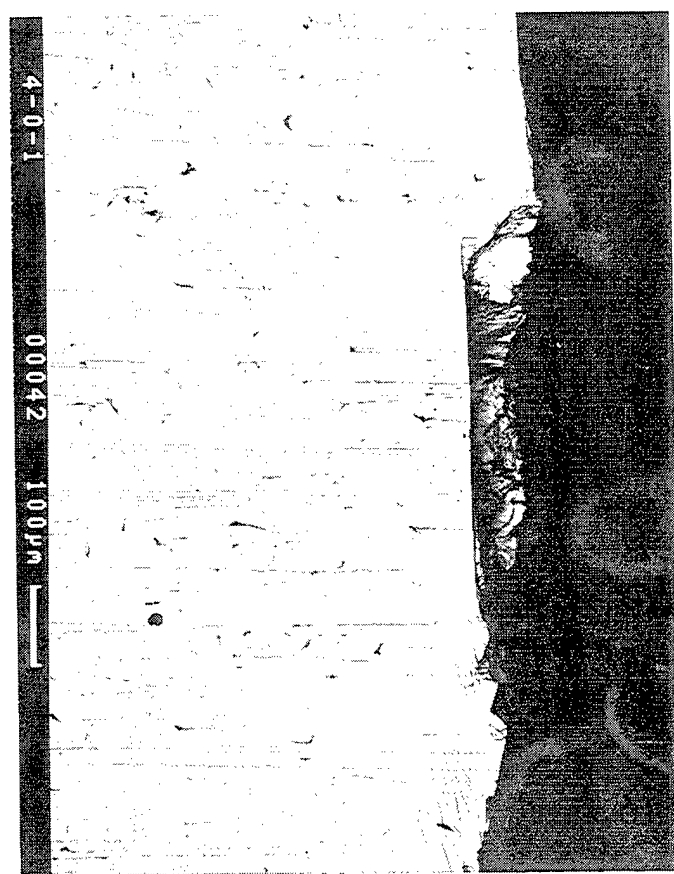
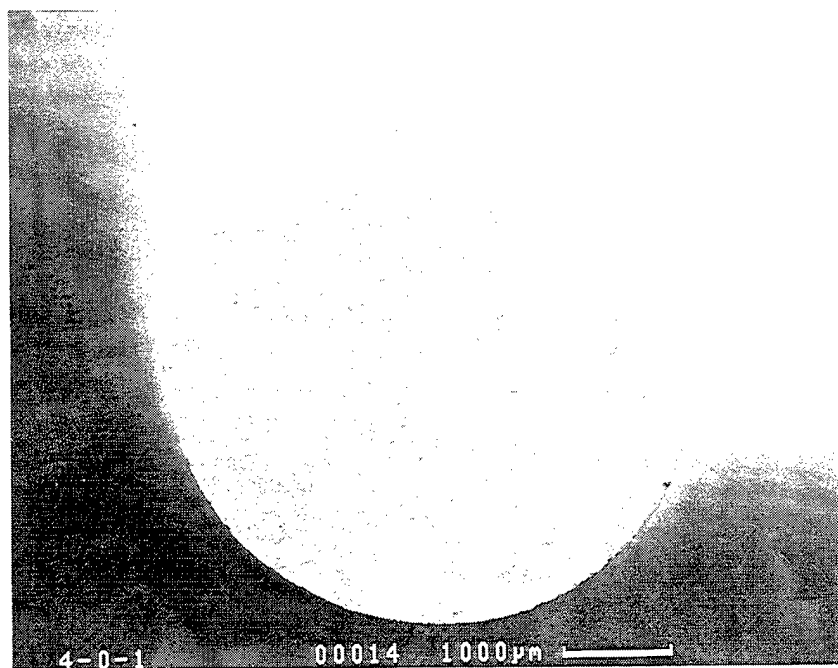


Figure 274. Fractography of an uncoated alpha-2 sample that failed after 1508 TMF cycles.

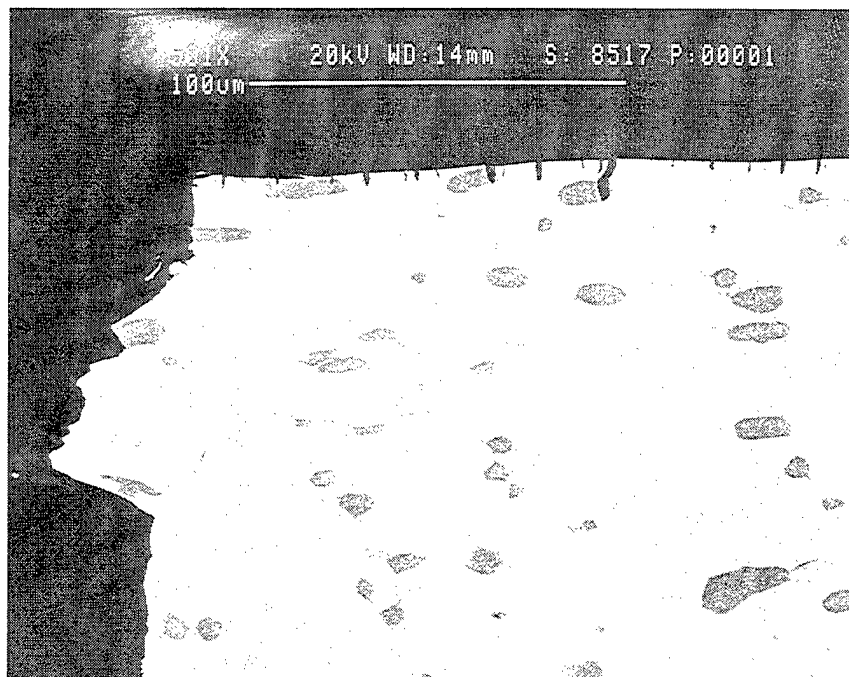


Figure 275. Cross section of the uncoated alpha-2 sample that failed after 1508 TMF cycles.

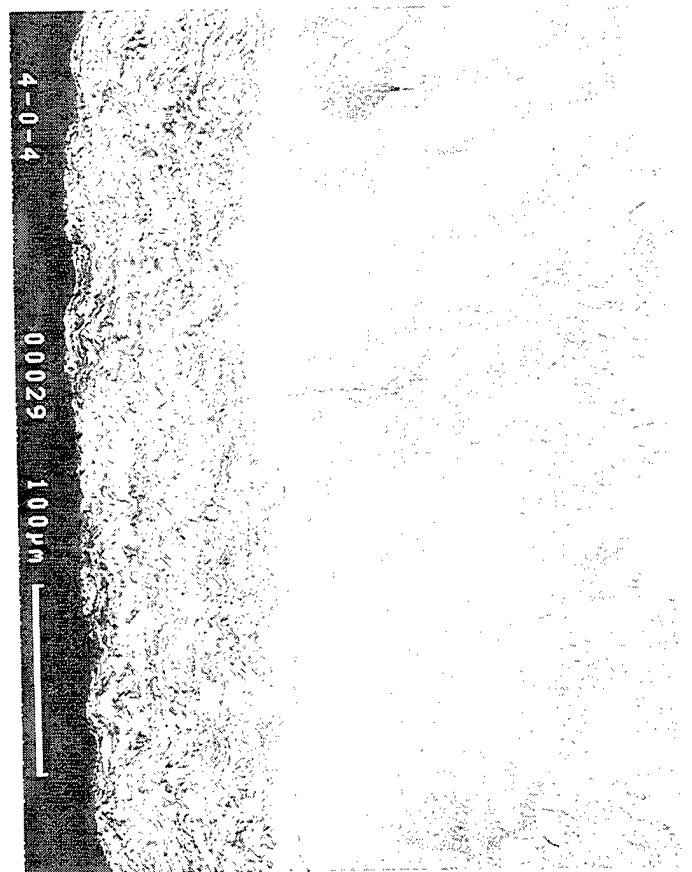
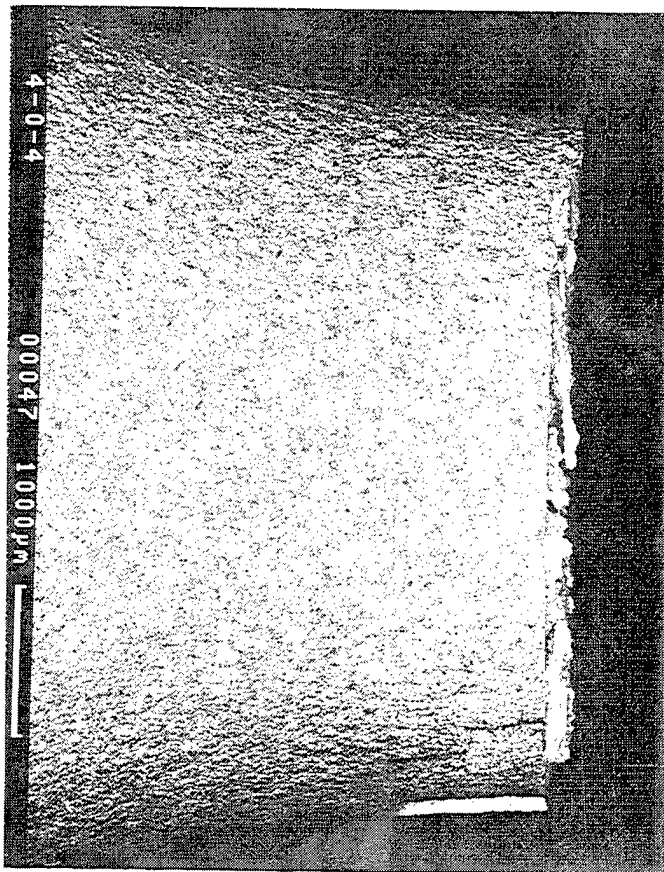
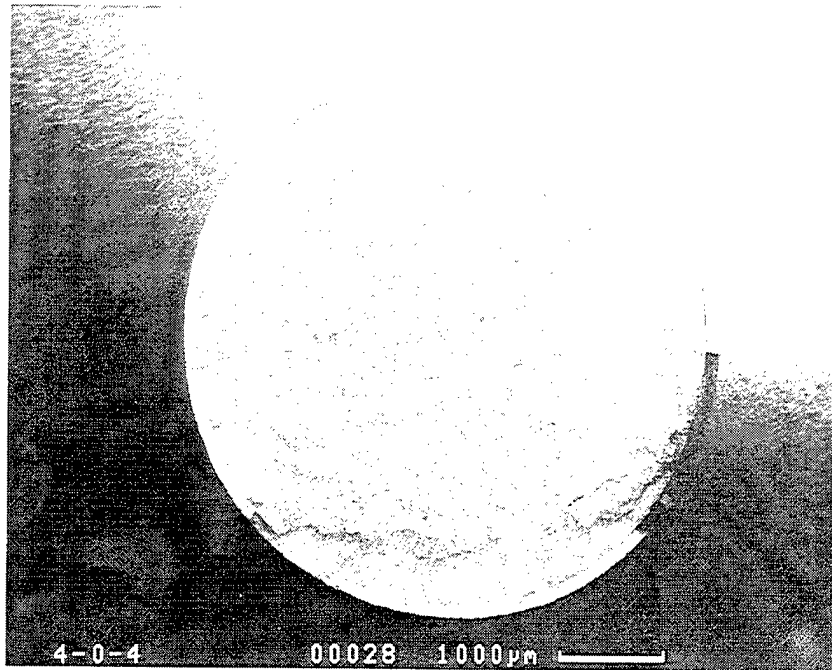


Figure 276. Fractography of a cermet coated alpha-2 sample that failed after 952 TMF cycles.

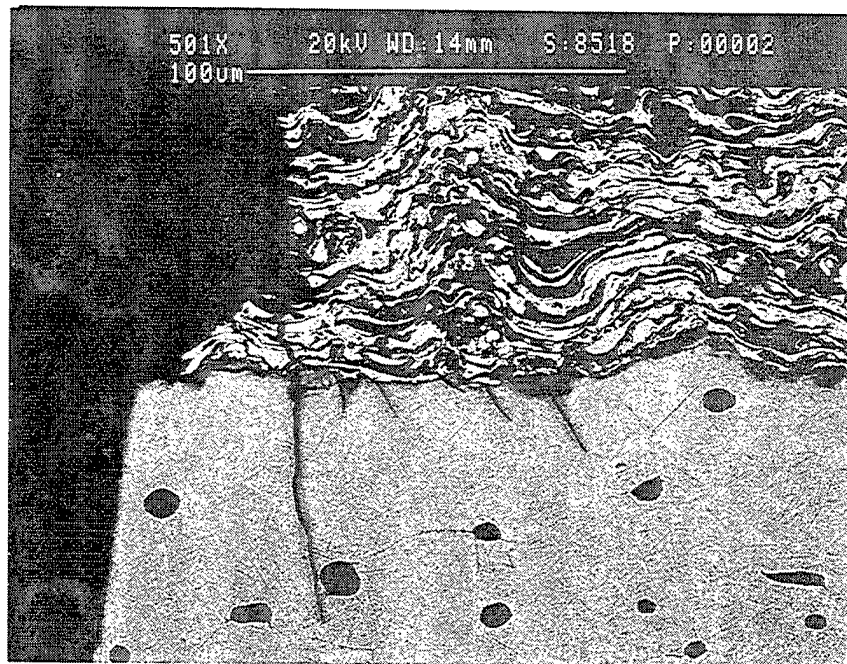
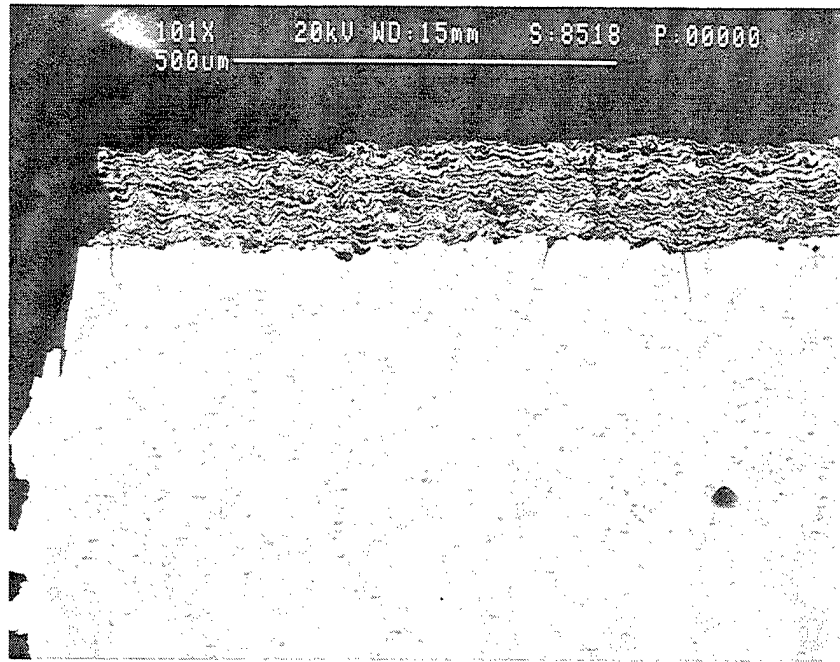


Figure 277. Cross section of the cermet coated alpha-2 sample that failed after 952 TMF cycles.

BLANK PAGE

TABLES

BLANK PAGE

Attributes:

1. Small Thermal Expansion Mismatch between Coating and Substrate
2. Limited Interdiffusion between Coating and Substrate
3. Strain Accommodation between Coating and Substrate
4. Coating Forms a Protective Scale
5. An Effective Coating Process

Coating Candidate	Attribute	Example	Substrate	
			α_2	γ
TiCrAl	1,2,4	Ti-44Al-28Cr	x	x
Modified g	1,2,4	Ti-48Al-2Cr-6Nb	x	
TBC	2,5	ZrO ₂ -8Y ₂ O ₃		x
Superalloy	3,4,5	IN 718	x	
MCrAlY	3,4,5	CoCr(WSiC)		x
Cermet	1,2,3,4,5	NiCrAlY/Al ₂ O ₃	x	x

Table 1. Coating candidates for α_2 and γ substrates for the program.

Coating Class	Composition	Process Variation	Substrate	
			Gamma	Alpha-2
TiCrAl	Ti-44Al-28Cr	Sputtered	X	X
	Ti-44Al-28Cr	HVOF	X	
	Ti-44Al-28Cr	LPPS	X	X
	Ti-55Al-9Cr	Sputtered	X	X
TBC	ZrO ₂ - 8 wt.%Y ₂ O ₃	APS	X	
composite	Al ₂ O ₃ +Ni-24Cr- 12Al-0.2Y	LPPS	X	
	Al ₂ O ₃ +René 80	LPPS	X	X
MCr	Co-32Cr-4.5C-2Si- 1W	HVOF	X	
Superalloy	Alloy 718	APS		X
	Alloy 718	Sputtered	X	

Table 2. The Table indicates the class, composition and coating process for the coatings applied to the substrates for the first round of environmental testing in Task 2.

1st Iteration

Evaluate Coatings Sub-Task 2.5	Cyclic Oxidation Sub-Task 2.2	HSSCC Sub-Task 2.3	CHC/O Sub-Task 2.4	Iteration Sub-Task 2.6
Optical & SEM Hardness XRD Hardness Auger? AEM?	For Gamma 900°C 1Hr Cycles	Salt/400°C/ σ exposure + Tensile Test	Turbine: 760/900°C 2ppm Sea Salt	Modification of Coating/Process
	For Alpha-2 760°C 1Hr Cycles	Salt/565°C/ σ exposure + Tensile Test	Compressor: 648/760°C 0.25ppm Sea Salt	Tests: Cyclic Oxidation HSSCC CHC/O
		Salt/565°C/ σ long exposure + Tensile Test		
Min. # Coatings	4 Coatings	3 Coatings	3 Coatings	1 Coating

2nd Iteration

	Hot Salt Stress Corrosion Cracking	Cyclic Oxidation/Hot Corrosion	High Velocity Oxidation
Test Conditions	Hi Temp/Long Time Exposure at 565°C for 750h with 0.1-0.2 mg/cm ² sea salt + RT Tensile Test	<u>Turbine</u> 900°C(5min) + 760°C(5min) + 1-2 ppm sea salt in Burnt Jet A @ 0.8Mach for 3000cycles (500h hot)	<u>Turbine</u> 900°C(5min) + 760°C(5min) in Burnt Jet A @ 0.8Mach for 3000cycles (500h hot)
		<u>Compressor</u> 760°C(5min) + 648°C(5min) + 1ppm sea salt in Burnt Jet A @ 0.8Mach for 3000cycles (500h hot)	
M ³ Coating Systems	Gamma : 3 Alpha-2 : 3	Gamma : 3 Alpha-2 : 3	Gamma : 3 Alpha-2 : 3

Table 3. The test plan for Task 2. HSSCC stands for hot salt stress corrosion cracking and CHC/O refers to cyclic hot corrosion - oxidation burner rig testing.

Coating	Rank	$\Delta Wt/A$ 760°C, mg/cm ²	Rank	$\Delta Wt./A$ 900°C, mg/cm ²	Δ Rank
Sputtered Ti-55Al-8.5Cr	3	0.602	3	2.319	0
Sputtered Ti-44Al-28Cr	5	0.635	2	2.167	3
None	9	1.133	7	3.324	2
M ³ NiCrAlY/Al ₂ O ₃	8	0.906	1	2.093	7
LPPS Ti-44Al-28Cr	6	0.715	9	7.032	3
HVOF Ti-44Al-28Cr	2	0.460	8	3.559	6
CoCr(W,Si,C)	7	0.883	4	2.391	3
Sputtered Alloy 718	4	0.611	6	2.775	2
APS YSZ	1	0.367	5	2.509	4

Table 4. Summary of the normalized weight change/area for the coated gamma alloy substrates after 500Hr. of cyclic oxidation at 760°C (1400°F) and 900°C (1650°F) in air. The rank represents the magnitude of the data with 1 being the lowest and presumably the best since visually little spalling was noted. Delta (Δ) rank is a relative measure of change in coating behavior between test temperatures.

Coating	Rank	$\Delta Wt/A$ 760°C, mg/cm ²	Rank	$\Delta Wt./A$ 900°C, mg/cm ²	Δ Rank
Sputtered Ti-55Al-8.5Cr	1	0.550	2	2.679	1
Sputtered Ti-44Al-28Cr	2	0.570	1	2.442	1
None	3	0.727	5	4.001	2
M ³ René 80/Al ₂ O ₃	6	1.369	3	2.687	3
LPPS Ti-44Al-28Cr	4	0.820	6	8.272	2
APS 718	5	1.039	4	4.141	1

Table 5. Summary of the maximum weight change/area for the coated alpha-2 alloy substrates after 500Hr. of cyclic oxidation at 760°C (1400°F) and 900°C (1650°F) in air. The rank represents the magnitude of the data with 1 being the lowest and presumably the best since little spallation was noted. Delta (Δ) rank is a relative measure of change in coating behavior between test temperatures.

Coating/Process	Coating Phases	Substrate Phases
Ti-44Al-28Cr/Sputtered	Amorphous : $d \approx 2.18$	L10 : $a_0=3.998$ $c_0=4.063$ DO ₁₉ ?
Ti-55Al-8.5Cr/Sputtered	FCC : $a_0=3.984$	L10 : $a_0=3.993$ $c_0=4.064$ DO ₁₉ ?
Ti-44Al-28Cr/LPPS	MgZn ₂ : $a_0=5.059$ $c_0=8.265$ FCC : $a_0=3.965$ cubic : $a_0=4.20$	L10 : $a_0=3.999$ $c_0=4.065$ DO ₁₉ ?
Ti-44Al-28Cr/HVOF	BCC : $a_0=3.095$ BCC : $a_0=2.890$	Not Examined
Alloy 718/Sputtered	FCC : $a_0=3.590$	L10 : $a_0=3.996$ $c_0=4.066$ DO ₁₉ ?

Table 6. X-ray diffraction results for some as-processed coatings on the Ti-48Al-2Cr-2Nb gamma alloy substrate. Lattice parameters are given in angstroms.

Coating/Process	Oxide Phases 1650°F/500Hr
Uncoated Gamma	Major - Tetragonal - TiO_2 (ss) Minor - Rhombohedral - Al_2O_3 Minor - L10 - Gamma : $a_0 = 3.981$ $c_0 = 4.060$
Ti-44Al-28Cr/Sputtered	Major - L10 - Gamma Minor - Rhombohedral - Al_2O_3 (ss) Unidentified Phase
Ti-55Al-8.5Cr/Sputtered	Major - MgZn_2 : $a_0 = 5.063$ $c_0 = 8.271$ Rhombohedral - Al_2O_3 (ss) : $a_0 = 4.767$ $c_0 = 13.013$ Unidentified Phase
Ti-44Al-28Cr/LPPS	Major - Tetragonal - TiO_2 : $a_0 = 4.604$ $c_0 = 2.962$ Minor - Rhombohedral - Al_2O_3 (ss)
Ti-44Al-28Cr/HVOF	Major - Tetragonal - TiO_2 Minor - Rhombohedral - Al_2O_3 (ss)
M ³ /NiCrAlY Type	Major - FCC : $a_0 = 3.550$ Major - Cubic - NiO : $a_0 = 4.183$ Major - Cubic - Spinel (ss) : $a_0 = \sim 8.150$ Minor - Al_2O_3 (ss) Unidentified
M ³ /René 80 Type	Major - Cubic - NiO $a_0 = 4.189$ Major - Cubic - Spinel : $a_0 = \sim 8.150$ Major - FCC $a_0 = 3.550$ Minor - Al_2O_3 (ss) Unidentified

Table 7. X-ray diffraction results for coated Ti-48Al-2Cr-2Nb alloys after cyclic oxidation testing in air at 900°C (1652°F) for 500Hr. Identification was made in conjunction with microprobe and metallographic results. Lattice parameters are in angstroms.

Coating/Process	Coating Phases	Substrate Phases
Ti-44Al-28Cr/Sputtered	Amorphous : $d \approx 2.23$	Orthorhombic : $a_0=5.941$ $b_0=9.828$ $c_0=4.676$ BCC : $a_0=3.252$
Ti-55Al-8.5Cr/Sputtered	FCC : $a_0=3.984$	Orthorhombic : $a_0=5.921$ $b_0=9.810$ $c_0=4.663$
Ti-44Al-28Cr/LPPS	MgZn ₂ : $a_0=5.059$ $c_0=8.265$ FCC : $a_0=3.97$ Cubic : $a_0=4.20$	DO ₁₉ : $a_0=5.80$ $c_0=4.685$ BCC : $a_0=3.250$
Alloy 718/APS	FCC : $a_0=3.590$ FCC : $a_0=3.531$ Spinel (Cr,Fe) ₃ O ₄ : $a_0=8.150$ Amorphous : $d \approx 4.31$	Orthorhombic : $a_0=5.923$ $b_0=9.813$ $c_0=4.665$ BCC : $a_0=3.250$

Table 8. X-ray diffraction data from as-coated alpha-2 samples. Lattice parameters are given where appropriate in angstroms.

Coating/Process	Oxide Phases 1650°F/500Hr
Uncoated Alpha-2	Major - Tetragonal - TiO ₂ (ss) Minor - Rhombohedral - Al ₂ O ₃
Ti-44Al-28Cr/Sputtered	MgZn ₂ - TiCrAl Rhombohedral - Al ₂ O ₃ Tetragonal - TiO ₂
Ti-55Al-8.5Cr/Sputtered	Major - Tetragonal - TiO ₂ (ss) Minor - Rhombohedral - Al ₂ O ₃

Table 9. X-ray diffraction results for various coated alpha-2 samples after cyclic oxidation for 500Hr. in air at 900°C(1650°F). The phases were identified in combination with metallography and energy dispersive analysis.

Reaction Layer Phase	Composition, atom percent
16	Ti-34Ni-14Al-9.5Fe-1Nb-0.7Cr-0.4Mo-0.3Co
17	Ti-17Ni-16Al-11Nb-4.4Fe-1.3Mo-0.3Cr-0.1Co
18	Ti-24.2Al-14.7Nb-1.9Ni-1.8Mo-0.5Fe
19	Ti-23.7Al-10.8Nb-1.32Mo-1.1Ni-0.2Fe

Table 10. Composition of reaction layer phases after an exposure of 1000Hr in air at 760°C (1400°F).

<u>Coating System</u>	<u>DWeight Salt,</u> <u>mg</u>	<u>Rinsed DW/A,</u> <u>mg/cm²</u>
Uncoated g	-1.2	0.2
LPPS cermet/g	-2.3	-8.0
Sputtered Ti-44Al-28Cr/g	-1.6	0.2
APS YSZ/g	-3.9	-12.9
Uncoated a2	-1.3	0.2
APS Alloy 718/a2	-6	-9.5
LPPS Modified g/a2	-3	0.4
Sputtered Ti-44Al-28Cr/a2	-1.2	0.1
Alloy 718	-1.5	-0.1

Table 11. Table showing the weight change of samples during a rinsing procedure that removed salt and debris after the high pressure compressor test. The last column indicated rinsed weight change/area data.

Coating System	DW Salt, mg	DW/A after Rinsing, mg/cm ²	Dia. Change, μ m
Uncoated Gamma	-102	0.02	0
Sputtered Ti-44Al-28Cr/g	-102	-3.5	-38
LPPS cermet/g	-141	-8.4	13
APS YSZ/g	-167	-14.2	-25
Uncoated Alpha-2	-75	-0.76	13
Sputtered Ti-44Al-28Cr/a2	-104	0.47	13
APS Alloy 718/a2	-152	-23.8	-267
LPPS Mod g /a2	-157	1.34	13
René 77	-108	-26.8	-368
René 80	-96	-22.4	-292

Table 12. Weight change data for candidate coating systems after the 498 cycle low pressure turbine test and rinsing. Large negative weight changes indicate systems that had coating spallation. The chart also indicates the amount of water soluble debris (salt) that was rinsed off the surface and the change in diameter of the sample during the test.

Coating	Test	Sea Salt Deposit	Creep Exposure		RT Tensile	
			% Deformed	Time, hours	UTS, ksi	% elongation
None	Baseline	None	NA	NA	67.6	2.5
			750°F/50ksi			
None	Interstitial Embrittlement	None	0.100	100	59.4	0.4
None	HSSCC	0.1mg/cm ²	0.074	100	57.2	0.5
TiCrAl	HSSCC	0.1mg/cm ²	0.114	100	56.9	0.9
APS YSZ	HSSCC	0.1mg/cm ²	0.095	100	59.8	0.7
cermet	HSSCC	0.1mg/cm ²	0.083	100	40.0	0.3
			1050°F/40ksi			
None	Interstitial Embrittlement	None	0.091	100	54.5	0.7
None	HSSCC	0.1mg/cm ²	0.167	100	52.9	0.3
TiCrAl	HSSCC	0.1mg/cm ²	0.148	100	44.5	0.3
APS YSZ	HSSCC	0.1mg/cm ²	0.176	100	54.0	0.6
cermet	HSSCC	0.1mg/cm ²	0.067	100	61.6	1.1
None	Interstitial Embrittlement	None	0.157	750	58.8	0.8
None	HSSCC	0.1mg/cm ²	0.186	750	0	0
TiCrAl	HSSCC	0.1mg/cm ²	0.170	750	55.8	1.3
APS YSZ	HSSCC	0.1mg/cm ²	0.208	750	55.4	2.3
cermet	HSSCC	0.1mg/cm ²	0.140	750	58.8	0.8

Table 13. Results of HSSCC testing for coated and uncoated gamma substrates as part of Task 2.4. Based on the data here, salt totally embrittled the bare gamma alloy after a 1050°F/40ksi/750h exposure.

Coating	Test	Sea Salt Deposit	Creep Exposure		RT Tensile	
			% Deformed	Time, hours	UTS, ksi	% elongation
None	Baseline	None	NA	NA	173.6	3.2
			750°F/50ksi			
None	Interstitial Embrittlement	None	0.012	100	165.3	0.9
None	HSSCC	0.1mg/cm ²	0.059	100	60.6	0.6
TiCrAl	HSSCC	0.1mg/cm ²	0.017	100	165	0.8
Mod g	HSSCC	0.1mg/cm ²	0.077	43.2	NA	NA
Alloy 718	HSSCC	0.1mg/cm ²	0.037	100	158.7	2.2
			1050°F/40ksi			
None	Interstitial Embrittlement	None	0.248	100	143.8	0.7
None	HSSCC	0.1mg/cm ²	0.2	39.1	NA	NA
TiCrAl	HSSCC	0.1mg/cm ²	0.163	22.5	NA	NA
Mod g	HSSCC	0.1mg/cm ²	0.477	100	31.5	0.2
Alloy 718	HSSCC	0.1mg/cm ²	0.186	100	148.5	0.6
None	Interstitial Embrittlement	None	0.707	750	132.5	2.3
None	HSSCC	0.1mg/cm ²	0.191	28.5	NA	NA
TiCrAl	HSSCC	0.1mg/cm ²	0.109	12.5	NA	NA
Mod g	HSSCC	0.1mg/cm ²	0.022	1.1	NA	NA
Alloy 718	HSSCC	0.1mg/cm ²	0.896	750	93.8	1.0

Table 14. Results of HSSCC testing for coated and uncoated alpha-2 substrates as part of Sub-Task 2.4. The alpha-2 was severely embrittled in the presence of sea salt. The only sample to survive both 1050°F creep exposures with salt was coated with air plasma sprayed Alloy 718. "NA" means non-applicable because of failure during creep exposure.

<u>Exposure Conditions</u>	<u>Secondary Crack Depth,</u> μm	<u>Distribution</u>
None	1	very few
750°F/50ksi/100h	2	evenly spaced (7 μm)
1050°F/40ksi/100h	4-5	evenly spaced (25 μm)
1050°F/40ksi/750h	22	evenly spaced (42 μm)

Table 15. Depth and distribution of cracks in exposed (without salt) and unexposed bare alpha-2. The secondary cracking was an indication of interstitial embrittlement at the surface

% Deformation	Time, Hours	
	Uncoated Alpha-2 (no salt)	Coated ⁶ /Alloy 718 (salt)
0.1	16,18	15,9
0.2	50,62	65,~129
0.5	375	430
0.75	~825	~913

Table 16. Time to 0.1, 0.2, 0.5 and 0.75% creep for the alpha-2 exposed at 1050°F/40ksi. Approximate values listed were linearly extrapolated from data at shorter times. A transient loading strain of 0.224% was subtracted from one of the Alloy 718 data sets.

System of Interest	Avg. Linear Expansion Coefficient, $\times 10^{-6}/^{\circ}\text{F}$	% Mismatch Relative to NiCrAlY
Al_2O_3	4.5	-43
Ti-22Al-27Nb (ortho)	5.3	-32.9
Ti-24.5Al-12.5Nb-1.5Mo (A2)	5.9	-25.3
Ti-48Al-2Cr-2Nb (gamma)	6.9	-12.7
Alloy 718	8.3	5
NiCrAlY	7.9	0

Table 17. Average linear expansion coefficients are shown for Ti-aluminides over the temperature range of expected application. Mismatch between MCrAlY and Ti-aluminides is a strong function of refractory metal content.

	Gamma	Alpha-2
<i>Alloy 718</i> Ni-18.5Cr-18.5Fe-5Nb-3Mo-0.9Ti- 0.5Al-0.04C (Ni-20.7Cr-19.3Fe-3.2Nb-1.8Mo- 1Ti-1Al-0.2C)	80% Alloy 718 + 20% Alumina	45% Alloy 718 + 55% Alumina
<i>Ni-Cr-Al-Y</i> Ni-20Cr-10Al-0.3Y (Ni-19.7Cr-19Al-0.2Y)	50% NiCrAlY + 50% Alumina (in First Iteration)	60% NiCrAlY + 40% Alumina
<i>Co-Cr-Al-Y</i> Co-17.4Cr-8.3Al-0.5Y (Co-17.6Cr-16Al-0.3Y)	85% CoCrAlY + 15% Alumina	45% CoCrAlY + 55% Alumina
<i>Ni-Co-Cr-Al-Y</i> Ni-22Co-17.2Cr-12.5Al-0.6Y (Ni-18.6Co-17Cr-23Al-0.3Y)	85% NiCoCrAlY + 15% Alumina	*

Table 18. The compositions of composite coatings applied to the Ti-aluminide substrates. The composite compositions are listed in terms of volume percent of constituent. The MCrAlY compositions are listed in weight and atomic percent (parentheses). A NiCrAlY-based composite coating had previously been determined to be protective on gamma substrates in the first iteration of environmental testing.

	Hot Salt Stress Corrosion Cracking	Cyclic Oxidation/ Hot Corrosion	High Velocity Oxidation
Test Conditions	<u>Hi Temp/Long Time</u> Exposure at 565°C/40ksi for 750h with 0.1-0.2 mg/cm ² sea salt + RT Tensile Test	<u>Turbine</u> 871°C(5min) + 760°C(5min) + 2 ppm sea salt (1 st 50Hr.) then 1ppm in comb. Jet A @ 0.8Mach for 3000cycles (500h hot)	<u>Turbine</u> 900°C(5min) + 760°C(5min) in comb. Jet A @ 0.8Mach for 1778cycles; then 900°C(5min) only for 2639 cycles (516h hot)
		<u>Compressor</u> 760°C(5min) + 648°C(5min) + 1ppm sea salt in comb. Jet A @ 0.8Mach for 3749cycles (625h hot)	
Composite MCrAlY Coatings	Gamma : 3 Alpha-2 : 3	Gamma : 3 Alpha-2 : 3	Gamma : 3 Alpha-2 : 3

Table 19. Table shows the tests used for the second iteration of environmental testing under Sub-Task 2.6.

Coating	Test	Substrate	Creep Exposure		RT Tensile	
			% Deformed	Time, hours	UTS, ksi	% elongation
None	RT Tensile	Alpha-2	NA	NA	173.6	3.2
None	RT Tensile	Gamma	NA	NA	67.6	2.5
			1050°F/40ksi		Strain Rate = 0.005/min	
cermet-Alloy 718	HSSCC	Alpha-2	NA	0.1	NA	NA
cermet-CoCrAlY	HSSCC	Alpha-2	0.224	63.6	NA	NA
cermet-NiCrAlY	HSSCC	Alpha-2	0.567	750	147.9	1.1
cermet-Alloy 718	HSSCC	Gamma	0.189	750	38.6	0.4
cermet-CoCrAlY	HSSCC	Gamma	0.289	750	48.7	0.6
cermet-NiCoCrAlY	HSSCC	Gamma	0.234	750	60.4	0.5

Table 20. Results of a 1050°F/40ksi HSSCC exposure followed by a RT tensile test of cermet coatings on Ti-aluminide substrates. All of the gamma samples failed in the radius away from the salt coating.

<u>Pin</u>	<u>Avg. Deposit Removed±s,</u> <u>mg/cycle</u>
Bare Gamma	0.210±0.67
Bare Alpha-2	0.212±0.61
Bare Preoxidized Hast X	0.243±0.07
NiCrAlY/Al ₂ O ₃ Alpha-2	0.291±0.09
CoCrAlY/Al ₂ O ₃ Alpha-2	0.315±0.10
NiCoCrAlY/Al ₂ O ₃ Gamma	0.318±0.10
CoCrAlY/Al ₂ O ₃ Gamma	0.348±0.12
Alloy 718/Al ₂ O ₃ Alpha-2	0.382±0.11
Alloy 718/Al ₂ O ₃ Gamma	0.389±0.13

Table 21. The average amount of deposit removed during each rinsing is displayed with the standard deviation.

Peak Temperature, °C	External Scale, μm	Substrate Attack, μm	Interstitial Layer, μm	Total Attack, μm
760	2	3.3	0.7	6
704	0.3	1.0	0.5	1.8
648	1.7	0	0	1.7
398	0	0	0	0

Table 22. Summary of the attack observed on the uncoated Ti-24.5Al-12.5Nb-1.5Mo Alpha-2 alloy after 520Hr of testing.

<u>Pin</u>	<u>Avg. Deposit Removed\pms,</u> <u>mg/cycle</u>
Bare Preoxidized Hast X	0.175 \pm 0.09
Codep Rene 80	0.223 \pm 0.11
Bare Gamma	0.224 \pm 0.11
Bare Alpha-2	0.231 \pm 0.10
CoCrAlY/Al ₂ O ₃ Alpha-2	0.251 \pm 0.11
NiCrAlY/Al ₂ O ₃ Alpha-2	0.252 \pm 0.11
NiCoCrAlY/Al ₂ O ₃ Gamma	0.283 \pm 0.13
CoCrAlY/Al ₂ O ₃ Gamma	0.325 \pm 0.15
Alloy 718/Al ₂ O ₃ Alpha-2	0.337 \pm 0.13
Alloy 718/Al ₂ O ₃ Gamma	0.404 \pm 0.16

Table 23. The average amount of deposit removed during rinsing is displayed with the standard deviation. The deposit taken after 50Hr was ~2-4X the values listed because of the extra salt and was ignored in the calculations.

Tensile						Fatigue						HSSCC				
Exp	DB	Ctg	RT	ET		Exp.	DB	Ctg	RT	ET		Exp	DB	Ctg	Salt	ET
N	N	N	1			N	N	Y	1			N	N	N		1
N	N	N		1		N	N	Y		1		N	N	N	Y	1
N	N	N		1		N	N	Y		1		N	N	Y		1
N	N	N		1		N	Y	Y	1			N	N	Y	Y	1
Y	N	N	1			N	Y	Y		1		Y	N	N		1
Y	N	N		1		N	Y	Y		1		Y	N	N	Y	1
Y	N	N		1		Y	N	Y	1			Y	N	Y		1
Y	N	N		1		Y	N	Y		1		Y	N	Y	Y	1
N	N	Y	1			Y	N	Y		1		N	Y	Y		1
N	N	Y		1		Y	Y	Y	1			N	Y	Y	Y	1
Y	N	Y	1			Y	Y	Y		1		Y	Y	Y		1
Y	N	Y		1		Y	Y	Y		1		Y	Y	Y	Y	1
N	Y	Y	1			N	N	N	1					total		12
N	Y	Y		1		N	N	N	1							
N	Y	Y		1		N	N	N		1						
N	Y	Y		1		N	N	N		1						
Y	Y	Y	1			N	N	N		1						
Y	Y	Y		1		N	N	N		1						
Y	Y	Y		1		Y	N	N	1							
Y	Y	Y		1		Y	N	N	1							
		total	6	14		Y	N	N		1						
						Y	N	N		1						
						Y	N	N		1						
						Y	N	N		1						
						total			8	16						

Table 24. The test plan for Task 3. Tensile, fatigue and HSSCC tests will be performed to determine the effect of coating (CTG), exposure (EXP), salt and diffusion barrier (DB) at room (RT) and elevated temperature (ET).

Alloy	Specimen Type	Cermet	W Diff. Barrier	Color	Cracking	Spalling	del Wt 50cyc
Gamma	Creep	N	N	B (tint)	N	N	13.4
Gamma	Creep	N	N	B (tint)	N	N	15.5
Gamma	Creep	Y	N	Gray	N	N	-194.4
Gamma	Creep	Y	N	Y (tint)	N	N	-265.2
Gamma	Creep	Y	Y	YW (THDS)	N	N	-141
Gamma	Creep	Y	Y	Y (tint)	N	N	-149.8
Gamma	Fatigue	N	N	Gray	N	N	11.8
Gamma	Fatigue	N	N	Gray	N	N	12.8
Gamma	Fatigue	N	N	Gray	N	N	12
Gamma	Fatigue	N	N	Gray	N	N	14.7
Gamma	Fatigue	N	N	Gray	N	N	7.5
Gamma	Fatigue	Y	N	Y (tint)	N	N	-299.5
Gamma	Fatigue	Y	N	Y (tint)	N	N	-323.7
Gamma	Fatigue	Y	N	Y (tint)	N	N	-283.3
Gamma	Fatigue	Y	Y	Y (tint)	N	N	-240.6
Gamma	Fatigue	Y	Y	Y (tint)	N	N	-193.5
Gamma	Fatigue	Y	Y	Y (tint)	N	N	13.4
Gamma	Tensile	N	N	B (tint)	N	N	0.7
Gamma	Tensile	N	N	B tint YW (thds)	N	N	1.4
Gamma	Tensile	N	N	B (tint)	N	N	0.4
Gamma	Tensile	N	N	B (tint)	N	N	0.8
Gamma	Tensile	Y	N	Gray	N	N	-43.4
Gamma	Tensile	Y	N	YW (THDS)	N	N	-21.5
Gamma	Tensile	Y	Y	YW	N	N	-11.1
Gamma	Tensile	Y	Y	YW	N	N	-31.7
Gamma	Tensile	Y	Y	YW	N	N	-47.5
Gamma	Tensile	Y	Y	YW	N	N	-18.6
Alpha2	Creep	N	N	YW	N	N	31.9
Alpha2	Creep	N	N	YW	N	N	34.2
Alpha2	Creep	Y	N	B (tint)	N	N	-287.2
Alpha2	Creep	Y	N	YW	N	N	-233.6
Alpha2	Creep	Y	Y	YW (THDS)	N	N	-105.1
Alpha2	Creep	Y	Y	YW (THDS)	N	N	-64.8
Alpha2	Fatigue	N	N	B (tint)	N	N	7.4
Alpha2	Fatigue	N	N	B (tint)	N	N	5
Alpha2	Fatigue	N	N	B (tint)	N	N	3.6
Alpha2	Fatigue	N	N	B (tint)	N	N	5.7
Alpha2	Fatigue	N	N	B (tint)	N	N	5.6
Alpha2	Fatigue	N	Y	Y (tint)	N	N	-301.8
Alpha2	Fatigue	N	Y	Y (tint)	N	N	-291.5
Alpha2	Fatigue	N	Y	Y (tint)	N	N	-675.6
Alpha2	Fatigue	Y	Y	Y (tint)	N	N	-129.9
Alpha2	Fatigue	Y	Y	Y (tint)	N	N	-150
Alpha2	Fatigue	Y	Y	Y (tint)	N	N	-306.3
Alpha-2	Tensile	N	N	YW	N	Y	12.8
Alpha-2	Tensile	N	N	YW	N	Y	12.8
Alpha-2	Tensile	N	N	YW	N	Y	15.2
Alpha-2	Tensile	N	N	YW	N	Y	16.7

Table 25. Table summarizing color, spalling and W/A observations for mechanical specimens that were cyclically exposed at 760°C in air for 100 1-hour cycles. Nomenclature: N=No; Y=Yes; B=blue; Y=yellow; and YW=yellowish white.

ID	Stock	Exp	DB	Cermet	Temp, C	Temp, F	Loc	UTS, ksi	YS, ksi	%e
19-14-1	Gam	N	N	N	22.22	72	gage	76.3	62.7	2.1
19-14-2	Gam	N	N	N	204.4	400	thread	•	•	•
19-14-3	Gam	N	N	N	482.2	900	gage	77.9	55.9	3.4
19-14-4	Gam	N	N	N	704.4	1300	gage	78.6	52.4	5.7
19-14-5	Gam	Y	N	N	22.22	72	thread	•	•	•
19-14-6	Gam	Y	N	N	204.4	400	gage	54.7	54.2	1.7
19-14-7	Gam	Y	N	N	482.2	900	gage	77	55.8	3.9
19-14-8	Gam	Y	N	N	704.4	1300	gage	59.2	51.8	2.3
19-14-9	Gam	N	N	Y	22.22	72	thread	•	•	•
19-14-10	Gam	N	N	Y	704.4	1300	gage	55.2	•	•
19-14-11	Gam	Y	N	Y	22.22	72	thread	•	•	•
19-14-12	Gam	Y	N	Y	704.4	1300	gage	53.3	53.3	0.5
19-14-13	Gam	N	Y	Y	22.22	72	thread	•	•	•
19-14-14	Gam	N	Y	Y	204.4	400	thread	•	•	•
19-14-15	Gam	N	Y	Y	482.2	900	gage	67.2	59.3	1.5
19-14-16	Gam	N	Y	Y	704.4	1300	thread	•	•	•
19-14-17	Gam	Y	Y	Y	22.22	72	thread	•	•	•
19-14-18	Gam	Y	Y	Y	204.4	400	gage	64.3	55.2	2.7
19-14-19	Gam	Y	Y	Y	482.2	900	gage	72.5	60.4	2.9
19-14-20	Gam	Y	Y	Y	704.4	1300	gage	77.1	50.9	•
45-1	A2	N	N	N	22.22	72	gage	114.6	99	8
45-2	A2	N	N	N	204.4	400	gage	119.8	91.6	21.9
45-3	A2	N	N	N	482.2	900	gage	130.7	82.7	23.1
45-4	A2	N	N	N	704.4	1300	gage	97.4	73.5	14.8
45-5	A2	Y	N	N	22.22	72	gage	121.6	97	5.8
45-6	A2	Y	N	N	204.4	400	gage	105.9	84.3	9.1
45-7	A2	Y	N	N	482.2	900	gage	116.8	76.7	12.2
45-8	A2	Y	N	N	704.4	1300	gage	88.1	74.2	8.2
45-9	A2	N	N	Y	22.22	72	gage	130	112.2	2.8
45-10	A2	N	N	Y	704.4	1300	gage	108.9	90	11.9
45-11	A2	Y	N	Y	22.22	72	gage	119.8	97.1	2.9
45-12	A2	Y	N	Y	704.4	1300	gage	88.4	78.5	•
45-13	A2	N	Y	Y	22.22	72	gage	127.3	127	1
45-14	A2	N	Y	Y	204.4	400	gage	131.8	99	5
45-15	A2	N	Y	Y	482.2	900	gage	137.3	100.3	16.6
45-16	A2	N	Y	Y	704.4	1300	gage	108.5	83.8	9
45-17	A2	Y	Y	Y	22.22	72	gage	118.5	96.3	2.9
45-18	A2	Y	Y	Y	204.4	400	gage	127.5	90.7	5.3
45-19	A2	Y	Y	Y	482.2	900	gage	120.3	84.5	10.7
45-20	A2	Y	Y	Y	704.4	1300	gage	87.1	74	6

Table 26. Tensile Results for Coated and Uncoated Gamma and Alpha-2 Under Task 3.

Sample	Alloy	Exp.	Diff	Ctg	Salt	Stress	Def'n	Exp time	UTS	%e	Thread
			Bar.			ksi	%	Hr	ksi		Failure
	G	N	N	N	N	N		0	76.3	2.1	N
19-5-1	G	N	N	N		20	20.12	500	60.09	1.2	N
19-5-2	G	N	N	N	Y	20	20.41	500	54.01	0.72	N
19-5-3	G	N	N	Y		20	10.99	500	52.55	0.48	N
19-5-4	G	N	N	Y	Y	20	10.2	500	50.66	0.83	N
19-3-5	G	N	Y	Y		20	18.81	500	46.97	1.2	N
19-3-6	G	N	Y	Y	Y	20	20	500	59.06	1.47	N
19-5-5	G	Y	N	N		20	48.49	499.6			N
19-5-6	G	Y	N	N	Y	20	30.81	500	61.95		N
19-5-7	G	Y	N	Y		20	9.788	500	49.16		N
19-3-4	G	Y	N	Y	Y	20	11.41	500	6.547		N
19-3-7	G	Y	Y	Y		20	22.13	500	57.66		N
19-6-4	G	Y	Y	Y	Y	20	40.95	418.7			N
	A2	N	N	N	N	N		0	114.6	8	N
1-1-4	A2	N	N	N		10	2.887	500	116.1	1.76	N
1-1-5	A2	N	N	N	Y	10	3.645	500	97.68	1.76	N
2-1-1	A2	N	N	Y		20/10	4.85	500	98.97		Y
2-1-2	A2	N	N	Y	Y	10	2.06	500	77.15		Y
2-0-13	A2	N	Y	Y		20/10	9.16	500	104.1	1.6	Y
2-0-14	A2	N	Y	Y	Y	10	4.134	500	114.7	1.96	Y
2-1-3	A2	Y	N	N		20	25	187.1			N
2-1-4	A2	Y	N	N	Y	20	29.76	175.8			N
2-1-5	A2	Y	N	Y		20	30.34	244.3			N
2-0-12	A2	Y	N	Y	Y	20	26.65	220.4			N
2-0-15	A2	Y	Y	Y		20	30.6	131			N
2-0-16	A2	Y	Y	Y	Y	20	24.3	131.1			N

Table 27. Summary of Task 3 HSSCC Test Results.

Sample	Alloy	GB	Exp	Cermet	DB	Temp	%ε	MAX stress	Cyc	Eo	Fail Loc'n
19-12-1	Gamma	N	N	N	N	72	0.4	62.96	200000	24.7	ro
19-12-2	Gamma	Y	N	N	N	72	0.4	59.59	200000	21.7	ro
19-12-3	Gamma	N	N	N	N	1200	0.4	50.86	237611	18.4	ro
19-12-4	Gamma	N	N	N	N	1200	0.5	53.09	200000	20	ro
19-12-5	Gamma	N	N	N	N	1400	0.4	49.36	282641	19	ro
19-12-6	Gamma	N	N	N	N	1400	0.3	45.94	207583	19.1	ro
19-13-1	Gamma	Y	N	N	N	1400	0.4		200000		ro
19-8-1	Gamma	N	N	Y	N	72	0.3	59.3	1		rad
19-8-4	Gamma	N	N	Y	Y	72	0.3	61.8	2		goext
19-8-2	Gamma	N	N	Y	N	1400	0.25	41.5	248746	23.1	ro
19-8-3	Gamma	N	N	Y	N	1400	0.4	52.1	345	20.3	giext
19-8-6	Gamma	N	N	Y	Y	1400	0.3	45.7	5168	26.7	ctg
19-13-3	Gamma	N	Y	N	N	72	0.25	50.9	1		thr
19-13-5	Gamma	N	Y	N	N	72	0.25	55.38	200000	25.1	ro
19-13-4	Gamma	N	Y	N	N	1200	0.4	49.92	1549	21.1	giext
19-13-6	Gamma	N	Y	N	N	1200	0.25	41.31	200000	20.8	disc
19-13-2	Gamma	N	Y	N	N	1400	0.4	49.166	200005	21.2	ro
19-7-2	Gamma	N	Y	Y	N	1200	0.4	49.5	1		
19-7-3	Gamma	N	Y	Y	N	1200	0.25	44.7	43825	22.3	thr
19-7-1	Gamma	N	Y	Y	N	1400	0.4		3		int
1	Alpha-2	N	N	N	N	72	0.9	131.8	13458	16.6	giext
2	Alpha-2	N	N	N	N	72	0.8	128.2	200000	16.9	ro
4	Alpha-2	Y	N	N	N	72	0.8	120.6	200000	15.7	ro
3	Alpha-2	N	N	N	N	800	0.8	108	165173	14.2	thr
5	Alpha-2	N	N	N	N	1200	1	107	10138	14	goext
6	Alpha-2	N	N	N	N	1200	0.8	97.79	200000	13.8	ro
7	Alpha-2	Y	N	N	N	1200	0.8		200000		ro
A3-1	Alpha-2	N	N	Y	N	72	0.8	124.3	378	15.5	giext
A3-4	Alpha-2	N	N	Y	Y	72	0.8	123.4	523	16	giext
A3-2	Alpha-2	N	N	Y	N	800	0.8	106.1	3308	14.6	goext
A3-3	Alpha-2	N	N	Y	N	1200	0.8	97.44	1610	14.4	goext
8	Alpha-2	N	Y	N	N	72	0.8	114.8	323	15.9	giext
9	Alpha-2	N	Y	N	N	800	0.8	103.9	4198	15	goext
12	Alpha-2	N	Y	N	N	800	0.6	80.57	4953	14.8	giext
10	Alpha-2	N	Y	N	N	1200	0.8	91.91	3608	14.6	giext
11	Alpha-2	N	Y	N	N	1200	0.6	74.94	1187	14.4	goext
A3-7	Alpha-2	N	Y	Y	N	72	0.8	113.4	172	14.8	ctg
A3-9	Alpha-2	N	Y	Y	N	800	0.6	81.93	3565	15.3	goext
A3-8	Alpha-2	N	Y	Y	N	1200	0.8	86.7	530	13.3	giext

Table 28. Task 3 Fatigue Results. Failure location terminology: ro = runout; rad=radius failure; goext= gage outside of extensometer; giext= gage inside of extensometer; thr = thread failure; and ctg=coating spall.

Region	C	Ca	Ti	O	Al	Cl
Blue 0Å	42.7	1.7	6.2	33.2	16.2	*
Blue 100Å	23.5	1.2	9.2	45	21.1	*
Brown 0Å	36.8	2	7	36.9	17.1	0.2
Brown 100Å	21.1	2	9.6	47.1	19.6	*

Table 29. Auger Spectroscopy Results on Tinted Oxides.

ID	Alloy	Coating	Max/Min Strain	Max/Min Stress @ N2, ksi	Nf, cycles	Failure Location
19-9-1	Gamma	None	0.0005/ -0.0005	58.1/ -43.5	108	Inside Extens.
19-9-2	Gamma	None	0.003/ -0.003	49.3/ -52.5	3	Inside Extens.
19-9-3	Gamma	Cermet	0.002/ -0.002	On Loading	0.25	Inside Extens.
19-9-4	Gamma	Cermet	0/0	42.84/ -2.22	0.5	Inside Extens.
19-9-5	Gamma	Cermet	0/0	48.67/ -49.27	1	Outside Extens.
4-0-1	Alpha-2	None	0.002/ -0.002	101.6/ -35.6	1508	Outside Extens.
4-0-2	Alpha-2	None	0/0	41.22/ -35.67	2465	Outside Extens.
4-0-3	Alpha-2	Cermet	0.002/ -0.002	88.6/-34.5	660	Inside Extens.
4-0-4	Alpha-2	Cermet	0.001/ -0.001	64.7/-30	952	Outside Extens.
4-0-5	Alpha-2	Cermet	0/0	53.76/ -22.89	1094	Outside Extens.
4-0-6	Alpha-2	Cermet	Power	Failure	Aborted	Test

Table 30. Summary of Task 4 TMF results on uncoated and coated Ti-aluminides.